VOL. 556 NOS. 1 + 2 SEPTEMBER 6, 1991
COMPLETE IN ONE ISSUE

Georges A. Guiochon Honour Volume
Part I

RNAL OF
HROMATOGRAPHY
LUDING ELECTROPHORESIS AND OTHER SEPARATION METHODS

SPECIAL VOLUME

ELSEVIER

Scope. The *Journal of Chromatography* publishes papers on all aspects of chromatography, electrophoresis and related methods. Contributions consist mainly of research papers dealing with chromatographic theory, instrumental development and their applications. The section *Biomedical Applications*, which is under separate editorship, deals with the following aspects: developments in and applications of chromatographic and electrophoretic techniques related to clinical diagnosis or alterations during medical treatment; screening and profiling of body fluids or tissues with special reference to metabolic disorders; results from basic medical research with direct consequences in clinical practice; drug level monitoring and pharmacokinetic studies; clinical toxicology; analytical studies in occupational medicine.

Submission of Papers. Manuscripts (in English; *four* copies are required) should be submitted to: Editorial Office of *Journal of Chromatography*, P.O. Box 681, 1000 AR Amsterdam, The Netherlands, Telefax (+31-20) 5862 304, or to: The Editor of *Journal of Chromatography, Biomedical Applications*, P.O. Box 681, 1000 AR Amsterdam, The Netherlands. Review articles are invited or proposed by letter to the Editors. An outline of the proposed review should first be forwarded to the Editors for preliminary discussion prior to preparation. Submission of an article is understood to imply that the article is original and unpublished and is not being considered for publication elsewhere. For copyright regulations, see below.

Publication. The *Journal of Chromatography* (incl. *Biomedical Applications*) has 38 volumes in 1991. The subscription prices for 1991 are:

J. Chromatogr. (incl. *Cum. Indexes, Vols. 501–550*) + *Biomed. Appl.* (Vols. 535–572):
Dfl. 7220.00 plus Dfl. 1140.00 (p.p.h.) (total *ca.* US$ 4400.00)

J. Chromatogr. (incl. *Cum. Indexes, Vols. 501–550*) only (Vols. 535–561):
Dfl. 5859.00 plus Dfl. 810.00 (p.p.h.) (total *ca.* US$ 3510.00)

Biomed. Appl. only (Vols. 562–572):
Dfl. 2387.00 plus Dfl. 330.00 (p.p.h.) (total *ca.* US$ 1430.00).

Subscription Orders. The Dutch guilder price is definitive. The US$ price is subject to exchange-rate fluctuations and is given as a guide. Subscriptions are accepted on a prepaid basis only, unless different terms have been previously agreed upon. Subscriptions orders can be entered only by calender year (Jan.–Dec.) and should be sent to Elsevier Science Publishers, Journal Department, P.O. Box 211, 1000 AE Amsterdam, The Netherlands, Tel. (+31-20) 5803 642, Telefax (+31-20) 5803 598, or to your usual subscription agent. Postage and handling charges include surface delivery except to the following countries where air delivery via SAL (Surface Air Lift) mail is ensured: Argentina, Australia, Brazil, Canada, Hong Kong, India, Israel, Japan*, Malaysia, Mexico, New Zealand, Pakistan, PR CHina, Singapore, South Africa, South Korea, Taiwan, Thailand, USA. * For Japan air delivery (SAL) requires 50% additional charge of the normal postage and handling charge. For all other countries airmail rates are available upon request. Claims for missing issues must be made within three months of our publication (mailing) date, otherwise such claims cannot be honoured free of charge. Back volumes of the *Journal of Chromatography* (Vols. 1–534) are available at Dfl. 208.00 (plus postage). Customers in the USA and Canada wishing information on this and other Elsevier journals, please contact Journal Information Center, Elsevier Science Publishing Co. Inc., 655 Avenue of the Americas, New York, NY 10010, USA, Tel. (+1-212) 633 3750, Telefax (+1-212) 633 3990.

Abstracts/Contents Lists published in Analytical Abstracts, Biochemical Abstracts, Biological Abstracts, Chemical Abstracts, Chemical Titles, Chromatography Abstracts, Clinical Chemistry Lookout, Current Contents/Life Sciences, Current Contents/Physical, Chemical & Earth Sciences, Deep-Sea Research/Part B: Oceanographic Literature Review, Excerpta Medica, Index Medicus, Mass Spectrometry Bulletin, PASCAL-CNRS, Pharmaceutical Abstracts, Referativnyi Zhurnal, Research Alert, Science Citation Index and Trends in Biotechnology.

See inside back cover for Publication Schedule, Information for Authors and information on Advertisements.

0021-9673/91/$03.50

This issue is printed on acid-free paper.

Printed in The Netherlands

For Contents, see p. VII

An authoritative review... highly recommended...

Optimization of Chromatographic Selectivity

A Guide to Method Development

by **P. Schoenmakers,** *Philips Research Laboratories, Eindhoven, The Netherlands*

(Journal of Chromatography Library, 35)

"The contents of this book have been put together with great expertise and care, and represent an authoritative review of this very timely topic... highly recommended to practising analytical chemists and to advanced students." (Jnl. of Chromatography)

"...an important contribution by a worker who has been in the field almost from its inception and who understands that field as well as anyone. If one is serious about method development, particularly for HPLC, this book will well reward a careful reading and will continue to be useful for reference purposes." (Mag. of Liquid & Gas Chromatography)

This is the first detailed description of method development in chromatography - the overall process of which may be summarized as: method selection, phase selection, selectivity optimization, and system optimization. All four aspects receive attention in this eminently readable book.

The first chapter describes chromatographic theory and nomenclature and outlines the method development process. Guidelines are then given for method selection and quantitative concepts for characterizing and classifying chromatographic phases. Selective separation methods (from both GC and LC) are given - the main parameters of each method are identified and simple, quantitative relations are sought to describe their effects. Criteria by which to judge the quality of separation are discussed with clear recommendations for different situations. The specific problems involved in the optimization of chromatographic selectivity are explained. Optimization procedures, illustrated by examples, are described and compared on the basis of a number of criteria. Suggestions are made both for the application of different procedures and for further research. The optimization of programmed analysis receives special attention, and the last chapter summarizes the optimization of the chromatographic system, including the optimization of the efficiency, sensitivity and instrumentation.

Those developing chromatographic methods or wishing to improve existing methods will value the detailed, structured way in which the subject is presented. Because optimization procedures and criteria are described as elements of a complete optimization package, the book will help the reader to understand, evaluate and select current and future commercial systems.

Contents: 1. Introduction. 2. Selection of Methods. 3. Parameters Affecting Selectivity. 4. Optimization Criteria. 5. Optimization Procedures. 6. Programmed Analysis. 7. System Optimization. Indexes.

1986 1st repr. 1987 xvi + 346 pages
US$ 110.50 / Dfl. 210.00
ISBN 0-444-42681-7

ELSEVIER SCIENCE PUBLISHERS

P.O. Box 211, 1000 AE Amsterdam, The Netherlands
P.O. Box 882, Madison Square Station, New York, NY 10159, USA

1991 Joint Meeting
FACSS/Pacific Conference

Eighteenth Annual FACSS Conference
and Thirtieth Pacific Conference

October 6-11, 1991

Disneyland Hotel and Convention Center
Anaheim, California

This joint meeting will focus on emerging technologies in analytical and chemical sciences.

* **Technical Program** - Approximately 1000 papers will be presented in all fields of chemistry and spectroscopy.

* **Workshop Program** - Twelve instructional workshops will be held covering a variety of analytical techniques.

* **Instrumentation Exhibit** - Instrument and laboratory equipment manufacturers, chemical companies, and publishers will be exhibiting.

For registration information and a copy of the 1991 preliminary program, contact:

FACSS
P.O. Box 278
Manhattan, KS 66502-0003
(301)-846-4797

JOURNAL OF CHROMATOGRAPHY

VOL. 556 (1991)

JOURNAL of CHROMATOGRAPHY

INCLUDING ELECTROPHORESIS AND OTHER SEPARATION METHODS

SPECIAL VOLUME

ELSEVIER
AMSTERDAM — LONDON — NEW YORK — TOKYO

J. Chromatogr., Vol. 556 (1991)

0021-9673/91/$03.50

SPECIAL VOLUME

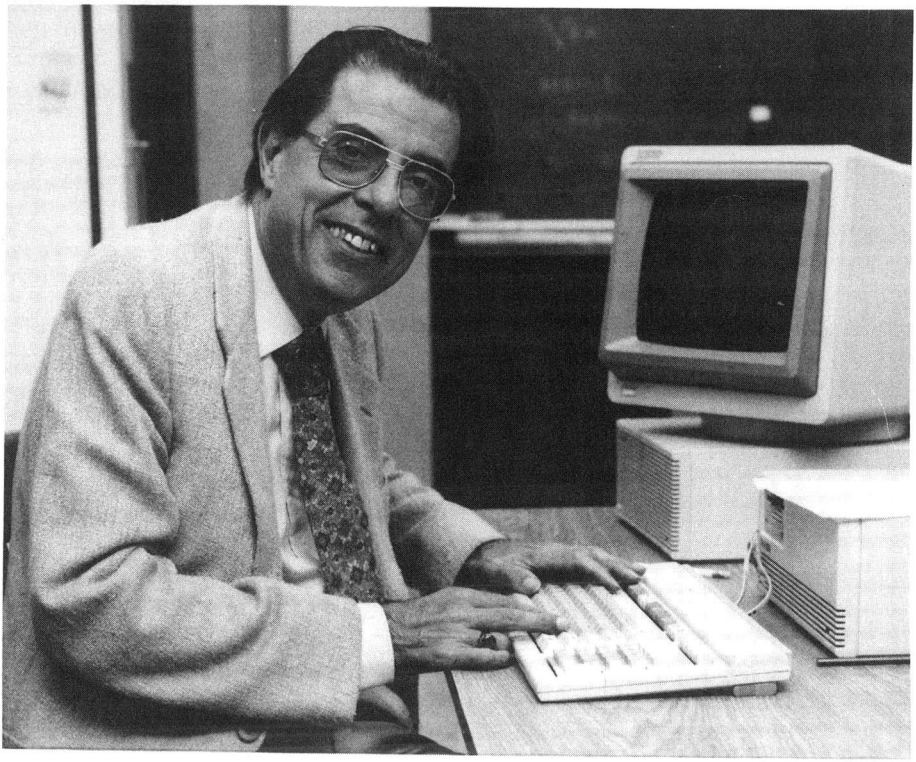

HONOUR VOLUMES

on the occasion of the 60th birthday of

GEORGES A. GUIOCHON

PART I

The papers submitted in honour of Professor **Georges A. Guiochon** on the occasion of his 60th birthday are published in two consecutive volumes of the *Journal of Chromatography*: Vols. 556 and 557 (1991). The Contents of both volumes are published in each of the volumes. A Preface by B. L. Karger appears in Vol. 556 and a Foreword by M. Martin in Vol. 557; a combined Author Index of both volumes is included in Vol. 557.

VOL. 556, NOS. 1+2 JOURNAL OF CHROMATOGRAPHY SEPTEMBER 6, 1991

CONTENTS

HONOUR VOLUMES ON THE OCCASION OF THE 60TH BIRTHDAY OF GEORGES A. GUIOCHON

PART I: VOLUME 556

PART II: VOLUME 557

In articles with more than one author, the name of the author to whom correspondence should be addressed is indicated in the article heading by a 6-pointed asterisk (*)

Journal of Chromatography, 556 (1991) XIII–XV
Elsevier Science Publishers B.V., Amsterdam

PREFACE

It is a great personal pleasure to offer some comments on the professional career of Georges Guiochon to whom this special issue of the *Journal of Chromatography* is dedicated on the occasion of his 60th birthday. It is very hard to imagine Georges is 60 years old, given his vigor and continuing prodiguous scientific productivity.

Georges Guiochon is one of the towering figures of chromatography of the past 30 years. He has been extremely productive with over 500 publications spanning all aspects of the field. His impact has been enormous, and he has often changed people's thinking on various topics, including column design, instrumentation and optimization. While this summary could simply enumerate his accomplishments, many of which are well known to the chromatographic community, I think a more suitable approach is to summarize personal recollections of Georges in the context of his scientific career.

Georges Guiochon began his scientific research in 1954 with his doctoral thesis under the direction of Professor Jacque on the topic of the kinetics of decomposition of ammonium nitrate, or exploding fertilizer. His work earned him an intimate relationship with gas chromatography in its infancy, French bureaucracy (since his findings led to regulations on the storage and transport of nitrogen fertilizers) and a Doctorate degree from École Polytechnique in 1958.

He joined École Polytechnique as an Associate Professor in the laboratory of Leon Jacque in 1958. During the next decade much of his work in gas chromatography was developed. He was greatly influenced during this time by István Halász who always kept Georges' nose pointed in the direction of relevant science. I am sure Georges would agree on the major impact István had on his career. Indeed, many active chromatographers owed a debt of gratitude to Professor Halász, including Csaba Horváth, Heinz Engelhardt and myself. Sadly, István Halász passed away in 1988.

I first came in contact with Georges in the middle 1960s after two papers on time normalization optimization in gas chromatography, based on my Ph.D. thesis, were published. I received this lengthy letter in broken English from someone I had only passing knowledge of. Most of Georges' papers at this time were written in French. Of course, Georges' remarks led to major works on his part dealing with column optimization and design.

We first met each other in 1967 when he visited Boston for the first time. Our friendship has continued for almost 25 years. Georges was introduced to one of his great loves during that visit —the lobster. One rapidly learns that it is mandatory to arrange a lobster meal for Georges anytime he is near the New England area.

By the late 1960s Georges had already become a major figure on the international scene of chromatography. He could be characterized as a theoretician, but his work had then (and still has) the ability to address the practical and significant issues of the day. Theory was always driven by experiment, and one invariably comes away from his papers with the recognition that something important has been learned. We need only to recall his major contributions to gas–solid adsorption theory, in line with the studies of Professor Kiselev of the USSR, preparative gas chromatography, ultra-

high-precision retention measurements and the characterization of column type and design. He summarized his vast knowledge with the 1988 publication of the book Quantitative Gas Chromatography, coauthored with C. Guillemin.

Based on his accomplishments and rèputation, in 1968 he was appointed as Director of the Laboratoire de Chimie Analytique Physique at École Polytechnique as well as Associate Professor, University of Paris VI. It was during this time that I spent three months in his laboratory, in early 1972. It was an experience I will never forget. I learned how blessed Georges was with the quality of his students at École Polytechnique. But without his leadership and direction, these budding scientists would never have reached their true potential. Undoubtedly, Georges derives a great deal of satisfaction from the high regard in which he is held by his former students, many of whom have gone on to very successful careers. In 1974 he rose to the rank of Professor, École Polytechnique and the University of Paris VI, a very distinghuished position.

It was in this period that he began his work in liquid chromatography. By the end of the 1970s he was clearly a dominant figure in this field. He not only dealt with the problems of analysis but focused carefully on this issue of column design and resolution optimization. He delineated the relationship of normal packed (4.6 mm I.D.), to microbore (1 mm I.D. or less), to packed capillary and finally to capillary liquid chromatography columns. This work remains today of high importance, particularly as capillary electrophoresis has become intertwined with liquid chromatography, and both techniques are increasingly coupled to mass spectrometry.

I recall the major commitment Georges had during this period to a joint French–Soviet project to analyze the atmosphere of Venus. Georges was brought into the program because of his expertise in gas analysis. While he left France before the project could come to fruition, he nevertheless clearly enjoyed the great challenge to design a gas chromatograph suitable for space and the Venetian atmosphere.

Another of Georges' great loves in life is America, and especially science in the USA. From afar, he always felt we were less bureaucratic than France, but I am not sure he would agree after experiencing first hand the USA. Because of his enthusiasm, Georges decided in the early 1980s it was an opportune time to come to America. Many of us admired the courage of his decision to leave a very productive laboratory and in essence begin a new career.

In 1984 he moved to Georgetown University where he remained until 1987 when he joined the University of Tennessee as a Distinguished Professor, with a joint appointment with the Oak Ridge National Laboratory. As any new immigrant, Georges struggled a little at first, particularly in procuring government funding of his research. This struggle was rapidly overcome so that today he is well-funded on his research program.

Georges likes to joke about the irony of an urbane Frenchman living in Knoxville, TN. But the truth is he appears very happy. He has been more productive than at any time in his career, if that were at all possible. Many of us are jealous of the time he has available for science. His wife, Lois Beaver, works for the Food & Drug Administration in Washington, but they see each other every other weekend. Also, invariably they will be together at scientific conferences.

Since coming to the USA, Georges has focused his program on non-linear behaviour in chromatography. His excellent models of overloading have led to im-

portant simulations of competitive adsorption behavior in chromatography, comparison of displacement *vs.* overloaded elution, and the general optimization of preparative scale chromatography. His work has had a major impact on the role of chromatography as a purification tool.

In the course of his very full career, he has collected a number of kudos. For example, the Hungarians honored him with a Doctor Honoris Causa from the Technical University in Budapest in 1982. In 1974 he was made an Honorary member of the Chromatography Discussion Group of the UK (the first foreigner to be so honored). In 1980 the same Group awarded him the A. J. P. Martin Medal. The Spanish recognized him in 1980 when they inducted him into the Socio de Honor of the Real Sociedad Espanola de Fisica y Quimica. There is a story around the awarding of the Tsvet Memorial Medal by the Academy of Sciences of the USSR in 1978 which is best told by the honoree. Of course, the French have given him numerous awards, including the Chevalier des Palmes Academiques, the Chevalier de l'Ordre National du Merite and the Silver Medal of the Centre National de la Recherche Scientifique. Recently, he has been honored with the American Chemical Society Award in Separation Science and Technology.

Dissemination of separation science has been a continuing interest of Georges as evidenced by his career in academia, his 500 plus publications, his editorial functions, and his organization of over twenty-five symposia, four of which were major international meetings attended by a total of 4500 scientists. In keeping with his active pursuit of scientific information exchange, Georges Guiochon was selected by Clark Hamilton, the inventor and manufacturer of microsyringes for chromatography, to manage a Foundation which supported exchanges of scientists between Eastern and Western Europe and distributed research grants. During the ten years under his management, the Scientific Exchange Agreement Foundation awarded about 150 research grants and permitted several hundred scientists, mainly from Czechoslovakia, Hungary and Poland to attend symposia and to work with Western scientists.

In conclusion, on behalf of the whole community, I wish to congratulate Georges Guiochon on his enormous impact on the advancement of the field of chromatography. It has been a personal pleasure knowing Georges as a friend and colleague. It is fitting that a special honorary volume of the *Journal of Chromatography* containing the papers of his friends be published. May he continue to be productive for another 20 years or more!

Boston, MA (USA) B. L. KARGER

Journal of Chromatography, 556 (1991) 1–24
Elsevier Science Publishers B.V., Amsterdam

CHROM. 23 409

Review

Methods of equilibrium concentration for the gas chromatographic determination of trace volatiles

A. G. VITENBERG
Chemistry Department, Leningrad State University, Petrodvorets, University Prospekt 2, Leningrad 198904 (USSR)

ABSTRACT

This review deals with a gas chromatographic technique based on the use of equilibria in the condensed phase–gas system, which is currently in the stage of intense development. Problems bearing on the usefulness of different variants of headspace analysis and of related methods in reducing the threshold of the gas chromatographic determination of volatile impurities in objects taken in any aggregate state are considered. When analysing impurities in solid and liquid objects, major attention is focused on the specific features of headspace analysis and methods of improving its sensitivity. For gas objects the same problems are treated in the context of the reverse technique, *i.e.*, equilibrium saturation of a condensed phase with the gas to be analysed.

The theory and practice of equilibrium concentration, including headspace analysis techniques, are developing so fast that even fairly recent reviews and monographs no longer reflect the state of the art of this area in organic analysis. The methods of headspace analysis and its new modifications provide fairly accurate and selective determinations of a variety of impurities present in complex mixtures at the $\mu g/l$ level or lower, and find broad application in the analysis of environmental samples and in biology, medicine, geochemistry, oceanology, power engineering, etc.

The review covers studies made in the field of headspace concentration and related methods in the last 10–12 years. Attention is focused primarily on the description of the fundamentals of these methods and the areas of their applicability.

CONTENTS

0021-9673/91/$03.50

1. INTRODUCTION

The present-day requirements concerning the sensitivity of methods used to measure the content of harmful volatile impurities are so stringent that direct injection of a sample into the chromatograph may not ensure the desired detection limit. Indeed, transfer of liquid or gaseous samples to a chromatograph equipped with a flame ionization detector permits the determination of impurities at a level of a few milligrams per litre of liquid or per cubic metre of gas. The allowable concentrations in such essential objects as natural or tap water and atmospheric air are one to five orders of magnitude lower. Therefore, in common analytical practice one frequently uses various adsorption, absorption and cryogenic methods of concentration. While these traditional methods based on complete extraction of an impurity from an object under study are employed widely in trace analysis (see, *e.g.*, ref. 1), they possess a number of drawbacks associated with the need to remove water, or exclude its adverse action, to prevent or take into proper account the breakthrough of the analyte, etc. Some shortcomings of the traditional methods of concentration can be eliminated by using, in place of complete absorption, the principle of equilibrium concentration[a] [2,3] where the impurity to be trapped distributes in a trap between the condensed phase and the gas in accordance with a simple law governing the partitioning of a compound in a heterogeneous system:

$$K = C_L/C_G \tag{1}$$

where K is the partition coefficient and C_L and C_G are the equilibrium concentrations of the compound in the condensed and gas phases, respectively.

In contrast to complete trapping, the equilibrium mode tolerates breakthrough of the analyte and is used in most instances under conditions which do not require measuring the gas volume. The methods of equilibrium concentration are based on the laws governing gas extraction and headspace analysis (HSA) [4–9]. The latter occupies a key place among modern techniques for the determinations of volatile organic impurities.

The concentration methods currently in use can be classified according to the aggregate state of the object under study and to the actual approach used for the adsorption and absorption trapping of impurities in gas objects, frontal (sorption) and absorption concentration of volatile impurities present in liquids and solids.

The equilibrium-concentration of impurities present initially in gas objects

[a] The term "equilibrium concentration" was introduced by Ioffe *et al.* [9] and applied for the first time to the absorption concentration of atmospheric air impurities with their subsequent gas chromatographic characterization.

differs from the concentration of compounds extracted from liquids and solids in the absence of the gas extraction stage and may be considered as an inverse method to headspace analysis. In the course of trapping, the compound likewise distributes between the condensed and gas phases, but in the direction opposite to that typical of HSA, namely, the condensed phase extracts impurities out of the gas. This imparts certain features to the concentration methods based on sorption, the most essential being the constancy of the analyte content in the gas under study and predominant use of dynamic conditions in the concentration process.

Combining HSA with preconcentration before injecting the enriched sample into the chromatographic column can be done in several ways, namely, when the equilibrium gas extraction of compounds from a solution or a solid object occur under static or dynamic conditions, and the concentration in an adsorption or absorption trap is carried out in the complete or equilibrium trapping mode. Cryogenic concentration can be used only under the complete trapping conditions.

The above methods of concentration differ in technical detail, are described by radically different relationships and are characterized by different possibilities of sensitivity and selectivity improvement.

2. EQUILIBRIUM CONCENTRATION OF IMPURITIES PRESENT IN GAS OBJECTS

Outwardly, the process of equilibrium concentration differs little from methods involving complete trapping of analytes from gases. There is, however, a radical distinction between these methods in that under the complete trapping conditions the gas under study can be passed only before the breakthrough of the analyte. Further saturation of the concentrator with the gas results in a loss of the accumulating compound and, eventually, in large analytical errors. Equilibrium concentration is achieved by passing the gas through the absorber until the impurity concentrations in the gas flow at the entrance to and exit from the trap become equal, *i.e.*, until the absorption capacity of the trap has become exhausted. As a result of this difference in the concentrator saturation regime, in order to calculate the initial impurity concentration under total trapping one has to measure the gas volume passed and to avoid exceeding a certain maximum volume (V_g^{max}) for which the breakthrough volume just reaches the allowable limit (δ). In equilibrium concentration, however, one has to pass a minimum volume of gas (V_g^{min}) at which the impurity concentration throughout the absorber volume reaches the equilibrium value. Further streaming of the gas will no longer change the analyte concentration (mass) in the trap, the analytical result being calculated based on the parameters of the analyte partitioning between the two phases. Thus the equilibrium concentration, in contrast to complete trapping, ensures more efficient use of the sorbent and does not require measurement of the gas flow volume.

Two variants of equilibrium concentration in non-volatile and volatile liquids have been developed, experimentally verified and put into service. They are technically different and possess different possibilities and limitations.

Equilibrium concentration in non-volatile liquids (stationary phases for gas chromatography) was proposed in 1965 [10] and was used subsequently by Novák, Janak and co-workers [11,12], Dravnieks, Krotoszynski and co-workers [13–16] and others [17–19] in the 1970s and 1980s for the concentration of multi-component

mixtures of volatiles of complex composition [19] and of compounds emitted from polymer materials into the atmosphere [17]. The theory of the method proposed by Novák *et al.* [10] was subsequently developed and refined [17,20–22].

Equilibrium concentration in volatile liquids (allowing the use of low-volatility liquids) was proposed by Ioffe, Vitenberg and co-workers [9,23–26] for the determination of toxic microimpurities in gases, the method having been applied also to the determination of alcohols in air [27].

There is an essential difference between these two variants of the equilibrium concentration. Direct injection into the chromatograph of a solution in a non-volatile solvent is undesirable. Accumulation of a non-volatile liquid in a chromatographic column may result in a substantial change in the retention parameters and a sharp drop in the separation efficiency, as it is difficult to realize the instantaneous release of volatiles from a non-evaporating solvent. Therefore, equilibrium concentration in non-volatile solvents is achieved in the form of frontal saturation of a thin liquid film deposited on a solid support [10–13,15–17] (*i.e.*, chromatographic packing) or directly on the tube walls [14]. The concentrate obtained in this way in the non-volatile liquid is subsequently subjected to thermal desorption in a carrier gas flow, with the total amount (rather than a fraction) of the volatile components absorbed in the trap being determined in a single measurement.

Equilibrium concentration in volatile liquids is achieved through absorption of the impurities present in a gas by bubbling it through a layer of a well mixed trapping liquid. Therefore, it differs from the frontal adsorption variant primarily in that the impurity concentration in the liquid increases uniformly throughout the volume in the course of saturation. Apart from this, the concentrate in a volatile liquid can be injected directly into the chromatograph, with the analysis being repeated as many times as needed.

As a result of these specific features of the adsorption and absorption variants of the equilibrium concentration method developed for impurities in gaseous objects, these processes are described by radically different relationships.

2.1. Equilibrium frontal concentration

This is based not only on the solution of the impurity vapours in a thin layer of a non-volatile liquid but also on adsorption on the surface of the liquid and the solid support [28–30]. The actual contributions of each of these effects to the trapping of a compound in the absorption column (or to retention in the case of chromatography) are determined by the nature and properties of the packing and of the liquid phase, and by their relative amounts. Therefore, the theory of frontal concentration is based on the retention parameters of a chromatographic column which has the same size and packing as the concentrator, *i.e.*, the same retention volume V_R^0. The quantity V_R^0 takes into account automatically the adsorption and absorption effects affecting the amount of the trapped compound.

Having determined gas chromatographically (usually by means of thermal desorption) the mass of the concentrated compound (m_c), one can calculate the analyte concentration (C_G^0) by a simple relationship:

$$C_G^0 = m_c/V_R^0 \tag{2}$$

The minimum gas volume (V_g^{min}) required to ensure equilibrium concentration along the trap can best be determined from the retention parameters (see p. 180 in ref. 7):

$$V_g^{min} = V_R^0 + \Delta V_R^0 \tag{3}$$

where ΔV_R^0 is the gas volume required for elution of half of the chromatographic band out of the column.

The sensitivity (S) of frontal concentration can likewise be expressed in terms of the retention parameters [7,8]:

$$S = fV_R^0 \tag{4}$$

where f is a coefficient accounting for the sensitivity of the chromatographic detector used to the analyte in question.

The possibilities of the method can be illustrated more graphically than is revealed by eqn. 4 by introducing the relative sensitivity (α) of the frontal equilibrium concentration, *i.e.*, the degree of reduction of its detection threshold compared with direct injection of the analyte gas into the chromatograph:

$$\alpha = V_R^0/v_g \tag{5}$$

where v_g is the volume of the gas sample pulse-injected into the chromatograph. This relationship may serve as a criterion in evaluating the usefulness of frontal equilibrium concentration to reduce the gas chromatographic detection threshold for volatile impurities in gaseous objects.

Eqns. 4 and 5 show that in order to improve the sensitivity of frontal concentration one has to increase V_R^0. For large V_R^0, however, the time required to remove an analyte from the concentration column in the cours of thermal desorption becomes substantially longer, which results in a reduced efficiency of chromatographic separation and puts a limit on the possibilities of the method in the variant of direct and complete desorption proposed by Novák *et al.* [10]. The ultimate possibilities of the method as related to reducing the impurity detection limit are usually limited by the value $\alpha = 100$.

The analytical aspects of equilibrium frontal concentration on polymer sorbents with subsequent capillary column gas chromatographic analysis were studied by Novotny *et al.* [19]. As a sorbent for mixtures of complex composition (food odours, volatile components of biological samples or atmospheric pollutants), one can recommend Tenax GC, which is capable of concentrating both polar and non-polar compounds. However, the chromatogram quality and also the possibility of quantitative analysis and of the identification of individual components depend to a considerable extent on the actual conditions of sample injection into the capillary column.

Pulsed injection of a thermally desorbed compound into the chromatographic column can be obtained by incomplete removal of the impurity from the concentrator [7,8]. The sensitivity of frontal concentration can also be improved by accumulating the impurities in a cryogenic trap prior to their transfer to the chromatographic column [13,14].

Equilibrium frontal concentration was tested on model vapour–gas mixtures of lower aromatic hydrocarbons, acetone and methanol in air over the concentration range 0.3 mg/l–0.3 μg/l [10]. Direct injection of the analyte gas into the chromatograph was used as a reference method. This technique was employed to analyze the air in factory shops polluted by benzene, chlorobenzene and nitrobenzene [11] and the air in surgery rooms for the presence of halothane [12] and to study the composition of the volatiles evolving from polymer materials [17]. The equilibrium and chromato-distributive [31] concentrations were combined [18] to identify the impurities present in air.

2.2. Equilibrium absorption concentration

This removes the complications arising from the need for thermal elution of the trapped impurities from non-volatile liquids or adsorbents. This method consists in saturating a few millilitres of a pure volatile liquid with a finely dispersed analyte gas. A small sample (1–5 μl) of the concentrate thus obtained is then injected directly into the chromatograph.

The theory of the method [23,24,26] yields the following equation:

$$C_L = KC_G^0 \cdot \frac{f_s}{1 - FK}\left[1 - \left(1 - F \cdot \frac{V_g}{V_L^0}\right)^{\frac{1-FK}{FK}}\right] \tag{6}$$

which describes the variation of the impurity concentration in the trapping liquid (C_L) as the gas under study is passed through it, as a function of the content in the former of the microimpurity of interest (C_G^0), its partition coefficient (K), initial volume (V_L^0) and volatility (F) of the absorbing liquid: $F = p_L M/RTd_L$ (here M is the molecular mass and p_L and d_L are the saturated vapour pressure and trapping liquid density at temperature T, R is the universal gas constant), as well as of a coefficient $f_s = (p_a - p_L)/p_a$, which accounts for the change in the volume of the gas after its passage through the solution of the volatile absorbing liquid (p_a is the atmospheric pressure).

An analysis of eqn. 6 shows the method to be useful only for $FK < 0.5$. In other words, for the equilibrium absorption concentration to be applicable in analytical practice, the volatility of the trapping liquid should be less than half that of the analyte which is characterized by $1/K$.

For a non-volatile trapping liquid $F \to 0$, and eqn. 6 transforms into an exponential function:

$$C_L = KC_G^0 \cdot \left[1 - \exp\left(-\frac{V_g}{KV_L^0}\right)\right] \tag{7}$$

One can refrain from measuring the volume of the gas passed through the absorber and calculate the analyte content in the gas by the equation

$$C_G^0 = \frac{C_L^{lim}}{K} \cdot \frac{1 - FK}{f_s} \tag{8}$$

if the gas volume passed has become larger than

$$V_g^{min} = \frac{V_L^0}{F}\left(1 - \delta^{\frac{FK}{1-FK}}\right) \quad (9)$$

where C_L^{lim} is the limiting impurity concentration in the solution differing from the equilibrium value by not more than the error of its measurement δ.

The sensitivity of equilibrium absorption concentration depends primarily on the numerical value of K. This is clearly seen from the relationship

$$\alpha = \frac{m_L}{m_g} = \frac{v_L}{v_g} \cdot K \cdot \frac{f_s}{1 - FK} = \frac{K}{10^3}\frac{f_s}{1 - FK} \approx \frac{K}{10^3} \quad (10)$$

which characterizes the change in the analytical sensitivity compared with direct introduction of the gas under study into the chromatograph. Here m_L and m_g are the masses of the analyte introduced into the chromatograph in the form of a liquid concentrate of volume v_L or of a gas sample of volume v_g, respectively.

It has been shown [32] that in the case of a concentrate injected directly into the column, equilibrium absorption concentration permits the lowering of the gas chromatographic detection threshold by more than an order of magnitude while being slightly inferior to the variants involving impurity trapping on the column packing.

Thus, apart from different degrees of enrichment, the principal difference between the above two methods of equilibrium concentration of impurities present in gaseous objects is that using the absorption technique one determines the concentration of the trapped analyte rather than its total amount. In addition, it becomes possible to choose a suitable solvent from a large number of compounds, while the elimination of the thermal desorption stage permits the characterization of unstable compounds and improves the reliability of analysis.

One should also point out an essential distinction between the absorption and frontal concentration techniques connected directly with the specific features of impurity build-up in the concentrator. In frontal concentration, the mass of the trapped impurity (m_L) increases linearly (Fig. 1) with the volume of the gas passed through the concentrator, as long as $V_g^{max} \leqslant V_R^0 - \Delta V_R$. The first part of the concentration curve limited by the volume V_g^{max} corresponds to total trapping of the analyte (with no breakthrough). The calculation of the initial concentration C_G^0 within this section includes the gas volume passed. A further increase in V_g in the interval $V_R^0 - \Delta V_R \leqslant V_g \leqslant V_R^0 + \Delta V_R$ results in a non-linear increase of the mass of the concentrated impurity. The behaviour of the $m_L(V_g)$ relationship in the second part of the plot is determined by the shape of the analyte distribution isotherm in the concentrator, usually remains unknown, and is not used in analytical practice. In this part of the concentration curve, partial breakthrough of the impurity through the absorbent begins (Fig. 2). Equilibrium concentration occurs in the third part of the curve for $V_g > V_R^0 + \Delta V_R$. This regime is characterized by a constant content of the trapped impurity in the concentrator (Fig. 1), *i.e.*, by a total breakthrough of the impurity or a linear increase in the mass of the impurity passing through the concentrator (Fig. 2).

The absorption concentration has a distinctive feature in that the impurity starts partially to break through the trap with the very first portions of the gas flow, the

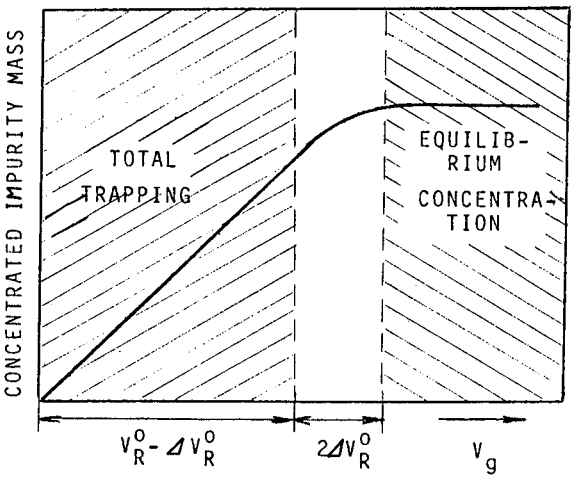

Fig. 1. Variation of the mass of the trapped analyte in the course of frontal sorption concentration.

build-up of the analyte in the concentrator up to the equilibrium state occurring exponentially. The regime of total trapping (Fig. 3) is limited by the allowable difference between the impurity concentrations achieved in the absence of breakthrough (curve I) and the absorption build-up (curve II). This difference should not usually exceed the error in the analyte concentration measurement in the absorbing solution (δ). The absorption equilibrium concentration regime sets in after the condition in eqn. 9 for V_g^{min} has been met.

The above equations describing the principal relationships which govern the absorption concentration not only permit one to calculate the equilibrium concentration parameters but can also be used to evaluate the optimum absorber volume and the allowed volume of the gas (V_g^{max}) passed under the total absorption conditions. The

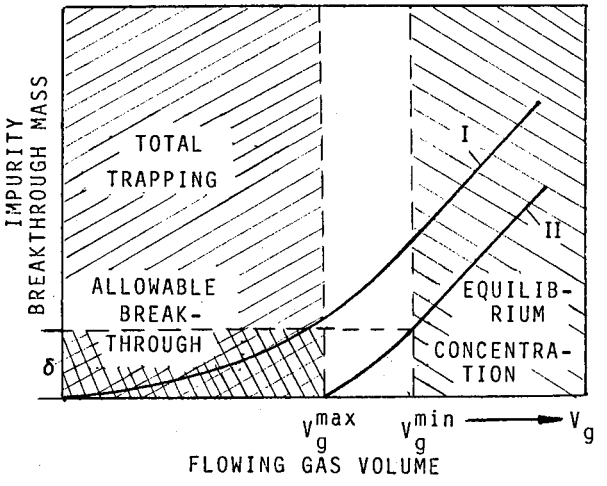

Fig. 2. Analyte breakthrough in (I) absorption and (II) frontal equilibrium concentration.

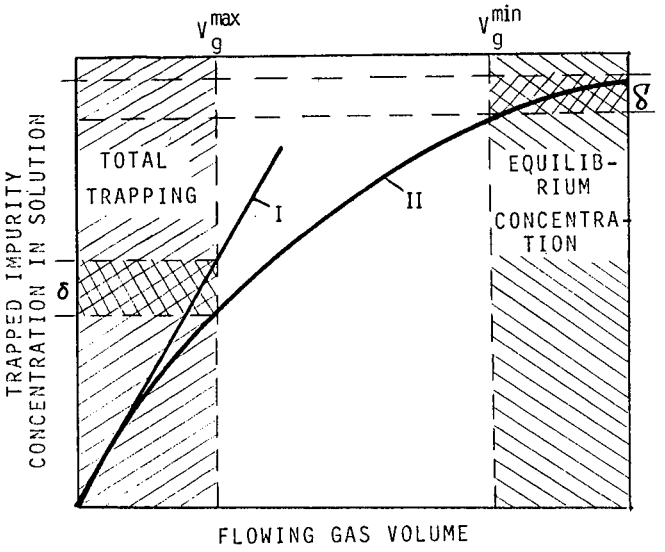

Fig. 3. Variation of analyte concentration in liquid absorber in the course of absorption concentration. (I) Total analyte absorption; (II) equilibrium concentration.

concentration parameters are still chosen arbitrarily without taking into proper account the absorbing capacity of the trapping liquid and the volatility of the analytes. As a result, the chosen volumes of the absorbent and of the analyte gas, and also the flow-rate of the latter, may turn out to be far from the optimum values. Apart from this, the combination of the total absorption and equilibrium concentration regimes in one sampling cycle eliminates errors in the analysis of the mixtures whose components differ substantially in the boiling temperature and solubility in the trapping liquid. High-volatility compounds can be trapped under the equilibrium concentration conditions, the less volatile being captured totally in the trap.

The basic points of the theory of equilibrium absorption concentration were checked for the absorption of aromatic hydrocarbon vapours with acetic acid, and also for some oxygen compounds and diethylamine with water [25,26]. Concentration of compounds with variable partition coefficients has also been considered [33,34].

In addition to these impurities, absorption equilibrium concentration has been used to develop gas chromatographic methods for the determination of gas moisture content [32,35] (with *n*-butanol as absorbent and *ca.* 1 μg/l detection threshold), of aliphatic alcohols in atmospheric air (trapping in air with a detection threshold of *ca.* 1 mg/m^3) [27] and of unstable lower thiols together with sulphides in natural gas and air [36] (benzene as absorbent, flame ionization detection, detection threshold at the *ca.* 1 mg/m^3 level).

The possibility of determining unstable impurities is the most essential asset and a distinctive feature of equilibrium concentration. Whenever the analytes undergo chemical transformations in the course of sampling, any method based on the total absorption of impurities during concentration will result in large errors. The collection of gas samples containing unstable compounds without introducing substantial

distortions is made possible by the fact that the loss of the impurities trapped in the concentrator is compensated for by their inflow with the subsequent gas portions, the volume of the gas passed not entering into the calculations.

Another feature of the equilibrium methods of concentrating impurities present in gaseous objects lies in the selectivity of impurity build-up in the absorber [7,8]. This opens up the possibility of separation from concomitant components in the concentration stage, which can be done only in the case of compounds with very different partition coefficients.

3. HEADSPACE CONCENTRATION OF VOLATILE IMPURITIES PRESENT IN LIQUID AND SOLID OBJECTS

Headspace concentration (HSC) is employed to increase the sensitivity of HSA and to reduce the detection limit of the gas chromatographic detection of volatiles present in liquids and solids. In the literature, by headspace concentration one usually understands the modifications of analysis involving intermediate (cryogenic, adsorption or absorption) accumulation of the compounds present in the gas phase above the sample under study before their injection into the chromatographic column. The sensitivity of these variants of HSA is increased by increasing the single-injection dose of the equilibrium gas. This is seen readily from the equation [7,8,32] describing the sensitivity of the principal HSA variant, *i.e.*, single gas extraction:

$$S = f \cdot \frac{v_g}{K + r} \tag{11}$$

whence it follows that, in addition to increasing the sample volume (v_g) injected into the chromatograph, the HSA sensitivity (S) can also be enhanced by reducing the partition coefficient (K), choosing an optimum ratio of the gas (V_g) to condensed phase (V_L) volumes ($r = V_G/V_L$) and by using selective detection (the factor f taking into account the sensitivity of the detector used to the analyte in question). Such modifications of HSA resulting in an improvement in its sensitivity and a reduction in the gas chromatographic detection limit should also be classified among HSC methods.

The gain in the gas chromatographic sensitivity obtained in direct HSA compared with direct injection of a sample into the chromatograph can be written as [32]

$$\alpha = \frac{10^3}{K + r} \tag{12}$$

and is reached at $\alpha > 1$, *i.e.*, when $K < (10^3 - r)$. The values of the partition coefficients between water and air for a number of compounds of interest for environmental monitoring range within 4–5 orders of magnitude (Table 1). The sensitivity and threshold of the HSA determination of these compounds also vary accordingly. Indeed, whereas gaseous hydrocarbons (methane, ethane, ethylene, etc.) present in water solutions can be detected in the most favorable cases at a level of 0.1–1 μg/l, for higly soluble compounds with $K > 10^3$ (alcohols, phenols, volatile fatty

TABLE 1

PARTITION COEFFICIENTS OF VOLATILES IN THE AIR–WATER SYSTEM AT 25°C

Compound	$K \pm \Delta K^a$	Ref.	Compound	$K \pm \Delta K^a$	Ref.
Methane	0.034	8	Acrolein	180	39
Ethane	0.045	8	Propionaldehyde	330	43
Propane	0.037	8	Dibutyl ether	5.3 ± 0.2	32
Ethylene	0.12	8	Methyl acetate	190 ± 5	32
Propylene	0.18	8		190	44
Acetylene	1.01	8	Ethyl acetate	150 ± 2	32
Methylacetylene	1.7	8		144	44
Benzene	4.0 ± 0.1	37	*n*-Butyl acetate	87 ± 2	32
Toluene	3.6 ± 0.2	37		87	44
m-Xylene	4.6 ± 0.3	37	Methyl propionate	130 ± 5	32
Chloroform	8.5 ± 1.4 (20°C)	38		141	43
Carbon tetrachloride	9.9 ± 1.9 (20°C)	38	Methyl butyrate	90 ± 5	32
Hydrogen sulphide	2.5	8		120	43
Ethanethiol	5.4 ± 0.3 (20°C)	45	Dioxane	5750 ± 450	32
Dimethyl sulphide	14.8 ± 1.4 (20°C)	45		5400	41
Dimethyl disulphide	20.2 ± 2.0 (20°C)	45	Methanol	5500	39, 40
Acetone	580 ± 45	32	Ethanol	5260 ± 610	32
	630	39		4800	40
	610	42		5700	41
Methyl ethyl ketone	380 ± 40	32	Propanol	4090 ± 390	32
	430	39		3600	40

[a] $n = 5$–7.

acids) the detection limit exceeds 1 mg/l, which is usually unacceptably high for the determination of toxic compounds. In such instances one frequently resorts to the methods of enhancing HSA sensitivity which involve reducing K or r and are now well studied [4–8].

To reduce K, one frequently increases the equilibrium onset temperature or uses salting-out (when determining impurities in aqueous solutions). Each of these techniques permits one to reduce K from 5 to 10, so that by combining them the detection limit can be decreased by 1.5–2 orders of magnitude. One can facilitate the characterization of impurities in volatile solvents (alcohol, acetic acid, dioxane) by diluting them with water [32]. A promising approach for reducing the detection limit of gas chromatographic HSA of readily soluble and chemically reactive compounds (such as lower aliphatic alcohols, carboxylic acids and phenols in water) lies in their conversion into more volatile and less soluble derivatives (see, *e.g.*, ref. 46). However, the most widely recognized among the various HSC methods are currently those involving intermediate cryogenic or sorption concentration.

Intermediate headspace accumulation of compounds in a trap before their introduction into the chromatographic column is needed in cases where direct injection either does not provide a sufficiently high analytical sensitivity or reduces the separation efficiency, as this may occur when using a capillary column.

The actual magnitude of the sensitivity enhancement of HSA with intermediate impurity concentration depends on the volume of the gas passed through the trap and may be as high as 2–4 orders of magnitude. A correct choice of the concentrator parameters is of particular significance here. The search for the optimum regimes and

the potential and limitations of the HSA techniques involving concentration have been discussed [47–54]. In cryogenic accumulation these critical points are the trap design and the temperatures required for total absorption of the analytes, their separation from concomitant compounds (*e.g.*, water) and their subsequent quantitative removal from the concentrator. The factors essential for the adsorption accumulation are the nature and volume of the adsorbent in the trap and the adsorption and desorption temperatures. The conditions and relationships governing the build-up in the trap of a compound stripped by the gas from the object under study differ substantially, depending on the properties of the analyte and of the sorbent, and on the actual concentration technique chosen.

Various modifications of HSC have been developed for use under static and dynamic conditions. The latter variant (frequently referred to as purge and trap) is more efficient, because by using a large volume of the extracting gas one can achieve a higher degree of enrichment. Apart from this, for the same gas volumes continuous gas extraction (CGE) ensures a more complete removal of the analyte from the sample [55]. Indeed, static HSA is employed much less frequently than that under dynamic conditions [7,8]. The method of CGE with subsequent accumulation of the impurities stripped by the carrier gas has found broad applications in the analysis of a wide variety of objects, ranging from the determination of volatile organic compounds in water and aqueous solutions to the characterization of complex aromas [7,8,51,56–67]. Dynamic HSA with intermediate concentration has also been applied to the analysis of foodstuffs [68–72], wine [73], cigarette filters [74], volatiles evolving from plants [75–77] and polymer materials [78–80], and to the chemotaxonomy of insects [81]. However, despite the high efficiency of CGE, the difficulties encountered in carrying out dynamic gas extraction under equilibrium conditions in the case of incomplete removal of an analyte from a sample, in addition to the high cost and long time taken up by an analysis, the artefacts related to thermal desorption and the presence of impurities in the extracting gas, make the static regime sometimes preferable in quantitative analysis [58,59,82–84]. From the technical standpoint this method is simpler, it provides gas extraction under equilibrium conditions and a high reproducibility of the degree to which one approaches phase equilibrium and, hence, of the fraction of the total amount of the analyte that enters the gas phase.

The equipment and techniques of headspace concentration which are based on dynamic and static HSA are described in reviews [56,57], monographs [4,5,7,8] and original papers [58,82–85]. One can find publications on commercial instrumentation and laboratory set-ups designed for routine analytical work in automatic and semi-automatic modes [82,83,86–89].

3.1. Cryogenic trapping of impurities

Cryogenic trapping of the impurities stripped with a gas from a solution or solid sample under study is employed only under conditions of complete trapping of the analyte, when the total mass of the impurity evolving from the object to be analysed into the gas phase is deposited in the trap and, after the latter has been heated, is injected into the chromatograph in a single step. A review [90] describes the various systems used to achieve cryogenic focusing.

For this analysis to be quantitative, the low-temperature traps have to be highly efficient. As traps one usually employs empty glass or quartz capillary tubes, and

sometimes the initial part of a capillary column or capillaries filled with glass beads. The latter are more efficient and are capable of retaining alkanes quantitatively. When using open capillaries, one should take into account not only the trapping temperature (which should be chosen as low as possible) but also the carrier gas flow-rate, trap geometry and the analyte concentration.

The enhancement of the analytical sensitivity depends on the amount of the analyte removed from the solution under study. In dynamic HSA, the fraction of the analyte extracted from a solution (Z_d) is dependent on the amount of the initial solution, its temperature and the volume of the gas passed, and for a system with a non-volatile solvent is described by the equation [91–93]

$$Z_d = 1 - \exp(-r/K) \tag{13}$$

For instance, in order to reach the detection threshold of a few fractions of a μg/l when $K = 10^3$, one will have to extract the analyte nearly completely ($Z_d > 0.95$) with a flow of a pure gas from 10 ml of solution. The required volume of the extracting gas should be about 30 l. If, however, the impurity is extracted from 100 ml of the solution, less than 10 l of pure gas will have to be passed to reach the same detection limit. A similar effect can be obtained by raising the solution temperature in CGE. A positive effect is given also by addition to aqueous solutions of large amounts of inorganic salts, because this usually results in a pronounced change of the vapour composition in favour of the analytes. To illustrate the potential of this technique, consider the detection of Freons in sea water [94]. Stripping of Freon 11 and 12 dissolved in 30 ml of water with their subsequent cryogenic focusing permits the determination of these compounds using a packed column with an electron-capture detector at levels down to a few hundredths of 1 pmol/kg in solution.

The appropriate regime of analyte extraction from solutions in a volatile solvent can be chosen based on the CGE relationships [95].

Under static conditions, the fraction of a volatile analyte (Z_s) removed from a system by passing through the trap the total volume of the gas phase is given by the expression

$$Z_s = \frac{r}{K + r} \tag{14}$$

When the analyte is accumulated in the concentrator under the conditions of partial sampling of equilibrated gas from a vial [96], *e.g.*, as is done in the pneumatic headspace sampling technique [83,97–99], the amount of the analyte (m) collected in n samplings depends on, in addition to the numerical values of K and r and the total amount of the compound in the sample vial (M_0), also the pressure drop in the system ($\Delta P = p/p'$) before (p') and after (p) the sample collection. For known K and r, the corresponding calculations are carried out using the expression

$$\sum_1^n m_n = M_0\left[1 - \left(\frac{K + rp/p'}{K + r}\right)^n\right] \tag{15}$$

If K and r are unknown, the mass of analyte removed is determined from the

measurement of the chromatographic peak areas (A_G^i) and (A_G^{i+1}) corresponding to the ith and ($i + 1$)th samplings:

$$\sum_1^n m_n = M_0[1 - (A_G^{i+1}/A_G^i)^n] \tag{16}$$

More precise results are usually obtained when characterizing systems with known K and r and using eqn. 15 for the calculations.

For illustration of the potential and specific features of static HSA with cryogenic concentration, compare the detection limits for halogenated hydrocarbons in water using flame ionization detection by direct injection of an equilibrium gas into the capillary column and with preliminary concentration in its initial part. Pneumatic sampling of equilibrium gas [84] was used for this purpose. Cryogenic headspace concentration was shown to reduce the detection limit of methylene chloride, chloroform, carbon tetrachloride and 1,2-dichloroethane by a factor of 12–20, and to allow the determination of halogenated hydrocarbons at the level of a few fractions of 1 μg/l.

The sensitivity of the determination of microimpurities in aqueous solutions can be further increased by removing moisture from the equilibrium gas by means of special condensers. For this purpose one employs quartz capillaries (30 cm × 0.32 mm I.D., sometimes coated with a thin film of liquid phase) [100], or Nafion desiccating membranes [100,101] (manufactured by DuPont).

Low detection limits with HSC and capillary column analysis can be achieved by using special techniques to narrow the initial chromatographic band, which may involve reducing the gas-to-liquid phase volume ratio in the trap, thermal focusing, etc. [102].

3.2. Adsorption headspace concentration

Adsorption headspace concentration with subsequent thermal desorption of the trapped analytes removes the principal drawback of the cryogenic concentration of impurities in aqueous solutions associated with the limited volume of the humid equilibrated gas passed through the trap. As adsorbers one employs [51] activated charcoal, Amberlite XAD, Chromosorbs or Tenax TA; however, the most widely recognized owing to its hydrophobic properties is Tenax GC, which has been proposed for the accumulation of organic impurities by Zlatkis and co-workers [103,104]. It should be pointed out that the use of Tenax materials meets with problems associated with the appearance of artefacts [105]. Thermal desorption brings about decomposition of Tenax GC with the formation of acetophenone, benzaldehyde, benzoic acid, ethylene oxide, phenol, etc. [106]. In addition, interaction with mineral acids (particularly those containing sulphur) may also result in the decomposition of Tenax GC and, eventually, in the formation of 2,6-diphenylbenzoquinone [107]. In addition to the oxidation products of Tenax GC, one observes unidentified high-molecular-weight products [108]. One may expect also the appearance of other artefacts, *e.g.*, when analysing air containing chlorine, ozone or nitrogen oxides [109]. The adsorbent intended for trapping volatile impurities in HSC should meet certain requirements [110–112].

The adsorption variant provides a further reduction in the detection limit of

impurities by gas chromatographic headspace analysis and can be used under the conditions of complete trapping and equilibrium concentration, each of them imposing certain restrictions on the volume of gas passed through the tube with the sorbent.

As follows from the above description of the equilibrium frontal concentration method [10], the impurity trapping remains complete as long as the sweeping gas volume does not exceed $V_R - \Delta V_R$. This volume of the sweeping gas places a limit on the amount of the analyte extracted from the object under study that can be concentrated under the total trapping conditions. If the amount of the analyte adsorbed under these conditions turns out to be insufficient for achieving the desired detection limit, one will have to increase the packing mass and the sorbent layer length in the concentrator which, consequently, will increase V_R.

If the sweeping gas volume satisfies the condition $V_g \geqslant V_R + \Delta V_R$, we come to the equilibrium concentration regime, *i.e.*, a total breakthrough of the impurity. The headspace adsorption concentration differs radically from the frontal equilibrium concentration of impurities present in gases in that the content of the analytes in the gas passing through the concentrator gradually decreases. In the case of CGE it occurs by an exponential law, and in discontinuous extraction in steps. Therefore, if the gas volume passing through the trap is too large, *i.e.*, $V_g \geqslant V_R + \Delta V_R$, this may result in the removal of the analyte from the concentrator and, thus, in reduced analytical sensitivity. So far only the total trapping regime has been used in adsorption headspace concentration.

Thermal desorption is a process occurring in time and, hence, it frequently involves a decrease in the efficiency of the chromatographic column. This effect is removed by using the cryogenic focusing technique. Werhoff and Bretschneider [51] studied the possibility of quantitative measurements using dynamic HSA with concentration. Optimum HSC conditions were found, and quantitative data obtained, in an analysis of eleven volatile aromatic compounds (primarily terpenes). With Tenax GC used under optimum volatile trapping conditions (gas flow-rate 50 ml/min, trapping time 2 h at 80°C), subsequent desorption at 250°C and a carrier gas flow-rate of 30 ml/min for 30 min and a cryogenic trap temperature of −130°C, the analyte losses did not exceed 4%.

In analyses for the presence of halogenated hydrocarbons in water [84], a transition from cryogenic to adsorption concentration brings the detection limit down to a few hundredths of 1 mg/l, but the reproducibility of measurements on the same solutions decreases. The high sensitivity of HSA with intermediate adsorption concentration can be illustrated by the determination of the volatiles present in human blood (Fig. 4).

Despite the widespread recognition of dynamic HSC, data on the quantitative characterization of volatile impurities with headspace concentration are scarce (see, *e.g.*, refs. 84, 89 and 113–115). Most of the studies are either of an illustrative character or are aimed at finding qualitative characteristics of the objects of interest. The approach to choosing the analytical conditions is predominantly empirical. Inadequate attention is focused on the relationships governing the extraction of volatiles from liquid and, particularly, solid materials, *i.e.*, in the CGE stage. The various models of this process and their mathematical description have been discussed [93,116].

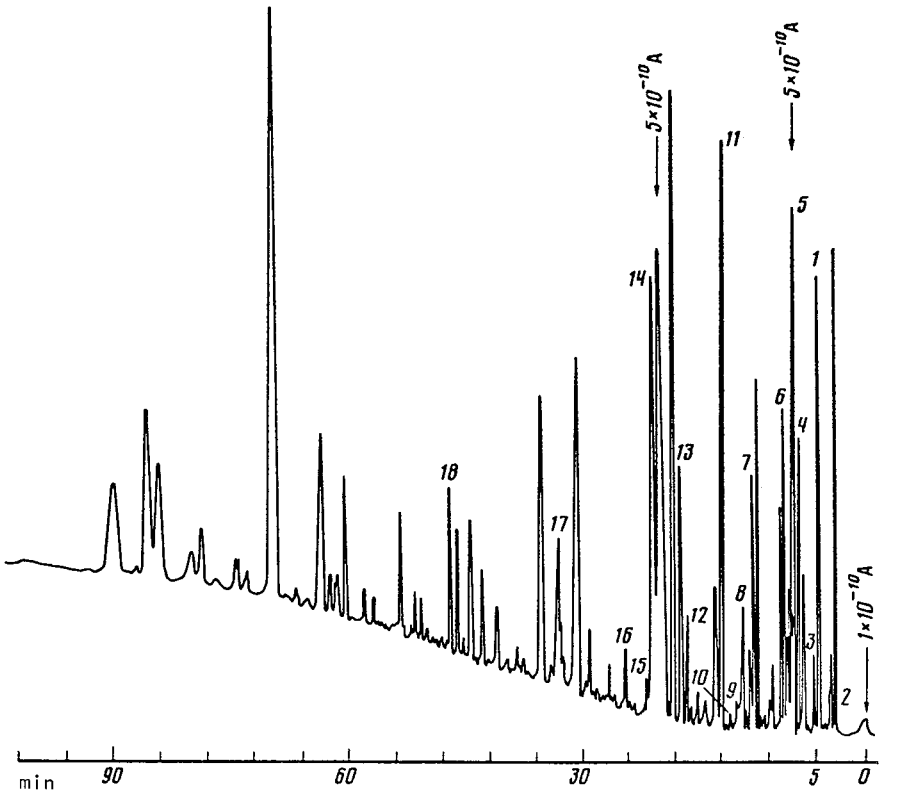

Fig. 4. Chromatogram of volatile organic impurities concentrated on Tenax GC from a sample collected from the headspace above human blood [84]. Conditions: blood sample volume, 3 ml; gas-phase volume, 20 ml; temperature and equilibrium onset time, 60°C and 45 min; sampling, pneumatic under static conditions; number of gas-phase samplings, 3, with pressure drop of 5 atm (507 MPa); capillary column with dinonyl phthalate (45 × 0.25 mm I.D.); carrier gas (helium) flow-rate, 1 ml/min; column temperature, 50°C for 5 min, increased to 130°C at 2°C/min. Peaks: 1 = acetaldehyde; 2 = methanol; 3 = isoprene; 4 = acetone; 5 = ethanol; 6 = dichloroethane; 7 = methyl ethyl ketone; 8 = heptane; 9 = carbon tetrachloride; 10 = chloroform; 11 = benzene; 12 = methyl propyl ketone; 13 = dioxane; 14 = octane; 15 = butanol; 16 = toluene; 17 = nonane; 18 = *n*-decane.

3.3. Absorption headspace concentration

Absorption headspace concentration removes the limitations inherent in the cryogenic and adsorption variants and stemming from the adverse effects of water and the need for thermal desorption and for prevention of analyte breakthrough. In addition, if the absorbing liquid has been chosen correctly, and proper techniques to enhance the HSA sensitivity have been used, equilibrium absorption concentration not only reduces the detection limit but also permits one to improve the selectivity of discrimination between the various components in the mixture under analysis.

Wahlroos and Nikkila [117] were the first to strip volatile impurities from solutions with a carrier gas with their subsequent accumulation in a non-volatile liquid as far back as 1966. This study was not extended, however, because there was only a small gain in sensitivity. Nearly 20 years later, Vitenberg and Kostkina [118]

considered a more general variant of headspace absorption concentration of impurities in volatile solvents, and found ways to improve the degree of concentration and to reduce further the detection limit of volatiles in solutions.

Headspace absorption concentration of volatile impurities by CGE actually represents a combination of extraction with a gas flow of analytes from the solution of interest with their subsequent equilibrium concentration in a volatile liquid. The fairly cumbersome equations describing this process have been validated experimentally [118] for the case of absorption concentration in glacial acetic acid of benzene, toluene and *m*-xylene present in aqueous solutions.

A major criterion for the practical use of headspace absorption concentration is the difference between the partition coefficient in the stage of stripping from the solution under study (K_1) and of the absorption coefficient in the trapping liquid (K_2), as the degree of concentration is $b = f(K_2/K_1)$. This difference should be as large as possible. The values of K_1 and K_2 and the calculated and experimentally confirmed values of b in Table 2 indicate that the gain in sensitivity observed on injecting acetate concentrate into the chromatographic column compared with direct introduction of the original aqueous solution is in excess of two orders of magnitude, the threshold of gas chromatographic detection of aromatic hydrocarbons in aqueous solutions being as low as 1–10 mg/l. The detection limit can be reduced by two more orders of magnitude down to a few hundredths of 1 mg/l if one uses headspace analysis of the concentrate after neutralization of the acetic acid with an alkali, similar to the technique proposed by Vitenberg and Tsibul'skaya [119].

The absorption concentration of volatile microimpurities present in solutions by CGE offers a substantial improvement in the selectivity of analyte discrimination against the background of concomitant components with strongly differing partition coefficients. For instance, in the above case the selectivity of characterization of aromatic hydrocarbons increases in all stages of the analysis. The CGE of the components of the aqueous solution and their equilibrium concentration in acetic acid is accompanied by depletion of the absorbing liquid in concomitant impurities with small partition coefficients (*n*-hexane, *n*-octane), which are removed almost completely not only from the aqueous solution but also from the absorber. The selectivity of discrimination against the concomitant impurities having large partition coefficients (alcohols, carbonyl compounds, carboxylic acids) stems from the fact that for them to be extracted nearly completely from the aqueous solution, one has to pass

TABLE 2

PARTITION COEFFICIENTS OF AROMATIC HYDROCARBONS IN WATER (K_1) AND GLACIAL ACETIC ACID (K_2) AT 20°C, AND THE DEGREE OF ENRICHMENT IN LIQUID ABSORBER (b) IN ABSORPTION CONCENTRATION OF HYDROCARBONS FROM AQUEOUS SOLUTIONS IN GLACIAL ACETIC ACID

Impurity to be concentrated	K_1	K_2	b
Benzene	4.0	900	115
Toluene	3.6	2480	242
m-Xylene	4.6	6370	287

much larger gas volumes. Therefore, the degree of concentration of such concomitants is considerably smaller than that of the analytes. Apart from this, after neutralization of the acetate concentrate, the equilibrium gas phase becomes depleted in the compounds that are more soluble in aqueous solutions.

3.4. Circulation concentration

This was proposed and used by Grob and co-workers [120–123] for the determination of hydrophobic compounds (*i.e.*, compounds with small K) in aqueous solutions. Later, Drozd and co-workers [124,125] employed the circulation arrangement in the analysis of hydrophilic (*i.e.*, with large K) compounds in aqueous solutions.

The essence of this method lies in the multiple use in a closed system of the same volume of extracting gas for the concentration of impurities present in solutions. In practice this is done by pumping the gas into the solution with a special pump [124].

The principal and essential advantage of this method over the conventional (direct-flow) variant of CGE is that when large volumes of the stripping gas are swept through a system, its own impurities do not build up in the concentrator. In addition, because the extracting gas volumes are small, the volatility of the main solvent may be neglected.

The calculations of HSA with circulation concentration made by Novák *et al.* [124] and, subsequently, by others [57,126] are based on the equation

$$C_L = C_L^0 \exp\left(-\frac{V_g}{KV_L + V_G}\right) \tag{17}$$

Other equations have also been proposed for CGE [116,127]. A comprehensive study of the CGE of volatiles from a non-volatile solvent [116] showed that the various expressions describing CGE are based on different models of the process. Realization of the conditions approximating each of these models would require the development of the corresponding experimental set-ups, and this could complicate substantially the analytical procedure.

Of particular importance for practical implementation of the process and the correct choice of the basic equation is the ratio of the phase volumes in the extraction vial. If the condition $KV_L \gg V_G$ is met, one can use for the calculations the approximate equation

$$C_L = C_L^0 \exp\left(-\frac{V_g}{KV_L}\right) \tag{18}$$

which describes with acceptable accuracy any CGE model and does not require additional complication of the analytical procedure. The stages of the adsorption and absorption trapping of impurities from the gas flow which represent an integral part of the calculation variant of CGE are described by the relationships given in preceding sections.

The possibilities and limitations of the calculation HSC were explored by Curvers *et al.* [126] in a study of the determination of hydrocarbons, halogenated hydrocarbons and ketones in water, stripping in closed systems having been used [128]

to detect bromoalkanes in aqueous solutions. The detection limit of non-polar impurities is a few thousandths of 1 mg/l. The reproducibility of the extracted fraction of the analyte is 10–15% over the concentration range 0.2–20 mg/l.

Circulation concentration can be used to advantage when determining impurities in solutions with high partition coefficients present in very low concentrations (less than 1 mg/l). Compounds with small K can be determined more simply and accurately under static conditions. This procedure provides virtually complete extraction of an impurity from a solution by simpler technical means.

Circulation concentration can be employed with any quantitative HSA technique [6,7,32]. Novák *et al.* [124] recommended the method of addition. We believe a more preferable approach to be absolute calibration, which does not require double chromatographic analysis of the concentrate. For systems with unknown K one can use the discontinuous technique [125] or the method involving complete extraction of the analyte from the solution under study.

3.5. Liquid–gas distributive chromatography (LGDC)

This technique, proposed in 1982 by Moskvin *et al.* [129] and subsequently developed [130,131], was used to analyse gases dissolved in liquids [131,132]. This method may be considered as a variant of HSC which differs from CGE only in that the mobile phase here is the solution under study, the extracting gas remaining fixed. LGDC is based on the degassing of a liquid as it is filtered through a column filled with a porous packing, which holds a volume of gas acting as a fixed gaseous extractant. LGDC actually represents a counterpart of the frontal concentration of impurities present in gas objects which, in contrast to the latter, has been implemented also in an elution-type procedure. The analytical calculations used in LGDC are based on relationships [132,133] assuming that the retention volume (mobile liquid phase) depends proportionally on the volume of the stationary gas phase. Whereas this method offers a considerable increase in the sensitivity of chromatographic determination of gases dissolved in water, the detection limits for oxygen, nitrogen and hydrogen in water [134] are comparable to those obtained with direct HSA under static conditions.

4. COMBINATION OF EQUILIBRIUM ABSORPTION CONCENTRATION WITH HEADSPACE ANALYSIS

The possibilities inherent in the equilibrium absorption concentration of impurities present in gas and liquid objects can be broadened substantially if one measures the content of an analyte in the absorber by headspace analysis rather than by its direct injection into the chromatograph. This variant may include enrichment of the equilibrium gas with the impurity, or may be implemented without it.

4.1. Direct headspace analysis of the concentrate

Direct headspace analysis of the concentrate solution saturated preliminarily with the analyte gas under study is the simplest case. No enrichment occurs, as the content of impurities in the gas equilibrated with the concentrate hardly differs from the initial concentration C_G^0. This method may be considered only as a means of collecting samples which permit one to store the gas samples of interest for long

periods of time. The liquid phase acts as a certain buffer which stabilizes the microimpurity concentration in the collected gas sample as a result of suppression of sorption on the vial walls and of the possible analyte losses in the gas phase being compensated for by the impurity entering the gas from the solution.

The above principles underlie a technique for the determination of lower aromatic hydrocarbons in humid air [135], its remarkable feature consisting in the use of water as the trapping liquid. Direct introduction into the chromatograph of an aqueous solution saturated with the analyte gas is not reasonable here as this would reduce drastically the analytical sensitivity. Therefore, after equilibrium has been reached in the absorbing vial, it is recommended to analyse the headspace above the liquid concentrate.

The distinctive features of this technique are its simplicity and short operating time. The sample collection with the gas bubbled through 10–20 ml of water does not take more than 2–5 min, as V_g^{min} is only 100–130 ml. The use of such a small volume of air increases the sensitivity because the concomitant impurities with high partition coefficients ($K > 10^3$; alcohols, carbonyl compounds, amines, acids, etc.) do not have time to build up in the liquid, their equilibrium concentration in the gas phase therefore being extremely low. This technique permits the determination of aromatic hydrocarbons in humid air over the concentration range 1–50 mg/m^3 and can be employed to analyse the exhaust fumes from internal combustion engines, the air in industrial sites, garages, etc.

4.2. Headspace analysis of the concentrate with equilibrium gas enrichment of the analyte

This involves the inclusion in the procedure of an additional operation resulting in a dramatic reduction in the original impurity partition coefficient between the liquid concentrate and the air (such as raising the temperature, salting out or dilution of a solution in organic solvent with water). After such a treatment the analyte concentration in the gas above the solution (C'_g) is related to C_L^0 through

$$C'_G = C_L^0 \cdot \frac{KV_L}{K'V'_L + V'_G} \cdot \frac{f_s}{1 - FK} \tag{19}$$

(the primes denoting the parameters obtained after the reduction of the partition coefficient). As shown by this equation, the degree of enrichment of the gas under study with an analyte (C'_G/C_G^0) depends primarily on the relative magnitude of K and K', as the factor $f_s(1 - FK)$ differs very little from unity, the volume ratio V'_G/V'_L usually varying from one to five. Recalling the possibility of improving the HSA sensitivity by reducing the partition coefficients, we see that the detection threshold can be decreased by 1–3 orders of magnitude.

The procedure combining absorption concentration with HSA and providing a substantial enrichment of an analyte in the gas phase can be illustrated by the determination of aromatic hydrocarbons in air by trapping them in acetic acid, a subsequent sharp reduction of the original value of K through neutralization of the acetic acid with a solution of potassium hydroxide and the analysis of the gas equilibrated with the aqueous salt solution thus obtained [119]. The partition coefficients of benzene, toluene and *m*-xylene in the aqueous solution of potassium

acetate are much lower than those in water (the salting-out effect), and 10^3–10^4 times lower than those in acetic acid [136]. Therefore, a transition from direct gas chromatographic analysis of the acetate concentrate to an investigation of the equilibrium vapour after the neutralization of the solution, a procedure carried out under the conditions proposed by Vitenberg and Tsibul'skaya [119], permits an increase in the sensitivity of determination of aromatic hydrocarbons in air by two orders of magnitude.

The technique for the determination of aromatic hydrocarbons in atmospheric air based on combining the absorption concentration with HSA has been approved by the USSR Ministry of Health for use in environmental monitoring stations [137].

This procedure is fairly simple and consists in saturation of 2 ml of 80% (at temperatures above 0°C) or 65% (at temperatures from 0 to −24°C) acetic acid with atmospheric air, neutralization of the concentrate thus obtained with an alkaline solution in a closed volume and subsequent gas chromatographic analysis of the headspace above the aqueous salt solution. A calibration solution with a known content of aromatic hydrocarbons in acetic acid is also analysed under identical conditions. An essential asset of the technique is the capability of determining aromatic hydrocarbons at the level of a few hundredths of 1 mg/m^3 in air with a high absolute humidity (up to 23 mg/l).

Apart from stabilization of the impurity content in the gas under study, in addition to improved sensitivity and selectivity of analysis, the combination of absorption concentration with HSA has the following attractive features: a higher precision of measurement, as the reproducibility of injection into the chromatograph of gas samples is much better than that of liquids; and the possibility of automating the analytical procedure by employing headspace analysers and special attachments to the all-purpose gas chromatographs produced by various instrument manufacturers.

Selyutina and Vinnikov [138] used the combination of CGE with absorption trapping (under the total trapping conditions) for the headspace concentration and gas chromatographic determination of volatile amines in water. Aniline and ethyl-, diethyl- and triethylamines present in the aqueous solution were removed with a gas flow at 70–90°C, 0.1 *M* sulphuric acid being employed as the absorber. To increase the efficiency of CGE, potassium hydroxide was added before the analysis to the solution under study at a concentration of 40–50 g/l. At an elevated gas temperature and an air flow-rate of 1 l/h, such an alkali content ensures virtually complete extraction of primary amines from 1.6 l of aqueous solution in 90 min and of secondary and ternary amines in 60 and 30 min, respectively. Aniline is more difficult to remove from solution, so that even after 90 min only 70% of it is extracted. More complete removal can be achieved by increasing the alkali concentration in the solution to 120 g/l.

The amine content in the sulphate concentrate obtained in the first stage after its neutralization with solid potassium hydroxide is determined by static HSA. For this purpose the authors employed a laboratory set-up [139] based on the pneumatic arrangement which is used in Hewlett-Packard instrumentation [83]. The detection limit for amines in water with this set-up is about 0.5 μg/l.

5. CONCLUSIONS

Equilibrium concentration of volatile impurities based on the distribution of the

compounds under study between the condensed and gas phases broadens substantially the scope and potential of the traditional methods of concentration assuming total extraction of the analyte from the object in question, and represents not only a useful addition to the list but, in a number of instances (*e.g.*, characterization of unstable microcomponents in atmospheric air and water), the only reasonable approach. The use of the gas extraction and related methods permits the development of acceptably simple, partially or totally automated procedures for sample preparation based on the available commercial equipment.

Headspace analysis provides a reduction in the gas chromatographic detection thresholds for volatiles with partition coefficients below 10^3. Combining equilibrium concentration with the headspace techniques improves the sensitivity and selectivity of the gas chromatographic determination of volatile impurities and brings their detection threshold in liquid and gas objects down to a few ppb and lower.

REFERENCES

1 G. R. Umbreit, in R. L. Grob (Editor), *Modern Practice of Gas Chromatography*, Wiley, New York, 1977, p. 365.
2 A. G. Vitenberg, B. V. Ioffe and V. N. Borisov, *Zh. Anal. Khim.*, 29 (1974) 1785.
3 B. V. Ioffe, *Zh. Anal. Khim.*, 36 (1981) 1663.
4 H. Huchenberg and A. P. Schmidt, *Gas Chromatographic Headspace Analysis*, Heyden, London, 1977.
5 H. Huchenberg and A. P. Schmidt, *Gas Chromatographic Analysis of Equilibrium Vapor Phase* (in Russian), Mir, Moscow, 1979.
6 B. Kolb, *Applied Headspace Gas Chromatography*, Heyden, London, 1980.
7 A. G. Vitenberg and B. V. Ioffe, *Gas Extraction in Chromatographic Analysis* (in Russian), Khimiya, Leningrad, 1982.
8 B. V. Ioffe and A. G. Vitenberg, *Headspace Analysis and Related Methods in Gas Chromatography*, Wiley-Interscience, New York, 1984.
9 B. V. Ioffe, A. G. Vitenberg and V. N. Borisov, *Zh. Anal. Khim.*, 27 (1972) 1811.
10 J. Novák, V. Vasák and J. Janák, *Anal. Chem.*, 37 (1965) 660.
11 M. Selucky, J. Novák and J. Janák, *J. Chromatogr.*, 28 (1967) 285.
12 J. Gelbicova-Ruzickova, J. Novák and J. Janák, *J. Chromatogr.*, 64 (1972) 15.
13 A. Dravnieks and B. K. Krotoszynski, *J. Gas Chromatogr.*, 6 (1968) 144.
14 A. Dravnieks and B. K. Krotoszynski, *J. Gas Chromatogr.*, 4 (1966) 367.
15 A. Dravnieks, B. K. Krotoszynski, J. Whifield, A. O'Donnell and T. Burgwald, *Environ. Sci. Technol.*, 5 (1971) 1220.
16 A. Dravnieks and A. O'Donnell, *J. Agric. Food Chem.*, 19 (1971) 1049.
17 G. J. Rudenko, V. V. Mal'tsev and V. N. Studenichnik, *Zh. Anal. Khim.*, 40 (1985) 1119.
18 N. G. Karabanov, I. N. Prusakova and L. E. Reshetnikova, *Zh. Anal. Khim.*, 40 (1985) 1675.
19 M. Novotny, M. L. Lee and K. D. Bartle, *Chromatographia*, 7 (1974) 333.
20 L. Ya. Gavrilina, V. I. Zheivot and I. D. Emel'yanov, *Izv. Sib. Otd. Akad. Nauk SSSR, Ser. Khim.*, 3, No. 7 (1982) 97.
21 C. Vidal-Madjar, M. F. Gonnord, F. Benchah and G. Guiochon, *J. Chromatogr. Sci.*, 16 (1978) 190.
22 A. A. Khvostikov, S. A. Reznikov, R. I. Sidorov, L. P. Zaitseva and G. I. Vakhrusheva, *Zh. Anal. Khim.*, 30 (1975) 1001.
23 A. G. Vitenberg, M. A. Kuznetsov and B. V. Ioffe, *Dokl. Akad. Nauk SSSR*, 219 (1974) 921.
24 A. G. Vitenberg, M. A. Kuznetsov and B. V. Ioffe, *Zh. Anal. Khim.*, 30 (1975) 1051.
25 V. N. Borisov, B. V. Ioffe and A. G. Vitenberg, *Zh. Anal. Khim.*, 30 (1975) 1289.
26 B. V. Ioffe, A. G. Vitenberg, V. N. Borisov and M. A. Kuznetsov, *J. Chromatogr.*, 112 (1975) 311.
27 V. D. Yablochkin, *Gig. Sanit.*, 5 (1978) 63.
28 V. G. Berezkin, V. P. Pakhomov, L. L. Starobinets and L. L. Berezkina, *Neftekhimiya*, 5 (1965) 438.
29 B. G. Belen'kii, A. G. Vitenberg, L. D. Turkova and N. N. Chernyshkov, *Izv. Akad. Nauk SSSR, Ser. Khim.*, (1967) 269.
30 V. G. Berezkin, *Gas–Liquid–Solid Chromatography* (in Russian), Khimiya, Moscow, 1986.
31 V. G. Berezkin, V. D. Loshchilova, V. D. Pankov and V. D. Yagodovskaya, *Chromato-Distributive Methods* (in Russian), Nauka, Moscow, 1967.

32 A. G. Vitenberg, *D. Sc. Thesis*, Leningrad State University, 1988.
33 I. A. Tsibul'skaya, A. G. Vitenberg and B. V. Ioffe, *Zh. Anal. Khim.*, 34 (1979) 557.
34 I. A. Tsibul'skaya, A. G. Vitenberg and A. F. Osokin, *Vestn. Leningr. Univ. Fiz. Khim.*, 10 (1980) 90.
35 B. V. Stolyarov and A. G. Vitenberg, *Abstracts of All-Union Meeting on Gas Chromatography in National Economy, Chelyabinsk*, 1977, p. 88.
36 V. V. Tsibul'skii, A. G. Vitenberg and I. A. Khripun, *Zh. Anal. Khim.*, 33 (1978) 1184.
37 B. V. Ioffe, A. G. Vitenberg and I. A. Tsibul'skaya, *J. Chromatogr.*, 186 (1979) 851.
38 I. Sliwka, P. Rotocki, E. Bros and J. Lasa, *Chem. Anal. (Warsaw)*, 28 (1983) 3.
39 J. R. Snider and G. A. Dowson, *J. Geophys. Res.*, 90 (1985) 3797.
40 R. G. Buttery, J. L. Bomben, D. G. Guadagni and L. C. Ling, *J. Agric. Food Chem.*, 19 (1971) 1045.
41 L. Rohrschneider, *Anal. Chem.*, 45 (1973) 1241.
42 A. G. Vitenberg, B. V. Ioffe, Z. St. Dimitrova and I. L. Butaeva, *J. Chromatogr.*, 112 (1975) 319.
43 R. G. Buttery and D. G. Guadagni, *J. Agric. Food Chem.*, 17 (1969) 385.
44 T. G. Kleckbusch and C. G. King, *J. Chromatogr. Sci.*, 17 (1979) 273.
45 A. G. Vitenberg, I. L. Butaeva, L. M. Kuznetsova and M. D. Inshakov, *Anal. Chem.*, 49 (1977) 129.
46 G. Triebig, in *Vortrage zum 2. Internationalen Colloquium über die Gas-Chromatographische Dampfraumanalyse in Uberlingen*, Perkin-Elmer, Bodenseewerk, 1978, p. 24.
47 E. R. Adlard and J. N. Davenport, *Chromatographia*, 17 (1983) 421.
48 J. F. Pankov, L. M. Isabelle and T. J. Kristensen, *Anal. Chem.*, 54 (1982) 1815.
49 J. F. Pankov, *J. High Resolut. Chromatogr. Chromatogr. Commun.*, 9 (1986) 18.
50 A. Hagman and S. Jacobson, *J. Chromatogr.*, 448 (1988) 117.
51 P. Werhoff and W. Bretschneider, *J. Chromatogr.*, 405 (1987) 99.
52 H. Borén, A. Grimvall, J. Palmborg, R. Sävenhed and B. Wigilius, *J. Chromatogr.*, 348 (1985) 67.
53 S. Jacobsson, *J. High Resolut. Chromatogr. Chromatogr. Commun.*, 7 (1984) 185.
54 W. V. Ligon and M. C. George, *J. Polym. Sci. Polym. Chem. Ed.*, 16 (1978) 2703.
55 A. G. Vitenberg, *Zh. Anal. Khim.*, 46 (1991) 764.
56 J. Drozd and J. Novák, *J. Chromatogr.*, 165 (1979) 114.
57 A. Nunez and L. F. Gonzalez, *J. Chromatogr.*, 300 (1984) 127.
58 C. G. Poole and S. A. Schuette, *J. High Resolut. Chromatogr. Chromatogr. Commun.*, 6 (1983) 526.
59 M. E. McNally and R. L. Grob, *Am. Lab. (Fairfield)*, 17 (1985) 20.
60 M. E. McNally and R. L. Grob, *Am. Lab. (Fairfield)*, 17 (1985) 106.
61 E. Jones, M. Davis, R. Gibson, B. Todd and R. Wallen, *Am. Lab. (Fairfield)*, 16 (1984) 74.
62 J. W. Washall and T. P. Wampler, *Am. Lab. (Fairfield)*, 20 (1988) 70.
63 D. J. Chichester-Constable, M. E. Barbeau, S. L. Liu, S. R. Smith and J. D. Stuart, *Anal. Lett.*, 20 (1987) 403.
64 J. Shou and Y. Ho, *J. Chromatogr. Sci.*, 27 (1989) 91.
65 M. Duffy, J. N. Driscoll, S. Pappas and W. Sanford, *J. Chromatogr.*, 441 (1988) 73.
66 S. A. Vandergrift, *J. Chromatogr. Sci.*, 26 (1988) 513.
67 J. F. Pankow, *J. High Resolut. Chromatogr. Chromatogr. Commun.*, 10 (1987) 409.
68 T. H. Wang, H. Shanfield and A. Zlatkis, *Chromatographia*, 17 (1983) 411.
69 A. M. Galt and G. Macleod, *J. Agric. Food Chem.*, 32 (1984) 59.
70 S. Adam, in P. Schreier (Editor), *Analysis of Volatiles*, Walter de Gruyter, Berlin, New York, 1984, p. 419.
71 J. Suzuki and M. E. Bailey, *J. Agric. Food Chem.*, 33 (1985) 343.
72 A. J. Nunez and H. Maarse, *Chromatographia*, 21 (1986) 44.
73 P. Etievant, H. Maarse and F. van den Berg, *Chromatographia*, 21 (1986) 379.
74 K. Fukuhara, T. Sakaki, H. Sakuma and S. Sugawara, *Agric. Biol. Chem.*, 49 (1985) 2177.
75 V. A. Isidorov, I. G. Zenkevich and B. V. Ioffe, *Dokl. Akad. Nauk SSSR*, 263 (1982) 893.
76 V. A. Isidorov, I. G. Zenkevich and B. V. Ioffe, *Atmos. Environ.*, 19 (1985) 1.
77 H. Termonia and G. Alaerts, *J. High Resolut. Chromatogr. Chromatogr. Commun.*, 8 (1985) 622.
78 F. Poy, L. Cobelli, S. Banfi and F. Fossati, *J. Chromatogr.*, 395 (1987) 281.
79 W. V. Ligon and M. C. George, *J. Polym. Sci. Polym. Chem. Ed.*, 16 (1978) 2703.
80 A. Hagman and S. Jacobson, *J. Chromatogr.*, 395 (1987) 271.
81 J. H. Brill and W. Bertsch, *J. High Resolut. Chromatogr. Chromatogr. Commun.*, 9 (1986) 461.
82 F. Poy and L. Cobelli, *J. Chromatogr. Sci.*, 23 (1985) 114.
83 P. L. Wylie, *Chromatographia*, 21 (1986) 251.
84 A. G. Vitenberg and M. I. Kostkina, *Zh. Anal. Khim.*, 44 (1988) 318.
85 K. Grob and A. Habich, *J. Chromatogr.*, 321 (1985) 45.

86 R. P. M. Dooper, *Chrompack News*, 11 (1984) 1.
87 H. T. Badings, C. Jong and R. P. M. Dooper, *J. High Resolut. Chromatogr. Chromatogr. Commun.*, 8 (1985) 755.
88 B. Kolb, D. Boege and L. Ettre, *Am. Lab. (Fairfield)*, 20 (1988) 33.
89 S. Nitz, F. Drawert and E. Julich, *Chromatographia*, 18 (1984) 313.
90 T. P. Wampler, W. A. Bowe, J. Higgins and E. J. Levy, *Am. Lab. (Fairfield)*, 17 (1985) 82.
91 A. G. Vitenberg and B. V. Ioffe, *Dokl. Akad. Nauk SSSR*, 235 (1977) 1071.
92 B. V. Ioffe and A. G. Vitenberg, *Chromatographia*, 11 (1978) 282.
93 A. G. Vitenberg and B. V. Ioffe, *J. Chromatogr.*, 471 (1989) 55.
94 R. F. Weiss, J. L. Bullister, R. H. Gammon and M. J. Warner, *Nature (London)*, 314 (1985) 608.
95 A. G. Vitenberg and B. V. Ioffe, *Dokl. Akad. Nauk SSSR*, 238 (1978) 352.
96 B. V. Ioffe, A. G. Vitenberg and T. L. Reznik, *Zh. Anal. Khim.*, 37 (1982) 902.
97 A. G. Vitenberg, *Dokl. Akad. Nauk SSSR*, 267 (1982) 113.
98 A. G. Vitenberg, *J. Chromatogr. Sci.*, 22 (1984) 122.
99 A. G. Vitenberg and T. L. Reznik, *J. Chromatogr.*, 287 (1984) 15.
100 Th. Noij, A. van Es, C. Cramers, J. Rijks and R. Dooper, *J. High Resolut. Chromatogr. Chromatogr. Commun.*, 10 (1987) 60.
101 B. E. Foulder and P. G. Simmons, *Anal. Chem.*, 51 (1979) 1089.
102 G. Takeoka and W. Jennings, *J. Chromatogr. Sci.*, 22 (1984) 177.
103 A. Zlatkis, H. A. Lichtenstein and A. Tishbee, *Chromatographia*, 6 (1973) 67.
104 W. Bertsch, R. C. Chang and A. Zlatkis, *J. Chromatogr. Sci.*, 12 (1974) 175.
105 B. Middleditch, A. Zlatkis and R. D. Schwartz, *J. Chromatogr. Sci.*, 26 (1988) 150.
106 E. D. Pollizzari, B. Demian and K. J. Krost, *Anal. Chem.*, 56 (1984) 793.
107 M. B. Neher and P. W. Jones, *Anal. Chem.*, 49 (1977) 512.
108 E. L. Atlas, K. F. Sullivan and C. S. Giam, *Anal. Chem.*, 57 (1985) 2417.
109 E. D. Pellizzari and K. J. Krost, *Anal. Chem.*, 56 (1984) 1813.
110 J. Delcourt, J. P. Guenier and J. Muller, *Chromatographia*, 17 (1983) 88.
111 P. Ciccioli, E. Brancaleoni, A. Cecinato, C. Di Palo, A. Brachetti and A. Liberti, *J. Chromatogr.*, 351 (1986) 433.
112 G. Macleod and J. M. Ames, *J. Chromatogr.*, 355 (1986) 393.
113 W. E. Hammers and H. F. P. M. Bosman, *J. Chromatogr.*, 360 (1986) 425.
114 C. E. Higgins, W. H. Griest and G. Olerich, *J. Assoc. Off. Anal. Chem.*, 66 (1983) 1074.
115 T. P. Wampler, W. A. Bowe and E. J. Levy, *J. Chromatogr. Sci.*, 23 (1985) 64.
116 A. G. Vitenberg and M. I. Kostkina, *Zh. Anal. Khim.*, 34 (1979) 1800.
117 O. Wahlroos and O. E. Nikkila, *Acta Chem. Scand.*, 20 (1966) 197.
118 A. G. Vitenberg and M. I. Kostkina, *Zh. Anal. Khim.*, 39 (1984) 1679.
119 A. G. Vitenberg and I. A. Tsibul'skaya, *Zh. Anal. Khim.*, 34 (1979) 1380.
120 K. Grob, *J. Chromatogr.*, 84 (1973) 255.
121 K. Grob and G. Grob, *J. Chromatogr.*, 90 (1974) 303.
122 K. Grob, K. Grob, Jr. and G. Grob, *J. Chromatogr.*, 106 (1975) 299.
123 K. Grob and F. Zuercher, *J. Chromatogr.*, 117 (1976) 285.
124 J. Novák, J. Golias and J. Drozd, *J. Chromatogr.*, 206 (1981) 421.
125 J. Drozd and J. Vodakova, *J. Chromatogr.*, 354 (1986) 47.
126 J. Curvers, Th. Noij, C. Cramers and J. Rijks, *J. Chromatogr.*, 289 (1984) 171.
127 M. G. Burnett, *Anal. Chem.*, 35 (1963) 1567.
128 V. Janda, K. Marha and J. Mitara, *J. High Resolut. Chromatogr. Chromatogr. Commun.*, 11 (1988) 541.
129 L. N. Moskvin, A. I. Gorshkov and M. F. Gumerov, *Dokl. Akad. Nauk SSSR*, 265 (1982) 378.
130 L. N. Moskvin, A. I. Gorshkov and M. F. Gumerov, *Zh. Fiz. Khim.*, 57 (1983) 1979.
131 J. C. Giddings and M. N. Meyers, *J. High Resolut. Chromatogr. Chromatogr. Commun.*, 6 (1983) 381.
132 A. I. Gorshkov, M. F. Gumerov, E. I. Leont'eva and L. N. Moskvin, *Zh. Anal. Khim.*, 41 (1986) 146.
133 A. I. Gorshkov, M. F. Gumerov and L. N. Moskvin, *Teploenergetika*, 10 (1980) 25.
134 A. G. Vitenberg, N. V. Pozdnyakov, G. A. Mayevskii and N. I. Pipko, *Zh. Anal. Khim.*, 46 (1991) 361.
135 V. V. Tsibul'skii, I. A. Tsibul'skaya and N. N. Yaglitskaya, *Zh. Anal. Khim.*, 34 (1979) 1300.
136 B. V. Ioffe, A. G. Vitenberg and I. A. Tsibul'skaya, *J. Chromatogr.*, 186 (1979) 851.
137 A. G. Vitenberg and I. A. Tsibul'skaya, *Recommendations for Gas Chromatographic Determination of Benzene, Toluene, Ethylbenzene and Xylenes in Air* (in Russian), Ministry of Health of the USSR, Moscow, 1982.
138 E. L. Selyutina and Yu. Ya. Vinnikov, *Zh. Anal. Khim.*, 43 (1988) 2060.
139 Yu. Ya. Vinnikov, V. V. Derbenev and N. S. Tambieva, *Zavod. Lab.*, 6 (1986) 7.

Journal of Chromatography, 556 (1991) 25–80
Elsevier Science Publishers B.V., Amsterdam

CHROM. 23 314

Review

Is chromatography a separation process?

The zonoid answer

PATRICK VALENTIN
Société Nationale Elf–Aquitaine, Elf–Solaize Research Centre, B.P. 22, 69360 St. Symphorien d'Ozon (France)

ABSTRACT

The separation state of a physical system is defined as a geometric entity called a *zonoid* and a brief account of the mathematical properties of zonoids is given. Visual representations of (2-D and 3-D) zonoids enhance the intuitive grasp of the theory and calculation of their volume gives a useful (although degraded) measure of separation. The answer to the title question is then, on rigorous grounds, that chromatography is not a separation, but a "sepmix" process, *i.e.*, it is both a separation and a mixing process. In linear chromatography, loss in 2-volume of separation between a solute and carrier increases along the column approximately according to $\sqrt{N}$, where N is the number of theoretical plates. 3-Volume of separation between two solutes and carrier first increases and then decreases. More intricate topics such as selectivity of separation are defined and discussed. Examples of problem solving with zonoids are given and it is shown that Rony's extent of separation results from a problem of approximation and reflects only part of separation produced by the column.

CONTENTS

0021-9673/91/$03.50

1. INTRODUCTION

This paper presents a brief account of a new geometric approach to separation engineering, called zonoid theory and shows its potential by application to chromato-

graphy. A small part of this theory has been presented elsewhere [1,2]. In order to be self-consistent, we recall and complete, in an abstract setting, relevant parts of the backbone of the theory, definitions and theorems without proofs or validity statements, in Section 2. Long or technical proofs are relegated to the Appendix. This will allow differently inclined categories of readers to linger on what they like most, without having to extract it painfully. Such an abstract setting is intended to ease application to other processes as well. Section 2 also develops further basic mathematical tools for comparison and classification of separation states.

Column chromatography makes a challenge to separation engineering, a keystone to its methodology. It is a transient process since the flow-rate of species is a function of time t and abscissa z, which involves at least three species, *i.e.*, two solutes and a carrier. Any correct theory of separation must cope with these two basic facts without recourse to simplification *ab initio*. Conversely, if such a theory can treat chromatography successfully, it will presumably be able to do so for any other process.

Previous theories [3,4] on separation failed mainly on two grounds: first, they did not take in account the fact that, as stated above, the primary "product" of a column is, by nature, a flow, the composition of which is a *continuous* function of time. Failure occurred possibly because recovering and managing a large number of small samples would be "uneconomic", or even "unthinkable". Second, these theories concentrate on the separation of solutes, "forgetting" the eluent, which is however an essential part of the process and of its thermodynamic consistency.

The aim of this paper is to show that zonoid theory removes these limitations: the evolution of separation between three species in the column can be computed as a function of z, without the need to resort to any (arbitrary) "cut point".

The ability to cope with multi-component *differential* families is the core of the new separation theory presented here. In fact, a discretization of the outlet flow into "cuts" is unavoidable, but we must do it thoughtfully. Indeed, zonoid theory will give us a safe procedure: to minimize the loss of separation by mixing induced by the trapping procedure, after taking due account of the separation really produced by the column. This task will be addressed in further work.

Is chromatography a separation process? This seemingly strange question stands behind the interesting and paradoxical paper from Golay [5] on entropy (im)balance in chromatography, but has not, up to now, been considered in all of its aspects. We shall leave for further study the pinpointing of the reasons why Golay [5] finds a discrepancy between entropy balance in chromatography and the second law of thermodynamics, noting for the moment only that the solution to this problem would clarify our understanding of chromatography.

In contrast to entropic theories, a remarkable feature of the present theory is that *the very nature, or selectivity type, of a process can be established by pure observation of conserved species evolution.* It is *model independent.* It is also *independent of the nature of these conserved species* (including, *e.g.*, energy).

Section 3 identifies the chromatographic counterpart to the mathematical entities given in Section 2. It also states the methodology for the study of separation states.

Section 4 is a rather qualitative presentation of tools and geometric objects, using simple linear models of the process. The various degrees of selectivity of chromatographic separation are studied.

Section 5 deals with the title question not on "intuitive" grounds, but by a quantitative study of separation zonoids. As it becomes increasingly apparent in Section 4 that chromatography is not a separation process (at least according to the given definition), we must assess clearly which type of process really chromatography is. Here comes into play the new type of process called the "sepmix" process, coined in Section 3 for a process (or transformation) that is neither a separation nor a mixing process. Chromatography will be revealed to be the first example of a sepmix process.

Section 6 lists some other questions that the theory of zonoids asks (and requires answers for), in order of importance. It also shows how the extent of separation defined by Rony [3] fits into the scheme.

On a point of terminology, in the following, zonoids, convex sets of mixtures (CSM) and separation content are really the same object, they are all the embodiment (of the concept) of the separation state, seen from different points of view.

One could give many variant forms to the results of this paper, according to which parameters on which one wishes to make the separation state depend. We have chosen to use variables more natural to users of chromatography. Readers with a deeper interest in zonoids are referred to refs. 6–12.

2. THEORY OF ZONOIDS, A SUMMARY

We outline here, without an attempt to justify the concepts axiomatically, or to give proofs or make precise conditions of the validity of the theorems, as would require a correct mathematical exposition, the main concepts and results of zonoid theory, in a restricted frame suited to column chromatography. The mathematical theory of zonoids is treated in detail in refs. 6–12.

2.1. Systems, linear space E and differential families

A formalization of the concept of a (uniaxial) "physico-chemical system" leads to the following definition.

Definition

Given a vector space E of finite dimension n, state Σ of a system $\mathscr{S}$ is a 1-differential form on the real line R, with value in the positive orthant E^+, and such that coefficient $\mathbf{F}$ of Σ is a Lebesgue integrable vector valued function:

$$\Sigma = \mathbf{F}(t)\mathrm{d}t, \quad t \in \Delta t \subset R$$

E is called the space of (conservative) quantities, and a vector $\mathbf{N} \in E$ is called a quantity vector. E is referred to as an n-dimensional (n-D) space. In accordance with tensor notations, (contravariant) coordinates are indexed as superscripts.

$$E \text{ is given norm } L_1, \ \|\mathbf{N}\|_1 = \sum_{i=1}^{n} |N^i|$$

A problem of evolution arises when **F** depends on a parameter z, *i.e.*, we consider the evolution of state of the system as a function of z. We note

$$\Sigma(z) = \mathbf{F}(z,t)\mathrm{d}t, \quad t \in \Delta t(z) \subset R, \quad z \in L \subset R$$

In the following, we consider $n = 3$, and diffuse, smooth states, *i.e.*,

$$\mathbf{F}(z,t) = (F^1(z,t), F^2(z,t), F^3(z,t)), t \in \Delta t, F^i \text{ of class } C^2(\Delta t) \cap C^1(L)$$

Let Δ_2 be the standard simplex of E:

$$\Delta_2 = \{\mathbf{x} \in E^+ | x^1 + x^2 + x^3 = 1\}$$

Calling $F^0 = F^1 + F^2 + F^3$, $\|\mathbf{F}(z,t)\| > 0$ on $L \times \Delta t$, we associate to **F** the composition function **x** (point valued in Δ_2):

$$\mathbf{x}(z,t) = \left(\frac{F^1}{F^0}(z,t), \frac{F^2}{F^0}(z,t), \frac{F^3}{F^0}(z,t)\right), \quad t \in \Delta t, \quad z \in L$$

Formally (and for a better physical grasp), the 1-differential form Σ may be thought of as a set of "infinitesimal" quantity vectors "d**N**" in E,

$$\mathscr{F} = \{\mathrm{d}\mathbf{N}(t) | t \in \Delta t\} = \{\mathbf{F}(t)\mathrm{d}t\}_{t \in \Delta t}$$

which is called a 1-differential (1-d) family and generically noted $\mathscr{F}$. System state and families or 1-differential forms are therefore the same concept. A problem of evolution will therefore involve a 1-d family depending on a parameter, *e.g.*, $\mathscr{F}(z)$.

The concept of a family of vectors is central to zonoid theory as the family contains all the relevant information to characterize separation present in the system.

The mixing convention is that a state (family) is said to be reduced iff all its colinear vectors in E^+ have been added together. The mixing convention avoids trivial complications, and is natural as we are looking at separations. Note that many physically different systems can map into same reduced state.

Invariance of families or states by change of variables

The change of variables follows a chain rule, or, more precisely, let $t = f(\tau)$, f, continuous, derivable, monotonic on segment Δt, $\tau = f^{-1}(t)$:

$$\{\mathrm{d}\mathbf{N}(t)\}t \in \Delta t = \{\mathbf{F}(t)\mathrm{d}t\}t \in \Delta t = \left\{\mathbf{F} \circ f(\tau) \left|\frac{\mathrm{d}f}{\mathrm{d}\tau}(\tau)\right| \mathrm{d}\tau\right\}_{\tau \in f^{-1}(\Delta t)} \tag{1}$$

This is really a property of differential forms. Note that inclusion of dt in the notation of differential families allows for the automatic use of the chain rule and that the absolute value is taken to conserve positivity in the case when f is decreasing. Eqn. 1 expresses conservation of quantity in the form of an invariant property associated with $\mathscr{F}$.

Integration of families

Any interval (or reunion of disjoint intervals, generically called a region), $\omega \subset \Delta t$ generates a *quantity vector* by

$$\mathbf{N}(\omega) = \int_{\omega} \mathbf{F}(t)\mathrm{d}t = \int_{\mathbf{R}} \chi_{\omega}\mathbf{F}(t)\mathrm{d}t, \mathbf{N}(\omega) \in E \tag{2}$$

where the characteristic function, $\chi_{\omega}: \mathbb{R} \to \{0,1\}$ (or discrete sampling function) is defined by

$\chi_{\omega}(t) = 1$ if $t \in \omega$
$\chi_{\omega}(t) = 0$ if $t \notin \omega$

$\mathbf{N}_0 = \int_0^{\Delta t} \mathbf{F}(s)\mathrm{d}s$ is called the sum (or distal) vector of family $\mathscr{F}$. In an evolution problem, a system is isolated iff $\mathbf{N}_0(z)$ is fixed.

Approximation of families

A partition of Δt into p intervals (or sub-regions) $\omega_1, \ldots, \omega_p$ defines a discrete sampling (approximation) of system state by the (discrete) family of quantity vectors:

$$\left\{\mathbf{N}_j\right\}_{\mathbf{J}} = \left\{\mathbf{N}_j \in E \,|\, j \in J = \{1,2,\ldots,p\}\right\} = \left\{\mathbf{N}_1, \mathbf{N}_2, \ldots, \mathbf{N}_p\right\}$$

If needed, $\mathbf{N}_j$ can be looked at as columns of the non-negative quantity matrix $[N]$, whose entry N_j^i represents the quantity of species i in region j.

2.2. *Zonotopes and zonoids (convex sets of mixtures)*

Taking advantage of the vector space structure of E, we define a geometric operation on sets. The Minkowski sum of sets A and B is the set

$$A + B = \{\mathbf{M} + \mathbf{N} \,|\, \mathbf{M} \in A, \mathbf{N} \in B, A, B \subset E\} \tag{3}$$

with E considered as an affine (point) space.

To a quantity vector $\mathbf{N}$ we associate, in a straightforward way, a segment denoted $[0,N]$ or $\mathbf{N}$ for short, with $\mathbf{N} = \{\lambda\mathbf{N} \,|\, \lambda \in [0,1], \mathbf{N} \in E\}$. Here E is considered as a vector space.

Definition (Coxeter [6,7])

A zonotope Z is the Minkowski sum of a finite set (family) of segments of E:

$$\mathbf{Z} = \sum_{j=1}^{p} [0,\mathbf{N}_j]$$

Simple examples of zonotopes (zonohedra if $n = 3$) are a parallelogram, plane polygon with central symmetry, cube and parallelepiped.

Theorem 1

A zonoid Z is the limit (norm L_1, Hausdorff distance on the set of conpact convex polytopes induced by norm L_1 on E) of a convergent sequence of zonotopes.

Examples of zonoids are a circle, closed plane curve with central symmetry, sphere and ellipsoid.

Let $\mathbf{Z}$ be the closed set of n-dimensional zonoids. In fact, if $\mathbf{K}$ is the set of zonotopes in E, $\mathbf{Z}$ is the closure of $\mathbf{K}$.

2.2.1. Projections

Any partition of a base of E in two subsets and their spanned subspaces V, $V^{\perp}$, defines a canonical projection in E, that is, a projection parallel to $V^{\perp}$ onto V. The projected object inherits the indexes of base of V, *e.g.*, if V = linear span $(\mathbf{e}_1, \mathbf{e}_2)$ then Z_{12} is the projection of Z onto $V^{\perp}$ = linear span $(\mathbf{e}_3)$.

Theorem 2

The image of a zonoid $Z\{\mathscr{F}\}$ by a linear transformation T (*e.g.*, projection), $T(Z)$, is the zonoid generated by the transformed family $T\mathscr{F}$, *i.e.*,

$$T(Z\{\mathscr{F}\}) = Z\{T(\mathscr{F})\} \tag{4}$$

Definition

The separation content Z of a system state Σ of system $\mathscr{S}$ is as follows:
for a discrete system state with p vectors, the zonotope

$$Z\{\mathbf{N}_1, \mathbf{N}_2, \ldots, \mathbf{N}_p\} = \left\{\mathbf{M} \in E \,|\, \mathbf{M} = \sum_{j=1}^{p} \lambda^j \mathbf{N}_j, \lambda^j \in [0,1], j = (1, \ldots, p)\right\} \tag{5}$$

for a diffuse system, the zonoid

$$Z\{\mathbf{F}(t)\mathrm{d}t\}_{\Delta t} = \left\{\mathbf{M} \in E \,|\, \mathbf{M} = \int_{\Delta t} \lambda(t)\mathbf{F}(t)\mathrm{d}t, \lambda \in [0,1]\right\} \tag{6}$$

$\lambda(t)$, called the sampling function, is a measurable function of t on Δt.

If Σ is a discrete (diffuse) system state, its separation content $Z(\Sigma)$ is a zonotope (or zonoid) said to be generated by the discrete (or differential) family of quantity vectors. In both cases, $Z(\Sigma)$ is defined as the set of mixtures feasible by sampling from Σ.

Liapunov's convexity theorem asserts that Z is convex and closed. The Krein–Milman theorem shows that we may take sampling functions λ (eqn. 6) in the smaller (included) set χ_{ω}, that is, we may restrain the sampling function to be characteristic functions without loss in possible mixtures. Therefore, eqn. 6 can be restated as the following theorem.

Theorem 3

Z is the range of the vector measure μ, whose density is $\mathbf{F}(t)$ relative to the Lebesgue measure on Δt.

From theorem 3 we obtain the fundamental property of zonoids.

Theorem 4

A necessary and sufficient condition for $\mathbf{M} \in E$ to be feasible by sampling from a family $\mathscr{F}$ is that $\mathbf{M}$ belongs to zonoid $Z\{\mathscr{F}\}$.

2.2.2. Exterior product of vectors

Define the exterior (or cross) product of two vectors $\mathbf{N}_1, \mathbf{N}_2 \in E = R^2$ as

$$\mathbf{N}_1 \wedge \mathbf{N}_2 = \mathrm{Det}[\mathbf{N}_1, \mathbf{N}_2] = N_1^1 N_2^2 - N_1^2 N_2^1 \tag{7}$$

and for $n = 3$, $\mathbf{N}_1, \mathbf{N}_2 \in E = R^3$ is a vector (in a 3-D space denoted $\Lambda^2 E$)

$$(\mathbf{N}_1 \wedge \mathbf{N}_2)^k = = N_1^i N_2^j - N_1^j N_2^i, 1 \leqslant i < j \leqslant 3, i,j \neq k,k = 1,2,3 \tag{8}$$

If $\mathbf{N}_1, \mathbf{N}_2, \mathbf{N}_3 \in E = R^3$, the exterior (or mixed) product is

$$\mathbf{N}_1 \wedge \mathbf{N}_2 \wedge \mathbf{N}_3 = \mathrm{Det}[\mathbf{N}_1, \mathbf{N}_2 . \mathbf{N}_3] \tag{9}$$

The properties of an exterior product generalize those of determinants.

2.2.3. Regular selectivity

Definition

A family of p vectors in 3-D space E has the 3-regular selectivity property iff its elements can be linearly ordered in such a way that

$$\mathbf{N}_{j_1} \wedge \mathbf{N}_{j_2} \wedge \mathbf{N}_{j_3} \geqslant 0, \forall\, 1 \leqslant j_1 < j_2 < j_3 \leqslant p \tag{10}$$

Similarly, a 1-differential family has the 3-regular selectivity property if a regular parameter exists such that

$$\mathbf{F}(s) \wedge \mathbf{F}(t) \wedge \mathbf{F}(u) \geqslant 0, \forall\, 0 \leqslant s < t < u \leqslant \Delta t \tag{11}$$

Theorem 5

If $\mathbf{F}$ is two times differentiable, a local requirement for 3-regular selectivity is that the Wronskian determinant $W(\mathbf{F})$ be non-negative:

$$W(\mathbf{F}) = \mathbf{F}(t) \wedge \mathbf{F}'(t) \wedge \mathbf{F}''(t) \geqslant 0, \forall\, 0 \leqslant t \leqslant \Delta t \tag{12}$$

Selectivity can be monitored directly from the graph γ of $\mathbf{x}(t)$ in simplex Δ_2, as shown by the following theorem.

Theorem 6

Selectivity is 3-regular iff γ is convex.

Selectivity between species i, j, $i \neq j$, is 2-regular iff one of the equivalent properties holds for any straight line KQ, K the vertex of Δ_2 (extremity of $\mathbf{e}_k$), $k \neq i, j$, Q on γ:

(i) KQ rotates uniformly when Q follows γ uniformly;

(ii) no line KQ has another point on γ than Q.

Definition

A 1-differential family of n species has totally regular selectivity iff it has r-regular selectivity for any $1 \leqslant r \leqslant n$.

For $n = 3$, a study of selectivity involves study of 2×2 minors of Wronskian matrix 12.

Definition (Karlin [13])

A function f: $R \to R^+$ is a Polya frequency (PF) function iff all minors of the matrix $n \times p$ of elements K_j^i, $K_j^i = f(y_j - x_i)$, are positive for any two finite linearly ordered sequences: $x_1 < x_2 < \ldots < x_n$, $y_1 < y_2 < \ldots < y_n$; f is a Polya frequency density if further it is integrable on R.

PF functions are stable by certain transformations:

(1) if $f(u)$ is PF, then $f(au + b)$ is PF, a, b given real numbers;

(2) if $f(u)$ is PF, $\psi(u)$ strictly increasing, then $f(\psi(u))$ is PF.

Theorem 6a

A family $\mathbf{F}(t)$ such that $F^i = f(t - t_i)$, where f is a Polya frequency function, has totally regular selectivity.

These definitions generalize themselves to constant sign in eqns. 12. Note that selectivity is conserved for a family $\lambda(t)\,\mathscr{F}$, $\lambda \geqslant 0$, but not conserved in general linear operations.

2.2.4. Boundary of zonoids

Call ∂Z the boundary of zonoid Z and consider 3-D zonoids.

Lemma 6

Every tangent plane to Z is spanned by two vectors $\mathbf{F}(t_1)$, $\mathbf{F}(t_2)$, $\quad t_1, t_2 \in [0, \Delta t]$.

Definition

A zone $L(t_1)$ is the set of points M on ∂Z, where the tangent (support) plane T_M contains direction of $\mathbf{F}(t_1)$.

Theorem 7

$L(t_1)$ is a closed line and the set of tangent planes envelopes a cylinder whose generatrix is parallel to $\mathbf{F}(t_1)$.

Theorem 8

In the case of 3-regular selectivity, ∂Z is split in two parts, ∂Z^+, ∂Z^- by the

cumulate curve. For ∂Z^+, called the "upper" (or "positive") part of ∂Z, we obtain a two-parameter expression of the surface:

$$\partial Z^+ : \mathbf{M}(t_1, t_2) = \int_0^{t_1} \mathbf{F}(\tau)\mathrm{d}\tau + \int_{t_2}^{\Delta t} \mathbf{F}(\tau)\mathrm{d}\tau, 0 \leqslant t_1 \leqslant t_2 \leqslant \Delta t \tag{13}$$

or

$$\partial Z^+ : \mathbf{M}(t_1, t_2) = \mathbf{N}_0 + \mathbf{N}(t_1) - \mathbf{N}(t_2),\ 0 \leqslant t_1 \leqslant t_2 \leqslant \Delta t$$

For the "lower" part, ∂Z^-, we obtain

$$\partial Z^- : \mathbf{M}(t_1, t_2) = \int_{t_1}^{t_2} \mathbf{F}(\tau)\mathrm{d}\tau, 0 \leqslant t_1 \leqslant t_2 \leqslant \Delta t \tag{14}$$

Clearly points **M** with same arguments in eqns. 13 and 14 are antipodal (*i.e.*, they sum to $\mathbf{N}_0$) in line with central symmetry of Z.

In the general case we obtain an equation for any point on ∂Z^+:

$$\left|\begin{array}{l} \partial Z^+ : \mathbf{M}(t_1, t_2) = \displaystyle\int_{\omega^+(t_1,t_2)} \mathbf{F}(\tau)\mathrm{d}\tau,\ 0 \leqslant t_1 < t_2 \leqslant \Delta t \\ \\ \omega^+(t_1, t_2) = \{\tau \in [0, \Delta t] \,|\, \mathbf{F}(t_1) \wedge \mathbf{F}(t_2) \wedge \mathbf{F}(\tau) \geqslant 0\} \end{array}\right. \tag{15}$$

where the integration domain is defined by the solution of a (non-linear) equation.

2.2.5. n-Volume of zonoids

Ξ, the volume of the n-dimensional body Z, provides a numerical value (in fact, an antisymmetric tensor) for separation, called the n-volume of separation. If one considers a separation between a subset of species, *e.g.*, 1, 2, the volume is labelled accordingly, Ξ_{12}.

The differential volume element is, for a 2-d zonoid,

$$\mathrm{d}\Xi = |\mathbf{F}(s) \wedge \mathbf{F}(t)|\mathrm{d}s\mathrm{d}t$$

where we may drop the absolute value if

$$\mathbf{F}(s) \wedge \mathbf{F}(t) \geqslant 0,\ 0 \leqslant s < t \leqslant \Delta t$$

Theorem 9

The 2-volume of separation of the differential family **F** is given by

$$\Xi = \iint\limits_{0 \leqslant s < t \leqslant \Delta t} |\mathbf{F}(s) \wedge \mathbf{F}(t)| \, \mathrm{d}s\mathrm{d}t \tag{16}$$

In this case, multi-linearity of the exterior product gives, through integration, if selectivity is 2-regular:

$$\Xi = \int\limits_{0 \leqslant t \leqslant \Delta t} \mathbf{N}(t) \wedge \mathbf{F}(t) \mathrm{d}t \tag{17}$$

with cumulate vector $\mathbf{N}(t)$, defined as

$$\mathbf{N}(t) = \int_0^t \mathbf{F}(s) \mathrm{d}s$$

Note that eqn. 17 is a classical expression for signed area (seen from the origin) generated by a plane curve given by parametric equations.

These equations extend readily to zonotopes and zonoids in spaces of higher dimension (compare eqns. 16 and 19).

In the discrete case, *i.e.*, for a 3-D zonotope, 3-volume is (from ref. 10)

$$\Xi = \sum_{1 \leqslant j_1 < j_2 < j_3 \leqslant p} |\mathbf{N}_{j_1} \wedge \mathbf{N}_{j_2} \wedge \mathbf{N}_{j_3}| \tag{18}$$

For a diffuse family, the equivalent of eqn. 18 is

$$\Xi = \iiint\limits_{0 \leqslant r < s < t \leqslant \Delta t} |\mathbf{F}(r) \wedge \mathbf{F}(s) \wedge \mathbf{F}(t)| \, \mathrm{d}r\mathrm{d}s\mathrm{d}t \tag{19}$$

2.3. Geometric comparison of separation contents

2.3.1. The existence ordering

Definition

A discrete system state Σ represented by family $\mathscr{F} = \{\mathbf{N}_j | j \in J\}$ is said to contain a greater separation than system state Σ', or $\mathscr{F}' = \{\mathbf{M}_k | k \in K\}$ iff family $\mathscr{F}'$ can be made by sampling from family $\mathscr{F}$, that is, iff a $J \times K$ matrix $[\mu]$ exists such as

$$\mathbf{M}_k = \sum_{j\in J} \mu_k^j \mathbf{N}_j, k \in K \tag{20}$$

$$0 \leqslant \mu_k^j, \quad j \in J, \quad k \in K, \quad \sum_{k\in K} \mu_k^j = 1, \quad j \in J \tag{20a}$$

As $N_0 = \sum_{k\in K} \mathbf{M}_k = \sum_{j\in J} \mathbf{N}_j$, families $\mathscr{F}$ and $\mathscr{F}'$ have the same sum vector, and therefore we compare two states of an isolated system. If $n = 1$, we recover the rule of conservation of quantity.

For diffuse systems represented by 1-differential families, we make the following definition.

Definition
A system state (family):

$$\mathscr{F}_2 = \{\mathbf{F}_2(\tau)\mathrm{d}\tau\}_{\tau\in[\tau_1,\tau_2]=I_2\subset R}$$

has a greater separation content than a system state (family):

$$\mathscr{F}_1 = \{F_1(t)\mathrm{d}t\}_{t\in[t_1,t_2]=I_1\subset R}$$

iff a non-negative function λ, called a sampling kernel, $\lambda: I_1 \times I_2 \to R^+$ exists such that

$$\mathbf{F}_1(t) = \int_{I_2} \lambda(t,\tau)\mathbf{F}_2(\tau)\mathrm{d}\tau, \quad t \in I_1 \tag{21}$$

$$\int_{I_1} \lambda(t,\tau)\mathrm{d}t = 1, \quad \tau \in I_2 \tag{21a}$$

Both eqns. 21 and 21a imply, through Fubini's theorem,

$$\int_{I_1} \mathbf{F}_1(t)\mathrm{d}t = \int_{I_2} \mathbf{F}_2(\tau)\mathrm{d}\tau = \mathbf{N}_0$$

Sampling kernels generalize sampling functions defined in eqn. 6.

Sampling kernels generate a partial order relation, called existence, on separation states or zonoids, *i.e.*, on $\mathbf{Z}$: one writes

$$Z(\Sigma') \prec Z(\Sigma) \tag{22}$$

and reads eqn. 22 as: separation state Σ' *exists* in separation state Σ. We have

$$Z(\Sigma') \prec Z(\Sigma) \text{ and } Z(\Sigma) \prec Z(\Sigma') \Rightarrow \Sigma = \Sigma'$$

By a theorem from Blackwell [12], if $\dim E = 2$, the existence order is equivalent to inclusion of zonoids, but is a stronger order in general.

The physical meaning of inequality 22 is that (the whole) system state Σ' can be made by sampling of system Σ.

As subtraction has no meaning for zonoids, we cannot simplify these as for scalar inequalities. However, we have a simplification property:

$$\text{If } Z' = Z'_1 + Z_2, Z = Z_1 + Z_2, \text{ then } Z' \prec Z \Leftrightarrow Z'_1 \prec Z_1 \tag{23}$$

2.3.2. A classification of transformations

Definition

A transformation T, $\Sigma \to \Sigma' = T(\Sigma)$, occurring in a isolated system is qualified as:

a pure separation iff $(Z(T(\Sigma)) \prec Z(\Sigma)$, *i.e.*, separation content increases;
a pure mixing iff $(Z(\Sigma)) \prec Z(T(\Sigma))$, *i.e.*, separation content decreases;
a sepmix iff neither case holds, *i.e.*, separation contents are incomparable.

3. OVERALL SEPARATION BALANCE IN CHROMATOGRAPHY

Our primary interest will be in the overall separation balance and we shall not attempt here to go to the root of the process and discover how the separation evolution is governed by partial differential equations of propagation themselves, together with their initial and boundary conditions and their thermodynamic constraints.

3.1. Identification of flow families

The separation of two species by chromatography is basically a ternary process, as it involves necessarily some spending of a third species called carrier: space E of quantities is three-dimensional, $\dim E = 3$.

A natural base for E is formed on unit quantity of each pure species, *e.g.*, axes will be labelled in moles of species 1, 2 (solutes), 3, carrier. In this base we associate, for any mixture of carrier and solutes, a vector of components (N^1, N^2, N^3). Note the superscript species label. A formal distinction is that species will be all chemical components injected into the column and solutes will be only those one wishes to analyse or separate. We make the convention that solutes are numbered by increasing retention times and the carrier is put as the last species.

The composition of a mixture is now expressed by a molar fraction vector $\mathbf{x}$ and associate point in Δ_2, the molar fraction simplex.

From this point on, we shall use consistently notations linked with the physical nature of the represented entity: $\mathbf{F}$ for a (vector) flow of species, $\mathbf{N}$ for a (vector) quantity of species, $\mathbf{x}$ for a (vector) molar fraction.

A (hypothetical) selective detector placed at a fixed point on the abscissa z in the chromatographic column would record a chromatogram of concentrations of solutes in the mobile phase (and, consequently, flow-rates), from which we calculate the coefficient function $\mathbf{F}$ of 1-differential family of quantities:

$$\mathbf{F}(z,t) = (F^1(z,t), F^2(z,t), F^3(z,t)), \quad t \in \Delta t, \quad z \in R$$

Carrier flow is usually calculated by difference, from

$$F^3(z,t) = F^0(z,t) - F^1(z,t) - F^2(z,t)$$

where $F^0(z,t)$ is the total molar flow-rate, assumed to be known or to be measured.

A family is denoted $\mathscr{F}(z) = \{\mathbf{F}(z,t)\mathrm{d}t\}_{t \in \Delta t}$

Alternatively, one may obtain a family by simulation through a differential model of the propagation involving a balance equation for all species, a necessity when only the sum $F^1(z,t) + F^2(z,t)$ is the one physical quantity that can be monitored.

Clearly we obtain a *diffuse* system (except at $z = 0$), as components of $\mathbf{F}$, flow of species through the section of a column at abscissa z, are smooth functions.

3.2. *Parameters and intervals*

The natural parameter t of the family is time and the evolution problem has parameter z, abscissa in the column.

In principle, owing to the nature of diffusion, the cycle or interval of time of collection $\Delta t(z)$ (and therefore carrier quantity and zonoids) is unbounded. To avoid mathematical complications, we shall often consider that essentially all the injected feed is recovered in a finite time interval called a cycle, a good assumption since for all of our models, the solute i flow ($i = 1, 2$) will follow Gaussian or near Gaussian laws centred at $\bar{t}_i$, with variance σ_i^2. For rigorous study, we must take $\Delta t = (-\infty, +\infty)$. However, for most practical purposes

$$\Delta t = [\bar{t}_1 - 3\sigma_1, \bar{t}_2 + 3\sigma_2] \tag{24}$$

or

$$\Delta t = [0, \bar{t}_2 + 3\sigma_2] \tag{24a}$$

will be appropriate. In the last case we shall slightly abuse the notation by confusing the interval Δt with its upper bound. For an isovariant case, eqn. 24 defines an interval $6\sigma + \bar{t}_2 - \bar{t}_1$ centred on the mid-point between peak maxima.

A column is of bounded length L, so that we may put $0 \leqslant z \leqslant L$.

The system state is obtained from observation of flow-rates given by a detector located at z as a function of time, during time interval Δt. Passing to space of quantities E is straightforward since $\mathrm{d}\mathbf{N}(z,t) = \mathbf{F}(z,t)\mathrm{d}t$ represents formally the (infinitesimal) quantity that would be collected in the mobile phase between t and $t + \mathrm{d}t$ at z in the column.

A parallel theory could have been developed, reversing z and t, using lineic concentrations instead of flows, *i.e.*, considering the system (state) Σ as the content of a volume Ω of the column with the problem of evolution in time. However, it would be less natural for the present application.

Although flows are the more natural variables, we may also consider chromatography as a spatial process and, in a sense, this must always be ultimately so, thinking as if elements of the family were in different regions (or tanks), the produced family $\{\mathbf{F}(z,t)\mathrm{d}t\}_{t \in \Delta t}$ going into a fraction collector which collects during a time interval $\mathrm{d}t$

flow vector $\mathbf{F}(z,t)$ passing through point z into a differential (volumic) region of volume $\mathrm{d}V$, whose content has concentration $\mathbf{C}(z,V)$. As we have

$$\{\mathbf{F}(z,t)\mathrm{d}t\}_{t\in\Delta t} = \{\mathbf{C}(z,V)\mathrm{d}V\}_{V\in\Delta V} \text{ with } \mathrm{d}V = Q\mathrm{d}t$$

this new family results from the flow family by a simple change of parameter and use of a chain rule and therefore is completely equivalent to it.

In elution chromatography, an inlet (discrete) family consists of two vectors:

$$\mathscr{F}(0) = \left\{ \begin{bmatrix} N_0^1 \\ N_0^2 \\ 0 \end{bmatrix}, \begin{bmatrix} 0 \\ 0 \\ F_0^3 \Delta t \end{bmatrix} \right\}$$

the former being the quantity of feed and the latter the quantity of pure carrier taken in by the column during the cycle time, taking the flow of carrier as $F^3(z,t) = F_0^3 =$ constant. The outlet family produced by the column is $\mathscr{F}(L) = \{\mathbf{F}(L,t)\mathrm{d}t\}_{t\in\Delta t}$. The overall species balance imposes that these two families acquire the same sum vector, at least to a reasonable approximation. However, the flow-rate of carrier F_0^3 must be such that solutes are sufficiently diluted in the column so that hypotheses of the model hold. In practice, taking in account the cycle time given by eqn. 24, this will impose a minimum quantity of carrier N_0^3. Using the simplification property given in eqn. 23, we see that any quantity of virtually pure carrier recovered at the column outlet can be "subtracted" from the pure carrier vector in the inlet family. This allows the minimum cycle time to be taken.

Fig. 1 shows chromatograms, the starting point of our investigation.

3.3. *Problem of evolution*

We identify now the problem of evolution: clearly we are interested in comparing separation states of flow families for increasing values of z, length along column and, especially, initial (inlet) and final (outlet) flow families. The inlet zonoid is generated by the (differential) family of inlet quantity vectors in the cycle and the outlet zonoid is

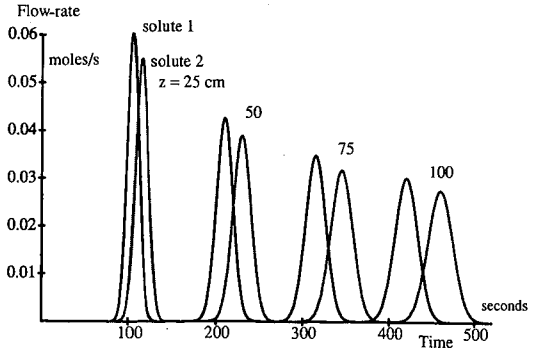

Fig. 1. Chromatograms at different locations in the column. L = 25, 50, 75, 100 cm. Conditions: HETP = 0.1 cm; u = 5 cm/s; k^1 = 20; k^2 = 22; α = 1.10; quantity injected per cycle, 1, 1, 26 mol; carrier flow-rate, 0.2 mol/s; cycle time, Δt = 130 s.

generated by the family of outlet quantity vectors. From species conversion, these two zonoids have the same sum vector.

In other words, a cycle transforms a system state Σ into a system state Σ'. From this point of view, the inlet (or outlet) family can also be called the initial (or final) family.

For theoretical and design purposes, the evolution of a zonoid together with all of its canonical projections has to be considered, *i.e.*, projections on planes of coordinates (1,2), (2,3), (2,3), which indicate the binary separation evolution between solutes or a solute and the carrier. Note also that separation between linear combinations of species can be considered, *e.g.*, separation between carrier and total flow of solutes (1,2) will be monitored in the vertical bisector plane.

The above material is all we need in order to assess and compare, in two and three dimensions, separation states.

However, two intermediate geometric tools will be useful, namely, graph Γ of cumulated quantities, in E, for the construction of a zonoid, and, graph γ of molar fractions function, in Δ_2, for the study of selectivity.

3.4. Graph Γ of cumulated quantities

By time integration of $\mathbf{F}(z,t)$ as shown in eqn. 2, from $\tau = 0$ to $\tau = t$, we obtain the cumulate family, $\mathbf{N}(z,t)$, which is shown for $z = 25$ in Fig. 2.

As a one-dimensional "object", Γ, the graph of $\mathbf{N}(t)$, is a skewed curve (Fig. 2) and bears no evident connection with the three-dimensional zonoid Z it generates. When t increases, point $\mathbf{N}$ goes from the origin towards the distal point on Γ. Although it is clear that Γ belongs to Z, there is no guarantee that it belongs to ∂Z. Hence one needs either some algorithm to calculate and represent the zonoid from experimental data, or some equation to obtain the boundary if the model is known. Such an algorithm is currently under development. Here we adopt the second approach as equations are simple to conceive and implement, at least for some simple models considered below.

Remark

In all 3-D drawings of zonoids or simplexes, the orientation will always be the

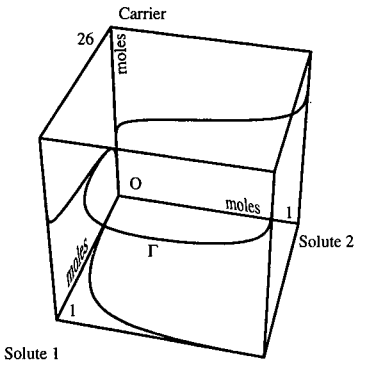

Fig. 2. Graph of cumulated quantity vector $\mathbf{N}(t)$ with canonical projections. $z = 25$ cm; $F_0^3 = 0.2$ mol/s.

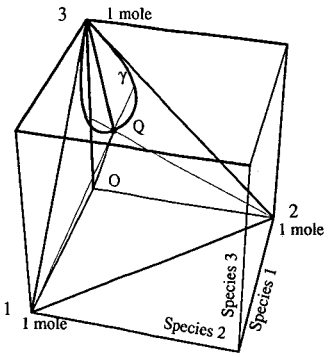

Fig. 3. Evolution of the composition $\mathbf{x}(t)$ in Δ_2. Conditions as in Fig. 1, $L = 25$ cm.

same, namely with the origin at the lower, back and left vertex, with the species 1 (the less retained) axis pointing towards the front, the species 2 axis horizontal parallel to the plane of the drawing and the carrier axis vertical parallel to the plane of the drawing. The cube is assumed to be transparent and the vertical scale has been contracted by a factor of 26.

3.5. Graph γ of molar fractions family

Evolution of the composition [molar fraction vector, $\mathbf{x}(t)$] of the outlet flow is represented by a curve $\gamma(t)$ in the molar fraction simplex Δ_2 on a cycle (Fig. 3). This curve belongs also to the hodograph cone of Γ (the set of rays starting at the origin, parallel to a tangent vector to Γ).

γ is a closed curve in Δ_2 if t is allowed to vary from $-\infty$ to $+\infty$. Note that γ is "nearly closed", *i.e.*, on most practical grounds if Δt is given by eqn. 24. In our convention that species 1 is less retained than species 2, point $\mathbf{x}$ rotates counter-clockwise when t increases.

4. LINEAR MODELS OF CHROMATOGRAPHY

We shall consider two types of linear models of propagation of elution bands into the column. For ease of interpretation in zonoid theory, these models are written (a rather unusual feature) in terms of flow-rates, but they could be transformed easily into concentrations, since $C^i = QF^i$.

4.1. Basic hypotheses

Strong hypotheses are made to arrive at an explicit solution of the propagation model of chromatography.

By linearity of a process we mean that a linear combination of injection functions $\mathbf{F}^1(0,t)$, $\mathbf{F}^2(0,t)$ with positive coefficients a, b produces the same linear combination of outlet flow-rates function $\mathbf{F}^1(z,t)$, $\mathbf{F}^2(z,t)$:

$$a\mathbf{F}^1(0,t) + b\mathbf{F}^2(0,t) \text{ gives } a\mathbf{F}^1(z,t) + b\mathbf{F}^2(z,t) \quad \forall z \in R^+$$

Linearity allows us to normalize quantities of species, as zonoids will transform themselves by linearity and n-volumes will be multiplied by an appropriate scalar quantity. Therefore, a yield of 3-volume can be defined as

$$\xi = \frac{\Xi}{N_0^1 N_0^2 N_0^3} \tag{25}$$

where $N_0^1 N_0^2 N_0^3$ represents the 3-volume of total separation between species.

The linearity hypothesis involves high dilution both in the stationary phase, *i.e.*, constant partition coefficients and the assumption of a small injection of solutes, both in quantity and in injection time, into the carrier (superscript 3). Then, we have

$$F^3(z,t) = F^0 - F^1(z,t) - F^2(z,t) \approx F^0 \tag{26}$$

where F^0, the flow-rate at the column inlet, is a known constant. In the following we admit also that the carrier is not adsorbed or absorbed on the stationary phase.

Anyway, this assumption is not necessary since a differential family with coordinate functions (F^1, F^2, F^0) results from (F^1, F^2, F^3) by a linear transformation, and the results upon separation can therefore be transposed immediately (Theorem 2) from one family to the other.

The solution of the balance equation of species, in the form of Partial Differential Equations in the case of superimposition of diffusion upon a plug flow (with suitable limit conditions), or of a discrete model of the column in the form of Ordinary Differential Equations (the plate model), leads in the former instance to an (approximate) Gaussian and in the latter to a Poisson distribution of flow-rate of a solute; see, *e.g.*, Villermaux [14] for a comparison of these models. From the central limit theorem in probability theory, both of them are asymptotically identical, that is, when the number of plates or, equivalently, the length of column approach infinity, a result which allows both of them to be expressed with the same parameters.

Hence parameters of the plate model, more acceptable to chromatographers, will be used throughout: a column is equivalent to N perfectly agitated vessels called theoretical plates, set in series. On the above asymptotic common solution, N and D, the dispersion coefficient (supposed to be identical for all the species), are related by

$$\text{HETP} = \frac{L}{N} = \frac{2D}{u} \tag{27}$$

where HETP (denoted H) is the height equivalent to a theoretical plate and u is the linear flow-rate of the carrier. σ_i, the standard deviation of the Gaussian distribution of the flow-rate (as a function of time), depends on the mean residence time $\bar{t}_i$ of solute i:

$$\sigma_i = \frac{\bar{t}_i}{\sqrt{N}} \tag{28}$$

Of course, more realistic expressions for H *vs.* u could be used, taking account different contributions to dispersion.

As $z = NH$, $\bar{t}_i$ at location z is given by

$$\bar{t}_i = \frac{z}{u}(1 + k^i) \approx \frac{(1 + k^i)NH}{u} \tag{29}$$

Although in the following, for the sake of simplicity, we adopt the "no pressure drop" hypothesis, such a requirement could be relaxed as far as separation between species is concerned. In the case of a moderate pressure drop, and for a carrier following the law of perfect gases, flow vectors do not depend explicity on pressure p, a distinct advantage of the present formulation, and we have simply to take into account the dependence of p and u on z. By straight integration of Darcy's law we obtain

$$u(z)p(z) = u(L), \quad p(0) = P, \quad p(L) = 1, \quad p^2 = P^2 - \frac{z}{L}(P^2 - 1)$$

which, by integration of eqn. 29, written in a differential form relating dz and $d\bar{t}_i$, gives the dependence of retention time on pressure:

$$\bar{t}_i = \frac{2}{3} \cdot \frac{P^3 - p^3}{P^2 - 1} \cdot \frac{1}{Lu(L)}(1 + k^i)$$

Similarly, eqn. 27 for the mean HETP (H) should be modified to

$$H = \frac{9}{8} \cdot \frac{(P^4 - p^4)(P^2 - 1)}{(P^3 - p^3)^2} \cdot \frac{2D(L)}{u(L)}$$

A complete study of separation would, however, take into account another conserved quantity, namely momentum, but, although feasible in principle, this would complicate the study tremendously.

4.2. Three linear models

4.2.1. Model I, asymptotic Gaussian

From the well known equation for Gaussian peaks, valid for a pulse injection of a small quantity of mixture into a column of infinite length (at both ends), we may deduce, using a staged model, asymptotically valid, *i.e.*, for $N \to +\infty$, the following expression for the flow-rate of solute i:

$$F^i(N,t) = N_0^i \frac{\sqrt{N}}{\sqrt{2\pi t_i}} e^{-\frac{1}{2}N\left(1 - \frac{t}{\bar{t}_i}\right)^2}, \quad t \in R, \quad i = 1,2 \tag{30}$$

(note that in a strict sense, eqn. 30 cannot be valid for $t < 0$, as it would violate the principle of causality). $\bar{t}_i$ is equal to the retention time of the maximum of the peak.

4.2.2. Model II, Gaussian, isovariance assumption

For computational simplicity, and as interest in chromatography focuses mainly

on difficult separations, that is with differences between retention times much lower than the retention times themselves, we may assume that σ_i in eqn. 28 depends not on i, but on some mean retention time for the group of solutes. Physically, this means that although the two peaks translate at different speeds, they enlarge at the same rate, depending on z or N but not on the species. The injected quantity of species acts only through a vertical affinity on the peak. We shall set (although other mean values could be chosen)

$$\bar{t} = \frac{1}{2}(\bar{t}_1 + \bar{t}_2)$$

From eqn. 28, we obtain (isovariance assumption)

$$\bar{\sigma} = \frac{\bar{t}}{\sqrt{N}} = \frac{(\bar{t}_1 + \bar{t}_2)}{2\sqrt{N}} \tag{31}$$

Therefore, the flow-rate vector for solutes becomes

$$F^i(N,t) = N_0^i \frac{\sqrt{N}}{\sqrt{2\pi t}} e^{-\frac{1}{2}N\left(\frac{\bar{t}_i - t}{\bar{t}}\right)^2}, \quad i = 1,2 \tag{32}$$

4.2.3. Model III, Poisson

The final linear model considered is the plate model, a classical one in chemical engineering, the solution of which can also be derived by a probabilistic argument assuming for each species an independent Poisson law with parameter λ_i. Let $P(N,\lambda)$ be the probability for a molecule of given λ to be at stage N:

$$P(N,\lambda) = \frac{1}{N!} e^{-\lambda} \lambda^N \tag{33}$$

Parameter λ_i, depending on the species i, is

$$\lambda_i = \frac{u}{(1 + k^i)H} = \frac{N}{\bar{t}_i}$$

is the mean number of plates "seen" by a molecule of species i during the unit time interval if the molecules distribute themselves randomly upon the $t \geqslant 0$ axis. By replacement of λ_i with its above value, multiplied by t, the flow-rate vector acquires the form

$$F^i(N,t) = N_0^i \frac{N}{\Gamma(N)\bar{t}_i} e^{-\frac{Nt}{\bar{t}_i}} \left(\frac{Nt}{t_i}\right)^{N-1}, \quad t \in R^+, \quad i = 1,2 \tag{34}$$

where we have extended to real (rather than integer) values of N using $\Gamma(N)$, the gamma function (recall $\Gamma(N) = (N-1)!$ if N is an integer). For $t < 0$, $F^i(N,t) = 0$.

Note that if N is an integer, eqn. 34 is the solution for a Dirac injection at time $t = 0$ into the first cell of a series of N perfectly agitated cells (modelled by a system of ordinary differential equations). Therefore, the results of model III will be valid for a larger class of separation processes than chromatography, *e.g.*, liquid–liquid extraction.

All families resulting from these models are summarized in Table 1. According to our conventions, **F** is the flow-rate family and N is the quantity (cumulated starting from the initial time of the cycle). The following definition has been used:

$$N(u) = \mathrm{erf}(u) = \frac{1}{\sqrt{2\pi}} \int_{-\infty}^{u} \mathrm{e}^{-\frac{t^2}{2}} \mathrm{d}t \tag{35}$$

Eqn. 35 is slightly different from the other definition of error function often used, *i.e.*,

$$\mathrm{Erf}(u) = \frac{2}{\sqrt{\pi}} \int_{0}^{u} \mathrm{e}^{-t^2} \mathrm{d}t$$

We have: $\mathrm{erf} = {}^1/_2(\mathrm{Erf} + 1)$.

The incomplete gamma function $\gamma(a,u)$ is defined as usual by

$$\gamma(a,u) = \int_{0}^{u} t^{a-1} \mathrm{e}^{-t} \mathrm{d}t, a > 0$$

$W(\mathbf{F})$ are the corresponding (Wronskian) matrices, *i.e.*, lines of the matrix are for species 1, 2, 3 and columns for time derivatives of order 0, 1, 2 of **F**.

4.3. A qualitative study of zonoids evolution

Unless specified otherwise, we shall use the Gaussian model I although other models would give similar results, except for some details. That we may study a 1-differential family and zonoid independently of the quantity and composition of injected mixture can be deduced from the following.

From linearity, **F**, or the 1-differential, family is proportional to the corresponding coordinate of $\mathbf{N}_0$, that is, the zonoid obtained from injected vector $\mathbf{N}_0$ is deduced from the zonoid calculated for the mixture (1,1,1) by the product of affinities N_0^i along axes $\mathbf{e}_i$ ($i = 1,2,3$). Also, canonical projection (1,2) does not depend on the dilution of the injection in the carrier, as long as injection time is short.

The curve $\Gamma = \mathbf{N}(t)$, as the primary ingredient for the zonoid construction, is drawn in Fig. 2. Direct examination of Γ and its projections on base planes reveals that the vertical projection of Γ on the ground plane (1,2) is convex, but projections on planes (1,3) and (2,3) are not. It suffices to note here that a plane arc of curve generates a two-dimensional zonoid and bounds it if the arc is convex. Therefore, canonical projection of Γ on the ground plane shows directly the projection of the 3-D zonoid.

Clearly there is a large difference between the separation of solutes 1 and 2 and

TABLE I

FLOW-RATE VECTOR FUNCTION F(t) AND WRONSKIAN MATRIX

Model	$\mathbf{F}(N,t)\mathrm{d}t$	$\mathbf{N}(N,t)$	Wronskian matrix
I	$\begin{bmatrix} N_0^1 \cdot \frac{\sqrt{N}}{\sqrt{2\pi}\bar{t}_1} \cdot \mathrm{e}^{-\frac{1}{2}N\left(1-\frac{t}{\bar{t}_1}\right)^2} \mathrm{d}t \\ N_0^2 \cdot \frac{\sqrt{N}}{\sqrt{2\pi}\bar{t}_2} \cdot \mathrm{e}^{-\frac{1}{2}N\left(1-\frac{t}{\bar{t}_2}\right)^2} \mathrm{d}t \\ F_0^3 \mathrm{d}t \end{bmatrix}$	$\begin{bmatrix} N_0^1 \operatorname{erf}\left(\sqrt{N}\cdot\frac{\bar{t}_1 - t}{\bar{t}_1}\right) \\ N_0^2 \operatorname{erf}\left(\sqrt{N}\cdot\frac{\bar{t}_2 - t}{\bar{t}_2}\right) \\ F_0^3 t \end{bmatrix}$	$\begin{bmatrix} 1 & -\frac{t-\bar{t}_1}{\bar{t}_1^2} & \frac{1}{\bar{t}_1^2}\left\{N\left(\frac{(t-\bar{t}_1)}{\bar{t}_1}\right)^2 - 1\right\} \\ 1 & -\frac{t-\bar{t}_2}{\bar{t}_2^2} & \frac{1}{\bar{t}_2^2}\left\{N\left(\frac{(t-\bar{t}_2)}{\bar{t}_2}\right)^2 - 1\right\} \\ 1 & 0 & 0 \end{bmatrix}$
II	$\begin{bmatrix} N_0^1 \cdot \frac{\sqrt{N}}{\sqrt{2\pi}\bar{t}} \cdot \mathrm{e}^{-\frac{1}{2}N\left(\frac{\bar{t}_1 - t}{\bar{t}}\right)^2} \mathrm{d}t \\ N_0^2 \cdot \frac{\sqrt{N}}{\sqrt{2\pi}\bar{t}} \cdot \mathrm{e}^{-\frac{1}{2}N\left(\frac{\bar{t}_2 - t}{\bar{t}}\right)^2} \mathrm{d}t \\ F_0^3 \mathrm{d}t \end{bmatrix}$	$\begin{bmatrix} N_0^1 \operatorname{erf}\left(\sqrt{N}\cdot\frac{\bar{t}_1 - t}{\bar{t}}\right) \\ N_0^2 \operatorname{erf}\left(\sqrt{N}\cdot\frac{\bar{t}_2 - t}{\bar{t}}\right) \\ F_0^3 t \end{bmatrix}$	$\begin{bmatrix} 1 & -(t-\bar{t}_1) & N\left(\frac{(t-\bar{t}_1)}{\bar{t}}\right)^2 - 1 \\ 1 & -(t-\bar{t}_2) & N\left(\frac{(t-\bar{t}_2)}{\bar{t}}\right)^2 - 1 \\ 1 & 0 & 0 \end{bmatrix}$
III	$\begin{bmatrix} N_0^1 \cdot \frac{N}{\Gamma(N)\bar{t}_1} \cdot \mathrm{e}^{-\frac{Nt}{\bar{t}_1}} \cdot \left(\frac{Nt}{\bar{t}_1}\right)^{N-1} \mathrm{d}t \\ N_0^2 \cdot \frac{N}{\Gamma(N)\bar{t}_2} \cdot \mathrm{e}^{-\frac{Nt}{\bar{t}_2}} \cdot \left(\frac{Nt}{\bar{t}_2}\right)^{N-1} \mathrm{d}t \\ F_0^3 \mathrm{d}t \end{bmatrix}$	$\begin{bmatrix} N_0^1 \cdot \frac{\gamma\left(N,\frac{Nt}{\bar{t}_1}\right)}{\Gamma(N)} \\ N_0^2 \cdot \frac{\gamma\left(N,\frac{Nt}{\bar{t}_2}\right)}{\Gamma(N)} \\ F_0^3 t \end{bmatrix}$	$\begin{bmatrix} 1 & -\frac{N}{\bar{t}_1} + \frac{N-1}{t} & \frac{N^2}{\bar{t}_1} - 2\cdot\frac{N}{\bar{t}_1}\cdot\frac{N-1}{t} + \frac{(N-1)(N-2)}{t^2} \\ 1 & -\frac{N}{\bar{t}_2} + \frac{N-1}{t} & \frac{N^2}{\bar{t}_2} - 2\cdot\frac{N}{\bar{t}_2}\cdot\frac{N-1}{t} + \frac{(N-1)(N-2)}{t^2} \\ 1 & 0 & 0 \end{bmatrix}$

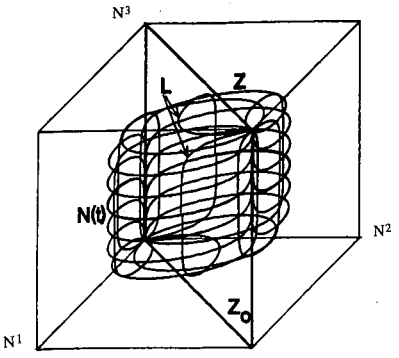

Fig. 4. Injected and recovered 3-d zonoids. Two solutes + carrier; Gaussian model; $z = 25$ cm.

separation of the carrier with solute 1 or solute 2. We shall consider the meaning and significance of convexity in Section 5.5, under the heading "Selectivity" at the end of this section. A quantitative study of the growth and decrease or increase in separation in three-dimensional space and in ground planes will be given in Section 7.

We wish now to acquire some visual grasp of the 3-D zonoid itself, that is, we want to draw its boundary. Although different shapes of the boundary of the zonoid are possible, the simplest type of lines covering Z is provided by zonal lines or zones. Let us postpone the construction of such lines and suppose here that we have constructed a set of such lines.

We are in position to "see" the 3-D separation balance defined in Section 4. Recall the fundamental property of zonoids: **M** is feasible by mixing from the effluent of the column iff it belongs to Z.

The initial or injected zonoid, Z_0 (Fig. 4), is a vertical parallelogram constructed on the vectors (1, 1, 0) and (0, 0, 26). The final or outlet zonoid, Z, may be drawn as a slanted ovoidal box: the quasi-vertical part of Z corresponds to almost pure carrier (part in front, part to the rear of the peaks), and the top and bottom correspond to an effective separation between solutes.

Clearly zonoids Z_0 and Z intersect themselves (in the sense that they have common points although none is contained in the other), a general fact of great importance in view of the fundamental property of CSM: more precisely, mixtures $\mathbf{M} \in Z$, $\mathbf{M} \notin Z_0$, feasible from the final separation state are not feasible from the initial state because they do not have the initial composition in solutes and conversely, mixtures $\mathbf{M} \notin Z$, $\mathbf{M} \in Z_0$ feasible from the initial separation state are not feasible from the final state because they are too rich (or too poor) in carrier.

Finally, one may look at canonical projections of Z on coordinate planes, which of course are zonoids and therefore centrally symmetric convex sets (Fig. 5).

4.4. Drawing the boundary of a zonoid

We give a projective construction of zones using simplex Δ_2, which provides also a geometric rationale for eqns. 13–15.

Consider a plane Π_M passing through the origin. Π_M intersects simplex Δ_2 along

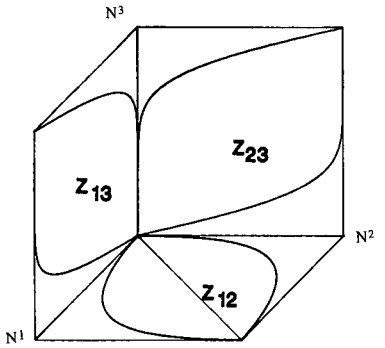

Fig. 5. Canonical projections of the zonoid Z on coordinate planes: Z_{12}, Z_{13}, Z_{23}. Conditions as in Fig. 4.

line PQ. Suppose P, Q are on γ, located at parameter values t_1, t_2, *i.e.*, they have coordinates $\mathbf{x}(t_1)$, $\mathbf{x}(t_2)$. Therefore, Π_M is an oriented plane spanned by $\mathbf{F}(t_1)$, $\mathbf{F}(t_2)$.

As Z is convex, we associate to Π_M a pair of tangent (or, more generally, support) planes T_{M_1}, T_{M_2} with $\mathbf{M}_1$, $\mathbf{M}_2$ the contact point on ∂Z. Recall that domain of integration ω^+ for any point M on ∂Z is defined by a value τ such that eqn. 15 holds:

$$\mathbf{F}(t_1) \wedge \mathbf{F}(t_2) \wedge \mathbf{F}(\tau) \geqslant 0 \text{ or } \mathbf{x}(t_1) \wedge \mathbf{x}(t_2) \wedge \mathbf{x}(\tau) \geqslant 0 \tag{36}$$

Therefore, ω^+ is the set of the points of γ which are in the positive half simplex plane defined by PQ. ω^- would be defined symmetrically by inequalities $\leqslant 0$ in eqn. 36.

To generate zone $L(t_1)$ we just rotate line PQ in Δ_2 around fixed point P. We obtain two symmetrical points on the zone, $\mathbf{M}_1, \mathbf{M}_2 \in L(t_1)$ by integrating flow-rate family upon ω^+, ω^-. Now two cases arise:

(a) γ is a convex curve, *i.e.*, selectivity is 3-regular: PQ has no other intersection point with γ. Letting $t = t_2$ vary, we obtain a parametric expression of zonal line $L(t_1)$ as the sum of the union of the two subfamilies:

$$\left\{ \{\mathbf{F}(\tau)\mathrm{d}\tau\}_{\tau \in [0,t_1]} \cup \{\mathbf{F}(\tau)\mathrm{d}\tau\}_{\tau \in [t,\Delta t]} \right\}$$

which is exactly eqn. 13. The first subfamily does not depend on t and its sum defines point $\mathbf{N}(t_1)$ on the cumulate curve. When t varies, the sum vector of the second subfamily is just what is obtained by drawing, in the reverse order, this part of the initial family, going from Δt to t. The zonal line can be completed through symmetry about the centre of Z, or the above reasoning can be made, with $0 < t < t_1$ as the complementary subfamily defines the symmetrical part of $L(t_1)$.

(b) γ is not convex, *i.e.*, selectivity is not 3-regular: the above construction has to be modified. For each position of line PQ one must look at all cut points of PQ with γ. If only one other than P exists, we obtain the same case as before and construct $\mathbf{M}(t)$ accordingly. If more than one exists, *e.g.*, of argument t_2, t_3, $\mathbf{M}(t)$ is the sum of the union of all subfamilies whose elements point in the positive half-space defined by Π_M.

Indeed, γ need not to be a convex curve in Δ_2. In fact, convexity requires, as we

shall see in Section 5.5, $N \leqslant N_c$, where N_c is the critical number of plates, or, equivalently, $z \leqslant z_c$, where z_c is the critical abscissa in column.

Note the geometric rationale for eqn. 15: contact points $\mathbf{M}_1$ or $\mathbf{M}_2$ are attained when planes parallel to Π_M passing through M, the sum of any subfamily, cannot recede further from the origin. But the plane recedes or not on adding $\mathbf{F}(\tau)\mathrm{d}t$ to the subfamily according to the sign of the dot product $<\eta, \mathbf{F}(\tau)>$, where η is the coefficient vector of plane Π_M. Now, in view of the well known fact that mixed product $\mathbf{F}(t_1) \wedge \mathbf{F}(t_2) \wedge \mathbf{F}(\tau) = <\eta, \mathbf{F}(\tau)>$, this amounts to including $\mathbf{F}(\tau)\mathrm{d}t$ in the subfamily according to the sign of the mixed product, which is exactly the meaning of eqn. 15.

Zones form a system of lines which cover ∂Z and do not intersect themselves, except trivially, at the origin and at S, the distal point of Z, and at two antipodal points. In Fig. 4, the shape of the zonoid corresponding to Fig. 1 is sketched, as a perspective view, by such zones. Each zone, such as L in Fig. 4, is defined by its starting point (and tangent vector) on Γ and therefore $\Gamma \in \partial Z$. It is smooth except at O, S and at points on Γ.

4.5. A study of 3-regular selectivity

One may note in Fig. 4 that every zone passes through O and $S = N_0$. Such a property is not guaranteed in general and results from what we have called the 3-regularity of the differential family. This is the first time that selectivity acquires an intrinsic (geometric) definition, that is, one independent of any model involving, *e.g.*, affinity ratios. n-Regular selectivity (n-RS) is a rather intricate topic, but a crucial one in both separation and zonoid theory. We leave a thorough study of selectivity for further work, noting only that one may conjecture that the "ordered" ion-exchange systems defined by Tondeur [15] exhibit n-RS [although not $(n+1)$-RS, taking into account the carrier]. One could study also the "selectivity reversal" along the same lines. It will be more and more apparent that the properties of Z depend heavily on the convexity properties of the plane curve γ, in the molar simplex Δ_2 defined in Section 4. Here, we shall study selectivity from geometric, then algebraic, points of view and show how the loss of selectivity can be monitored directly on the chromatogram.

4.5.1. A general geometric condition

Selectivity can be monitored directly from γ in simplex Δ_2. Indeed, the physical meaning for 3-regular selectivity stems from Theorem 6:

Family $\mathscr{F} = \{\mathbf{F}(t)\mathrm{d}t\}_{t \in \Delta t}$ is 3-regular iff $\mathbf{F}(t)$ is extreme in $\mathscr{F}$, *i.e.*, a mixture of composition $\mathbf{x}(t)$ cannot be made by mixing from other elements of $\mathscr{F}$.

Therefore, in some way, each differential vector (or composition) delivered by a 3-regular process is "new". Looking at Fig. 3, we see that selectivity is 3-regular (or seems geometrically to be so). Taking each vertex of Δ_2 in turn we obtain that the selectivity between species 1, 2 is 2-regular: any $3Q$ line cuts the curve γ only once (from convexity of γ). In contrast, selectivity between species 1, 3 (or 2, 3) is not 2-regular: $2Q$ (or $1Q$) lines cut the curve γ (convex and closed) at two points.

It is now apparent that selectivity is not stable by projection. We may say that 3-regular selectivity reversal occurs at points (if any) where γ acquires an inflection tangent. However, selectivity (or, as we shall see, values of critical parameters for selectivity reversal) do not depend on the injected quantities of solutes as long as the model remains linear.

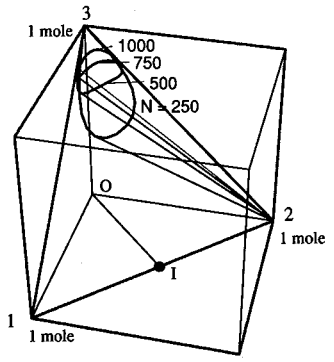

Fig. 6. Curves γ in Δ_2 in the case of 3-regular selectivity ($N = 250$), near 3-regular selectivity ($N = 500$) and non-3-regular selectivity ($N = 750$, 1000 plates).

To see the influence of the abscissa in the column on selectivity, the curves γ at different values of N are drawn in Fig. 6.

Notes

(1) The rule of decreasing maximum flow-rate (or concentration) of peaks on progressing along the column materializes into a monotonic rotation of tangents to γ around the vertices relative to pure species 1 or 2 in Fig. 6. γ shrinks to point 3 when N increases.

(2) The overall shape of γ depends on N: for $N \geqslant 500$, a depression appears on γ; γ is discontinuous for initial family $\mathscr{F}(0)$: it is composed of two points I, and vertex 3, which stresses the fact that the flow at the column inlet is not a smooth (and not even continuous) function of time.

4.5.2. An algebraic condition for 3-selectivity

The results will show the similarities and differences between models I, II and III. A study of the Wronskian matrix allows one to locate singularities in the plane of independent variables (N,t), for differential families (in the sense of 3-selectivity reversal), in terms of pairs (N_c, t_c), where N_c is the number of plates at which singularity occurs, t_c, the time of appearance, on the chromatogram taken at N_c.

$\mathbf{F}(t)$ has continuous derivatives of any order, then, from Theorem 5, convexity of γ is equivalent to condition 13 involving the Wronskian matrix of the flow-rate $F^i(t)$, $i = 1,2,3$, $W(\mathbf{F})$ (in another context, see Karlin [13], Theorems 2-1 and 2-3).

Taking in turn matrices in the last column in Table 1 (where the maximum of possible factorization in lines or columns of (strictly) positive common terms comprising $F^1F^2F^0$ has already been made), we obtain, after expansion, the following.

The general idea is that, in view of the linearity in N of $W(\mathbf{F})$, we look for the maximum value of N such that $W(\mathbf{F})$ remains non-negative for all values of t. For different models, see the corresponding entries in Table 2.

Taking, for example, model II, selectivity is 3-regular iff $W(\mathbf{F}) \geqslant 0$, *i.e.*,

$$N \leqslant N_c = \operatorname*{Max}_{t \in]\bar{t}_1, \bar{t}_2[} \left(\frac{-1}{\left(\frac{t}{\bar{t}_1} - 1\right)\left(\frac{t}{\bar{t}_2} - 1\right)} \right) \tag{37}$$

using linearity in N. Clearly, the product containing t in eqn. 37 is negative, and the minimum for $t = t_c$ with

$$t_c = \bar{t} = \frac{\bar{t}_2 + \bar{t}_1}{2} \tag{38}$$

Max is attained for t_c and leads to the following condition on N:

$$N_c = \frac{(\bar{t}_2 - \bar{t}_1)^2}{4\bar{t}^2} \tag{39}$$

We may rewrite the selectivity condition relevative to model II as a function of equilibrium parameters:

$$N \leqslant N_c = \left(\frac{\bar{t}_2 + \bar{t}_1}{\bar{t}_2 - \bar{t}_1}\right)^2 = \left(\frac{2 + k^1 + k^2}{k^2 - k^1}\right)^2 \approx \left(\frac{\alpha + 1}{\alpha - 1}\right)^2 \tag{39a}$$

Models I and III lead to a slightly more intricate Wronskian matrix and condition, but the method is similar and the results are given in Table 2.

Remarkably (see Table 2), N_c given by condition 39a appears to be model independent, *i.e.*, its value is the same for models I, II and III. However, the critical times t_c given in Table 2 differ slightly, reflecting the difference between the peak shapes in these models. A geometric interpretation will be given below.

Note that except for the leading factor $\bar{t}_2 - \bar{t}_1$ that is in line with the fact that $W(\mathbf{F})$ tends to 0 when α tends to 0 (solutes tend to be identical), $W(\mathbf{F})$ is, for all models, a second-degree polynomial in t, which means that γ will have two inflection points for $N > N_c$, the parameters of which are roots of these polynomials (see Fig. 6, case N = 750 and 1000).

Therefore, 3-regular selectivity inversion $N = N_c$ is just the condition for the existence of a "double" inflection point (*i.e.*, a point where the tangent has a contact of order 4) on γ and this point occurs at parameter t_c.

Under the conditions of Fig. 1, the formulae in Table 2 give for models I and III N_c = 484 plates and t_c = 112 s. With the isovariance assumption, N_c = 484 plates

TABLE 2

WRONSKIAN AND CRITICAL PARAMETERS

Model	$W(\mathbf{F})$	N_c	t_c
I	$N\left(\frac{t}{\bar{t}_1} - 1\right)\left(\frac{t}{\bar{t}_2} - 1\right)\left(\frac{t}{\bar{t}_1} + \frac{t}{\bar{t}_2} - 1\right) + 1$	$\left(\frac{\bar{t}_2 + \bar{t}_1}{\bar{t}_2 - \bar{t}_1}\right)^2$	$2 \cdot \frac{\bar{t}_1 \bar{t}_2}{\bar{t}_2 + \bar{t}_1}$
II	$N\left(\frac{(t - \bar{t}_1)(t - \bar{t}_2)}{\bar{t}^2}\right) + 1$	$\left(\frac{\bar{t}_2 + \bar{t}_1}{\bar{t}_2 - \bar{t}_1}\right)^2$	$\frac{\bar{t}_2 + \bar{t}_1}{2}$
III	$Nt^2 - t(N-1)(\bar{t}_2 + \bar{t}_1) - (N-1)\bar{t}_2\bar{t}_1$	$\left(\frac{\bar{t}_2 + \bar{t}_1}{\bar{t}_2 - \bar{t}_1}\right)^2$	$2 \cdot \frac{\bar{t}_1 \bar{t}_2}{\bar{t}_2 + \bar{t}_1}$

and $t = 110$ s, results not significantly different from the other (more rigorous) values. In any case, separation is far from complete at the critical number of plates.

If, for model I, II or III, the (unique) condition 39a is not fulfilled, *i.e.*, if the number of plates at the location of observation exceeds the critical number, γ is not convex and this introduces many complications in the study of zonoids and separation, including the fact that the volume of the zonoid must be computed as the integral of the absolute value of a function changing sign on a domain which may be intricate.

4.5.3. Comparing 2- and 3-selectivity for solutes

We may now compare algebraic conditions for 3- and 2-selectivity for solutes. In view of the constant carrier flow-rate, these two conditions involve only minors extracted from the two first lines of the Wronskian matrix relative to the model. Therefore, working on this sub-matrix gives all the information needed regarding selectivity for solutes.

For curve Γ_{12}, the canonical projection of the graph of $\mathbf{N}(t)$ into plane (1,2), *i.e.*, dropping the last coordinate in **N** and **F**, 2-regular selectivity amounts to

$$\mathbf{N}'(t) \wedge \mathbf{N}''(t) = \mathbf{F}(t) \wedge \mathbf{F}'(t) > 0 \tag{40}$$

which simply means that the curvature vector always stands on the same side relative to the tangent vector, a classical condition for convexity.

It is clear that the 3-regular selectivity condition $W(\mathbf{F}) \geqslant 0$ reduces and implies, in the case of a constant total flow-rate, a higher order (stronger) condition on derivatives of flow of solutes only, namely

$$\mathbf{N}''(t) \wedge \mathbf{N}'''(t) = \mathbf{F}'(t) \wedge \mathbf{F}''(t) \geqslant 0 \tag{41}$$

These conditions are linked geometrically: if condition 42 is fulfilled, Γ_{12}, or the curve γ_{12} defined by $(F^1(t), F^2(t))$, in plane (1,2) is convex. The vertical translate of γ_{12} with length F^3 (which means dilution by a constant flow of carrier) defines a convex cone with apex O, the intersection of which with Δ_2 is γ. Therefore, γ must be convex in Δ_2: we recover the condition of constant sign for the Wronskian determinant in three dimensions.

4.5.4. Reading 3-selectivity condition on chromatogram

In practice, it is very easy to monitor the loss of 3-selectivity for model I, II or III (which is usually the one flow or concentration experimentally monitored). Indeed, a sufficient condition for following eqn. 42 to be satisfied as an equality at the limit of $t = t_c$

$$\mathbf{F}'(t_c) \wedge \mathbf{F}''(t_c) = 0 \tag{42}$$

is clearly $\mathbf{F}''(t_c) = 0$. As, in fact, $\mathbf{F}''$ depends on N, we simply obtain, for two solutes, two non-linear equations in two unknowns, t_c and N_c:

$$F^{1\prime\prime}(t_c, N_c) = 0, \quad F^{2\prime\prime}(t_c, N_c) = 0 \tag{43}$$

where derivatives are understood to be relative to t. Dimensionally, there is room for a solution of this system. Indeed, a solution of the system of eqn. 43 gives back those found through annulation of the Wronskian determinant.

A geometric interpretation of this result is the proposition that if inflection points on the chromatogram of solutes appear at the same time t at location x in the column, 3-selectivity reversal occurs at (x,t). Clearly this holds for any model with a constant flow of carrier. Therefore, any composition of injected quantities will satisfy eqn. 43 and especially $(F^1 + F^2)'' = 0$.

On the chromatogram of total flow-rate of solutes, $F^1 + F^2$, such a point of coincidence will correspond to a tangent of order 2 at the 3-regular selectivity reversal time, since clearly $(F^1 + F^2)'' = 0$. Further, in any linear model, the coincidence point will stay fixed for any composition (or quantity) of injected mixture.

For model II, at time t_c, the tangent will have a slope proportional to

$$-N_0^2 \cdot \frac{t - \bar{t}_2}{\bar{t}} - N_0^1 \cdot \frac{t - \bar{t}_1}{\bar{t}} \text{ or } (x_0^2 - x_0^1)\frac{t_c - \bar{t}_1}{\bar{t}} \text{ or } (x_0^2 - x_0^1)\frac{\bar{t}_2 - \bar{t}_1}{\bar{t}_2 + \bar{t}_1} \approx (x_0^2 - x_0^1)\frac{\alpha - 1}{\alpha + 1}$$

Therefore, half-way between the maxima of peaks, an inflection tangent begins to appear at 3-selectivity reversal on the total flow-rate $F^1 + F^2$ (Fig. 7; see Fig. 1 for chromatogram of individual species, especially the corresponding chromatograms for $z = 50$ cm, and conditions).

It should be noted that the simple expression of ∂Z in Section 4.4 as a parameterized surface does not hold true in the case of non-3-regular selectivity: some depressions would appear on the surface given by equation 13 which therefore could not be the boundary of a convex body.

The link with the bitangent line and the depression nascent between peaks and non-3-regular selectivity shows that the *loss of 3-regular selectivity is a necessary phenomenon to obtain a good separation.* This could be expected from the simplest translation model of rectangles, the study of which is left to the reader.

Hence the effect of diffusion is twofold: diffusion smooths out discontinuities in γ, and ensures a progressive shrinking of γ into vertex 3 of Δ_2 when z increases.

We shall return to the study of zonoid projections and evolution in Section 6.

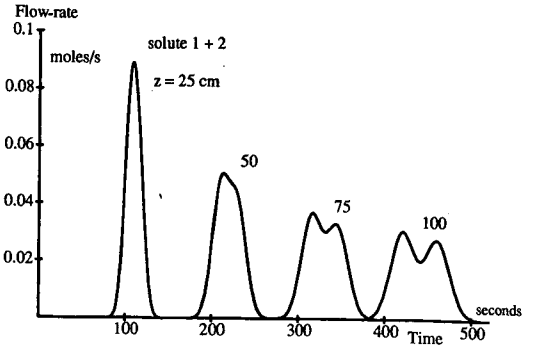

Fig. 7. Total flow-rate of solutes in the case of 3-regular selectivity ($z = 25$ cm), just after selectivity inversion ($z = 50$ cm), in the case of non-3-regular selectivity ($z = 75$, 100 cm).

4.6. *Generalizations and comments*

Canonical projections of zonoids give the separation state of subsets of species. The number of such canonical projections depends on n. For $n = 3$, we may group canonical projections into four subsets with (1 3 3 1) elements, that is, one 3-d zonoid (ternary separation), three 2-d zonoids (binary separations) and three 1-d zonoid (segments on the axes). Adding further the "dummy" 0-d zonoid, reduced to the origin point, we complete the variety of zonoids necessary to obtain a full picture of a ternary separation. It is significant that for 1-d zonoids, the separation balance reduces to a species balance; therefore, the latter appears as a special case (in one dimension) of the former.

This leads us to infer that, in general, the number of r-d zonoids to study for the separation of n species is the kth coefficient of the binomial expansion of nth order, which is indeed true. Hence there are $2^n - 1$ non-zero zonoids to study in the general case. These should be completed by the choice of appropriate projections or intersection with planes to fit special problems if needed.

Even in the simple models presented here, one finds complex features for selectivity, including changes along the column:

(1) 3-regular selectivity or not;

(2) absence of 2-selectivity between carrier and any solute;

(3) 2-selectivity between the two solutes.

Combined with the above comment, this gives a hint of how intricate and rich the study of separations can be for even a moderate number of species.

5. IS CHROMATOGRAPHY A SEPARATION PROCESS?

A quantitative (although not scalar) assessment of separation evolution in chromatography involves the evolution of zonoids "passing through" the abscissa z in the column, in addition to its canonical projections as a function of z.

The motivation for the study of projections comes from the following: a canonical projection has physical meaning; we neglect the content of species along which we project and consider only (partial) separation associated with remaining species. Therefore, although we are "interested" only in separation between solutes, we must consider in turn the three canonical projections of $Z(z)$, then the 3-d zonoid itself.

5.1. *Separation between a solute and carrier*

5.1.1. *2-Selectivity and convexification in the plane*

The condition for 2-selectivity of separation of a solute i and a carrier is

$$\mathrm{proj}_{i3}\mathbf{F}(t) \wedge \mathrm{proj}_{i3}\mathbf{F}'(t) \geqslant 0$$

and the left-hand member is the corresponding minor on the Wronskian matrix $W(\mathbf{F})$. For model I, II or III, we obtain (see first two columns in square matrices, Table 1)

$$t_i - t \geqslant 0$$

Therefore, 2-selectivity reversal occurs at the maximum of the peak of the solute. As we consider only two species, we can apply the mixing convention (which would not be possible in three dimensions). That 2-selectivity between a solute and carrier is not regular could be anticipated by comparing projections of cumulated curves on planes (1,3) and (2,3) in Fig. 2 with corresponding projections of Z in Fig. 5.

Instead of a canonical projection of ∂Z to obtain, *e.g.*, ∂Z_{13}, we may construct ∂Z_{13} directly from the chromatogram of solute 1 in species 3 or from its cumulate curve C, using a method that we shall call convexification. Customizing eqn. 15 for 2-d space, we obtain

$$\partial \mathbf{Z}^{+}: \mathbf{M}(t_1) = \int_{\omega^{+}(t_1)} \mathbf{F}(\tau)\mathrm{d}\tau,\ 0 \leqslant t_1 \leqslant \Delta t$$
$$\omega^{+}(t_1) = \{\tau \in [0,\Delta t] \,|\, \mathbf{F}(t_1) \wedge \mathbf{F}(\tau) > 0\} \tag{44}$$

Eqn. 44 can be recast, using a new (reduced) family $\mathscr{F}^*$ obtained through use of the mixing convention on $\mathscr{F}$, both of these generating same separation state. Although in essence the mixing convention amounts on the chromatogram of the sum of the flow-rates at same molar ratio of species i to the carrier, care must be taken of the very nature of a 1-differential family (which contains $\mathrm{d}t$). In the following, boundaries 0 and Δt are assumed to be taken such that the molar flow-rate of solutes are equal (and arbitrary near to zero).

Reduction of family $\mathscr{F}$

Let $t_{\max}$ be the retention time of the peak maximum and consider $\mathscr{F}$ as the union of two sub-families,

$$\mathscr{F} = \mathscr{F}_1 \cup \mathscr{F}_2, \mathscr{F}_1 = \{\mathbf{F}(t)\mathrm{d}t\}_{t\in[0,t_{\max}]}, \mathscr{F}_2 = \{\mathbf{F}(t')\mathrm{d}t'\}_{t'\in[t_{\max},\Delta t]}$$

Given $t \in [0, t_{\max}]$, we consider the solution $t' \in [t_{\max}, \Delta t]$ of the equation

$$\mathbf{F}(t) \wedge \mathbf{F}(t') = 0$$

As $\mathbf{F}(t) = (F^1(t), F^3)$, and F^3 = constant, this amounts to the scalar condition

$$F^1(t) = F^1(t')$$

For any "peaked model", this implicit equation defines a monotonically decreasing function $t' = f(t)$ of class C^1. We may therefore apply eqn. 1 for change of variable in $\mathscr{F}_2$, noting that $f^{-1}([t_{\max}, \Delta t]) = [0, t_{\max}]$, and we obtain

$$\mathscr{F}_2 = \left\{ -\mathbf{F} \circ \mathbf{f}(t)\frac{\mathrm{d}f}{\mathrm{d}t} \cdot \mathrm{d}t \right\}_{t\in[0,t_{\max}]}$$

Owing to the definition of function f, $\mathbf{F} \circ f(t) = \mathbf{F}(t)$. Evaluation of the derivative is straightforward by use of the implicit function theorem

$$\frac{\mathrm{d}f}{\mathrm{d}t} = \frac{\dfrac{\mathrm{d}F^1}{\mathrm{d}t}(t)}{\dfrac{\mathrm{d}F^1}{\mathrm{d}t}(t')}$$

Adding sub-families $\mathscr{F}_1$ and $\mathscr{F}_2$, which are now expressed with the same parameter t, we obtain identification

$$\mathbf{F}^*(t) = \mathbf{F}(t)\left(1 - \frac{\dfrac{\mathrm{d}F^1}{\mathrm{d}t}(t)}{\dfrac{\mathrm{d}F^1}{\mathrm{d}t}(t')}\right), \quad t \in [0, t_{\max}] \tag{45}$$

$\mathscr{F}^* = \{\mathbf{F}^*(t)\mathrm{d}t\}\ 0 \leqslant t \leqslant t_{\max}$ is called the reduced family and allows one to construct ∂Z_{i3} directly by drawing the cumulate curve of $\mathscr{F}^*$ through

$$\partial \mathbf{Z}^+ : \mathbf{M}(t) = \int_t^{t_{\max}} \mathbf{F}^*(\tau)\mathrm{d}\tau, \quad 0 \leqslant t \leqslant t_{\max} \tag{46}$$

$$\partial \mathbf{Z}^- : \mathbf{M}(t) = \int_0^t \mathbf{F}^*(\tau)\mathrm{d}\tau, \quad 0 \leqslant t \leqslant t_{\max}$$

In the case when F^i is even (*e.g.*, models I and II), symmetry around $t_{\max}$ implies $t' = 2t_{\max} - t$, and therefore eqn. 45 reduces to an explicit result: $\mathbf{F}^* = 2\mathbf{F}$. However, it is not so in more general cases (*e.g.*, model III) and t' is, in general, not known explicitly.

Fig. 8 shows how points A and A' on cumulated curve C with parallel tangents map onto a unique point A^* on the convexified curve $C^* = \Gamma$.

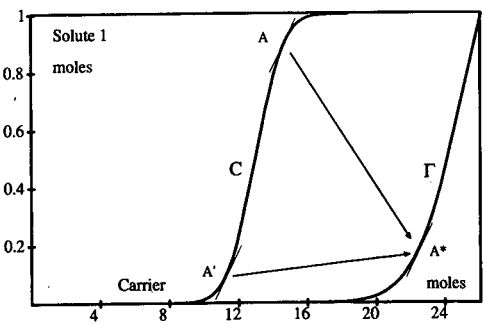

Fig. 8. Sigmoid curve C of cumulated quantities (solute, carrier). Convex boundary curve $\Gamma = C^*$.

This method extends itself readily to a non-unimodal chromatogram of solute i (including more than one cycle, for example) but is, in general, not valid in n-D space, $n > 2$.

5.1.2. Construction of 2-D zonoid

Let **F** be given by eqn. 30. Then, for a unique solute i and carrier 3, we obtain the equation of Γ_{i3} in the parameterized form (for model I or II):

$$\left|\begin{array}{l} N^i(N,t) = 2N_0^i \operatorname{erf}\left(\sqrt{N}\cdot\dfrac{\bar{t}_i - t}{\bar{t}_i}\right),\ i = 1,2\ \ -\infty < t < \bar{t}_i \\ \\ N^3(N,t) = 2F^3(\bar{t}_i - t) \end{array}\right. \tag{47}$$

Convexity of Γ_{i3} stems from construction and can be shown directly through convexity of the function $\operatorname{erf}(x)$ for $x \in [-\infty, 0]$.

Some remarks are in order:

(a) The mixing convention is applied here only to the projected family: in the complete family, the simultaneous presence of solute j prevents colinearity occurring at times $t_i - \Delta$, $t_i + \Delta$. Therefore, it is clear that the mixing convention will give, in general, different results depending on the canonical projection, that is, on the species i.

(b) $Z(z)$ is unbounded in the time axis direction as support of the solution of the diffusional model extends to the whole time axis (or the positive axis R^+ for the Poisson model). As already noted, we restrict ourselves to an interval Δt of R^+ supporting "essentially" all the peak. Note that a rigorous study would involve unbounded zonoids. It is not too difficult to show by extending the boundaries of segment $[0, \Delta t]$ that this would not change the final conclusions concerning separation evolution (inclusion), but would give a useless (infinite) 2-volume of separation, thus showing a major drawback of use of these volumes as an index of separation.

Applying this to model II (isovariance assumption), we obtain a simple result (which was to be expected as in model II peaks of solutes at given z deduce themselves by translation).

The separation zonoid between species and carrier is independent of species (for model II):

$$Z_{12} = Z_{13}$$

[except for a trivial linear dependence (linearity) on injected quantity of species, and as long as the time interval is sufficient].

5.1.3. Evolution of separation state

Making first a geometric study, let us compare families of curves $\Gamma_{i3}(N)$, $i = 1, 2$. One uses the geometric invariance of Γ_{i3} in a regular change of parameter (depending on species i). Then (Gaussian model I or II), taking $\theta_i = t_i - t$ leaves Γ invariant; this

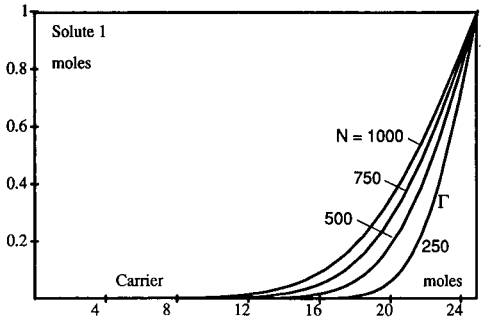

Fig. 9. Evolution of 2-d zonoid (solute 1, carrier) lower boundary. z = 25, 50, 75, 100 cm.

amounts to set time zero at the peak maximum and to reverse orientation of the time line (F is an even function).

In a second parameter change, $\tau_i = \sqrt{N}\frac{\theta_i}{\bar{t}_i}$, eqn. 47, of Γ_{i3} becomes

$$N^i(\tau_i) = 2N_0^i \operatorname{erf}(\tau_i), i = 1 \text{ or } 2,\ 0 < \tau_i < \infty \tag{48}$$

$$N^3(\tau_i) = 2F_0^3 \cdot \frac{\bar{t}_i}{\sqrt{N}}\tau_i$$

That is, all curves Γ_{i3} map onto the graph of erf(x) over R^- by a linear application of diagonal matrix [A] with elements $\left(\frac{1}{2N_0^i}, \frac{1}{2F_0^3\frac{\bar{t}_i}{\sqrt{N}}}\right)$. Then curves Γ_{i3} do not intersect (except at the origin; note that this precludes these curves from having exactly the same sum vector) and lie above one another for increasing values of N. A decrease of the 2-d zonoid Z_{13} is clearly visible in Fig. 9.

We have thus established inclusion (recall $\text{proj}_{i3}\ Z = Z_{i3}$)

$$Z_{i3}(z') \supset Z_{i3}(z) \text{ if } z' < z,\ i = 1,2$$

which amounts here to be *existence* order between canonical projections of $Z(z)$ and $Z(z')$ on planes (1,3) or (2,3).

$$Z_{i3}(z) \prec Z_{i3}(z') \text{ if } z' < z, i = 1,2$$

This leads us to an important and simple conclusion: *linear diffusional chromatography is a mixing process between carrier and a solute.*

5.1.4. Mixing kernel

Making now an analytical study, we give direct proof that solute propagation is a mixing process between solute and carrier by exhibiting a sampling kernel.

In view of the definition of a mixing process given in Section 2.3, we may enquire directly about the nature of the process. We must exhibit a mixing kernel λ according to eqn. 21 and 21a which allows one to obtain a differential family of flow-rate vectors obtained at $N + \Delta N$ plates from that obtained at N plates.

Looking, *e.g.*, at solute 1, the flow-rate family at N (see Table I) is similar for models I or II:

$$\mathscr{F}(N) = \begin{bmatrix} N_0^1 \cdot \dfrac{\sqrt{N}}{\sqrt{2\pi}\bar{t}_1} \cdot e^{-\frac{1}{2}N\left(1-\frac{t}{\bar{t}_1}\right)^2} dt \\ F_0^3 \, dt \end{bmatrix}_{-\infty < t < +\infty}$$

As the second component of flow is constant, eqn. 21a will directly ensure the mixing properties for carrier species. Therefore, we need only to study the flow of the solute.

Starting from the following identity, which expresses the classical property of additivity of variances (see Appendix for a proof using Fourier transformation):

$$\frac{1}{\sqrt{2\pi}\sqrt{\sigma^2 + \sigma'^2}} e^{-\frac{\tau^2}{2(\sigma^2+\sigma'^2)}} = \int_{-\infty}^{+\infty} \frac{e^{-\frac{w^2}{2\sigma^2}}}{\sqrt{2\pi}\sigma} \cdot \frac{e^{-\frac{(w-\tau)^2}{2\sigma'^2}}}{\sqrt{2\pi}\sigma'} \cdot dw$$

we obtain, on identification of the left-hand term with the flow-rate at $N + \Delta N$ plates, calling σ'' the square root of variance at this location, and use of eqns. 27 and 29,

$$\sigma = \frac{(1 + k^1)\sqrt{NH}}{u}, \qquad \sigma'' = \frac{(1 + k^1)\sqrt{N + \Delta N}H}{u}$$

hence

$$\sigma' = \sqrt{\sigma''^2 - \sigma^2} = \frac{(1 + k^1)\sqrt{\Delta N}H}{u}$$

Therefore, family $\mathscr{F}(N + \Delta N)$ (up to translations of time scale to obtain centred distributions, *i.e.*, $w = t - \bar{t}_1$, $\tau = t' - \bar{t}_2$) results from family $\mathscr{F}(N)$ by a mixing process with the mixing kernel:

$$\lambda(t - \bar{t}_1, t' - \bar{t}_2) = \frac{e^{-\frac{(t - t' + \bar{t}_2 - \bar{t}_1)^2}{2\sigma'^2}}}{\sqrt{2\pi}\sigma'} = \frac{1}{\sqrt{2\pi}} \sqrt{\frac{N + \Delta N}{\Delta N}} \cdot \frac{1}{\bar{t}_2} \cdot e^{-\frac{N + \Delta N}{\Delta N} \cdot \frac{(t - t' + \bar{t}_2 - \bar{t}_1)^2}{2\bar{t}_2^2}}$$

and property 21a stems from normalization of the area under a Gaussian curve.

Note that the above mixing kernel derives also from a Gaussian function and is a convolution kernel. Also, the above result holds for an unbounded quantity of carrier, *i.e.*, for $t \in R$.

Of course, the existence of a mixing kernel is linked with the fundamental fact that diffusion (as represented here by the increase in variance of a Gaussian curve) is basically a mixing process, a fact that can be traced back to the diffusion equation and will be emphasized in future work.

5.1.5. 2-Volume of separation between solute and carrier

Although a direct integration can be made using eqn. 48, it is simpler to use the linear transformation T of matrix $[A]$ defined in Section 5.1.3.

In view of the fact that for the unbounded (rigorous) case, when the quantity of carrier is infinite, the area in the rectangle of total separation, under the curve Γ_{i3}, stays finite, we introduce the following.

Definition

The loss of 2-volume is the area ζ_{i3} of the complement of 2-d zonoid to the rectangle of total separation.

Let ζ be the area under the graph of erf(x) over R^-, *i.e.*, $\zeta = \int_{-\infty}^{0} \mathrm{erf}(s)\mathrm{d}s = \frac{1}{\sqrt{2\pi}}$. Through transformation T^{-1}, ζ will be multiplied by dat $[A]^{-1}$, so that we obtain

$$\zeta_{i3} = 8\zeta N_0^i F_0^3 \cdot \frac{\bar{t}_i}{\sqrt{N}} = 8\zeta N_0^i F_0^3 \sigma_i$$

Therefore, for separation 2-volume (pairs 1,3 or 2,3) we obtain

$$\Xi_{i3}(N) = \Xi_0 - \frac{8}{\sqrt{2\pi}} N_0^i F_0^3 \sqrt{N} \cdot \frac{1 + k^i}{u} \cdot H \tag{49}$$

as long as sufficient carrier is allowed to contain virtually all the solute. Recall that area $\Xi_0 = N_0^i F_0^3 \Delta t$ is unbounded if $\Delta t \to \infty$.

At a given retention time for solute i, we obtain ζ_{i3}, proportional to $\bar{t}_i/\sqrt{N}$, *i.e.*, the loss of 2-volume diminishes if we increase the number of plates or, for a given z, if we decrease the HETP.

Eqn. 49 may be given in a different form: introducing τ_1^i, the residence time of solute per plate, $\tau_1^i = H \cdot \frac{1 + k^i}{u}$, an interesting statement can be made: in linear diffusional chromatography, ζ_{i3}, the loss in 2-volume of separations between carrier and solute i, increases as the square root of the number of plates and as the residence time of solute per plate. The rate of decrease in 2-volume of separation between solute i and carrier is given by

$$\Xi_{i3}(N) = \Xi_0 - 8\zeta N_0^i F_0^3 \sqrt{N} \tau_1^i$$

A conclusion may be drawn in another way: although the separation between a solute and a given quantity of carrier decreases when z increases, *i.e.*, zonoids become smaller as the column length increases, nevertheless, a given increment of length has less and less influence on mixing; this can be related to Fick's law, which states that the flux is proportional to the gradient of concentration. Indeed, the effect of a constant increment of column length on the mixing is clearly visible in Fig. 9, as the relative loss area ratios are 1, 1.41, 1.73 and 2.

These conclusions all fit fairly well the "intuitive" (qualitative) thinking about what the effect of these parameters on separation should be.

5.2. *Separation between two solutes*

Consider now the separation between solutes 1 and 2, that is, the canonical projection on the plane (1,2) of the three-dimensional zonoid. We must first construct proj(Z) and then study its variation with N.

5.2.1. *Study of 2-selectivity*

Model I: taking the leading minor in $W(\mathbf{F})$ in Table 1, we obtain the 2-selectivity condition

$$\operatorname{sgn}(\operatorname{proj}_{12}\mathbf{F}(t) \wedge \operatorname{proj}_{12}\mathbf{F}'(t)) = \operatorname{sgn}\begin{vmatrix} 1 & -\dfrac{(t-\bar{t}_1)}{(\bar{t}_1)^2} \\ 1 & -\dfrac{(t-\bar{t}_2)}{(\bar{t}_2)^2} \end{vmatrix} \tag{50}$$

$$= \operatorname{sgn}(\bar{t}_1 - \bar{t}_2)\left(t - \frac{\bar{t}_1\bar{t}_2}{\bar{t}_1 + \bar{t}_2}\right) = -1 \text{ for } t > \frac{\bar{t}_1\bar{t}_2}{\bar{t}_1 + \bar{t}_2} > \frac{\bar{t}_1}{2}$$

The sign is constant for any practical conditions, as the above inequality in t is always satisfied when a non-negligible flow of solute 1 or 2 occurs, for sufficiently high N. This means that, on the cumulate curve Γ_{12}, the inflection point is very near to the origin. Presumably this inflection point is an artefact of the approximation of the peak shape by a Gaussian curve.

To make this point precise, let us make a comparison with model II. Now $W(\mathbf{F})$ leads to the 2-regular selectivity condition taken from Table 1, or just equating denominators to $\bar{t}$ in the determinant of eqn. 50. Similarly, model III leads to a 2-regular selectivity condition also taken from Table 1:

$$1 = \operatorname{sgn}\begin{vmatrix} 1 & -\dfrac{N}{\bar{t}_1} + \dfrac{N-1}{t} \\ 1 & -\dfrac{N}{\bar{t}_2} + \dfrac{N-1}{t} \end{vmatrix} = \operatorname{sgn}(\bar{t}_2 - \bar{t}_1) \tag{51}$$

which is clearly always satisfied since $\bar{t}_2 > \bar{t}_1$.

The family of flow-rate vectors (models II and III) therefore possesses 2-regular selectivity properties. Then, from the chromatogram, the construction of a convex set of mixtures is very simple: integrate **F** from 0 to t, to obtain ∂Z^-. The tangent to Z at point $\mathbf{N}(t)$ is parallel to $\mathbf{F}(t)$.

Returning to model I, we can trace the lack of 2-regular selectivity to the following: the peak of species 2 is slightly more diffuse than that of species 1 ($\bar{t}_2 > \bar{t}_1$), and indeed this stems from the influence of retention time on the variance in eqn. 28. Therefore, at some early value of t, species 2 will supersede species 1. In fact, model I is valid only asymptotically for the Dirac inlet distribution and high N. This view is confirmed by the fact that, if we equate the variances of the two peaks, that is, if we pass to model II, Γ is convex on R as the factor containing t in eqn. 50 drops out. Hence a lack of 2-regular selectivity points to a discrepancy between the model and physical reality, a satisfactory result.

Physically, 2-selectivity for species 1, 2, means that in the flow passing through location z, species 2, the more retained species, increases in purity as time goes on.

5.2.2. Construction of 2-D zonoid

Consider, *e.g.*, the Gaussian model I, neglecting the above-mentioned inversion of selectivity. Projection Γ_{12} of the cumulate curve $\mathbf{N}(t)$ is a convex curve. Therefore, the (half) boundary of Z_{12} has a parametric equation:

$$\left|\begin{array}{l} N^1(N,t) = N_0^1 \operatorname{erf}\left(\sqrt{N}\cdot\dfrac{\bar{t}_1 - t}{\bar{t}_1}\right), \quad t\in[0,\Delta t] \\ \\ N^2(N,t) = N_0^2 \operatorname{erf}\left(\sqrt{N}\cdot\dfrac{\bar{t}_2 - t}{\bar{t}_2}\right) \end{array}\right. \tag{52}$$

Convexity of Γ_{12} is towards the axis of the more retained species.

5.2.3. Evolution of separation state

A quantitative study of the growth of zonoid Z_{12} with z covers both relative positions of Z and area growth. Through a change of parameters (already done in Section 6.1.3.),

$$\tau = \sqrt{N}\cdot\frac{t}{\bar{t}}, \quad \bar{t} = \frac{\bar{t}_1 + \bar{t}_2}{2}$$

we obtain

$$N^i(\tau) = N_0^i \operatorname{erf}(\tau_i - \tau), \tau\in\left[0, \sqrt{N}\cdot\frac{\Delta t}{\bar{t}}\right], \quad i = 1,2$$

Accordingly, the peaks representing the flow-rate are translates of affine Gaussian curves with δ, the reduced translation parameter:

$$\delta = \tau_2 - \tau_1 = \sqrt{N}\cdot\frac{\bar{t}_2 - \bar{t}_1}{\bar{t}} \approx 2\cdot\frac{\alpha - 1}{\alpha + 1}\cdot\sqrt{N} \tag{53}$$

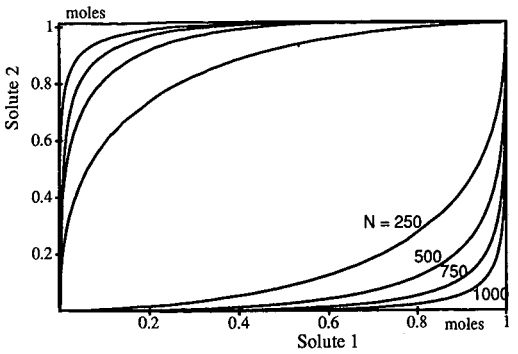

Fig. 10. Growth of separation, zonoid Z_{12}. L = 25, 50, 75, 100 cm.

Evolution of the zonoid of separation is therefore a function of δ, valued in the set of zonoids (of given sum vector in 3-D space) (Fig. 10).

Inclusion is then simple to show: at any given τ, increasing δ makes the second peak recede from the first, thus $N^2(\tau)$ decreases. The point on ∂Z^- moves towards axis 1 on the vertical above $N^1(\tau)$, thus proving inclusion. Note that slope of the tangent at $N^1(\tau)$ decreases if $\tau < \tau_1 + \delta$ and increases if $\tau > \tau_1 + \delta$.

5.2.4. 2-Volume of separation

Calculation of the law of increase of 2-volume of separation with δ is less easy (see Appendix) but gives a simple result, both as a first-order expansion of Ξ and in general.

From eqn. (A5) (see Appendix), we obtain for the Gaussian isovariant model

$$\Xi_{12} = 2\,\mathrm{erf}\left(\frac{\delta}{\sqrt{2}}\right) - 1 \tag{54}$$

and at first order, for small δ (*i.e.*, for $N \ll N_c$)

$$\Xi_{12} \approx \frac{\delta}{\sqrt{\pi}} = \frac{1}{\sqrt{\pi}}\sqrt{N}(\alpha - 1)$$

where the last inequality amounts to $N \leqslant N_c$. Therefore, at incipient separation, 2-volume increases as only as $\sqrt{N}$ or, conversely, the rate of growth of 2-volume is infinite at $N = 0$, and decreases as $1/\sqrt{N}$ because

$$\frac{\mathrm{d}\Xi_{12}}{\mathrm{d}N} = -\frac{1}{\sqrt{\pi}} \cdot \frac{1}{2\sqrt{N}}(\alpha - 1)$$

This relative inefficiency of theoretical plates in the process can be traced back to the fact that separation is produced only in part of the column, the width of the signal being approximately proportional to $\sqrt{N}$. Remarkable also is the grouping of α and

N into a single factor, which is indeed linked with resolution $R = R_{12} = 2\left(\frac{\bar{t}_2 - \bar{t}_1}{w_1 + w_2}\right)$ (where w_i is the distance between the intercept of the inflection tangents with the baseline), since (for two Gaussian peaks of equal area) $\delta = 4R$, we obtain

$$\Xi_{12} \approx \frac{4R}{\sqrt{\pi}}$$

However, the use of these approximations is severely restricted, as first-order expansion (eqn. A8) is valid only in the cases of difficult separation ($\alpha \approx 1$) and incipient separation [$\sqrt{N}(\alpha - 1) \ll 1$]. That condition of incipient separation is usually not satisfied in practice as one aims for a resolution of about unity between peaks. However, R is restricted to be lower than about 5 if the above equation is to have any chance of being valid, *i.e.*, to give a value lower than 1 (and, in this instance, it is hardly measurable from the chromatogram). Finally, as concerns resolution, it is not difficult to prove that at the 3-selectivity inversion point, N_c, $R = 0.5$ for model II.

We may state that for a difficult separation, when peaks are not too well separated, the rate of 2-volume production for solutes 1, 2 is proportional to $\sqrt{N}$. Note, however, that area is of limited interest here and can even be misleading; a complete study should encompass growth of the zonoid itself.

The study of canonical projections of Z leads to a remarkable conclusion concerning binary separations, namely that linear chromatography (models II and III) with diffusion is a separation process between two solutes, a mixing process between a solute and carrier. As linear diffusional chromatography is neither a pure separation nor a pure mixing process, it must be a sepmix process. Note that, although drawn from studies of binary separations, this conclusion also holds for ternary separations. Indeed it is a sufficient condition for a process to be sepmix that two 2-D projections exist in which the initial and final zonoids are not ordered in the same way.

5.2.5. A generalization to n solutes

We generalize the results in Section 5.2.1. to the separation of any number of solutes: using Polya's frequency functions (PF) we obtain the following general theorem, holding for any number of solutes.

Theorem

Gaussian isovariant and Poisson models give rise to 1-differential families endowed with regular selectivity of any order between solutes.

Proof

Refer to Section 2.2.3. on PF functions. Clearly K_j^i may depend on i and j through constant multipliers, *e.g.*, N_i^0.

Take model II. We show first that $e^{-\frac{\eta^2}{2}}$ is a PF density. Let $L(x,y) = e^{xy}$. Clearly all minors of the generalized Vandermonde matrix $n \times p$ of elements L_j^i, $L_j^i = e^{x_i y_j}$ are positive for any two finite linearly ordered sequences: $x_1 < x_2 < \ldots < x_n$,

$y_1 < y_2 < \ldots < y_n$. Therefore, through multiplication of lines and rows by constant factors,

$$e^{-\frac{y_j^2}{2}} e^{x_i y_j} e^{-\frac{x_i^2}{2}} = e^{-\frac{(x_i - y_j)^2}{2}}$$

enjoys the same property and is of the required form for a PF function. As it is integratable on the real line, it is a PF density. Use of transformation property 1 of PF functions given under Theorem 6 gives immediately the desired result that F^i, for model II, *i.e.*, for a fixed variance (eqns. 31 and 32) is generated by the PF function

$$f(\eta) = \frac{1}{\sqrt{2\pi\sigma}} \cdot e^{-\frac{\eta^2}{2\sigma^2}}$$

For model III, we show first that $P(N,\lambda) = \frac{1}{\Gamma(N)} \cdot e^{-\lambda} \lambda^N$ is a totally positive kernel. Starting anew from the generalized Vandermonde matrix generated (this time directly) by λ^N, we obtain the result by multiplication with $1/\Gamma(N)$ and $e^{-\lambda}$. F^i in eqn. 34 is a PF function replacing y_j with $\ln t_j$, x_i with $\ln \bar{t}_i$.

5.3. Separation between solutes and carrier

An overview of the character of chromatographic separations is gained by a three-dimensional representation of the zonoid rather than from the two-dimensional projections, as done above. 3-Selectivity was studied in Section 4.4, as it was necessary to draw the boundary of Z. Calculation of the volume of the zonoid is not a simple matter, so we shall attempt first to draw qualitative "visual" conclusions.

5.3.1. 3-d Zonoid comparison

The influence of z for given operating conditions can be seen in Fig. 11. Only the bottom half of the zonoid boundary has been represented.

At $z = 0$, the injected zonoid is a vertical parallelogram, as the mixture of solutes and the pure carrier are separately available. Therefore, clearly, if solutes are to be separated to some extent, the resulting zonoid must not project on a segment, *i.e.*, no inclusion property between zonoids can hold: the process must be a sepmix. In fact, the construction of zones used assumed 3-regular selectivity, which is true in the cases in Fig. 11a and b, approximately true in Fig. 11c and false in Fig. 11d.

Note that increasing the time cycle Δt by δt would add a vector $(\varepsilon_1, \varepsilon_2, F^3 \delta t)$ with small $\varepsilon_1, \varepsilon_2$ to the initial and final families, or, equivalently, expand all zonoids with an (almost) vertical cylinder of length $F^3 \delta t$ without adding any really interesting information. The 3-volume of Z would then increase by $\Xi_{12} F^3 \delta t$.

The general deformation trends are as follows when z increases:

(1) Z becomes thinner (maximum vertical width decreases): for a given carrier quantity, this means a more homogeneous medium as a given mixture of solutes 1, 2 can be made with less and less different minimal and maximal quantities of carrier;

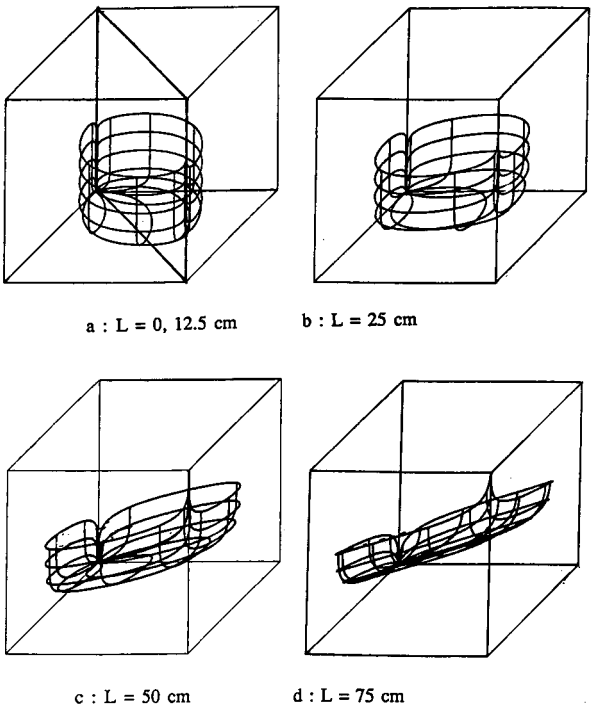

Fig. 11. Evolution of three-dimensional zonoid along the column. Axes labelling and orientation are similar to those in Fig. 4.

(2) Z becomes larger in horizontal projection (the smallest vertical cylinder containing Z grows).

5.3.2. Evolution of 3-volume

We first give a remarkable expression for 3-volume.

Theorem

For a family $\mathscr{F}$ given by model II or III, when $N < N_c$, *i.e.*, for 3-regular selectivity,

$$\Xi = N_0^1 N_0^2 N_0^3 \left\{ \xi_{12} - \frac{(\bar{t}_2 - \bar{t}_1)}{\Delta t} \right\}$$

Proof

As selectivity is 3-regular, one may drop absolute values and sum for r, in eqn. 19, which gives

$$\Xi = \iint_{0 \leqslant s < t \leqslant \Delta t} \mathbf{N}(s) \wedge \mathbf{F}(s) \wedge \mathbf{F}(t) \, \mathrm{d}s\mathrm{d}t \tag{55}$$

Similarly, summing on t from s to Δt,

$$\Xi = \int_{0 \leqslant s \leqslant \Delta t} \mathbf{N}(s) \wedge \mathbf{F}(s) \wedge (\mathbf{N}(\Delta t) - \mathbf{N}(s))\mathrm{d}s$$

Using linearity and antisymmetry properties of the exterior product we obtain

$$\Xi = \mathbf{N}(\Delta t) \wedge \int_{0 \leqslant s \leqslant \Delta t} \mathbf{N}(s) \wedge \mathbf{F}(s)\,\mathrm{d}s \tag{56}$$

We need simply to integrate the three components of the integrand (in $\Lambda^2 E$) and then to make the exterior product with the sum vector $\mathbf{N}(\Delta t) = \mathbf{N}_0$.

For the separation of two solutes with carrier by chromatography, the selectivity is 2-regular for pair (1,2) but is not so for pairs (1,3) and (2,3). Therefore, eqn. 56 leads to

$$\Xi = N_0^1 \phi_{23} - N_0^2 \phi_{13} + N_0^3 \Xi_{12} \tag{57}$$

where

$$\phi_{13} = \int_{0 \leqslant s \leqslant \Delta t} \begin{pmatrix} \mathbf{N}^1(s) \\ \mathbf{N}^3(s) \end{pmatrix} \wedge \begin{pmatrix} \mathbf{F}^1(s) \\ \mathbf{F}^3(s) \end{pmatrix} \mathrm{d}s \quad \phi_{23} = \int_{0 \leqslant s \leqslant \Delta t} \begin{pmatrix} \mathbf{N}^2(s) \\ \mathbf{N}^3(s) \end{pmatrix} \wedge \begin{pmatrix} \mathbf{F}^2(s) \\ \mathbf{F}^3(s) \end{pmatrix} \mathrm{d}s$$

Integrands do not have a fixed sign in these expressions. They also depend on Δt. A geometrical interpretation of these expressions is that they give the algebraic area of curve $\mathbf{N}(s)$ seen from the origin, in plane (1,3) or (2,3). However, a remarkable feature is that $N_0^1 N_0^2$ can be put into the first two terms of eqn. 57, in such a way that $N_0^1 N_0^2(\varphi_{23} - \varphi_{13}) \cdot \varphi_{13}, \varphi_{23}$ are mapped on $[0,1] \times R$ to form a curve closed at infinite [*i.e.*, with $\varphi_{13}(-\infty) = \varphi_{23}(-\infty) = 0$ and $\varphi_{13}(\infty) = \varphi_{23}(\infty) = 1$]. Then $\varphi_{23} - \varphi_{13}$ is the area inside this curve. As in model II peaks are translated by $\bar{t}_2 - \bar{t}_1$, and so are $\varphi_{13}, \varphi_{23}$, this oriented area is finite and equal to $\varphi_{23} - \varphi_{13} = -(\bar{t}_2 - \bar{t}_1)[\varphi_{23}(\infty) - \varphi_{23}(-\infty)] = -(\bar{t}_2 - \bar{t}_1)$. Therefore, as long as $N < N_c$ holds,

$$\Xi = N_0^1 N_0^2 F^3 \Delta t \xi_{12} - N_0^1 N_0^2 F^3 (\bar{t}_2 - \bar{t}_1) \tag{58}$$

or

$$\xi = \left\{ \xi_{12} - \frac{(\bar{t}_2 - \bar{t}_1)}{\Delta t} \right\} \tag{59}$$

which concludes the proof since $N_0^3 = F^3 \Delta t$.

Geometrically, one may understand this result as follows. Let us split eqn. 58

into two terms, in same way as in eqn. 49. $N_0^1 N_0^2 F^3 \Delta t \xi_{12}$ is 3-volume of a vertical cylinder with base Z_{12}, height $N_0^3 = F^3 \Delta t$, which would be obtained if the carrier was not an integral part in the process and could be spared (of course a hypothetical case). Note that this 3-volume is unbounded when $\Delta t = \infty$.

$N_0^1 N_0^2 F^3 (\bar{t}_2 - \bar{t}_1)$ is, dimensionally, a (bounded) 3-volume. Formally, this term represents 3-volume of total separation between pure solutes and the quantity of carrier which flows between the retention times of the peaks. It does not depend on either Δt, and therefore it is finite, or directly on the efficiency of the process (HETP or N). As this term is subtracted from the first term in eqn. 58, it can be appropriately called *loss of 3-volume*.

Finally, one obtains for the Gaussian isovariant model, $N < N_c$,

$$\xi = \left\{ 2 \operatorname{erf}\left(\sqrt{\frac{N}{2}} \cdot \frac{\bar{t}_2 - \bar{t}_1}{\bar{t}_1} \right) - 1 - \frac{(\bar{t}_2 - \bar{t}_1)}{\Delta t} \right\} \tag{60}$$

where t_i can be evaluated using eqn. 29. Therefore, the yield of 3-volume is given by (Fig. 12)

$$\xi = \left\{ 2 \operatorname{erf}\left(\sqrt{\frac{N}{2}} (\alpha - 1) \right) - 1 - \frac{(\alpha - 1)}{\Delta t} \cdot \frac{(1 + k^1) NH}{u} \right\} \tag{61}$$

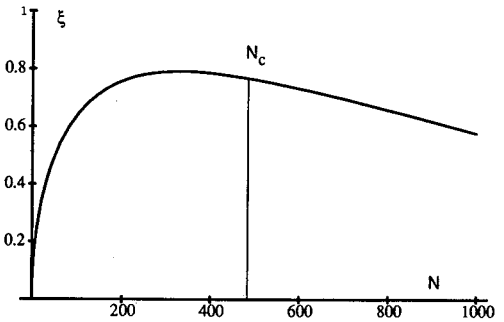

Fig. 12. 3-Volume yield *vs.* number of plates. Conditions as in Fig. 1, $\Delta t = 100$ s.

Especially interesting is the rapid (in $\sqrt{N}$) increase in 3-volume creation at the beginning, followed by a step-up and a decrease. The mean rate of creation of 3-volume per plate, ξ/N, goes to zero at a certain number of plates. Clearly, the existence of such a maximum on ξ is a very important feature for optimization: it indicates that one should consider some way of enhancing the efficiency of the process beyond this point.

5.3.3. *Evolution of 3-volume for three solutes*

For 3 solutes, in the special case of totally regular selectivity, we recognize that the components in eqn. 56 are exactly the 2-volumes of canonical projections of Z and,

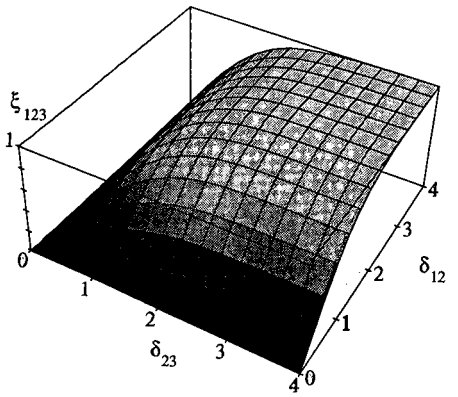

Fig. 13. 3-Volume yield between three solutes *vs.* translation parameters.

therefore, we derive the simple and useful expression that 3-volume is a linear function of 2-volumes:

$$\Xi = N_0^1 \Xi_{23} - N_0^2 \Xi_{13} + N_0^3 \Xi_{12} \tag{62}$$

which can also be recast yields in 3- and 2-volume (eqn. 25), with coefficients independent of quantities of species:

$$\xi = \xi_{23} - \xi_{13} + \xi_{12} \tag{63}$$

Combining the results in Section 5.2.4. and the generalization in Section 5.2.5. we obtain for the Gaussian isovariant model the expression of 3-volume of separation between three solutes:

$$\xi = 2\left\{\mathrm{erf}\left(\frac{\delta_{23}}{\sqrt{2}}\right) - \mathrm{erf}\left(\frac{\delta_{13}}{\sqrt{2}}\right) + \mathrm{erf}\left(\frac{\delta_{12}}{\sqrt{2}}\right)\right\} - 1 \tag{64}$$

where δ_{ij}, given by eqn. 53, is the translation parameter between peaks of solutes i and j. As $\delta_{13} = \delta_{12} + \delta_{23}$, ξ is a symmetric function of two independent variables (Fig. 13).

6. PROBLEM SOLVING WITH ZONOIDS

A good theory should first integrate previous knowledge and then ask new questions whose answers open new avenues. Many separation problems can be recast geometrically and given innovative answers. We consider below five problems, in order of increasing complexity, but clearly they only scratch the surface of a vast subject. For many of these problems, the fundamental property of a convex set of mixtures will be the critical property. Meanwhile, we shall encounter the extent of separation, proposed by Rony [3], and show how well it fits into zonoid theory. Although economy (*e.g.*, marginal costs and linear programming) is assumed to give answers to these problems, this is not so in most instances owing to the overwhelming complexity of the calculations. We then need first to answer on a technical basis, and zonoid theory gives the answer.

6.1. A problem of recovery with minimum dilution

Given a process delivering a family of mixtures by use of a (conservative) separation agent, and a mixture of solutes, find the sampling (if any) which will allow them to be recovered with minimum dilution in separation agent.

It is not commonly considered that a sampling function λ may, in principle, oscillate wildly between 0 and 1. There is no real reason why only "gentle" sampling procedures should be the best.

The answer is given below for $\dim E = 3$, but can be generalized.

Consider a family $\mathscr{F}$ and $\mathbf{M} = (M^1, M^2)$, a mixture of solutes. If $\mathbf{M} \in Z_{12}(\mathscr{F})$, $\mathbf{M}$ is feasible, and the problem amounts to determining geometrically the point on the boundary ∂Z^- above $\mathbf{M}$. In the case of 3-regular selectivity, in view of eqn. 14, it is equivalent to finding t_1, t_2 such that

$$\mathbf{M} = \int_{t_1}^{t_2} \mathbf{F}(\tau)\mathrm{d}\tau, 0 \leqslant t_1 \leqslant t_2$$

or, a segment equipollent to $\mathbf{M}$ can be put as a chord on ∂Z_{12}.

The minimum quantity of separation agent will then be

$$M^3_{\min} = \int_{t_1}^{t_2} F^3(\tau)\mathrm{d}\tau$$

If selectivity is not 3-regular, a more complicated sampling function (deduced from a variant of eqn. 15) will be necessary, but it remains gentle.

6.2. A problem of yield

Given a family $\mathscr{F}$, characterize all mixtures $\mathbf{M}$ with a given content M^i of a given solute i (*i.e.*, all mixtures with a given yield of solute i). Geometrically, this is equivalent to finding the intersection of Z_{12} ($\mathscr{F}$) by a plane, the equation of which is $N^i = M^i$, and must be solved by computer to be represented graphically.

Strongly related is the problem of chromatographic design. Let us consider the existence of a real problem in preparative chromatography (overlooked until now). To choose the sampling valves for continuous outlet flow $\mathbf{F}(t)$, the designer must answer first the question: Is it best to actuate the sampling valve through an "all or nothing" command (called bang–bang in control theory) or through an arbitrary, bounded command? In the first instance the sampling function is as in eqn. 2 and in the second as in eqn. 6. In other words, are they mixtures which can be sampled in the latter (and more general) way but not in the former? A sideways question is whether the answer depends on the number of chemical species in the flow. The answer is (through the Krein–Milman theorem, referred to in Section 2; see comments on Theorem 3) that any mixture which can be made by the general sampling approach can also be made by, at least, one bang–bang command, a result which justifies everyday practice.

6.3. A problem of approximation

Given a family $\mathscr{F}$, find a criterion for the optimum recovery of a fixed number p of cuts and find the corresponding set of optimum p-1 cut-points.

The answer is to take the p cuts to minimize loss of n-volume.

This is a problem of approximation of a differential family by a discrete family. Clearly we may consider the approximation in the full space in n dimensions (*i.e.*, take into account the separation agent), or a projected subspace defined by r "preferred species", *e.g.*, solutes. We must have $p \geqslant n$ or $p \geqslant r$ depending on the case.

With $n = 3, r = 2$, the second procedure would involve minimizing 2-volume lost in the plane of solutes 1,2. Let us consider in the following $p = 2$. We have to find one cut-point.

Now, recall that for a binary mixture $\mathbf{N}_0$ split into two mixtures, N_1, N_2, Rony [3,4] has defined the extent of separation as

$$\xi = \mathrm{Abs}\left(\frac{1}{N_0^1 N_0^2}\begin{vmatrix} N_1^1 N_2^1 \\ N_1^2 N_2^2 \end{vmatrix}\right) = \frac{1}{N_0^1 N_0^2}|\mathbf{N}_1 \wedge \mathbf{N}_2|$$

and this definition has been generalized by Valentin [2] to a vector extent of separation. We shall take $\mathbf{N}_0 = (1,1)$. In the present theory we should call ξ a yield of 2-volume. Zonoid theory gives a physical interpretation which was lacking in Rony's index. ξ is the yield of 2-volume of $Z\{\mathbf{N}_1, \mathbf{N}_2\}$ (a parallelogram). Now, it is natural, if $\mathbf{N}_1$ and $\mathbf{N}_2$ are obtained from a 1-differential family of parameter t by a 1-cut point sampling at τ, to ask for ξ^*, the maximum $\xi(\tau)$. Clearly, ξ^* is the 2-volume of a (best) approximation of Z_{12} by a parallelogram.

In the case of linear chromatography (model II), Rony [4] showed that the optimum cut point is located at $\tau^* = \delta/2$ and

$$\xi^* = 2\,\mathrm{erf}\left(\frac{\delta}{2}\right) - 1 \tag{65}$$

From the corresponding eqn. 54 it is clear that loss of 2-volume induced by the two-cut trapping procedure is then independent of δ, as long as the linear expansion is valid, and therefore,

$$\frac{\xi^*}{\Xi} = \frac{1}{\sqrt{2}} = 0.707$$

Eqns. 54 and 65 set in perspective the effect of recovering only two cuts on the length of the column: to obtain the same 2-volume of separation between solutes in chromatography with 1-cut point, as in differential chromatography, one needs a two times longer column.

Thus ξ^*, the extent of separation, as defined by Rony [3,4], reflects only part of the separation produced by the column. Further, returning to the full dimensional approximation, one may take into account dilution of the solutes in the carrier, *i.e.*, a ternary separation. Now it is clear that a 2-cut procedure cannot be optimal as the

3-volume recovery would be zero. This strongly suggests that optimizing a 3-cut recovery should be considered for recovering a better part of the separation produced by the column and that classification of processes by Rony [17] should be re-worked accordingly.

6.4. *A problem of basestock management*

Given a family of mixtures, what should be the criterion for fabrication of a required mixture if the next mixture to be made is unknown?

This problem, also called the paint dealer problem, has been elegantly solved [16] using the fact that the probability of hitting a zonoid by a point is proportional to its n-volume (for a uniform density of probability of demand).

6.5. *A problem in design*

This last problem is certainly the most difficult and rewarding: how can one match a given separation (*e.g.*, by purity and yield) with some set of elementary devices (*e.g.*, equilibrium stages)?

The problem can be recast in term of zonoids, as the required separation can be represented by a convex set of mixtures Z_0 (or a set of these if the separation is not fully specified). Therefore, the problem is to find an arrangement of these stages which produces a zonoid Z_1 such that

$$Z_0 \prec Z_1$$

A simpler form of the problem is to determine the minimum number of stages in a column to obtain products $N_1, \ldots, N_p$. Formalization of this problem is

$$\operatorname*{Min}_{N} \left\{ Z(N) \mid N = 1, 2, \ldots, Z(N) \prec Z_0 \right\}$$

with

$$Z_0 = Z\{N_1, \ldots, N_p\} \text{ and } Z(N) = Z\left\{ \{\mathbf{F}(N,t)\mathrm{d}t\}_{t \in \Delta t} \right\}$$

7. CONCLUSIONS

Zonoid theory has been applied to very simple types of models of chromatography, namely the linear diffusional models. The results apply, of course, to all processes that can be modelled in this way, *e.g.*, liquid–liquid extraction. The method is general and should be a safe guide to the optimization or design of any process, including those which deliver families diffuse in 3-D space and time. Although the tools may seem very sophisticated and the applications remote at this stage, one must stress the probable long-term importance of this theory. Mathematical foundations and developments reflect an inherently complex situation and shed light on the specific features of chromatography.

Chromatography is not a separation process but a sepmix process. From this example, one may infer the importance of taking into account properly all the species involved, not forgetting the carrier. We have been able to study the three-dimensional zonoid of separation and its projections. The separation between species or mixing between one species and the carrier depends on the square root of the length of the column or of the number of theoretical plates, and is proportional to $\alpha - 1$. Chromatography exhibits how the interplay between separations and mixing operations may be a delicate one. Indeed, each species mixes with the carrier at the same time as it separates from other species. The important concept of r-regular selectivity has been defined.

The same methodology will be used in subsequent work to study non-linear effects on separations in chromatography where the power of the theory will be at its best; even though the inclusion of a zonoid of separation between solutes is valid in the simple model used, there are hints that the general situation is much more intricate. It certainly may happen that, owing to different diffusion or strong specific interaction effects, one species is better separated from the others when the feed quantity is increased. Then no inclusion property of zonoids will hold true and, *a fortiori*, no existence property.

This study has shown also that fundamental definitions in separation science are independent of concepts specific to thermodynamics. The former must define and study separation on a "stand-alone" basis. Then the latter may indicate subsequently how much separation production can occur, due to restraints imposed by the laws of thermodynamics (and also other sciences of matter, such as mass transfer kinetics). Basic independence will provide a firm ground for linking the evolution of separation in a system with the second principle of thermodynamics; more precisely, this will be made through a new general theorem expressing that separation between a carrier and solutes cannot increase (in the sense given by zonoid theory) in an isothermal, isobaric chromatographic column.

Among the fundamental questions to be investigated for a foundation in separation science along the lines developed here is the following: what are the springs of the separation and mixing creation hidden in the equations of motion in fluid mechanics and thermodynamics? In this respect the basic simplicity and the global nature of zonoids should allow one to concentrate only on salient features of solutions.

8. SYMBOLS

C	Concentration (mol/cm^3)
D	Diffusion or dispersion coefficient (cm^2/s)
E	Vector space of quantities (mol)
$\mathbf{e}$	Base vector of E
$\mathbf{F}$	Flow-rate vector
H(HETP)	Height equivalent to a theoretical plate (cm)
I	Interval of natural numbers $\{1, \ldots, n)$
i	Chemical species
J	Interval of natural numbers
k	Equilibrium coefficient, ratio of number of moles
L	Length of a column

N	Number of theoretical plates
$\mathbf{M,N}$	Quantity vector
$\mathbf{N}_0$	Overall (or sum) quantity vector or distal point
n	Dimension of the space E; number of species
O	Origin
P	Hyperplane, point; relative inlet pressure
p	Number of regions or of cuts; relative pressure at location z
Q	Volume flow-rate (cm^3/s)
R	Vector space of real numbers $(-\infty, +\infty)$
R	Resolution
R^3	Usual Euclidean space
t	Time, retention time; current parameter on a curve
$\bar{t}$	Arithmetic mean of retention times
$\bar{t}_1$	Retention time of species 1
u	Speed of carrier
$\mathbf{x}$	Molar fraction vector
Z	Zonoid, convex set of mixtures
$\mathbf{Z}$	Set of Zonoids in R^n
z	Spatial coordinate in R or R^3

Greek letters

α	Relative volatility, $\alpha = k^2/k^1$
Γ,γ	Curve, boundary of a convex
Δ_{n-1}	$n-1$ Dimensional simplex (of molar fractions in E, $\dim E = n$)
δ	Dirac measure; dimensionless translation operator, $\delta = \sqrt{N} \cdot \frac{\bar{t}_2 - \bar{t}_1}{\bar{t}}$
∂	Operator taking boundary of an open set
Ξ	n-Volume of Z, $(Z \subset E, \dim E = n)$ $(\text{mol})^n$
ξ	Extent of separation
Σ	System state
σ	Reduced variance
τ	Reduced time, parameter on a curve

Superscripts

i,k	Chemical species
$+$	Positive orthant, upper part

Subscripts

j	Region
0	Entering in the system

Symbols

[ ]	Matrix
$\{\ldots\}$	A set of elements
$\circ$	Composition of functions: $f \circ g(x) = f(g(x))$
$+$	Sum or Minkowski sum

$\wedge$	Exterior product of vectors
n-D	n-Dimensional (space)
1-d	1-Differential (family)
sgn(x)	$+1$ if $x > 0$, -1 if $x < 0$
$\prec$	Exists in
O	Of the order of

9. ACKNOWLEDGEMENTS

Part of this work was carried out when the author was a lecturer with Professor G. Guiochon at the École Polytechnique. The author gratefully acknowledges many discussions with L. Tartar (now at Carnegie Mellon University) and M. Schoenauer of the Applied Mathematics Department of this School. The continuous interest of P. J. Laurent, D. Girard and B. Lacolle from IMAG (Université Joseph Fourier, Grenoble) was important for completion of this work. The support of Société Nationale Elf-Aquitaine for part of this work has been substantial.

10. APPENDIX: CALCULATION OF 2-VOLUME OF SEPARATION

We give a general expansion for Ξ_{12} for the case when $\mathbf{F}(t)$ is generated by a Polya frequency (PF) function (in fact 2-selectivity would be sufficient here) and obtain an explicit equation in the special case of a Gaussian isovariant model.

10.1. A general expansion for Ξ

In the case of a Polya frequency function let us write

$$F^1(u) = F(u), F^2(u) = F(u - \delta)$$

dropping the indexes of solutes and taking unit total quantities of each solute, from eqn. 19, using Theorem 6a to discard absolute values:

$$\mathrm{d}\Xi = \begin{vmatrix} N(u) & F(u) \\ N(u-\delta) & F(u-\delta) \end{vmatrix} \mathrm{d}u \tag{A1}$$

We also make the hypothesis that $N(u)F(u)$ and $N(u)F^{(k)}(u)$, $k \geqslant 1$, is zero for $u = \pm\infty$.

We insert the Taylor development of F and N around u:

$$F(u - \delta) = F(u) - \delta F'(u) + (1/2)\delta^2 F''(u) - (1/6)\delta^3 F^{(3)}(u) + \ldots$$

$$N(u - \delta) = N(u) - \delta F(u) + (1/2)\delta^2 F'(u) - (1/6)\delta^3 F''(u) + \ldots$$

taking into account $N'(u) = F(u)$ in eqn. A1 and develop $\mathrm{d}\Xi/\mathrm{d}u$ in powers of δ. From the multi-linearity property of determinants, we obtain

$$\mathrm{d}\Xi = \sum_{k=1}^{\infty} \frac{(-1)^k}{k!} \cdot \delta^k \begin{vmatrix} N(u) & F(u) \\ F^{(k-1)}(u) & F^{(k)}(u) \end{vmatrix} \mathrm{d}u$$

where the superscripts in parentheses represent derivation. On integration on R we obtain the Taylor expansion of Ξ in powers of δ. From integration by parts of the general determinant, we obtain

$$\int_{-\infty}^{+\infty} \begin{vmatrix} N(u) & F(u) \\ F^{(k-1)}(u) & F^{(k)}(u) \end{vmatrix} \mathrm{d}u = \int_{-\infty}^{+\infty} N(u)F^{(k)}(u) - F(u)F^{(k-1)}(u)\mathrm{d}u$$

$$= -2\int_{-\infty}^{+\infty} F(u)F^{(k-1)}(u)\mathrm{d}u + [N(u)F^{(k-1)}(u)]_{-\infty}^{\infty}$$

where the last term is zero in view of the hypothesis. The general expansion can be written as

$$\Xi = 2\sum_{k=1}^{\infty} \frac{(-1)^{k+1}}{k!} \cdot \delta^k \int_{-\infty}^{+\infty} (F(u)F^{(k-1)}(u))\mathrm{d}u \tag{A2}$$

Each coefficient in eqn. A2 is a well behaved integral which can be calculated numerically fairly easily and reduces the calculation of Ξ to quadratures. However, the series is slowly convergent for values of δ over 2.

For any even Polya frequency function, expression A2 loses its terms with even k, as $F^{(k-1)}(u)$ is odd.

Limiting eqn. A2 to its first terms, we obtain

$$\Xi = 2\delta \int_{-\infty}^{+\infty} F(u)^2\mathrm{d}u - \delta^2 \int_{-\infty}^{+\infty} F(u)F'(u)\mathrm{d}u + \frac{1}{3}\delta^3 \int_{-\infty}^{+\infty} F(u)F''(u)\mathrm{d}u + O(\delta^4)$$

Applying eqn. A2 to the Gaussian isovariant model, we obtain the seven-term expansion, without even terms as $F(u)$ is even:

$$\Xi = \frac{1}{\sqrt{\pi}} \cdot \delta - \frac{1}{12} \cdot \frac{1}{\sqrt{\pi}} \cdot \delta^3 + \frac{1}{80} \cdot \frac{1}{\sqrt{\pi}} \cdot \delta^5 - \frac{1}{672} \cdot \frac{1}{\sqrt{\pi}} \cdot \delta^7 + O(\delta^9)$$

In view of the classical expansion of the error function around $x = 0$:

$$\mathrm{erf}(x) = \frac{1}{2} + \frac{1}{\sqrt{2\pi}}\left(x - \frac{x^3}{3} + \frac{x^5}{2!5} - \frac{x^7}{3!7} + \ldots\right) \tag{A3}$$

rewriting eqn. A2 with $x = \dfrac{\delta}{\sqrt{2}}$:

$$\Xi = \frac{2}{\sqrt{2\pi}}\left[\frac{\delta}{\sqrt{2}} - \frac{1}{3}\left(\frac{\delta}{\sqrt{2}}\right)^3 + \frac{1}{2!5}\left(\frac{\delta}{\sqrt{2}}\right)^5 - \frac{1}{3!7}\left(\frac{\delta}{\sqrt{2}}\right)^7 + \ldots\right] \tag{A4}$$

gives through identification the final expression of 2-volume for the Gaussian isovariant model:

$$\Xi = 2\,\mathrm{erf}\left(\frac{\delta}{\sqrt{2}}\right) - 1 = \mathrm{Erf}\left(\frac{\delta}{\sqrt{2}}\right) \tag{A5}$$

10.2. Fourier transformation

Eqn. A5 may also be derived through the use of Fourier transformation, which proves to be an interesting tool for the calculation of volumes of zonoids. Starting from eqn. A1, we note that, on integration on R,

$$\Xi = \int_{-\infty}^{+\infty} [N(u)F(u-\delta) - N(u-\delta)F(u)]\mathrm{d}u \tag{A6}$$

Integrating by parts the second term in eqn. A6, we obtain

$$\Xi = 2\int_{-\infty}^{+\infty} N(u)F(u-\delta)\mathrm{d}u - 1$$

As we may write this as

$$\Xi = 2\int_{-\infty}^{+\infty} N(u)F(-(\delta-u))\mathrm{d}u - 1 \tag{A7}$$

Using the definition of the convolution integral

$$f*g(v) = \int_{-\infty}^{+\infty} f(u)g(v-u)\mathrm{d}u \tag{A8}$$

we recognize from eqn. A8 that Ξ results from convolution of $N(u)$ with $F(-u)$. Alternatively, this can be recast, using the correlation integral

$$h(v) = \int_{-\infty}^{+\infty} f(u)g(u+v)\mathrm{d}u$$

to say that $\Xi(-\delta)$ results from correlation of $N(u)$ with $F(u)$. Indeed, eqn. A8 reduces, if F is even, *i.e.*, $F(u-\delta) = F(\delta-u)$, to the convolution

$$\Xi(\delta) = 2N*F - 1$$

Ξ, as a function of δ, results from a convolution between N and F.

Now we consider classical results linking Fourier transforms and convolution. Call $J(f;z)$ the Fourier transform J of f, and $J^{-1}(f;z)$ the inverse Fourier transform:

$$J(f:z) = \frac{1}{\sqrt{2\pi}} \int_{-\infty}^{+\infty} f(u)\, e^{-iuz}\, du, \quad J^{-1}(f;u) = \frac{1}{\sqrt{2\pi}} \int_{-\infty}^{+\infty} f(z)\, e^{iuz}\, dz \tag{A9}$$

Let us introduce explicit (heavy) notations about the Fourier transform specifying the initial function, its variable and the variable of the transform, *i.e.*, $J(f(u);z)$. We write classical properties, *e.g.*,

$$J\left(f\left(\frac{u}{\sigma}\right);z\right) = |\sigma| J(f(u);\sigma z)$$

the equation for the Fourier transform of a derivative:

$$J(f'(u);z) = izJ(f(u);z)$$

and the equation for the Fourier transform of a convolution:

$$f*g(u) = \sqrt{2\pi}\, J^{-1}(J(f(u);z)\, J(g(u);z);u) \tag{A10}$$

The equation for the Fourier transform of a correlation involves the conjugate of the Fourier transform of one function (and is not symmetric):

$$h = \sqrt{2\pi}\, J^{-1}(J(f;z)\, \overline{J(g;z)};u)$$

The convolution equations apply to $F(u)$ and $N(u)$ as defined in model II, as $F(u)$ is even. Now, it is well known that a normal centred distribution is stable by operator J, *i.e.*,

$$J(F(u);z) = F(z)$$

From the derivation rule,

$$J(N;z) = \frac{1}{iz} J(F;z) = \frac{1}{iz} F(z)$$

Then we obtain, from eqn. A7

$$\Xi(\delta) + 1 = 2J^{-1}(\sqrt{2\pi}\, J(F;z)\, J(N;z);\delta) \tag{A11}$$

from which follows eqn. A5 through

$$\Xi(\delta) + 1 = 2J^{-1}\left(\frac{1}{\sqrt{2\pi}} \cdot \frac{1}{iz} \exp(-z^2);\delta\right)$$

$$= 2J^{-1}\left(J\left(N\left(\frac{u}{\sqrt{2}}\right);z\right);\delta\right) = 2\,\mathrm{erf}\left(\frac{\delta}{\sqrt{2}}\right)$$

as

$$\frac{1}{\sqrt{2\pi}}\cdot\frac{1}{iz}\exp(-z^2)=\sqrt{2}\cdot\frac{1}{\sqrt{2\pi}}\cdot\frac{1}{is}\exp\left(-\frac{s^2}{2}\right)\text{with}\,s=\frac{s}{\sqrt{2}}$$

$$=J(\sqrt{2}\,N(u);s)=J(\sqrt{2}N(u);z\sqrt{2})=J\left(N\left(\frac{u}{\sqrt{2}}\right);z\right)$$

10.3. A basic equation for Gaussian mixing kernel

Let

$$f(\tau)=\int_{-\infty}^{+\infty}\frac{e^{-\frac{w^2}{2\sigma^2}}}{\sqrt{2\pi}\sigma}\cdot\frac{e^{-\frac{(w-\tau)^2}{2\sigma'^2}}}{\sqrt{2\pi}\sigma'}dw\ \text{and}\ g(\eta)=\frac{e^{-\frac{\eta^2}{2}}}{\sqrt{2\pi}}$$

We apply Fourier transformation to f, seen as a convolution equation of simple normalized transforms of g

$$J(f(\tau);z)=\sqrt{2\pi}\,J\left(g\left(\frac{\tau}{\sigma}\right);z\right)J\left(g\left(\frac{\tau}{\sigma'}\right);z\right)$$

$$=\sqrt{2\pi}\,J(g(\tau);\sigma z)\,J(g(\tau);\sigma' z)$$

$$=\frac{1}{\sqrt{2\pi}}\cdot g(\sqrt{\sigma^2+\sigma'^2}\,z)=\frac{1}{\sqrt{\sigma^2+\sigma'^2}}\cdot J\left(g\left(\frac{\tau}{\sqrt{\sigma^2+\sigma'^2}}\right);z\right)$$

Hence

$$f(\tau)=\left(\frac{1}{\sqrt{\sigma^2+\sigma'^2}}\right)g\left(\frac{\tau}{\sqrt{\sigma^2+\sigma'^2}}\right)$$

Therefore, a Gaussian mixing kernel, applied to a Gaussian family, gives a Gaussian family whose variance is the sum of variances.

REFERENCES

1 P. Valentin, *Cours de Génie de la Séparation*, Ecole Polytechnique, Paris, 1977.
2 P. Valentin, in A. Rodrigues and D. Tondeur (Editors), *Percolation Process and Applications* (*NATO ASI Series*, E33), Sijthoff and Noordhoff, Netherlands, 1980, pp. 141–195.
3 P. R. Rony, *Sep. Sci.*, 3 (1968) 239.
4 P. R. Rony, *Sep. Sci.*, 3 (1968) 357.
5 M. J. E. Golay, in D. Goldup (Editor), *Gas Chromatography 1964*, Institute of Petroleum, London, 1965, p. 2.

6 H. S. M. Coxeter, *J. Math. Pures Appl.*, 41, No. 9, (1962) 137.
7 H. S. M. Coxeter, *Regular Polytopes*, Macmillan, New York, 2nd ed., 1963.
8 E. D. Bolker, *Trans. Am. Math. Soc.*, 145 (1969) 323.
9 P. McMullen, *Trans. Am. Math. Soc.*, 159 (1971) 91.
10 G. C. Shephard, *Can. J. Math.*, 26 (1974) 302.
11 R. Schneider and W. Weil, *Applications of Convexity*, Birkhauser, Basle, 1982, pp. 296–317.
12 D. Blackwell, in *Proceedings of the Second Berkeley Symposium on Mathematical Statistics and Probability* (1950, Berkeley), Berkeley University Press, Los Angeles, 1951, pp. 93–102.
13 S. Karlin, *Total Positivity*, Stanford University Press, Stanford, CT, 1968.
14 J. Villermaux, in A. Rodrigues and D. Tondeur (Editors), *Percolation Process and Applications* (*NATO ASI Series*, E33), Sijthoff and Noordhoff, Netherlands, 1980.
15 D. Tondeur, *Ph.D. Thesis*, University of Nancy, 1969.
16 D. Girard and P. Valentin, in J. P. Penot (Editor), *New Methods in Optimization and Their Industrial Uses*, (*International Series of Numerical Mathematics*, Vol. 87), Birkhauser, Basle, 1989 pp. 57–71.
17 P. R. Rony, *AIChE Symp. Ser.*, 68, No. 120 (1972) pp. 89–104.

Journal of Chromatography, 556 (1991) 81–94
Elsevier Science Publishers B.V., Amsterdam

CHROM. 23 285

Review

Some aspects of optimization in planar chromatography

A.-M. SIOUFFI
Laboratoire de Génie Chimique et Chimie Appliquée, Université Aix-Marseille 3, 13397 Marseille Cedex 13 (France)

ABSTRACT

A survey of published optimization procedures in thin-layer chromatography (TLC) is presented. In one-dimensional TLC the mobile phase selection is performed through either computerized or non-computerized methods. Most of the latter methods are similar to those utilized in high-performance liquid chromatography and have been advocated for planar chromatography (simplex, overlapping resolution map). Resolution-based criteria have been criticized and others are proposed. Some procedures are predictive whereas others are not, such as principal component analysis. In two-dimensional TLC the aim is to find two systems exhibiting the least correlation. In this respect no attempt has been made to optimize the stationary phase.

CONTENTS

1. INTRODUCTION

It is often considered that efficiencies achieved in planar chromatography (PC) are low in comparison with high-performance liquid chromatography (HPLC) and, as

0021-9673/91/$03.50

a consequence, efforts to optimize PC are not numerous. This is emphasized by the fact that many runs can be carried out within a short period of time in classical PC [thin-layer chromatography (TLC)], thus supplying the analyst with a large amount of data. The best conditions for separation are determined by trial and error, relying on the expertise of the chromatographer.

Fortunately, PC has evolved toward an instrumentalized technique capable of producing a high degree of sensitivity, selectivity and efficiency with reliable reproducibility.

In the more general case, the goal of the optimization process must be to improve the separation between all the peaks representing the individual components of a mixture in order to obtain a chromatogram in which each peak will correspond to one and only one component. This goal is achieved by adjusting a set of experimental factors. Optimization in PC is important as the length of the plate and the time of analysis are fixed and there is no way to couple plates in series. Moreover, the unique feature of PC is its two-dimensional capability and it has been demonstrated by Guiochon and co-workers [1,2] that the peak capacity in two-dimensional TLC is much larger than those obtained with the best HPLC columns.

Optimization involves three steps: (i) definition of the criterion, (ii) definition of the parameter space and (iii) logical procedure.

We shall not consider the "one-variable-at-a-time" (univariate) methods to focus on multivariate optimization. Optimization of one variable is performed on discrete variables such as particle size, pH and ionic strength. Multivariate methods deal with related variables such as the amount of each type of solvent used in the mobile phase. These are related variables as the sum of all solvents must total 100%. The first paper on the topic was from Guiochon *et al.* [3], who determined the relationships between development length, analysis time and particle diameter to achieve the best performances (see, *e.g.*, Fig. 17 in ref. 3).

At present the analyst selects one stationary phase and searches for the optimum solvent. Although many ways of changing selectivity in chromatography are possible, the most powerful is to change the composition of the mobile phase. In HPLC the majority of separations are carried out with alkyl-bonded phases. Conversely, bare silica is still widely used in PC. Smith and Cooper [4] described a stationary phase selectivity triangle in which only polar bonded phases are displayed. Mixtures of stationary phases are unusual. One attempt was made by Righezza and Siouffi [5], who demonstrated that it works well with non-polar solutes whereas peak broadening occurs with polar solutes [6]. Published optimization procedures deal with the selection of the solvent, which can be a time-consuming operation.

We shall distinguish one-dimensional classical TLC from more advanced techniques and computerized methods from non-computerized methods. It does not seem that special optimization procedures devoted to forced flow or high-pressure PC have been published.

2. ONE-DIMENSIONAL PLANAR CHROMATOGRAPHY

2.1. Grid search procedures

A graphical method has recently been published by Issaq and Seburn [7]. The system is based on a plot of observed R_F values *versus* the composition of a binary

mobile phase. The method is said to be simple and has been applied to both normal- and reversed-phase TLC. Two primary solvents, A and B, are selected and five data from five mixtures are required to plot R_F values *versus* mobile phase composition. This procedure is only experimental. Unfortunately, A and B are not single solvents, *e.g.*, A is acetonitrile–water and B is methanol–water in a reversed-phase system. The selection of primary solvents A and B is not straightforward and it does not seem that this procedure can be used with complex mixtures.

Oscik-Mendyk [8] proposed displaying the R_F data on a Gibbs triangle in the form of isolines, *i.e.*, lines connecting the points corresponding to the same R_F values. These lines are not parallel and regions where R_{F_1}/R_{F_2} is higher permits the selection of the appropriate solvent. It is particularly useful with ternary mobile phases but it is time consuming as a large number of experiments are required and there is no means to predict the retention behaviour.

The PRISMA model developed by Nyiredy and co-workers [9–11] is a three-dimensional model correlating the solvent strength and the selectivity of mobile phases. Silica is used as the stationary phase and solvent selection is performed according to Snyder's solvent classification [12]. Preliminary experiments are carried out with different solvents from the eight groups of the classification. The solvent strength has to be reduced or increased so that the substance zones are distributed between $R_F = 0.2$ and 0.8. For this purpose, when R_R values are too high or too low modifiers (hexane or water) are added. Water saturation can be used. The PRISMA model has three parts: an irregular frustum, a regular middle part and a platform (Fig. 1). The three top corners of the model represent the selected three individual solvents which can be diluted with hexane (eluotropic strength = 0). The solvent strength is represented by the height of the prism, points along the edges stand for combination of two solvents, points on the sides for combination of three and points in the interior of the prism for mixtures of four solvents. The prism is similar to that proposed by Glajch and Kirkland [13] for experimental design approach for gradient elution.

The PRISMA model includes all combinations of one to five solvents for the separation of compounds from low to high polarity. With non-polar samples the initial solvent composition corresponds to the centre of the triangular top face of the regular prism. This composition is diluted with hexane to bring solutes into the convenient R_F range. The solvent strength is maintained and a further three chromatograms are run at solvent compositions corresponding to selectivity points near the apices of the triangle. From these initial runs further chromatograms with different compositions are obtained until the best solvent mixture is reached. With polar samples the upper face of the frustum is utilized and the optimization proceeds in a very similar way. The last step is the selection of the appropriate development mode (linear, circular, anticircular, etc.). The PRISMA is a structured trial-and-error method. The TLC system is not computerized. In our opinion, the PRISMA is very powerful for the selection of mobile phase in over-pressurized layer chromatography. However, when four or five components are selected as the best mobile phase the TLC experiments may be tedious because of demixing.

2.2. *Computer-assisted methods*

These can be divided into two categories: simultaneous and sequential methods.

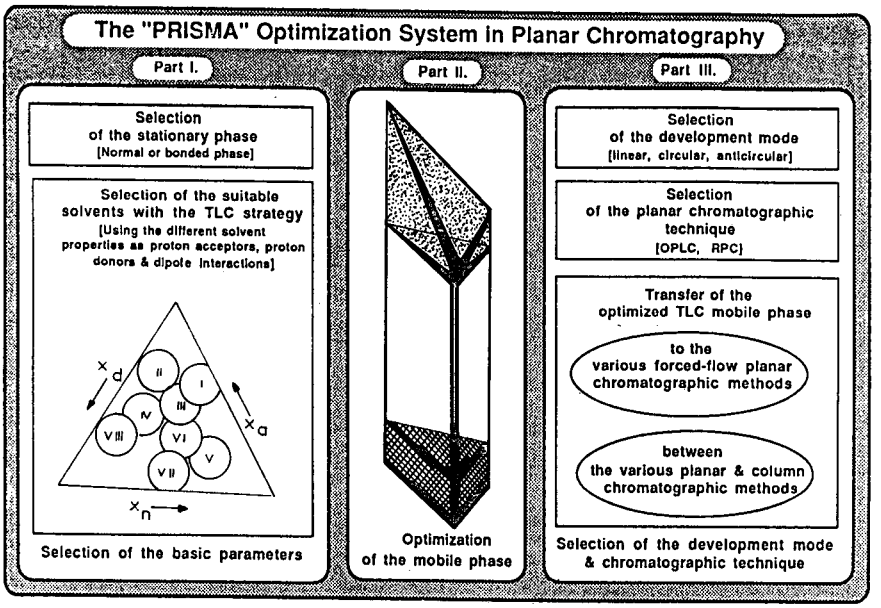

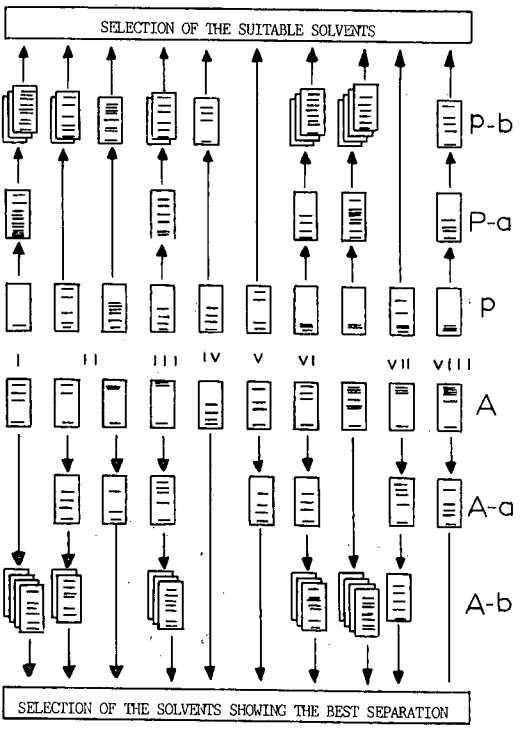

Fig. 1. Illustration of the PRISMA optimization procedure (reprinted from ref. 11, with permission).

In every case a response criterion summarizes the quality of the chromatogram in a single numerical value. In many instances binary eluents are utilized, which permit the use of the linear relationship between R_M (or log k') and log X_s, where X_s, is the mole fraction of the component of greater eluting strength. In normal-phase chromatography the binary eluent is formed with an apolar diluent (*e.g.*, hexane) and a polar modifier; in the reversed-phase mode X_s is the proportion of organic modifier in the water–organic solvent mixture.

$$R_M = a \log X_s + b \tag{1}$$

This relationship holds true in both systems; a and b are constants characteristic of a given compound. One important feature is that the comparison of theoretically equieluotropic mixtures shows that this is only true for a given reference solute and there is an individual contribution from the solute molecular structure [14]. This means that two different binary mixtures of the same calculated eluotropic strength will yield different R_F values for different solutes on the same stationary phase. This precludes the *a priori* selection of isoeluotropic mixtures when dealing with samples containing very different species.

Nurok and Richard [15] used the above linear relationship to calculate R_F values for pairs of solutes at different mole fractions of a binary mixture of solvents to determine the ΔR_F. Plots of ΔR_F *versus* the mole fraction of the polar modifier in the normal-phase mode exhibit a maximum. Moreover, a plot of ΔR_F *versus* solvent polarity parameter exhibits another ΔR_F maximum corresponding to another binary mixture (Fig. 2). This $\Delta R_{F_{max}}$ criterion is used in many schemes as it is related to capacity factors through

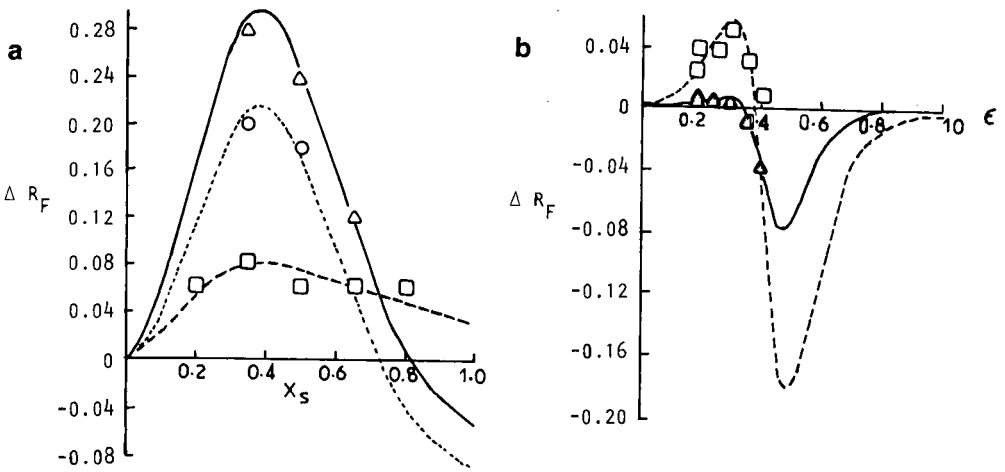

Fig. 2. (a) Plot of ΔR_F *vs.* X_s, the mole fraction of the polar modifier in an acetone–cyclohexane binary mixture. △, ○, □, Experimentally determined ΔR_F values. Pairs of solutes are as follows: solid line, hydroquinone–*o*-cresol; dotted line, hydroquinone–phenol; dashed line, phenol–*o*-cresol. (b) Plots of ΔR_F *vs.* the solvent polarity parameter for a chloroform–carbon tetrachloride binary mixture. Solutes are dyes: solid lines, butter yellow/sudan green; dashed line, oil orange/sudan green. (Reprinted from ref. 15, with permission.)

$$\Delta R_F = \frac{k'_j - k'_i}{(1 + k'_j)(1 + k'_i)} \tag{2}$$

2.3. Computerized method through a data base

This procedure was proposed by Matyska and co-workers [16,17]. Two experiments are required to determine constants a and b and many data were gathered by the authors. The optimization program has five steps: input section where names (as codes) of solutes are introduced, computation of R_F values, sorting and calculation of R_F, choice of the best eluent composition corresponding to the largest value for minimum R_F and output section. R_F values in the range 0.3–0.4 are considered when the volume percentage of polar modifier is low. The program is written in BASIC. The aim is to analyse toxic substances and rapidly select a solvent that differentiates two solutes exhibiting same retention in one system.

From eqn. 1 we can write for two solutes i and j

$$\log \alpha = \log X_s (a_j - a_i) + (b_j - b_i) \tag{3}$$

and

$$\frac{\mathrm{dlog}\ \alpha}{\mathrm{dlog}\ X_s} = a_j - a_i \tag{4}$$

when $a_j > a_i$ the selectivity will increase with increasing amount of the modifier, and when $a_j < a_i$ the reverse is observed.

A different equation was proposed by Oscik [18] to relate the R_M value of a chromatographed substance using a multi-component mobile phase to R_M values of the same substance in a single mobile phase. However, it requires the determination of excess adsorption isotherms and its application looks tedious.

2.4. Window diagrams

This technique was introduced in gas chromatography by Laub and Purnell [19]. It has recently been advocated for the selection of mobile phases in HPTLC [20]. It is based on the same equation as eqn. 1 but rewritten in the form

$$R_F = \frac{1}{1 + \exp(a \ln X_s + b)} \tag{5}$$

The separation between two spots is

$$\Delta R_F = R_{F_i} - R_{F_j} = \frac{1}{1 + \exp(a_i \ln X_s + b_i)} - \frac{1}{1 + \exp(a_j \ln X_s + b_j)} \tag{6}$$

A window diagram is used to plot the ΔR_F *versus* mobile phase composition. The maxima at the top of the window represent the mobile phase composition giving the best separation for the least separated pair (Fig. 3). A perpendicular from the tallest window to the abscissa identifies the optimum composition. This procedure requires the same number of experiments as the previous one. The location of peak cross-overs is easier.

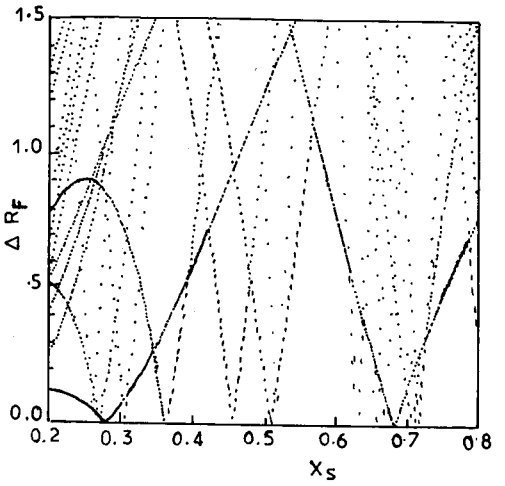

Fig. 3. Typical window diagram utilized for determining the optimum solvent composition in the separation of pesticides (reprinted from ref. 27, with permission).

2.5. Sequential optimization procedures

The simplex method is based on the principle of stepwise movement toward the set goal with simultaneous changes of several variables. The simplex itself is a geometric shape with one more vertex than the number of variables under study. In the optimization each vertex corresponds to a set of operating parameters and it is necessary to run a chromatogram with these conditions. The quality of the separation achieved is assessed for each vertex and ranked from best to worst. The worst separation is discarded and a new vertex is constructed by reflecting it through the plane joining the remaining vertex. A modified simplex with expansion or contraction is more convenient for TLC.

Turina [21] proposed the following course with simplex: input data, simplex design, experiments, testing the experiments, rejection of the worst vertex, centroid, new vertex, new experiment, new simplex. There are several disadvantages to the sequential approach: the optimum that is located is not *a priori* the global optimum and is dependent on the choice of the response function and the initial setting of the experimental variables. For HPLC Berridge [22] proposed the chromatographic response function, $CRF = \Sigma \ln (P_i)$, where P_i is the peak separation.

In the separation of three dyes, Sabate and Tomas [23] considered that the distance between spots and the response is

$$S = \frac{4\,(R_{F_3} - R_{F_2})(R_{F_2} - R_{F_1})}{(R_{F_3} - R_{F_1})} \tag{7}$$

where the denominator is the distance between the highest and lowest spots. Some rules were given to transform the "rigid" simplex and accelerate the location of the optimum.

According to De Spiegeleer *et al.* [24], comparison of literature data with

a resolution-based criterion is tedious or even not possible owing to the lack of information on the spot widths. They proposed a multi-peak response function:

$$\frac{[hR_F(\max) - hR_F(n)][hR_F(l) - hR_F(\min)] \prod_{i=1}^{n-1} (hR_F(i+1) - hR_F(i)]}{\{[hR_F(\max) - hR_F(\min)]/(n+1)\}^{n+1}} \cdot 100\% \quad (8)$$

The criterion is expressed as a percentage (0–100%) and it has an intrinsic and universal meaning which permits the comparison of published separations. The idea is that the optimum solvent is the one that yields a chromatogram where all the spots lie at equal distances from each other and from chosen boundaries. In this mode the R_F range may be selected. According to the authors [24], eighteen vertices are required to reach a 99.1% response in order to select a suitable solvent for the complete separation of platinum complexes.

2.6. Statistical mixture design with isoresponse curves

The overlapping resolution map (ORM) technique has been successfully introduced in HPLC by Glajch *et al.* [25]. In this procedure three selectivity-adjusting solvents for either mode [methanol, tetrahydrofuran (THF) and acetonitrile for the reversed-phase (RP) mode and diethyl ether, methylene chloride and chloroform for the normal-phase (NP) mode] plus a strength-adjusting solvent for either mode (water for RP, hexane for NP) require the use of a total of four solvents to carry out the selectivity optimization. The three apices of the selectivity triangle represent isoeluotropic binary mixtures of the diluent and the modifier. A series of 7–10 experimental runs are necessary to calculate the coefficients of the response function. The chromatographic optimization function (COF) describes the resolution between pairs of compounds inside the triangle (the factor space). Overlapping of these maps permits the selection of the optimum mobile phase. It must be pointed out that the selectivity triangle can be used with any three parameters. In this way, Tecklenburg *et al.* [26] plotted plate length, binary solvent composition and analysis time to optimize the TLC separation of fifteen steroids. A similar plot has been published recently for the separation of thirteen pesticides [27].

The ORM technique has been adapted to HPTLC by Issaq *et al.* [28] for the separation of four naphthalene derivatives on C_{18} plates. Bayne and Ma [29] used the resolution function

$$R_s(j, j+1) = 2(D_{j+1} - D_j)/W_j + W_{j+1} \quad (9)$$

where D_j and D_{j+1} are migration distances of two adjacent spots and W_j and W_{j+1} are the spot diameters. As an NP system with propylamino-bonded silica gel plates was utilized, the diluent was hexane and benzene (group 7 of Snyder's selectivity triangle), chloroform (group 8) and THF (group 3) were the selected modifiers. As usual in HPLC, a Scheffe's second-order polynomial was used for predicting the resolution of each pair of adjacent spots:

$$Y = A_1X_1 + A_2X_2 + A_3X_3 + A_1A_2X_1X_2 + A_1A_3X_1X_3 + A_2A_3X_2X_3 \quad (10)$$

where Y is the response, X_i the proportions of solvents 1, 2 and 3 with $X_1 + X_2 + X_3 = 1$, A_i are the expected responses for pure components and A_iA_j are synergistic coefficients. Ten experiments were carried out for the eleven dyes of interest and the optimum was located. The authors compared the results with those obtained with the ideal separation (*IS*) function they advocated previously.

Bayne and Ma [30] used statistical mixture experiments to find the best solvent system to separate twelve structurally related benzo[*a*]pyrene metabolites. Starting with n solvents an $n - 1$ dimensional simplex was defined. Preliminary tests were carried out to estimate the solvent strength capable of yielding R_F values of the solutes within a selected range. Some regions were of no interest and truncations were performed, which yielded a polyhedron. As the authors considered five solvents, the domain was a truncated four-dimensional simplex. The separation response model had fifteen coefficients and five additional runs were performed to estimate the experimental error. A total of 20 runs were required. Response functions were tested and four were discarded [maximizing overall distances, minimizing inverse distances, maximizing a function based on the difference ln $(R_{F_j} - R_{F_i})$, maximizing adjoining distances]. All these functions exhibited failures when eccentric spots were observed. The ideal response function is the sum of an ideal spacing term and an ideal spread term. The ideal separation of q components would have R_F values equally spaced on the unit interval (0–1). The ideal value for the jth ordered R_F value would be $(j - 1)/(q - 1)$. The idea is similar to that of De Spiegeleer *et al.* [24]. To account for spreading, Bayne and Ma [32] suggested the use of the standardized fourth central moment of the R_F values:

$$b_2 = (M_4/M_2)^2 \tag{11}$$

For q components equally spaced

$$B_2 = 3(3q^2 - 7)/[5(q - 1)(q + 1)] \tag{12}$$

and

$$IS = \left(\sum [(R_F)_j - (j - 1)/(q - 1)]^2 + (b_2 - B_2)^2 \right)^{1/2} \tag{13}$$

The aim is to reach the lowest value of *IS*. The search considered 41 469 cases!

ORM and *IS* methods resulted in different mobile phase compositions. From the authors' conclusion, the ORM method focuses on the separation of the nearest pair of spots whereas the *IS* approach maximizes the overall separation of all spots.

2.7. Statistical approach

Computer-assisted multivariate techniques offer the possibility of evaluating all retention data simultaneously. Principal component analysis (PCA) provides an approximation of a data matrix. In PCA one considers each row in the data matrix to be a point in a multi-dimensional space with coordinates defined by the values corresponding to the appropriate n columns in the data matrix. Each solute is treated as a point in a space defined by its retention coordinates along the different solvent composition axes. The PCA extracts axes (or eigenvectors) that best span the data

matrix. The first eigenvector is computed such as the sum of the magnitudes of the projections of all points on that vector is a maximum. The second eigenvector is chosen orthogonal to the first so that as much of the remaining variation lies along this vector. The data matrix is thus decomposed into two matrices, the row cofactor matrix and the column cofactor matrix.

Cserhati and co-workers [31–33] used PCA and spectral mapping techniques to optimize the selectivity of mixed packings in amino acid analysis. Glycine and glutamine give rise to severely overlapped zones [34] and from PCA results together with target transformation quantification, capabilities were estimated and compared with the Kalman filter. Two recent papers examined the separation of steroids on silica gel with fifteen mobile phases [35] and on both silica gel and RP-18 plates [36]. It permits the mobile phases to be selected that provide the highest selectivity.

A Plackett–Burman factorial design at two levels has been proposed by Olsson *et al.* [37] in lipid analysis. In this mode a plot of principal properties of organic solvents was drawn in the form of a quadrant where the axes are linear combinations of those physical variables. Two solvents were chosen from each of the quadrants, one near the origin (low level, $-$) and one far from the origin ($+$ level). These factors were varied together with chromatographic conditions. From this screening procedure a principal component map of the design space is drawn, followed by a multivariate regression model.

2.8. Gradient in TLC

Markowski [38] has developed equations to predict R_{F_g}, *i.e.*, the R_F value of a solute chromatographed under stepwise gradient conditions. A binary mobile phase is utilized in such a way that the total volume introduced in the layer is equal to the void volume. A relative resolution is selected as a criterion where the distance between spots and spreading of a solute spot in R_F units are involved. The program is written in BASIC.

3. PLANAR CHROMATOGRAPHY: SPECIAL TECHNIQUES

3.1. Continuous development

In this mode solvent is allowed to evaporate from the end of the plate and spots continue to migrate until they reach the end of the plate or the plate is removed from the solvent.

Extensive work has been performed by Nurok [39]. The distance migrated by a solute in continuous development TLC is given by a modification of eqn. 1:

$$M_D = \frac{1}{1 + \exp(a \ln X_s + b)} \left[\frac{l^2 - 2lx_0 + \kappa t_l}{2l} \right] \tag{14}$$

where l is the solvent path length, x_0 the spotting distance, κ the solvent velocity constant and t_l the analysis time.

Plots of M_D *versus* X_s permit solvent systems to be compared. To draw the plots l is arbitrarily specified and t is selected such that the least retained solute migrates to the end of the fixed l at the highest mole fraction of X_s. A glance at this plot permits the variation in selectivity to be checked.

3.2. Two-dimensional TLC

In this mode the usual approach is to make use of two developments along two orthogonal directions using two different mechanisms, provided that the sample is spotted in the corner of a square plate. The worst situation is that where all spots lie on a straight line, which means a high degree of correlation. To exploit the capabilities of two-dimensional TLC fully, spots would be spread over the whole plate. Clearly, the larger the spreading the less is the correlation. This is the basis of a very simple strategy proposed by De Spiegeleer *et al.* [40]. Each spot is located and identified by its coordinates x and y and a correlation coefficient R provides a measure of the linearity (or similarity) of the systems. The data matrix contains the hR_F ($R_F \times 100$) values of the k components in the n different chromatographic systems. The correlation matrix of these systems ($n \times n$) is calculated. The lowest absolute value gives the best combination of systems:

$$D\ (k \times n) \rightarrow C\ (n \times n) \rightarrow \min |R| \tag{15}$$

To obtain a percentage value, the correlation criterion is expressed as $100(1 - R)\%$. Silica gel HPTLC plates were used and eleven mobile phases tested. The selection is performed by searching for the lowest absolute correlation coefficient.

Gonnord *et al.* [41] previously used x and y coordinates and proposed two functions:

$$D_A = \sum_{i=1}^{k} \sum_{j=i+1}^{k} [(x_i - x_j)^2 + (y_i - y_j)^2] \tag{16}$$

$$D_B = \sum_{i=1}^{k} \sum_{j=i+1}^{k} \frac{1}{(x_i - x_j)^2 + (y_i - y_j)^2} \tag{17}$$

where D_A sums the square of all possible distances between any pair of spots, the aim being to maximize D_A, and D_B sums the inverse of these distances, the aim being to minimize D_B.

D_B would be undefined for unresolved pairs which are either eliminated or replaced by a distance equal to the average spot width. The response function was tested with nineteen amino acids and the optimization according to D_B yielded a better resolved chromatogram. It must be noted that Bayne and Ma [30] pointed out that one eccentric point may dominate the distance measure. Nurok *et al.* [42] used modifications of D_A and D_B in the two-dimensional TLC separation of steroids. *DF* and *IDF* [43] are of the same form as D_A and D_B but use distances rather than the squares of distances and the *PRF* which is defined by

$$PRF = \sum_{i=1}^{k-1} \sum_{j=i+1}^{k} \ln \left(\frac{S_D^{ij}}{S_D^{spec}} \right) \tag{18}$$

where S_D^{ij} is the actual spot separation and S_D^{spec} is the desired spot separation. All solute pairs with $S_D^{ij} > S_D^{spec}$ are assigned a value of S_D^{spec} and have a zero contribution to the *PRF*. The continuous development mode was selected and the different M_D

values were calculated. Plots of computed migration for each steroid *versus* mole fraction of the polar modifier were drawn and visual inspection permitted the scatter of the spots to be checked. According to Nurok [39], *IDF* is less sensitive than *DF* to the presence of poorly resolved pairs.

Visual inspection is difficult to handle since 1681 chromatograms were simulated. To overcome this problem, Steinbrunner *et al.* [44] constructed contour diagrams (Fig. 4). In these diagrams the solvent compositions for the two developments are independent variables and spot separation is the dependent variable. The curves are isoresponse curves for the distance between the most poorly separated pair of solutes. The darkened area indicates the optimum solvent composition. Good agreement was claimed between the simulated and the experimental chromatograms on a dual plate consisting of a strip of C_{18} layer adjacent to silica gel.

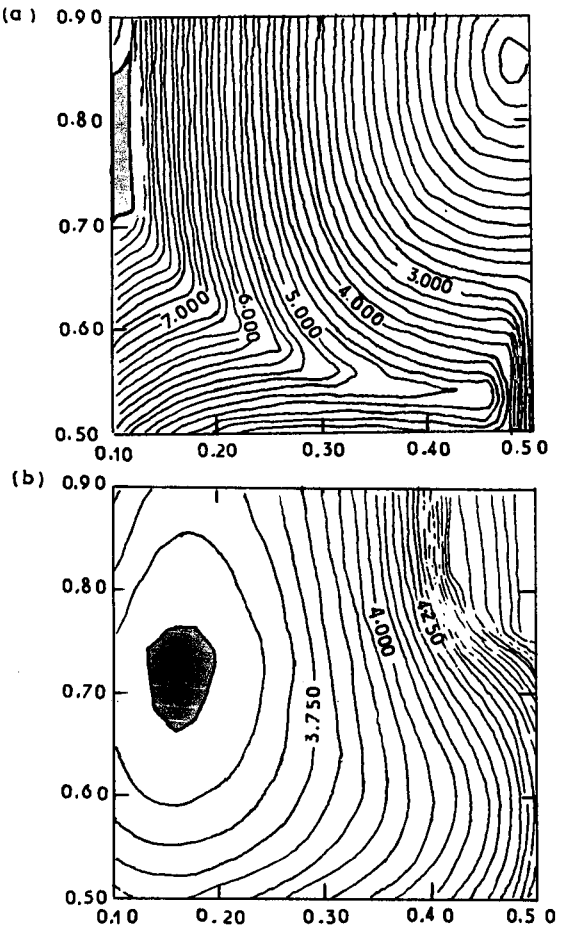

Fig. 4. Two-dimensional contour diagram for the separation of steroids on a dual-phase plate. The shaded area represents the region of the solvent domain where all solutes are separated by an appropriate distance (reprinted from ref. 44, with permission).

However, in our experience discrepancies occur between simulated and experimental runs because a small gap exists between the two layers. In the second development the NP-type solvent is strongly eluting the solutes on the C_{18} layer, which acts as a concentration zone. Solutes are located in the solvent front and spots are elongated perpendicular to the development direction. On reaching the interface between the two layers some mixing occurs, resulting in disturbed zones. It would be very valuable to use a homogeneous plate and polar bonded phases are potentially useful.

4. CONCLUSION

Compared with HPLC, TLC looks simple and rapid. However, in both instances the optimization procedures are time consuming. With the notable exception of the work of Nurok *et al.* [42] little has been done on two-dimensional TLC and continuous development and nothing has appeared on computer-assisted methods for automated multi-development (AMD). Similarly, procedures for the reversed-phase mode are scarce and nothing has appeared on optimization with cyano-bonded phases, which look promising as they can be used in both NP and RP modes [45].

At present silica gel packings are generally considered and the selection of mobile phase is more tedious in TLC than in HPLC owing to the possible solvent demixing and front formation. As it is very difficult to differentiate between spots in the R_F range 0–0.1, the retention of solutes should be limited to the range 0.1–0.8, which means in the ideal case a k' range of 0.25–9. From compilations in the literature, two strategies are utilized: either keeping the solvent simple and considering binary mixtures only, or tuning selectivity by additing more solvents, thus leading to very complex mixtures. In the first instance a limited number of experiments are required (theoretically two) and a window diagram is simple to look for separation and peak cross-overs. A large amount of data is available from the literature but the experimental conditions are not very often clearly indicated. In the second instance the PRISMA model looks powerful.

Some of the criteria proposed for computer-assisted methods in HPLC have been utilized in TLC optimization. In our opinion, resolution-based criteria which make use of spot width are meaningless as the plate count is not constant in TLC. The approach proposed by De Spiegeleer *et al.* [24] looks well suited for TLC.

For the same purpose the *CRF* function should be tried with a procedure other than the simplex method. As visual inspection is still very often used in PC, the analyst has no idea of the peak shape and peak separation is obviously the most useful parameter. When dealing with sample mixtures containing different amounts of solutes, the discrimination factor [46] would be used as a criterion.

REFERENCES

1 G. Guiochon, M.-F. Gonnord, A.-M. Siouffi and M. Zakaria, *J. Chromatogr.*, 250 (1982) 1.
2 G. Guiochon, L. A. Beaver, M.-F. Gonnord, A.-M. Siouffi and M. Zakaria, *J. Chromatogr.*, 255 (1983) 415.
3 G. Guiochon, F. Bressolle and A.-M. Siouffi, *J. Chromatogr. Sci.*, 17 (1979) 368.
4 P. L. Smith and W. T. Cooper, *Chromatographia*, 25 (1988) 55.
5 M. Righezza and A.-M. Siouffi, *Analusis*, 12 (1984) 535.

6 A.-M. Siouffi, M.-F. Gonnord, M. Righezza and G. Guiochon, in *Proceedings of the International Symposium on TLC with Special Emphasis on OPLC, Szeged, Hungary, September 1984*, Labor MIM, Budapest, 1985, p. 232.
7 J. J. Issaq and K. E. Seburn, *J. Liq. Chromatogr.*, 12 (1989) 3121.
8 B. Oscik-Mendyk, *J. Liq. Chromatogr.*, 12 (1989) 891.
9 Sz. Nyiredy, C. A. J. Erdelmeier, B. Meier and O. Sticher, *Planta Med.*, 51 (1985) 241.
10 K. Dallenbach-Toelke, Sz. Nyiredy, B. Meier and O. Sticher, *J. Chromatogr.*, 365 (1986) 63.
11 Sz. Nyiredy, K. Dallenbach-Toelke and O. Sticher, *J. Planar Chromatogr.*, 1 (1988) 336.
12 L. R. Snyder, *J. Chromatogr. Sci.*, 16 (1978) 223.
13 J. L. Glajch and J. J. Kirkland, *Anal. Chem.*, 54 (1982) 2593.
14 M. Matyska and E. Soczewinski, *J. Planar Chromatogr.*, 3 (1990) 144.
15 D. Nurok and M. J. Richard, *Anal. Chem.*, 53 (1981) 563.
16 M. Matyska and E. Soczewinski, *J. Planar Chromatogr.*, 3 (1990) 264.
17 M. Matyska, M. Dabek and E. Soczewinski, *J. Planar Chromatogr.*, 3 (1990) 317.
18 B. Oscik, *J. Liq. Chromatogr.*, 8 (1985) 1363.
19 R. J. Laub and J. H. Purnell, *J. Chromatogr.*, 112 (1975) 71.
20 Q.-S. Wang, R.-Y. Gao and H.-Y. Wang, *Chromatographia*, 28 (1989) 285.
21 S. Turina, in R. E. Kaiser (Editor), *Planar Chromatography*, Vol. 1, Hüthig, Heidelberg, 1988, p. 15.
22 J. C. Berridge, *J. Chromatogr.*, 485 (1989) 3.
23 L. G. Sabate and X. Tomas, *J. High Resolut. Chromatogr. Chromatogr. Commun.*, 7 (1984) 104.
24 B. J. M. De Spiegeleer, P. H. M. De Meloose and G. A. S. Seghers, *Anal. Chem.*, 59 (1987) 62.
25 J. L. Glajch, J. J. Kirkland, K. M. Squire and M. M. Minor, *J. Chromatogr.*, 199 (1980) 57.
26 R. E. Tecklenburg, Jr., G. H. Fricke and D. Nurok, *J. Chromatogr.*, 290 (1984) 75.
27 Q.-S. Wang and H.-Y. Wang, *J. Planar Chromatogr.*, 3 (1990) 15.
28 H. J. Issaq, J. R. Klose, K. L. McNitt, J. E. Haky and G. M. Muschik, *J. Liq. Chromatogr.*, 4 (1981) 2091.
29 C. K. Bayne and C. Y. Ma, *J. Liq. Chromatogr.*, 12 (1989) 235.
30 C. K. Bayne and C. Y. Ma, *J. Liq. Chromatogr.*, 10 (1987) 3529.
31 G. Gullner, T. Cserhati, B. Bordas and M. Szogyi, *J. Liq. Chromatogr.*, 9 (1986) 1919.
32 T. Cserhati, *Chromatographia*, 25 (1988) 908.
33 T. Cserhati and B. Bornas, *J. Chromatogr.*, 286 (1984) 131.
34 S. C. Rutan and C. B. Motley, *Anal. Chem.*, 59 (1987) 2045.
35 H. Lamparczyk, R. J. Ochocka, P. Zaricki and J. P. Zielinski, *J. Planar Chromatogr.*, 3 (1990) 34.
36 G. Windhorst, J. Kelder and J. P. De Kleijn, *J. Planar Chromatogr.*, 3 (1990) 300.
37 U. Olsson, P. Kaufmann and B. G. Herslof, *J. Planar Chromatogr.*, 3 (1990) 55.
38 W. Markowski, *J. Chromatogr.*, 485 (1989) 517.
39 D. Nurok, *LC · GC Int.*, 1 (1988) 28.
40 B. De Spiegeleer, W. Van Den Bossche, P. De Merloose and D. L. Massart, *Chromatographia*, 23 (1987) 407.
41 M.-F. Gonnord, F. Levi and G. Guiochon, *J. Chromatogr.*, 264 (1983) 1.
42 D. Nurok, S. Habibi-Goudarzi and R. Kleyle, *Anal. Chem.*, 59 (1987) 2424.
43 E. K. Johnson and D. Nurok, *J. Chromatogr.*, 302 (1984) 135.
44 J. Steinbrunner, D. J. Malik and D. Nurok, *J. High Resolut. Chromatogr. Chromatogr. Commun.*, 10 (1987) 560.
45 W. Jost and H. E. Hauck, in R. E. Kaiser (Editor), *Proceedings of the 2nd International Symposium on Instrumental HPTLC, Würzburg, 1985*, Institute for Chromatography, Bad Dürkheim, 1985, p. 83.
46 M. Z. Elfallah and M. Martin, *Analusis*, 16 (1988) 317.

Journal of Chromatography, 556 (1991) 95–110
Elsevier Science Publishers B.V., Amsterdam

CHROM. 23 231

New approach for calculating ideal chromatograms from arbitrary composite distribution isotherms

H. POPPE
Laboratory for Analytical Chemistry, University of Amsterdam, Nieuwe Achtergracht 166, 1018 WV Amsterdam (Netherlands)

ABSTRACT

A new method for the calculation of ideal chromatograms is presented. It is based on the solution of the eigenvector problem as occurs in the consideration of system peaks. As the resulting eigenvectors are tangential to the paths governing the shape of ideal chromatograms, these paths can be found by following the direction of the eigenvectors in composition space, this process being equivalent to the numerical integration of simultaneous differential equations, with the eigenvectors as the derivatives. The method has the advantage that new shapes of composite isotherms do not require more mathematical effort than inserting the corresponding expressions in the program source. So far the method has been developed for describing the phenomena at the front and the rear of a rectangular band that still has a region where the injected concentration is preserved. However, the application to fully deformed bands peaks and to systems with more than two components seems entirely feasible.

INTRODUCTION

As argued by Guiochon and Katti [1], the prediction of overloaded chromatograms can be approached from two extremes: on the one hand one can start from the solution of the chromatographic transport equations for the infinite dilution, linear situation, and treat the non-linearity as a perturbation to that solution. The treatment by Haarhof and van der Linde [2] has been shown to be extremely useful in that respect [1,3–5]. On the other hand, one can start with the solution for dispersionless or ideal chromatography. Often, *i.e.*, in heavily overloaded situations, this gives already [1,6,7] a fairly accurate impression of the chromatogram that is obtained when dispersion is also active both in experiment and in simulations of the process. A next step could be to try to correct these ideal chromatograms for dispersion, without resorting actually to carrying out experiments or simulations, which are both time consuming and expensive.

As the first approach is limited to relatively small overload (the perturbation should be small), the second approach is probably of great future importance for the development of preparative liquid chromatography (LC). It is therefore very unfortunate that ideal solutions in themselves can be calculated only for a few specific cases.

0021-9673/91/$03.50

The best known solution of the ideal chromatography problem is probably that given decades ago by Helfferich and Klein in their classic book [8] on multi-component chromatography. However, their solution with the *h*-transform applies only to the case of so-called stoichiometric exchange, with constant selectivity coefficients. This is an appropriate model for ion exchange, but a great variety of phase systems in use in high-performance liquid chromatography (HPLC) cannot be forced into this model.

Recently, Golshan-Shirazi and Guiochon [6,7,9] performed the tremendous task of solving the ideal chromatography problem for a two-component competitive Langmuir equilibrium. First [6], they derived the solution in a new way, solving the equation for the "paths" (see Theory section) with the Clairaut and Offord equations, and then derived the complete elution pattern for the two components, for different degrees of separation. Second, they compared these results with an adapted version of the *h*-transform (already indicated as being useful by Helfferich and Klein [8]) and showed mathematical equivalence [9].

As indicated by them, the prospects for using this analytical approach for more complicated cases, *e.g.*, for more complicated isotherm expressions and for three- or more-component cases, look poor. The analytical equations become very complicated, and it is probably too much to expect that the path analysis can be performed in such cases.

The approach taken during this work was to use a numerical version of the path analysis.

THEORY

Paths and hodogram

As explained at length in Helfferich and Klein's book [8], the concept of coherence is central to the understanding of ideal multi-component chromatography with interference. Briefly, it appears that coherence is the ultimate situation towards which these systems tend to develop. Coherence means that a given concentration of a component is accompanied by the same set of concentrations of the n-1 other components, although the time and position of the observation point may vary. A propagation velocity is associated with each of such sets of concentrations.

These coherent changes in concentrations may occur in two versions: those with finite slope of concentration against time (or position) curves, *i.e.*, continuous changes, and abrupt, *i.e.*, discontinuous changes. Which one occurs depends on the mathematical properties of the system, which are complicated and abstract to formulate, but can be derived easily from physical principles, as will be discussed below. However, the continuous changes, indicated by Helfferich and Klein [8] as diffuse boundaries, will be discussed first.

When a given concentration of one component is associated with a given set of n-1 other concentrations, this represents a point in an n-dimensional space, the composition space. A two-dimensional example is shown in Fig. 1. A diffuse boundary is represented in this composition space by a line, each point of which connects a concentration with n-1 others. A collection of such lines may be called a hodogram. Each point on such a line, called a path (or Γ [10]), is associated with a retention parameter such as the equivalent of the capacity factor k' or of the R_F value. This

retention parameter tells how fast the particular point will move through the column in relation to the mobile phase velocity. When the coherent boundary is present immediately after the injection (this often occurs at the rear of the peak), the position in the column after a given time, or the retention time, *i.e.*, the time of occurrence of that concentration at the column exit, can be predicted by familiar equations such as

$$z(c_1,c_2,c_3...c_n) = vtR_F = vt \cdot \frac{1}{(1 \pm k')} \tag{1}$$

$$t(c_1,c_2,c_3...c_n) = (L/v)(1 + k') = (L/v) \cdot \frac{1 - R_F}{R_F} \tag{2}$$

where

$(c_1,c_2,c_3...c_n)$	represents the particular combination of concentrations;
v	is the mobile phase velocity;
t	is time, from injection to the moment that the combination $(c_1,c_2,c_3...c_n)$ elutes;
L	is the column length
z	is the position in the column of the combination $(c_1,c_2,c_3...c_n)$
k'	is the "capacity factor"; and
R_F	is the retardation factor.

It is important to distinguish the "capacity factor" k' as used here from the meaning usually associated with it, namely the ratio of amounts of a solute in the stationary and mobile phases. Here the value of k' just describes the migration velocity of the particular point in concentration space.

Consider a simple case of a transition from one composition, A, to another, B, *i.e.*, when both points A and B are on the same path, and B is the injected solution (with a long injection block and chosen carefully to be on the path of A) and A is the composition of the mobile phase. The retention along the path will vary (see the Langmuir hodogram in Fig. 1). Assume that it continuously decreases (it does for the Langmuir case when both concentrations in B are larger) when moving from A to B. Drawing the rear of such a peak presents no problems; the concentrations close to B have moved fast, those close to A have moved less and a "reasonable", *i.e.*, physically acceptable shape is obtained. However, at the front the procedure would yield double-valued concentrations, a curve that retreats in space or time, which is physically unacceptable.

The mathematics of such phenomena is that of shock waves, as discussed by Golshan-Shirazi and Guiochon [6]. It is abstract and difficult. In this paper the mathematical approach to deal with this will not be taken, rather physical arguments will be used to handle situations such as these. However, it should be recognized that eventually, if the approach given here is to be of much use, formal rules for substituting the physical reasoning often applied here have to be found in the literature or be derived.

Anyway, rather than an impossible retreating diffuse boundary, a steep concentration change, discontinuity, from B to A, occurs at the front of the band. The analysis of it is easiest when B represents the composition of the injected solution, and

is not yet deformed after or before the shock. Its velocity can then be derived from consideration of mass preservation. This is most easily done when graphs (such as used here) plot total concentration against position in column, or when elution functions of mobile phase concentrations against time are used. In both instances the position of the shock can be found as the mean value of the found positions or times, respectively (retreating), as this is the position of the shock that gives the proper amount of material. "Mean value" is to be understood here as the integral of position integrated with respect to concentration, divided by concentration difference. That this gives a mass-preserving solution can be derived as follows.

The retreating solution of the differential equation is one that "conserves mass"; the total amount present does not change with time. This amount equals the integral with respect to position of the total concentration, or of the mobile phase concentration with respect to time. Taking the average position or time in both graphs therefore does gives the proper location of the shock.

However, this reasoning can be applied only in this simple form when the two extreme composition points of the shock remain the same during column transport; if there is no flat profile on both sides, the intensity of the shock is changing all the time and a more intricate form of the mass balance has to be applied.

The Followpath procedure

In a previous paper [11] and a paper by Golshan-Shirazi and Guiochon [12] it was discussed how the eigenvectors and eigenvalues describe the properties of system peaks and the possibilities for indirect detection, in both chromatography and electrophoresis. In the following we shall limit the discussion to chromatography. Briefly, it was shown [11,12] that, for small deviations from the mobile phase composition, the distribution equilibrium in general can be described by a matrix equation, given the vector, $\boldsymbol{c}_s$, consisting of the changes in each of the n stationary phase concentrations $c_{s,j}$, as a function of the vector $\boldsymbol{c}_m$ of changes in the mobile phase concentrations, $c_{m,j}$:

$$\boldsymbol{c}_s = \boldsymbol{S\_from\_M} \cdot \boldsymbol{c}_m \tag{3}$$

The matrix $\boldsymbol{S\_from\_M}$ usually has n eigenvalues, λ_0 through λ_{n-1} with associated eigenvectors $\boldsymbol{e}_0$ through $\boldsymbol{e}_{n-1}$. The n values of λ represent capacity factors, k', at which the particular coherent disturbances are eluted. The set of n resulting eigenvectors describe the proportions in which the n constituents vary in concentration in each of the n disturbances. That is, if one injected a composition that differs from the mobile phase by exactly the $e_{j,i}$ values multiplied by a small number (j giving the number of the eigenvalue, i giving the number of the component to which the component of eigenvector $\boldsymbol{e}_j$ applies), it is transported as one peak with capacity factor λ_j. Injected compositions that cannot be described as one eigenvector will be split up, in general into n peaks of which the capacity factors are the λ's.

This approach has been shown [12–15] to give an adequate description of system peaks and indirect detection phenomena, which had previously puzzled many workers. However, it was also noted in the earlier paper [11] that the eigenvectors thus obtained are the tangents to the paths in the n-dimensional composition space and that they describe the coherent boundaries that would develop in ideal chromatography.

It follows that one can move approximately from one point on a path to another in its vicinity, after the eigenvector has been calculated. Thus there is a way, at least an approximate one, to find a full path starting from a given point in composition space. It consists of repeatedly computing the eigenvector and moving to a new point on the path. By starting at several points one can derive the picture of the hodogram with any degree of detail.

The program that forms the basis of this report relies on a procedure called "Followpath", taking a starting solution, "**sol**", as the argument. **Sol** is a vector of n numbers (2 in the implementations described in this paper), giving the concentrations in the mobile phase. With any given expression for the distribution of the n components to the stationary phase (*e.g.*, Langmuir, ion-pair distribution equations) the concentrations of the stationary phase can be calculated. (A short comment on the forms used, especially the omission of certain factors such as the phase ratio and the surface necessities for a composite Langmuir adsorption is to be found at the end of this section.)

As the eigenvector treatment works with the changes in the concentrations, the derivatives of these expressions are needed. These have been obtained during this work by numerical differentiation: the concentrations of compounds $j = 0$ to n-1, $c_{m,j}$, are changed by a small amount, "eps", successively and the resulting changes in the stationary phase concentrations $c_{s,i}$ are noted. Divided by eps these form the elements $[i,j]$ of the matrix that is needed. This matrix was above indicated by "***S*_from_*M***".

Numerical differentiation has the important advantage that the study of a new type of distribution behaviour merely involves introducing other distribution equations in integral form; the often painstaking analytical differentiation to obtain all the matrix elements is not needed. The full procedure could be carried out by just using ***S*_from_*M*** with, as indicated, eigenvalues corresponding to capacity factors, k'. However, it is useful to consider also other matrices carrying the same information; these are as follows:

(i) ***M*_from_*S***, calculation of mobile phase concentration changes from stationary phase concentration changes. This is unusual; however, at least one [16] model exists where explicit expressions are obtainable only for this case. ***M*_from_*S*** is the inverse of ***S*_from_*M***, and numerical values were obtained by the Gauss–Jordan algorithm. Its eigenvalues correspond to $1/k'$.

(ii) ***T*_from_*M***, calculation of the total concentration changes (see the remark at the end of the section on expressions and units) from the mobile phase concentration changes. It is obtained by adding 1 to the diagonal elements of ***S*_from_*M***. The eigenvalues equal $k'+1$.

(iii) ***M*_from_*T***, calculation of the mobile phase concentration changes from the changes in the total concentrations. This matrix is obtained by inversion of ***T*_from_*M***. Its eigenvalues are the R_F values of the corresponding disturbances. The use of this form might be useful in cases where mass preservation is to be considered in studies involving spatial distribution, rather than elution function (see below).

It should be noted that when finding eigenvalues and eigenvectors for all these four matrices one obtains different eigenvalues [although the one set can be easily found from the other, *e.g.*, by $R_F = 1/(1+k')$], but the same eigenvectors. This is easily seen when one considers that for an eigenvector $\boldsymbol{e}_j$ with eigenvalue λ_j it holds that

$$\boldsymbol{S\_from\_M} \cdot \boldsymbol{e}_j = \lambda_j \cdot \boldsymbol{e}_j \tag{4}$$

Stationary phase and mobile phase changes are in the same proportion λ_j for all components. Thus the changes of, *e.g.*, the sum of both concentrations are also in proportion.

After the n eigenvectors have been found for the first time it is to be decided which one of these gives the direction to be followed (*e.g.*, one can choose the one with the largest capacity factor). Denoting this one by $j = f$ (f for "follow this one"), a next point on the path is found by adding the components of the vector e_f to the components of "**sol**". The size of the step is controlled by a parameter β, by which the eigenvector components are multiplied before carrying out the addition. Thus, for the two-component system considered in this paper:

$$\begin{aligned} \mathrm{sol}_0 &= \mathrm{sol}_0 + \beta \cdot e_{f,0} \\ \mathrm{sol}_1 &= \mathrm{sol}_1 + \beta \cdot e_{f,1} \end{aligned} \tag{5}$$

In fact, as the $\boldsymbol{e}_j$ emerge normalized from the eigenvector procedure (*i.e.*, the sum of the squares of the components is 1, the euclidic length is 1), the value of β is the distance travelled in composition space during such a step.

For the new point described by the new value of "**sol**", the eigenvector is again calculated, and a new step is taken in the new direction. It might occur during the Followpath procedure that the step size, β, is too large: following the tangent rather than the path curve itself is only sufficiently accurate if either the curvature is small or the step size is small. Therefore, after each tentative step it is checked if the direction indeed has changed only insignificantly.

The change in direction is measured by the correlation coefficient, r, sum of the cross-products of the elements of previous and newly considered vector (division by the square root of the euclidic lengths of both is not needed as both are 1). A value $r = 1$ corresponds to exactly the same direction. In that case the path is linear in composition space, a situation occurring with competitive Langmuir adsorption, as discussed at length by Guiochon and co-workers.

Values of r larger than 0.9999 were treated as acceptable. When smaller values occurred, the value of β was decreased repeatedly by a factor of two until a sufficiently large value of r was obtained. When r exceeded 0.99999, the step size β was doubled, in order to speed up calculations.

A rough guess of the errors made this way can be made as follows. A correlation coefficient of 0.9999 means that the angle between the vectors equals $\sqrt{(1-r)} = 0.01$ rad. Thus on each step of size β one deviates 0.01 β from the correct path. Suppose a path is a full circle (an extreme case; for useful phase systems curvature in general will not be very strong) with radius 1. One return to the point of origin there would be a deviation of 0.0628. Thus the procedure is probably accurate to better than a few percent in composition space.

The calculation of r was needed for another reason: as indicated, from each point in composition space n paths emerge (2 in this work). The eigenvalue–eigenvector procedure gives the n results in an unpredictable order, and precautions have to be taken to avoid hopping from one direction to another that is more or less orthogonal

to it. Thus, each time the relevant eigenvalue λ_f and corresponding vector $\boldsymbol{e}_f$ were identified as the one having the highest correlation, r, with the previous vector.

As indicated, the eigenvalues obtained during the iteration, either in terms of k' (when ***S*_from_*M*** is used) or in terms of R_F (when ***M*_from_*T*** is used) contain essential information; they can be used to predict either the retention time or the spatial position in the column of the specific composition point. Thus, the full information on the behaviour of the components in the phase system used is contained in an $(n+1)$-dimensional plot, composition space with an additional dimension in which the λ (k' or R_F) value is plotted. In Figs. 1, 3 and 5 this is approached by inserting the numbers for the k' values on the path lines.

The program needs additional tricks for the following reasons:

(1) To make sure that a path is followed in both directions. Thus, after a path is followed until the edge of considered composition space is reached, one has to return to the original composition and "go the other way".

(2) To make sure that the n (2 here) paths emerging form one point are plotted. Thus, *e.g.*, first the higher capacity factor (at the point of origin) is handled, and next the smaller capacity factor. Altogether, $2n$ (here 4) "rays" emanate from a point.

(3) To obtain a reasonable distribution of plotted paths over the composition space considered to be of interest. This was done here by choosing a rather arbitrary starting composition. In each of the resulting four main "rays", a stop was made when a given distance had been travelled. From there the other path was followed leading to two new rays. In this way usually a reasonably filled but not overcrowded hodogram was obtained.

Description of the distribution equilibrium

In the following the two-component composite Langmuir isotherm will be used to demonstrate the principles used here.

The concentration in the stationary phase, either per unit of surface area or per gram of adsorbent, is generally modelled as

$$c_{s,j} = \frac{K_i c_{m,j}}{1 + K_1 c_{m,1} b_1 + K_2 c_{m,2} b_2} \tag{6}$$

where the bs represent the areas covered by a mole of material. They have been the subject of interesting discussions [17], when it was noted that widely different b's for the two components can lead to intersecting isotherms, *i.e.*, at low concentration the one component is better adsorbed, whereas at higher concentrations the reverse case occurs.

In order to correlate the k' values in the column with eqn. 4, one needs in addition the phase ratio, q, *e.g.*, in square metres per millilitre of mobile phase. Altogether, one ends up with unwieldy expressions that are especially impractical in general considerations, because of the lengthy equations, and in simulations, because of increased program run times. It is our opinion that in such general discussions, as well as in simulations, it is very profitable to "normalize out" the b's in addition to q. This can be done as follows.

In the first place the concentrations in the stationary phase are defined as the

amount adsorbed in a given infinitesimal part of the column, divided by the volume of *mobile* phase in that part. As there is a constant ratio between square metres and the mobile phase volume, there is no loss of generality when doing this. The result is that k' and the distribution constant K are the same. The sum of c_m and c_s is now equal to the "total concentration" used above, c_t, total amount in an infinitesimal section of the column over the associated volume of mobile phase.

In the second place, it can be noted that the way amounts and concentrations are expressed is arbitrary. Also, different units can be used for different components. It lies at hand to multiply the concentration $c_{m,j}$ by b_j to form normalized concentrations (in both phases). Again, there is no loss in generality, and all situations can still be expressed. The Langmuir expression can then be written as

$$c_{s,j} = \frac{K_j c_{m,j}}{1 + K_1 c_{m,1} + K_2 c_{m,2}} \tag{7}$$

the K's being the same as those in eqn. 6. From this approach, which is used throughout this work, it follows, *e.g.*, that special phenomena brought about by strongly differing b values can be studied (simulation, analytical) by means of the regular model given in eqn. 7, by simply increasing the amount injected of compounds having a large b.

The advantage of this is that the great multitude of different cases met with in discussions or preparative chromatography are at least partly reduced. All situations that can be modelled, *e.g.*, by the simple composite Langmuir expressions can be represented by choosing proper values for K's and the injected concentrations.

EXPERIMENTAL

All programs were written in Turbo Pascal (Borland International, Scotts Valley, CA, USA) version 4.0. For the present two-component case the eigenvector problem was solved by solving the quadratic equation, with the procedure as described in ref. 18. For three and higher component systems the procedures ELMHES, HQR and SVDCMP from the same source were applied. A custom-written package for translating graphic calls in Turbo 4.0 into graphics commands for a laser printer was used to obtain the figures shown.

Column transport simulations were implemented according to the approach described by Golshan-Shirazi and Guiochon [19]. However, the code as described by them was first translated into Pascal, and next modified to allow the presentation of spatial distributions in the column rather than elution functions. Also, in many cases another choice of the time and position increments, Δt and Δz, was made. In those cases the numerical dispersion was made practically zero (at least for the most retained disturbance), rather than equal to a predetermined amount of dispersion, as the purpose here was to compare results from two approaches for ideal chromatography. The simulation program was thoroughly checked for conceptual or programming errors by running experiments with predictable results, such as those with only one component, or with minor disturbance injections leading to "system peaks" and indirect detection phenomena. Retentions and peak intensities as well as mass conservation agreed entirely satisfactorily (*i.e.*, deviations could be explained as the result of numerical truncations).

RESULTS AND DISCUSSION

Langmuir case

Fig. 1 gives the paths as calculated for a two-component Langmuir isotherm, according to eqn. 5, with $K_0 = 2$ and $K_1 = 3$. This result is trivial, in the sense that the lines can be much more easily calculated according to the procedure given by Golshan-Shirazi and Guiochon [6] using the Offord and Clairaut equations. Indeed, doing this produces (not shown) an identical figure.

In Fig. 1 the numbers written along the lines represent the capacity factor, k', corresponding to the retention of the path at that position. Thus, if the path exists from the very start of the elution, the position of the composition point in the chromatogram, or in the column at a given time, can be predicted. This concept, in combination with the general method for finding the paths, would allow the prediction of the column history for any kind of composite distribution isotherm.

The implementation of this concept is, however, not without difficulties, and at present requires the application of intuitive notions or physical insight. This will be illustrated while discussing the results obtained with this form of isotherm, although in themselves these results are no more than a partial reproduction of the results of Golshan-Shirazi and Guiochon [6] who derived the complete set of expressions for the elution curves of a still partially mixed band.

In Fig. 1 point I represents a hypothetical composition of an injected plug. This

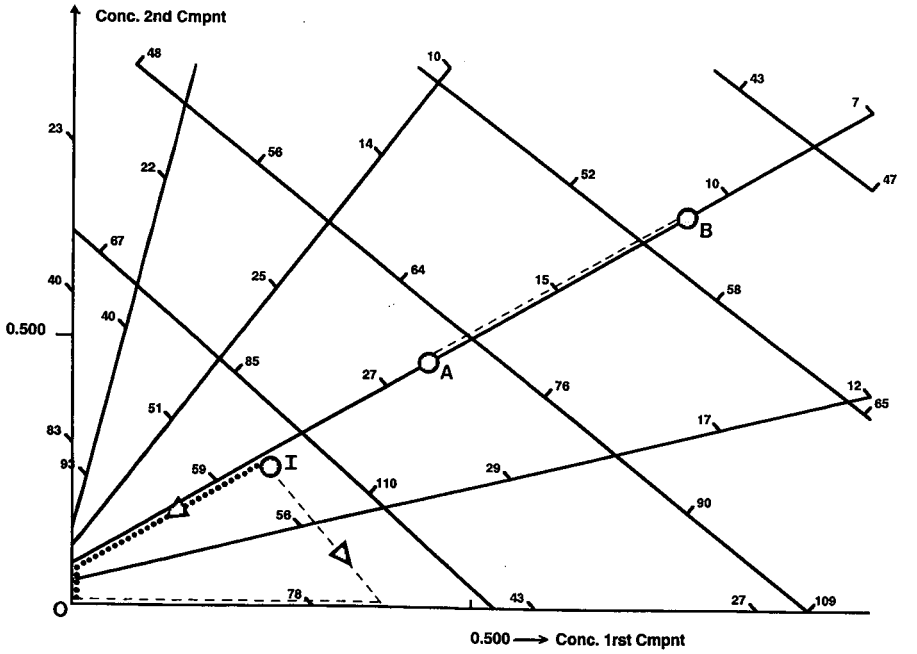

Fig. 1. Hodogram for Langmuir isotherm, according to eqn. 7, with $K_0 = 2$, $K_1 = 3$. Numbers on the path lines are capacity factors, multiplied by 100. Concentrations on axes are mobile phase concentrations. Cmpnt = Component.

is supposed to be already in equilibrium with the stationary phase, so that in fact much more is injected. (This rather artificial modelling of injection is chosen in these first exercises just to facilitate insight; in later, more practical, applications one should of course consider the influx of a solution into an empty column.)

The rear of this plug represents a transition in the composition space from the origin, O, the empty solvent, to I; at the front the opposite transition occurs. For such transitions, following the paths in the hodogram, there are in general two routes (in fact, the Langmuir case gives three routes, as can be seen, but one is ruled out for physical reasons). Which way is taken depends on whether the front or the rear of the peak is considered. At the very rear of the band, still close to the origin, one should find a path with the highest capacity factor. That is the path coinciding with the vertical axis ($c_{m,0} = 0$), corresponding to pure component 1 (the most retained one). This path is followed until arrival on the intersection with the path through I. Next this mixed band path is followed; see the dotted lines in Fig. 1 starting at point I.

Note that on both paths the capacity factor decreases, and position increases, while following the path, and thus approaching the original injected concentration at the (still) flat top of the band. This indicates that no physical impossibilities are implied by this solution and indeed a diffuse boundary is described.

As noted by Golshan-Shirazi and Guiochon [9], the difference in k' value for the two paths at the same composition (the intersection point) explains the occurrence of a plateau of constant concentration of component 1, where it seems that this component leaks out of the mixed band.

It should be noted that in the algorithm (Followpath) that produced the circles in, *e.g.*, Fig. 2, the opposite route was followed, starting from the injected concentrations. For the description of the rear of the band the path with the smallest capacity factor was first followed, making sure that both concentrations decreased. When the concentration of the least retained component was found to be zero (the procedure was targeted to reach that point), the procedure switched to the alternative path, that following the vertical axis in Fig. 1, leading to a classical one-component Langmuir boundary.

In the algorithm for the calculation of the front of the band the path with the highest capacity factor was first followed, making sure that the concentration of component 1 decreased, that of 0 increased, because (one of the physical reasonings resorted in this work to make the system work) it is known that by displacement a concentration effect on the less retained component occurs. When the concentration of the most retained component was found to be zero, the procedure switched to the alternative path, that again giving a classical one-component Langmuir boundary, albeit retreating. This route corresponds to that indicated by the dashed lines starting at point I in Fig. 1.

All R_F values found were multiplied with the time (velocity assumed to be 1), added to the starting position of the rear or front, respectively, and plotted in Fig. 2 as circles. Fig. 2 shows the graphical implementation in terms of column "maps" for the two components. The full line gives the results of a simulation with this distribution equilibrium. Best efforts were made to make dispersion as small as possible in this simulation experiment; for one thing it takes several hours to reach this point of $t = 4000$. Superimposed on this are circules that were calculated from the Followpath approach. As the starting point the injection was taken.

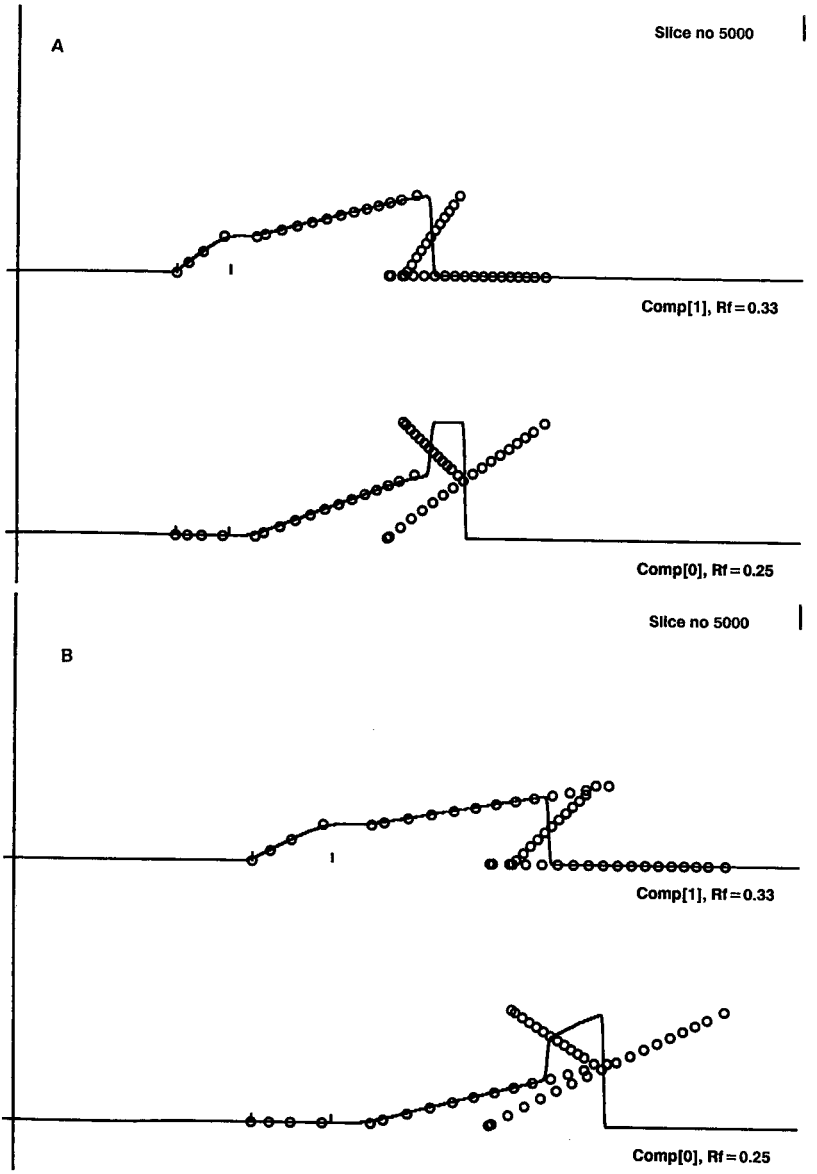

Fig. 2. Distribution of the two components along the length of the column after a time lapse of (A) 4010 units or (B) 6007 units, for Langmuir isotherm as in Fig. 1. Injection was done by saturating slice No. 50 (vertical line at left) to 1050 with a mobile phase with $c_0 = 0.2$ and $c_1 = 0.2$, and forcing the stationary phase concentration to be in equilibrium with that mobile phase. Mobile phase velocity assumed to be 1 slice per time unit. Component concentrations plotted are total concentrations, $c_t = c_s + c_m$. Full line, results of Guiochon-type simulation; circles, results from path calculation.

As can be seen in Fig. 2, the Followpath approach yields a fairly accurate estimate of the distribution functions for the components. Where diffuse boundaries occur, the (full) lines obtained by simulation are a very good match with the circles

obtained with the Followpath procedure. At the front of the peak the two lines formed by the circles represent physically impossible retreating lines. However, the shocks given by the numerical simulation are indeed at the average position of the circles. Note that two paths follow the axis of component 0 or component 1 in the hodogram, *i.e.*, the circles in the column map in Fig. 2 are on the axis for one of the components.

However, as soon as the flat top of the band at the injected concentration is "eroded away" [9], the applied procedure fails (Fig. 2B). As indicated above, the shocks then no longer have a constant intensity, and their positions have to be calculated with a more complicated mass balance consideration. Also, another diffuse boundary develops. The latter can be handled in the indicated way, with the exception that its time and place of birth differ from the injection time and either front or rear of the injection plug. Rather the place and time of birth should be calculated separately.

Such problems cannot be handled yet, although we have confidence that they can be solved and that the solutions can be put into fairly general code. However, at this stage meaningful results can only be obtained for situations where the injected concentrations are still present in the band.

Quadratic Langmuir-type equilibrium expression

Guiochon's group [20] have argued that the composite Langmuir expression can be generalized by substituting polynomes in the various mobile phase concentrations for the expressions $K_i c_i$. In order to demonstrate the flexibility of our approach, we carried out calculations with such an isotherm. Its exact shape was as follows:

$$c_{s,0} = \frac{K_{00}c_{m,0} + Q_{00}c_{m,0}^2 + Q_{01}c_{m,0}c_{m,1}}{1 + K_{00}c_{m,0} + K_{11}c_{m,1} + Q_{00}c_{m,0}^2 + Q_{11}c_{m,1}^2 + Q_{01}c_{m,0}c_{m,1}}$$

$$c_{s,1} = \frac{K_{11}c_{m,1} + Q_{11}c_{m,1}^2 + Q_{01}c_{m,0}c_{m,1}}{1 + K_{00}c_{m,0} + K_{11}c_{m,1} + Q_{00}c_{m,0}^2 + Q_{11}c_{m,1}^2 + Q_{01}c_{m,0}c_{m,1}} \quad (8)$$

Followpath calculations were carried out and compared with transport simulations for such an isotherm with $K_{00} = 1$, $K_{11} = 1.5$, $Q_{00} = 2$, $Q_{11} = 3$, $Q_{01} = 1$. The results are shown in Fig. 3 as a hodogram and in Fig. 4 as a prediction of column maps (circles), together with the result of the numerical simulation (full lines).

Inspection of the hodogram shows that the paths are curves, as is to be expected. Still, the structure of the Langmuir hodogram can be distinguished. More important, on a number of paths (those with a negative slope) the retention does not change monotonously, but first goes up and then goes down. This means that, no matter if one considers the front or the rear of the band, a transition is possible consisting partly of a shock and partly of a diffuse boundary. This is similar to what occurs in the one-component case when the isotherm has a sigmoid shape, *i.e.*, the second derivative changes sign over the range of interest.

Fig. 4, given the results of the Followpath procedure in comparison with those of the simulation, clearly shows this behaviour. Considering first the rear part of the curves, coming down from the injected concentration one first has a "normal" boundary, and in this part the agreement with the simulation is very good. However,

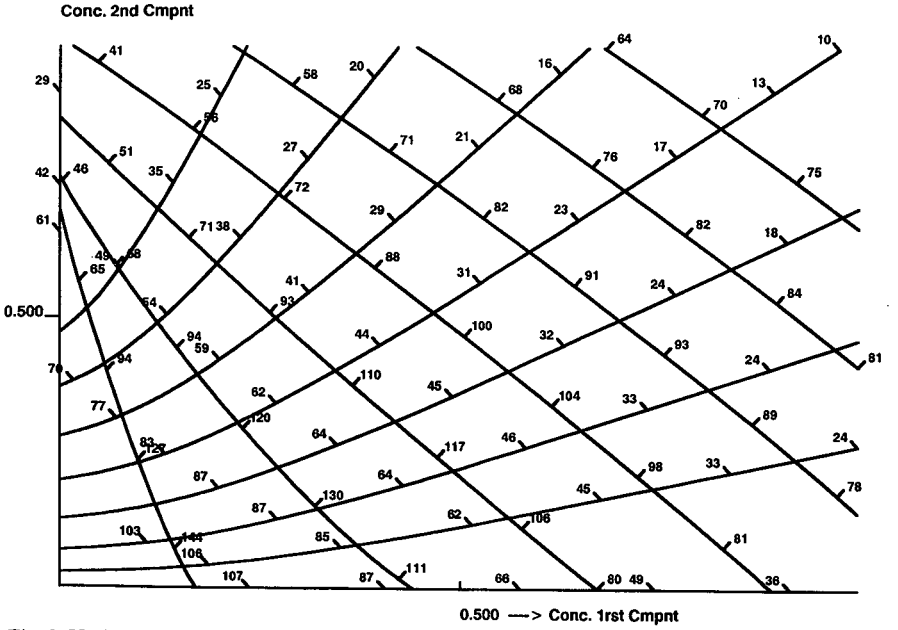

Fig. 3. Hodogram for quadratic Langmuir isotherm, according to eqn. 8, with $K_{00} = 1$, $K_{11} = 1.5$, $Q_{00} = 2$, $Q_{11} = 3$, $Q_{01} = 1$. Numbers on the path lines are capacity factors, multiplied by 100. Concentrations on axes are mobile phase concentrations.

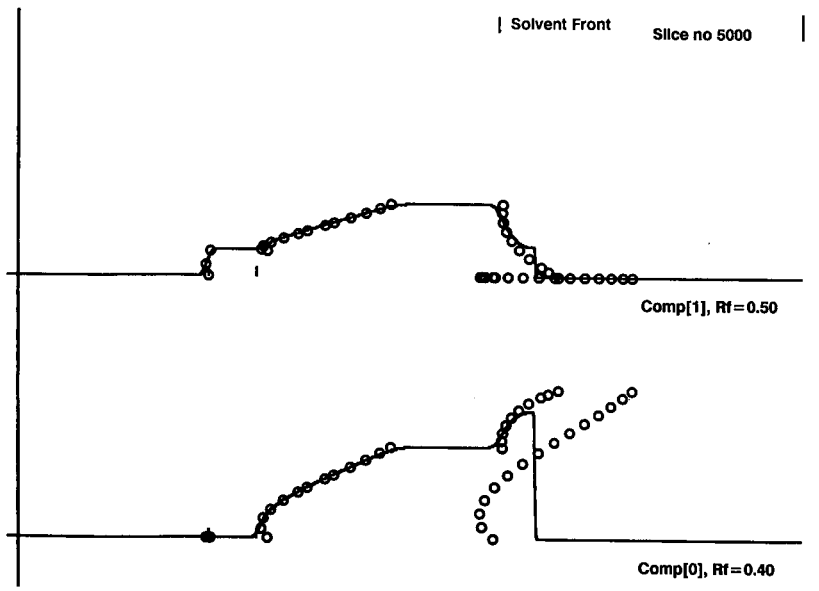

Fig. 4. Distribution of the two components along the length of the column after a time lapse of 3005 units, for quadratic Langmuir isotherm as in Fig. 3. Injection was done by saturating slice No. 50 (vertical line at left) to 1550 with a mobile phase with $c_0 = 0.7$ and $c_1 = 0.5$, and forcing the stationary phase concentration to be in equilibrium with that mobile phase. Mobile phase velocity assumed to be 1 slice per time unit. Component concentrations plotted are total concentrations, $c_s + c_m$. Full line, results of Guiochon-type simulation; circles, results from path calculation.

when the concentration of component 1 approaches zero, the curve formed by the circles changes to a retreating line, predicting a shock. This is not apparent from the simulation (full line); this is probably due to the influence of (numerical) dispersion. The line describing the transition to where both concentrations are zero (far left side of the band in Fig. 4) shows a similar behaviour. Also here the shock nature is not visible in the simulation.

The front part of the band in Fig. 4 shows reasonable agreement for the onset of the concentrated band of component 0, pushed forward by the other component. However, it can be seen that the Followpath procedure does predict a much higher concentration for component 0 than is actually observed. This can be explained as follows. The program as it is moves along the path until the concentration of component 1 is zero. However, at that point its velocity is higher than that of the shock described by the alternative path starting from the point of injection composition; the upper part of the diffuse boundary moves faster than that shock. Thus the path should have been followed up to a point P where its velocity equals that of the shock connected with the transition from P to zero.

Synergistic sorption

Another example considered is that of synergistic sorption, an adequate model, *e.g.*, for ion-pair chromatography. Here the isotherm is

$$c_0 = K_{00}c_0 + Q_{01}c_0c_1$$

$$c_1 = K_{11}c_1 + Q_{01}c_0c_1 \qquad (9)$$

where the term with Q_{01} stands for, *e.g.*, ion-pair formation and the K's for simple sorption of the constituent ions. The hodogram obtained with $K_{00} = 2$, $K_{11} = 3$ and $Q_{01} = 2$ is shown in Fig. 5.

Note that the capacity factors along the axis are constant, 2 and 3, respectively, for the two components, in agreement with the fact that when the other component is absent eqn. 9 gives simple linear partition. The curvature of the paths is striking, as is the fact that above a given concentration of 1 there appear to be no intersections with the corresponding axis.

The prediction of column maps is given in Fig. 6, again compared with the simulation experiment. As can be seen, the concentration of component 1 at the end of the band is predicted, with good quantitative agreement. Note that all paths are "natural"; there are no shocks. The paths with one component (far left and far right of the band) are vertical in the column map, as there is a constant capacity factor.

CONCLUSIONS

It has been shown that numerical procedures can be applied to derive the shape of paths in composition space, together with the corresponding retention data. The prediction of elution functions and column maps for ideal chromatography seems to be possible with this approach. The main drawback of the present implementation of the idea is that physical, more or less intuitive, arguments have to be used to decide

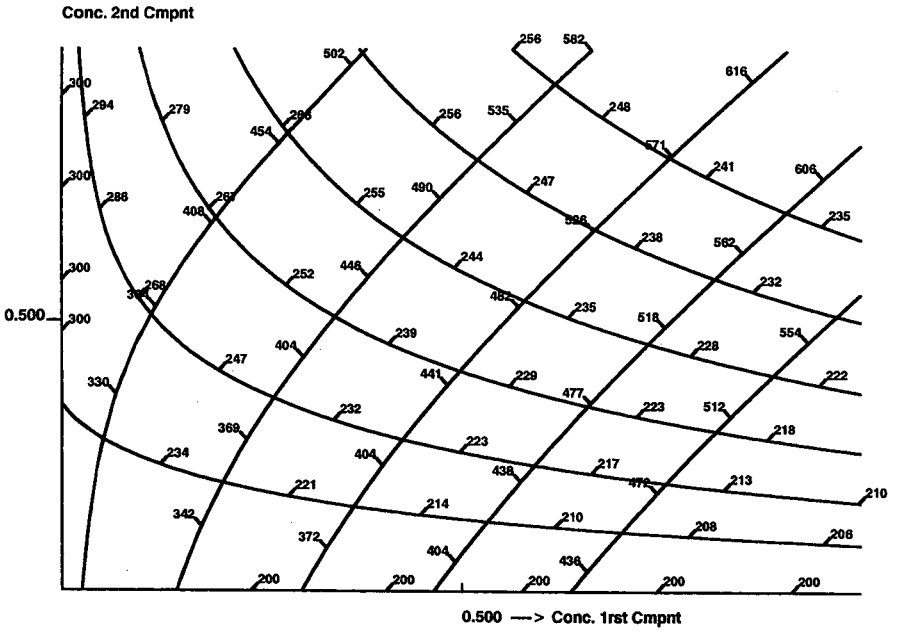

Fig. 5. Hodogram for synergistic isotherm, according to eqn. 9, with $K_{00} = 2$, $K_{11} = 3$, $Q_{01} = 2$. Numbers on the path lines are capacity factors, multiplied by 100. Concentrations on axes are mobile phase concentrations.

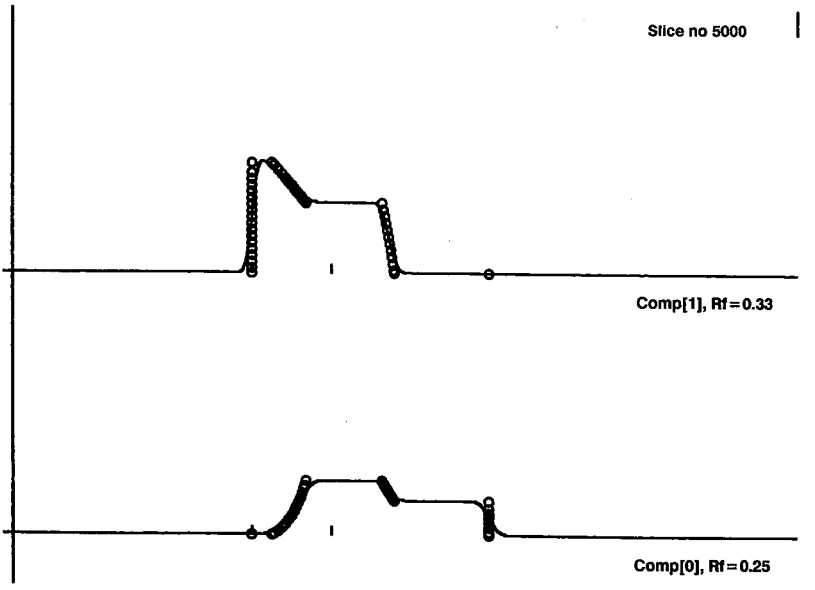

Fig. 6. Distribution of the two components along the length of the column after a time lapse of 6111 units, for synergistic isotherm as in Fig. 5. Injection was done by saturating slice No. 50 (vertical line at left) to 1050 with a mobile phase with $c_0 = 0.2$ and $c_1 = 0.2$, and forcing the stationary phase concentration to be in equilibrium with that mobile phase. Mobile phase velocity assumed to be 1 slice per time unit. Component concentrations plotted are total concentrations, $c_s + c_m$. Full line, results of Guiochon-type simulation; circles, results from path calculation.

which path is to be followed, and to what limit, and when to change path. Also, only a simple situation, just a broad band that broadens on one side and leading to displacement on the other, can be properly handled at this stage. However, it is believed that the rules for choosing paths can be formalized and put into automatic code. In addition, it is believed that the application of the calculation scheme can be extended, by proper calculation and decision schemes, to cases where, *e.g.*, a diffuse band or shock originates during the chromatographic transport.

The potential advances that could be obtained when these aims can be reached are significant. It would be possible to predict ideal chromatograms in an easy manner, by just inserting the code for the distribution equilibrium into the program, for arbitrary isotherm shapes. There also appear to be no unsurmountable problems in applying this approach to systems with more than two components.

ACKNOWLEDGEMENTS

This work would not have been possible without support from Georges Guiochon, Anita Katti and Martin Czok. They made their effective program for simulations available to me at an early stage and interesting discussions with them were an incentive to carry out the ideas in this work.

REFERENCES

1 G. Guiochon and A. Katti, *Chromatographia*, 24 (1987) 165.
2 P. C. Haarhof and H. J. van der Linde, *Anal.Chem.*, 38 (1966) 573.
3 H. Poppe and J. C. Kraak, *J.Chromatogr.*, 255 (1983) 395.
4 J. A. Eble, R. L. Grob, P. E. Antle and L. R. Snyder, *J. Chromatrogr.*, 384 (1987) 25.
5 C. A. Lucey, J. L. Wade and P. W. Carr, *J. Chromatogr.*, 484 (1989) 61.
6 S. Golshan-Shirazi and G. Guiochon, *J. Phys. Chem.*, 93 (1989) 4143.
7 S. Golshan-Shirazi and G. Guiochon, *Anal. Chem.*, 61 (1989) 462.
8 F. Helfferich and G. Klein, *Multicomponent Chromatography*, Marcel Dekker, New York, 1970.
9 S. Golshan-Shirazi and G. Guiochon, *J. Chromatogr.*, 484 (1989) 125.
10 H. K. Rhee and N. R. Amundson, *Chem.Eng. Sci.*, 27 (1972) 199.
11 H. Poppe, *J. Chromatogr.*, 506 (1990) 45.
12 S. Golshan-Shirazi and G. Guiochon, *Anal. Chem.*, 62 (1990) 923.
13 J. Crommen, G. Schill, D. Westerlund and L. Hackzell, *Chromatographia*, 24 (1987) 252.
14 E. Arvidsson, J. Crommen, G. Schill and D. Westerlund, *Chromatographia*, 24 (1987) 460.
15 J. Crommen, G. Schill and P. Herné, *Chromatographia*, 25 (1988) 397.
16 P. deBokx, in preparation.
17 S. Golshan-Shirazi and G. Guiochon, *Anal. Chem.*, 62 (1990) 217.
18 W. H. Press, B. P. Flannery, S. A. Teukolsky and W. T. Vetterling, *Numerical Recipes: the Art of Scientific Computing*, Cambridge University Press, Cambridge, 1985.
19 S. Golshan-Shirazi and G. Guiochon, *J. Phys. Chem.*, 93 (1989) 4143.
20 B. Lin, Z. Ma, S. Golshan-Shirazi and G. Guiochon, *J. Chromatogr.*, 475 (1989) 1.

Journal of Chromatography, 556 (1991) 111–118
Elsevier Science Publishers B.V., Amsterdam

CHROM. 23 237

Improved computer algorithm for characterizing skewed chromatographic band broadening

I. Method

W. W. YAU* and J. J. KIRKLAND

E. I. du Pont de Nemours and Company, Central Research and Development Experimental Station, B-228, P.O. Box 80228, Wilmington, DE 19880-0228 (USA)

ABSTRACT

A method of extracting column band-broadening parameters from skewed and noisy chromatographic peaks is derived from an exponentially modified Gaussian peak model. In the proposed method of determining peak variance and peak skew, only four peak parameters need to be measured from an experimental chromatographic peak: peak retention time, peak height, peak area and the first moment or center of gravity of the peak. This proposed method is more accurate and less susceptible to baseline noise than those previously described.

INTRODUCTION

Extracting accurate information from real chromatographic peaks is a challenging task that requires sophisticated computational approaches. It is well known that use of the Gaussian peak model gives significant errors in determining plate number, peak asymmetry factor and resolution [1]. Because of this, various studies have proposed many approaches, the most accepted being based on the exponentially modified Gaussian (EMG) model [2–6]. Uses of the EMG model have been reviewed [7][a], and the effect of random noise on the accuracy of measurements by the EMG model has been presented [8].

This paper presents a new method of extracting information from skewed and noisy peaks, based on the EMG model. This method is more accurate than previous approaches; susceptibility to errors from baseline noise is also substantially reduced. The method has been used with excellent results for more than 4 years in our laboratory for many high-performance liquid chromatographic, size-exclusion chromatographic and field-flow fractionation studies.

[a] A review of EMG function since 1983 has just been published [13].

0021-9673/91/$03.50

THEORY

The following EMG peak-shape model is used:

$$h(t) = \left(\frac{A}{2\tau}\right) \exp\left(\frac{\sigma^2}{2\tau^2} - \frac{t - t_R}{\tau}\right)[1 + \text{erf}(Z/\sqrt{2})] \quad (1)$$

where

$$Z = \frac{t - t_R}{\sigma} - \frac{\sigma}{\tau} \quad (2)$$

and

$$\text{erf}(x) = \frac{2}{\sqrt{\pi}} \int_0^x e^{-y^2}\, dy \quad (3)$$

Fig. 1 depicts the EMG peak-shape model as described by eqn. 1, where h_p is the peak height, t_p is the peak retention time, t_R is the retention time of the Gaussian input function, σ is the standard deviation of the Gaussian component, τ is the time constant of the exponential modifier and M_1 is the first moment of the skewed experimental peak. The M_1 value denotes the centroid retention time of the skewed experimental peak. Peak moments are defined by

$$\text{peak area } (A) = M_0 = \int_{\text{all } t} h(t)\, dt \quad (4)$$

$$\text{peak centroid} = M_1 = \int_{\text{all } t} th(t)\, dt / M_0 \quad (5)$$

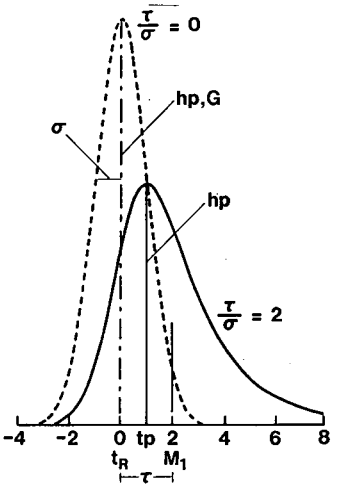

Fig. 1. Peak shape model: exponentially modified Gaussian.

With this peak-shape model, the following useful properties of peaks are described [3,9,10]:

$$M_1 = t_R + \tau \tag{6}$$

$$\text{peak variance} = \sigma^2 + \tau^2 \tag{7}$$

$$\text{peak skew} = Sk = 2\tau^3/(\sigma^2 + \tau^2)^{3/2} \tag{8}$$

$$\text{peak excess} = (3\sigma^4 + 6\sigma^2\tau^2 + 9\tau^4)/(\sigma^2 + \tau^2)^2 - 3 \tag{9}$$

and

$$\text{plate number } (N) = (t_R + \tau)^2/(\tau^2 + \sigma^2) \tag{10}$$

From the above equations, other useful properties of peaks can be defined:

$$h_p = \frac{A}{\sigma\sqrt{2\pi}} \cdot \exp(-\gamma^2/2) \tag{11}$$

where

$$\gamma = \text{peak displacement} = (t_p - t_R)/\sigma \tag{12}$$

and

$$\frac{\tau}{\sigma} = \sqrt{\pi/2}\,\exp(Z_p^2/2)[1 + \operatorname{erf}(Z_p/\sqrt{2})] \tag{13}$$

where

$$Z_p = Z\text{-value at peak} = (t_p - t_R)/\sigma - \sigma/\tau \tag{14}$$

The τ/σ and the γ values for a broadened peak of a particular Z_p value can be calculated from eqns. 12–14, as exemplified in Table I.

To conserve computer time, the $\operatorname{erf}(Z_p/\sqrt{2})$ in eqn. 13 can be calculated with the following approximation:

$$\operatorname{erf}(Z_p/\sqrt{2}) = \operatorname{erf}(x), \qquad \text{for } Z_p > 0 \tag{15a}$$

$$\operatorname{erf}(Z_p/\sqrt{2}) = -\operatorname{erf}(x), \qquad \text{for } Z_p < 0 \tag{15b}$$

where

$$x = |Z_p/\sqrt{2}| = \text{absolute value of } Z_p/\sqrt{2} \tag{15c}$$

and

$$\operatorname{erf}(x) = 1 - (a_1 t + a_2 t^2 + a_3 t^3 + a_4 t^4 + a_5 t^5)e^{-x^2} \tag{15d}$$

where

$$t = \frac{1}{1 + px}$$

$$|\varepsilon(x)| < 1.5 \cdot 10^{-7}$$

where $p = 0.3275911$, $a_1 = 0.254829592$, $a_2 = -0.284496736$, $a_3 = 1.421413741$, $a_4 = -1.453152027$, $a_5 = 1.061405429$ and $\varepsilon(x)$ is the limit of approximation error for $0 < x < \infty$ [11].

METHOD

Experimental measurements

Four peak parameters are to be measured from the experimental chromatographic peak, t_p, h_p, A and M_1. The peak retention time can be read directly from the experimental peak. For high accuracy in determining band broadening factors with the proposed method, t_p and M_1 values should be measured accurately. It is important to note that the determined σ and τ values can only be as accurate as the measured t_p and M_1 values. In the integration of the peak for peak area (A) and peak controid (M_1) with eqns. 4 and 5, care should be taken so that baseline noise does not affect the accuracy of the A and M_1 values.

Derived equations

In the proposed method, an iterative search algorithm is used to determine the σ and τ value of the experimental peak from measured t_p, h_p, A and M_1 values. For this purpose, equations were derived from the basic characteristics of the EMG peak model. By eliminating t_R from eqns. 6 and 14, we obtain

$$Z_p = \frac{t_p - (M_1 - \tau)}{\sigma} - \frac{\sigma}{\tau} \tag{16}$$

also, from eqns. 12 and 14,

$$\gamma = Z_p + \frac{\sigma}{\tau} \tag{17}$$

and, from eqn. 11,

$$\sigma = \frac{A}{h_p\sqrt{2\pi}} \cdot \exp(-\gamma^2/2) \tag{18}$$

By grouping together the experimentally measured information from the peak-shape factors, we find the following property of the EMG peak model:

$$\frac{M_1 - t_p}{\left(\frac{A}{h_p\sqrt{2\pi}}\right)} = \left(\frac{\tau}{\sigma} - \gamma\right) \exp(-\gamma^2/2) \tag{19}$$

We define

$$\beta = \left(\frac{\tau}{\sigma} - \gamma\right) \exp(-\gamma^2/2) = \left(\frac{\tau}{\sigma} - \gamma\right) \Gamma \tag{20}$$

where

$$\Gamma = \text{peak-height factor} = \exp(-\gamma^2/2) \tag{21}$$

which gives the peak-height ratio of the exponentially modified peak *versus* the original Gaussian peak, and

$$\beta^* = \frac{M_1 - t_p}{\frac{A}{h_p\sqrt{2\pi}}} = \text{the experimental } \beta \text{ value} \tag{22}$$

The following equations were developed to simplify the τ/σ calculations with improved accuracy: for $Z_p < -4$,

$$\frac{\tau}{\sigma} \approx \frac{1}{|Z_p|}\left[1 + \sum_{m=1}^{6} (-1^m) \frac{(2m-1) \cdots 3 \cdot 1}{Z_p^{2m}}\right] \tag{23a}$$

for $-4 < Z_p < 0$,

$$\frac{\tau}{\sigma} \approx \sqrt{\frac{\pi}{2}} \sum_{n=1}^{5} a_n t^n \tag{23b}$$

for $Z_p > 0$,

$$\frac{\tau}{\sigma} \approx \sqrt{2\pi} \exp(Z_p^2/2) - \sqrt{\frac{\pi}{2}} \sum_{n=1}^{5} a_n t^n \tag{23c}$$

where a_n and t^n have been defined in eqn. 15.

Table I gives a few examples of calculated τ/σ, γ, Γ, β and Sk values.The τ/σ and β values from Table I are also plotted as a function of Z_p in Fig. 2. The characteristic relationships between τ/σ, Γ and Sk with β for the EMG model are depicted in Figs. 3 and 4.

Note that the semi-logarithmic β *versus* Z_p plot is nearly linear in the β range of experimental interest. We have taken advantage of this linear relationship to develop a much simplified computer algorithm. The linear approximation to the β *versus* Z_p plot takes the mathematical form

$$Z_p = 1.2028 + 2.474 \log \beta \tag{24}$$

Simplified computer algorithm

With a measured β^* value from an experimental chromatographic peak, one can quickly use Fig. 2 or 3 to read off the τ/σ value for an experimental chromatographic

TABLE I

CHARACTERISTICS OF EXPONENTIALLY MODIFIED GAUSSIAN PEAK

Z_p	τ/σ	γ	Γ^a	β^b	Sk
−10	0.0990	0.0981	0.9952	0.0009	0.002
−7	0.1401	0.1375	0.9906	0.0026	0.005
−6	0.1624	0.1584	0.9875	0.0039	0.008
−5	0.1928	0.1870	0.9827	0.0060	0.014
−4	0.2366	0.2265	0.9747	0.0099	0.024
−3	0.3046	0.2829	0.9608	0.0208	0.049
−2.5	0.3544	0.3215	0.9496	0.0312	0.075
−2.0	0.4214	0.3732	0.9327	0.0450	0.117
−1.5	0.5158	0.4388	0.9082	0.0699	0.193
−1.0	0.6560	0.5244	0.8715	0.1147	0.330
−0.75	0.7526	0.5787	0.8458	0.1471	0.435
−0.50	0.8761	0.6414	0.8141	0.1911	0.572
−0.25	1.0381	0.7133	0.7754	0.2518	0.747
0	1.2533	0.7979	0.7274	0.3313	0.955
0.25	1.5487	0.8957	0.6696	0.4372	1.186
0.50	1.9639	1.0092	0.6010	0.5737	1.415
0.75	2.5687	1.1393	0.5226	0.7470	1.618
1.00	3.4774	1.2876	0.4365	0.9559	1.775
1.50	7.2047	1.6388	0.2611	1.4533	1.944
2.00	18.1011	2.0552	0.1210	1.9416	1.991
2.50	56.5477	2.5177	0.0320	2.2708	1.999
3.00	225.3349	3.0044	0.0110	2.4372	2.000

[a] $\Gamma = \exp(-\gamma^2/2)$.

[b] $\beta = \left(\frac{\tau}{\sigma} - \gamma\right) \exp(-\gamma^2/2)$.

peak by finding the point on the β axis that corresponds to the β^* value. From that point, the τ/σ value is read directly at the corresponding Z_p value at β^*. The corresponding Z_p and τ/σ values are determined digitally in the following way:

(1) Estimate Z_p:

(a) obtain the initial estimate $(Z_p)_0$ by substituting β^* for β in eqn. 24:

$$(Z_p)_0 = 1.2028 + 2.474 \log \beta^* \tag{25}$$

(b) update the Z_p value by using the following iterative calculations:

$$(\Delta Z_p)_n = 2.474 \log (\beta^*/\beta_n) \tag{26}$$

and

$$(Z_p)_{n+1} = (Z_p)_n + (\Delta Z_p)_n \tag{27}$$

(2) Calculate τ/σ from Z_p by using eqn. 23 or 13.

(3) Calculate γ from eqn. 17.

(4) Calculate β from eqn. 20.

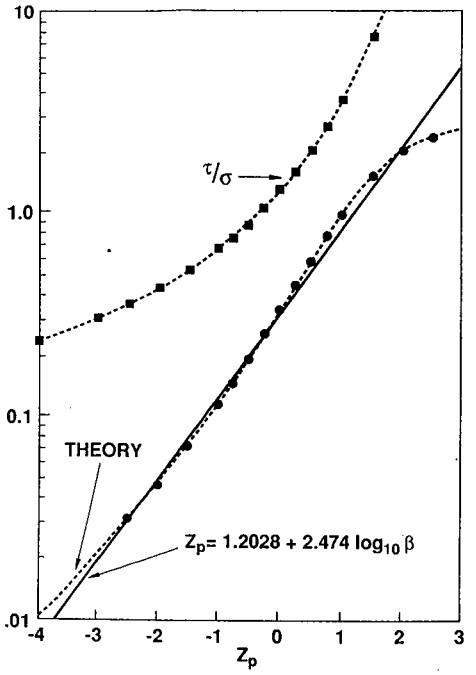

Fig. 2. Characteristics of exponentially modified Gaussian peak.

(5) Check the ΔZ_p value to terminate the iteration:

(a) if $|\Delta Z_p| > \delta$, go back to (1);

(b) if $|\Delta Z_p| < \delta$, end the iteration and continue to calculate σ from eqn. 18.

Proceed to calculate τ, peak skew, peak variance and other peak performance parameters described earlier. The value of δ is the search accuracy limit that can be adjusted to control the desired accuracy of the peak τ/σ value. We suggest a beginning

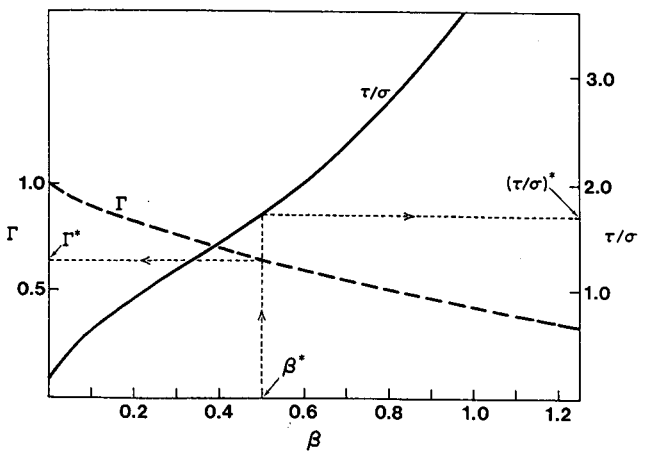

Fig. 3. Nomograph for extracting EMG peak functions.

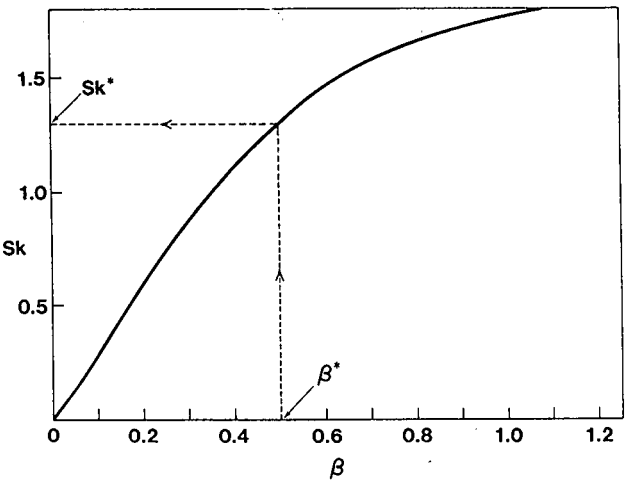

Fig. 4. Relationship between *Sk* and β value for EMG peak.

δ value of 0.02, as this produces a τ/σ value that is within about ± 0.01 of the actual value.

Computer program

The peak characterization method described above has been programmed for IBM-PC in BASIC and HP-1000 in FORTRAN-77. Special attention was paid to interpolate data points at the peak maximum so that an accurate determination of the experimental t_p value can be made. As was mentioned earlier, the accuracy of the present method is directly affected by how well t_p and M_1 values can be determined.

RESULTS AND DISCUSSION

The performance of the proposed method has been tested by a computer simulation study and by application to actual chromatographic data. The results of these studies will be presented in Part II [12].

REFERENCES

1 J. J. Kirkland, W. W. Yau, H. J. Stoklosa and C. H. Dilks Jr., *J. Chromatogr. Sci.*, 15 (1977) 303.
2 E. Grushka, *Anal. Chem.*, 44 (1972) 1733.
3 W. W. Yau, *Anal. Chem.*, 49 (1977) 395.
4 R. E. Pauls and L. B. Rogers, *Anal. Chem.*, 49 (1977) 625.
5 R. E. Pauls and L. B. Rogers, *Sep. Sci. Technol.*, 12 (1977) 395.
6 J. P. Foley and J. G. Dorsey, *Anal. Chem.*, 55 (1983) 730.
7 J. P. Foley and J. G. Dorsey, *J. Chromatogr. Sci.*, 22 (1984) 40.
8 J. V. H. Schudel and G. Guiochon, *J. Chromatogr.*, 457 (1988) 1.
9 J. C. Sternberg, *Adv. Chromatogr.*, 2 (1966) 205.
10 W. W. Yau, J. J. Kirkland and D. D. Bly, *Modern Size-Exclusion Liquid Chromatography*, Wiley, New York, 1979, Ch. 4 and 9.
11 M. Abromowitz and I. A. Stegun (Editors), *Handbook of Mathematical Functions*, Dover, New York, 1965, equation 7.1.26.
12 W. W. Yau, S. W. Rementer, J. M. Boyajian, K. B. Lim, J. J. DeStefano and J. J. Kirkland, *J. Chromatogr.*, in press.
13 M. S. Jeansonne and J. P. Foley, *J. Chromatogr. Sci.*, 29 (1991) 258.

Journal of Chromatography, 556 (1991) 119–143
Elsevier Science Publishers B.V., Amsterdam

CHROM. 23 371

Analysis of isotachic patterns in displacement chromatography

FIROZ D. ANTIA and CSABA HORVÁTH*
Department of Chemical Engineering, Mason Laboratory, Yale University, P.O. Box 2159, Yale Station, New Haven, CT 06520 (USA)
(Received November 20th, 1990)

ABSTRACT

Most previous theoretical treatments of displacement chromatography have been confined to systems that follow the competitive Langmuir isotherm. With the assumption of such idealized multi-component adsorption behavior, in a sufficiently long column the final outcome of the process is always expected to be an isotachic displacement train having a series of adjacent separated bands of increasing concentration. Several recent reports, however, suggest that no such train forms when the single-component isotherms of the separands cross. In order to examine the possibility of separation under such conditions, the stability of the isotachic pattern is analyzed and criteria for displacement and for stability of the resulting boundaries are established. The approach requires the knowledge of the multi-component isotherm that governs the adsorption of the separands. As the competitive Langmuir isotherm completely fails to represent such behavior, the pertinent multi-component isotherms are generated from Langmuir single-component isotherms within the framework of the ideal adsorbed solution model. The results obtained with such a multi-component isotherm in binary separations show that three operating regions in displacement chromatography can be identified when the single-component isotherms of the separands cross. In one region at sufficiently low concentrations, the two components separate and appear in the same order as in linear chromatography. In a second region at sufficiently high concentrations, the bands are predicted to separate but appear in the reverse order. In the third region at intermediate concentrations, complete separation is not possible, and the resulting isotachic pattern contains a mixed zone. The stability analysis presented here facilitates the prediction of the outcome of displacement without the need for arduous computation; it is fairly general and may be applied to systems that follow other multi-component isotherms.

INTRODUCTION

Displacement is one of the three operational modes of chromatography identified by Tiselius [1,2]. In it, a feed mixture is followed into the column by a solution containing a substance called the displacer, which binds so strongly to the stationary phase that it drives the feed components ahead of its front. Under favorable conditions, the components eventually separate into adjacent bands that all move at the velocity of the displacer front, thus forming an isotachic pattern known as the displacement train. Displacement is a *non-linear* chromatographic method; the displacer and separand concentrations have to be high enough that the equilibrium relationship governing the simultaneous adsorption of the components, *i.e.*, the multi-component adsorption isotherm, is both competitive and *non-linear*. As a consequence,

0021-9673/91/$03.50

migrating molecules interfere strongly with one another as they traverse the column and, under appropriate conditions, the interference facilitates separation. This is in contrast with *linear* elution chromatography, most commonly employed in analytical practice, where concentrations are kept low so that adsorption isotherms are *linear* and components migrate through the column without interference.

The rudiments of the displacement process were already recognized by Tswett in 1906, but it was not until the Tiselius' formal classification and the pioneering work of Glückauf [3] that its principles were placed on a firm footing. Glückauf's theoretical approach was quite general, but, for the sake of mathematical simplicity, he used only the competitive Langmuir isotherm. The subsequent treatment of Helfferich and Klein [4] also hinged upon the use of this isotherm. As a result, the prevalent understanding of non-linear chromatography in general and displacement chromatography in particular was, until recently, restricted to systems that would obey the competitive Langmuirian model.

However, the competitive Langmuir isotherm model is valid only when the saturation capacities of the stationary phase for all the various adsorbing components are identical, and thus it has very limited practical relevance. Another characteristic feature of this model is that the selectivity between any pair of components is constant, independent of concentration. As a consequence, the requirements for a displacement separation would merely be that the displacer be retained more strongly than the feed components and that its concentration be above a certain minimum value [3]. Then, in the absence of axial dispersion and given a suitably long column, a displacement train would eventually be formed, with the components fully separated and arranged in order of increasing initial slopes of their respective single-component isotherms.

Early success [5,6] and the implicit assurance from theory that separation would be achieved upon fulfilling such simple criteria encouraged experimental efforts in the 1940s and 1950s. Displacement chromatography was used for a brief period to separate a variety of compounds, from petroleum products to rare earths and biochemicals (see refs. 7 and 8 for reviews). Thereafter it was overshadowed by the development of linear chromatography and, after a hiatus of more than 20 years, was revived in the early 1980s [9–11]. The efficient columns and sorbents of today's high-performance era have made displacement chromatography practicable, and it has established itself in a number of preparative applications, including the purification of antibiotics, peptides and even proteins (see refs. 8 and 12 for reviews).

On the other hand, when the method has failed, researchers have been perplexed and frustrated. Recent experimental studies, both from this and from other laboratories, have shown that displacement is likely to be unsuccessful if the single-component isotherms cross one another when drawn on the same plane [13–16]. In an adsorption process it is generally true that larger molecules bind more strongly to the sorbent than smaller ones and their individual isotherms therefore have a larger initial slope. However, because the larger molecules may occupy more space on the surface of the sorbent they would be expected to have lower saturation capacities, in molar terms. Isotherms of larger and smaller molecules would therefore often cross. Indeed, from these considerations, crossing isotherms are more likely to be the rule than the exception, and a thorough investigation is necesary to gain insight into the mechanisms that dictate the sucess or failure of displacement processes under such circumstances.

In many instances, the isotherms of the components often individually fit the Langmuir single-component model. However, because of the different saturation capacities of the components, the competitive, or multi-component Langmuir isotherm model is not thermodynamically consistent [17–19] and, even when forced into service despite this limitation, cannot account for the observed behavior. This was noticed in an early qualitatiative study by Tiselius's group [20], where it was found that the selectivity between a feed component and the displacer may actually reach unity and even undergo a reversal, leading to the loss of a sharp front between displacer and feed component.

Evidently, adsorption isotherms other than the competitive Langmuir model are needed to describe such behavior. One means of generating thermodynamically consistent multi-component isotherms from single-component data is provided by the ideal adsorbed solution (IAS) method, introduced first for gas–solid adsorption [21] and later extended to liquid systems [22]. Using the IAS approach, it has been shown that selectivity inversion, *i.e.*, the reversal in the order of band appearance on going from low to high concentration, may occur in systems where the respective single-component isotherms cross [23]. The treatment of Frey [24], which is based on considerations of free energy consumption at concentration discontinuities within the column and requires information only about single-but not multi-component isotherms, also implies selectivity reversal in such systems. What is not clear from either study, however, is whether complete separation always occurs in the final pattern, or if a mixed band, indicative of an adsorption azeotrope, or "adsorbotrope", forms instead.

Here we tackle afresh the issue of selectivity reversal and the formation of azeotropes by analyzing the stability of the displacement train. The approach is general and may be applied also to other multi-component isotherm formalisms. The Langmuir and IAS multi-component isotherms are compared for their ability to predict the observed behavior and their advantages and shortcomings are exposed.

THEORY

In developing our theory, we shall assume that conditions of "ideal" chromatography prevail, *i.e.*, there is no axial dispersion and instantaneous equilibrium is reached everywhere in the column. This allows us to focus on the fundamental characteristic that distinguishes non-linear processes, such as displacement, from linear chromatography, *viz.*, the effect of the competitive adsorption behavior. This assumption has been used in the past and found to provide respectable approximations to observed behavior in non-linear systems [3].

For brevity, single-component adsorption isotherms will be referred to either as "SC" or as "parent" isotherms, and multi-component isotherms as "MC" isotherms. As we are concerned for the most part with liquid chromatography, it is understood that the term "SC isotherm" alludes to the adsorption of a component from a solvent that by definition is assumed to be absent from the adsorbed phase [25,26]. We shall restrict our attention to SC isotherms that can be fitted to the one-component Langmuir model, given for a component i by [27]

$$q_i = \frac{\lambda_i b_i c_i}{1 + b_i c_i} \tag{1}$$

where q_i and c_i are the concentrations of i in the stationary and and mobile phases, respectively, and λ_i and b_i are the pertinent isotherm parameters; λ_i represents the largest possible value of q_i, and is known as the saturation capacity of the stationary phase for component i. The initial slope of this isotherm is $a_i = \lambda_i b_i$. In liquid chromatography, SC isotherms of the separands and displacer can often be fitted successfully to eqn. 1 [28–30]. We use such isotherms for the sake of simplicity; the results of our treatment can be extended to many cases where the SC isotherms are not so well behaved. However, additional factors must be taken into account when the isotherms have features such as inflection points, and these are not addressed here.

We have already referred to the competitive Langmuir model, which is an example of a multi-component or MC isotherm which is constructed to describe the simultaneous adsorption of several components. In general, such an isotherm must be obtained by fitting an appropriate function to equilibrium adsorption data over the composition range of interest. This is a tedious task, however, and only very few such measurements have been made in liquid chromatographic systems [31,32]. For shortage of experimental data multi-component adsorption behavior is usually described by a formalism that uses parameters derived from SC isotherm data. In the past, the competitive Langmuir equation has been widely used in the past for this purpose and is given by [33]

$$q_i = \frac{\lambda_i b_i c_i}{1 + \sum_{j=1}^{n} b_j c_j} \qquad i = 1, 2, \ldots, n \tag{2}$$

where n is the total number of adsorbed components. In eqn. 2, as with all MC isotherms, the stationary phase concentration of a component i is a function of the mobile phase concentrations of all the components the system and it can be represented by an n-dimensional surface in an $(n + 1)$-dimensional space.

One remarkable feature of the competitive Langmuir model is that it predicts a constant selectivity for any two components, regardless of their respective concentrations or that of any additional components. The selectivity, or separation factor, for two species A and B, α_{BA}, is defined as the ratio $q_B c_A / q_A c_B$. Constant selectivity is what makes the competitive Langmuir isotherm attractive for mathematical treatment, but is an artifact which narrowly restricts the applicability of the model.

A property that is common to most MC isotherms is that the isotherm of one component, when measured in the presence of a fixed concentration of another, is "suppressed" compared with its SC isotherm, *i.e.*, it has a lower initial slope and possibly also a lower saturation level as well. This suppression has important consequences in displacement, as we shall see later.

The competitive Langmuir model is valid only in the case where the SC saturation capacities for all n components are equal, *i.e.*, when

$$\lambda_1 = \ldots = \lambda_i = \ldots = \lambda_n = \lambda \tag{3}$$

Nevertheless, because of its mathematical simplicity, eqn. 2 has often been used even when eqn. 3 does not hold. In such cases, however, eqn. 2 fails to satisfy the Gibbs adsorption equation and therefore violates the second law of thermodynamics [17–

19]. Consequently, any predictions about non-linear chromatography obtained by applying eqn. 2 in this manner are of dubious value.

With these preliminary remarks, we now turn our attention to displacement chromatography. The salient feature of displacement, according to the Tiselian concept [1], is that in the process the various feed components separate into a series of successive bands, followed by the displacer, all moving at the same velocity. When the isotachic conditions is achieved, the characteristic velocity of the train is the species velocity of the displacer, u_D, given by [4]

$$u_D = \frac{u_0}{1 + \phi \frac{q_D^*}{c_D^*}} \tag{4}$$

where u_o is the velocity of the bulk mobile phase, q_D^* and c_D^* are the equilibrium concentrations of the displacer in the stationary and mobile phases, respectively, and ϕ is the phase ratio. Under isotachic conditions, the species velocities of all the pure components, A, B, etc., in the displacement train are identical, so that

$$\frac{q_A^*}{c_A^*} = \frac{q_B^*}{c_B^*} = \ldots = \frac{q_D^*}{c_D^*} \equiv \Delta \tag{5}$$

As each band contains a single feed component, their concentrations in the displacement train are determined graphically from the points at which the respective single-component isotherms intersect the so-called "operating line" having slope Δ and intercept zero. It follows that in order for a species to be part of the displacement train, its single-component isotherm must not lie wholly below the operating line. This is Glückauf's condition for displacement [3].

For predicting behavior in displacement chromatography, one consequence of using the competitive Langmuir model given by eqn. 2 is that Glückauf's condition is sufficient to ensure a successful displacement separation. Thus, if the system were to follow the Langmuir MC isotherm, the ultimate outcome of a displacement run can be completely determined from the SC isotherms and the operating line, according to the picture described above.

Whereas this beguilingly simple construction seems wholly adequate in many instances [8,9,34], it appears to break down when the parent isotherms of the separands cross one another. Experimental results under such conditions show only partial, or no, separation even when Glückauf's conditions is met [14–16].

Conditions for establishment of the displacement train

Evidently, in the case of crossing SC isotherms, Glückauf's condition is insufficient, and the model with the Langmuir MC isotherm fails. Consequently, another MC isotherm function is required and new conditions for displacement must be formulated. First, we intend here to derive such conditions from an analysis of the stability of the displacement train; an appropriate MC isotherm is discussed later. The stability analysis is fairly general and applicable to most MC isotherms generated

from monotonically concave downward SC isotherms which have no inflection points. Extension to other more complex SC isotherm shapes may be possible but requires further investigation. The analysis is prefaced with the following comments.

In an ideal chromatographic system with concave downward parent isotherms, as long as Glükauf's conditions is met and an appropriate displacer is chosen, all displacement processes will, in a column of sufficient length, attain the isotachic state. This happens because Glükauf's condition ensures that the individual feed components would, on their own, move slower than the displacer. However, the displacer does not allow any feed components behind its front, and so forces the components to move at its velocity; any differences in local velocity of the feed components eventually disppear. (It suffices for present purposes that the displacer be one whose isotherm completely overlies that of the feed components; a more general idea of an "appropriate" displacer will emerge from the following discussion.) In the terminology of Helfferich and Klein [4], the train reaches a "coherent" state, *i.e.*, all concentration discontinuities in the system propagate at a constant velocity, and the velocities of the bands on either side of these boundaries meet the coherence conditions. In the following discussion it will be assumed that the coherence and Glükauf conditions, together termed the "zeroth" displacement conditions, are satisfied.

Stability of the displacement train

The desired outcome of a displacement experiment is the completely separated coherent pattern predicted by the Tiselian model. However, as seen experimentally in the case of crossing isotherms, it does not appear that this state is always achieved. One may then ask whether there are other possible coherent states and, if so, which of them is the likely result in a given displacement run? The answer to this question will be sought here by carrying out "Gedanken experiments" to examine the stability of the Tiselian train. If the train is found to be stable to small perturbations, there exists by implication a driving force that propels the system towards and maintains it in the separated state. This is not to say that such stability guarantees the formation of the separated state from every previously mixed state, but that there is at least a pathway towards separation from the perturbed state. If the train is not stable, such a driving force is absent and the separation cannot proceed to completion, so that some alternative coherent state containing mixed bands may result.

Consider a displacement train with a pair of successive bands of feed components A and B which are separated by a sharp boundary. The respective concentrations of the pure bands are c_A^* and c_B^* as dictated by the operating line given by eqn. 5. In the first "Gedanken experiment", imagine that a trace amount of the leading component, A, is brought into the domain of the trailing component B without noticeably changing the concentration of either band. For the system to return to the sharply separated state, the velocity of that trace of A must be greater than the characteristic velocity of the displacement train.

The velocity of A under these conditions is given by

$$(u_A)^0_{c_B=c_B^*} = \frac{u_0}{1+\phi\left(\frac{q_A}{c_A}\right)^0_{c_B=c_B^*}} \tag{6}$$

where the superscript 0 and the subscript $c_B = c_B^*$ indicates that the quantities are evaluated as $c_A \to 0$ and at $c_B = c_B^*$. For the system to be stable to the perturbation, it therefore follows that

$$\left(\frac{q_A}{c_A}\right)^0_{c_B = c_B^*} < \Delta \tag{7}$$

where Δ is the ratio q_B^*/c_B^* or q_A^*/c_A^* as determined by the operating line (see eqn. 5).

In a second "Gedanken experiment", let us consider that a trace amount of the trailing component B encroaches into the domain of the leading component A. Following an argument similar to that above the condition for stability in this case is

$$\left(\frac{q_B}{c_B}\right)^0_{c_A = c_A^*} > \Delta \tag{8}$$

Eqns. 7 and 8 will be termed the first and second stability conditions, respectively. Note that in the eqns. 7 and 8, c_A^* and c_B^* depend on Δ.

When both stability conditions are satisfied the boundary between A and B is stable to small perturbations. Unlike Glückauf's condition which is determined solely from the parent single-component isotherms, the terms $(q_A/c_A)^0_{c_B = c_B}$ and $(q_B/c_B)^0_{c_A = c_A}$ in the stability conditions expressed by eqns. 7 and 8 depend on the multi-component isotherm that describes the simultaneous adsorption of the components. As we shall see later, the stability conditions will be used to determine the result of a displacement run. It ought to have been obvious that the outcome should depend on the MC isotherm, and not just the SC isotherms. In the past, however, this fact has been clouded by the employment of the competitive Langmuir isotherm because only this MC formalism allows the final pattern to be determined from the SC isotherms alone.

A closer examination shows that the first stability condition, eqn. 7, is an affirmation of the driving force for displacement, *i.e.*, the trailing component, B, must suppress the isotherm of the leading component, A, sufficiently so that it is never allowed to fall behind. The second condition, eqn. 8, essentially ensures that the front of B is self-sharpening. In the absence of the leading component the front of B would self-sharpen naturally because of its concave downward isotherm [4]. Since as a rule A also suppresses the isotherm of B, the condition assures that the self-sharpening effect is still operative.

Whereas an SC isotherm is a line on a two-dimensional plot, an MC isotherm of a binary mixture, as mentioned before, is represented by a pair of two-dimensional planes in a three-dimensional space. However, little information can be gained from such illustration of the MC isotherms, and a graphical analysis of displacement is facilitated by projecting certain key features from the three-dimensional space to a two-dimensional plot of c_B *versus* c_A, which is known as a "hodograph". In order to visualize the stability conditions graphically, we consider points on the hodograph at which the stability criteria are just satisfied. For the first conditions this point is

$$\left(\frac{q_A}{c_A}\right)^0_{c_B = c_B^*} = \frac{q_B^*}{c_B^*} \tag{9}$$

and for the second

$$\left(\frac{q_B}{c_B}\right)^0_{c_A=c_A^*} = \frac{q_A^*}{c_A^*} \tag{10}$$

In the hodograph, eqns. 9 and 10 represent points along the c_B and c_A axes, respectively, at which the selectivity, α_{BA}, is unity. The two conditions in eqns. 7 and 8 thus indicate that a final pattern of complete separation in which the bands have the order AB is stable when the selectivities at the points $(0, c_B^*)$ and $(c_A^*, 0)$ in the hodograph both exceed unity. On the other hand, if the selectivities at both of these points are lower than unity, a train with the order BA is predicted to be stable. However, the stability conditions are violated if the respective selectivities at $(0, c_B^*)$ and $(c_A^*, 0)$ are greater and lower than unity, or *vice versa*. As a result, under these conditions the final pattern of complete separation is unstable, and some alternative coherent state will be reached. The problem of determining the stability of the displacement train thus reduces to that of finding the points of unit selectivity, if they exist at all, on the c_B and c_A axes, and ensuring that the lcoations of $(0, c_B^*)$ and $(c_A^*, 0)$, as dictated by the operating line, lie on the appropriate sides of line connecting these points. Graphical illustrations of the analysis are shown later.

Multi-component isotherms generated by the IAS method

The constant selectivity feature of the competitive Langmuir isotherm precludes any possibility of finding in the hodograph points or regions of unit selectivity (except in the degenerate case where the SC isotherms are identical), and thus makes any discusison of stability pointless: with this MC isotherm, as long as the zeroth conditions are satisfied, all displacement trains are stable, and the only final patterns reached are those of complete separation. In practice, constant selectivity is unlikely to be realized, and MC isotherms that allows for variable selectivity are necessary.

As already mentioned, the Langmuir MC isotherm violates the Gibbs adsorption equation unless eqn. 3 is satisfied. The Gibbs equation relates adsorbed amounts to the spreading pressure, defined as the difference of the interfacial tensions between the multi-component solution–sorbent and the pure principal solvent–sorbent systems. The ideal adsorbed solution (IAS) method, so called because it uses an analogue of Raoult's-law ideality to describe the adsorbed phase, provides a framework to generate a multi-component isotherm that satisfies Gibbs equation from any set of single-component isotherms [21,22]. The antecedents of this approach and a useful general result are presented in Appendix A. Our interest here is to use the IAS method to obtain multi-component isotherms from Langmuir parent isotherms. In this case the calculation proceeds in two steps (see Appendix A). First, the reduced spreading pressure, Π, is determined for the given set of Langmuir SC isotherm parameters and concentrations of the components in the mobile phase from the implicit equation (see Appendix A)

$$\sum_{j=1}^{n} \frac{b_j c_j}{\exp(\Pi/\lambda_j) - 1} = 1 \tag{11}$$

The numerical solution of eqn. 11 is greatly facilitated by using as an initial guess the approximation to Π put forward by LeVan and Vermeulen [19]. Next, for a known value of Π, the multi-component isotherm is calculated from

$$q_i = \frac{b_i c_i/[\exp(\Pi/\lambda_i) - 1]}{\sum_{j=1}^{n} b_j c_j \exp(\Pi/\lambda_j)/\{\lambda_j[\exp(\Pi/\lambda_j) - 1]^2\}} \qquad i = 1, 2, \ldots, n \tag{12}$$

The relationship given in eqn. 12 is hereinafter termed the IAS/L isotherm. In the case where eqn. 10 is satisfied, eqn. 12 reduces to the competitive Langmuir isoherm (eqn. 9), which is therefore a special case of the IAS/L equation.

Computation of displacement profiles

The stability criteria have been applied to the displacement of a binary mixture in the light of IAS/L isotherms. The results are illustrated by computer simulations of displacement profiles under various conditions. Exact solutions for the ideal case, *i.e.*, without dispersion in the system, cannot be found; instead, the calculations are carried out using the so called "semi-ideal" model [35,36]. The finite difference scheme for the solution of the resulting first-order partial differential equations introduces a numerical error that can be made to approximate the desired amount of dispersion in the system, quantified by a plate number N ($= u_0 L/2\mathscr{D}$, where L is the column length and $\mathscr{D}$ the effective axial dispersion coefficient that accounts for all dispersive processes in the system; N is also equal to L/H, where H is the plate height). The numerical scheme also introduces some additional errors but at sufficiently high values of N these do not significantly effect the calculations [36]. For convenience, in the calculations it is assumed that the phase ratio is unity. In addition, a constant plate height was used, so that the plate number gives an indication of the column length required. The results are presented as plots of the outlet concentration of the components *versus* the column volumes of mobile phase that have passed through the system. Note that with this representation, as long as the plate number is fixed, the actual values employed for the plate height and flow-rate need not be specified.

RESULTS AND DISCUSSION

Our goal here is to use the stability criteria put forward above to examine in detail the deviations from the classical Tiselian displacement picture observed when the parent isotherms of the separands cross. For this purpose, we shall consider the separation of pairs of components A and B, whose single-component isotherms intersect, as depicted in Fig. 1a. The displacement will be driven by a displacer whose isotherm overlies those of the separands. As the stability criteria are general, they ought to be applicable to any displacement system. For simplicity, however, we shall confine our attention to those that obey the IAS/L multi-component isotherm given in eqn. 12. In Appendix B, the treatment is extended to systems obeying another thermodynamically consistent MC isotherm; the results differ only marginally from those obtained with the IAS/L isotherm.

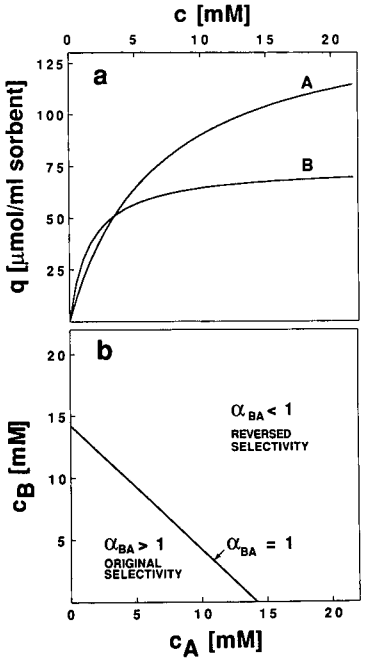

Fig. 1. (a) Plots of crossing single-component isotherms of components A and B and (b) the corresponding line of unit selectivity in a hodograph. The latter was calculated from eqn. 15 with the isotherm parameters λ_A = 150 μmol/ml sorbent, b_A = 0.15 l/mmol, λ_B = 75 μmol/ml sorbent, b_B = 0.62 l/mmol; c_x was obtained as 14.22 m*M*.

Selectivity inversion

As is evident from eqns. 9 and 10, a stability analysis is necessary only in those systems where the selectivity between the separands becomes unity at some points. In general, for separands A and B, such points define a line that demarcates regions of opposite selectivity in the hodograph space. We must therefore first examine under what conditions such regions exist.

The IAS/L isotherm allows for variable selectivity and can be used in the description of systems where selectivity inversion takes place [23]. It must be noted at the outset that, as with all MC isotherms generated only from SC isotherm data, the predictive power of the IAS/L isotherm is limited to "well behaved" systems. In case of the IAS method, "well behaved" implies that activity coefficients of the components in the moble and adsorbed phases are close to unity (for definition of adsorbed phase activity coefficients, see refs. 37 and 38). Even with this restriction, however, the IAS/L isotherm represents a distinct improvement over the competitive Langmuir isotherm, which cannot describe systems with changing selectivity.

From eqn. 12, the selectivity between two components, α_{BA}, is given by

$$\alpha_{BA} = \frac{b_B[\exp(\Pi/\lambda_A) - 1]}{b_A[\exp(\Pi/\lambda_B) - 1]} \tag{13}$$

where Π is a function of the concentrations c_A and c_B and is determined from eqn. 11. To locate points of unit selectivity, α_{BA} is set to unity in eqn. 13; the result is an implicit equation that can be solved for Π', the reduced spreading pressure that corresponds to all points of unit selectivity:

$$\frac{b_B[\exp(\Pi'/\lambda_A) - 1]}{b_A[\exp(\Pi'/\lambda_B) - 1]} = 1 \tag{14}$$

Introducing Π' into eqn. 11 and multiplying the result by $[\exp(\Pi'/\lambda_A) - 1]/b_A$ yields

$$c_A + c_B = \frac{[\exp(\Pi'/\lambda_A) - 1]}{b_A} \equiv c_x \tag{15}$$

In Appendix A, eqn. 15 is generalized for all MC isotherms generated by the IAS method, regardless of the shape of the parent isotherms. The result expresses an important property of the IAS isotherms: all points of unit selectivity between two components, if they exist at all, are connected by a straight line of slope -1 on a hodograph. The unit selectivity line intersects both the c_A and c_B axes at the value c_x, which is given by $[\exp(\Pi'/\lambda_A) - 1]/b_A$ in the case of the IAS/L isotherm.

An analysis of eqn. 14 shows that it has a real solution for Π' only if $b_B > b_A$, then $\lambda_B < \lambda_A$ and *vice versa*. When the parent isotherms of A and B cross, *i.e.*, $\lambda_B b_B > \lambda_A b_A$, and $\lambda_B < \lambda_A$ or *vice versa*, these criteria for a real solution for Π' are always satisfied. It would appear that they could also be satisfied without requiring the SC isotherms to intersect. However, in order to be physically acceptable, Π' must be positive (see eqn. 15), and this is found to occur *only* when the isotherms cross. Thus, according to the IAS/L isotherm model, selectivity inversion occurs only when the parent isotherms of the two components cross and the two regions of opposite selectivity are demarcated by a line of unit selectivity with slope -1 in the hodograph space.

A pair of crossing single-component isotherms and the corresponding unit selectivity line in a hodograph are shown in Fig. 1a and b, respectively. It is seen that whenever the sum of the concentrations $c_B + c_A$ is less than c_x, the selectivity, α_{BA}, is greater than unity, *i.e.*, $\alpha_{BA} > 1$, and *vice versa*. The two regions will be termed the regions of original and reversed selectivity, respectively. Fig. 1 also shows that the concentrations corresponding to points of unit selectivity along the c_B and c_A axes do not coincide with the intersection point of the parent isotherms. Indeed, this latter intersection point on two-dimensional plots has no physical significance *per se*. Within the hermeneutics of the IAS method the true concentration of unit selectivity, c_x, can be found by numerically solving eqn. 14 for Π' and substituting the result in eqn. 15. The dependence of c_x on the initial selectivity, *i.e.*, the selectivity at infinitesimal concentrations of both components A and B, α^0 ($= \lambda_b b_B/\lambda_A b_A$, or a_B/a_A, the ratio of the Henry's-law constants), is plotted for different values of the ratio of the saturation capacities λ_B/λ_A in Fig. 2. The results indicate that for a fixed saturation capacity ratio, c_x increases with increasing α^0, whereas for fixed α^0, c_x decreases with decreasing λ_B/λ_A. This is the same trend expected for the intersection point of the parent isotherms, and hence one may formulate a crude rule of thumb: if the sum of the

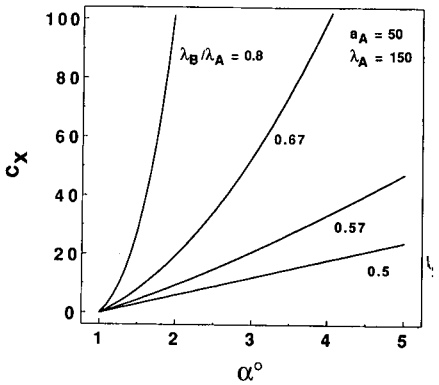

Fig. 2. Plots of the total concentration of unit selectivity, c_x, *versus* the initial selectivity $\alpha^0 = a_A/a_B$, calculated from eqn. 15 for the parameter values shown. The trends predicted in this diagram are independent of the actual parameter values chosen.

concentrations of the two components do not exceed that of the intersection point at any location in the column, selectivity in version is avoided altogether. This is valid for all three modes of frontal, elution or displacement chromatography. Our results show that, within the framework of the IAS/L isotherm, the true selectivity reversal

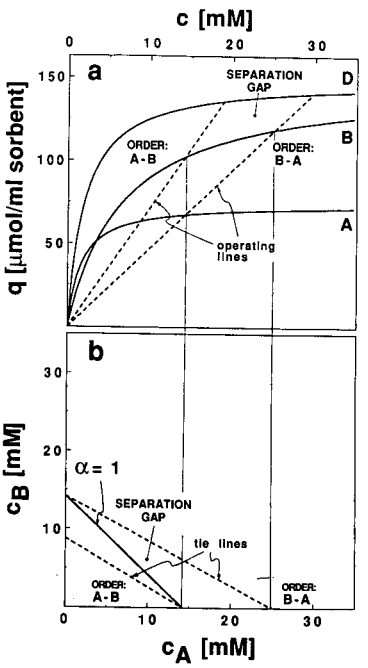

Fig. 3. (a) Crossing SC isotherms of components A and B, and the displacer, along with operating lines, and (b) the corresponding hodograph showing tie lines and the unit selectivity line. The operating and tie lines shown demarcate the space into three operating regions, as discussed in the text. Displacer parameters: λ_D = 150 μmol/ml sorbent, b_D = 0.5 l/mmol; other parameters as in Fig. 1.

concentration, c_x, is always greater than the apparent crossing point, and the rule of thumb is therefore always conservative.

Displacement chromatography with crossing isotherms

More precise rules for displacement chromatography can be formulated by considering the stability conditions in eqns. 7 and 8. Consider the displacement of a mixture of two components A and B whose SC isotherms cross, and whose multicomponent isotherm follows the IAS/L equation. The isotherms of A, B and that of a displacer are shown in Fig. 3a and a corresponding hodograph of c_A *versus* c_B is depicted in Fig. 3b. Operating lines are drawn on the isotherm plot from the origin to the point on the displacer isotherm corresponding to the displacer concentration. Two such lines are shown in Fig. 3a. The operating lines transformed into the hodograph space are termed here "tie lines" and are shown on the hodograph in Fig. 3b. It is seen that each tie line is constructed from an operating line and connects the concentrations c_A^* and c_B^* determined by the intersection of the operating lines with the respective parent isotherms. A tie line merely serves to highlight the concentrations c_A^* and c_B^* on the axes of the hodograph that are the predicted concentrations of the bands in a completely separated Tiselian displacement train; apart from this it does not appear to have physical significance within the hodograph space. The unit selectivity line, $c_B + c_A = c_x$ is also drawn on the hodograph. The two tie lines and corresponding operating lines shown are for the cases where $c_A^* = c_x$ and $c_B^* = c_x$.

As mentioned in the discussion following eqn. 10, the stability conditions indicate that a separated isotachic sequence AB is stable if the corresponding concentrations c_A^* and c_B^* both lie below the line of unit selectivity, *i.e.*, below the tie line passing through $c_A^* = c_x$. On the other hand, when both c_A^* and c_B^* lie above the unit selectivity line, *i.e.*, when the tie line lies above the one passing through $c_B^* = c_x$, a stable isotachic pattern with the opposite order, in this case BA, is expected. Further, the stability conditions require that when c_A^* and c_B^* lie on opposite sides of the unit selectivity line, *i.e.*, the operating lines and corresponding tie lines lie between those shown in Fig. 3a and b, a completely separated pattern is not obtained. The operating region between these lines will be termed the "separation gap". Operating lines to the left of the gap yield displacement trains with original selectivity and those to the right of it trains with reversed selectivity. In the gap, no complete separation is possible. The construction in Fig. 3 allows us to visualize on a plot of the SC isotherms the separation gap that has been obtained from the stability analysis based on the corresponding MC isotherm.

To illustrate the results of operating in the different regions, simulations of displacement separations were carried out with the IAS/L isotherm as described earlier. With conditions chosen such that the operating line lies to the left of the gap, as shown in Fig. 4a, the calculated displacement profiles in Fig. 4b show that components A and B have separated into individual bands, with order AB. It is interesting to note that, because in this case the operating line lies above the intersection point of the parent isotherms, the concentration reached by A is higher than that of B, unlike in the classical picture of a displacement train [11]. This serves to emphasize that although the crossing of the SC isotherms is indicative of selectivity reversal, the location of their intersection point *per se* does not correspond to the concentration of unit selectivity as might have been inferred from a superficial examination.

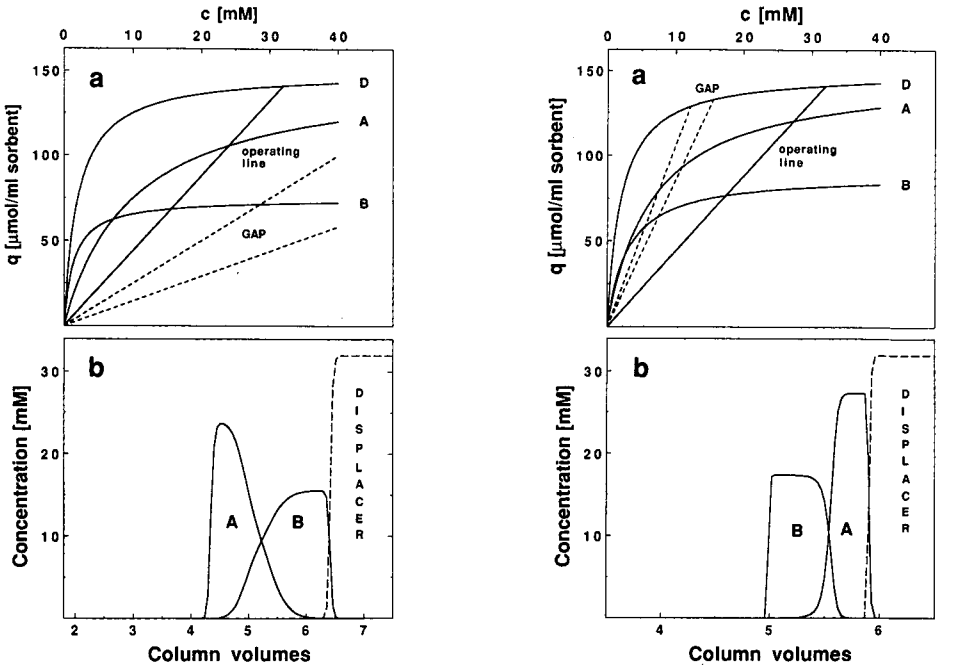

Fig. 4 (a) Crossing SC isotherms of components A and B and isotherm of the displacer showing an operating line lying to the left of the separation gap, and (b) displacement profiles calcualted using the IAS/L isotherm for the same conditions. Plate number, N = 2800; feed, 20 mM A and 20 mM B in one column volume. Isotherm parameters: λ_A = 150 μmol/ml sorbent, b_A = 0.1 l/mmol, λ_B = 75 μmol/ml sorbent, b_B = 0.7 l/mmol; c_x was calculated from eqn. 15 to be 50 mM. Displacer parameters as in Fig. 3; displacer concentration, 32 mM.

Fig. 5. (a) Crossing SC isotherms of components A and B and isotherm of the displacer showing an operating line lying to the right of the separation gap and (b) displacement profiles calculated using the IAS/L isotherm for the same conditions. Plate number, N = 10 000; feed, 5 mM A and 5 mM B in 1.25 column volumes. Isotherm parameters: λ_A = 150 μmol/ml sorbent, b_A = 0.15 l/mmol, λ_B = 90 μmol/ml sorbent, b_B = 0.33 l/mmol; c_x was calculated from eqn. 15 to be 7.34 mM. Displacer parameters and concentrations as in Fig. 4.

With conditions such that the operating line lies to the right of the separation gap, as depicted in Fig. 5a, the calculated displacement profiles shown in Fig. 5b display reversed selectivity, with bands appearing in the order BA as predicted from the above analysis. The plate number, N, chosen for this example was 10 000, indicative of a fairly difficult separation. A high plate number requirement for the calculation translates in practice into the need for a long column.

For the sake of comparison, we also carried out simulations by forcing the SC isotherms into the competitive Langmuir formalism. The results under conditions identical with those in Figs. 4 and 5 are shown in Fig. 6a and b, respectively. The bands in Fig. 6a appear in the same order and at the same concentrations, but are better separated than those in Fig. 4b. This is because the competitive Langmuir isotherm predicts a constant selectivity, $\alpha^0 = a_B/a_A$, at all concentrations, whereas with the IAS/L isotherm the selectivity ranges from α^0, its highest value at very low concentration, to some value close to unity at the higher concentrations of the final

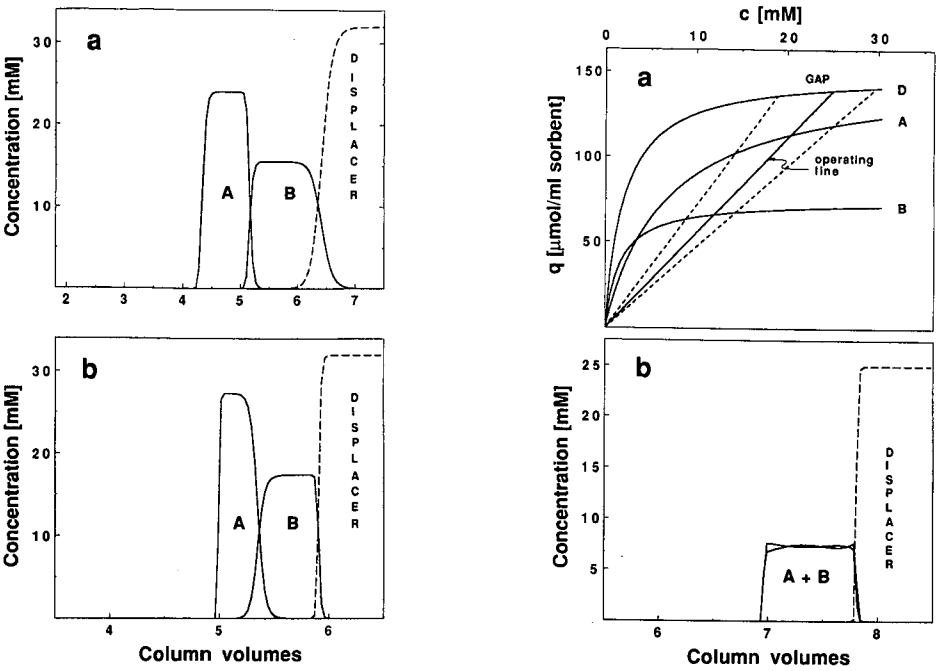

Fig. 6. Displacement profiles calculated with the competitive Langmuir isotherm under conditions given in (a) Fig. 4b and (b) Fig. 5b.

Fig. 7. (a) Crossing SC isotherms of components A and B and isotherm of the displacer showing an operating line lying in the separation gap, and (b) displacement profiles calculated using the IAS/L isotherm under the same conditions. Plate number, N = 10 000; feed, 20 mM A and 20 mM B in 0.5 column volume. Isotherm parameters as in Figs. 1 and 3; displacer concentration, 25 mM.

pattern. Therefore, in the latter instance, the overall selectivity is lower, and the separation is consequently more difficult. Under conditions where a reversed order is predicted by the IAS/L as the final outcome, the calculations with the Langmuir isotherm in Fig. 6b continue to show the bands appearing in the order of original selectivity. Fig. 6 therefore confirms the inadequacy of the competitive Langmuir isotherm for use in dynamic adsorption systems discussed earlier.

A crude estimate of the difficulty of the separation can be determined from the selectivities at the inlet feed concentration and in the final pattern. For example, in the case shown in Fig. 4, the selectivity at the composition of the feed is 1.12, and at (c_A^*, 0) and (0, c_B^*) it is 1.59 and 1.57, respectively. In contrast, the selectivity given by the ratio of Henry's-law constants is 3.5. On the other hand, in the separation shown in Fig. 5, the selectivity, α_{BA}, at the column inlet is 0.933 (*i.e.*, α_{AB} = 1.07), at (c_A^*, 0) it is 0.646 (α_{AB} = 1.55) and at (0, c_B^*) it is 0.827 (α_{AB} = 1.21); however, the ratio of Henry's-law constants, α^0, is 1.33. The long development required for this separation is largely due to the very low initial selectivity. It is interesting that the selectivities at the end points of the tie lines are different from each other; the consequence of this in Fig. 5B is that the tail of B is somewhat sharper than the front of A.

In order to investigate how the feed concentration affects the profiles calculated with the IAS/L isotherm, we have carried out numerous simulations with the same parent isotherms and operating lines as in Figs. 4a and 5a, but with feed concentrations that, in the hodograph space, lie across the line of unit selectivity from the predicted separated pattern. Although higher plate numbers were required to bring about the separation, final patterns of complete separation were always achieved. Thus, at least within the hermeneutics of the IAS/L isotherm, the stability criterion appears to provide a sufficient condition for a given final pattern to eventually prevail.

The separation gap: formation of azeotropes

When the operating line lies in the separation gap, as illustrated in Fig. 7a, according to the stability analysis no completely separated state can be reached because the pattern would be unstable. Indeed, the calculated profiles in Fig. 7b show no sign of any separation. This kind of mixed displacement profile has been reported [16,39].

When operating in the separation gap, the final state eventually reached depends on the composition of the feed. Let us consider a displacement process, with the operating line in the gap, that has reached a coherent state, *i.e.*, with concentration profiles that no longer change as the bands continue to traverse the column. As shown above, the final pattern of complete separation is unstable and hence a mixed zone must form. For the mixed zone to persist at a given composition, it must travel at the velocity of the displacer and the composition of the components must be such that the selectivity is unity (or else there is a tendency for change). Thus the composition of the mixed zone must lie on the line of unit selectivity in the hodograph. If the proportion of the two components in the feed differs from that of such a mixed zone, conservation of mass dictates that there must be at least one other zone. In general, there could be several mixed zones that have the requisite properties; however, when adsorption is governed by the IAS/L isotherm, there is only one such mixed zone. Thus the other zone must be that of a pure substance. Depending on the relative amounts of the separands in the feed with respect to those of the mixed zone, the pure band contains either component A or B.

The mixed zone represents an "azeotropic" composition, *i.e.*, a mixed band that persists in the course of the displacement process. Unlike azeotropes in distillation which form only at one composition, all compositions along the unit selectivity line appear to be potential azeotropic points. Also, unlike in distillation, the azeotrope may be broken, at least in principle, simply by changing the displacer concentration so that the operating line moves out of the gap. Further, the elimination of any potential selectivity inversion or azeotropy by addition of another component may be possible as has been proposed [23,40] and is discussed later.

What order of appearance is expected for the train of mixed and pure zones? Consider the situation where the pure band is component A. As in the "Gedanken experiments" conducted earlier, let us bring a trace of B from the mixed band into the domain of A. The hodograph in Fig. 3b shows that when the operating and tie lines lie in the separation gap, the point $(c_A^*, 0)$ is in the region of reversed selectivity. Thus the trace of B should move more rapidly than A and be pushed ahead. If the pure band were B instead, a trace of A brought into its domain would likewise be pushed ahead because the point $(0, c_B^*)$ is in the region of original selectivity. This forces us to

the conclusion that whether the pure band is of A or B, it must be located behind the mixed band.

In an attempt to confirm these assertions, several simulations were performed with the operating line in the separation gap and with feed concentrations such that either A or B were in excess with respect to the anticipated mixed-zone composition. Under such conditions, the displacement train evolved extremely slowly; *e.g.*, with parameters similar to those in Fig. 7, more than 15 000 plates were typically required before an unequivocal trend towards the expected final state could be discerned. The slow development is not surprising, because at the concentrations in question the selectivity is always close to unity.

In order to circumvent the lengthy calculations, another approach was taken to examine the order of the mixed and pure bands. In the simulations the feed itself was introduced in the anticipated final state, *i.e.*, with a mixed zone at the relevant composition along the unit selectivity line, either preceded or followed by a pure band of A or B. (The anticipated mixed-zone composition was found by searching the unit selectivity line numerically for the point where its velocity is equal to that of the displacer). It was reasoned that if the feed pattern closely resembled the actual final state, the concentration profiles would show very little change, apart from dispersion,

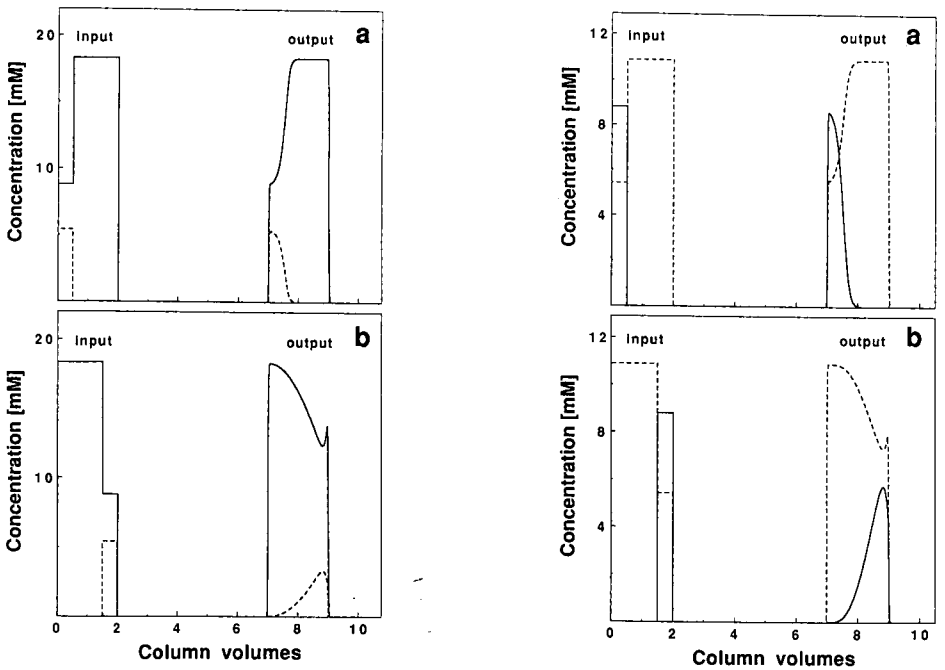

Fig. 8. Displacement profiles calculated with input profiles having a pure zone of component A (——) and a mixed zone containing components A (——) and B(- - - -). In (a) the mixed zone precedes the pure zone into the column and in (b) the inlet order of zones is reversed. Parameters as in Fig. 7 with a displacer concentrations of 23 mM. The mixed zone composition lies along the unit selectivity line in Fig. 3b with c_A = 8.8 and c_B = 5.42. The displacer profile is not shown.

Fig. 9. Displacement profiles calculated with input profiles composed of a pure zone of B and a mixed zone containing components A and B as shown in the plots. All other conditions as in Fig. 8.

when the displacement proceeds over a significant length of column. The feed and corresponding effluent patterns from a 10 000-plate column when the pure band of A follows and precedes the mixed band are shown in Fig. 8a and b, respectively. The results are in accord with our expectations: when the pure band follows the mixed band, the change in the concentration profiles is minimal when the bands traverse the column. When the order of mixed and pure bands is reversed, however, the concentration profiles in the effluent no longer resemble the input profiles. In Fig. 9a and b, similar results are shown when the pure band is component B.

Azeotropy with non-IAS multi-component isotherms

All systems that display selectivity inversion are not likely to behave as the IAS/L isotherm predicts. In Appendix A, a result is derived that shows that all MC isotherms based on the IAS theory, regardless of the form of the parent isotherms (as long as they do not have points at which $dq/dc \rightarrow \infty$), are constrained in such a way that points of constant selectivity lie on straight lines in hodograph space. Further, it is shown that in such systems, if points of unit selectivity exist, they must lie on a line of slope -1; eqn. 15 is a special case of this for Langmuir parent isotherms. Much as constant selectivity over the entire composition range is an artifact of the competitive Langmuir equation, this constraint is a shortcoming of IAS isotherms. The IAS approached represents a significant improvement over the MC Langmuir isotherm, as it can describe systems with variable selectivity, but it is by no means the only correct MC isotherm. Indeed, to describe real systems, non-idealities must often be incorporated, and the behavior may be considerably different form that predicted by the IAS method [22,37,38]. With this background, a brief discussion of selectivity reversal and azeotropy in non-IAS/L systems is presented here.

With the IAS/L isotherm, the concentration c_x always lies beyond the intersection points of the SC isotherms. As a consequence, the operating lines in the hodograph, *i.e.*, the tie lines, which lie in the separation gap are always less steep than the unit selectivity line, as shown in Fig. 3a. Thus, for tie lines within the gap, the points $(0, c_B^*)$ and $(c_A^*, 0)$ always lie in the region of initial and opposite selectivity and the argument given above for the order of the mixed and pure bands always holds. On the other hand, if the adsorption were governed by some other MC isotherm so that the pertinent tie lines were now steeper than the unit selectivity line (which is not necessarily straight), the point $(c_A^*, 0)$ for a tie line that crosses the unit selectivity line would lie in the region of original selectivity, whereas $(0, c_B^*)$ would now lie in the region of reversed selectivity. The "Gedanken experiment" above would then yield the opposite result, and the pure band would be expected to precede the mixed one. With some MC isotherms the unit selectivity line may coincide with a tie line, and there is no separation gap or azeotropy even though the system exhibits selectivity reversal, as shown in Appendix B for the generalized multi-component Langmuir isotherm.

These are only two examples of departure from the IAS/L MC isotherm. In a study of azeotropy in frontal chromatography, Basmadjian *et al.* [41] have pointed out several further possibilities for azeotropic systems that do not fall within the purview of the IAS method. For example, they consider two cases where the hodograph space is broken up into more than two regions of inverted selectivity. In such a system, if a suitable displacer were to be found, mere meeting of the stability

conditions discussed above may be insufficient to obtain separated displacement pattern from any previously mixed state. There is then no recourse but to search for all points on the concentration axes and the unit selectivity lines that have species velocities equal to that of the displacer, and decide which combinations of such points would eventually evolve as the final state from a given feed composition.

One system that shows simpler behavior than what has just been described, but is unlike that predicted by the IAS approach, is that of benzenesulfonic acid and *p*-nitrophenol adsorbed from aqueous solutions onto activated carbon [41]. Here the unit selectivity line appears to project outward from the origin of the hodograph. If a suitable displacer were chosen for this system, all possible tie lines would be found to intersect the unit selectivity line. It would therefore be impossible to obtain a completely separated displacement train in this system regardless of the displacer concentration. By performing an analysis akin to that mentioned above, one can predict for such systems that the final pattern ought to be one where a pure band of either component, depending on the relevant feed and azeotropic compositions, precedes a mixed band.

Eliminating azeotropes by adding another component

The results of this study show that selectivity reversal is in general detrimental to displacement chromatography, even when stable patterns of complete separation are expected. As suggested in previous studies, the addition of another component can be used to eliminate an possibility of azeotropy [23,40]. As we have not yet found a strategy by using a component merely added to the feed, we are considering here the addition of another component to the carrier. In order to determine the concentration of a component C required to ensure that there are no longer any points of unit selectivity in the c_A–c_B hodograph, we rearrange eqn. 11, written for three components and evaluated at $\Pi = \Pi'$ (see eqn. 14) to obtain

$$c_A + c_B = \frac{\exp(\Pi'/\lambda_A) - 1}{b_A}\left(1 - \frac{b_C c_C}{\exp(\Pi'/\lambda_C) - 1}\right) = c_x(c_C) \tag{16}$$

The total concentration of unit selectivity, c_x, is now seen to be a function of the concentration of the additive, c_C. This concentration goes to zero at $c_C = [\exp(\Pi'/\lambda_C) - 1]/b_C$; above this the value of Π is always greater than Π', and there will no longer be a unit selectivity line. However, the addition of a third component in such a manner is accompanied by both a reduction in the retention and the sorption capacity of components A and B. When this effect is large it may render the system useless for preparative separations [23,40]. The reduction in retention and the sorption capacity depends on Π', which is determined from the isotherm parameters of A and B alone and is thus largely independent of the particular components C employed. As a consequence, in systems where the reduction in sorption capacity by addition of a particular additive is too severe, it is not likely that the use of another additive will be successful. In such cases, it would be necessary to change other conditions, such as pH, temperature or even the sorbent itself in order to eliminate completely the unwanted selectivity reversal.

ACKNOWLEDGEMENTS

This work was supported by Grant No. GM20993 from the National Institutes of Health, US Department of Health and Human Resources and by the National Foundation for Cancer Research.

APPENDIX A

After presenting an outline of the IAS method an expression is derived for the points of constant selectivity in hodograph space that is generally valid for multi-component isotherms based on the ideal adsorbed solution (IAS) approach and facilitates the analysis of such MC isotherms.

The IAS method

The IAS approach provides a framework to generate thermodynamically consistent multi-component adsorption isotherms from any set of single-component isotherm data [21,22]. The basic hypothesis is that the adsorbed phase is "ideal" in sense corresponding to Raoult's law in liquid–vapor equilibria. That is, the fluid phase concentration, c_i, of a component i in equilibrium with the adsorbed phase is related to a standard state concentration, c_i^s by

$$c_i = z_i c_i^s \qquad i = 1, \ldots, N \tag{A-1}$$

where z_i is the mole fraction of i in the adsorbed phase and N is the total number of adsorbed components. In adsorption from liquid solutions, the adsorbed phase is defined by the "solvent-not-adsorbed" convention and therefore the mole fraction does not include the principal solvent [22]. The standard state is defined as a system containing only the component i (and the principal solvent) at the same temperature and spreading pressure as the multi-component system being considered. The spreading pressure, π, is the difference between the solution–sorbent interfacial tension and the pure reference solvent–sorbent interfacial tension. A reduced spreading pressure, Π, is defined as $\pi A/RT$, where A is the surface area of the sorbent assumed to be equally accessible to all adsorbates, R is the gas constant and T is the temperature. The standard state concentration c_i^s is not a constant at a given temperature, as is the saturation vapor pressure in Raoult's law, but depends on Π which varies with the composition of the multi-component mixture. The relationship between Π and c_i^s is determined from the Gibbs' adsorption equation and the adsorption isotherm for a single component using the expression [22]

$$\Pi = \int_0^{c_i^s} \frac{q_i(c_i)}{c_i} \cdot \mathrm{d}c_i \qquad i = 1, \ldots, N \tag{A-2}$$

where $q_i(c_i)$ is the pertinent SC isotherm. Note that since q_i and c_i are always positive, in the absence of conditions under which $\mathrm{d}q_i/\mathrm{d}c_i \to \infty$, Π is a single-valued function of c_i^s and *vice versa*. As the concentrations, c_i, in multi-component solution are

known, and the sum of the mole fractions in the adsorbed phase is unity, Π can be determined in principle form the single equation

$$\sum_{j=1}^{N} \frac{c_j}{c_j^s(\Pi)} = 1 \tag{A-3}$$

This equation can be employed in practice only when an explicit relationship for c_i^s as a function of Π can be found from eqn. A-2. For example, eqn. 11 corresponds to this equation written for the case where the single-component isotherms have the Langmuirian form. If the integral in eqn. A-2 cannot be solved analytically and the function cannot be inverted explicitly, other numerical methods must be employed to determine Π [42]. Once Π and therefore c_i^s are known, then z_i for each component can be found from eqn. A-1.

It can be shown that the total adsorbed amount on the stationary phase, q_T, is given by [22]

$$q_T = \frac{1}{\sum_{j=1}^{N} \frac{z_j}{q_j^s}} \tag{A-4}$$

where q_i^s is the stationary phase concentration of i in equilibrium with c_i^s in the respective single-component system. The adsorbed amounts of each component, q_i, are then simply given by

$$q_i = z_i q_T \tag{A-5}$$

Eqn. 12 is a combination of eqns. A-4 and A-5 written in terms of Π and c_i for the case of SC Langmuir isotherms.

Constant selectivity with IAS isotherms

Here it is shown that the selectivity for any two components, in the case of MC isotherms obtained by the IAS method, is a function of the reduced spreading pressure, Π. Further, it is shown that for nearly all forms of the parent isotherms in a binary system with two components A and B, the locus of constant selectivity, α_{BA}, in a hodograph of c_B *versus* c_A, is a straight line of slope $-1/\alpha_{BA}$. It follows then that, if they exist, points of unit selectivity in any binary IAS isotherm lie on a straight line of slope -1.

Combining eqns. A-1 and A-5 yields

$$q_i = \frac{c_i}{c_i^s(\Pi)} \cdot q_T \tag{A-6}$$

The selectivity for two components, α_{BA}, is defined as $q_B c_A / q_A c_B$; from eqn. A-6 the selectivity is thus seen to be

$$\alpha_{BA} = \frac{c_A^s(\Pi)}{c_B^s(\Pi)} \tag{A-7}$$

which is a function of Π only (besides the parameters of the parent isotherms).

Combining equation A-3 written for a binary system with eqn. A-7 and rearranging the result yields

$$c_B = c_B^s(\Pi) - \frac{c_A}{\alpha_{BA}(\Pi)} \tag{A-8}$$

Thus the loci of constant α_{BA} (or of constant Π) are straight lines of slope $-1/\alpha_{BA}$ in the hodograph space. Eqn. A-8 is meaningful only when c_A^s and c_B^s are single-valued functions of Π, which is always the case as long as there are no points on the SC isotherms at which $dq_i/dc_i \to \infty$. Note that in general there could be several values of Π for which the selectivity is the same, and consequently several parallel lines in the hodograph having the same selectivity. Eqn. 15 in the text is a special case of eqn. A-8 written for $\alpha_{BA} = 1$ and Langmuir SC isotherms.

APPENDIX B

Generalized multi-component Langmuir isotherm with selectivity inversion

Here another thermodynamically consistent MC isotherm is presented that can account for cases where the individual components have different saturation capacities. The derivation is essentially a simple extension of the equilibrium arguments that lead to the competitive Langmuir isotherm, and it is therefore called the generalized multi-component Langmuir (GML) isotherm. (The isotherm may well have been described before, but we could not find any reference to it. It is formally similar to the multivalent ion-exchange isotherm [43], with the exception that no electroneutrality condition must be satisfied at the sorbent surface). This isotherm formalism will then be used in the same way as he IAS/L isotherm was in the main body of the text, to examine the different operating regions of displacement chromatography.

The generalized multi-component Langmuir isotherm

Consider the set of binding reactions

$$i + \nu_i\Theta \Leftrightarrow \overline{i\Theta_{\nu_i}} \qquad i = 1, \ldots, N \tag{B-1}$$

where i is one of N species in the liquid phase, Θ is a free binding site on the sorbent, ν_i is a stoichiometric coefficient and $\overline{i\Theta_{\nu_i}}$ represents i in the adsorbed state on the stationary phase. The equilibrium constants, K_i, for the process are represented by

$$K_i = \frac{q_i}{c_i[\Theta]^{\nu_i}} \qquad i = 1, \ldots, N \tag{B-2}$$

where q_i and c_i are the respective concentrations of i in the stationary and mobile phases and $[\Theta]$ represent the concentration of free binding sites. If the total concentration of binding sites is Λ, one can write

$$[\Theta] + \sum_{j=1}^{N} \nu_j q_j = \Lambda \tag{B-3}$$

Substitution of eqn. B-2 into eqn. B-3 yields

$$[\Theta] + \sum_{j=1}^{N} \nu_j K_j c_j [\Theta]^{\nu_j} = \Lambda \tag{B-4}$$

Although eqn. B-4 can in general have multiple solutions, it has only one solution that lies in the range $0 < [\Theta] < \Lambda$, as more than one stationary phase composition in equilibrium with a given mobile phase condition is excluded from this treatment. When this solution is found for $[\Theta]$, the concentrations of the N species in the stationary phase are obtained on rearranging eqn. B-2 as

$$q_i = K_i c_i [\Theta]^{\nu_i} \qquad i = 1, \ldots, N \tag{B-5}$$

It is noted that eqns. B-5 and B-4 reduce to the competitive Langmuir equation when all the stoichiometric coefficients, ν_i, are unity.

The corresponding parent isotherm for component i is given by the implicit expression

$$q_i = K_i c_i (\Lambda - \nu_i q_i)^{\nu_i} \qquad i = 1, \ldots, N \tag{B-6}$$

This isotherm has the initial slope $K_i \Lambda^{\nu_i}$ and saturation capacity Λ/ν_i. Fitting of experimental single-component isotherm data to this equation is a non-trivial exercise because, in order to ensure a unique value of Λ, all the isotherms involved must be fit simultaneously. These difficulties are not germane here, however, as the concern is how a set of components that follow such an isotherm would behave in displacement chromatography.

Selectivity inversion

The selectivity, α_{BA} when eqn. B-5 holds is given by

$$\alpha_{BA} = \frac{q_B c_A}{q_A c_B} = \frac{K_B [\Theta]^{\nu_B}}{K_A [\Theta]^{\nu_A}} \tag{B-7}$$

Thus, when α_{BA} is unity, the corresponding concentration of free sites, $[\Theta]'$, is

$$[\Theta]' = \left(\frac{K_A}{K_B}\right)^{\frac{1}{\nu_B - \nu_A}} \tag{B-8}$$

As mentioned above, $[\Theta]'$ must lie between 0 and Λ. Thus, with the GML isotherm, selectivity inversion will occur only when

$$\Lambda > \left(\frac{K_A}{K_B}\right)^{\frac{1}{\nu_B - \nu_A}} \tag{B-9}$$

This condition is satisfied for $\nu_B > \nu_A$ when $K_B\Lambda^{\nu_B} > K_A\Lambda^{\nu_A}$, and *vice versa, i.e.,* whenever the parent isotherms cross.

On substituting eqn. B-8 into eqn. B-4 we find that the locus of unit selectivity in c_A-c_B hodograph space is a straight line given by

$$c_B = c'_B - \frac{\nu_A}{\nu_B} \cdot c_A \tag{B-10a}$$

This line has slope $-\nu_A/\nu_B$, and intercept c'_B given by

$$c'_B = \left[\Lambda - \left(\frac{K_A}{K_B}\right)^{\frac{1}{\nu_B - \nu_A}}\right] \Bigg/ \left[\nu_B K_B \left(\frac{K_A}{K_B}\right)^{\frac{\nu_B}{\nu_B - \nu_A}}\right] \tag{B-10b}$$

Operating regimes for displacement chromatography

To determine the different operating regimes in the case of crossing isotherms for the multi-component isotherm formalism given by eqn. B-5, we examine first the equation of the tie line that connects those points on the c_A and c_B axes in the hodograph which correspond to the intersections of the respective parent isotherms with an operating line of slope Δ. The intersection points with the parent isotherms can be found from eqn. B-6 to be

$$c_i^* = \left[\Lambda - \left(\frac{\Delta}{K_i}\right)^{\frac{1}{\nu_i}}\right] \Big/ \nu_i \Delta \qquad i = A, B \tag{B-11}$$

The tie line that connects $(0, c_B^*)$ and $(c_A^*, 0)$ in the hodograph is given by the equation $c_B = c_B^* - (c_B^*/c_A^*)c_A$. Expressing the pertinent concentrations from eqn. B-11 we obtain that the slope of this tie line, m_T, is given by

$$m_T = -\left[\frac{\Lambda - \left(\frac{\Delta}{K_B}\right)^{\frac{1}{\nu_B}}}{\Lambda - \left(\frac{\Delta}{K_A}\right)^{\frac{1}{\nu_A}}}\right] \frac{\nu_A}{\nu_B} \tag{B-12}$$

The term in square brackets on the right-hand side of eqn. B-12 becomes unity at

$$\Delta = \left(K_B^{\frac{1}{\nu_B}} / K_B^{\frac{1}{\nu_B}}\right)^{\frac{\nu_A \nu_B}{\nu_B - \nu_A}} \equiv \Delta^* \tag{B-13}$$

After some algebraic manipulation, it can be shown that at this value of Δ, $c_B^* = c'_B$. Thus the tie line passing through c'_B has the same slope, $-\nu_A/\nu_B$, as the unit selectivity line. Additionally, one can show that no tie line actually crosses the unit selectivity line. Thus, within the framework of the GML isotherm, when the parent isotherms of A and B cross there are two operating regions, separated from each other by an operating line of slope Δ^*. These regions correspond to final patterns of complete separation with different order of the components: for operating lines of slope greater than Δ^* the order is AB, and for those with slope lower than Δ^* it is BA.

REFERENCES

1 A. Tiselius, *Kolloid Z.*, 105 (1943) 101.
2 F. D. Antia and Cs. Horváth, *Ber. Bunsenges. Phys. Chem.*, 93 (1989) 961.
3 E. Glückauf, *Proc. R. Soc. London, Ser. A*, 186 (1946) 35.
4 F. Helfferich and G. Klein, *Multicomponent Chromatography*, Marcel Dekker, New York, 1970.
5 A. Tiselius, *Ark. Kemi, Mineral. Geol.*, 16A, No. 18 (1943) 1.
6 F. H. Spedding, E. I. Fulmer, T. A. Butler and J. E. Powell, *J. Am. Chem. Soc.*, 72 (1950) 2349.
7 Cs. Horváth, in F. Bruner (Editor), *The Science of Chromatography*, Elsevier, New York, 1985, p. 179.
8 J. Frenz and Cs. Horváth, in Cs. Horváth (Editor), *High Performance Liquid Chromatography: Advances and Perspective*, Vol. 5, Academic Press, New York, 1988, pp. 211–314.
9 Cs. Horváth, A. Nahum and J. Frenz, *J. Chromatogr.*, 218 (1981) 365.
10 H. Kalász and Cs. Horváth, *J. Chromatogr.*, 215 (1981) 295.
11 Z. El Rassi and Cs. Horváth, *J. Chromatogr.*, 266 (1983) 319.
12 F. D. Antia and Cs. Horváth, in R. S. Hodges and C. T. Mant (Editors), *HPLC of Peptides and Proteins: Separation, Analysis and Conformation*, CRC Press, Boca Raton, FL 1990, p. 809–821.
13 Cs. Horváth, A. L. Lee, A. Velayudhan and G. Subramanian, presented at *Dal Nogare Symposium at the Pittsburgh Conference, Atlantic City, NJ, March 9–13, 1987.*
14 A. L. Lee, *Ph.D. Thesis*, Yale University; New Haven, CT, 1990.
15 G. Vigh, G. Quintero and G. Farkas, *J. Chromatogr.*, 506 (1990) 481.
16 G. Subramanian and S. M. Cramer, *Biotechnol. Prog.*, 5 (1989) 92.
17 D. B. Broughton, *Ind. Eng. Chem.*, 40 (1948) 1506.
18 C. Kemball, E. K. Rideal and E. A. Guggenheim, *Trans. Faraday Soc.*, 44 (1948) 948.
19 D. M. LeVan and T. Vermeulen, *J. Phys. Chem.*, 85 (1981) 3247.
20 L. Hagdahl, R. J. P. Williams and A. Tiselius, *Arkiv Kemi Miner. Geol.*, 4 (1951) 193.
21 A. L. Myers and J. M. Prausnitz, *AIChE J.*, 11 (1965) 121.
22 C. J. Radke and J. M. Prausnitz, *AIChE J.*, 18 (1972) 761.
23 A. K. Velayudhan, *Ph. D. Thesis*, Yale University, New Haven, CT, 1990.
24 D. D. Frey, *J. Chromatogr.*, 409 (1987) 1.
25 F. Riedo and E. sz. Kováts, *J. Chromatogr.*, 239 (1982) 1.
26 W. R. Melander, J. F. Erard and Cs. Horváth, *J. Chromatogr.*, 282 (1983) 211.
27 I. Langmuir, *J. Am. Chem. Soc.*, 38 (1916) 2221.
28 J. Jacobson, J. Frenz and Cs. Horváth, *J. Chromatogr.*, 316 (1984) 53.
29 J. X. Huang and Cs. Horváth, *J. Chromatogr.*, 406 (1987) 275.
30 J. X. Huang and Cs. Horváth, *J. Chromatogr.*, 406 (1987) 285.
31 M. J. Jacobson, H. J. Frenz and Cs. Horváth, *Ind. Eng. Chem. Res.*, 26 (1987) 43.
32 J. X. Huang and G. Guichon, *J. Colloid Interface Sci.*, 128 (1989) 577.
33 G. M. Schwab, *Ergebnisse der exakten Naturwissenschaften*, Vol. 7, Julius Springer, Berlin, 1928, p. 276.
34 J. Frenz and Cs. Horváth, *AIChE J.*, 31 (1985) 400.
35 G. Guiochon and S. Ghodbane, *J. Phys. Chem.*, 92 (1988) 3682.
36 M. Czok and G. Guiochon, *Anal. Chem.*, 62 (1990) 189.
37 O. Talu and I. Zwiebel, *AIChE J.*, 32 (1986) 1263.
38 A. L. Myers, in A. I. Liapis (Editor), *Fundamentals of Adsorption*, Engineering Foundation, New York, 1987, pp. 3–25.
39 A. W. Liao, *Ph. D. Thesis*, Yale University, New Haven, CT, 1990.
40 F. D. Antia and Cs. Horváth, *J. Chromatogr.*, 550 (1991) 411.
41 D. Basmadjian, P. Coroyannakis and C. Karayannopoulos, *Chem. Eng. Sci.*, 42 (1987) 1737.
42 J. A. O'Brien and A. L. Myers, *Ind. Eng. Chem. Process Des. Dev.*, 24 (1985) 1188.
43 A. Velayudhan and Cs. Horváth, *J. Chromatogr.*, 443 (1988) 13.

Journal of Chromatography, 556 (1991) 145–158
Elsevier Science Publishers B.V., Amsterdam

CHROM. 23 388

Method for characterization of selectivity in reversed-phase liquid chromatography

V. Calibration of the retention scale for chromatographic systems with low concentrations of organic solvents in the mobile phase

PAVEL JANDERA* and JITKA ROZKOŠNÁ
Institute of Chemical Technology, Department of Analytical Chemistry, Nám. Legií 565, 53210 Pardubice (Czechoslovakia)

ABSTRACT

The method for the characterization and prediction of selectivity and absolute retention in reversed-phase liquid chromatography based on two indices (a lipophilic and a polar one) has been previously applied to chromatographic systems with mobile phases containing 50% and more of one or two organic solvent(s). Because of a high retention, the homologues series of *n*-alkylbenzenes is not suitable for the direct calibration of the retention scale in mobile phases with lower concentrations of organic solvents, and the extrapolation of the calibration parameters based on the data for this series in mobile phases with low water content yields predicted retention data that are subject to significant errors. To circumvent this inconvenience and to expand the application possibilities of the above method to mobile phases with higher concentrations of water, three homologous series were tested as potential candidates for calibration standards: 3-*n*-alkyl-6-methyluracils, 3-alkoxycarbonyl-2-pyrazolines and alkan-2-ones. All three homologous series tested were found to be suitable substitutes for *n*-alkylbenzenes as calibration standards in mobile phases containing 25–50% methanol in water. The selection of suitable calibration standards for acetonitrile–water mobile phases is more difficult because of a curvature of the dependence of log k' on the concentration of acetonitrile at low concentrations of this solvent in aqueous mobile phases. Here, the alkoxycarbonyl pyrazolines and alkan-2-ones proved useful as calibration standards in mobile phases containing 30–50% acetonitrile. The agreement between the predicted and experimental k' was within 10% or better of the experimental k'.

INTRODUCTION

Because of the restricted availability of a number of physico-chemical constants involved in various theoretical models of retention in reversed-phase liquid chromatography, precise prediction of retention using these complex models is not possible at present without preliminary experimental data. Hence, most prediction methods rely on calibration of the retention scale using suitable reference data. Some prediction methods are based on correlations of the retention data with various structur-

0021-9673/91/$03.50

al descriptors and related parameters; other use a scale of retention indices similar to the Kováts retention indices in gas chromatography, based on alkyl aryl ketones [1,2], alkan-2-ones [3,4] or polyaromatic hydrocarbons [5,6] as the reference compounds. Because of various specific solute–solvent interactions, the retention indices are usually sensitive to changes in the composition of the mobile phase [7], and the single-index approach is reliable only within a narrow composition range of mobile phases. The prediction method based on the interaction indices [8,9] also cannot take full account of these effects over a broad range of mobile phase compositions [10].

To avoid the necessity of recalibration of the retention scale with changing mobile phase composition, the retention indices or their structural contributions were expressed as a quadratic function of the concentration of the organic solvent in the mobile phase, and it was suggested that the coefficients of these equations be used in the predictive calculations [7].

Another solution to this problem was introduced earlier. In this, two indices are used simultaneously to characterize the retention of each sample solute [10]. One index, n_{ce}, accounts for the hydrophobicity of the solute matrix, and the other, q_i, for the polarity of the functional groups in the molecule of the solute and its effects on the interactions with the components of the mobile phase. The retention scale is calibrated using a reference homologous series over a wide range of mobile phase compositions and the retention, expressed in terms of capacity factors, k', is predicted using eqn. 1:

$$\log k' = (a_0 + a_1 \cdot n_{ce}) \cdot (1 - p \cdot x) - q_i \cdot x \qquad (1)$$

where n_{ce} and q_i are the lipophilic and polar indices of a given solute, respectively, x is the concentration of the organic solvent in the water–organic solvent mobile phase [in % (v/v) $\cdot 10^{-2}$] and a_0, a_1 and p are the constants of the calibration equation, valid for a given type of column packing (stationary phase), organic solvent and calibration homologous series [10]. The index n_{ce} has the meaning of a hypothetical equivalent number of carbon atoms in the alkyl chain of the calibration homologous series and depends on the type of the calibration series; ideally, it should depend only slightly on the column packing material and on the type of organic solvent in the mobile phase. On the other hand, the index q_i is a measure of solute–solvent interactions and is expected to depend strongly on the organic solvent.

Homologous *n*-alkylbenzenes were found to be suitable for the calibration of the retention scale using eqn. 1 in binary mobile phases containing 50–90% methanol, acetonitrile, 1,4-dioxane or tetrahydrofuran [10,11] and in ternary mobile phases of methanol–acetonitrile–water [12], and the use of this method was later adapted also for reversed-phase chromatography with gradient elution [13].

The indices n_{ce} and q_i can be calculated from the data plot of $\log k'$ *versus* x, using linear regression. It is also possible to use the quadratic regression for the analysis of strongly curved data plots; in this case an additional second-order term with respect to x is introduced in eqn. 1 [10,11]. The constants a_0, a_1 and p are determined from the experimental data of the dependence of k' of the calibration homologous series on x and on the number of carbon atoms in the alkyl chain, n_c, of the individual homologues [14]:

$$\log k' = (a_0 + a_1 \cdot n_c) \cdot (1 - p \cdot x) - q \cdot x \qquad (2)$$

The accuracy of the prediction of k' is significantly improved when the differential indices, Δn_c and Δq, related to a standard reference compound (such as toluene, the alkylbenzene with $n_c = 1$) are used instead of n_{ce} and q_i in eqn. 1 to calculate the relative retention with respect to the standard:

$$\alpha = k'/k'_s \tag{3}$$

Eqn. 1 is then transformed to:

$$\log \alpha = a_1 \cdot (1 - p \cdot x) \cdot \Delta n_c - x \cdot \Delta q \tag{4}$$

where $\Delta n_c = n_{ce} - n_{c,s}$ $\quad \Delta q = q_i - q_s$ (5a and b)

and k'_s, $n_{c,s}$ and q_s are the capacity factor k' and the indices n_{ce} and q_i of the reference standard compound (*e.g.* toluene) [11,12].

This calibration method was found to be useful in explaining the experimental behaviour of various oligomeric series, including occasionally occurring changes in the order of elution depending on the composition of the mobile phase and on the type of the functional end group [15].

In mobile phases containing low concentrations of organic solvent, even the lowest homologous alkylbenzenes are strongly retained ($k' > 10$), which makes the use of the alkylbenzene calibration series unpractical. To allow the use of the above method of calibration and prediction of retention in water-rich mobile phases, another suitable less retained calibration homologous series should be found with less bulk and/or a more polar functional end group than the benzene ring. For this purpose, three homologous series are tested in this work, namely 3-*n*-alkyl-6-methyluracils, 3-alkoxycarbonyl-2-pyrazolines and alkan-2-ones, all of which are UV-absorbing and thus can be readily used in reversed-phase chromatography with UV detection.

Earlier attempts at using the parameters a_1 and p of the alkylbenzene homologous series, determined in water poor mobile phases, in mobile phases with low concentrations of organic solvents were not successful. Instead of using the extrapolated constants, we decided to measure a few experimental data for toluene, ethylbenzene and, possibly, for *n*-propylbenzene in the investigated range of mobile phase compositions to determine the constants of the calibration eqn. 4, even though the values determined from a small number of experimental data may not be very precise, in order to get some idea of the performance of the other potential calibration homologous series in comparison with alkylbenzenes.

For the test solutes, we selected some simple aromatic compounds and some structurally more complex pesticides and their metabolites of practical importance.

EXPERIMENTAL

The equiment used included a Model 6000A pump, a U6K injector and a Model 440 UV detector, operated at 254 nm, all from Waters–Millipore (Milford, MA, USA). The detector signal was registered using a TZ 4100 line recorder (Laboratory Instrument Works, Prague, Czechoslovakia). The chromatographic column was stainless steel, 300 × 3.8 mm I.D., packed in the laboratory with Silasorb C_{18},

10 μm, octadecylsilica (Lachema, Brno, Czechoslovakia), using a high-pressure slurry-packing technique.

The mobile phases were prepared by mixing water (double-distilled in glass with addition of potassium permanganate) with either methanol or acetonitrile (spectroscopic grade, Lachema) in desired volume ratios. All the solvents were filtrated using a Millipore 0.45-μm filter and the premixed mobile phases were degassed by ultrasonication before use.

The column dead volume, V_M, was determined as the retention volume of ^2H_2O in each mobile phase employed, using a Model R 401 refractometric detector (Waters). The experimental values of V_M were in the range from 2.36 to 2.25 cm^3 in 25–50% methanol and from 2.64 to 2.05 cm^3 in 25–50% acetonitrile.

The capacity factors, $k' = (V_R/V_M - 1)$, were calculated from the arithmetic means of two or three experimental retention volumes, V_R, in repeated experiments. From the plots of the experimental k' at different compositions of the mobile phase, the parameters a and m of eqn. 6 were determined using linear regression (Table II):

$$\log k' = a - m \cdot x \tag{6}$$

The constants a_0, a_1 and m of the homologous series tested were determined from the constants a and m of the individual homologoues as described elsewhere [11]. The indices n_{ce} and q_i were calculated after combining eqns. 1 and 6 as:

$$n_{ce} = (a - a_0)\, a_1 \tag{7}$$

$$q_i = m - p \cdot a \tag{8}$$

where a and m relate to the individual test solutes and a_0, a_1 and p to the calibration homologous series. Eqn. 5a and b was used to calculate the indices Δn_c and Δq, related to toluene as the reference compound [11].

The capacity factors of the test solutes were predicted from their differential indices Δn_c, Δq, using eqns. 3 and 4 for each of the calibration series tested.

The sample solutes were purchased or obtained from different sources or synthesized at the Departments of Organic Chemistry and Analytical Chemistry, Institute of Chemical Technology, Pardubice, Czechoslovakia. *n*-Alkyl-3-alkoxycarbonyl-2-pyrazolines were prepared by derivatization of alkyl acrylates with diazomethane, as described previously [16]. Table I lists the chromatographed homologous and test compounds.

RESULTS AND DISCUSSION

As is demonstrated by the values of the correlation coefficients in Table II, most compounds studied show good linearity of the log k' *versus* methanol concentrations plots in the concentration range investigated, *i.e.* 25–50% methanol in water, in agreement with eqn. 6. In acetonitrile–water mobile phases, the correlation coefficients are lower than in methanol–water mobile phases for some compounds, such as homologous alkyluracils and alkoxycarbonylpyrazolines, aromatic amides and phenylureas with methoxy substituents on both the nitrogen and the benzene ring. This

TABLE I

LIST OF THE CALIBRATION HOMOLOGOUS SERIES AND TEST COMPOUNDS

I. Calibration compounds

(A) n-Alkylbenzenes

(1) Methylbenzene
(2) Ethylbenze
(3) *n*-Propylbenzene

(B) 3-n-Alkyl-6-methyluracils

(4) 3,6-Dimethyluracil
(5) 3-Ethyl-6-methyluracil
(6) 3-*n*-Propyl-6-methyluracil
(7) 3-*n*-Butyl-6-methyluracil

(C) 3-Alkoxycarbonyl-2-pyrazolines

(8) 3-Methoxycarbonyl-2-pyrazoline
(9) 3-Ethoxycarbonyl-2-pyrazoline
(10) 3-*n*-Propyloxycarbonyl-2-pyrazoline
(11) 3-*n*-Butyloxycarbonyl-2-pyrazoline
(12) 3-*n*-Pentyloxycarbonyl-2-pyrazoline

(D) Alkan-2-ones

(13) Acetone
(14) Methyl *n*-propyl ketone
(16) Methyl *n*-butyl ketone

II. Test compounds

(17) Benzonitrile
(18) Anisole
(19) Acetophenone
(20) Nitrobenzene
(21) Phenetole
(22) Phenyl acetate
(23) Methyl benzoate
(24) Ethyl benzoate
(25) Benzaldehyde
(26) Benzylalcohol
(27) Aniline
(28) Phenol
(29) *o*-Cresol
(30) *p*-Cresol
(31) Linuron (N-(3,4-dichlorophenyl)-N′-methoxy-N′-methylurea)
(32) Ethyl phenylcarbaminate
(33) Benzene
(34) *m*-Bromonitrobenzene
(35) Benzamide
(36) N-Methylbenzamide
(37) Phenylurea
(38) Phenylsulphamide
(39) N,N-Dimethylbenzamide
(40) N-Methylphenylsulphamide
(41) Metoxuron (N-(3-chloro-4-methoxyphenyl)-N′,N′-dimethylurea)
(42) Deschlorometoxuron (N-(4-methoxyphenyl)-N′N′-dimethylurea)
(43) Hydroxymetoxuron (N-(3-chloro-4-hydroxyphenyl)-N′,N′-dimethylurea)
(44) Methomyl (1-methylthio-O-(N-methylcarbamoyl)acetaldoxime)
(45) Simazine (2-chloro-4,6-bis-ethylamino-1,3-5-triazine)
(46) Atrazine (2-chloro-4-ethylamino-6-isopropylamino-1,3,5-triazine)

behaviour obviously originates in the curvature of the log k' *versus* acetonitrile concentration plots in mobile phases containing 25% acetonitrile. The dependence of log k' on the concentration of acetonitrile in the range 30–50% is fairly linear, as in water–methanol mobile phases.

Table III lists the constants a_0, a_1, p and q of eqn. 2 for the four potential calibration homologous series, determined by linear regression of the log k' data in dependence on both n_c and x. Prior to the determination of these constants, good linearity of the plots of log k' and of the constants a and m (eqn. 6) *versus* the number of carbon atoms in the individual homologues, n_c was verified (the results are not shown here). The values of a_0, a_1, p and q for the homologous *n*-alkylbenzenes may be subject to errors resulting from the strong retention of higher homologues in mobile phases with lower contents of organic solvent, which did not allow measurement of their retention data. Only the capacity factors of toluene could be determined over the full concentration range of the mobile phases investigated, with the aim of calculating the constants of eqn. 2; the additional data used for this purpose included only k' of *n*-propylbenzene in 35%-50% acetonitrile (three data points), and k' of *n*-butylbenzene in 40 and 50% acetonitrile; in water–methanol mobile phases only the k' of *n*-propylbenzene in 40 and 50% methanol was used.

TABLE II

CONSTANTS a AND m OF EQN. 6 FOR THE CALIBRATION HOMOLOGOUS COMPOUNDS AND TEST SOLUTES IN METHANOL–WATER (I) AND ACETONITRILE–WATER (II) MOBILE PHASES

R = correlation coefficient. The numbers of the solutes are as in Table I.

Solute	I			II		
	a	m	R	a	m	R
n-Alkylbenzenes						
1	2.547	2.917	0.9932	2.558	3.749	0.9932
2	3.102	3.441	[a]	2.837	3.844	0.9967
3	–	–	–	3.149	3.985	[a]
3-n-Alkyl-6-methyluracils						
4	0.425	2.688	0.9999	−0.023	2.419	0.9535
5	0.824	2.762	0.9990	0.258	2.527	0.9867
6	1.365	3.176	0.9989	0.512	2.538	0.9759
7	1.984	3.699	0.9998	0.904	2.824	0.9975
3-Alkoxycarbonyl-2-pyrazolines						
8	0.624	2.631	0.9967	0.155	1.604	0.9182
9	1.048	2.729	0.998	0.478	1.894	0.9928
10	1.673	3.240	0.9999	0.944	2.427	0.9936
11	2.319	3.825	0.9994	1.513	3.076	0.9970
12	2.877	4.250	[a]	2.012	3.589	0.9936
Alkan-2-ones						
13	0.158	1.688	0.9985	−0.075	0.851	0.9640
14	0.675	1.951	0.9964	0.505	1.583	0.9983
15	1.232	2.352	0.9982	0.940	1.976	0.9952
16	1.884	2.948	0.9995	1.513	2.691	0.9987

TABLE II (*continued*)

Solute	I			II		
	a	*m*	*R*	*a*	*m*	*R*
Test solutes						
17	1.790	3.022	0.9970	1.630	2.905	0.9972
18	2.199	2.935	0.9981	2.064	3.311	0.9977
19	2.005	3.265	0.9986	1.493	2.702	0.9985
20	1.919	2.848	0.9989	1.905	3.181	0.9978
21	2.810	3.714	[a]	2.460	3.642	0.9950
22	1.965	3.755	0.9978	1.485	2.650	0.9970
23	1.996	3.229	0.9990	1.721	2.973	0.9978
24	3.023	4.024	[a]	2.402	3.567	0.9937
25	1.739	2.983	0.9992	1.432	2.635	0.9976
26	1.289	2.508	0.9987	0.856	2.234	0.9984
27	1.075	2.178	0.9974	1.104	2.226	0.9990
28	1.260	2.418	0.9963	1.076	2.421	0.9950
29	1.881	3.042	0.9980	1.533	2.934	0.9972
30	1.899	3.128	0.9978	1.491	2.946	0.9981
31	3.441	4.758	[a]	2.823	4.559	0.9923
32	2.410	3.804	0.9949	1.806	3.001	0.9957
33	1.971	2.448	0.9887	2.058	3.170	0.9979
34	–	–	–	2.588	3.910	0.9955
35	1.021	2.801	0.9995	0.554	2.471	0.9903
36	1.167	2.816	0.9994	0.664	2.317	0.9996
37	1.109	2.798	0.9987	0.614	2.462	0.9946
38	0.886	2.957	0.9978	0.621	2.147	0.9886
39	1.700	3.409	0.9994	0.933	2.455	0.9959
40	1.474	3.046	0.9986	1.175	2.686	0.9955
41	2.382	4.576	0.9996	1.446	3.206	0.9947
42	1.601	3.577	0.9982	0.894	2.573	0.9941
43	1.429	3.649	0.9978	0.816	2.847	0.9970
44	1.052	3.252	0.9985	0.474	1.958	0.9993
45	2.436	3.987	0.9965	1.456	2.819	0.9967
46	2.876	4.228	0.9986	1.969	3.422	0.9961

[a] The constants *a* and *m* were determined using only two data points of capacity factors (for only two different mobile phase compositions), as in other mobile phases the solute is either too strongly or too weakly retained.

Note that the constants a_1 and p in water–methanol mobile phases do not depend significantly on the type of homologous series, in contrast to acetonitrile–water mobile phases. This is in agreement with the earlier results for other homologous series [14]. In acetonitrile–water mobile phases, alkylbenzenes and alkyluracils have values of a_1 and p approximately 2–3 times lower than the corresponding constants for alkoxycarbonylpyrazolines and alkanones, which are however close to each other.

The values of a_0 decrease with decreasing overall retention in a given homologous series, *i.e.* with increasing polarity and decreasing size of the end group (structural residue in the series). The index q increases in the same direction in methanol–water mobile phases, whereas no straightforward structural dependence of this constant is apparent in acetonitrile–water mobile phases.

TABLE III

CONSTANTS a_0, a_1, p AND q OF EQN. 2 FOR THE HOMOLOGOUS SERIES OF *n*-ALKYLBENZENES (A), 3-*n*-ALKYL-6-METHYLURACILS (B), 3-ALKOXYCARBONYL-2-PYRAZOLINES (C) AND ALKAN-2-ONES (D) IN METHANOL–WATER (I) AND ACETONITRILE–WATER (II) MOBILE PHASES

Homologous series	Mobile phase	a_0	a_1	p	q
A	I	1.981	0.563	0.878	0.705
	II	2.296	0.282	0.401	2.718
B	I	−0.300	0.560	0.771	2.116
	II	−0.447	0.342	0.483	2.361
C	I	−0.174	0.616	0.840	1.849
	II	−0.639	0.545	1.109	1.375
D	I	−0.561	0.605	0.828	1.372
	II	−0.527	0.510	1.107	0.992

TABLE IV

INDICES Δn_c AND Δq OF SAMPLE SOLUTES RELATED TO TOLUENE (SOLUTE NO. 1) AS THE REFERENCE STANDARD (EQN. 5a AND b) IN METHANOL–WATER (I) AND ACETONITRILE–WATER (II) MOBILE PHASES, USING *n*-ALKYLBENZENES (A), 3-*n*-ALKYL-6-METHYLURACILS (B), 3-ALKOXYCARBONYL-2-PYRAZOLINES (C) AND ALKAN-2-ONES (D) AS THE CALIBRATION HOMOLOGOUS SERIES

Numbers of solutes are as in Table I.

Solute	Mobile phase	A		B		C		D	
		Δn_c	Δq	Δn_c	Δq	Δn_c	Δq	Δn_c	Δq
17	I	−1.35	0.77	−1.35	0.69	−1.23	0.74	−1.25	0.73
	II	−3.29	−0.47	−2.72	−0.39	−1.71	0.19	−1.82	0.18
18	I	−0.62	0.32	−0.62	0.29	−0.57	0.31	−0.58	0.31
	II	−1.75	−0.24	−1.45	−0.20	−0.91	0.11	−0.97	0.11
19	I	−0.96	0.82	−0.97	0.77	−0.88	0.80	−0.90	0.80
	II	−3,78	−0.62	−3.12	−0.53	−1.96	0.14	−2.09	0.13
20	I	−1.12	0.48	−1.12	0.42	−1.02	0.46	−1.04	0.45
	II	−2.32	−0.30	−1.91	−0.25	−1.20	0.16	−1.28	0.15
21	I	·0.47	0.57	0.47	0.59	0.43	0.58	0.44	0.58
	II	−0.35	−0.06	−0.29	−0.06	−0.18	0.00	−0.19	0.00
22	I	−1.03	0.75	−1.04	0.69	−0.95	0.73	−0.96	0.72
	II	−3.80	−0.67	−3.14	−0.58	−1.97	0.09	−2.10	0.09
23	I	−0.98	0.80	−0.98	0.74	−0.90	0.78	−0.91	0.77
	II	−2.97	0.44	−2.45	−0.37	−1.54	0.15	−1.64	0.15
24	I	0.84	0.69	0.85	0.74	0.77	0.71	0.79	0.71
	II	−0.55	−0.12	−0.46	−0.10	−0.29	−0.01	−0.31	−0.01
25	I	−1.43	0.78	−1.44	0.69	−1.31	0.74	−1.34	0.73
	II	−3.99	−0.66	−3.30	−0.57	−2.07	0.14	−2.21	0.13
26	I	−2.24	0.70	−2.25	0.56	−2.04	0.65	−2.08	0.63
	II	−6.04	−0.83	−4.98	−0.69	−3.13	0.37	−3.34	0.37
27	I	−2.62	0.55	−2.63	0.40	−2.39	0.45	−2.44	0.48
	II	−5.48	−0.90	−4.52	−0.77	−2.84	0.19	−3.23	0.18

TABLE IV (*continued*)

Solute	Mobile phase	A		B		C		D	
		Δn_c	Δq	Δn_c	Δq	Δn_c	Δq	Δn_c	Δq
28	I	−2.28	0.63	−2.30	0.49	−2.09	0.58	−2.13	0.57
	II	−5.26	0.73	−4.34	−0.61	−2.72	0.32	−2.91	0.31
29	I	−1.15	0.78	−1.16	0.71	−1.08	0.68	−1.10	0.68
	II	−3.63	−0.40	−3.00	−0.32	−1.88	0.32	−2.01	0.32
30	I	−1.18	0.71	−1.19	0.64	−1.05	0.76	−1.07	0.75
	II	−3.78	−0.37	−3.12	−0.28	−1.96	0.38	−2.09	0.38
31	I	1.59	1.06	1.59	1.15	1.45	1.09	1.48	1.10
	II	0.94	0.71	0.77	0.68	0.48	0.52	0.52	0.51
32	I	−0.24	1.01	−0.25	0.99	−0.22	1.00	−0.23	1.00
	II	−2.67	−0.44	−2.20	−0.38	−1.38	0.09	−1.48	0.08
33	I	−1.02	0.04	−1.03	−0.02	−0.94	0.01	−0.95	0.01
	II	−1.77	−0.38	−1.47	−0.33	−0.92	−0.02	−0.98	−0.03
34	I	0.48	0.56	0.48	0.59	0.44	0.57	0.45	0.58
	II	0.11	0.15	0.08	0.15	0.05	0.13	0.06	0.13
35	I	−2.71	1.22	−2.73	1.06	−2.48	1.17	−2.53	1.15
	II	−7.11	−0.47	−5.86	−0.31	−3.68	0.95	−3.93	0.94
36	I	−2.45	1.11	−2.46	0.96	−2.24	1.06	−2.28	1.04
	II	−6.72	−0.67	−5.54	−0.51	−3.48	0.67	−3.71	0.66
37	I	−2.55	1.14	−2.57	0.99	−2.34	1.09	−2.38	1.07
	II	−6.89	−0.50	−5.69	−0.34	−3.57	0.87	−3.81	0.86
38	I	−2.95	1.50	−2.97	1.32	−2.70	1.44	−2.75	1.42
	II	−6.87	−0.82	−5.67	−0.66	−3.56	0.55	−3.80	0.54
39	I	−1.50	1.24	−1.51	1.15	−1.38	1.20	−1.40	1.19
	II	−5.76	−0.64	−4.75	−0.51	−2.99	0.51	−3.19	0.50
40	I	−1.90	1.07	−1.92	0.96	−1.74	1.03	−1.78	1.02
	II	−4.90	−0.51	−4.05	−0.39	−2.54	0.47	−2.71	0.47
41	I	−0.29	1.80	−0.30	1.79	−0.27	1.80	−0.27	1.80
	II	−3.94	−0.09	−3.25	0.00	−2.04	0.69	−2.18	0.69
42	I	−1.68	1.49	−1.69	1.39	−1.54	1.45	−1.57	1.44
	II	−5.90	−0.51	−4.87	−0.37	−3.06	0.67	−3.26	0.66
43	I	−1.98	1.71	−2.00	1.59	−1.82	1.67	−1.85	1.66
	II	−6.18	−0.20	−5.10	−0.06	−3.20	1.03	−3.42	1.02
44	I	−2.65	1.65	−2.67	1.47	−2.43	1.59	−2.47	1.57
	II	−7.39	−0.95	−6.10	−0.78	−3.83	0.52	−4.09	0.51
45	I	−0.19	1.17	−0.20	1.16	−0.18	1.16	−0.18	1.16
	II	−3.91	−0.48	−3.23	−0.39	−2.03	0.29	−2.16	0.29
46	I	0.59	1.02	0.59	1.06	0.53	1.04	0.54	1.04
	II	−2.09	−0.09	−1.73	−0.04	−1.08	0.33	−1.16	0.32

The differential structural indices Δn_c and Δq (eqn. 5a and b) of 30 test solutes, related to toluene as the reference standard and calculated using the constants a_o, a_1 and p of the four potential calibration series, are compared in Table IV. In water–methanol mobile phases, good agreement is observed between the differential indices Δn_c and Δq determined using all the individual homologous calibration series. The maximum difference between the individual Δn_c values for a given solute is 0.27, and only for seven compounds are these differences higher than 0.20. Only three differences between the indices Δq exceed 0.15, with the maximum value 0.18. For most

TABLE V

EXPERIMENTAL (E) AND PREDICTED (P) CAPACITY FACTORS k' OF SAMPLE SOLUTES IN METHANOL–WATER (I, 40 AND 25% METHANOL) AND IN ACETONITRILE–WATER (II, 40 and 30% ACETONITRILE) MOBILE PHASES

The prediction is based on calculations using eqns. 3–5 and the indices Δn_e and Δq listed in Table IV, with toluene as the reference standard and *n*-alkylbenzenes (A), 3-*n*-alkyl-6-methyluracils (B), 3-alkoxycarbonyl-2-pyrazolines (C) and alkan-2-ones (D) as the calibration homologous series. Numbers of solutes are as in Table I.

Solute	Mobile phase	k'				
		E	P(A)	P(B)	P(C)	P(D)
17	I, 40	3.83	3.62	3.64	3.64	3.65
	I, 25	10.13	9.89	9.60	9.94	9.97
	II, 40	2.81	2.79	2.76	2.76	2.80
	II, 30	5.98	6.29	6.25	6.24	6.31
18	I, 40	10.31	10.13	10.09	10.07	10.03
	I, 25	27.90	26.83	26.81	26.68	26.62
	II, 40	5.24	5.22	5.20	5.20	5.20
	II, 30	12.30	12.94	12.88	12.88	12.90
19	I, 40	4.82	4.80	4.75	4.79	4.74
	I, 25	14.86	14,26	14.13	14.22	14.10
	II, 40	2.48	2.45	2.44	2.43	2.46
	II, 30	4.91	5.28	5.26	5.24	5.28
20	I, 40	6.21	5.74	5.73	5.74	5.74
	I, 25	16.02	14.75	14.78	14.78	14.78
	II, 40	4.04	4.04	4.06	4.06	4.10
	II, 30	9.02	9.74	9.78	9.76	9.84
21	I, 40	21,12	20,12	20,23	20,12	20,23
	II, 40	9.12	9.49	9.55	9.58	9.59
	II, 30	24,62	25,42	25,54	25,62	25,66
22	I, 40	4.87	4.83	4.80	4.78	4.83
	I, 25	15.26	13.83	13.75	13.68	13.82
	II, 40	2.52	2.54	2.52	2.53	2.53
	II, 30	5.07	5.40	5.37	5.38	5.39
23	I, 40	5.22	4.81	4.84	4.78	4.83
	I, 25	15.35	14.14	14.22	14.06	14.19
	II, 40	3.24	3.23	3.22	3.23	3.24
	II, 30	6.98	7.40	7.39	7.40	7.42
24	I, 40	25.89	24.59	24.73	24.60	24.87
	II, 40	8.41	8.99	8.89	8.96	8.95
	II, 30	22.61	23.64	23.41	23.53	23.52
25	I, 40	3.60	3.36	3.36	3.37	3.36
	I, 25	9.65	9.07	9.07	9.09	9.03
	II, 40	2.26	2.27	2.26	2.25	2.27
	II, 30	4.43	4.81	4.79	4.78	4.81
26	I, 40	1.88	1.83	1.84	1.84	1.85
	I, 25	4.58	4.18	4.21	4.22	4.22
	II, 40	0.92	0.87	0.87	0.87	0.87
	II, 30	1.57	1.68	1.68	1.68	1.68
27	I, 40	1.52	1.52	1.52	1.52	1.52
	I, 25	3.44	3.11	3.10	3.11	3.09
	II, 40	1.33	1.26	1.25	1.26	1.27
	II, 30	2.26	2.42	2.42	2.42	2.44

TABLE V (*continued*)

Solute	Mobile phase	k'				
		E	P(A)	P(B)	P(C)	P(D)
28	I, 40	1.95	1.87	1.88	1.88	1.86
	II, 25	4.46	4.15	4.16	4.16	4.14
	II, 40	1.36	1.21	1.21	1.21	1.22
	II, 30	2.25	2.44	2.44	2.45	2.45
29	I, 40	4.67	4.24	4.23	4.43	4.40
	I, 25	12.61	12.04	12.00	12.17	12.11
	II, 40	2.16	2.17	2.17	2.18	2.17
	II, 30	4.67	4.94	4.93	4.95	4.94
30	I, 40	4.54	4.42	4.40	4.23	4.24
	I, 25	12.41	12.16	12.11	12.02	12.03
	II, 40	2.02	1.94	1.94	1.95	1.95
	II, 30	4.21	4.44	4.42	4.44	4.45
31	I, 40	34.46	32.87	32.79	32.89	33.03
	II, 40	8.83	9.43	9.47	9.41	9.55
	II, 30	31.81	31.20	31.27	31.09	31.49
32	I, 40	7.34	7.39	7.36	7.41	7.36
	I, 25	26.40	26,49	26.33	26.54	26.34
	II, 40	3.79	3.80	3.81	3.82	3.83
	II, 30	8.49	8.78	8.80	8.81	8.83
33	I, 40	9.75	9.36	9.31	9.36	9.37
	I, 25	20.71	21.03	20.91	20.94	21.02
	II, 40	5.92	5.87	5.79	5.82	5.88
	II, 30	13.31	14.09	13.90	13.98	14.10
34	I, 40	21.42	20.48	20.41	20.51	20.42
	II, 40	9.89	10.05	9.96	9.98	10.02
	II, 30	28.03	28.59	28.34	28.39	28.54
35	I, 40	0.77	0.76	0.76	0.75	0.75
	I, 25	2.13	1.93	1.91	1.91	1.90
	II, 40	0.34	0.35	0.35	0.35	0.35
	II, 30	0.69	0.71	0.71	0.71	0.71
36	I, 40	1.08	1.05	1.06	1.05	1.05
	I, 25	2.97	2.67	2.68	2.67	2.68
	II, 40	0.55	0.52	0.51	0.52	0.52
	II, 30	0.92	1.02	1.02	1.02	1.03
37	I, 40	0.94	0.94	0.93	0.93	0.93
	I, 25	2.57	2.37	2.35	2.34	2.35
	II, 40	0.41	0.40	0.40	0.40	0.41
	II, 30	0.79	0.82	0.82	0.82	0.83
38	I, 40	0.52	0.48	0.48	0.48	0.48
	I, 25	1.41	1.29	1.28	1.28	1.28
	II, 40	0.56	0.55	0.54	0.54	0.55
	II, 30	1.02	1.04	1.03	1.03	1.04
39	I, 40	2.18	2.07	2.07	2.07	2.08
	I, 25	7.15	6.48	6.47	6.45	6.48
	II, 40	0.86	0.85	0.85	0.84	0.85
	II, 30	1.64	1.73	1.73	1.71	1.73
40	I, 40	1.78	1.73	1.71	1.72	1.71
	I, 25	5.05	4.77	4.71	4.75	4.70
	II, 40	1.29	1.20	1.19	1.20	1.20
	II, 30	2.44	2.58	2.55	2.57	2.57

(Continued on p. 156)

TABLE V (*continued*)

Solute	Mobile phase	*k'*				
		E	P(A)	P(B)	P(C)	P(D)
41	I, 40	3.61	3.42	3.37	3.39	3.39
	I, 25	17.61	15.98	15.77	15.83	15.90
	II, 40	1.36	1.38	1.38	1.38	1.38
	II, 30	3.26	3.34	3.34	3.35	3.34
42	I, 40	1.46	1.41	1.41	1.41	1.41
	I, 25	5.12	4.68	4.67	4.67	4.65
	II, 40	0.70	0.70	0.69	0.69	0.70
	II, 30	1.41	1.46	1.45	1.45	1.46
43	I, 40	0.93	0.90	0.89	0.89	0.89
	I, 25	3.37	3.04	3.02	3.01	3.01
	II, 40	0.47	0.45	0.45	0.45	0.45
	II, 30	0.96	1.00	1.00	1.00	1.01
44	I, 40	0.58	0.54	0.54	0.54	0.54
	I, 25	1.77	1.60	1.59	1.59	1.60
	II, 40	0.49	0.46	0.46	0.46	0.47
	II, 30	0.78	0.84	0.84	0.84	0.85
45	I, 40	6.62	6.65	6.59	6.64	6.66
	I, 25	26.69	25.41	25.15	25.32	25.39
	II, 40	2.02	2.01	2.00	2.02	2.02
	II, 30	4.26	4.45	4.43	4.45	4.48
46	I, 40	15.08	14.71	14.61	14.48	14.54
	I, 30	39.91	43.42	43.15	42.78	42.91
	II, 40	3.76	3.78	3.76	3.77	3.79
	II, 30	9.31	9.60	9.55	9.60	9.61

compounds maximum deviations are observed with the indices determined using *n*-alkylbenzenes as the calibration series. This can be understood if we consider the impact of the strongly limited number of the experimental data on the precision of determination of the constants a_0, a_1 and p used for the calibration of the retention scale. Deviations from the mean values of Δn_c and Δq in the opposite direction were found for the indices based on alkyluracils as the calibration series, while the indices determined using alkoxycarbonylpyrazoline and alkanone calibration series were almost identical.

In acetonitrile–water mobile phases, the indices Δn_c and Δq determined with alkylbenzenes as the calibration homologous series differ significantly from those determined with the calibration series of alkyluracils and even more from the values determined on the basis of the two remaining calibration series. On the other hand, the values of Δn_c and Δq for alkoxycarbonylyrazolines and alkanones as the calibration series are close to each other, with only seven differences in Δn_c exceeding 0.20 and with maximum differences in Δq indices of 0.01. The deviations observed can be attributed to the lack of experimental data for precise determination of the constants of the calibration eqn. 4 with alkylbenzene calibration series and to slightly curved log *k' versus x* plots of alkyluracils.

Note that the least differences between the indices Δn_c determined in acetonitrile–water and in methanol–water mobile phases are obtained with alkoxycarbo-

nylpyrazolines and with alkanones as the calibration series. The differences between the n_{ce} indices are even less, < 0.5 for the great majority of the sample solutes tested. Toluene is one of the exceptions, which explains the better agreement observed between the n_{ce} than between the Δn_c indices. These results suggest that alkoxycarbonylpyrazolines and alkanones are better suited as the calibration homologous series than alkylbenzenes and alkyluracils in the tested range of mobile phase compositions.

As the final test of the prediction method, the capacity factors predicted using eqns. 4 and 5a and b with the differential indices Δn_c and Δq and the calibration constants a_0, a_1 and p, determined using the four tested calibration homologous series, were compared with the experimental k' (Table V). Only the results for two concentrations of methanol (40 and 25%) and acetonitrile (40 and 30%) are shown, even though other mobile phase compositions were also tested.

All the predicted k' differ from the experimental values by less than 10% (relative to k'_{exp}) and the values predicted using various calibration homologous series differ only insignificantly from each other, which means that all the series tested can in principle be used for the calibration of retention in reversed-phase systems with mobile phases containing 25–50% methanol or 30–50% acetonitrile in water. In mobile phases containing 50% organic solvent, the differences between the predicted and experimental values are even less than those for the mobile phases in Table V. However, these differences may be as high as 20% rel. for some test solutes in 25% aqueous acetonitrile as the mobile phase, because of the curvature of the log k' *versus* x plots in this range of relatively high water contents.

CONCLUSIONS

The application of the method for prediction of retention in reversed-phase systems based on the indices Δn_c and Δq and the *n*-alkylbenzene calibration homologous series failed in water-rich mobile phases when the parameters of the calibration eqn. 4 were determined in mobile phases containing more than 50% organic solvent, but proved feasible with a suitable calibration homologous series the retention of which could be measured in mobile phases containing 25–50% methanol or acetonitrile. In principle, it is possible to use homologous *n*-alkylbenzenes as the basis of calibration, with the calibration constants determined only from the retention data of toluene over the full composition range of mobile phases and two additional data for ethylbenzene, however the indices Δn_c and Δq determined in this way may be subject to significant errors.

For better accuracy and consistency, it is preferable to use another calibration homologous series which allows the experimental determination of the capacity factors of the first four or five members in the investigated range of composition of mobile phases. Although the four homologous series tested here provided similar results, with the predicted k' differing by 10% rel. or less from the experimental values in 25–50% aqueous methanol or in 30–50% aqueous acetonitrile, the homologous alkoxycarbonylpyrazolines or alkan-2-ones are to be preferred because of a better consistency of the indices n_{ce} and q_i (Δn_c and Δq) determined in methanol–water and in acetonitrile–water mobile phases.

This accuracy is similar to previous results achieved using the present method in mobile phases containing 50–90% organic solvent [11,12] and better than that report-

ed using the method based on the parameters of the concentration dependences of the structural increments to retention indices [7]. The advantage of the latter method is that fewer preliminary experimental data are required for its application. Apparently a common feature of all the methods of calibration and prediction of retention suggested so far is that a decreased number of necessary experiments should be traded for either a limited range of experimental conditions for which the method is applicable or a decreased accuracy of the predicted retention data.

Taking into account the better availability of the alkan-2-ones, this homologous series is recommended for calibration in water-rich mobile phases using the method based on the indices Δn_c and Δq, as a supplement to the *n*-alkylbenzene calibration series, and is suitable for mobile phases with 50% or less water.

REFERENCES

1 R. M. Smith, *J. Chromatogr.*, 236 (1982) 313.
2 R. M. Smith, *Anal. Chem.*, 56 (1984) 256.
3 J. K. Baker, *Anal. Chem.*, 51 (1979) 1693.
4 J. K. Baker and C.-Y. Ma, *J. Chromatogr.*, 169 (1979) 107.
5 M. Popl, V. Dolanský and J. Fähnrich, *J. Chromatogr.*, 146 (1978) 195.
6 F. Šmejkal, M. Popl, A. Čihová and M. Zázvorková, *J. Chromatogr.*, 197 (1980) 147.
7 R. M. Smith and C. M. Burr, *J. Chromatogr.*, 475 (1989) 57; 481 (1989) 71; 481 (1989) 85; 485 (1989) 325.
8 P. Jandera, H. Colin and G. Guiochon, *Anal. Chem.*, 54 (1982) 435.
9 H. Colin, G. Guiochon and P. Jandera, *Anal. Chem.*, 55 (1983) 442.
10 P. Jandera, *Chromatographia*, 19 (1984) 101.
11 P. Jandera, *J. Chromatogr.*, 352 (1986) 91.
12 P. Jandera, *J. Chromatogr.*, 352 (1986) 111.
13 P. Jandera and M. Špaček, *J. Chromatogr.*, 366 (1986) 107.
14 P. Jandera, *J. Chromatogr.*, 314 (1984) 13.
15 P. Jandera, *J. Chromatogr.*, 449 (1988) 361.
16 A. Horna, H. Pechová, A. Pikulová, L. Hornová and J. Churáček, *J. Chromatogr.*, 367 (1986) 155.

Journal of Chromatography, 556 (1991) 159–168
Elsevier Science Publishers B.V., Amsterdam

CHROM. 23 374

Analysis of the separability of plate height into overload and intrinsic contributions using the kinetic model of non-linear chromatography

CHARLES A. LUCY*
AECL Research, General Chemistry Branch, Chalk River Laboratories, Chalk River, Ontario, K0J 1J0 (Canada)
and
PETER W. CARR
Department of Chemistry and Institute for Advanced Studies in Bioprocess Technology, Kolthoff and Smith Halls, 207 Pleasant Street SE, University of Minnesota, Minneapolis, MN 55455 (USA)

ABSTRACT

In developing optimization strategies for preparative-scale chromatography it is very convenient, if not entirely valid, to the represent overall peak broadening in terms of the sum of two distinct, independent contributions to the plate height: that portion due to band broadening under linear chromatographic conditions and that due to the effect of mass overload. The kinetic model of non-linear elution chromatography is used to demonstrate that this separation of terms is a reasonable approximation under a wide range of chromatographic conditions and to define the limits of this approximation.

INTRODUCTION

In their seminal work on the optimization of sample throughput in preparative chromatography, Knox and Pyper [1] analyzed the effect of sample overload on peak width in terms of two distinctly different and assumed independent contributions to the plate height. For the present purposes, the first factor will be termed the intrinsic (H_{int}) contribution. This corresponds to the height equivalent to a theoretical plate for a column operating under perfectly linear isotherm conditions. The second contribution, that due to isotherm broadening, H_{iso}, results from overloading the isotherm by injection of a negligibly small volume of solution containing an excessively large amount of solute. Knox and Pyper [1] wrote an equation equivalent to

$$H = H_{int} + H_{iso} \quad (1)$$

Their justification for the decomposition of the total plate height into these two types of terms was based on the prior theoretical work of Haarhoff and Van der Linde [2] and the experimental work of De Jong *et al.* [3]. The peak-shape equation developed by Haarhoff and Van der Linde [2] was based on the assumption that the mobile and

0021-9673/91/$03.50

stationary phase solutes are in perfect equilibrium and that broadening under linear conditions, *i.e.*, at very low sample load, is due only to axial diffusion and eddy dispersion processes. Additionally, a parabolic isotherm was assumed to make the mathematics tractable, *i.e.* the relationship between the mobile (C) and stationary phase (q) solute concentrations was taken as

$$q = a_1 + a_2C + a_3C^2 \tag{2}$$

Under conditions where the volume injected *per se* does not broaden the peak, the concentration–time relationship derived by Haarhoff and Van der Linde [2] can be expressed as

$$\frac{C}{C_0} = \frac{\sqrt{P}(1+k')}{\sqrt{\pi}YC_0k'} \cdot \frac{\exp - \left[\frac{\left(\frac{\bar{t}}{1+k'} - 1\right)^2}{4P}\right]}{\left[\frac{1}{\exp\left(\frac{k'YC_0}{2P(1+k')^2}\right) - 1}\right] + 0.5\left[1 + \operatorname{erf}\left(\frac{\frac{\bar{t}}{1+k'} - 1}{2\sqrt{P}}\right)\right]} \tag{3}$$

where $P = D_{ax}t_o/L^2$ (dimensionless dispersion coefficient); $\bar{t} = t/t_o$ (dimensionless time); $k' = k'_{C=0}$ (thermodynamic k'); $Y = -1/k'\,(d^2q/dC^2)_{C=0}$; C_0 = (moles of solute injected)/(dead volume); D_{ax} is the axial dispersion coefficient, t_o is the column dead time and L is the column length. In the limit of a very small number of moles of solute, *i.e.*, under linear isotherm conditions, the above equation takes on the much simpler Gaussian form:

$$\frac{C}{C_0} = \frac{1}{2\sqrt{P\pi}(1+k')} \cdot \exp - \left[\frac{\left(\frac{\bar{t}}{1+k'} - 1\right)^2}{4P}\right] \tag{4}$$

with the dimensionless plate height given by

$$H_{\text{int,disp}} = 2P \tag{5}$$

P is directly related to D_{ax}, which is formally equivalent to the spreading by pure axial molecular diffusion, which in turn is formally inversely dependent on flow-rate. Therefore, eqn. 5 is only an approximate representation of the overall intrinsic plate-height behavior under overload conditions. However, physically D_{ax} is a dispersion coefficient which is coupled to the linear velocity, u [*i.e.*, $D_{ax} = f(u)$]. Thus,

$$P = \frac{D_{ax}t_0}{L^2} = \frac{f(u)}{uL}$$

Therefore, P has a complicated dependence on the linear velocity, and eqn. 5 is a

reasonable approximation of the band broadening under linear chromatographic conditions.

Recently, the solution to a very different model of non-linear elution chromatography was presented. Based on the work of Thomas [4], Heister and Vermuelen [5] and Arnold *et al.* [6,7], a solution was obtained to the non-linear boundary value problem in which the rate of transfer of solute between the phases is taken as the sole band-broadening process under linear conditions [8]. That is, interphase equilibrium is not assumed, rather the solute concentrations in the mobile and stationary phases were assumed to be related by

$$\frac{\partial q}{\partial t} = k_a(S_0 - q)C - k_d q \tag{6}$$

where S_o is the concentration of binding sites (M; same units as q). The rate constants k_a ($\mathrm{lmol^{-1}s^{-1}}$) and k_d ($\mathrm{s^{-1}}$) are "lumped" rate parameters corresponding to the net rate constants of solute adsorption and solute desorption.

In order to make the problem mathematically tractable, dispersion was assumed to be negligible ($D_{ax}=0$). One advantage of this particular theoretical approach is that a Langmuir isotherm is retained. This physically more realistic isotherm, in comparison with eqn. 2, allows this model to be used for higher degrees of column overload than the equilibrium model using a parabolic isotherm [9]. The solution for an impulse injection of sample is [8]

$$\frac{C}{C_0} = \left(\frac{1 - \exp(-\gamma K C_0)}{\gamma K C_0}\right)\left\{\frac{[\gamma\sqrt{k'/y}\, I_1(2\gamma\sqrt{k'y}) + \delta(y)]\exp[-\gamma(y + k')]}{1 - T(\gamma k', \gamma y)[1 - \exp(-\gamma K C_0)]}\right\} \tag{7}$$

where $y \equiv t/t_o - 1$; $\gamma \equiv k_d t_o$ (dimensionless rate parameter); $k' \equiv (k_a/k_d)S_o\varepsilon$ (thermodynamic k'); $K \equiv k_a/k_d$; $C_o \equiv$ (moles of solute injected)/(column dead volume).

In the above set of definitions, $S_o\varepsilon$ is the maximum adsorption capacity of the column. In eqn. 7, I_1 is a first-order modified Bessel function of the first kind, and the T-function is a Bessel function integral:

$$T(u,v) = \mathrm{e}^{-v}\int_0^u \mathrm{e}^{-t} I_0(\sqrt{vt})\,\mathrm{d}t \tag{8}$$

in which I_o is the zeroth-order Bessel function of the first kind. The T-function acts as a "switching" function which produces the skew in the peak profile when the column is overloaded.

In the limit of a very small number of moles of sample, *i.e.*, linear isotherm conditions, eqn. 7 takes on a much simpler form:

$$\frac{C}{C_0} = [\gamma\sqrt{k'/y}\, I_1(2\gamma\sqrt{k'y}) + \delta(y)]\exp(-\gamma y - \gamma k') \tag{9}$$

This result is mathematically identical with the Giddings–Eyring first-order stochastic model of chromatography [10]. The dimensionless plate height corresponding to this equation is

$$H_{\text{int}} = \frac{2k'}{(1+k')^2\gamma} = 2\frac{k'}{(1+k')^2}\cdot\frac{u}{k_d L} \tag{10}$$

Eqn. 10 is the usual result for a plate height resulting from resistance to interphase equilibrium originating in the stationary phase under linear chromatographic ($KC_o = 0$) conditions.

The separability of the total plate height into intrinsic and isothermal contributions is commonly used in theoretical treatments of preparative chromatography [11–13]. However, the justification for this separability thus far is based solely on the Haarhoff–Van der Linde model [2]. As the conditions for the validity of the Haarhoff–Van der Linde [2] and the kinetic models are in complete opposition, *i.e.*, one is an axial dispersion–equilibrium model and the other is based solely on slow kinetics, we felt that it would be of considerable importance to determine whether and under what conditions the non-linear kinetic equation (eqn. 7) would lead to the same separation of plate height contribution shown in eqn. 1.

COMPUTATIONS

The dimensionless plate heights were obtained from

$$H = m_2'/m_1^2 \tag{11}$$

where m_1 and m_2' are the first normalized and second normalized centralized statistical moments, respectively. The moments were computed for concentration–time profiles generated using eqn. 7 such that 75 evenly spaced points were taken on each side of the maxima. Integrations were performed using Simpson's 1/3 rule.

For the reversed-phase chromatographic simulations, k' was varied between 1 and 10, γ was varied from 100 to 1000 and KC_o was varied from 0 to 0.1. For high-performance affinity chromatography (HPAC), k' was 25, γ was varied from 4 to 40 and KC_o was varied from 0 to 2.0.

RESULTS AND DISCUSSION

At the outset of this work is was not at all clear to us that the separation of plate height as shown in eqn. 1 would be possible. Indeed, we were surprised that eqn. 1 had been given much credence at all [11–13]. In essence, our concern was as follows: the extent of peak broadening due to overload must depend on the *local* solute concentration averaged over the entire column. Obviously the local concentration under linear chromatographic conditions depends on both axial dispersion and broadening due to slow interphase transfer. Consequently, the intrinsic and isotherm broadening should be strongly coupled effects for overloaded columns, such that the contribution from isotherm broadening effects would diminish as the intrinsic broadening increased.

Despite this argument, we find that eqn. 1 is a surprisingly good approximation both for high-performance reversed-phase and affinity chromatographic conditions. The expected coupling between the intrinsic and isotherm broadening was observed, but was sufficiently small that it would generally be easily overwhelmed by experimental uncertainties in real chromatographic data.

Reversed-phase chromatography

The range of the model parameters (k', KC_o and γ) used in the computations here was based on the values observed in experimental studies of small uncharged solutes in preparative reversed-phase chromatography [9]. In that study, 3-phenylpropanol was studied from linear chromatographic conditions (KC_o = 0.0) to "moderate" column overload conditions (KC_o = 0.1) [9].

In the kinetic model of non-linear chromatography, axial dispersion is assumed to be negligible and band broadening under linear chromatographic conditions is described solely by γ, the dimensionless rate parameter. The magnitude of this rate parameter results from the combined effects of slow solute desorption ad slow interphase mass transfer. The effects of these two mechanisms are combined in the "lumped" desorption rate constant. In reversed-phase chromatography, the kinetics of solute desorption at the surface are fairly fast. Therefore, the "lumped" desorption rate constant reflects the effect of mass transfer, which is independent of k' and, if resistance to mass transfer resides in the stationary phase, it will be essentially independant of flow-rate. Therefore, k_d can be considered to be constant, and so the dimensionless rate parameter, γ, is directly related to the dead time of the column, t_0, or indirectly to the linear velocity. Thus, instead of the traditional H *versus* linear velocity plot, H *versus* $1/\gamma$ will used.

Fig. 1 shows a series of plots of H *vs.* $1/\gamma$ for the range of overload conditions previously studied [9] at k' values of 1, 3 and 10. At all values of k' the plots are qualitatively similar. For the case of zero overload ($KC_o = 0$), which corresponds to H_{int} in eqn. 1, the plot is exactly linear in accord with eqn. 10, and passes through the origin at $1/\gamma = 0$. As the column becomes slightly overloaded ($KC_o = 0.02$), the plot of H *vs.* $1/\gamma$ appears to translate upwards. Close inspection of the plots for KC_o = 0.02 reveals a slight curvature at low $1/\gamma$ (*i.e.*, low linear velocity). However, for higher degrees of overload this curvature is more gradual and less distinct. Experimentally it would be difficult to discern any curvature or change in slope given the expected random error in the measurement of H.

Thus all of the plots are roughly parallel and show an increase in the intercept at $1/\gamma = 0$ as the degree of overload increases. This is the qualitative behavior predicted by eqn. 1. The overload effect acts as a flow-rate-independent contribution to the overall H in these pseudo-Van Deemter plots.

In order to obtain a clearer view of the overload term, the computed H_{int} based on eqn. 9 was subtracted from the total H values shown in Fig. 1:

$$H_{iso} = H - H_{int} \quad \text{(eqn. 9)} \tag{12}$$

The results are summarized in Fig. 2. If H_{iso} were truly independent of the intrinsic broadening effects, then these plots should have a slope of zero. It is evident that H_{iso} does depend on the linear velocity ($1/\gamma$) and thus the separation of terms shown in eqn. 1 can not be perfect. As the intrinsic band broadening in the column increases

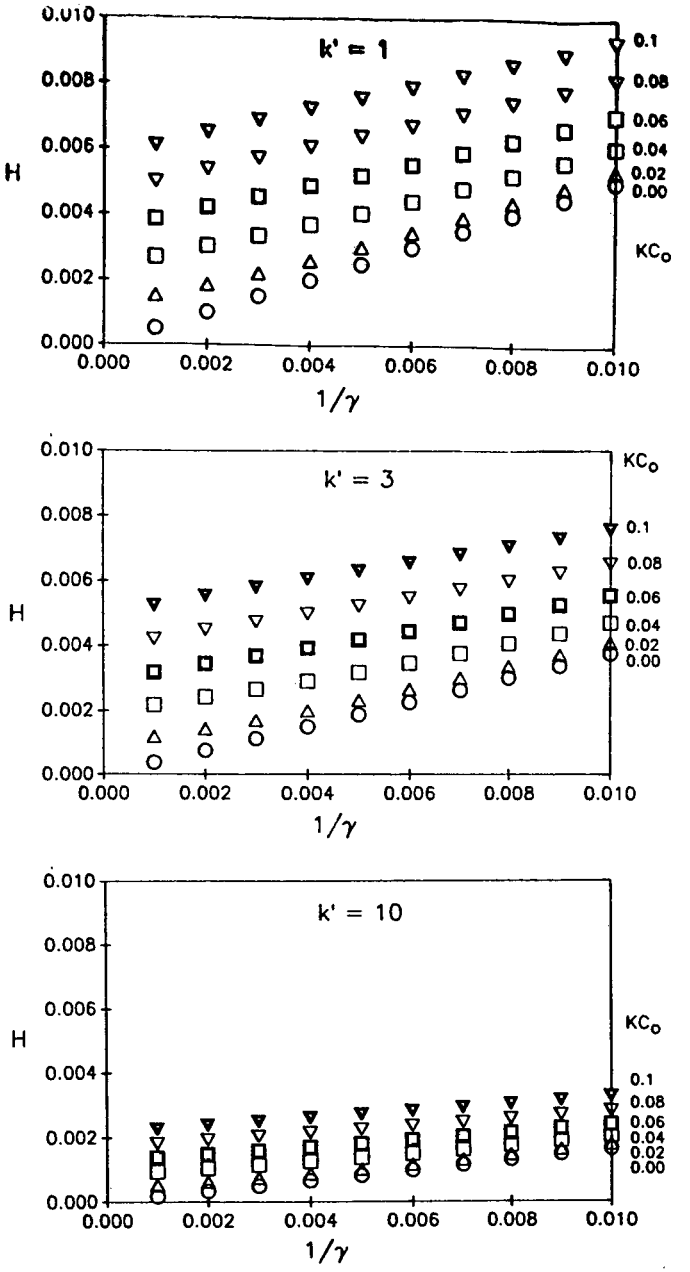

Fig. 1. H *vs.* $1/\gamma$ dependence under preparative reversed-phase conditions at $k' = 1$,3 and 10, for γ in the range 100–1000. The degree of column overload, KC_o, associated with each curve is indicated on the plots.

with increasing flow-rate, the average solute concentration in the sample band does decrease. Hence, as H_{iso} is concentration dependent, it will diminish. This is the behavior that we initially expected. However, as can be seen in comparing Figs. 1 and

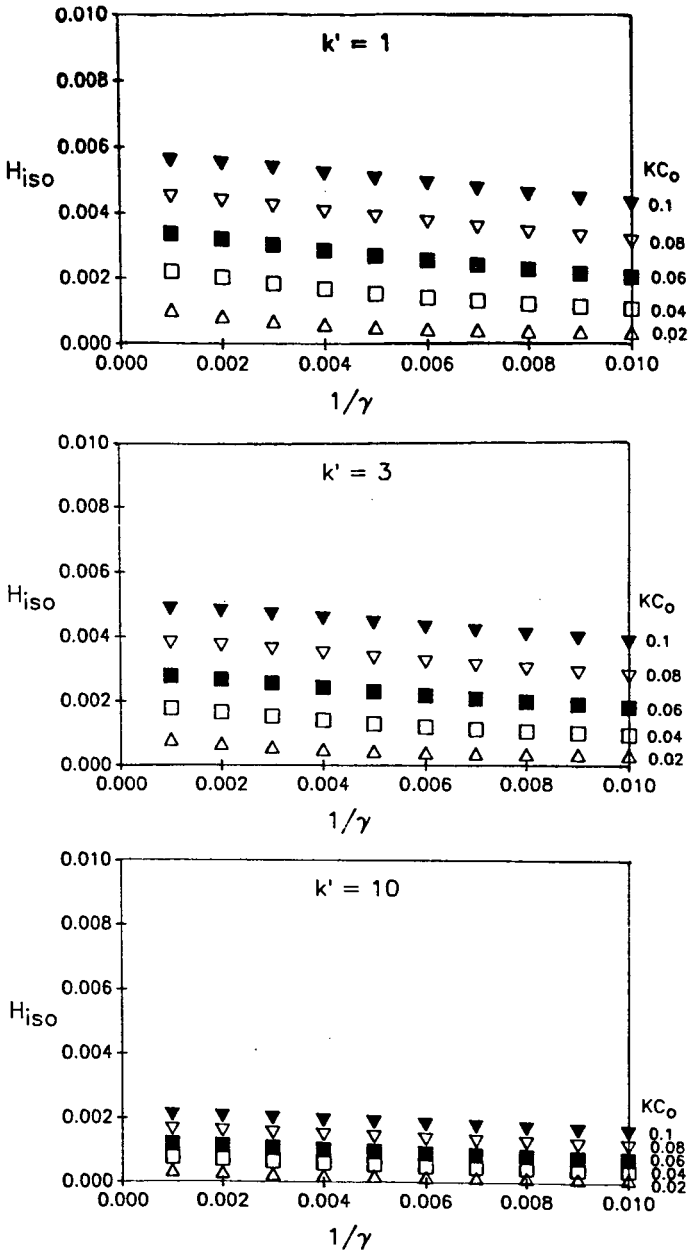

Fig. 2. H_{iso} *vs.* $1/\gamma$ dependence under preparative reversed-phase conditions for data given in Fig. 1. H_{iso} was calculated using eqn. 12.

2, the decrease in H_{iso} which results from this coupling is small enough relative to the change in the intrinsic plate height that eqn. 1 will appear to be obeyed in experimental studies.

It is also evident in Fig. 2 that for a given degree of column overload (KC_o), H_{iso}

decreases with increasing k'. This trend is observed at constant KC_o because m_1^2 increases more rapidly than m_2' with increasing k'. The net result of these two opposing processes is a decrease in H_{iso} with increasing k'. However, in any experimental study in which the number of moles injected is held constant, KC_o would not be constant but rather would increase linearly with increasing k'. The effect of this more realistic situation is given in Fig. 3, where it is shown that for a constant solute concentration given by a constant value of KC_o/k', H_{iso} increases with increasing k'. This is intuitively what one would expect.

Affinity chromatography

In high-performance affinity chromatography (HPAC), the low density of binding sites can result in overloading of the column under even analytical conditions and the strong binding constants between the immobilized ligand and the solute result in column efficiencies far below those associated with reversed-phase HPLC. Thus HPAC provides a distinctly different test of the separability of the plate height under non-linear chromatographic conditions from the preparative reversed-phase HPLC case discussed above.

To test the validity of the separation of plate height shown in eqn. 1 under HPAC conditions, H *vs.* u plots were calculated using conditions previously observed for the retention of *p*-nitrophenyl-α-D-mannopyranoside on a silica-bound concanavalin A affinity column [8]. One very approximate assumption that has been made is that the affinity medium is homogeneous, *i.e.*, all sites have the same dissociation rate constant, k_d, and thus the observed k_d is independent of the amount injected. Under these conditions $1/\gamma$ is proportional to linear velocity, u, for a constant k'. Fig. 4 shows the variation of (A) the total plate height and (B) H_{iso} with $1/\gamma$ for $k' = 25$. The plots in Fig. 4 display similar behavior to that observed in Figs. 1 and 2 despite the large differences in the parameter ranges between the two cases. Again there is evidence of significant coupling between the intrinsic band broadening and that caused by the overloading of the isotherm. However, the effect of the coupling is such that H_{iso} would in all likelihood appear constant in an experimental study of preparative HPAC.

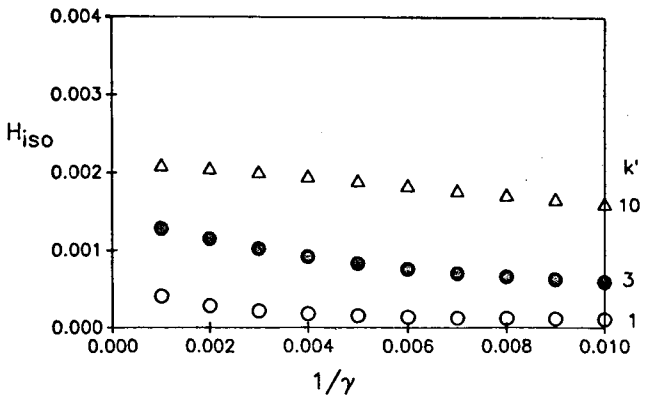

Fig. 3. Effect of k' on the H_{iso} *vs.* $1/\gamma$ dependence for a constant level of column overload under preparative reversed-phase conditions. KC_o/k' is constant at 0.01 for the three plots.

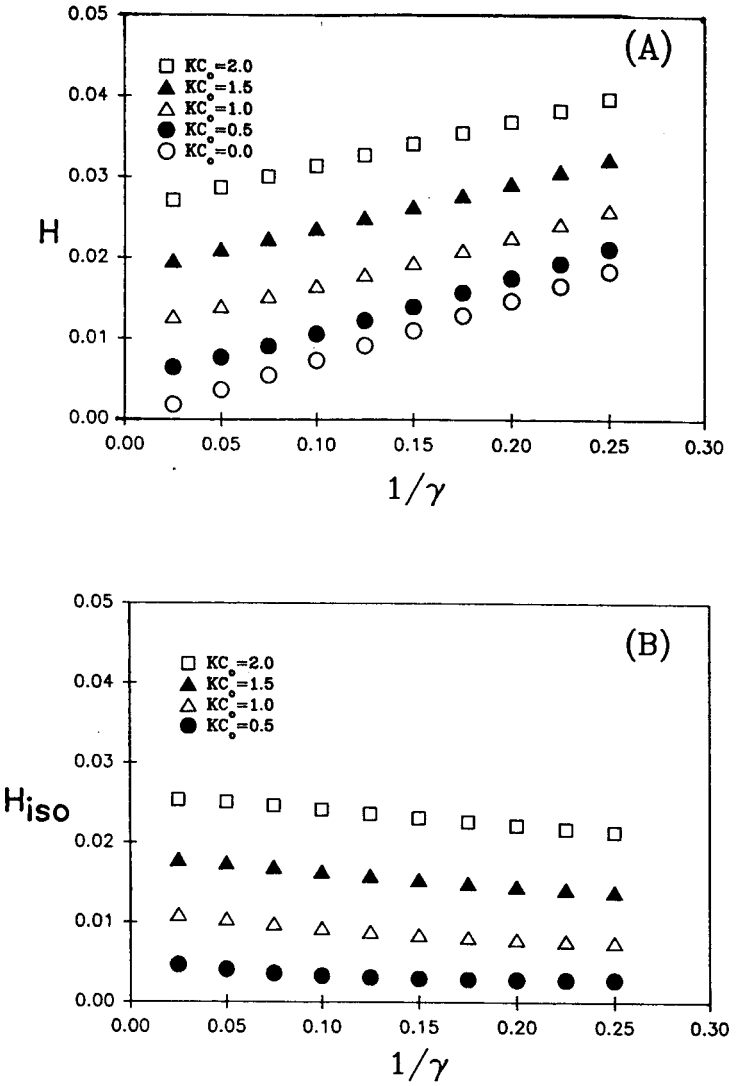

Fig. 4. Plate-height dependence under high-performance affinity chromatographic conditions. $k' = 25$; $\gamma = 4$–40; KC_o = (○) 0.0; (●) 0.5; (△) 1.0; (▲) 1.5 and (□) 2.0. (A) Total plate height H *vs.* $1/\gamma$; (B) H_{iso} *vs.* $1/\gamma$.

CONCLUSIONS

The kinetic model of non-linear chromatography has been used to test the validity of the separation of the total plate height observed in preparative chromatography into intrinsic and isotherm contributions. *H versus u* plots were generated using physico-chemical parameters typical of both high-performance reversed-phase and affinity chromatography. These plots indicate that regardless of the mode of

chromatography, the intrinsic and isotherm contributions to the plate height are coupled, such that increases in the intrinsic band broadening on the column will reduce the band broadening due to the isotherm overload. However, it was found that the degree of this coupling is sufficiently small that in most instances the two contributions could be considered independent.

Under conditions of extreme overload the peak width is dominated by the isotherm broadening effect and thus eqn. 1 will appear to be observed as H_{iso} will be much larger than H_{int}.

ACKNOWLEDGEMENTS

This work was supported in part by the Natural Sciences and Engineering Research Council of Canada and by the NSF Center for Bioprocess Technology, University of Minnesota.

REFERENCES

1 J. H. Knox and H. M. Pyper, *J. Chromatogr.*, 363 (1989) 1.
2 P. C. Haarhoff and H. J. Van der Linde, *Anal. Chem.*, 38 (1966) 573.
3 A. W. J. de Jong, J. C. Kraak, H. Poppe and F. Nooitgedacht, *J. Chromatogr.*, 193 (1980) 181.
4 H. C. Thomas, *J. Am. Chem. Soc.*, 66 (1944) 1664.
5 N. K. Heister and T. Vermeulen, *Chem. Eng. Prog.*, 48 (1952) 505.
6 F. H. Arnold, H. W. Blanch and C. R. Wilke, *J. Chromatogr.*, 330 (1985) 159.
7 F. H. Arnold, H. W. Blanch and C. R. Wilke, *Chem. Eng. J.*, 30 (1985) B9.
8 J. L. Wade, A. F. Bergold and P. W. Carr, *Anal. Chem.*, 59 (1987) 1286.
9 C. A. Lucy, J. L. Wade and P. W. Carr, *J. Chromatogr.*, 484 (1989) 61.
10 J. C. Giddings and H. Eyring, *J. Phys. Chem.*, 59 (1955) 416.
11 L. R. Snyder, G. B. Cox and P. E. Antle, *Chromatographia*, 24 (1987) 82.
12 S. Golshan-Shirazi and G. Guiochon, *Anal. Chem.*, 61 (1989) 462.
13 S. Golshan-Shirazi and G. Guiochon, *J. Chromatogr.*, 517 (1990) 229.

Journal of Chromatography, 556 (1991) 169–180
Elsevier Science Publishers B.V., Amsterdam

CHROM. 23 306

Factor analysis and experimental design in high-performance liquid chromatography

XI[a]. Factor analysis maps and chromatographic information

MICHEL RIGHEZZA
Laboratoire de Chimiométrie, Université d'Orléans, B.P. 6759, 45067 Orléans Cedex 2 (France)
and
JACQUES R. CHRÉTIEN*
Laboratoire de Chimiométrie, Université d'Orléans, B.P. 6759, 45067 Orléans Cedex 2 (France) and Institut de Topologie et de Dynamique des Systèmes, Associé au CNRS UA 34, 1 Rue Guy de la Brosse, 75005 Paris (France)

ABSTRACT

A progressive approach to the exploitation of chromatographic data, based on factor analysis, is presented. This approach is applied to the retention data k' of a large series of compounds in high-performance liquid chromatography. The chromatographic information, *i.e.*, affinity and selectivity, is extracted with help of principal component analysis (PCA) and correspondence factor analysis (CFA). The factor analysis gives rise to three factorial maps to present the chromatographic information: PCA affinity map, CFA trend analysis map and CFA distance analysis map. Examples of extraction of chromatographic information are given for the simultaneous exploitation of these maps. Possibilities and limitations of this approach are discussed.

INTRODUCTION

It is essential for the chromatographer to have a representation of the main information nested in huge series of data, and factor analysis is a good tool to extract and to represent this information [1,2]. The chromatographic properties, affinity, polarity and selectivity, can be revealed by factor analysis maps.

Up to now factor analysis has most often been used as a clustering technique [3]. Proximities between representative points, solutes or chromatographic systems, are considered to suggest similarities of the basic chromatographic phenomenon. In fact, the extracted factors most often remain abstract ones. In some instances it has

[a] For Part X, see ref. 12.

0021-9673/91/$03.50

been possible to give a real physicochemical meaning to these factors. For example, it has been shown that the first factorial axis can be assimilated to the contribution of the partition coefficient [4] or to the electronic factors [5].

Chromatographers can use factor analysis for the rapid and efficient selection of packings and/or eluents. Any data processing techniques or their representations generate a loss of minor information. These limitations need to be circumvented with the help of complementary factor analysis methods. The aim of this paper is to consider the complementarity evolved from the successive use of principal component analysis (PCA) and correspondence factor analysis (CFA). It will be shown how the chromatographer can retrieve required information in a series of factor analysis maps. Emphasis will be placed on affinity and/or selectivity with three maps: (1) PCA "affinity analysis" map, (2) CFA "trends analysis" map and (3) CFA "distances analysis" map.

DATA

Corresponding data have been published previously in a series of papers devoted to "factor analysis and experimental design in high-performance liquid chromatography (HPLC)" [4–12]. The original data set corresponds to 63 compounds studied on 43 systems. An overall view of these data has been presented in a previous paper in this series [12]. Therefore, the description of the solutes, a series of chalcones, $XC_6H_4CH=CHCOC_6H_4Y$, has been omitted in order to simplify the paper. The topic is focused on factor analysis maps, the art of the exploitation of chemometric techniques rather than on the physico-chemical exploitation of the data. The characteristics of the 43 chromatographic systems are presented Fig. 1: the packings, the eluents and the corresponding identifiers of the systems are given. References to the original papers are indicated at the top.

From the original incomplete data matrix of capacity factors (k'), two subsets have been considered. The first matrix is a set of 1548 k' relative to 36 compounds

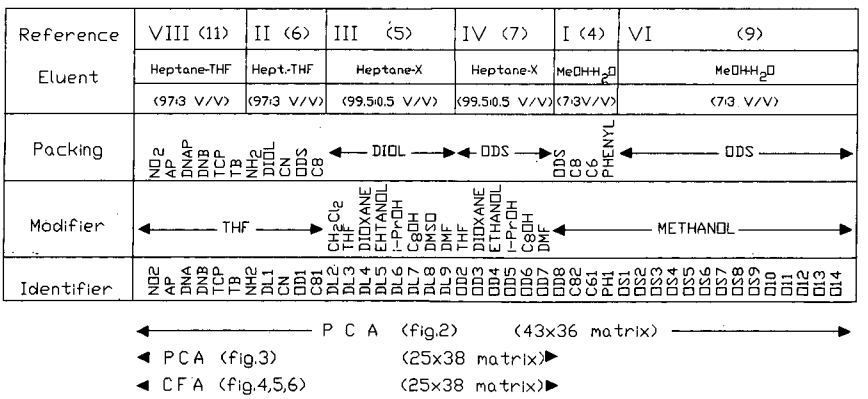

Fig. 1. Characteristics of the 43 studied chromatographic systems. These systems are the variables of an incomplete 43 × 38 retention data matrix of a series of 38 compounds. Factor analysis (PCA and CFA) was realized on the complete matrix and the reduced set of normal-phase data. MeOH = Methanol; i-ProH = isopropanol; C_8OH = Octanol-1.

eluted from 43 normal (NP) and reversed-phase (RP) chromatographic systems. The second matrix is a set of 950 k' relative to 38 compounds eluted from 25 normal-phase chromatographic systems.

DATA PROCESSING

Data were analysed with the use of PCA and CFA. Both approaches have been explained in previous papers [2,4,8].

The CFA method is particularly useful for a simultaneous comparison of the different characteristics of chromatographic systems and solutes. The usual maps obtained with CFA permit trends analysis of the chromatographic systems and solutes by means of their relative proximities. Hence, relative polarity, affinity and selectivity are accessible.

CFA can be extended to increase the analysis of the selectivity. The original maps of CFA are transformed by a translation of chromatographic systems (i) along the main axes (k). The translation factors are given by the eigenvalues (e_i) extracted from the data matrix. For a chromatographic system (i), the translation factor along the axis (k) is equal to $1/\sqrt{e_k}$. Because the chromatographic systems are translated far from the origin, they are drawn on the limit of the graph. The directions given by the chromatographic systems are then more useful for obtaining the relative selectivity of systems. This relative selectivity is related to the distance between the perpendicular projections of two solutes onto the directions defined by the systems. Hence, for a pair of solutes, it is possible to compare the selectivities of chromatographic systems by distance analysis.

RESULTS AND DISCUSSION

The factor analysis will be presented progressively by using PCA of the 43 × 36 complete matrix and of the 25 × 38 submatrix (Fig. 1) and CFA of the 25 × 38 submatrix.

The PCA of the matrix of normal and reversed-phases is presented Fig. 2. The projection of the 30 compounds is given on the plane defined by the first and second best factorial axes of inertia. These axes correspond to 60% and 34%, respectively, of the information content. Fig. 2 represents simultaneously the correlation circle of the chromatographic systems. Two main groups of systems defined two perpendicular directions which show clearly their independence. These groups correspond to the normal- and reversed-phase systems.

For the two chromatographic modes, a strong correlation of all the chromatographic systems was observed with the first two extracted factors. This separation into two groups can be related to the CFA of the same data matrix given elsewhere [12] (Fig. 4b). This CFA map has shown two clouds of the projected chromatographic systems with a large scattering of representative points for the NP systems due to the large and specific interactions involved. The representative points of the RP mode were closed, certainly owing to the simpler partition mechanism and the lack of various solvents. This type of information is not obvious in the above PCA map (Fig. 2). The latter gives some trends of the affinity of compounds for the system belonging to the two chromatographic modes. Each group of systems gives an average direction

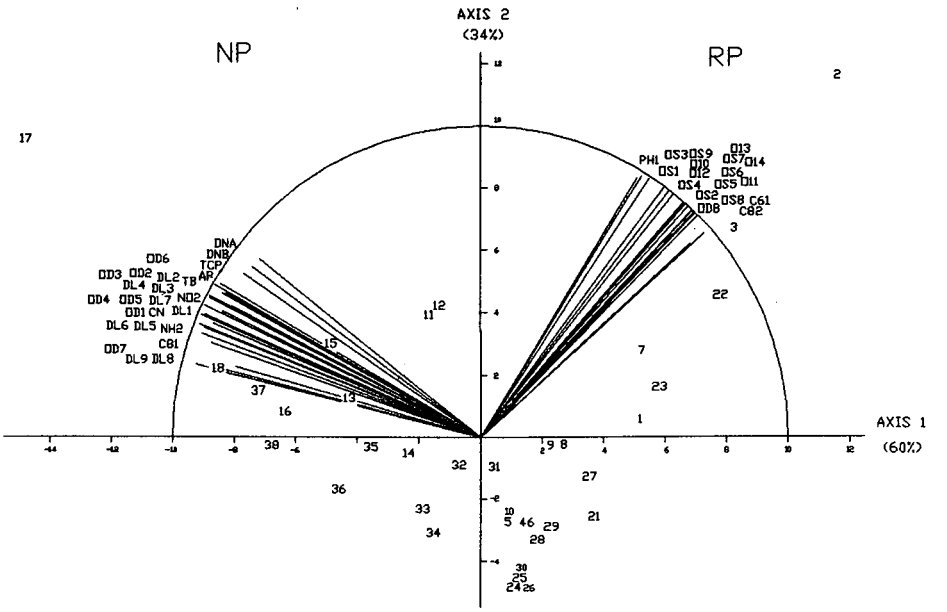

Fig. 2. Principal component analysis of a matrix of 1548 capacity factors in normal and reversed phases. The compounds are projected in the plane defined by the first and second best axes of inertia which represent 94% of the information content. On the correlation circle the independence of the two chromatographic modes appears clearly.

which presents a better dispersion for sets of compounds. For example, solutes 2, 3 and 7 have a better affinity for RP than for NP systems. In the same way, compounds 17, 18, 37 and 16 have a better affinity for NP systems. Compounds 5, 46, 29 and 28, which are located in the centre of the graph, present a similar affinity for RP and NP systems. The capacity factors increase according to the main directions defined by the NP and RP systems.

A submatrix of the main matrix is considered. It includes 950 k' data corresponding to the behaviour of the model series of chalcones on the normal phases only. This submatrix is studied by PCA. A projection of the compounds in the first factorial plane, defined by the first and second axes of inertia, which represent 89% and 6% of the information content, respectively, is shown in Fig. 3a. A simultaneous representation of the correlation circle confirms a strong correlation of each NP system principaly with axis 1 and secondarily with axis 2 and a similarity between all these systems. The average direction defined by the position of the systems on the correlation circle is superposed with axis 1. This graph gives a better in-depth analysis of similarities and differences of the systems. For example, the diol systems DL8 and DL9, with their strong modifiers (DMSO and DMF), are similar and relatively separated from the others. The group with ODS, C_8, diol and TB systems (OD1, $C_8$1, DL2–DL4, DL7, etc.) are not correlated with axis 2 and present the same affinity for the tested compounds. The non-commercially available phases TCP, DNAP (DNA) and DNB have the same specific affinity. The three groups reflect the three main trends of all the set of NP systems.

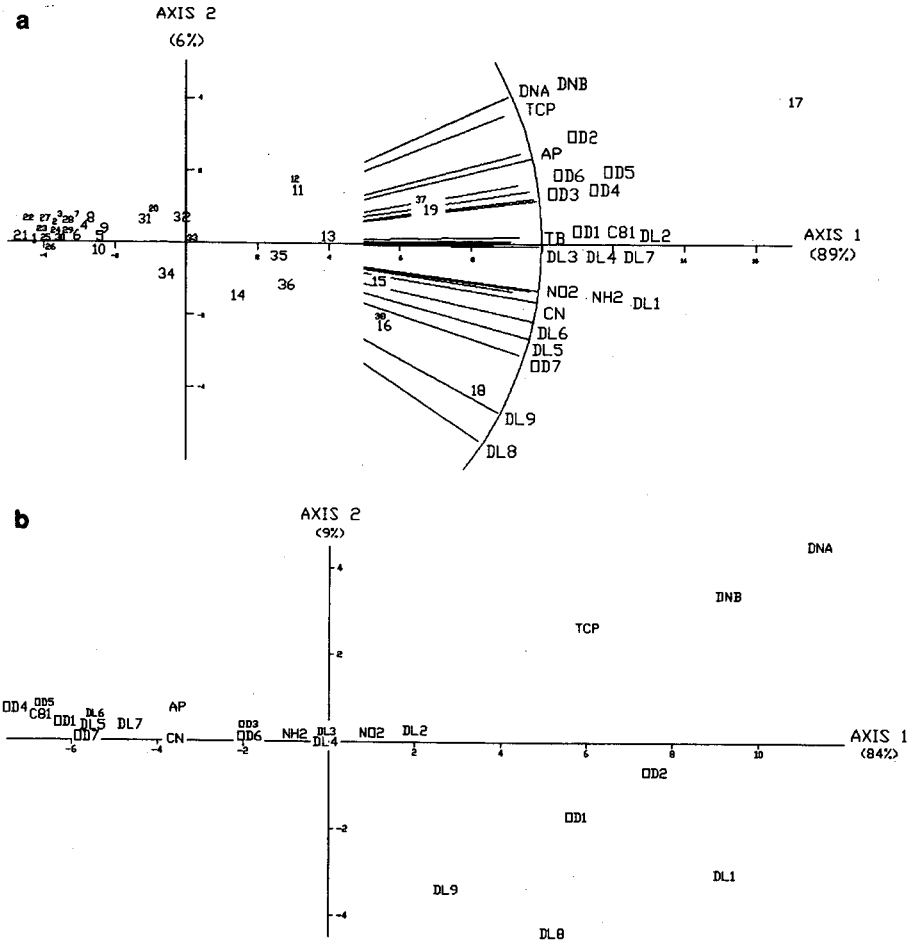

Fig. 3. (a) Principal component analysis of the submatrix of the 950 normal-phase capacity factor data. Projection of the compounds in the first plane (95% of the information content). The dispersion of the chromatographic systems on the correlation circle is related to their correlation with the extracted factors 1 and 2 and to their specific interactions with the compounds. (b) Principal component analysis of the normal-phase submatrix. Projection of the chromatographic systems in the first factorial plane (93% of the information content). This map gives the relative polarity of the chromatographic systems.

The above average direction defined by the chromatographic systems is related to the average value of the capacity factors; 89% of the information content of axis 1 reflects the weight of the k' when the main factor of inertia is extracted. In other words, axis 1 reflects k' variations. The dispersion of the previous three groups is due to the contribution of axis 2, which is the second extracted factorial axis. The differences in the chromatographic affinities of the compounds for all these NP systems can be linked to their contribution to the information content of the second axis.

The cloud of compounds located on the left-hand side of Fig. 3a contains those which have a low affinity for NP systems. These solutes have a better affinity for RP

systems, as was shown previously on the right-hand side of Fig. 2. The compounds that have the greatest k' values for NP systems are located on the right-hand side of Fig. 3a. On axis 2, the dispersion of solutes can be related to the dispersion of NP-systems. The trend analysis of the system directions and the solute projections can be linked qualitatively. For example, compound 17 has a great affinity for DNAP and DNB. Compound 18 has a great affinity for DL8.

The PCA of the NP matrix can also be used to analyse the behaviour of the chromatographic systems in the solute space. Fig. 3b gives the projection of these systems on the first factorial plane defined by axes 1 and 2, which take 84% and 9%, respectively, of the information content. Axes 1 and 2 also represent the variation of chromatographic polarity. Fig. 3b gives a more in-depth analysis of the dispersion of the systems than can be done with the correlation circle only (Fig. 3a). For any direction issued from the origin of the axes, the systems are classified according to their average chromatographic polarity. The systems which are located on the right-hand side of the graph contribute to the dispersion represented by the second factorial axis.

The complete PCA study must take into account projections of compounds (Fig. 3a) and systems (Fig. 3b). For example, compound 18 has a good affinity for DL9 and DL8 (Fig. 3a) but Fig. 3b shows that in the average direction of both systems, DL8 exhibits a greater polarity than DL9. Effectively, k' of compound 18 on DL8 is twice the k' value on DL9. In the same way, compound 17 has a relatively good affinity for DNA, DNB and RCP systems (Fig. 3a). Fig. 3b shows that this affinity increases in the order TCP < DNB < DNA. In order to optimize a separation of compounds, it is necessary to put the stress first on the affinity and second on the selectivity. Trends in affinity and selectivity can be elucidated simultaneously by CFA.

Trends in affinity are deduced from the relative proximity of compound and system projections. This exploitation must be conducted progressively. The different planes of projection are examined successively. The apparent trends must be weighted by the individual contributions of solutes and/or systems to the factorial axes. The usual CFA of the NP submatrix is given in Fig. 4a and b. Fig. 4a is the simultaneous projection of compounds and systems on the two main factorial axes of inertia. Axis 1 represents 55% of the information content and axis 2 24%. Fig. 4b shows the projections on the plane defined by the factorial axes 2 and 3. Axis 3 corresponds to 10% of the information content. Hence these factorial axes integrate 89% of the information content.

Compound 18 is projected near DL8 and DL9, on the first factorial plane (Fig. 4a). It exhibits a strong affinity for these two systems. The difference between the two systems is emphasized in Fig. 4b, where compound 18 is closer to DL8 than DL9. Hence this compound has a greater affinity for the DL8 system. Compound 17 has no particular proximity with any systems, but it has a strong contribution to the first and second axes. These axes are defined mainly by the DNB, TCP and DNA systems for axis 1 and by the OD6 and OD2 systems for axis 2. Hence, in this particular case compound 17 has a strong affinity for all these systems. The affinity increases with the proximity of the above systems. The DNA, TCP and DNB systems are closed to compound 19 in the first factorial plane. Owing to the lower contribution to the first and second axes of this compound, the exploitation of this map cannot determine the

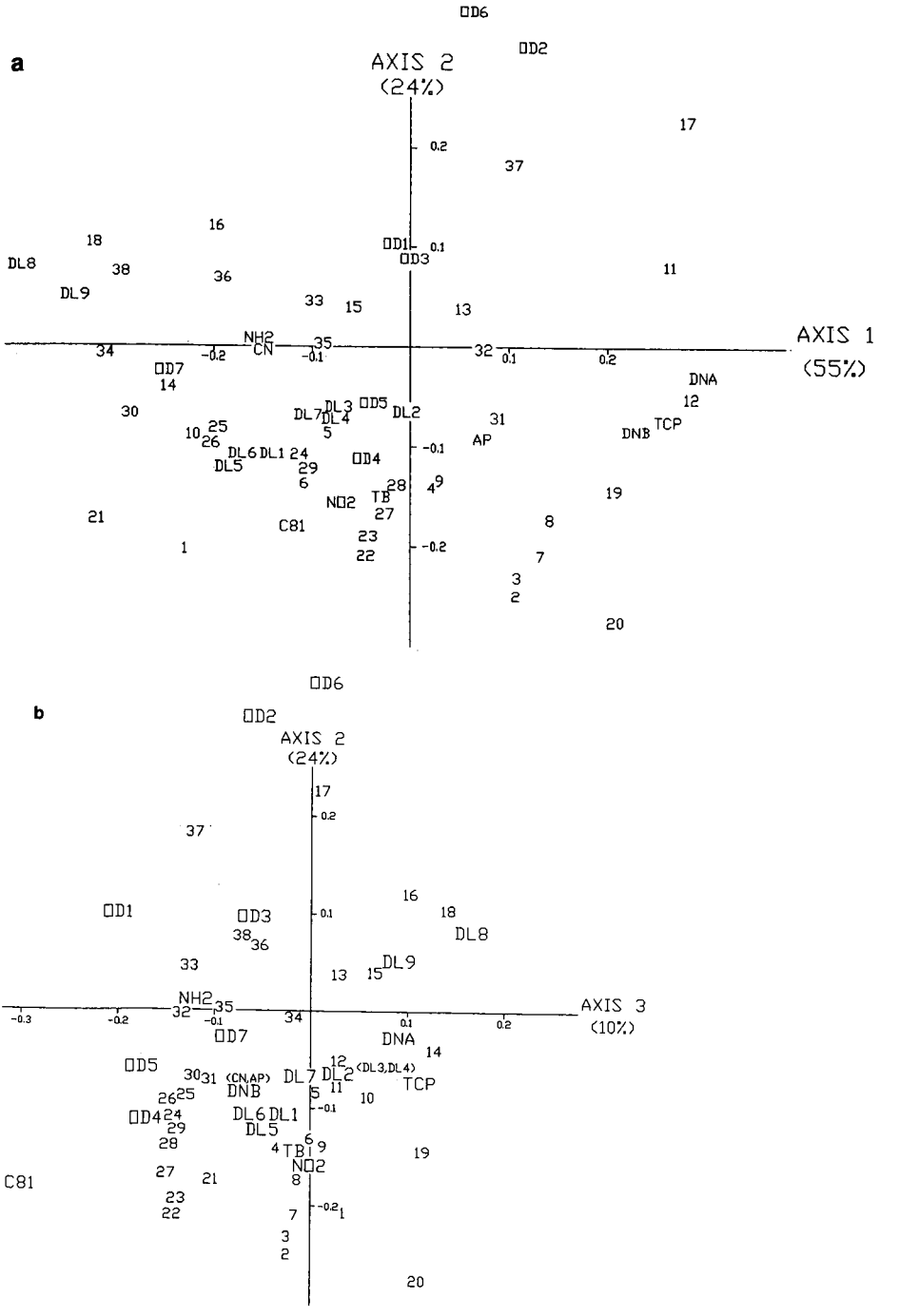

Fig. 4. (a) CFA trend analysis map. Simultaneous projection of the normal-phase chromatographic systems and compounds on the plane defined by the first and second best axes of inertia which represent 55% and 24%, respectively, of the information content. (b) CFA trend analysis map. Simultaneous projection of the normal-phase chromatographic systems and compounds on the plane defined by the second and third best axes of inertia which represent 24% and 10%, respectively, of the information content.

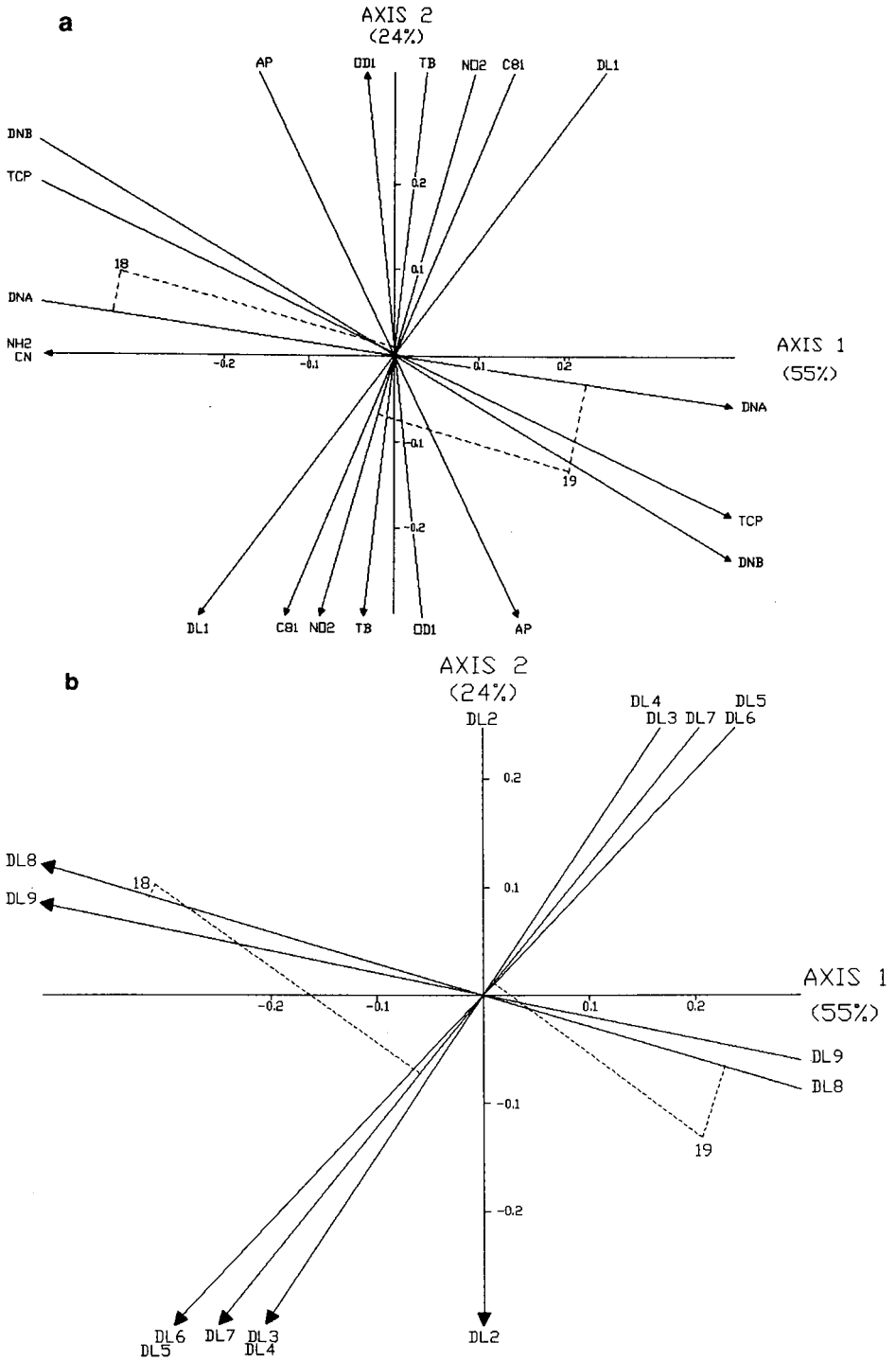

Fig. 5. (a) CFA distance analysis map. The chromatographic systems and compounds are selected from the previous CFA of the chromatographic normal-phase data matrix. The eleven presented chromatographic systems have the same eluent [heptane–THF (97:3, v/v)]. (b) CFA distance analysis map. The chromatographic systems and compounds are selected from the previous CFA of the complete normal-phase data matrix. The eight presented chromatographic systems have the same diol packing used with heptane plus different modifiers.

system which presents the greatest affinity. This is due to the determination of the principal factors, which are the average factors describing the behaviour of a large population of solutes and systems. Only "trends in affinity" can be reached here with different levels of reliability depending on the contribution to the extracted factors of solutes or systems analysed.

This common CFA map can be transformed to obtain the relative selectivity of the systems. Fig. 5a and b represent the transformed CFA maps from the previous ones limited to the example of solutes 18 and 19. Here, the eigenvalues of the first and second axes are 0.0428 and 0.0185, respectively. The selectivity is measured by the distance between the projections of two solutes on the axis defined by a transformed system. The relative selectivity of a chromatographic system, compared with the others, can be established. Two examples are proposed to illustrate the exploitation of the transformed CFA. In the first example (Fig. 5a), systems using the same eluent are extracted from the original CFA map. In the first factorial map, the eleven transformed systems define eleven directions drawn with solid lines. Arrows indicate that the true transformed projection of the systems are off the graph. Only two solutes are represented. The perpendicular projections of solutes on selected system axes are drawn with dashed lines. This map shows two main directions. The first is defined by the OD1, DL1, C81, NO2, TB and AP systems and the second by NH2, CN, DNB, TCP and DNA systems. These two directions are roughly perpendicular; the second main direction is parallel to the direction of solutes 18–19. The projection in dashed lines of these solutes are given on the directions of the DNA and NO2 systems. The observed distances between the projections of solutes 18–19 on the direction of a considered system are: (a) 12.3 arbitrary units for the DNA system and (b) 2.3 arbitrary units for the NO2 system. The corresponding selectivities of these two compounds, *i.e.*, their k' ratio, are 2.24 and 1.18 for the DNA and NO2 systems, respectively. The measure of the distances of the projections of solutes on particular system directions reflects the chromatographic selectivity.

For the chromatographer, the remaining problem is how to select a chromatographic system to separate this pair of solutes, *i.e.*, how to choose the best packing among others. It has been shown, in Fig. 5a, that the best selectivity is obtained with packings having the closest direction to the solute direction. For example, for the pair 18–19, the set of best packings is CN, NH2, DNA, TCP and DNB. The CFA map gives the relative affinity of solutes for these packings. To obtain an acceptable selectivity and a satisfactory affinity, the relative proximity of solutes and systems must be considered. For the pair 18–19, in Fig. 4a, the set of best packings is divided into two subsets. The first includes NH2 and CN systems and the second DNA, TCP and DNB systems. The first subset is between the two considered solutes whereas the second is close to solute 19. In the latter subset the best packing must be chosen. The selection of the retention time can be approached Fig. 3b.

The same type of map can be obtained to give a better understanding of the role of different eluents with the same diol packing (Fig. 5b). In this example the different contributions to factorial axes are not taken into account. Eight transformed chromatographic systems are presented. The projections of the model solutes 18–19 on DL7 and DL8 systems are drawn as dashed lines. Two main directions appear, the first for DL8 and DL9 systems and the second for DL2 up to DL7. The distances between the projections of compounds 18 and 19 on the two main directions are (a) 13 arbitrary

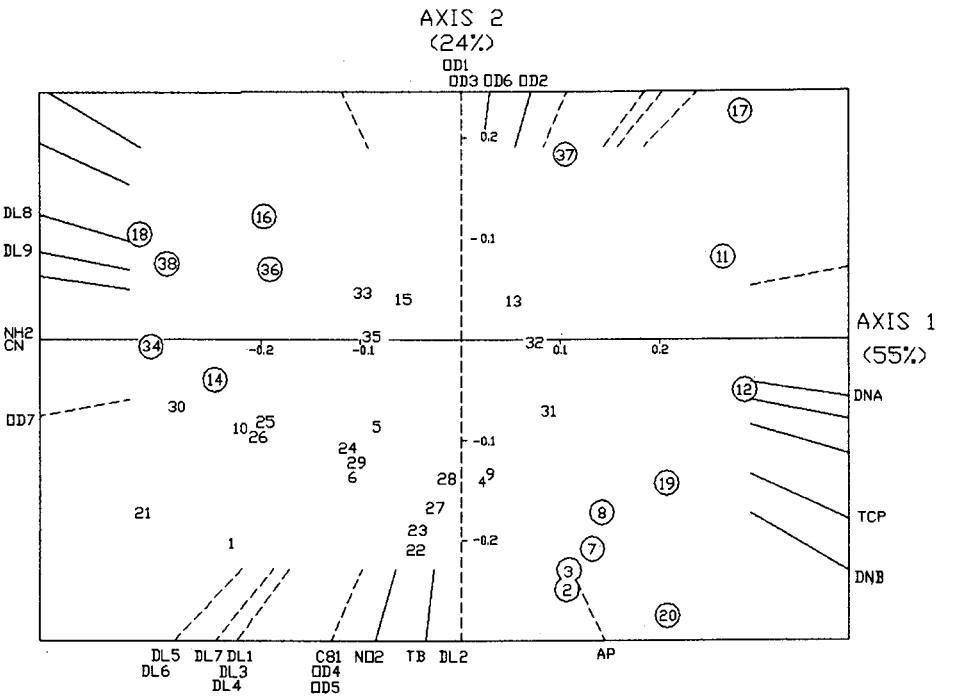

Fig. 6. CFA distance analysis map. The normal-phase data matrix is studied. Axes of the chromatographic systems are indicated. Axes of the chromatographic systems which have a lower contribution to inertia are drawn as dashed lines. Solutes which have a significant contribution to inertia of axes 1 and 2 are circled.

units for the DL8 system and (b) 2.5 arbitrary units for the DL7 system. The corresponding selectivities of these two compounds, *i.e.*, their k' ratio, are 2.7 and 1.2 for the DL8 and DL7 systems respectively. The best selectivity is obtained with solvents that have a parallel direction to the direction of the solute pair 18–19. DL8 and DL9 are selected, as they offer the greatest distance between the solutes projection. Systems have been selected regarding the selectivity by distances analysis. Now the affinity, *i.e.*, the time of chromatographic analysis, can be studied by "trends analysis" with CFA maps and by "affinity analysis" with PCA maps.

"Distance analysis" must be done carefully. The solute projections on the transformed systems are significant, at the first level of analysis, only if the chromatographic systems have a non-negligible contribution to the factorial axes. In the presented CFA, the most significant systems on axis 1 are DNA, DNB, NH2, TB, DL8 and DL9 and on axis 2 they are NO2, DNB, TCP, TB, CN, DL8, OD2 and OD6. With the other systems, their contribution to inertia must be considered to weight the distance analysis. The same restriction exists with solutes. On axis 1 solutes 11, 12, 14, 16–20, 34, 36 and 38 have a non-negligible contribution to inertia and on axis 2 solutes 2, 3, 7, 8, 16–20 and 37 have the same level of contribution to inertia.

A distances analysis map of the complete CFA is given Fig. 6. Systems that have a significant contribution to inertia are drawn as solid lines and other systems as dashed lines. Solutes that draw inertia of the solute cloud are circled.

Distances analysis of these solutes is possible with the eleven significant chromatographic systems. Specific treatment of chromatographic systems and solutes which have a weak contribution to the total inertia will be presented in a forthcoming paper. The interest in this map is that it offers an easy way to analyse the selectivity between two solutes. With this map, the selectivity is estimated by the distances between solute projections on chosen chromatographic systems. For example, let us consider the solute pair 2–3. Their own direction is approximatively perpendicular to axis 1 and parallel to axis 2. The best selectivity should be given with systems such as NO2, TB, OD2 or OD6. From the data matrix, OD6 is the most selective system. In the same manner, the best system, indicated by their identifier in parentheses, can be selected for some pairs of solutes such as 7 and 8 (OD6), 11 and 12 (NO2), 14 and 34 (TCP), 17 and 18 (DNA) and 20 and 37 (OD6).

CONCLUSIONS

To analyse a large set of homogeneous chromatographic data, it is necessary to use complementary chemometric methods. PCA and CFA do not extract the same factors.

With PCA the stress is put on the chromatographic affinity of solutes or on the chromatographic polarity of systems. The affinity of solutes and the polarity of systems are shown with two maps which are the projections of the solutes in their first factorial plane and the projection of the systems in their first factorial plane. The average direction(s) found on the correlation circle show the axis of variation of k'. When only NP or RP retention data are processed, the axis of k' variation is superimposed on the first factorial axis.

CFA puts the stress on relative chromatographic affinity and on selectivity. The data processing used in CFA hides the contribution of k' to the first factorial axis seen in PCA. CFA allows simultaneous solute and system projections on the same map. The relatives proximities of solutes and systems reflect the chromatographic affinity. The usual CFA maps give chromatographic trends of affinity and selectivity. Such projections could be called "trends analysis maps".

The selectivity analysis is improved with appropriate transformation of system projections. The distances between the solute projections on the system directions reflect the system selectivities. Selectivity analysis can be done easily with the transformed CFA maps, also called "distances analysis maps". Such a map can be exploited rapidly. The influent systems offering the best selectivity have the same direction as the two solutes considered.

Chromatographic analysis of a data set can be reduced to the study of factor analysis maps. The chromatographic properties, affinity and selectivity, are more or less nested in the three factor analysis maps: PCA affinity, CFA trends analysis map and CFA distances analysis map. An extensive study of chromatographic data requires the simultaneous grasping of the information content deduced from these three maps.

REFERENCES

1 E. R. Malinowski and D. G. Howery, *Factor Analysis in Chemistry*, Wiley, New York, 1980.

2 R. F. Hirsch, R. J. Gaydosh and J. R. Chrétien, *Anal. Chem.*, 52 (1980) 723.
3 D. L. Massart, B. G. M. Vandeginste, S. N. Deming, Y. Michotte and L. Kaufman, *Chemometrics: a Textbook (Data Handling in Science and Technology*, Vol. 2), Elsevier, Amsterdam, 1988, p. 371.
4 B. Walczak, M. Dreux, J. R. Chrétien, K. Szymoniak, M. Lafosse, L. Morin-Allory and J. P. Doucet, *J. Chromatogr.*, 353 (1986) 109.
5 B. Walczak, L. Morin-Allory, J. R. Chrétien, M. Lafosse and M. Dreux, *Chemometr. Intell. Lab. Syst.*, 1 (1986) 79.
6 B. Walczak, J. R. Chrétien, M. Dreux, M. Lafosse, L. Morin-Allory, K. Szymoniak and F. Membrey, *J. Chromatogr.*, 353 (1986) 123.
7 B. Walczak, J. R. Chrétien, M. Dreux, L. Morin-Allory and M. Lafosse, *Chemometr. Intell. Lab. Syst.*, 1 (1987) 177.
8 B. Walczak, M. Lafosse, J. R. Chrétien, M. Dreux and L. Morin-Allory, *J. Chromatogr.*, 369 (1986) 27.
9 J. R. Chrétien, B. Walczak, L. Morrin-Allory, M. Dreux and M. Lafosse, *J. Chromatogr.*, 371 (1986) 253.
10 B. Walczak, L. Morin-Allory, M. Lafosse, M. Dreux and J. R. Chrétien, *J. Chromatogr.*, 395 (1987) 183.
11 B. Walczak, M. Dreux, J. R. Chrétien, L. Morin-Allory, M. Lafosse and G. Felix, *J. Chromatogr.*, 464 (1989) 237.
12 M. Righezza and J. R. Chrétien, *J. Chromatogr.*, 544 (1991) 393–411.

Journal of Chromatography, 556 (1991) 181–194
Elsevier Science Publishers B.V., Amsterdam

CHROM. 23 270

Measurement of partition coefficients by various centrifugal partition chromatographic techniques

A comparative evaluation

NABIL EL TAYAR, RUEY-SHIUAN TSAI, PHILIPPE VALLAT, COSIMO ALTOMARE and BERNARD TESTA*

Institut de Chimie Thérapeutique, Ecole de Pharmacie, Université de Lausanne, BEP, CH-1015 Lausanne (Switzerland)

ABSTRACT

Using published and previously unpublished data, the present paper compares the value of four centrifugal partition chromatography systems for measuring partition coefficients. The best results (broad applicability, log P range -3 to $+3$, precision, effectiveness) were obtained with the Ito multilayer coil separator–extractor and the horizontal flow-through multilayer centrifugal partition chromatography model. Excellent correlations were found with published log P values obtained by the shake-flask method.

INTRODUCTION

Lipophilicity, as expressed by the partition coefficient P, has since the pioneering work of Meyer [1] and Overton [2] become a major physicochemical parameter in medicinal chemistry. This property is often a determinant of the pharmacokinetic and pharmacodynamic behaviour of xenobiotics [3–6]. Thermodynamically, partition coefficient is defined as a constant relating the concentration of a solute in two immiscible phases at equilibrium [7,8]. A number of experimental models are currently used to simulate partition processes in biological systems and to determine lipophilicity. The "shake-flask" (SF) method, using water and a poorly misible organic solvent, is the technique most widely used for measuring partition coefficients [9,10]. 1-Octanol–water is universally accepted as the standard biphasic solvent system [9], but other solvents are of value, for example in understanding the relative contribution of hydrogen-bonding capacity to lipophilicity [11–14]. However, despite its value, the SF method suffers from a number of practical limitations, such as lack of precision, solute stability or volatility, solute impurities, formation of microemulsions, time consumption, etc., as previously discussed by Dearden and Bresnen [15].

Partition chromatography has been explored as an alternative means for measuring lipophilicity. In particular, chromatographic retention parameters obtained by

0021-9673/91/$03.50

reversed-phase high-performance liquid chromatography (RP-HPLC) have become increasingly popular in replacing the 1-octanol–water partition coefficients measured by the SF method [16–19]. However, the assumption that the mechanism of retention in RP-HPLC should be similar to the mechanism of partitioning in a 1-octanol–water system is an oversimplification. Indeed, the chemically bonded solid phases are expected, owing to the restricted mobility of the bonded alkyl chains and the presence of a solid support with a non-negligible proportion of residual silanol groups, to display a partitioning behaviour different from that of a true liquid such as 1-octanol [20–22].

Recently, centrifugal counter-current chromatography, also known as centrifugal partition chromatography (CPC), has been explored as a novel technique for measuring liquid–liquid partition coefficients [23–30]. This is a unique form of liquid–liquid partition chromatography that eliminates the need for a solid support; in other words, adsorption is precluded by the absence of a solid support, and solute retention depends only on its partition coefficient. Two poorly miscible liquids are used as the stationary and mobile phase. A centrifugal force maintains the stationary phase, while the mobile phase is pumped through the system. During the last decade, various CPC systems have been developed, such as the flow-through multilayer coil planet centrifuge [31,32], the horizontal flow-through multilayer coil planet centrifuge [33,34], the toroidal coil planet centrifuge [35,36], and the multichannel cartridges CPC [37,38].

In this paper we attempt to asses the potential application of four different centrifugal counter-current chromatographic techniques, namely multichannel cartridges CPC, toroidal coil planet centrifuge, flow-through multilayer coil planet centrifuge and horizontal flow-through multilayer coil planet centrifuge, in measuring partition coefficients.

THEORY AND GENERAL CONSIDERATIONS

Centrifugal counter-current chromatography is a liquid–liquid chromatographic technique resembling to some extent droplet counter-current chromatography (DCCC). In DCCC, the stationary phase is retained in a series of vertical narrow-bore tubes, while the mobile phase, depending upon its density, is pumped through the system in the ascending or descending mode in the form of small droplets [39–41]. CPC differs from DCCC in that centrifugal and/or Archimedian screw forces maintain the stationary phase, while the mobile phase is pumped through. These features allow high partition efficiency and large retention capability of the stationary phase under a high flow-rate of the mobile phase.

In a recent review [42], Ito presented the historical background, development and mechanisms of distribution of stationary and mobile phases in the CPC coil, classifying CPC systems into two types, namely hydrostatic equilibrium systems and hydrodynamic equilibrium systems. Briefly, the hydrostatic systems use a stationary coil, for example PTFE tubing such as those used in the toroidal coil planet centrifuge chromatograph [35,36] or multichannel cartridges such as those used in the Sanki CPC chromatograph [37,38]. Measurements begin with filling the coil with the stationary phase; and then the mobile phase, depending on its density, in introduced at the head or the tail of the coil, displacing nearly half the volume of the stationary phase in the coil. Hence, solutes introduced at the inlet of the coil are subjected to a

continuous partitioning process between the two phases. In this system, the retention of the stationary phase and the distribution of stationary and mobile phases in the coil are governed mainly by the centrifugal force.

In hydrodynamic systems such as the flow-through multilayer coil planet centrifuge [31,32] or the horizontal flow-through multilayer coil planet centrifuge [33,34], the rotation of the coiled column around its own axis creates an Archimedean screw force which, in combination with a revolutionary centrifugal force towards the centre of the centrifuge, allows a continuous mixing of the two phases while retaining a high proportion of the stationary phase. Using a stroboscope, Ito [42] observed that under high centrifugal forces and flow-rates the mixing zone, located near the centre of the centrifuge where the centrifugal force is weakest, travels towards one end of the coil. This indicates that the two phases are subjected to a typical partitioning process of repetitive mixing and settling at a high rate of over 13 times per second while the mobile phase is steadily passing through the stationary phase. These features provide a high partition efficiency and a high retention capability of the stationary phase under a high flow-rate of the mobile phase in comparison with the hydrostatic systems. For more detail, the reader is referred to the excellent review of Ito [42].

In these systems, the partition coefficient ($\log P^{CPC}$) is defined as the ratio of solute concentration in the stationary phase and in the mobile phase. In solvent systems using water as mobile phase, the partition coefficient is calculated as:

$$\log P^{CPC} = \log [(V_R - V_M)/V_S] \quad (1)$$

where V_R is the retention volume of the solute, V_M is the dead volume (mobile phase volume) and V_S is the stationary phase volume. In our laboratory, the dead volume (V_M) was determined using potassium dichromate as the non-retained compound. Using the organic solvent as mobile phase, the partition coefficient is readily calculated as:

$$\log P^{PCP} = \log [(V_S)/V_R - V_M] \quad (2)$$

In this case, the dead volume (V_M) was determined using anthracene as the non-retained compound.

What distinguishes the toroidal coil centrifuge from other CPC apparatus is that movement of coloured solutes can be observed continuously through the transparent coil using a stroboscopic light source [35]. This feature allows the measurement of highly lipophilic or highly hydrophilic solutes which take a very long time to elute. In such cases, the retention time (t_R) can be calculated when the solute is still far from the column outlet by measuring the distance of the position of the centre of the solute band (X_t) at time t as:

$$t_R = t(X_R/X_t) \quad (3)$$

where X_R is the distance of the circumference of the support around which the coil is wound. Hence, V_R can be calculated from the predetermined flow-rate of the mobile phase [31].

EXPERIMENTAL

Multichannel cartridges CPC apparatus

A Model CPC-LLN chromatograph (Sanki Engineering, Kyoto, Japan) connected to a 2238 Uvicord II detector operating at 254 nm (LKB, Bromma, Sweden) and a 600 chart recorder (W + W Scientific, Basle, Switzerland) was used. The chromatograph was fitted with twelve Type 250W cartridges (total volume 250 ml) placed in the rotor of a centrifuge [38]. Each cartridge is composed of four poly(chlorotrifluoroethylene) plates and five PTFE sheets. The rotor is thermostated in a constant-temperature box, and all experiments were performed at 30°C. Solvent was delivered by a Sanki constant-flow pump (Model LBP-V, Sanki Engineering). The apparatus was first packed with the stationary phase and then the mobile phase was pumped through. Depending upon the density of the two phases, the eluent was pumped in a head-to-tail or tail-to-head mode. A systematic determination of the dead volume is very important in the Sanki CPC-LLN model because of continuous "bleeding" of the stationary phase [25].

Toroidal coil planet centrifuge

The original design of the toroidal coil centrifuge has already been described [30]. A helical column is mounted in the periphery of the column container located on the top of the rotor. The helical column was prepared by winding PTFE tubing (0.55 mm I.D.) (Zeus Industrial Products, Raritan, NJ, USA) around a nylon tube (110 cm × 4 mm O.D.) to make *ca.* 830 turns with a total capacity of 4.0 ml. The movement of coloured solutes was observed by stroboscopic illumination with a visible light source.

In a previous study [30], 1-octanol and 0.1 *M* phosphate aqueous buffer were used as stationary and mobile phases, respectively. The rotational speed was adjusted to 1000 rpm and the flow-rate was 0.4 ml/min.

Flow-through multilayer coil planet centrifuge

A preparative coil (2.6 mm I.D., 370 ml volume capacity) was fitted in an Ito multilayer coil separator-extractor (P.C. Inc., Kim Place, Potomac, MD. USA). For commuting between "head" and "tail" ends of the coil, an SRV-4 four-way valve (Pharmacia, Uppsala, Sweden) was installed. The solutes were injected through a Lobar six-port valve injector (Merck, Darmstadt, Germany) with a 2.5-ml loop mounted. A Uvikon 725 UV detector (Kontron, Zurich, Switzerland) equipped with a QS 1.000 80-μl UV cell was used. The chromatograms were recorded with a Model 3392A integrator (Hewlett-Packard, Meyrin, Switzerland). A more detailed description of the apparatus was reported by Slacanin *et al.* [43].

1-Octanol–aqueous buffer and *n*-heptane–aqueous buffer solvent systems were used. The rotation speed of the rotor was about 1000 rpm. Depending upon the estimated distribution coefficient values, the flow-rate and the volume ratio of stationary and mobile phases were selected so that reasonable and precise retention time of solutes could be obtained. Thus, a flow-rate of 0.5 ml/min and a 36:1 volume ratio of stationary and mobile phases were employed for hydrophilic compounds with log *P* values smaller than −2.3. The other experimental details were as previously reported [29].

Horizontal flow-through multilayer CPC

The horizontal flow-through multilayer CPC model, CCC-1000 (Pharma-Tech Research, Baltimore, MD, USA) consists of three columns, each being helically wound with five layers of PTFE tubing (3.00 mm I.D., 3.94 mm O.D., volume capacity 115 ml). A Kontron Model 432 UV detector and a Model 420 HPLC pump (Kontron) were used. The chromatograms were recorded with a 3392A integrator (Hewlett-Packard). The experimental procedure is the same as for the Ito multilayer coil separator–extractor.

Chemicals

All compounds were of highest available purity and were obtained from different pharmaceutical and chemical companies. Analytical grade 1-octanol, cyclohexane, *n*-heptane and 3-morpholinopropane sulfonic acid (MPS) were purchased from Merck.

RESULTS AND DISCUSSION

Comparison of partition coefficients measured by CPC instruments with literature values measured by the shake-flak method

Multichannel cartridge CPC. Terada *et al.* [23,24] have measured the partition coefficients of various organic compounds using the Sanki CPC model and a solvent system consisting of 1-octanol–*n*-hexane (20:80)–water solvent system. A good linear relationship between (1-octanol–*n*-hexane (20:80)–water partition coefficients (log P^{CPC}) and 1-octanol–water partition coefficients measured by the SF method (log P^{SF}) was found. The reason for using octanol–hexane mixtures as the organic solvent was to decrease the high viscosity of 1-octanol, which caused pressure problems. However, the decrease in polarity of the octanol resulting from the addition of *n*-hexane is known to influence dramatically the mechanism of partitioning compared with the 1-octanol–water solvent systems [44]. Berthod and Armstrong [25,26] showed that the Sanki CPC model can be used directly to determine 1-octanol–water partition coefficients over a log P range of -2 to 2 by changing the number of cartridges in the rotor.

A recent study [28] has also compared the partition coefficients obtained by the Sanki CPC model and the SF method. Two solvent systems were employed, namely 1-hexanol–aqueous buffer (0.02 *M* MPS, pH 7.4) and cyclohexane–aqueous buffer (0.02 *M* MPS, pH 7.4). The aqueous and organic phases were mutually saturated. Preliminary studies using a 1-octanol–aqueous buffer and *n*-hexane–aqueous buffer systems were not successful, probably because of the high viscosity of 1-octanol and the low density and/or viscosity of *n*-hexane, respectively. In the 1-hexanol–aqueous buffer system, 1-hexanol was used as the mobile phase and aqueous buffer as the stationary phase. The flow-rate was 1.8 ml/min and the pump pressure was 55 kg/cm^2 at a rotation rate of 500 rpm. In the cyclohexane–aqueous buffer system, water was used as the mobile phase and cyclohexane as the stationary phase; the flow-rate was 2.4 ml/min and the pump pressure was 50 kg/cm^2 at a rotation of 700 rpm. In 1-hexanol–water and cyclohexane–water systems, a good reproducibility of partition coefficient measurements was obtained (S.D. $< 4\%$) by the Sanki CPC model. 1-Hexanol–water and cyclohexane–water partition coeffcients expressed as log $P^{CPC}_{hexanol}$ and log $P^{CPC}_{cyclohex}$, respectively, are reported in Table I. Table I also reports literature

partition coefficents obtained by the SF method in the 1-octanol–water and hexane–water solvent systems and expressed as log P^{SF}_{oct} and log P^{SF}_{hex} [45], respectively. Good linear relationships between partition coefficients obtained by the Sanki CPC model (log P^{CPC}) and partition coefficients measured by the SF method (log P^{SF}) were obtained as follows:

$$\log P^{SF}_{oct} = 1.25(\pm 0.16) \log P^{CPC}_{hexanol} - 0.25(\pm 0.16) \quad (n = 20;\ r = 0.968;\ s = 0.15) \quad (4)$$

$$\log P^{SF}_{hex} = 1.05(\pm 0.31) \log P^{CPC}_{cyclohex} - 0.21(\pm 0.29) \quad (n = 8;\ r = 0.959;\ s = 0.26) \quad (5)$$

where n is the number of compounds, r is the correlation coefficient, and s is the standard deviation of regression. The values in parentheses are the 95% confidence limits of the regression coefficients. Eqns. 4 and 5 indicate that multichannel cartridges CPC is a useful method for measuring partition coefficients. However, the narrow range of measurable lipophilicites, the continuous "bleeding" of the stationary phase, the high pressure and the resulting breakage of tubing limit the usefulness of this technique.

Toroidal coil CPC. Toroidal coil CPC has been used by some to measure partition coefficients of a few coloured compounds [30]. The log P^{CPC} values measured by this technique are reported at the end of Table II. This technique proved its potential

TABLE I

PARTITION COEFFICIENTS OF VARIOUS ORGANIC COMPOUNDS MEASURED BY MULTICHANNEL CARTRIDGES CPC USING 1-HEXANOL–WATER AND CYCLOHEXANE–WATER SOLVENT SYSTEMS

Solute	Log $P^{CPC}_{hexanol}$	Log $P^{SF\,a}_{octanol}$	Log $P^{CPC}_{cyclohexane}$	Log $P^{SF\,a}_{hexane}$
Benzenesulphonamide	0.44	0.31	−2.28	−[b]
Phenylmethylsulphoxide	0.60	0.55	−1.29	−
Phenylmethylsulphone	0.69	0.49	−0.59	−
Benzamide	0.74	0.64	−1.92	−2.35
Acetanilide	0.99	1.16	−1.31	−1.80
Aniline	1.03	0.90	0.12	−0.05
Benzyl alcohol	1.08	1.10	−0.46	−0.76
Phenylethanol	−[b]	−	0.01	−0.39
Phenol	1.34	1.47	−0.69	−0.89
Phenyl acetate	1.32	1.49	−	−
Nitrobenzene	1.45	1.86	−	−
4-Aminophenol	0.11	0.04	−1.62	−
2-Aminophenol	0.70	0.52	−1.02	−
4-Nitroaniline	1.49	1.39	−0.92	−0.62
3-Nitroaniline	1.35	1.37	−	−
2-Nitroaniline	1.47	1.83	0.42	0.21
4-Pyridylmethanol	0.22	0.06	−	−
4-Pyridylethanol	0.30	0.10	−	−
4-Pyridylpropanol	0.80	0.58	−	−
4-Pyridylbutanol	1.01	0.90	−	−
4-Pyridylpentanol	1.47	1.39	−	−

[a] Taken from ref. 45.
[b] Not determined.

TABLE II

PARTITION COEFFICIENTS OF VARIOUS ORGANIC COMPOUNDS MEASURED BY THE ITO MULTILAYER COIL SEPARATOR EXTRACTOR (UNLESS OTHERWISE INDICATED) USING 1-OCTANOL–WATER AND *n*-HEPTANE–WATER SOLVENT SYSTEMS

Solute	Log $P^{CPC}_{octanol}$	Log $P^{SFa}_{octanol}$	Log $P^{CPC}_{heptane}$	Log $P^{SFa}_{heptane}$
Phenol	–[b]	1.46	−0.82	−0.70
2-Chlorophenol	2.05	2.14	–	–
4-Chlorophenol	–	2.39	−0.12	−0.11
2-Nitrophenol	1.68[c]	1.72[c]	–	–
3-Nitrophenol	1.74[c]	1.52[c]	−1.23	−1.40
4-Nitrophenol	1.77[c]	1.38[c]	−2.11	−2.00
2-Aminophenol	–	0.62	−2.46	−2.51
3-Aminophenol	0.15	0.17	–	–
3-Methoxyphenol	–	1.58	−0.88	−0.72
4-Methoxyphenol	–	1.34	−1.03	−1.16
4-Methylphenol	–	1.94	−0.19	−0.35
2,6-Difluorophenol	1.46[c]	–	–	–
Aniline	–	0.90	0.03	0.04
2-Nitroaniline	–	1.85	0.31	0.25
3-Nitroaniline	–	1.37	−0.46	−0.56
4-Nitroaniline	1.30[d]	1.39	−1.09	−1.13
4-Chloroaniline	2.01	1.88	–	–
N-Methylaniline	1.69	1.66	–	–
N,N-Dimethylaniline	2.32	2.31	2.40	2.23
m-Phenylenediamine	–	–	−2.51	−2.60
p-Phenylenediamine	–	−0.30	−3.01	−3.00
Benzene	2.05	2.13	2.37	2.29
Fluorobenzene	2.26	2.27	2.46	2.45
Chlorobenzene	–	2.81	2.99	2.95
Nitrobenzene	–	1.85	1.53	1.43
Toluene	2.54	2.73	2.85	2.85
Benzaldehyde	–	1.48	1.12	1.05
Benzamide	0.65	0.64	–	–
4-Fluorobenzamide	0.96	0.91	–	–
2-Chlorobenzamide	1.35	–	–	–
2-Bromobenzamide	0.71	0.73	–	–
Benzyl alcohol	1.22	1.10	−0.62	−0.55
2-Fluorobenzyl alcohol	1.31	–	–	–
4-Fluorobenzyl alcohol	1.36	–	–	–
2,6-Difluorobenzyl alcohol	1.12	–	–	–
Benzylamine	1.15	1.09	–	–
4-Chlorobenzoic acid	2.66	2.65	–	–
4-Bromobenzoic acid	2.74	2.86	–	–
4-Iodobenzoic acid	3.00	3.02	–	–
4-Hydroxybenzoic acid	1.56	1.58	–	–
Anisole	–	2.11	2.15	2.10
Acetophenone	–	1.58	1.20	1.14
2-Chloroacetanilide	1.35	1.28	–	–
2-Naphthol	2.85	2.84	–	–
Pyridine	–	0.65	−0.31	−0.30
2-Aminopyridine	0.51	0.49	–	–
4-Pyridylmethanol	−0.04	−0.02	–	–
4-Pyridylpropanol	0.59	0.60	–	–

(Continued on p. 188)

TABLE II (*continued*)

Solute	Log $P^{CPC}_{octanol}$	Log $P^{SFa}_{octanol}$	Log $P^{CPC}_{heptane}$	Log $P^{SFa}_{heptane}$
Catechol	–	–	−2.72	−2.85
Caffeine	–	−0.07	−2.21	−2.18
Pentobarbital	–	2.07	−1.22	−1.30
Secobarbital	–	1.97	−0.99	−1.00
Hexobarbital	–	1.49	−0.57	−0.70
Morphine	0.84	0.76	–	–
Sulpiride	0.52	0.58	–	–
Sulphamerazine	0.07	0.14	–	–
Sulphathiazole	0.04	0.05	–	–
Sulphanilamide	−0.85	−0.72	–	–
BzSA[e]	0.33	0.35	−2.54	–
4-Methyl-BzSA	0.83	0.80	−2.42	–
3-Methyl-BzSA	0.85	0.90	−2.35	–
4-Chloro-BzSA	–	1.10	−2.27	–
3-Chloro-BzSA	–	1.20	−2.21	–
4-Bromo-BzSA	–	1.38	−2.17	–
3-Bromo-BzSA	–	1.39	−2.04	–
4-Iodo-BzSA	1.77	1.59	−1.91	–
3-Iodo-BzSA	1.58	1.62	−1.91	–
4-Isopropyl-BzSA	1.96	1.75	−1.37	–
3-Isopropyl-BzSA	1.96	1.70	−1.41	–
4-Phenyl-BzSA	2.60	2.28	−1.24	–
4-Cyano-BzSA	0.40	0.22	−2.54	–
3-Cyano-BzSA	0.27	0.26	−2.33	–
4-Acetyl-BzSA	0.31	0.24	−2.74	–
3-Acetyl-BzSA	0.23	0.25	−2.74	–
4-Methoxy-BzSA	0.48	0.45	−2.71	–
3-Methoxy-BzSA	0.65	0.57	−2.33	–
4-Nitro-BzSA	0.72	0.75	−2.96	–
3-Nitro-BzSA	0.60	0.56	−2.98	–
4-Butyloxy-BzSA	2.19	2.09	−1.12	–
3-Butyloxy-BzSA	2.09	2.10	−0.94	–
4-Hexyloxy-BzSA	2.83	2.93	−0.41	–
4-Sulphonamido-BzSA	−0.70	−0.96	–	–
3-Sulphonamido-BzSA	−0.56	−0.46	–	–
4-Carboxyamido-BzSA	−0.66	−0.79	–	–
3-Carboxyamido-BzSA	−0.55	−0.80	–	–
4-Amino-BzSA	−0.64	−0.62	–	–
3-Amino.BzSA	−0.38	−0.28	–	–
4-Methylsulphonamido-BzSA	−0.73	−0.36	–	–
4-Acetanilido-BzSA	−0.10	0.00	–	–
4-Hydroxy-BzSA	−0.06	−0.06	–	–
4-ADS[f]	1.84	1.76	−0.97	–
4′-Methyl-4-ADS	–	2.40	−0.49	–
2′,4′-Dimethyl-4-ADS	2.69	2.73	−0.63	–
4′-Fluoro-4-ADS	2.17	2.01	−0.76	–
4′-Chloro-4-ADS	–	2.57	−0.91	–
4′-Bromo-4-ADS	3.15	2.85	−0.44	–
4′-Cyano-4-ADS	–	1.63	−1.43	–
4′-Acetyl-4-ADS	–	1.67	−1.34	–
4′-Methoxycarbonyl-4-ADS	2.13	2.25	−1.18	–
4′-Methoxy-4-ADS	1.99	1.96	−0.98	–

TABLE II (*continued*)

Solute	Log $P^{CPC}_{octanol}$	Log $P^{SFa}_{octanol}$	Log $P^{CPC}_{heptane}$	Log $P^{SFa}_{heptane}$
2',4'-Dimethoxy-4-ADS	1.65	1.63	−1.50	–
2',4',6'-Trimethoxy-4-ADS	–	1.03	−2.27	–
4'-Nitro-4-ADS	2.03	2.13	−1.00	–
2',4'-Dinitro-4-ADS	1.84	2.04	−1.22	–
4'-N,N-Diethylamino-4-ADS	–	1.44	−2.03	–
2'-Amino-4-ADS	1.75	1.56	−1.70	–
2',4'-Diamino-4-ADS	0.38	0.38	–	–
4'-N,N-Dimethylamino-4-ADS	1.93	2.04	−1.19	–
4'-N-Ethylamino-4-ADS	–	1.98	−1.38	–
4'-N-Hydroxylamino-4-ADS	–	0.88	−2.30	–
2',4',6'-Trihydroxy-4-ADS	1.75	1.53	–	–
Cytidine[g]	−2.32	−2.10	–	–
Adenosine[g]	−1.03	−0.98	–	–
Inosine[g]	−2.11	−2.00	–	–
Uridine[g]	−1.98	−1.89	–	–
Cytosine[g]	−1.51	−1.73	–	–
Guanosine[g]	−1.94	−0.92	–	–
Thymidine[g]	−1.19	−1.10	–	–
Uracil[g]	−1.14	−1.07	–	–
Thymine[g]	−0.61	−0.62	–	–
5-Fluorouracil[g]	−1.01	−0.95	–	–
Adenine[g]	−0.16	−0.09	–	–
Glycine[g]	−3.00[h]	−3.00[i]	–	–
Alanine[g]	−2.77[h]	−2.74[i]	–	–
Proline[g]	−2.62[h]	−2.54[i]	–	–
Phenylalanine[g]	−1.44[h]	−1.52[i]	–	–
Tryptophane[g]	−1.15[h]	−1.11[i]	–	–
Tyrosine[g]	−2.11[h]	−2.42[i]	–	–
Pararosaniline	−0.21[d]	–	–	–
Crystal violet	0.51[d]	–	–	–
Sudan III	2.11[d]	–	–	–
Phenol red	3.02[d]	–	–	–
MPTP[j]	2.71	2.61	–	–
4'-amino-MPTP	1.48	–	–	–
MPP^{+}[k]	−2.28	−1.04	–	–
4'-Methyl-MPP^{+}	−1.90	–	–	–

[a] Taken from ref. 45.
[b] Not determined.
[c] Log distribution coefficient (log *D*) at pH 7.4.
[d] Measured by toroidal coil CPC 31.
[e] BzSA = benzenesulphonamide.
[f] 4-ADS = 4-aminodiphenylsulphone.
[g] Measured by horizontal flow-through CPC.
[h] Log distribution coefficient (log *D*) at isoelectric point.
[i] Log distribution coefficient (log *D*) at pH 7.0.
[j] MPTP = 1-phenyl-4-phenyl-1,2,3,6-tetrahydropyridine.
[k] MPP^{+} = 1-methyl-4-phenyl-pyridinium iodide.

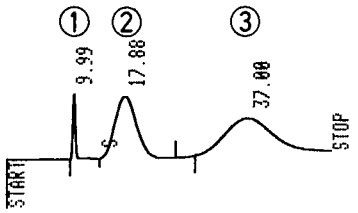

Fig. 1. A chromatogram of a mixture of 4-amino-BzSA and 4-acetanilido-BzSA using the flow-through multilayer CPC apparatus. The abscissa is the retention time in minutes and the ordinate is the UV spectral absorbance. Phosphate buffer (pH 7.4) and 1-octanol were used as the mobile and stationary phases, respectively. Peaks: 1 = potassium dichromate; 2 = 4-amino-BzSA; 3 = 4-acetanilido-BzSA.

to calculate the partition coefficient of highly lipophilic or hydrophilic coloured compounds from their movement observed in the transparent coil under stroboscopic light. Thus, the retention time of highly lipophilic or hydrophilic solutes, which take a very long time to elute, can be calculated using eqn. 3 when the solute is still far from the column outlet. Unfortunately, no literature log P^{SF} values are available for comparison except *p*-nitroaniline (log P^{SF} = 1.39; log P^{CPC} = 1.30). The most obvious limitation of the method is solute detection, which in the present state of development

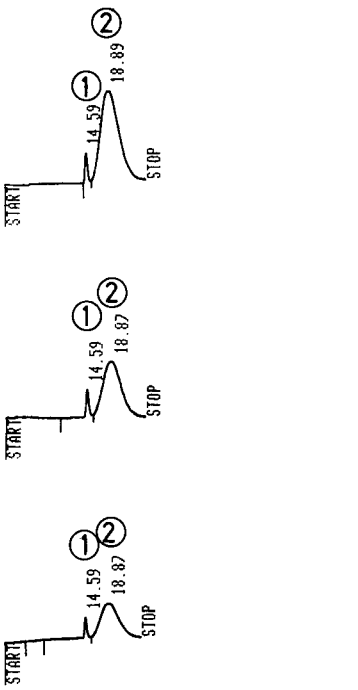

Fig. 2. A triplicate measurement of 5-fluorouracil at three different concentrations using the horizontal flow-through multilayer CPC. The abscissa is the retention time in minutes and the ordinate is the UV spectral absorbance. The volume of stationary and mobile phases is 262.5 ml and 87.5 ml, respectively. Aqueous MPS buffer (pH 7.4) was used as the mobile phase and 1-octanol as the stationary phase; the flow-rate was adjusted to 6 ml/min. Peaks: 1 = potassium dichromate; 2 = 5-fluorouracil.

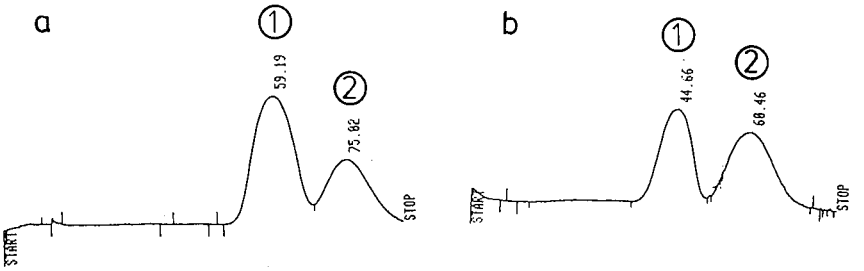

Fig. 3. Chromatograms of MPTP at different stationary and mobile phase volume ratios: (a) 5:1 and (b) 7:1. The abscissa is the retention time in minutes and the ordinate is the UV spectral absorbance. The distribution coefficient of MPTP was exactly the same (log D^{CPC} = 1.29). The flow-through multilayer CPC apparatus was used, 1-octanol being the mobile phase and phosphate buffer (pH 7.4) the stationary phase; the flow-rate was 1.00 ml/min. Peaks: 1 = anthracene; 2 = MPTP.

is restricted to coloured compounds. However, we believe that the method could be extended to all UV-active solutes by using a stroboscopic UV light source.

Flow-through CPC and horizontal flow-through CPC. 1-Octanol–aqueous buffer and *n*-heptane–aqueous buffer partition coefficients (log P_{oct}^{CPC} and log P_{hep}^{CPC}) measured by the Ito multilayer coil separator–extractor and the horizontal flow-through CPC (CCC-1000 model), are reported in Table II. The two techniques gave very satisfactory results. However, the Ito multilayer coil separator–extractore instrument is limited to a rotational speed of 800 rpm and the coil should be accurately balanced. The range of measurable log *P* values is −3.0 to +3.0 in the two solvent systems, and the average time of a triplicate measurement is about 2 h. The average time can be reduced by measuring a mixture of compounds, provided that their peaks are fully separated as illustrated in Fig. 1. An excellent reproducibility of partition coefficients was obtained (S.D. < 1%) by both the Ito multilayer coil separator–extractor and the horizontal flow-through CPC, as illustrated in Fig. 2. Fig. 2 also reveals that the retention time of solutes was constant in the usual concentration range. Furthermore, the precision of measurements by these techniques is not affected by changing the

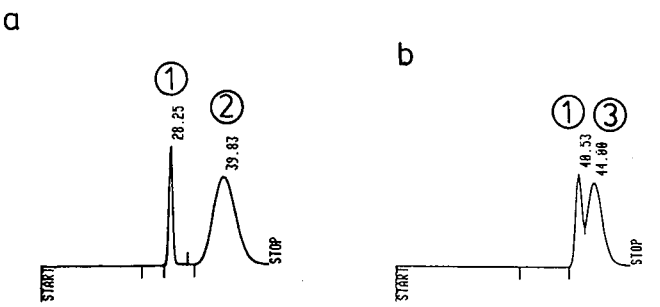

Fig. 4. Chromatograms of (a) 4′-amino-MPTP (log D^{CPC} = −0.19) and (b) 4′-methyl-MPP$^+$ (log D^{CPC} = −1.90) using the flow-through multilayer CPC apparatus. The abscissa is the retention time in minutes and the ordinate is the UV spectral absorbance. Phosphate buffer (pH 7.4) and 1-octanol were used as the mobile and stationary phase, respectively. The flow-rate was (a) 8.00 ml/min, and (b) 1.10 ml/min. Peaks: 1 = potassium dichromate; 2 = 4′-amino-MPTP; 3 = 4′-methyl-MPP$^+$.

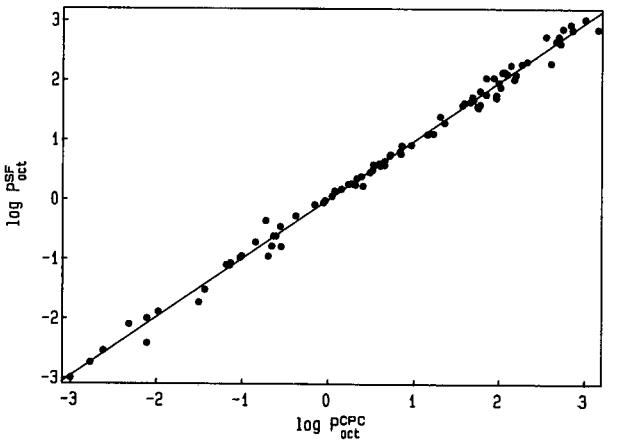

Fig. 5. Linear relationship between 1-octanol–water partition coefficients measured by the CPC and SF methods (eqn. 6).

flow-rate of the mobile phase and/or the volume ratio of stationary and mobile phases, as shown in Fig. 3. Both the aqueous and organic solvent can be employed as mobile phases depending on the lipophilicity of solutes. In both cases, very stable baselines, as shown in Fig. 3 and 4, were observed.

Excellent correlations were found with literature partition coefficients measured by the shake-flask method (log P^{SF}), as demonstrated in Figs. 5 and 6 and eqns. 6 and 7:

$$\log P^{SF}_{oct} = 0.99(\pm 0.01) \log P^{CPC}_{oct} - 0.01(\pm 0.02) \quad (n = 89;\ r = 0.997;\ s = 0.12) \qquad (6)$$

$$\log P^{SF}_{hep} = 0.99(\pm 0.01) \log P^{CPC}_{hep} - 0.04(\pm 0.02) \quad (n = 30;\ r = 0.999;\ s = 0.08) \qquad (7)$$

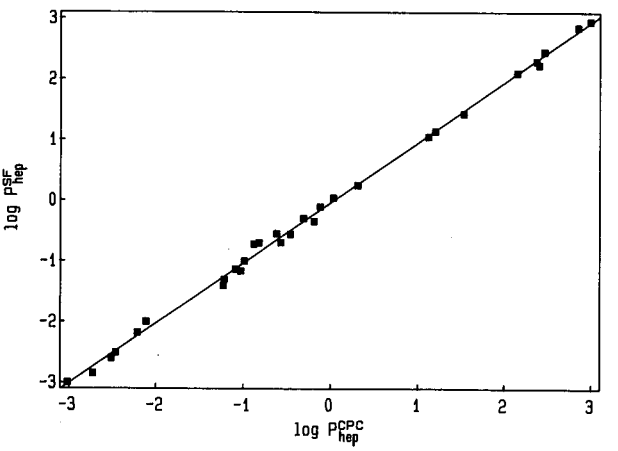

Fig. 6. Linear relationship between *n*-heptane–water partition coefficients measured by the CPC and SF methods (eqn. 7).

Guanosine and MPP^+ were excluded from eqn. 6, the deviations being most probably the result of some inherent limitations of the shake-flask method. These equations (6 and 7) clearly indicate that the same partitioning mechanism is operative in both CPC and SF methods, the slopes being equal to one and the intercepts to zero. In addition, these equations prove the potential applicability of CPC for measuring the partition coefficient of various drugs and many chemical compounds of chemical or biological interest (Table II).

CONCLUSIONS

CPC is demonstrated in this study to be a valuable alternative to the SF and RP-HPLC methods for measuring lipophilicity. Indeed, CPC combines the advantages of the SF method (ability to obtain genuine partition coefficients, possibility of using a variety of solvent systems) with those of RP-HPLC (rapidity, reproducibility, decreased interference by impurities). In our experience, solutes of log P values ranging from -3 to $+3$ can be measured in triplicate in about 2 h, and the results for a large number of compounds correlated very well with published log P values obtained by the SF method. The experimental conditions reported here result from a two-year effort in optimization, but more progress is to expected as CPC systems become dedicated to the measurement of partition coefficients.

ACKNOWLEDGEMENTS

B. T. and N. E. T. are indebted to the Swiss Science Foundation for Research Grant 31-27531.89. C. A. was supported by a post-doctoral NATO fellowship. The technical assistance of Gilles Boss is acknowledged.

REFERENCES

1 H. Meyer, *Arch. Exp. Pathol. Pharmakol.*, 42 (1899) 109.
2 E. Z. Overton, *Phys. Chem.*, 22 (1897) 189.
3 H. Kubinyi, in E. Jucker (Editor), *Progress in Drug Research*, Vol. 23, Birkhäuser, Basle, 1979, p. 97.
4 J. C. Dearden and P. K. Mays, *J. Pharm. Pharmacol.*, 37 (1985) 70P.
5 R. F. Rekker, *Farmaco Ed. Sci.*, 34 (1979) 346.
6 J. M. Mayer and H. van de Waterbeemd, *Environ. Health Perspec.*, 61 (1985) 295.
7 M. Berthelot and E. Jungfleisch, *Ann. Chim. Phys.*, 26 (1872) 396.
8 S. C. Valvani, S. H. Yalkowsky and T. J. Roseman, *J. Pharm. Sci.*, 70 (1981) 502.
9 A. Leo, C. Hansch and D. Elkins, *Chem. Rev.*, 71 (1971) 525.
10 A. Hersey, A. P. Hill, R. M. Hyde and D. J. Livingstone, *Quant. Struct.–Act. Relat.*, 8 (1989) 288.
11 P. Seiler, *Eur. J. Med. Chem.*, 9 (1974) 473.
12 T. Fujita, T. Nishioka and M. Nakajima, *J. Med. Chem.*, 20 (1977) 1071.
13 M. Gryllaki, H. van de Waterbeemd, B. Testa, N. El Tayar, J. M. Mayer and P.-A. Carrupt, *Int. J. Pharm.*, 51 (1989) 95.
14 N. El Tayar, R.-S. Tsai, P.-A. Carrupt, B. Testa and A. Leo, *J. Pharm. Sci.*, June 1991.
15 J. C. Dearden and G. M. Bresnen, *Quant. Struc.–Act. Relat.*, 7 (1988) 133.
16 N. El Tayar, H. van de Waterbeemd and B. Testa, *J. Chromatogr.*, 320 (1985) 305.
17 T. Braumann, *J. Chromatogr.*, 373 (1986) 191.
18 R. Kaliszan, in J. D. Winefordner (Editor), *Qantitative Structure–Chromatographic Retention Relationships*, Wiley-Interscience, New York, 1987.
19 D. J. Minik, J. J. Sabatka and D. A. Brent, *J. Liq. Chromatogr.*, 10 (1987) 2565.
20 A. Nahum and Cs. Horvath, *J. Chromatogr.*, 203 (1981) 53.

21 E. Bayer and A. Paulus, *J. Chromatogr.*, 400 (1987) 1.
22 N. El Tayar, A. Tsantili-Kakoulidou, T. Röthlisberger, B. Testa and J. Gal., *J. Chromatogr.*, 439 (1988) 237.
23 H. Terada, Y. Kosuge, N. Nakaya, W. Murayama, Y. Nunogaki and K.-I. Nunogaki, *Chem. Pharm. Bull.*, 35 (1987) 5010.
24 H. Terada, Y. Kosuge, W. Murayama, N. Nakaya, Y. Nunogaki and K.-I. Nunogaki, *J. Chromatogr.*, 400 (1987) 343.
25 A. Berthod and D. W. Armstrong, *J. Liq. Chromatogr.*, 11 (1988) 547.
26 A. Berthod and D. W. Armstrong, *J. Liq. Chromatogr.*, 11 (1988) 567.
27 C. Altomare, R.-S. Tsai, N. El Tayar, B. Testa, A. Carotti, S. Cellamare and P. G. De Benedetti, *J. Pharm. Pharmacol.*, 43 (1991) 191.
28 N. El Tayar, A. Marston, A. Bechalany, K. Hostettmann and B. Testa, *J. Chromatogr.*, 469 (1989) 91.
29 P. Vallat, N. El Tayar, B. Testa, J. Slacanin, A. Marston and K. Hostettmann, *J. Chromatogr.*, 504 (1990) 411.
30 R.-S. Tsai, N. El Tayar, B. Testa and Y. Ito, *J. Chromatogr.*, 538 (1991) 119.
31 Y. Ito and R. L. Bowman, *J. Chromatogr.*, 147 (1978) 221.
32 Y. Ito, *J. Chromatogr.*, 188 (1980) 33.
33 Y. Ito, *J. Chromatogr.*, 207 (1981) 161.
34 Y. Ito and H. Oka, *J. Chromatogr.*, 457 (1988) 393.
35 Y. Ito and R. L. Bowman, *Anal. Biochem.*, 85 (1978) 614.
36 Y. Ito, *J. Chromatogr.*, 192 (1980) 75.
37 W. Murayama, T. Kobayashi, Y. Kosuge, H. Yano, Y. Nunogaki and K. Nunogaki, *J. Chromatogr.*, 239 (1982) 649.
38 D. Armstrong, G. L. Bertrand and A. Berthod, *Anal. Chem.*, 60 (1988) 2513.
39 T. Tanimura, J. J. Pisano, Y. Ito and R. L. Bowman, *Science (Washington, D.C.)*, 169 (1970) 54.
40 Y. Ito, R. L. Bowman, *J. Chromatogr. Sci.*, 8 (1970) 315.
41 W. D. Conway and Y. Ito, *LC Mag.*, 2 (1984) 368.
42 Y. Ito, *CRC Crit. Rev. Anal. Chem.*, 17 (1986) 65.
43 I. Slacanin, A. Marston and K. Hostettmann, *J. Chromatogr.*, 482 (1989) 234.
44 S. Okada, H. Nakahara, C. Yomota and K. Mochida, *Chem. Pharm. Bull.*, 33 (1985) 4.
45 C. Hansch and A. Leo, *The Pomona Medicinal Chemistry Project*, Pomona College, Claremont, CA, 1983.

Journal of Chromatography, 556 (1991) 195–204
Elsevier Science Publishers B.V., Amsterdam

CHROM. 23 275

Experimental study on the effect of the sample size on the band profile for a binary mixture showing no competitive interaction

ANITA M. KATTI[a]
Ciba-Geigy, Central Analytic Department, CH-4002 Basle (Switzerland)

ABSTRACT

The effect of the sample size on the band profile of triphenylphosphine oxide and a piperidine derivative, for the pure components and for the binary mixture, were measured in reversed-phase chromatography. The experimental results showed reversal of the elution order with respect to the peak maximum. Deconvolution of the detector response for the mixture into individual component profiles was made by collecting fractions and subsequent analysis. The results show that the profile of the two components in the mixture is virtually the same as if they were injected alone. These results suggest that there is more than one type of adsorption site on the surface of the stationary phase and that each component interacts with a different site. Therefore, during the separation process there is hardly any competitive interaction between the two solutes.

INTRODUCTION

Single-component band profiles in overloaded elution chromatography can be predicted if the shape of the adsorption isotherm is accurately known [1,2]. This has been demonstrated experimentally in normal- and reversed-phase chromatography when the isotherm exhibits Langmuir shape [3–6]. Band profiles of binary mixtures can also be predicted when the competitive Langmuir isotherm is known [7,8]. This has been demonstrated experimentally with alcohols in reversed-phase chromatography [9], and with the separation of protected amino acid enantiomers on a bovine serum albumin stationary phase [10]. In the former case, a competitive Langmuir isotherm has been used empirically to fit the measured isotherm data. In the latter case a competitive biLangmuir isotherm has been employed in the light of a hypothesis of a two-site surface for interaction, one chiral and one non-chiral. Some solutes do not behave ideally and require more complex isotherm models to fit the empirical data [11,12]. For example, the separation of *cis*- and *trans*-androsterone at different

[a] Present address: Mallinckrodt Specialty Chemicals, St. Louis, MO, USA.
Je vous présente, en cette occasion, mes meilleurs voeux de bonheur et succés.

0021-9673/91/$03.50

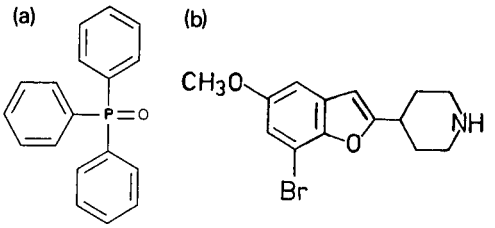

Fig. 1. Molecular structures of solutes used in this study: (a) triphenylphosphine oxide (PPO); (b) piperidine derivative (Pip).

sample sizes on a phosphate-buffer-modified silica could be predicted qualitatively by fitting the measured isotherm data to the LeVan-Vermeulen isotherm [13].

The prediction of non-traditional band shapes requires either the use of empirical models or an understanding of the basic mechanism of the separation, from which one can derive a model. In this paper, an unusual change of band shape with sample size, as seen in the detector response for a binary mixture, is described. A fundamental study is presented in order to understand the phenomenon that occurs. An interpretation of the results is made on the basis of binary and single-component band profile data.

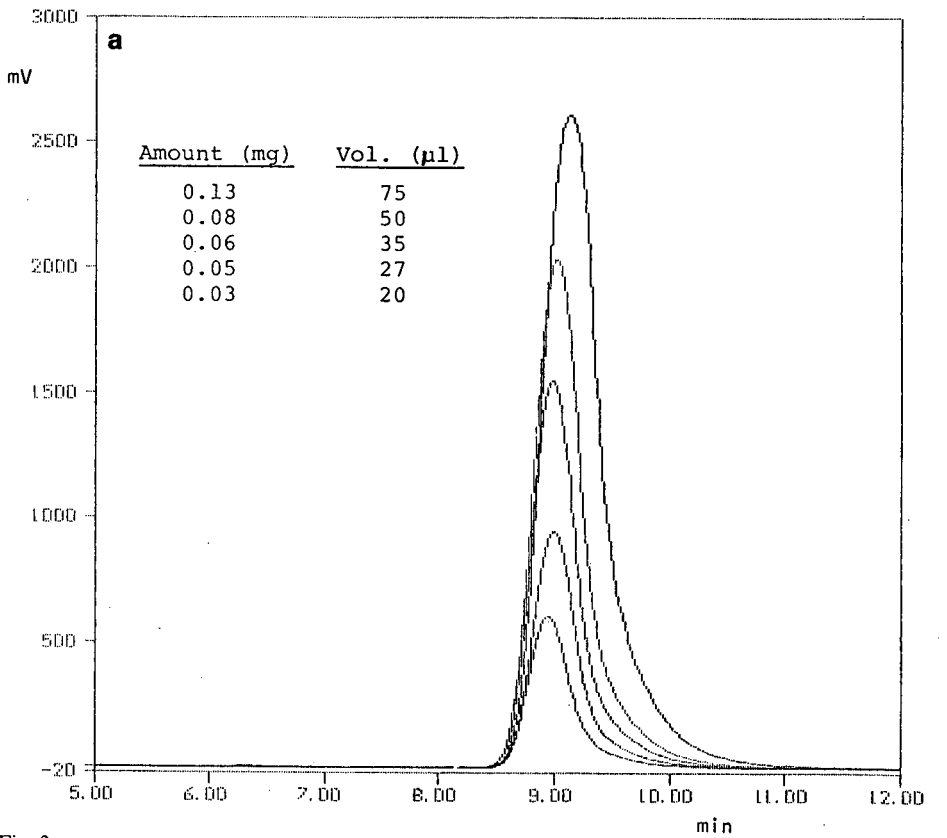

Fig. 2.

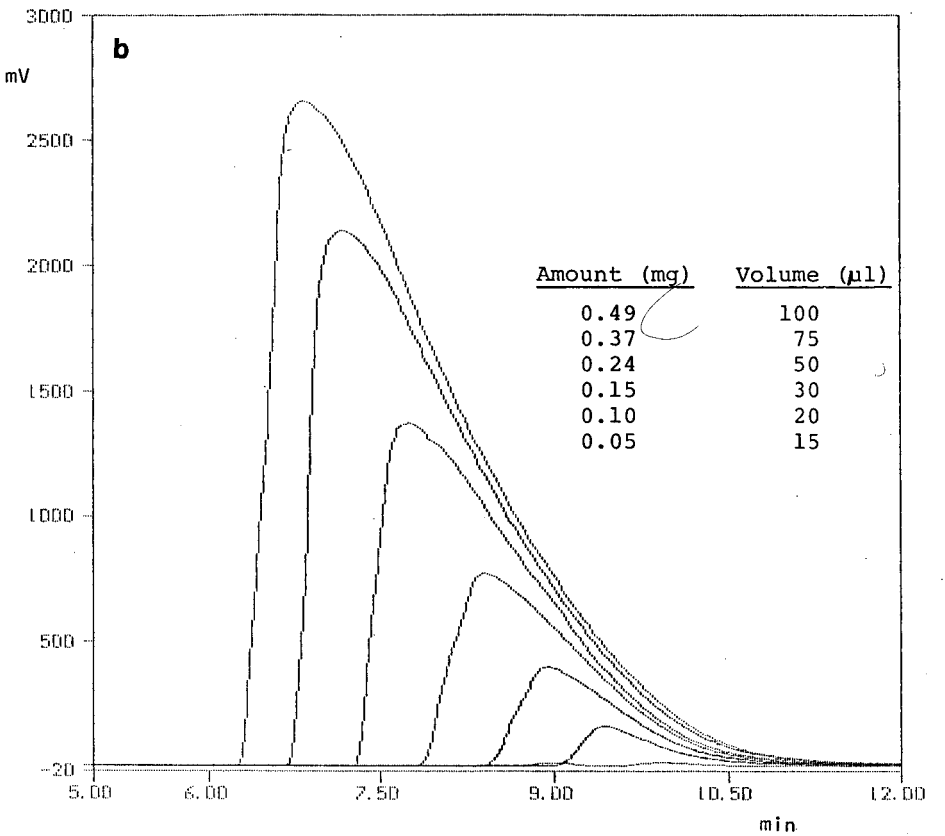

Fig. 2. Effect of the sample size on the pure components band profile. Column, 10-μm CN-Nucleosil, 25 × 0.46 cm I.D.; mobile phase, A–B (50:50) where A = acetonitrile–10 m*M* $(NH_4)_2SO_4$ (60:40) and B = 10 m*M* $(NH_4)_2SO_4$ in water; flow-rate, 1 ml/min; detection wavelength 230 nm. (a) Triphenylphosphine oxide; (b) piperidine derivative.

EXPERIMENTAL

Apparatus

Experiments were conducted on a modular high-performance liquid chromatograph consisting of a Kontron (Zurich, Switzerland) Model 425 low-pressure gradient controller and a Model 420 high-pressure pump, connected to the first Rheodyne (Cotati, CA, USA) Model 7010 valve of a Gilson (Middleton, WI, USA) Model 232/401 sample processor, a column, a Linear (Reno, NV, USA) Model 206 PHD rapid scanning detector. Then the outlet from the detector was connected to the second Rheodyne valve of the sample processor. The wires for control of the pump, the gradient former, the detector's output analog signal and the contact closures for the sample processor were connected to a Kontron multiport interface and to a Kontron adapted AT personal computer. Use of a Kontron data system Model 450-MT2 software, operating under MS-DOS version 3.3, allowed control of this modular system. The set-up and operation of the sample processor for this work were similar to that described previously [14].

Columns

Band profiles were determined on a 25 × 0.46 cm I.D. Nucleosil 10-μm CN column (Macherey-Nagel, Düren, Germany) packed in our laboratory. Analysis of the collected fractions was accomplished on a 25 × 0.46 cm I.D. CPS Hypersil, 5-μm CN column (Bischoff Chromatography, Wallisellen, Switzerland).

Chemicals

Triphenylphosphine oxide was purchased from Fluka (Buchs, Switzerland). The piperidine derivative (Ciba-Geigy, Basle, Switzerland) was obtained in our laboratory. The structures of the two solutes are shown in Fig. 1. Ammonium sulphate, (pro analysi) and Gradient-grade acetonitrile was purchased from Merck (Darmstadt, Germany). S.Q.S. HPLC-quality water was obtained from a Millipore system (Milford, MA, U.S.A.) All chemicals were used as received, without further purification.

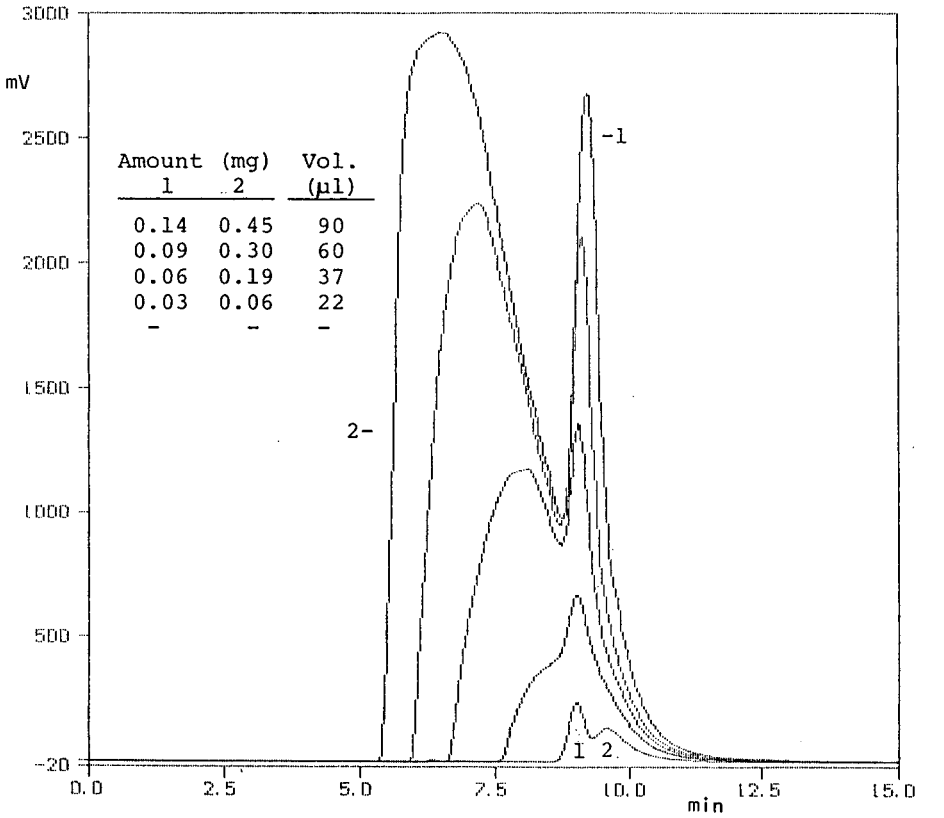

Fig. 3. Effect of the sample size on the binary mixture profile. Conditions as in Fig. 2. 1 = PPO; 2 = Pip.

RESULTS AND DISCUSSION

The effect of the sample size on the individual component band profiles of triphenylphosphine oxide (PPO) and a piperidine derivative (Pip) were measured (Fig. 2). The retention time of the peak maximum of the triphenylphospine oxide increases slightly with increasing sample size. This is indicative that the isotherm is slightly concave up. This is a moderate effect as no self-sharpening effect on the rear boundary is observed. The piperidine derivative takes on the typical profile of a compond with a Langmuir isotherm. As the sample size increases, the time of the peak maximum decreases, the front becomes self-sharpening, and the rear boundary tails to the value of its infinite dilution retention time.

When the two components are injected as a mixture (Fig. 3), at low concentration the PPO elutes first and the Pip elutes second with a separation factor, α, of 1.19. This has been confirmed by injection of the individual component in consecutive injections at low solute concentrations. As the sample size increases, however, it appears that the front of the second component passes the peak maximum of the first component. The roundness at the top of the band profile corresponding to the largest sample illustrated in Fig. 2b is due to detector saturation.

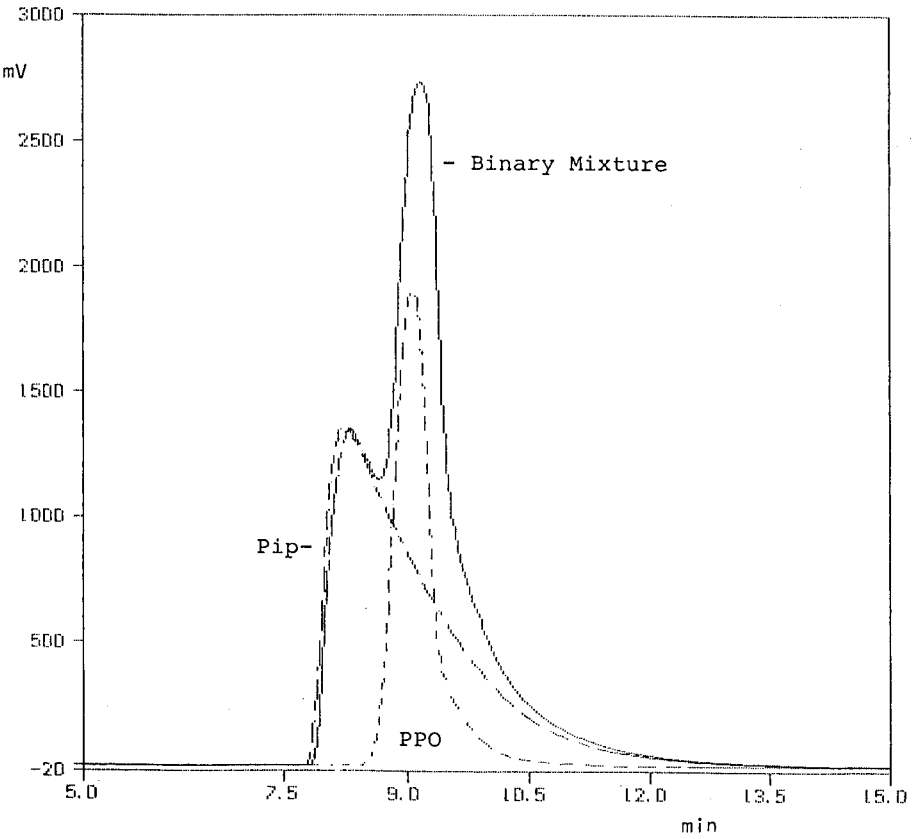

Fig. 4. Comparison on the single-component detector response profiles and that of the binary mixture at the same sample size. The conditions as in Fig. 2, except 50 μl injection (0.1 mg PPO and 0.25 mg Pip).

Fig. 4 illustrates an overlay of the individual detector response profiles of PPO and Pip compared with the total profile of the two component injected as a mixture. The amounts of PPO and Pip in the individual injections are the same as in the mixture. This figure suggests that the sum of the two individual profiles gives the total profile of the mixture; however, these data give no information about the individual profiles in the mixed zone.

One of the methods used to confirm the nature of the individual band profiles in the mixed zone is to collect fractions and develop a method for the quantitative analysis of each fraction [14]. Fig. 5a shows the detector response and Fig. 5b the result of the reanalysis of collected fractions. Several sets of data were taken with fraction collection and reanalysis. These experiments clearly show that the two data points at 8 min are outliers.

These results show that there is only a slight amount of competition and/or interaction between PPO and Pip. The simplest interpretation is that PPO and Pip interact with two independent sites for which the column saturation capacities are different. These results suggest that there are more sites available to PPO than to Pip, since the PPO remains practically linear in sample loading range where the Pip already exhibits a non-linear profile. Intermolecular interactions between the benzene

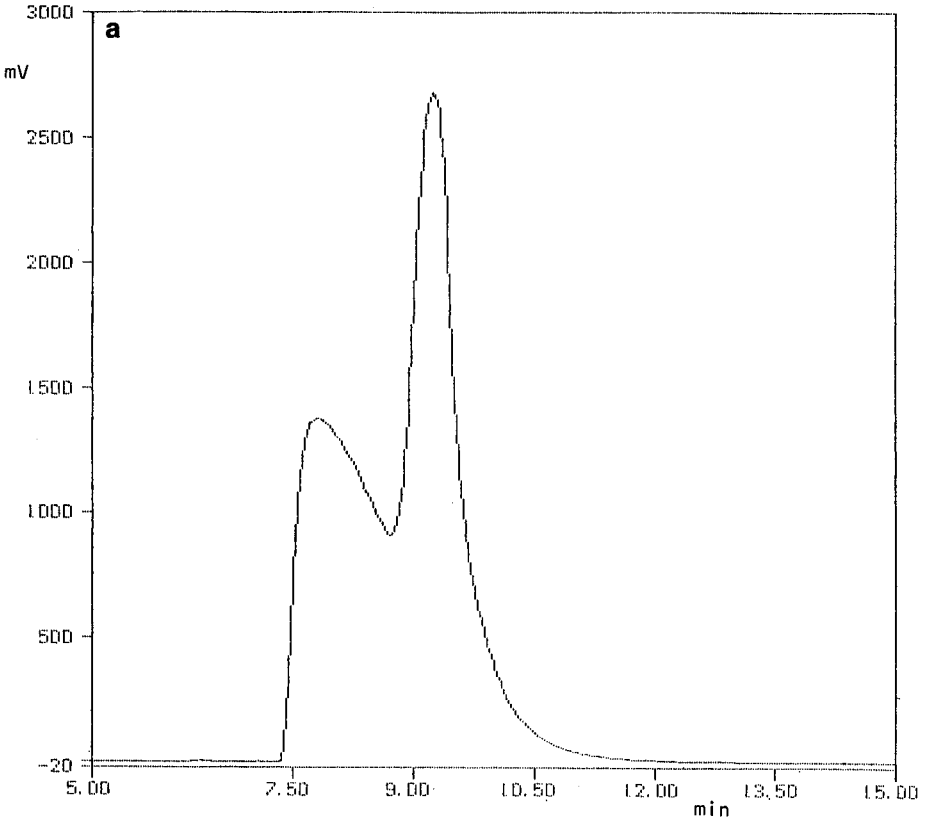

Fig. 5.

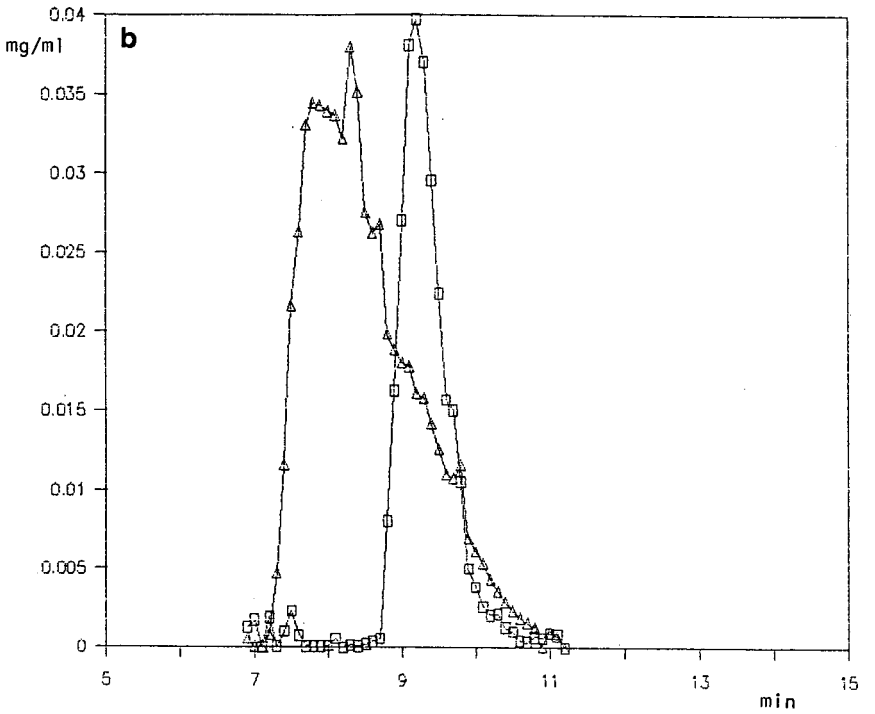

Fig. 5. Individual band profiles determined by fraction collection and reanalysis. Conditions as Fig. 2, except 50 μl injection (0.15 mg PPO and 0.31 mg Pip). (a) Detector Response; (b) individual profiles: □ = PPO; △ = Pip.

rings of the molecules of PPO could explain the slight increase in the retention time of the peak maximum, indicative of a convex isotherm. However, further experimental data on the surface properties of these would be required in order to draw a firm conclusion about the nature of the interactions [15].

The results in Fig. 5 also imply that the band profiles of the two-component mixture can be predicted quantitatively within a few per cent from only the single-component isotherm data. In the case of PPO the band profile at different sample sizes can be approximated with the estimation of coefficients for a linear isotherm or a slightly concave-up isotherm. The band profile of Pip can be predicted with the estimation of Langmuir isotherm coefficients. Isotherm data can be obtained in both cases directly from the band profiles [15–18] or by measurement of the single-component isotherm [19–21].

For analytical method development or preparative chromatography, it is important to increase the separation factor between the two components. By modifying slightly the mobile phase and increasing the $(NH_4)_2SO_4$ concentration in water from 10 mM to 50 mM, the chromatogram in Fig. 6a was obtained. The addition of salt decreases the retention of Pip below that of PPO, and the retention time of PPO increases slightly. The capacity factors (k') are summarized in Table I. This result

suggests that PPO interacts according to the hydrophobic effect, suggestive of an adsorption mechanism, whereas Pip appears to undergo an ionic interaction on sites that are relatively few in number. Under these experimental conditions, because Pip elutes before PPO and because of the larger separation factor, the non-linear effects do not lead to an interference chromatogram.

It is also possible to change the retention properties of the components by using a column packing material from another manufacturer. Using the same mobile phase as in Fig. 6a, but on a 5-μm CN-Hypersil column, a good separation was also obtained. The chromatogram illustrating the band profiles at different sample sizes is shown in Fig. 6b. With this material as well, the profile of Pip exhibits strong non-linear behavior. Comparing Fig. 6b and 2b, the retention time of Pip is observed to be only slightly less than on the other column with the same mobile phase conditions. In contrast, the retention time of PPO drops significantly compared with the retention of Fig. 2. The capacity factors are summarized in Table I. This change in the elution order suggests that the density of sites for PPO is lower on this latter column than on the former. However, with a separation factor of over 7, quantitative analysis is possible. In fact, this column under these experimental conditions was used for the

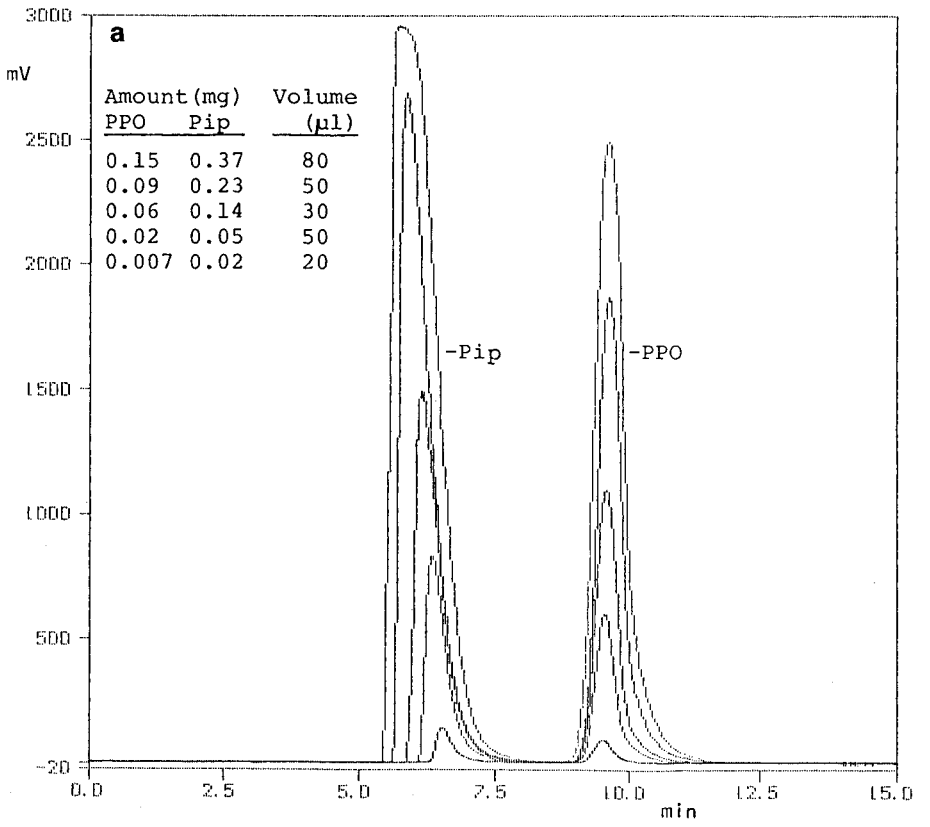

Fig. 6.

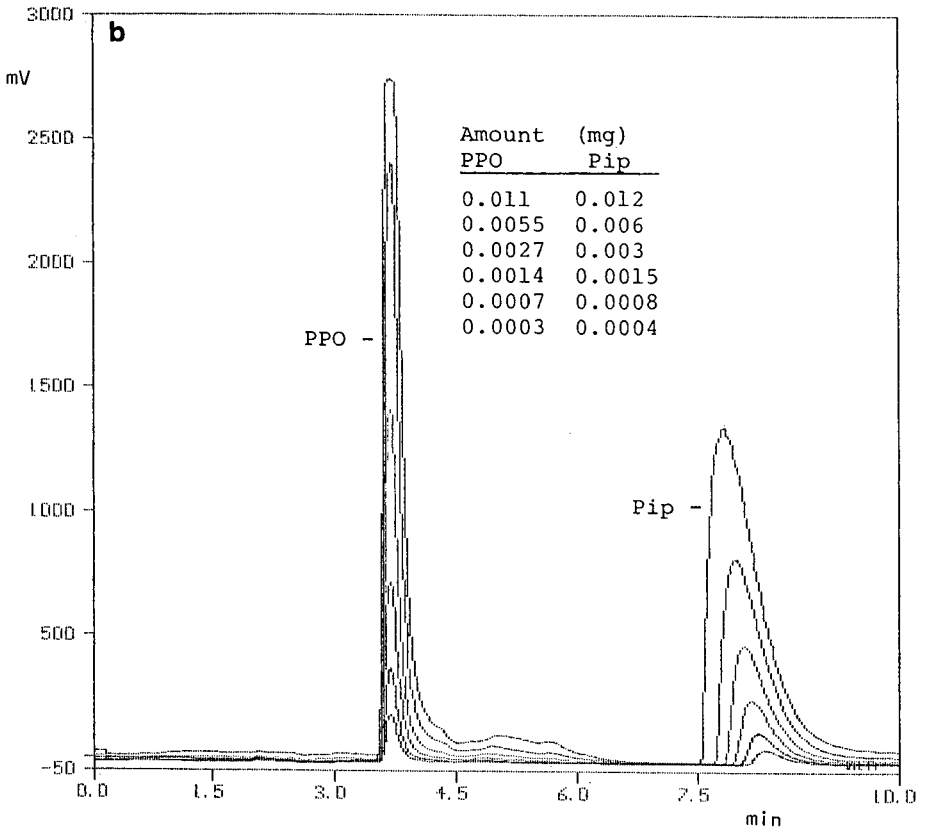

Fig. 6. Illustration of an improved method: (a) conditions as Fig. 1, except 50 mM $(NH_4)_2SO_4$ in solutions A and B; (b) new column, 5-μm CN-Hypersil, 25 × 0.46 cm I.D.; flow-rate, 1 ml/min; 50 mM $(NH_4)_2SO_4$ in A and B; detection wavelength 208 nm.

TABLE I

COMPARISON OF THE INFINITE DILUTION CAPACITY FACTORS

	k'_{PPO}	k'_{Pip}	α
Nucleosil			
10 mM salt	2.03	2.41	1.19
Nucleosil			
50 mM salt	1.18	2.17	1.84
Nucleosil			
10 mM salt	1.88	6.64	3.53
Hypersil			
50 mM salt	0.24	1.78	7.42

analysis of the fractions for Fig. 5b. Lastly, by decreasing the salt concentration from 50 mM to 10 mM, the capacity factor of both components is increased, but the separation factor is decreased (Table I).

CONCLUSIONS

The experimental chromatograms illustrate a situation in which two solutes in overloaded conditions behave as if there is virtually no interaction. This suggests that the solutes are absorbed on different sites, thus there is practically no competition. Band profiles under these conditions can be predicted quantitatively using only single-component isotherms.

ACKNOWLEDGEMENTS

The author is grateful to Ciba-Geigy, Basle, Switzerland, for supporting this work, and Kontron Inc. for their generous assistance in setting up and interfacing the sample processor to the data acquisition system.

REFERENCES

1 G. Guiochon, S. Ghodbane, S. Golshan-Shirazi, J.-X. Huang, A. Katti, B.-C. Lin and Z. Ma, *Talanta*, 36 (1989) 19.
2 A. Katti and G. Guiochon, *Adv. Chromatogr.*, 31 (1991) 1.
3 J. N. Wilson, *J. Am. Chem. Soc.*, 65 (1940) 532.
4 S. Golshan-Shirazi, S. Ghodbane and G. Guiochon, *Anal. Chem.*, 60 (1988) 2630.
5 S. Golshan-Shirazi and G. Guiochon, *Anal. Chem.*, 60 (1988) 2634.
6 A. M. Katti, J.-X. Huang and G. Guiochon, *Biotech. Bioeng.*, 36 (1990) 288.
7 J. I. Coates and E. Glueckauf, *J. Chem. Soc.*, (1947) 1308.
8 E. Glueckauf, *Proc. Roy. Soc. (London)*, A186 (1946) 35.
9 A. M. Katti, Z. Ma and G. Guiochon, *AIChE J.*, 36 (1990) 1722.
10 S. Jacobson, S. Golshan-Shirazi and G. Guiochon, *J. Am. Chem. Soc.*, 112 (1990) 6492.
11 J.-X. Huang and G. Guiochon, *J. Colloid Interface Sci.*, 128 (1989) 577.
12 J. Zhu, A. Katti and G. Guiochon, *J. Chromatogr.*, 552 (1991) 71.
13 S. Golshan-Shirazi, J.-X. Huang and G. Guiochon, *Anal. Chem.*, 63 (1991) 1147.
14 A. Katti and G. Guiochon, *Am. Lab.*, October (1989) 17.
15 E. C. Jenning and R. G. Brownlee, *Anal. Chem.*, 58 (1986) 2895.
16 A. J. P. Martin, *Discuss. Faraday Soc.*, 7 (1949) 332.
17 J. A. Jonsson and P. Lovkvist, *J. Chromatogr.*, 408 (1987) 1.
18 E. Dose, S. Jacobson and G. Guiochon, *Anal. Chem.*, 63 (1991) 833.
19 D. H. James and C. S. G. Phillips, *J. Chem. Soc.*, (1954) 1066.
20 G. Schay and G. Székely, *Acta Chim. Hung.*, 5 (1954) 167.
21 J. Jacobson, J. Frenz and Cs. Horváth, *J. Chromatogr.*, 316 (1984) 53.

Journal of Chromatography, 556 (1991) 205–218
Elsevier Science Publishers B.V., Amsterdam

CHROM. 23 239

Prediction of single and binary profiles in overloaded elution chromatography using various semi-ideal models

ANITA M. KATTI[a]

Department of Chemical Engineering, University of Tennessee, Knoxville, TN 37996-1600 (USA)

and

MARTIN CZOK[b] and GEORGES GUIOCHON*

Department of Chemistry, University of Tennessee, Knoxville, TN 37996-1600 and Division of Analytical Chemistry, Oak Ridge National Laboratory, Oak Ridge, TN 37831 (USA)

ABSTRACT

Experimental band profiles of 2-phenylethanol and 3-phenylpropanol were recorded for pure components in different amounts and for binary mixtures at different compositions in reversed-phase chromatography. The injection function was also measured. These experimental profiles are compared with those calculated using different finite difference methods (*i.e.*, the Craig and Rouchon *et al.* models). The results show that it is important to take into account the true injection profile. The different calculation procedures in most instances give profiles which are in close agreement with the experimental data. The Craig model gives profiles which are generally sharper than those given by the Rouchon *et al.* model. Differences between the experimental and calculated profiles are ascribed to mathematical properties of the method implemented.

INTRODUCTION

In several previous instances, we have shown that single- and multi-component band profiles can be predicted accurately in isocratic elution chromatography, provided that the adsorption equilibrium isotherm, the column efficiency, the mobile phase flow velocity and the column dead volume are known accurately [1–4]. While it is relatively easy to account for single-component adsorption equilibrium data and the Langmuir isotherm is usually satisfactory, accurate representation of multi-component adsorption data is much more difficult. When severe overloading occurs at low concentration and when the column saturation capacities are equal, such as in chiral systems, the competitive Langmuir isotherm gives excellent results [3]. However, when the column saturation capacities differ the LeVan–Vermeulen isotherm [5] derived using the ideal adsorbed solution theory of Myers and Prausnitz [6] can give good results over a limited concentration range [7]. In the general case, however, and

[a] Present address: Mallinckrodt Speciality Chemicals, St. Louis, MO, USA.
[b] Present address: Université de Paris-Sud, Centre d'Études Pharmaceutiques, F-92296 Chatenay-Malabry, France.

0021-9673/91/$03.50

especially when the mobile phase concentration range studied exceeds 100 mM, it is difficult to achieve good representation of the competitive isotherm, unless empirical equations are used [8].

Band profiles can be calculated by solving the system of partial differential equations which express the conservation of the mass for each component. Usually it is assumed that the solutes in the mobile phase are at or near equilibrium with the solutes in the stationary phase at each point and at any time. Therefore, the compositions in the stationary and mobile phases are given by the equilibrium isotherm. As a closed-form solution of the system of partial differential equations cannot be derived, numerical solutions are calculated. Either finiti difference [9–12] or finite element [13] calculation procedures can be used. The latter are much faster than the former in instances where the problem has several space dimensions (*e.g.*, in aeronautics). This is not the case in chromatography, as we can assume the column to be one-dimensional [9].

The finite difference algorithms have a simple physical representation which makes them easy to understand [12]. The column is divided into a number of cells, in the space domain [9]. Time is also discretized. The values of the concentrations at all the points of this (t,z) grid are calculated successively, starting from the initial values (at time $t = 0$) and the values derived from the boundary condition. The boundary conditions give the values of concentrations imposed at the column inlet during the injection and throughout the course of the experiment. Axial dispersion which accounts for axial diffusion and the finite rate of the mass transfer in the column is introduced in this model as a consequence of the discretization of the time and space dimensions [9,12]. There is a finite number of segments considered in the grid during propagation of the concentration signal and this leads to averaging the concentration across the segments. The consequence of this is numerical or apparent dispersion of the solute band in the column.

The aim of this paper is to compare several semi-ideal models which can be used to predict individual band profiles in overloaded elution chromatography. For binary mixtures, the profiles calculated with the Craig model [14] and the Rouchon *et al.* model [15] are compared with experimental results. The Craig model is a physical model which has been used widely to calculate band profiles in overloaded elution [14,16,17]. An analogous procedure that gives faster computation times has also proven utility in predicting band profiles [2,9].

THEORY

Mass balance equation

The individual band profiles are obtained as the solution of the mass balance equation for each component i in a chromatographic column [9,11]:

$$F \cdot \frac{\partial q_i}{\partial t} + \frac{\partial C_i}{\partial t} + u_0 \cdot \frac{\partial C_i}{\partial z} = D_a \cdot \frac{\partial^2 C_i}{\partial z^2} \tag{1}$$

where q_i and C_i are the stationary and the mobile phase concentrations of each component at equilibrium, z and t are the column length and time, respectively, F is the phase ratio, u_o the linear mobile phase velocity and D_a the apparent diffusion

coefficient. The apparent diffusion coefficient is related to the column height equivalent to a theoretical plate (HETP, H) under linear conditions by

$$D_a = \frac{HL}{2t_0} \tag{2}$$

where L is the column length and t_0 is the dead time.

Eqn. 1 represents the semi-ideal model of chromatography. It assumes the mass transfer kinetics in the column are fast and deviation from equilibrium is small [11]. The equilibrium concentrations of each component i in the two phases are related according to the functional form of the isotherm:

$$q_i = f(C_i) \tag{3}$$

In elution chromatography, the initial conditions are an empty column [$C_i(z,0) = 0$] and the boundary condition usually corresponds to the injection of a rectangular pulse of concentration C_i° and width t_p.

There is no closed-form solution for this problem when the number of components is two or greater. A numerical solution has to be calculated and several approaches are possible [11]. The simplest approach considers the migration of the chromatographic bands along the column as the propagation of a signal through a grid [12]. The numerical solution of the semi-ideal model consist of solving eqn. 1 with $D_a = 0$. When $D_a = 0$, the solution to eqn. 1 is called the ideal model. Two procedures are worthy of special consideration [12]. They are the Rouchon *et al.* [15] and the Craig model. In the Rouchon *et al.* model, the propagation requires that part of the cell content is frozen in time, which has no physical meaning. However, this procedure leads to fast computations. The partial differential equation in eqn. 1 is replaced by the following finite difference equantion:

$$u_0 \cdot \frac{C_{z,t} - C_{z-1,t}}{\Delta z} + \frac{C_{z-1,t} - C_{z-1,t-1}}{\Delta t} + F \cdot \frac{q_{z-1,t} - q_{z-1,t-1}}{\Delta t} = 0 \tag{4}$$

In the Craig model, where the propagation scheme resembles closely the separation process and implements the Craig machine, eqn. 1 is replaced by another finite difference equation:

$$u_0 \cdot \frac{C_{z,t-1} - C_{z-1,t-1}}{\Delta z} + \frac{C_{z,t} - C_{z,t-1}}{\Delta t} + F \cdot \frac{q_{z,t} - q_{z,t-1}}{\Delta t} = 0 \tag{5}$$

Numerical errors are made and they accumulate during the integration of the mass balance equation, because the increments Δz and Δt are finite. It can be shown that the overall contribution of these errors to the solution obtained is as a first approximation equal to the addition of a diffusion term of the mass balance equation. The coefficient D_a of this numerical diffusion term is related to the characteristics of the calculation by the equation for the Rouchon *et al.* [15] method:

$$D_a = \frac{\Delta z u_0}{2}(a - 1) \tag{6}$$

and for the Craig method:

$$D_a = \frac{\Delta z u_0}{2}(1 - a) \tag{7}$$

where a is the Courant number:

$$a = \frac{u_0 \Delta t}{(1 + k')\Delta z} \tag{8}$$

The theory of partial differential equations shows that in order to obtain a stable numerical solution, the Courant number must be larger than 1 in the Rouchon *et al.* [15] model and smaller than 1 in the Craig model. With $a = 1$ for the single-component system, the solution to the ideal model is obtained. By comparing eqns. 2 and 6–7 a relationship between the values of the HETP, the space and the time increment can be derived. For the Rouchon *et al.* [15] model this relationship is

$$H = -\Delta z + \frac{u_0}{1 + k'}\Delta t \tag{9}$$

and for the Craig model

$$H = \frac{k' \Delta z}{1 + k'} \tag{10}$$

In the Craig model, the linear velocity is related directly to the space and time increment:

$$u_0 = \frac{\Delta z}{\Delta t} \tag{11}$$

Proper selection of the space and time increments permits adjustment of the apparent column HETP to the value required to model exactly the experimental system.This results is rigorous for single-component bands in linear chromatography. For binary mixtures in non-linear chromatography, the consequence of eqns. 8 and 9 is that the HETP can be adjusted exactly to the amount of band spreading for one component. However, the efficiency (the apparent dispersion) of the two bands cannot be controlled independently. Moreover, eqns 8 and 9 do not give a realistic relationship between the column HETP and the retention factor. This effect is negligible for the prediction of single-component bands and small for many two-component problems, especially when the relative retention is small.

Another calculation method, the control diffusion procedure, has been presented [12]. In this method, small values of the space and time increments are selected, such that the extent of the numerical diffusion does not exceed the required amount of apparent diffusion for any of the component. Then, a diffusion term is added to the

finite difference equations (eqns. 4 and 5) representing the amount of diffusion missing for each component. This is calculated according to Fick's second law:

$$\frac{\partial C}{\partial t} = D_p \cdot \frac{\partial^2 C}{\partial z^2} \tag{12}$$

The apparent diffusion coefficient D_p is chosen so that $D_p = D_a - D_n$, where D_a is the required value of the apparent dispersion coefficient (eqn. 2) and D_n is the numerical diffusion resulting from the choice of the space and time increments and the local k' [12].

Isotherm model

The single-component isotherm data were fitted to the Langmuir equation:

$$q = \frac{aC}{1 + bC} \tag{13}$$

The values of the parameters are summarized in Table I.

The isotherm for the binary mixture was measured using the method of the hodograph transform [4] as applied to the competitive Langmuir isotherm model:

$$q_i = \frac{a_i C_i}{1 + \sum b_i C_i} \tag{14}$$

For practical purposes it is convenient to define the column saturation capacity

$$CSC = \frac{\sum_{i=1}^{n} \frac{a_i}{b_i} \cdot V_{sp}}{n} \tag{15}$$

as the maximum amount adsorbed as a monolayer on the surface of the stationary phase. Then the amount of sample injected can be made independent of the size of the column by using the loading factor:

$$L_{f,i} = \frac{m_i}{CSC} \tag{16}$$

where m_i is the amount of sample component i injected.

TABLE I

SUMMARY OF SINGLE-COMPONENT ISOTHERM DATA FOR 2-PHENYLETHANOL AND 3-PHENYLPROPANOL

Parameter	Column 1		Column 2	
	Phenylethanol	Phenylpropanol	Phenylethanol	Phenylpropanol
HETP (cm)	0.0167		0.009	
t_o (s)	180		176	
k'	0.72	1.31	0.71	1.42
a (ml/ml)	1.92	3.55	1.94	3.41
b (ml/mg)	0.0148	0.0255	0.0218	0.0592
CSC[a]	140	150	109	70

[a] Defined by eqn. 15.

EXPERIMENTAL

The isotherm data and the individual band profiles for large-sized samples were determined using a modular chromatograph expecially assembled for this purpose.

Apparatus

The modular liquid chromatograph was assembled from two Waters Assoc. (Milford, MA, USA) Model 510 pumps, a Valco (Houston, TX, USA) six-port electrically actuated valve fitted with a 100-μl sample loop and a Kratos Spectroflow (ABI, Ramsey, NJ, USA) variable-wavelength UV detector set at 272 nm for the measurement of the band profiles. The pumps were controlled and the detector signal was monitored via a Waters System Interface Module (SIM), using the Waters Maxima 860 Dynamic Solutions (Ventura, CA, USA) software installed on an NEC APCIV Powermate 2 microcomputer. The electrical outputs of the valve and the detector were connected to the SIM box for automatic data acquisition.

Products

Two 25 × 0.46 cm I.D. columns were packed in-house, at 9000 p.s.i., using 10-μm Vydac (Hesperia, CA, USA) octadecylsilica as stationary phase. The characteristics of these two columns are summarized in Table I. The flow-rate in all the experiments was 1.0 ml/min.

The solutes were 2-phenylethanol and 3-phenylpropanol purchased from Fluka (Ronkonkoma, NY, USA) and 2,6-dimethylphenol, purchased from Aldrich (Milwaukee, WI). The mobile phase was a mixture of methanol and water, purchased from Burdick and Jackson (Muskegon, MI, USA). All chemicals were used as received.

Procedures

The single-component elution profiles were derived from the detector trace and from a calibration graph determined by pumping directly into the detector a known concentration of sample. The detector response was strongly non-linear in the region of interest [18].

For binary mixtures, the individual component profiles were obtained by collecting fractions every 3 s with subsequent reanalysis using a Model 232/401 Automatic Sample Processor from Gilson (Middletown, WI, USA) [19]. With a linear calibration graph quantitative analysis of each sample was done using the Maxima software.

The injection profile was determined by placing the sample valve between the column and the detector, which permits a mobile phase stream with a stable flow. The concentrated samples of 2-phenylethanol were injected and their profiles recorded. Fig. 1 shows a typical results, with the corresponding ideal, rectangular profile overlaid. It can be seen that the measured profile gives a sharp front and diffuse rear boundary owing to dispersion in the tubes. Moreover, the maximum concentration injected is lower than that of the prepared sample solution. The measured injection profile was fitted to one half of the Gaussian function and this function form was used in the inlet boundary condition of the finite difference algorithms.

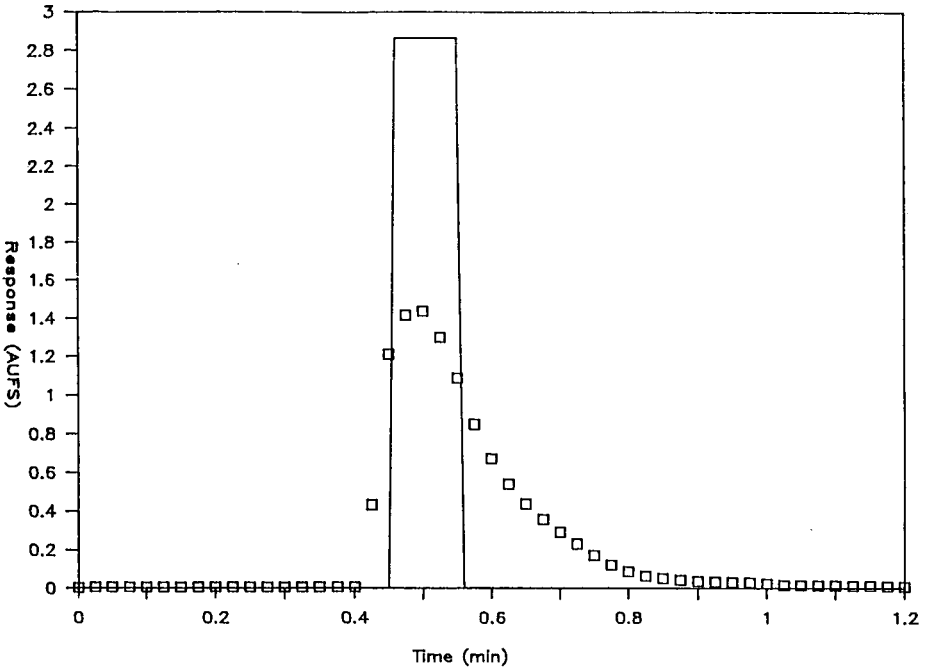

Fig. 1. Injection profile for a large-volume sample. Symbols, experimental profile; solid line, rectangular profile.

RESULTS AND DISCUSSION

Adsorption equilibrium isotherms were determined on the two columns using the classical techniques of frontal analysis for single components [1, 20, 21] and by the method of the Hodograph transform for binary mixtures [22]. The single-component parameters are given in Table I and the isotherms of phenylethanol and phenylpropanol are shown in Fig. 2. The differences between the isotherms measured on the two columns are almost negligible at low concentrations but significant at high concentrations. The values of the slope of the isotherm at the concentration origin (*i.e.*, the coefficient *a*) differ by less than 1% for 2-phenylethanol and by 4% for 3-phenylpropanol. Therefore, the isotherms corresponding to each component on both columns are tangential. In contrast, the isotherm curvature (*i.e.*, the coefficients *b*) differs by more than 50% between the two columns. This result suggests that columns for preparative liquid chromatography may be even more difficult to reproduce than analytical columns.

The values of the average hodograph parameters [4] employed in the prediction of the binary mixtures using the Craig, Rouchon *et al.* [15] and control diffusion models are $a_1 = 1.924$ ml/ml, $a_2 = 3.554$ ml/ml, $b_1 = 3.044$ ml/mmol and, $b_2 = 3.69$ ml/mmol.

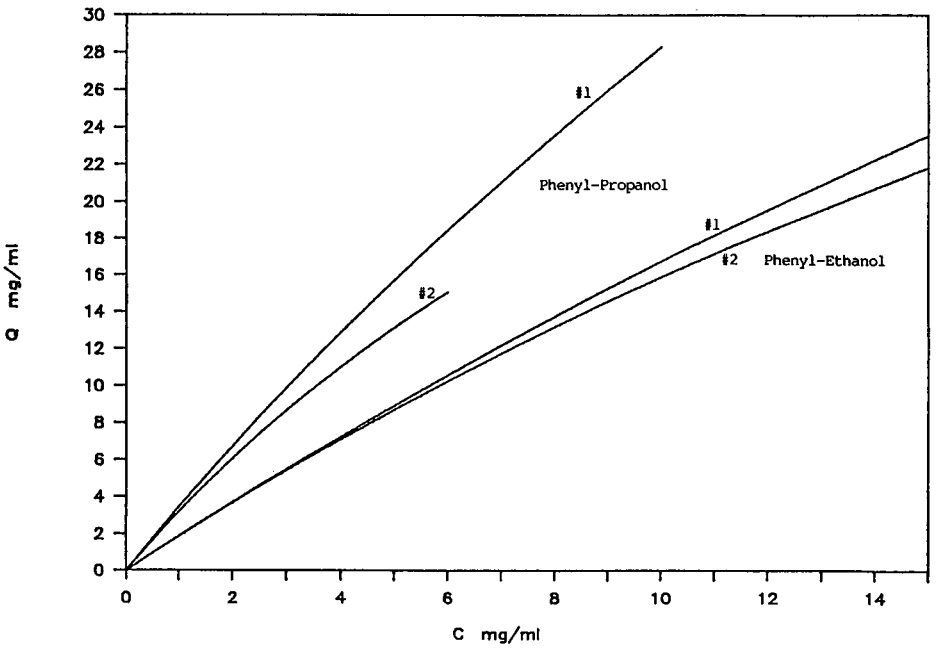

Fig. 2. Reproducibility of experimental isotherm data for phenylethanol and 3-phenylpropanol on two columns packed with C_{18}-bonded silica.

Single-component profiles

Single-component elution band profiles at increasing sample size were measured on both columns for 2-phenylethanol, 3-phenylpropanol and 2,6-dimethylphenol. Some of the profiles recorded on column 2 are shown in Figs. 3 (2-phenylethanol), 4 (3-phenylpropanol) and 5 (2,6-dimethylphenol). The single-component profiles for column 1 have been reported previously [2,23] and in all instances the agreement between the calculated and experimental profiles is good. The hump on the back of the 3-phenylpropanol peaks (Fig. 4) is due to a calibration problem. The detector response is very non-linear in the concentration range sampled and the polynomial used to fit the response is not a monotonic function in its first derivative. The serious tail at the end of the 2,6-dimethylphenol band is probably due to the interaction between the acidic hydroxyl group of the phenol molecule and some unreacted silanol groups at the surface of the silica. The adsorption data and the band profiles might be better accounted for by a biLangmuir isotherm, as has been reported previously [3,24,25].

Two-component band profiles

The individual band profiles of 2-phenylethanol and 3-phenylpropanol were determined experimentally for three different binary mixtures having relative compositions 1:1, 1:3 and 3:1. The volume of sample injected and the amounts of each component are reported in Table II. The total sample size is *ca.* 28% of the average of the column saturation capacities for the two compounds. This corresponds to a high degree of column overload.

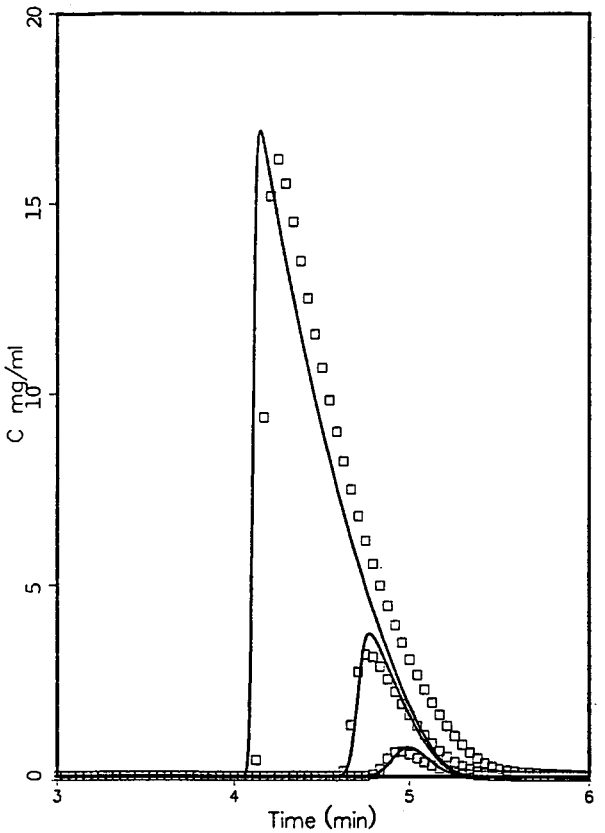

Fig. 3. Overloaded elution band profiles of samples of 2-phenylethanol on C_{18}-bonded silica. Symbols, experimental; solid lines, theoretical. 0.2 mg = 0.2% of CSC; 1.2 mg = 1% of CSC; 8.6 mg = 7.9% of CSC.

In the following sections, a comparison is made between various theoretical models and experimental data for binary mixtures on column 1.

Effect of the injection function using the semi-ideal model. Fig. 6 compares the theoretical profiles calculated assuming a rectangular profile (dashed lines) and the measured injection profile (solid lines) according to the Rouchon *et al.* [15] implementation of the semi-ideal model for 1:1, 1:3 and 3:1 mixtures. In many respects, the differences in the theoretical profiles predicted under these conditions are relatively minor, but they are not completely insignificant. In general, the profiles obtained with the experimentally correct injection profile give rise to shorter, broader peaks. The diffuse injection profile gives rise to slightly more diffuse exit profiles. Therefore, there is more interference and better agreement with the experimental data.

This comparison illustrates the influence that the injection profile may have on the resolution between bands in preparative chromatography. It is notable, but not extremely important, especially in view of displacement effects. Reducing the tailing will permit gains in the recovery yield and the production rate.

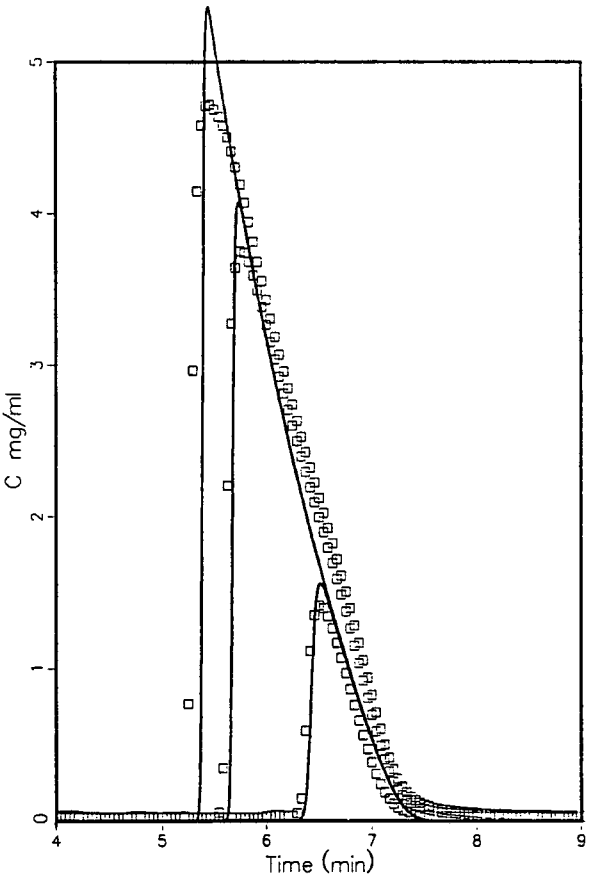

Fig. 4. Overloaded elution band profiles of samples of 3-phenylpropanol on C_{18}-bonded silica. Symbols, experimental; solid lines, theoretical. 0.9 mg = 1.3% of CSC; 3.7 mg = 5.3% of CSC; 5.5 mg = 7.8% of CSC.

Comparison of experimental data with the Craig and Rouchon et al. [15] models. The Craig (dashed line) and Rouchon *et al.* (solid lines) algorithms were used to calculate the band profiles. A comparison with experimental data is shown in Fig. 7. The measured injection profile was employed as the inlet boundary condition for this series of comparisons. Therefore, the solid line in Fig. 6 is the same as that line in Fig. 7.

In general, the Craig model gives sharper taller peaks than the Rouchon *et al.* model. This is a result of the differences in the calculation procedure for these two models. In both models, the HETP or the amount of band spreading is specified for one component for a known value of k'. As discussed under Theory, this approach leads to an artificial relationship between the amount of band spreading and k'. For the Rouchon *et al.* model, when k' is near zero there is more band spreading than at the specified reference k' value. For the Craig model, in the limit as k' goes to zero, the amount of band broadening goes to zero. Hence the amount of band spreading is less

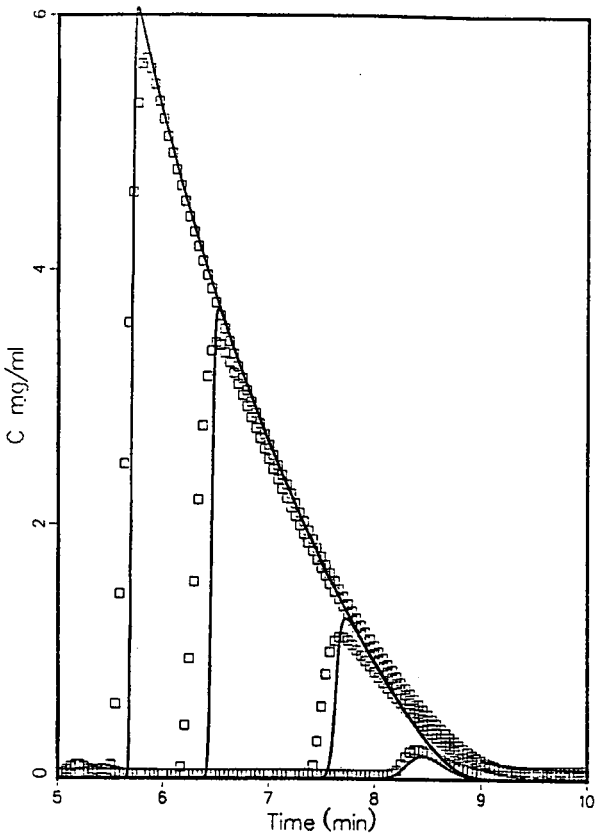

Fig. 5. Overloaded elution band profiles of samples of 2,6-dimethylphenol on C_{18}-bonded silica. Symbols, experimental, solid lines, theoretical. 0.08 mg = 0.1% of CSC; 0.8 mg = 1% of CSC; 3.9 mg = 4.9% of CSC; 7.8 mg = 9.7% of CSC.

than at the reference k' value. Because in these experiments the injection was made at high concentration, the velocity of the molecules associated with a given concentration is large so the local k' is near zero over a certain length of the column. Hence this leads to the Craig model giving sharper taller peaks than the Rouchon *et al.* model.

TABLE II

SUMMARY OF THE SAMPLE SIZES FOR THE BINARY DATA

Mixture	Total amount (mg)	2-Phenylethanol (mg)	3-Phenylpropanol (mg)	L_f [a] (%)	
				2-Phenylethanol	3-Phenylpropanol
1:1	20	10	10	7	7
1:3	28	7	21	5	15
3:1	40	30	10	21	7

[a] Defined by eqn. 16.

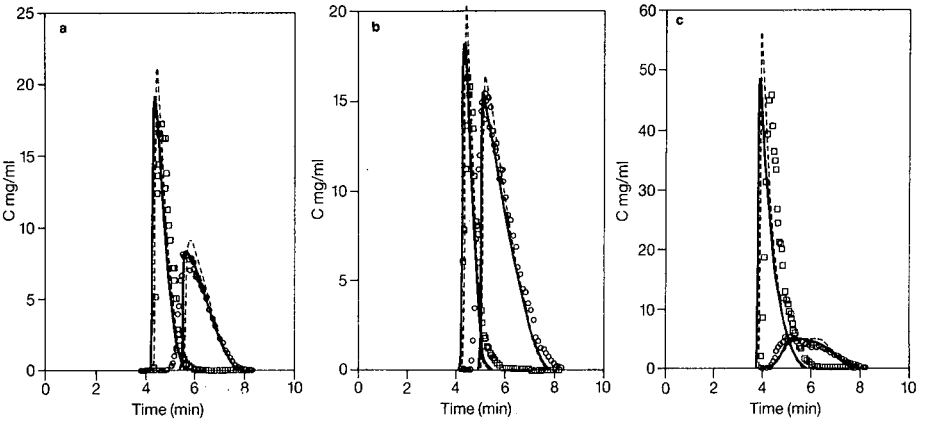

Fig. 6. Comparison of experimental data and predicted profiles using the Rouchon *et al.* [15] model with a rectangular injection function and the measured injection profile. Solid line, Rouchon *et al.* [15] with measured injection profile; dashed line, rectangular injection function. (□) 2-phenylethanol; (○) 3-phenylpropanol experimental data. (a) 1:1 mixture; (b) 1:3 mixture; (c) 3:1 mixture.

Comparison of the Craig and control diffusion model. In contrast with the Craig model, the control diffusion model allows independent specification of the diffusion coefficients of each solute [12]. Hence a more accurate prediction is obtained. Fig. 8 compares the predictions obtained by the Craig model and the controlled diffusion model for 1:1 and 3:1 mixtures. The profile for the early eluting component is the same for both models, but for the second component there are slight deviations. In Fig. 8a (1:1 mixture), the retention time of the front is slightly less and the concentration at the peak maximum slightly lower. In Fig. 8b (3:1 mixture), the front of the second component is only slightly more diffuse. For the 1:3 mixture, the control diffusion model and the Craig model give identical results.

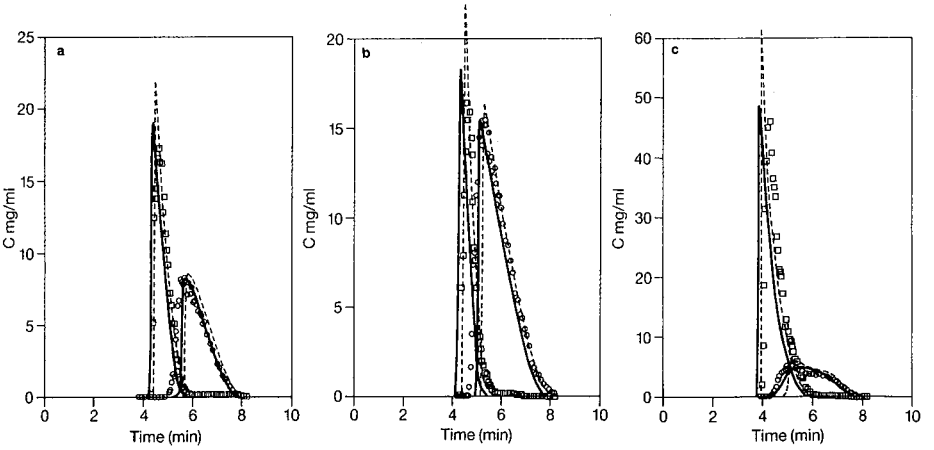

Fig. 7. Comparison of experimental data and predicted profiles using the (dashed lines) Craig and (solid lines) Rouchon *et al.* [15] semi-ideal models. (□) 2-Phenylethanol; (○) 3-phenylpropanol experimental data. (a) 1:1 mixture; (b) 1:3 mixture; (c) 3:1 mixture.

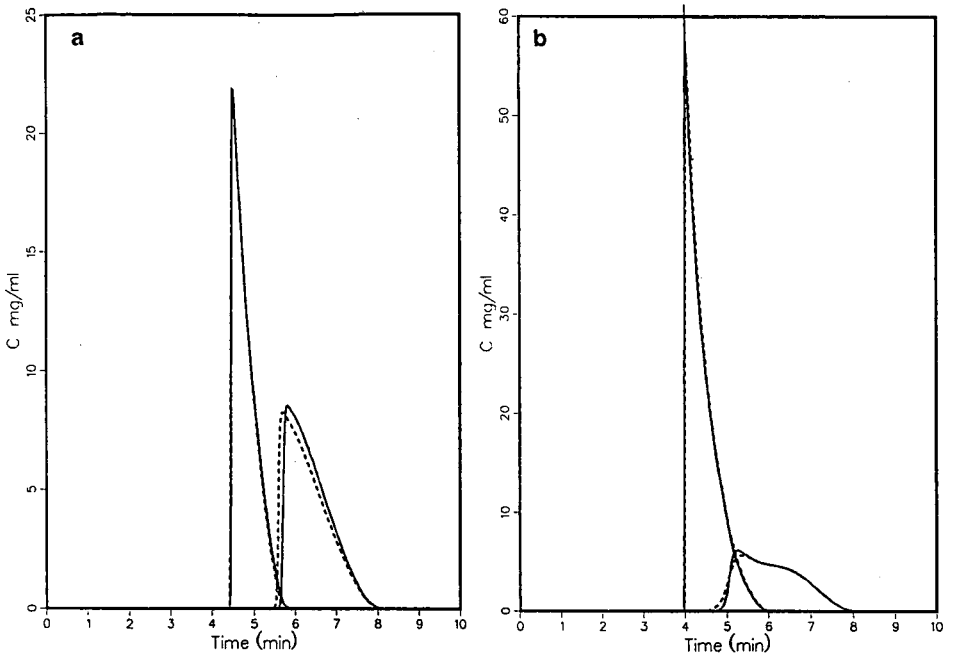

Fig. 8. Comparison of the (solid lines) Craig and (dashed lines) control diffusion models. (a) 1:1 Mixture; (b) 3:1 mixture.

CONCLUSIONS

Differences are observed between individual band profiles calculated using the Rouchon *et al.* [15], Craig and control diffusion procedures. These models correspond to slightly different ways of writing the finite difference equations. None of these calculation procedures gives profiles which are consistently in excellent agreement with all the experimental data, but all the models give good agreement with the experimental data. The present problem seems to be in finding an accurate model to predict competitive equilibrium isotherms from single-component data. Until more refined methods of determining competitive isotherms are developed and better models to fit the data are proposed, the differences between these theoretical profiles are not significant.

ACKNOWLEDGEMENTS

This work was supported in part by grant CHE-8901382 from the National Science Foundation and by the cooperative agreement between the University of Tennessee and the Oak Ridge National Laboratory. We acknowledge support of our computational effort by the University of Tennessee Computing Center.

REFERENCES

1 S. Golshan-Shirazi, S. Ghodbane and G. Guiochon, *Anal. Chem.*, 60 (1988) 2630.
2 A. M. Katti and G. Guiochon, *J. Chromatogr.*, 499 (1990) 21.
3 S. Jacobson, S. Golshan-Shirazi and G. Guiochon, *J. Am. Chem. Soc.*, 112 (1990) 6492.
4 A. M. Katti, Z. Ma and G. Guiochon, *AIChE J.*, 36 (1990) 1722.
5 M. D. LeVan and T. Vermeulen, *J. Phys. Chem.*, 85 (1981) 3247.
6 A. L. Myers and J. M. Prausnitz, *AIChE J.*, 11 (1965) 121.
7 S. Golshan-Shirazi, J.-X. Huang and G. Guiochon, *Anal. Chem.*, 63 (1991) 1147.
8 J. Zhu, A. M. Katti and G. Guiochon, *J. Chromatogr.*, 552 (1991) 71.
9 G. Guiochon, S. Golshan-Shirazi and A. Jaulmes, *Anal. Chem.*, 60 (1988) 1856.
10 B. C. Lin, Z. Ma and G. Guiochon, *J. Chromatogr.*, 484 (1989) 83.
11 B. C. Lin, S. Golshan-Shirazi, Z. Ma and G. Guiochon, *J. Chromatogr.*, 500 (1990) 185.
12 M. Czok and G. Guiochon, *Anal. Chem.*, 62 (1990) 189.
13 Z. Ma and G. Guiochon, *Comput. Chem. Eng.*, July 1991.
14 L. C. Craig, *J. Biol. Chem.*, 155 (1944) 519.
15 P. Rouchon, M. Schonauer, P. Valentin and G. Guiochon, *Sep. Sci. Technol.*, 22 (1987) 1793.
16 H. Poppe and J. C. Kraak, *J. Chromatogr.*, 255 (1983) 395.
17 J. E. Eble, R. L. Grob, P. E. Antle, G. B. Cox and L. R. Snyder, *J. Chromatogr.*, 405 (1987) 31.
18 A. M. Katti and G. Guiochon, *Am. Lab.*, 21, No. (1989) 17.
19 E. V. Dose and G. Guiochon, *Anal. Chem.*, 61 (1989) 2571.
20 D. H. James and C. S. G. Phillips, *J. Chem. Soc.*, (1954) 1066.
21 G. Schay and G. Szekely, *Acta Chim. Hung.*, 5 (1954) 167.
22 Z. Ma, A. M. Katti and G. Guiochon, *J. Phys. Chem.*, 94 (1990) 6911.
23 A. M. Katti, *Ph.D. Thesis*, University of Tennessee, Knoxville, TN, 1990.
24 S. Golshan-Shirazi and G. Guiochon, *J. Phys. Chem.*, 94 (1990) 495.
25 S. Jacobson, S. Golshan-Shirazi and G. Guiochon, *AIChE J.*, 37 (1991) 836.

Journal of Chromatography, 556 (1991) 219–234
Elsevier Science Publishers B.V., Amsterdam

CHROM. 23 157

Description of retention mechanism by solvophobic theory

Influence of organic modifiers on the retention behaviour of homologous series in reversed-phase liquid chromatography

S. HERON and A. TCHAPLA*
LETIAM, IUT d'Orsay Plateau du Moulon, B.P. 127, 91403 Orsay Cedex (France)

ABSTRACT

The retention behaviour of different homologous series ($2 \leqslant n_C \leqslant 22$) was studied on three different bonded chain lengths (C_1, C_{14} and C_{18}) and in aqueous–organic solvent mixtures commonly used in reversed-phase liquid chromatography [methanol, acetonitrile and tetrahydrofuran (THF)]. For all solutes (ligands) without π electrons, and regardless of bonded chain length, the plots $\log k'$ *vs.* φ (organic modifier ratio) in methanol–water or acetonitrile–water are correlated with the evolution of surface tension of these mixtures. On the other hand, for ligand which possess π electrons, there is a modification in these curves which is due to specific π–π interactions added to the pure solvophobic effect. In this respect, pure methanol was found to be a better eluent than pure acetonitrile excepted for the ligands with π electrons, for which the opposite was observed. For the THF–water mixtures, the plots of $\log k'$ *vs.* φ were always below those for methanol–water or acetonitrile–water. Moreover, the plots of $\log k'$ *vs.* n_C did not increase linearly. In this pure solvent, retention is due to an exclusion mechanism. These results were in agreement with conformational infrared studies of alkyl chains in THF, methanol and acetonitrile. The overall results could rationalize the fact that retention prediction based on methylene selectivity was often erroneous when THF was used. Nevertheless, they show the possibility of optimizing separations of homologous series from the results obtained from a single gradient experiment with any commonly used organic modifier.

INTRODUCTION

Separation of the constituents of homologous series by reversed-phase liquid chromatography (RPLC) is not the central theme of most chromatographic research. Nevertheless, the study of these ligands is of value from a general point of view, because it leads to a better understanding of the parameters determining the chromatographic process.

The rationalization of experimental results is based on the solvophobic theory [1], which explains all phenomena from the standpoint of energies and has been adapted to chromatography by Melander and Horváth [2]. Its mathematical expression is

0021-9673/91/$03.50

$$\text{Ln } k' = \ln\left(\frac{V}{V_m}\right) + \frac{1}{RT}\left[W_s + \Delta A\,(a_s + \gamma) + NA_s\,\gamma\,(\chi_e - 1) - \frac{\Delta Z}{\varepsilon}\right] + \ln\left(\frac{RT}{P_0 V_s}\right) \quad (1)$$

This leads to the prediction of the behaviour of ligands as a function of their hydrophobic volume [3] and their polarity, and to that of the nature of the modifier on their retention. It involves two simultaneous phenomena:

(1) Retention of homologues increases with increasing carbon number, n_C, since the size of the cavity ΔA increases with increasing carbon number [3]. Numerous experiments have been reported on this effect [4–10] and allowed the evaluation of the elution strength of solvents based on the reasoning of Snyder [11], in both partial aqueous reversed-phase liquid chromatography (PARP) [12–15] and non-aqueous reversed-phase liquid chromatography (NARP) [9,12].

(2) The retention of the same solute in different aqueous–organic solvent mixtures must be correlated with their surface tension. This has been shown for three alkanes for which it was possible to correlate log k' *vs.* φ (volume ratio of organic modifier) with the curves of the variation of the surface tension of mixtures [16] (methanol–water and acetonitrile–water). The generality of the phenomenon independent of the nature of the ligand, has not been established however.

Moreover, the particular role of the aromatic ring as a polar head has been reported previously, suggesting a particular behaviour for systems with π electrons [8,17–19].

The aim of this work was to define further the role of the type of polar head of the ligand on retention and on methylene selectivity as a function of the nature of the modifier: methanol, acetonitrile or tetrahydrofuran (THF). This was accomplished by a systematic study of the retention of different homologous series as a function of the percentage of water in the mobile phase. We also attempted to correlate variations in the surface tension curves of aqueous–organic solvent mixtures.

This study was carried out on long-chain (C_{18}, C_{14}) and short-chain (C_1) monofunctional phases (identical with the previously mentioned monomeric phase [8]) in order to detect the possible role of residual silanols in the retention mechanism. The effects of the chemical nature of the bonded phase, *e.g.*, propylphenyl, will be reported subsequently.

EXPERIMENTAL

Reagents

Methanol, acetonitrile and tetrahydrofuran were of high-performance liquid chromatographic (HPLC) grade (Carlo Erba, Milan, Italy and Merck, Darmstadt, Germany). All solvents were filtered through a 0.5-μm Millipore filter. Water was of ultra-high quality (18 MΩ cm) from an Elgastat UHQ system (Elga, Bucks, UK).

Solutions were made up precisely by volume and degassed by sonication.

Homologous series ($C_nH_{2n+1}Z$, where Z = H, Ph, Cl, COOMe, OCOPh, OH) were obtained from various sources [7,8]. Studies on C_{18} and C_{14} bonded chains were

carried out with $C_nH_{2n+1}Z$ with Z = H, OH, COOMe, Cl and Ph and studies on C_1 with Z = H, OH, COOMe and OCOPh; $1 \leqslant n \leqslant 22$.

Equipment

The LC system consisted of a Model 110B pump (Beckman, San Ramon, CA, USA), a Model 7125 injection valve with a 20-μl loop (Rheodyne, Cotati, CA, USA), a Model R401 refractive index detector (Waters Assoc., Milford, MA, USA), a UV detector (254 nm) (Beckman) and a Model DDL 21 light-scattering detector (Cunow, Cergy St. Christophe, France).

For all experiments, the precolumn, the loop and the column temperature was controlled using a Croco-cil oven (Cluzeau, Sainte-Foy-la-Grande, France) thermostated with water by means of a Model HS 40 cryostat (Huber, Offenburg-Elgersweier, Germany) with a precision of 0.1°C.

Five columns were used: Spherisorb ODS-1 (5 μm), 125 × 4.6 mm I.D. (SFCC, Neuilly-Plaisance, France); LiChrosorb RP-2 (10 μm), 250 × 4.6 mm I.D. (Merck); RP-14 (10 μm) 300 × 4.6 mm I.D., previously used [7,8]; LiChrosorb RP-18 (5 μm), 150 × 4.6 mm I.D. (Merck), laboratory packed; and Hypersil ODS (5 μm), 150 × 4.6 mm I.D. (Shandon, Runcorn, UK), laboratory packed.

The eluent flow-rate was 1 ml/min.

Methods

All retention values are reported in terms of capacity factor, k'. The calculation of this parameter requires the determination of the void volume of the column used. The weighing method has been used for this purpose [8]. Each k' value reported is the mean from at least three reproducible injections. The accuracy of the measurements and the mathematical treatment of the results were as described in previous papers [7–9].

IR

Fourier transform IR spectra were obtained with a Perkin-Elmer 1730 FTIR spectrometer equipped with a DGTS detector and operated to give 2 cm^{-1} resolution. Conventional sodium chloride windows (38.7 μm) or plates were used for pure samples. A calcium fluoride window (52 μm) was used for mixed ^2H_2O–organic modifier solutions. A total of 100 scans were collected for the neat reagents or ligands in solution, but bonded-phase samples required at least 500 scans.

The organic solvents (S.S.T., Champs sur Marne, France) were completely deuterated (^2H_2O, $C^2H_3O^2H$, C^2H_3CN, THF-$^2H_8$, C^2HCl_3) so the overlapping solvent peaks can be shifted to lower energies where they no longer interfere.

All spectra were recorded in transmission units between 1500 and 1300 cm^{-1}. Each time the solvent spectrum was subtracted from those of the ligands in solution. In order to compare different spectra, the data are normalized to the intensity of the methyl scissoring band at 1378 cm^{-1}. No modification of the wavenumber of the four absorption bands of interest appears when the organic solvent changes. The even-carbon alkanes were studied with $8 \leqslant n_C \leqslant 16$. Concentrations were calculated to be near the concentration corresponding to the phase ratio in the chromatographic column.

RESULTS AND DISCUSSION

Role of the modifier on the retention of the same solute: effect of surface tension

Behaviour of solutes of different polarity. In order to determine the possible influence of the physical nature of the ligate, we have drawn the plots of log k' *vs.* percentage of organic modifier (φ) compiled from data in ref. 12. This was done for each compound in five homologous series with both a monofunctional octadecyl linkage (Hypersil C_{18}) (Fig. 1) and a difunctional one (LiChrosorb RP-18) (Fig. 2). For purposes of clarity, only one compound per series is presented, but the same variations were observed, regardless of ligand chain length.

For all the series tested, (except phenylalkanes) and independently of the mono- or difunctional nature of the bonded phases, it was noted that the curves of variation of log k' obtained with methanol as organic modifier crossed those obtained with acetonitrile at about a 90% organic modifier content. This value was independent of the injected ligand length. For the phenylalkanes, we observed that the intersection of these curves was around a value of 95% of organic modifier instead of 90%. This difference may seem negligible, but this tendency to shift the crossover point of the two curves towards 100% organic modifier is supported by results published by Thevenon [16] and Thevenon-Emeric *et al.* [20] and the examination of those obtained by Chartier [17] showing that acetonitrile was a better eluent than pure methanol for components with π electrons.

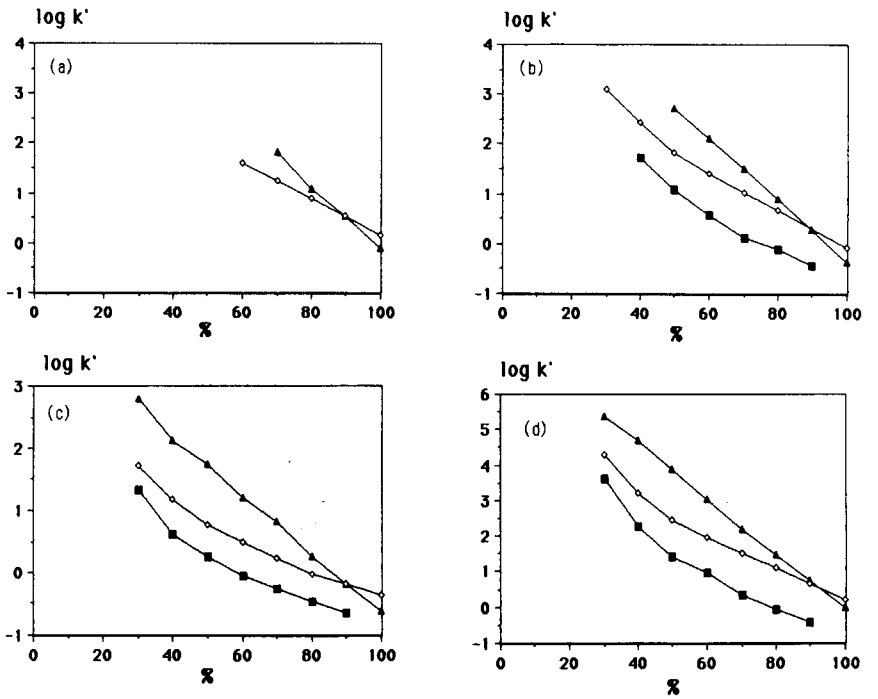

Fig. 1. Log k' *vs.* volume fraction of organic solvent in water on the Hypersil C18 column. ▲ = Methanol–water mixtures; ◇ = acetonitrile–water mixtures; ■ = THF–water mixtures. (a) *n*-Alkane with $n = 9$; (b) chloro-*n*-alkane with $n = 9$; (c) *n*-alkanol with $n = 9$; (d) phenyl-*n*-alkane with $n = 9$.

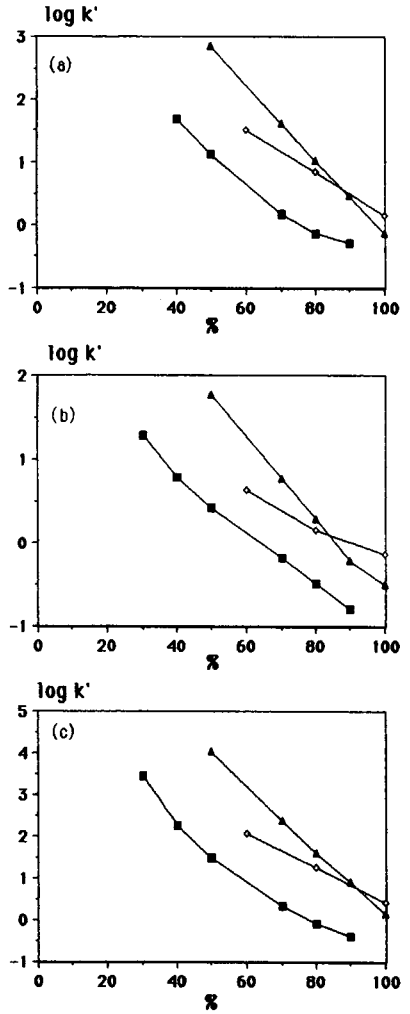

Fig. 2. Log k'*vs.* volume fraction of organic solvent in water on the RP-18 column. ▲ = methanol–water mixtures; ◇ = acetonitrile–water mixtures; ■ = THF–water mixtures. (a) Chloro-*n*-alkane with $n = 9$; (b) *n*-alkanol with $n = 9$; (c) phenyl-*n*-alkane with $n = 9$.

Similarly, the curves obtained with THF were systematically lower than those obtained with methanol and acetonitrile. The study of published data [21] for variously substituted aromatic compounds led to the same type of behaviour. This shows the general nature of the phenomenon, independently of the chemical nature of the ligand (aromatic or hydrocarbon chain substituted differently). Even though results with pure THF could not be obtained as a result of its particular behaviour [12], the variation of log k'*vs.* % THF was linear in the range studied. Extrapolating k' values for pure THF always furnished values much lower than those obtained with the other organic modifiers investigated.

Effect of bonded chain length. The same study was performed by using a methyl

phase. An example of the results is reported in Fig. 3. The general behaviour is similar to that observed with C_{18} phases.

Long-chain alkanols have an increased k'_{CH_3CN}/k'_{CH_3OH} selectivity in comparison with the other series tested. This is shown by a k' value in pure acetonitrile which is not aligned with those obtained with partially aqueous mixtures. This reflects the additional influence of residual silanols on retention and demonstrates a specific silanol–ligand interaction for this type of ligand via hydrogen bonds when this solvent is used. The covering of silica by methyl links permits easy access of residual silanols.

Relationship between retention characterized by k' and the surface tension of the mobile phase. Eqn. 1 according to Melander and Horváth [2] can be used to relate the change in the log k' value of a given ligand on a given column to the variation in surface tension, γ, of the mobile phase. We therefore plotted on the same curve the relative variation of this parameter for aqueous mixtures of three organic modifiers often used in PARP (Fig. 4).

If we consider only surface tension, it can be predicted that for organic modifier contents lower than 70%, the retention of the same ligand in aqueous–organic mixtures of the same volume composition would be in the order THF < CH_3CN < CH_3OH. For higher percentages, the order would be CH_3OH < THF ≈ CH_3CN.

The curves recorded for methanol–water and acetonitrile–water mixtures follow the above predictions relatively closely (Figs. 1 and 2). The difference between the

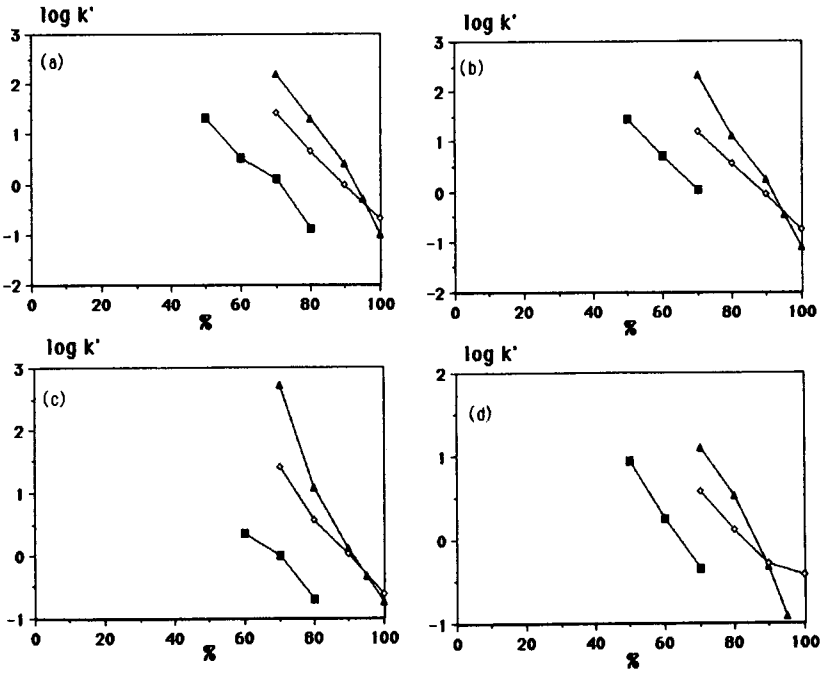

Fig. 3. Log k'*vs.* volume fraction of organic solvent in water on the RP-2 column. ▲ = methanol–water mixtures; ◇ = acetonitrile–water mixtures; ■ = THF–water mixtures. (a) Phenyl-*n*-alkane with n = 18. (b) *n*-alkyl benzoate with n = 18; (c) *n*-alkane with n = 18; (d) *n*-alkanol with n = 18.

experimental value and the theoretical value of 70%, predictable from Fig. 4, can be explained by χ_e, a factor which adjusts the macroscopic surface tension to molecular dimensions, especially since the 90% crossover is constant, regardless of the chain length and polarity of the ligand.

In the case of ligands with π electrons, there is a shift of the crossover point. This is the consequence of a smaller retention in acetonitrile than in methanol with regard to the pure effect from pure solvophobic theory. This can be interpreted as the result of the development of specific interactions between a ligand and the solvent, leading to better solvation of the complex and its faster elution.

With THF, the log k' *vs.* % organic modifier curves do not cross those obtained with methanol, and apparently call into question an interpretation based solely on surface tension. This led us to compare the homologous series in THF using both chromatography and infrared spectrometry in order to elucidate the particular role of this modifier.

Role of THF in the retention of homologous series

As reported in the Introduction, the retention of homologues must increase with increasing size of the cavity ΔA. A linear increase is not verified thermodynamically but is justified by the results of numerous experiments in methanol. We therefore tested whether same phenomenon can be observed with THF.

The results are reported Fig. 5. Regardless of the series, the variation of log k' *vs.* n_C is not represented by broken lines, but by curves. This was confirmed by plotting α *vs.* n_C curves (Fig. 6), which are much more sensitive to slight changes in selectivity, and which exhibit a regular decrease. The mean value of α was identical for all the series tested for the same limiting values of n_C, confirming the convex shape of the first type of plot (log k' *vs.* n_C). The effect observed is due to the solvent and not to the nature of the link. Indeed, with the same column the plots of α *vs.* n_C with methanol–water mixtures (or pure methanol) furnished a curve with a jump n_{crit} equal to 14, as already reported with other monofunctional C_{18}-bonded phases.

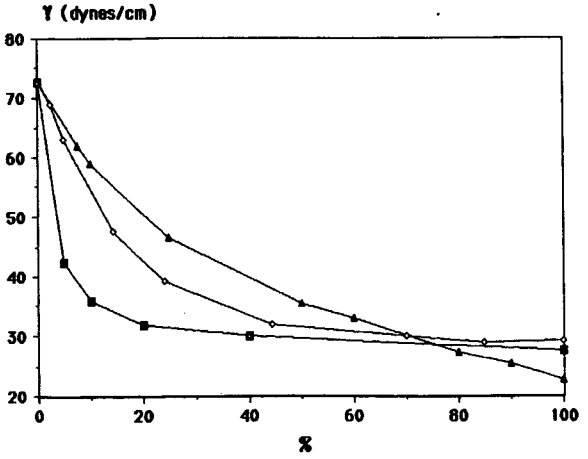

Fig. 4. Surface tension (γ) *vs.* volume fraction of organic solvent in water. ▲ = Methanol–water mixtures; ◇ = acetonitrile–water mixtures; □ = THF–water mixtures. From ref. 2.

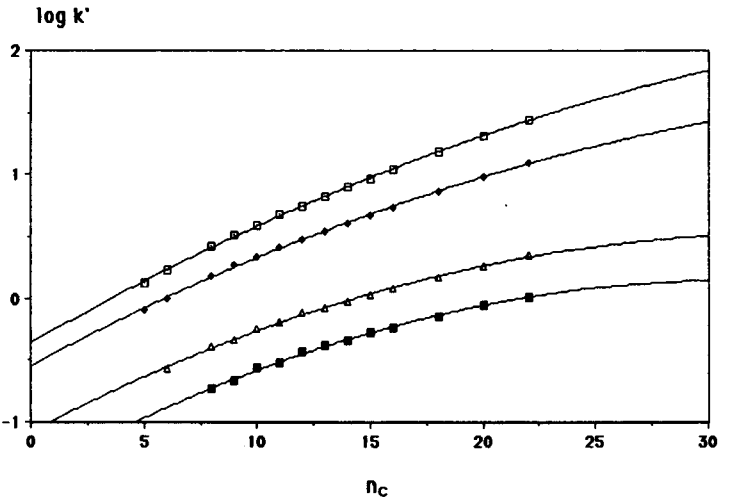

Fig. 5. Log k' *vs.* n_C plots on a Spherisorb ODS-1 column for *n*-alkyl benzoates in THF–water mixtures. THF: water ratio: □ = 55:45; ◆ = 60:40; △ = 70:30; ■ 75:25.

In another way, we were able to show that ligands are excluded by using pure tetrahydrofuran or tetrahydrofuran–chloroform mixtures, as had also been by others [11,22]. The results (Fig. 7) show that at water contents above 5% alkanes are well

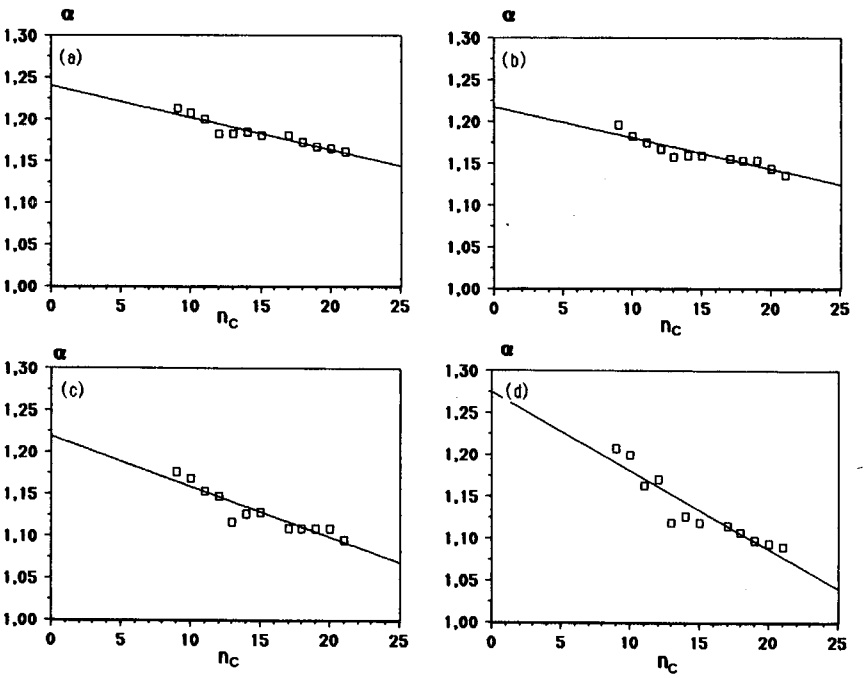

Fig. 6. Quadratic methylene selectivity [8] (α_n) *vs.* n_C plots on a Spherisorb ODS-1 column for *n*-alkyl benzoates in THF–water mixtures. THF: water ratio: (a) 55:45; (b) 60:40; (c) 70:30; (d) 75:25.

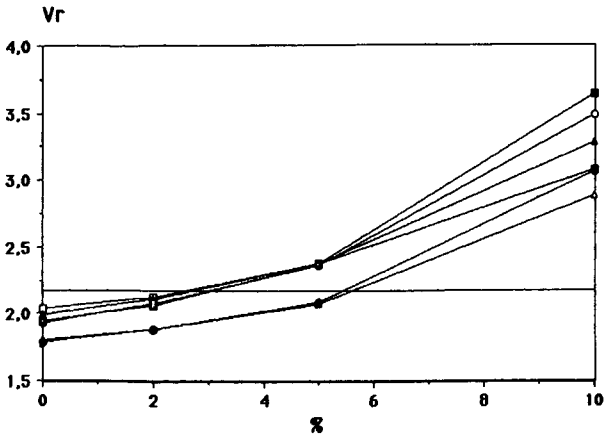

Fig. 7. Absolute retention volume (V_r) of ligands *vs.* volume fraction of water in THF on a C_{18} column. ■ = *n*-Alkane with $n = 36$; ○ = *n*-alkane with $n = 32$; ▲ = *n*-alkane with $n = 26$; □ = *n*-alkane with $n = 20$; △ = triglyceride with $n = 16$; ● = triglyceride with $n = 18$. Horizontal line, void volume of the column.

retained and a common point of intersection can be seen for a value of V_r close to but slightly higher than the column dead volume obtained with the method of two solvents. This phenomenon is the same for alkanes and triglycerides. The same study undertaken with tetrahydrofuran–chloroform mixtures (up to 25% chloroform) showed that the retention volume of each of the ligands used in this study remained the same as in pure tetrahydrofuran. The points on the log M *vs.* V_r plot are aligned for the ligands studied, contributing evidence for an exclusion phenomenon.

A conformation change of the chains in this modifier could explain all the above results. This will be described below.

Conformational infrared study

Calculations have shown [23] that four bands in the region 1480–1320 cm^{-1} were characteristic of the conformation of alkyl chains: $\nu = 1378$ cm^{-1}, all-*trans* conformation of the chain; $\nu = 1341$ cm^{-1}, end-*gauche* conformation; $\nu = 1354$ cm^{-1}, *gauche–gauche* conformation (two consecutive non-planar left bonds); $\nu = 1367$ cm^{-1}, kink model conformation (*gauche–trans–gauche* sequences).

Based on these attributes, we studied the conformation of different bonded alkyl phases and of the corresponding alkanes in different deuterated solvents. We observed that regardless of the solvent. THF-$^2H_8$, $C^2H_3O^2H$, C^2HCl_3 or C^2H_3CN, the four expected spectral bands were present in variable proportions. Solubilization in partially aqueous mixtures did not change the phenomenon qualitatively.

The results (Fig. 8) call for several comments. The proportion end-*gauche*, *gauche–gauche* and kink conformations increases consistently with the carbon number of the alkane in all four solvents tested. We confirmed the results of Sander *et al.* [24] and showed that the same changes occurred in the other three solvents. For an alkane of given chain length, the proportion of kink conformations in methanol and acetonitrile is similar to but lower than that in tetrahydrofuran or chloroform, whereas the inverse occurs for the weights of the *gauche–gauche* and end-*gauche* conformations.

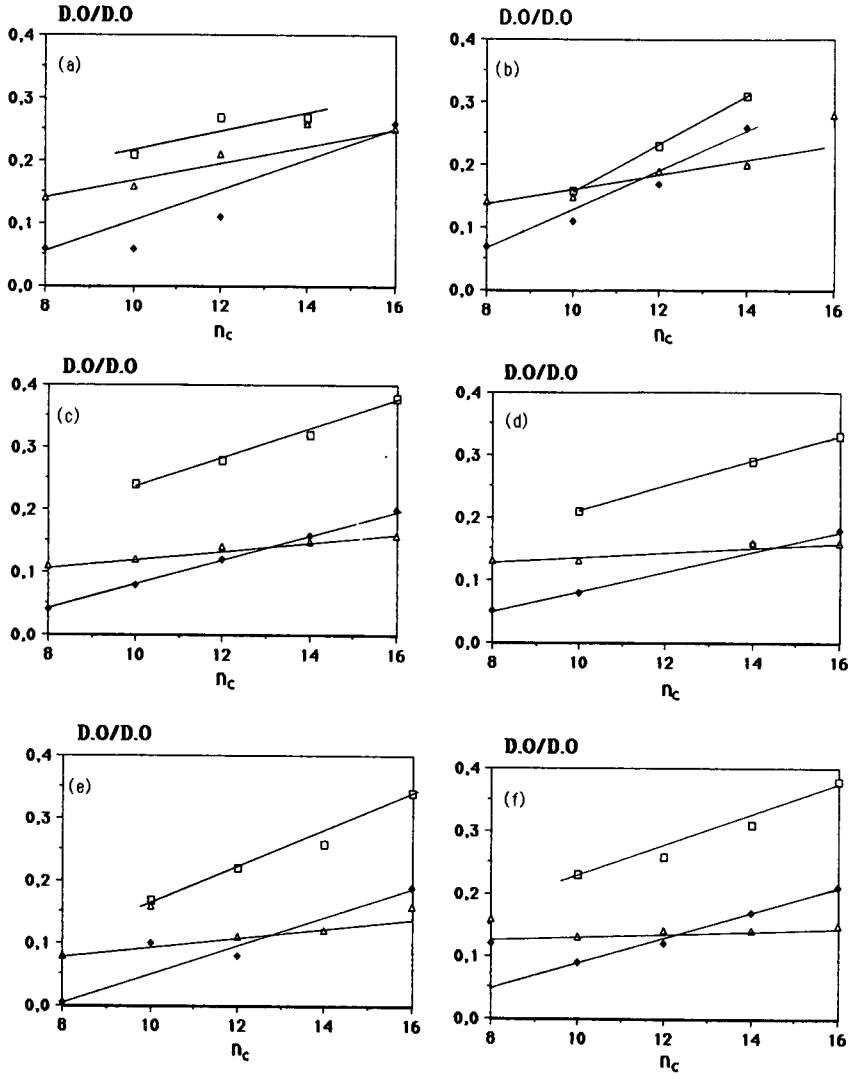

Fig. 8. Ratio of vibration band absorbances related to different alkyl chain conformations *vs.* alkane chain length. □ = Ratio D.O. kink/D.O. all-*trans*; △ = ratio D.O. *gauche–gauche*/D.O. all-*trans*; ◆ = ratio D.O. end-*gauche*/D.O. all-*trans*. (a) in $C^2H_3O^2H$; (b) in ^2H_3CN; (c) in THF-$^2H_8$; (d) pure ligand; (e) in C^2HCl3; (f) in THF-$^2H_8$–^2H_2O (90:10). D.O. = optical density.

Hence the fact that the values obtained in THF are different from those in methanol and acetonitrile confirm, as we have seen in chromatography, that THF has a particular behaviour towards alkyl chains.

The proportions of the conformations in both acetonitrile and methanol being similar, we studied the role of the first solvent with regard to the chromatographic process. We studied particularly ligands with π electrons.For all these ligands, the results are entirely comparable to those obtained with methanol [8] (Fig. 9). There is a

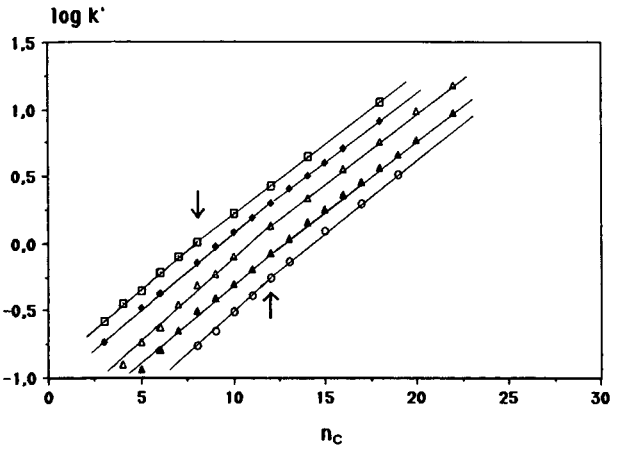

Fig. 9. Log k' *vs.* n_C plots on an RP-14 column [solvent: acetonitrile–water (95:5). □ = Phenyl-*n*-alkanes; ◆ = *n*-alkyl benzoates; △ = chloro-*n*-alkanes; ▲ = methyl esters of *n*-alkanecarboxylic acids; ○ = 2-*n*-alkanones.

break in the curve for a critical chain length, independent of the series tested, characteristic of the bonded chain length and independent of the percentage of water and temperature. A shift in this critical value, n_{crit} in the case of phenylalkanes and *o*-phthalates in comparison with the other homologous series tested confirms that these ligands penetrate the interior of the linkage by their aromatic part in acetonitrile–water mixtures as in methanol–water mixtures.

On the other hand, it should be noted that in NARP in pure acetonitrile the aromatic ring does not penetrate the linkage but rather remains at the exterior [16]. We have recently confirmed these results and showed that at least 5% acetonitrile in methanol is necessary for the development of a specific interaction between acetonitrile and the aromatic ring to cause non-insertion of this ring in the ligate. This phenomenon of non-insertion had been reported for alkyl benzoates [8] for all the solvent studied.

Acetonitrile is thus a particular modifier, introducing specific interactions with ligands having π electrons.

Interpretation of the results in relation to the solvophobic theory

Regardless of the modifier used, the behaviour of homologous series is directly related to the increase in the hydrophobic volume, ΔA, of the ligand with increasing n_C (eqn. 1).

IR results in methanol and acetonitrile show that regardless of the length of the chain, the all-*trans* conformation is the predominant one. However, when n_C increases, the proportion of kink and *gauche–gauche* conformations causes a deviation from linearity and flatness of the chains. This leads to a less intimate contact of solutes with the linkage, especially as the number of carbon atoms in the solute increases. If we consider the energy of contact of each methylene, the addition of an additional methylene does not cause a constant variation of the energy of interaction when n_C increases. Hence the methylene selectivity is not constant but declines slightly

with increasing carbon number. In THF, the solutes behave differently than in methanol and acetonitrile. The fact that in THF the proportion of the kink conformation is higher than that in the other two does not prevent penetration between the ligates. The contact of solutes is distributed according to the position of the kink in the linkage chain. This contact is less intimate and increases less regularly than with a ligate which is stretched. Hence methylene selectivity decreases slightly with increasing chain length and the plots of log k' *vs.* n_C are curved.

Moreover, the very low retention observed with this solvent cannot be explained only by surface tension. It reflects its high solvation power for hydrocarbon chains. Restricted movements in methanol [25,26] or acetonitrile [27] favour longer contact times between the alkyl chains and thus a more intimate contact than in chloroform or dioxane [25,26] (and by analogy THF), where movements are much freer. In eqn. 1, this may be related to the dielectric constant ε of THF, which is very low in comparison with those of acetonitrile and methanol. This is the third factor responsible for retention when surface tensions are similar.

Verification of the linear approximation in binary mixtures

The detailed study of log k' *vs.* % organic modifier shows apparent differences between the three solvent systems used.

The separation factors between two ligands L_1 and L_2 are represented by the vertical difference between the log k' *vs.* % organic modifier curves for a given composition of mobile phase:

$$\log \alpha_{L_1L_2} = \log k'_{L_1} - \log k'_{L_2} \tag{2}$$

In the case of homologous series, $\log \alpha_{L_1L_2}$ represents the methylene selectivity [15]. For mixtures with a high percentage of organic modifier, the separation factor increases in the order THF < acetonitrile < methanol. The reverse order is observed for mixtures poor in organic modifier (< 50%). Hence, in the case of solutes requiring analysis at a low percentage of organic modifier, more homologues can be separated in methanol than in tetrahydrofuran.

The curves of the different ligands are convergent, regardless of the modifier used. This had been noted with another series of ligands with different chemical structure, *i.e.*, differently substituted aromatic compounds [21]. The originality of the present results is that for homologous series this is also verified in acetonitrile, which is not the case for the other ligands tested. A practical application of this property permitting the separation of homologous series to be optimized is suggested below.

Application to the determination of parameters permitting the prediction of retention of homologous series

A scale of elution strength of different solvents used in HPLC is based on the value of the methylene selectivity [11,28]. This elution strength scale is defined by analogy with Snyder's processing [29] of adsorption on polar surfaces. It characterizes only the purely solvophobic effect and thus has a real basis provided that this effect is manifested by an increase in retention by a constant increment of the compounds in a homologous series. This property is not verified for THF–water mixtures.

We therefore attempted to predict the retention of ligands based on Snyder *et al.'s* processing [13] with

$$\log k' = \log k'_0 - S\varphi \tag{3}$$

This equation takes all interactions into account.

We determined the values of $\log k_0$ and S by rendering the curves in Figs. 1 and 2 linear for $\log k'$ values between 0 and 2. Regardless of the organic modifier, the correlation coefficients were systematically higher than 0.998. The linear correlation of these values of S and $\log k_0$ was made with eqn. 4:

$$S = p + q \log k_0 \tag{4}$$

Such a treatment had already been applied to methanol, with 32 aromatic ligands and with different columns. The values of p and q deduced permitted the successful prediction of the retentions of different ligands, using an isocratic mobile phase and a single gradient [30]. Application of the same treatment to the homologous series tested in this work resulted in S *vs.* $\log k_0$ curves shown in Fig. 10. As can be seen, and in contrast to previous results, the points are aligned regardless of the solvent (Table I), suggesting the possibility of optimizing the separation of homologous compounds or long-chain saturated compounds with different polarity by the use of a single elution gradient [31], without being required to start by using a mobile phase containing methanol.

CONCLUSIONS

This study has confirmed the application of the solvophobic theory to explain reversed-phase chromatography. Capacity factors increase with increasing hydrocarbon surface of ligand–ligate contacts. This is true regardless of whether the mechanism of molecular interaction occurs via an intimate contact of the ligand (in acetonitrile or methanol) or by a more or less loose contact (in THF or on methyl-bonded columns for all solvents).

The variation of the retention of solutes as a function of the percentage of organic modifier in the mobile phase is calculated based on the variation in the surface tension of the eluting mixture. In the most general case, this is realized with methanol or acetonitrile, whether or not the ligand penetrates the stationary phase and regardless of its polarity. Pure methanol is generally a better eluent than pure acetonitrile.

The development of specific ligand–modifier or ligate–modifier interactions causes a change in selectivity leading to a crossover of $\log k'$ *vs.* % organic modifier curves when the latter is higher than 90%. In some instance, acetonitrile is an even better eluent than methanol. The linearity of the $\log k'$ *vs.* n_C curves is unaffected, but the nature of the penetration mechanism may be modified depending on the nature of the polar head of the ligand. Thus, acetonitrile develops specific π–π interactions, in particular with aromatic or multi-double-bond systems. They may be profitably used in NARP to optimize the separation of these compounds.

As a result of its low dielectric constant, THF solvates hydrocarbon chains

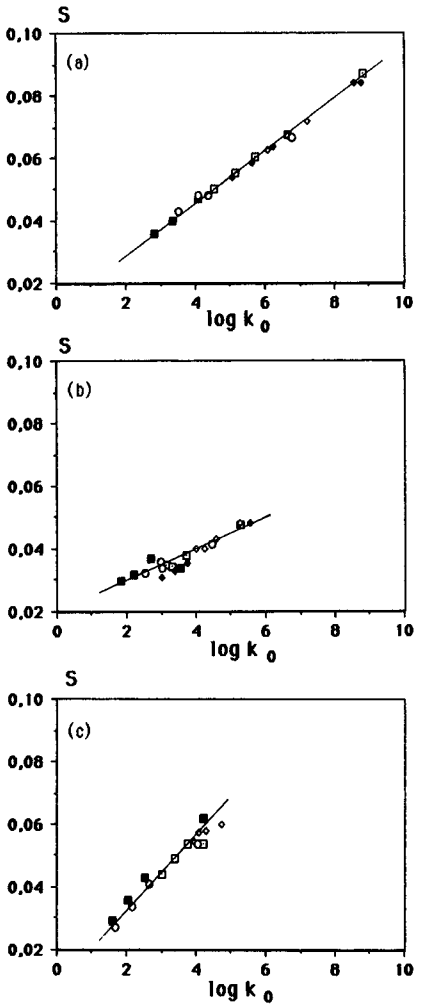

Fig. 10. S (slope of $\log k'$ *vs.* % organic modifier) *vs.* $\log k_0$ on a Hypersil C_{18} column. (a) Methanol–water mixtures; (b) acetonitrile–water mixtures; (c) THF–water mixtures. □ = Chloro-*n*-alkanes; ◆ = *n*-alkanes; ■ = *n*-alkanols; ◇ = phenyl-*n*-alkanes; ○ = methyl esters of *n*-alkanecarboxylic acids.

TABLE I

GRADIENT SHAPE PARAMETERS

Stationary phase	Modifier	p (eqn. 4)	q (eqn. 4)	r (correlation coefficient)
Hypersil C_{18}	Methanol	3.06	0.8	0.998
	Acetonitrile	4.26	0.53	0.936
	THF	2.85	1.07	0.980
Lichrosorb RP-18	Methanol	3.27	0.8	0.999
	Acetonitrile	1.61	0.87	0.992
Spherisorb ODS-1	THF	3.88	1.0	0.985

much better and even though the solvophobic effect is generally respected with this modifier when mixed with water, the retention of ligands is always lower than in other solvents. The mobility of chains and the wide range of conformations in this solvent (shown by IR and NMR) even lead to a phenomenon of exclusion when it is used pure. On the other hand, this property can be used to solubilize ligands with a large hydrocarbon volume by adding several percent of this modifier to methanol or acetonitrile, which will lead to a mechanism of interaction by insertion.

The non-linear behaviour of ligands in THF as a function of their chain length explains the erroneous predictions obtained when optimizing long-chain separations based on the idea of elution strength deduced from methylene selectivity. An approach to this problem on the basis of the p and q values deduced from studies of the linear variation of retention in binary mixtures is more appropriate.

SYMBOLS

a_s	Characteristic constant of solvent
$\Delta A =$	$A_L + A_1 - A_{L_1}$
A_L	Surface area of ligand (solute)
A_1	Surface area of ligate (stationary phase)
A_{L_1}	Surface area of complex
A_s	Surface area of solvent
k'	Capacity factor of ligand
k'_0	Extrapolation of the k' value in pure water
N	Avogradro's number
p_0	Atmospheric pressure
R	Gas constant
S	Slope of log k'*vs.* φ plot.
T	Absolute temperature
V_s	Molar volume of solvent
V_r	Absolute retention volume of ligand
V	Volume of stationary phase
V_m	Volume of mobile phase
W_s	Characteristic constant of solvent
$\Delta Z =$	$Z_{L_1} - Z_1 - Z_L$
Z_{L_1}	Partial electrostatic charge of complex
Z_1	Partial electrostatic charge of ligate
Z_L	Partial electrostatic charge of ligand
α	Methylene selectivity = log (k'_{n+1}/k'_n) ratio of capacity factors for two consecutive homologous ligands
α_n	Quadratic methylene selectivity = $(k'_{n+1}/k'_{n-1})^{1/2}$
$\alpha_{L_1L_2}$	Separation factor: ratio of capacity ratios between two ligands L_1 and L_2 for a given mobile phase composition
γ	Surface tension of bulk solvent
ε	Dielectric constat of solvent
χ_e	Factor adjusting the macroscopic surface tension to molecular dimension
φ	Volume ratio of organic modifier

REFERENCES

1 O. Sinanoglu, in B. Pullman (Editor), *Molecular Association in Biology*, Academic Press, New York, 1968, p. 427.
2 W. R. Melander and Cs. Horváth, in Cs. Horváth (Editor), *High Performance Liquid Chromatography*, Vol. 2, Academic Press, New York, 1980, p. 133.
3 A. P. J. Martin, *Biochem. Soc. Symp.*, 3 (1949) 4.
4 W. R. Melander and Cs. Horváth, *Chromatographia*, 15 (1982) 86, and references cited therein.
5 A. Tchapla, S. Heron, H. Colin and G. Guiochon, presented at *16th International Symposium on Chromatography, Paris, September 21–26, 1986.*
6 D. Morel, J. Serpinet, J. M. Letoffe and P. Claudy, *Chromatographia*, 22 (1986) 103.
7 A. Tchapla, H. Colin and G. Guichon, *Anal. Chem*, 56 (1984) 621.
8 A. Tchapla, S. Heron, H. Colin and G. Guiochon, *Anal. Chem.*, 60 (1988) 1443, and references cited therein.
9 M. Martin, G. Thevenon and A. Tchapla, *J. Chromatogr.*, 452 (1988) 157.
10 M. Czok and H. Engelhardt, *Chromatographia*, 27 (1989) 5.
11 L. R. Snyder, *J. Chromatogr.*, 6 (1961) 22.
12 H. Colin, G. Guiochon, Z. Yun, J. C. Diez Masa and P. Jandera, *J. Chromatogr. Sci.*, 21 (1983) 179.
13 L. R. Snyder, J. W. Dolan and J. R. Gant, *J. Chromatogr.*, 165 (1979) 3.
14 K. Karch, I. Sebestian, I. Halász and H. Engelhardt, *J. Chromatogr.*, 122 (1976) 171.
15 H. Colin and G. Guiochon, *J. Chromatogr. Sci.*, 18 (1980) 54.
16 G. Thevenon, *Ph. D. Thesis*, Université de Paris 6, Paris, 1986.
17 A. Chartier, *Ph. D. Thesis*, Université Claude Bernard Lyon I, Lyon, 1987.
18 H. Colin, A. M. Krstulović, G. Guiochon and Z. Yun, *J. Chromatogr.*, 255 (1983) 295, and references cited therein.
19 G. Felix and C. Bertrand, *Analusis*, 17 (1990) 326.
20 G. Thevenon-Emeric, M. Martin and A. Tchapla, *J.Chromatogr.*, 550 (1991) 267.
21 P. J. Schoenmakers, H. A. H. Billiet and L. de Galan, *J. Chromatogr.*, 185 (1979) 179.
22 E. Lundanes and T. Greibrokk, *J. Chromatogr.*, 322 (1985) 347.
23 R. G. Snyder, *J. Chem. Phys.*, 47 (1967) 1316.
24 L. C. Sander, J. B. Callis and L. R. Field, *Anal. Chem.*, 55 (1983) 1068.
25 M. E. MacNally and L. B. Rogers, *J.Chromatogr.*, 331 (1985) 23.
26 P. Shah and L. B. Rogers, *J. Chromatogr.*, 388 (1987) 411.
27 R. K. Gilpin and M. E. Gandola, *Anal. Chem.*, 56 (1984) 1470.
28 H. Colin, G. Guiochon and J. C. Diez Masa, *Anal. Chem.*, 53 (1981) 146.
29 L. R. Snyder, *Principles of Adsorption Chromatography*, Marcel Dekker, New York, 1968.
30 P. J. Schoenmakers, *Optimization of Chromatographic Selectivity (Journal of Chromatography Library*, Vol. 35), Elsevier, Amsterdam, 1986, p. 63.
31 P. J. Schoenmakers, H.A. H. Billiet and L. de Galan, *J. Chromatogr.* 205 (1981) 13.

Journal of Chromatography, 556 (1991) 235–248
Elsevier Science Publishers B.V., Amsterdam

CHROM. 23 200

Dispersion in round tubes and its implications for extra-column dispersion

A. SHANKAR[a] and A. M. LENHOFF*
Department of Chemical Engineering, University of Delaware, Newark, DE 19716 (USA)

ABSTRACT

Dispersion in connecting tubing represents a major contribution to extra-column band broadening in liquid chromatography, a factor that is particularly important in miniaturized high-performance liquid chromatographic systems. Although most analyses of extra-column effects are based on the Taylor–Aris theory of dispersion in tubes and the additivity of variances, these approaches are known to be inaccurate under some conditions, but alternative theoretical methods have not been verified experimentally. These aspects have been addressed by a combination of theory and experiment. Experimental elution curves in single tubes are shown to match closely the theoretical predictions based on solutions to the convective diffusion equation, without the need for any adjustable parameters. For tubes in series, use of a convolution relationship allows the accurate prediction of the response of the overall system when radial mixing between the two tubes is present. Although injection and detection systems have not been analysed in detail, they may contribute to discrepancies between theory and experiment if they are not well matched with the remainder of the chromatographic system.

INTRODUCTION

Extra-column contributions to overall peak width in chromatography arise from dispersion in injection and detection systems and in connecting tubing. Such dispersion, which results from the interaction of non-uniform velocity and concentration profiles in the component of interest, reduces the resolution of the separation, and efforts are thus made to minimize it relative to the band spreading occurring in the column itself. A crucial factor in such efforts is minimization of the volume of the extra-column component, but given the continuing development of miniaturized high-performance liquid chromatographic (HPLC) systems, even these endeavours have bounds. Analysis of the extra-column effects then becomes important. Although this in itself obviously does not reduce actual band spreading, it can aid in the analysis of affected data and in the design of components with improved performance characteristics as regards extra-column dispersion.

Most analyses of extra-column contributions to band spreading (*e.g.*, [1,2]) have been based on two assumptions. The first assumption is that the various contributions

[a] Present address: Hoffman-La Roche, 340 Kingsland St., Nutley, NJ 07010, USA.

0021-9673/91/$03.50

to band spreading are all independent, as a result of which the overall variance is simply the sum of the individual contributions [1,3]. The second refers specifically to dispersion in connecting tubing, where it is generally assumed that the Taylor [4]–Aris [5] result holds, namely that the axial spreading, in terms of the concentration averaged across the tube cross-section, is Fickian, with the dispersion coefficient equal to $u^2d^2/192D$, where u is the average velocity, d the tube diameter and D the solute diffusivity. The Taylor–Aris result predicts that an impulse input of solute will spread such that it always has a Gaussian axial profile.

That both these assumptions are questionable under at least some conditions was recognized by Golay and Atwood [6,7]. They noted that the variances contributed by successive components of the chromatographic system are additive only if there is complete radial mixing at the junction between the components. This is because the input–output relationship for each component is generally expressed in terms of average concentrations, with the implicit assumption that the concentration is, in fact, uniform across the cross-section of the stream concerned.

Golay and Atwood [6] also stressed that, as was clear from the original derivations [4,5], the Taylor–Aris result is valid only for sufficiently long tubes (length $L \gg ud^2/D$). They showed by both computations and experiment that the axial profile of average concentration follows a complex evolution in shape due to the interaction of axial convection and radial diffusion. This evolution, which has been widely documented [6–12], can be summarized as follows. The initial bolus of solute is distorted by the laminar velocity profile into a bullet shape, the length of which increases linearly with time. If the radially averaged concentration is considered, the axial profile adopts a "box-car" [6] shape which, as shown by Taylor [4], decays hyperbolically in concentration with time as it grows in length. The distortion caused by the velocity profile results in steep radial concentration gradients, down which radial diffusion thus occurs. This occurs most visibly near the rear, where solute is mainly in the region of steep velocity gradients near the wall; inward diffusion here gives rise to a bump at the rear of the box-car. At longer times, however, outward diffusion near the snout of the bullet-shaped profile into the slower moving region near the wall also dissipates the front end of the box-car, leading ultimately to the Gaussian profile predicted by the Taylor–Aris theory. Because of the simultaneous decrease in the box-car concentration and increase in the concentration of the Taylor–Aris (dispersion) peak, the elution profile at intermediate times may display a double peak comprising a hyperbolic convection peak followed by a dispersion peak. Such results have been observed experimentally [6,13–16].

Issues such as those outlined above are seldom taken into account in analyses of extra-column dispersion in chromatography, possibly owing in part to the complexity of the behaviour predicted and observed. However, in view of the wide availability of computational power, the routine implementation of more detailed approaches should be possible. It is therefore important to ensure the reliability of the theory in predicting observed experimental behaviour. Similar qualitative trends have been observed in both computational and experimental studies, but direct comparisons of theory and experiment [6,7] have been largely in terms of such parameters as peak variance. The objectives of this work were to perform direct comparisons of experimental data obtained on standard extra-column systems with the predictions of convective diffusion models. Both aspects discussed above, namely the responses of both single tubes and systems consisting of more than one component, are addressed.

THEORY

Dispersion in laminar tube flow

For fully developed laminar flow in a tube the local solute concentration $c(z, r, t)$ satisfies the convective diffusion equation

$$\frac{\partial c}{\partial t} + U\left[1 - \left(\frac{r}{a}\right)^2\right]\frac{\partial c}{\partial z} = D\left(\frac{1}{r}\cdot\frac{\partial}{\partial r}\cdot r\cdot\frac{\partial c}{\partial r} + \frac{\partial^2 c}{\partial z^2}\right) \tag{1}$$

where U is the centre-line velocity, r, z and t are the radial and axial coordinates and time, respectively, a is the tube radius and D is the solute diffusivity. For the problem of dispersion of a bolus of solute of mass M which is initially uniformly distributed across the tube cross-section, eqn. 1 is to be solved subject to the radial boundary condition

$$\frac{\partial c}{\partial r} = 0 \quad \text{at} \quad r = 0, a \tag{2}$$

denoting symmetry at the centre-line and no flux at the walls, and the initial condition

$$c(z, r, 0) = \frac{M\delta(z)}{\pi a^2} \quad \text{at} \quad t = 0 \tag{3}$$

Two axial boundary conditions are also required in principle; one is the absence of solute in fluid entering the system,

$$c = 0 \quad \text{at} \quad z = 0 \tag{4}$$

while the need for the other falls away because of the solution method used, as discussed below.

This problem has been studied extensively [6–12,17] and a number of solution procedures have been proposed. We have recently reported an approach which is particularly efficient to implement computationally [12]. It is based on the neglect of the axial diffusion term in eqn. 1, thus also eliminating the need for a second axial boundary condition. Omission of the axial diffusion term can be corrected for exactly using a Gaussian smoothing method [18], but this correction is unnecessary for the systems of interest here, as it is important only at very low flow-rates or at extremely short times. As full details of the solution procedure are given elsewhere [12], all that is noted here is that the solution provides values of the dimensionless concentration

$$C = \frac{\pi a^4 U c}{DM} \tag{5}$$

as a function of the dimensionless variables

$$\xi = \frac{r}{a} \qquad r = \frac{Dt}{a^2} \qquad \zeta = \frac{zD}{Ua^2} - \frac{\tau}{2} \tag{6}$$

Thus time is scaled relative to the characteristic time for radial diffusion, while the axial coordinate is transformed such that its origin moves with the mean velocity of the fluid. The solution is independent of any dimensionless parameters, an aspect which is significant in the presentation of computational results and the interpretation of experimental data.

Although the solution procedure provides local concentrations C, it is usually some average concentration that is of interest. The most widely studied average, which is also the one on which the Taylor–Aris result is based, is the straightforward area average.

$$\bar{C} = 2\int_0^1 C\xi d\xi \tag{7}$$

also referred to as the "slice content" [6,7]. However, as noted by Golay and Atwood [6], a different average is appropriate when the mean concentration in an eluting stream is examined. This average, usually called the cup-mixing average [19], weights the local concentration by the rate at which the fluid emerges from the tube, *i.e.*, by the velocity profile:

$$C_m = 4\int_0^1 C(1 - \xi^2)\xi d\xi \tag{8}$$

Multiplying the cup-mixing concentration by the mean velocity thus gives the rate at which solute emerges from the tube.

Because averaging eliminates dependence on ξ, $\bar{C}$ and C_m are functions of τ and ζ only. However, elution curves provide concentration data at a fixed value of $z = L$, and this introduces an independent parameter. This quantity is most conveniently expressed in dimensionless terms as a dimensionless minimum transit time (transit time based on the centre-line velocity U), $\tau_m = LD/Ua^2$. The elution curve is then just the value of the relevant average concentration as a function of τ at $\zeta = \tau_m - \frac{1}{2}\tau$. Fig. 1, which shows the predicted cup-mixing responses for a range of τ_m values, illustrates the evolution of the elution curve from an essentially hyperbolic convection peak, through a double-peaked response, to the near-Gaussian Taylor–Aris form where only the dispersion peak is seen.

Response of components in series

The response of a system consisting of multiple components in series is generally obtained by assuming additivity of mean retention times and varances, a result which may be obtained as shown by, for instance, Sternberg [3]. Such results are, however, a consequence of a more general set of results using the theory of residence time distributions or, more generally, age-distribution functions [20,21]. The residence time distribution (RTD) or exit age distribution $E(t)$ gives the distribution of time spent by fluid molecules leaving the system. In principle, it is found by marking all the molecules entering the system at a given instant, and then measuring the fraction of marked

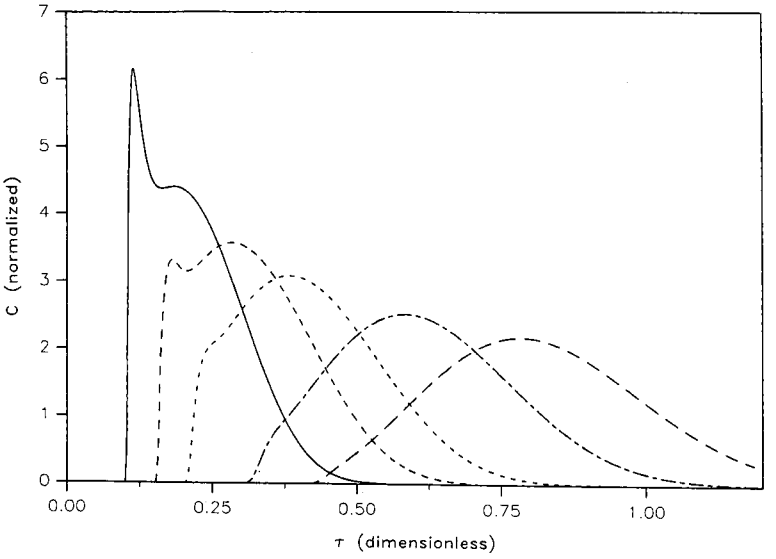

Fig. 1. Evolution of theoretical cup-mixing elution curves as a function dimensionless minimum transit time. τ_m values: —, 0.10; – –, 0.15; - -, 0.20; – – –, 0.30; ——, 0.40.

particles which emerge from the system as a function of time. For a solute leaving a chromatographic component, then, $E(t)$ is simply the normalized cup-mixing concentration, measured at the exit, for an experiment in which the input was a perfect impulse. In practice, however, the distinction between cup-mixing and other averages is not always noted, and in fact it is often implicitly assumed that the concentration across the exit is uniform.

There are other implicit assumptions in the use of RTDs which are worth bearing in mind, although they are rarely limiting. One is that of linearity of all components; in chromatography this may cause problems under overload conditions. Another assumption is that components in series are non-interacting, *i.e.*, the RTD of one component is not affected by that of any other. Further, as RTDs are based on the amounts entering or leaving components without regard for spatial inhomogeneities at the entrace and exit, treating components in series assumes that the stream leaving one component is well mixed before it enters another. Atwood and Golay [7] also recognized the need for this requirement for variances to be additive. If all these assumptions are satisfied, the overall RTD for a combination of two components in series can be obtained from the individual RTDs using the convolution equation [20,21]

$$E(t) = \int_0^t E_1(t_1)E_2(t - t_1)\mathrm{d}t_1 \tag{9}$$

This relationship can obviously be generalized to one for any number of components in series; it is, in fact, just a particular example of the use of a convolution equation to account for an arbitrary input function (*i.e.*, one other than a perfect impulse).

Using the definitions of the mean residence time

$$\bar{t} = \int_0^\infty tE(t)\mathrm{d}t \tag{10}$$

and the variance

$$\sigma^2 = \int_0^\infty (t - \bar{t})^2 E(t)\mathrm{d}t \tag{11}$$

of the RTD, it is easy to show [20,21] by substitution of eqn. 9 that both mean residence times and variances are additive. The more detailed RTD approach is thus consistent with the additivity of mean retention times and variances used ubiquitously in chromatography. The full RTD is used in this work, however, because it allows the full shapes of elution curves to be examined. This is particularly important in the context of extra-column effects, where the responses can be very different in form from the ideal Gaussian shape. This peak shape information can be more informative regarding the nature of extra-column dispersion processes, and it can also provide a more challenging test of model validity in comparisons with real experimental data. The experiments reported later in which two extra-column components were used in series are therefore compared with predictions based on eqn. 9, with the individual component RTDs based on results of the kind shown in Fig. 1.

EXPERIMENTAL

The aim of the experiments performed was to obtain solute response curves for impulse injections into components both individually and in series. The components of interest were simply straight sections of tubing of various dimensions, as discussed in more detail below, to allow comparison with the responses predicted using the theory outlined above. The experimental system was thus selected so as to match closely the idealized conditions on which the models are based.

As pressure drops in open tubes are relatively low, a Harvard Apparatus (South Natick, MA, USA) Model 909 syringe pump was used as the primary source of solvent under pressure. A syringe pump has the advantage of delivering steady flows without pulsation, unlike the delivery from a high-pressure dual-piston HPLC pump. However, to evaluate the effect of flow pulsation under standard chromatographic conditions, a Waters Assoc. (Milford, MA, USA) Model 6000 HPLC pump was also used and results were compared with the syringe pump results. Both pumps were calibrated by volume collection over a fixed period to time, but owing to differences in control of the two pumps, discrepancies of up to about 2% in the flow-rates for corresponding experiments were possible.

The injection valve was chosen so as to approach the impulse input condition in eqn. 3. A Rheodyne (Cotati, CA, USA) Model 7520 valve with a 0.5-μl injection passage on the stator was used. Detection was accomplished using an Isco (Lincoln,

TABLE I

TEST COMPONENT PARAMETERS

System	Diameter (cm)	Length (cm)	Volume (μl)	Diffusion time, a^2/D (s)
A	0.025	100.0	50.7	19.7
B	0.051	100.0	202.7	78.7
C	0.102	100.0	810.7	314.7
D	0.051	158.8	321.9	78.7

NE, USA) Model V4 UV–visible absorbance detector with computerized data acquisition and a response time as low as 0.05 s. The flow cell was a standard Z-pattern type with an illuminated volume of 1 μl and a path length of 0.5 cm. The connecting tubing joining the test section to the flow cell was 0.013 cm in diameter and about 10 cm long. Hence the volume of the injection and detection system was small enough (a few μl) that its effect on $\bar{t}$ and σ^2 was small, both in absolute terms and relative to the contributions of the test sections themselves.

The test components were cylindrical tubes of various diameters, purchased precut from Upchurch Scientific (Oak Harbor, WA, USA). Four different geometries were examined, as shown in Table I. For each set, the tube volume and the diffusion time scale a^2/D are also shown. The effect of placing components in series was examined in two ways, each for two pieces of tubing of equal length with the same combined length as shown in Table I. First, interaction of components without radial mixing was studied by using a zero dead volume connector (Alltech, Deerfield, IL, USA), intended to make two tubes in series behave as a single tube with the same overall length. Second, forced convective radial mixing was introduced by including a stainless-steel precolumn filter (Model A315; Upchurch Scientific) in the junction between components.

Benzyl alcohol (Aldrich, Milwaukee, WI, USA) was used as the solute and distilled, de-ionized water as the solvent. The binary diffusivity of benzyl alcohol in water has been measured experimentally as $0.82 \cdot 10^{-5}$ cm^2/s at 20°C, a value which is within less than 10% of the values predicted by three widely used equations for estimating diffusivities in liquids [22]. Detection was at the maximum absorbance wavelength, namely 252 nm.

RESULTS AND DISCUSSION

Single tubes

The experimental system was intended to approximate as closely as possible the model system described by eqns. 1–4. However, as more than one approach to averaging is possible, as is illustrated by eqns. 7 and 8, it is important to base comparisons between theory and experiment on the appropriate average. For the type of detector used here, in which the optical path is axial, the area-average concentration is clearly inappropriate. As discussed by Atwood and Golay [7], the cup-mixing is, strictly speaking, also inappropriate. There is, however, good reason to expect the cup-average to provide a reasonable approximation to the measured results. As the

Z pattern of the detector flow cell disrupts the laminar flow sufficiently to induce mixing of the stream entering the cell, the solute flux into the cell (product of volumetric flow-rate and concentration) should be determined by the cup-mixing, and not the area-average concentration. Further, as the volume of the flow cell is much smaller than that of the dispersive components being tested, the measured concentration will be only weakly dependent on flow cell characteristics relative to its dependence on the concentration in the entering stream.

Fig. 2 shows a comparison of normalized experimental elution curves for each of the two pumps with theoretical results for the cup-mixing and area-average concentration for a system with $\tau_m = 0.163$ (system D in Table I). The results here and in subsequent figures are presented with τ as the independent variable, *i.e.*, with time scaled by the diffusion time a^2/D, to allow subsequent comparison of multiple experimental systems on a single plot; real time scales can be recovered using the a^2/D values shown for each system in Table I. The cup-mixing concentration profile in Fig. 2 is clearly closer to the experimentally observed curves than is the mean concentration; it should be emphasized that the theoretical curves were found with no adjustable parameters. All comparisons shown below are thus with the computed cup-mixing concentration. It is interesting that experimental results obtained using a detector measuring absorbance across a cross-section of the tube [16] show better agreement with the theoretical curves for the mean concentration than for the cup-mixing concentration. In Fig. 2, the difference in behaviour between the experiments with different pumps is negligible. Most of the experimental curves below were obtained with the syringe pump, but in some cases the HPLC pump was used.

Figs. 3–6 show experimental and computed elution profiles for τ_m values of 0.108, 0.163, 0.218 and 0.447, respectively. In each instance except the first, experimental curves are shown for the four different tube geometries listed in Table I,

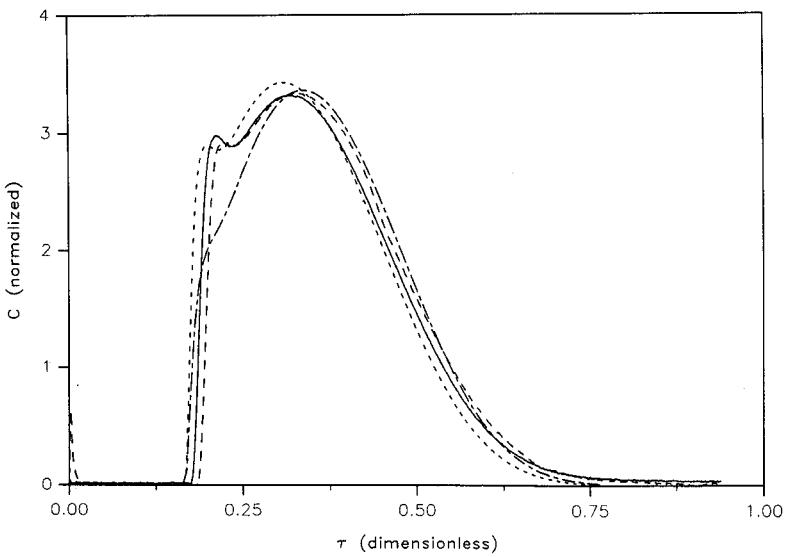

Fig. 2. Comparison of theoretical and experimental elution curves for single tube (system D) with τ_m = 0.163. Experimental: —, syringe pump; – –, HPLC pump. Theoretical: - -, cup mixing; ———, area average.

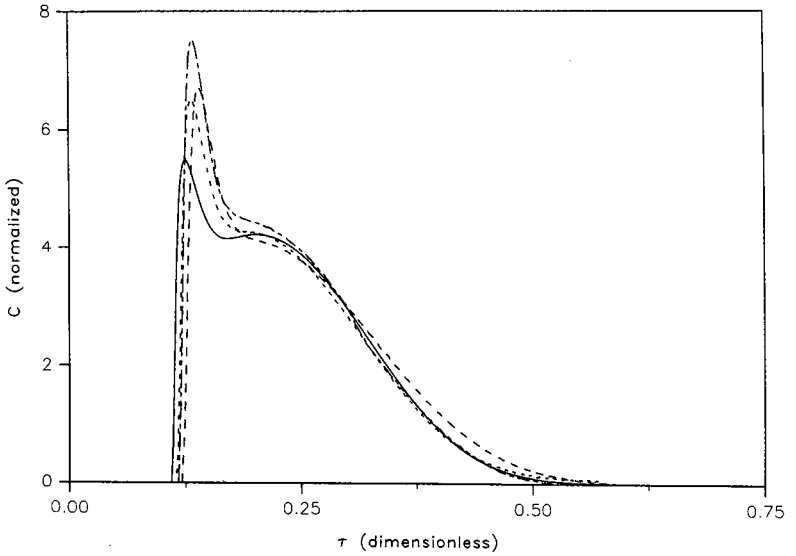

Fig. 3. Comparison of theoretical and experimental elution curves for single tubes of different geometries with $\tau_m = 0.108$. Experimental: ––, B; - -, C; – – –, D; —, theoretical.

with the appropriate τ_m value attained for different tubes by adjusting the flow rate. Although only one experimental curve is shown for each set of parameters, each experiment was replicated several times; the curves are highly reproducible, the only significant variation being that resulting from errors in recording the injection time. These errors, which were a consequence of using a manual injection valve and thus

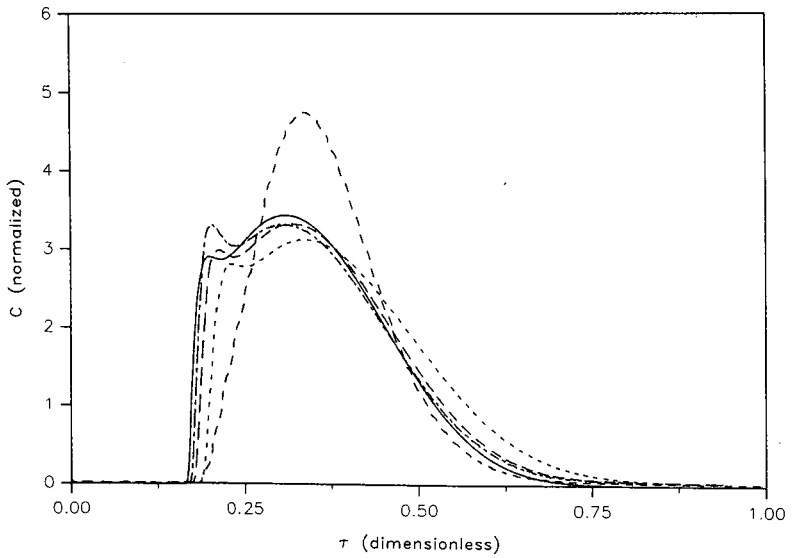

Fig. 4. Comparison of theoretical and experimental elution curves for single tubes of different geometries with $\tau_m = 0.163$. Experimental: ––, A; - -, B; – – –, C; ————, D; —, theoretical.

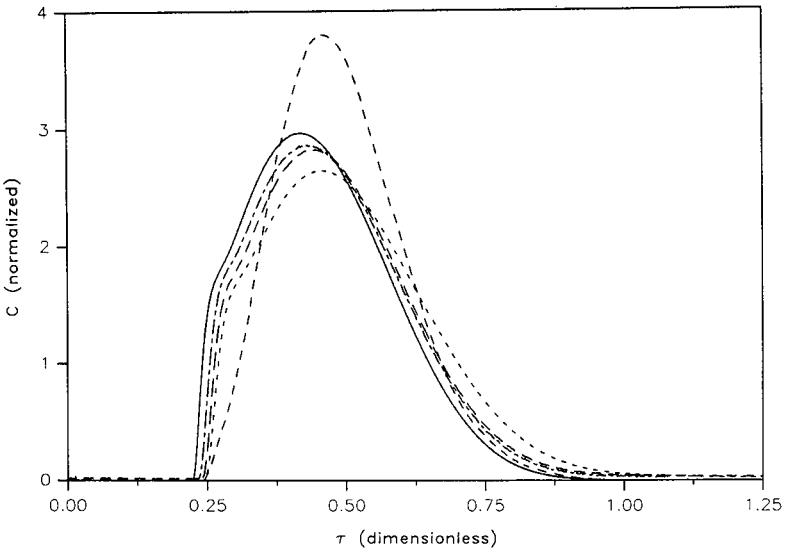

Fig. 5. Comparison of theoretical and experimental elution curves for single tubes of different geometries with $\tau_m = 0.218$. Lines as in Fig. 4.

were less than 1 s, are also the main reason for the shifts among the different curves on the plots. They become less noticeable at larger τ_m values as the time scales of the experiments increase. Agreement between theoretical and experimental curve shapes is generally excellent, especially considering, as noted previously, that the theoretical

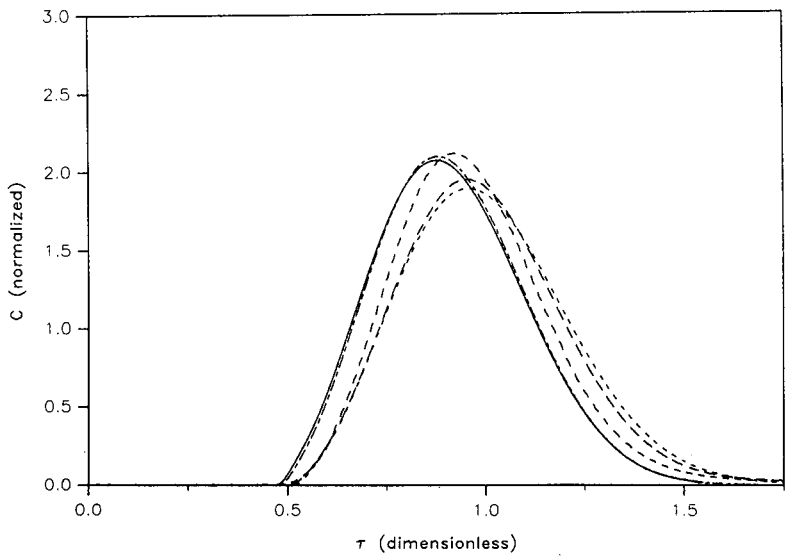

Fig. 6. Comparison of theoretical and experimental elution curves for single tubes of different geometries with $\tau_m = 0.447$. Lines as in Fig. 4.

computations involve no adjustable parameters. Agreement is poorest for system A, where the test-component volume is smallest, and the response is thus most likely to be significantly affected by transport in the injection and detection system. This is why a result for system A is not shown in Fig. 3, where the minimum transit time would be about 2 s. It is interesting, however, that in Fig. 4 the system A elution peak is of approximately the same width as predicted by theory.

A discrepancy between theory and experiment seen for small τ_m (Fig. 3, and system C result in Fig. 4) is that the experimental convective peaks are sharper than predicted by theory. A change of the order of 10% in τ_m would be sufficient to bring the theoretical curve into better agreement, but a more likely explanation for the discrepancy is one recognizing the nature of the injection. As noted previously, the injection valve tubing is in line with the test section. However, the former is of only 0.013 cm diameter, *i.e.*, smaller than any tubing used as a test section. Consequently, the injection may be biased toward the centre of the tube used as test section, instead of the uniform distribution denoted by eqn. 3. As the convection peak arises from material initially near the tube centre, an enlarged convection peak may result from the non-uniform initial distribution. That the widest tubing (system C) is the only one affected in Fig. 4 would appear to support this conjecture.

Tubes in series

The experiments to investigate interacting components in series were based on essentially the same systems for which results are shown in Figs. 3–6, the key difference being that each tube now consisted of two parts of equal length. These two parts were connected by either a zero dead volume fitting to minimize radial mixing or by an in-line solvent filter to maximize it. Fig. 7 shows a comparison of experimental and theoretical results for system B for the two linkage modes, for an overall τ_m of 0.163;

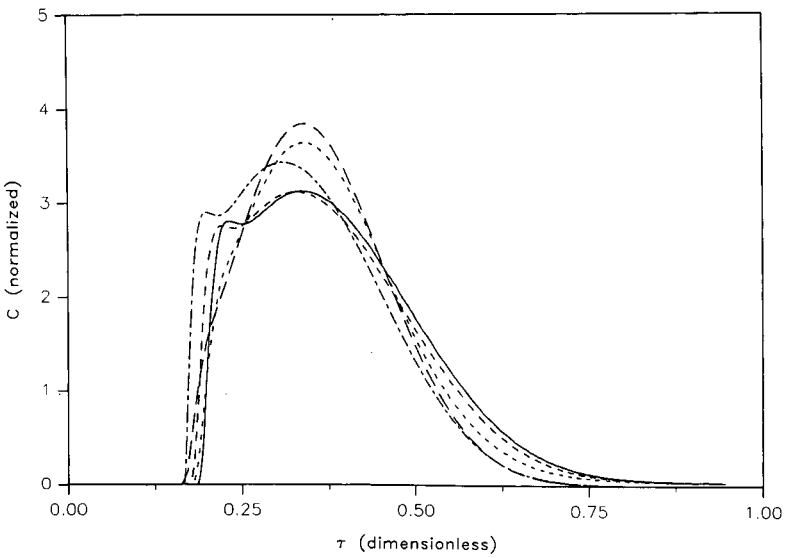

Fig. 7. Comparison of theoretical and experimental elution curves for system B with $\tau_m = 0.163$, showing effect of various tube configurations. Experimental: —, single tube; – –, two tubes with zero dead volume connector; - -, two tubes with filter. Theoretical: – – –, single tube; ——, convolution.

the corresponding single-tube experimental result is also shown for reference. Theoretical curves are shown for the convolution of two tubes (eqn. 9) and for a single tube of the same total length.

For the zero dead volume fitting, the response is very similar to the theoretical and experimental curves for a single tube. On the other hand, the convolution approach appears to allow the overall response to be calculated fairly accurately for the system incorporating the in-line filter between the two tubes, at least in the example shown. Both the theoretical and experimental curves here are significantly smoother than in the absence of mixing, and it is also noticeable that the standard parameters used to characterize response peaks, such as variances, peak widths at various ordinate values, etc., may be misleading regarding the nature of the responses. However, it follows from the accuracy of the convolution result that the overall variance of the response is equal to the sum of the two contributing variances, as is generally assumed in practice.

Additional comparisons of responses with the in-line filter are shown in Figs. 8–10 for three different τ_m values; the system A response is omitted from Fig. 8 for the same reason as in the corresponding single-tube case. Agreement between theory and experiment is again excellent for larger τ_m values, but for small τ_m, as in Fig. 8, the experimental curves display features such as convection peaks which are more characteristic of systems without mixing. This could be due to the steeper radial concentration gradients at small τ_m, making good radial mixing at the junction more difficult. As the nature of the mixing process due to the filter is poorly understood, it is not clear what the effect is of the higher rates used to attain small transit times. Here, as in Fig. 4 discussed above, it is again the widest tubing that appears most susceptible to enlargement of the convection peak, again supporting the suggestion that inadequate radial transport is involved.

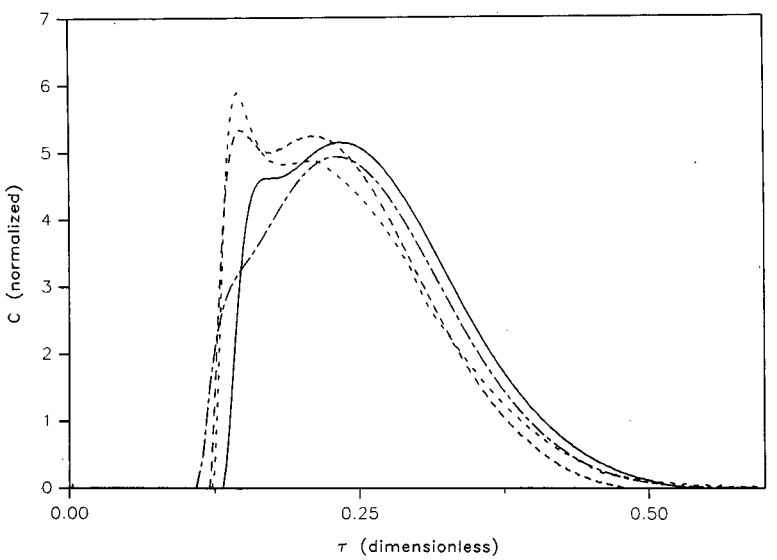

Fig. 8. Comparison of theoretical and experimental elution curves for tubes in series with $\tau_m = 0.108$. Experimental: – –, B; - -, C; – – –, D. —, Theoretical (convolution).

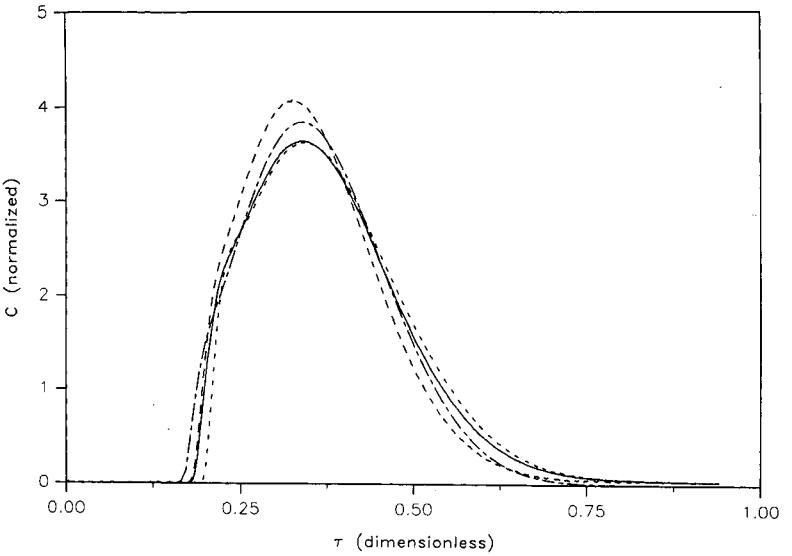

Fig. 9. Comparison of theoretical and experimental elution curves for tubes in series with $\tau_m = 0.163$. Lines as in Fig. 8.

CONCLUSIONS

Two issues concerning the modelling of extra-column dispersion have been addressed. First, we have shown that it is possible to predict the shape of elution peaks for single tubes fairly accurately, without the need for adjustable parameters. These

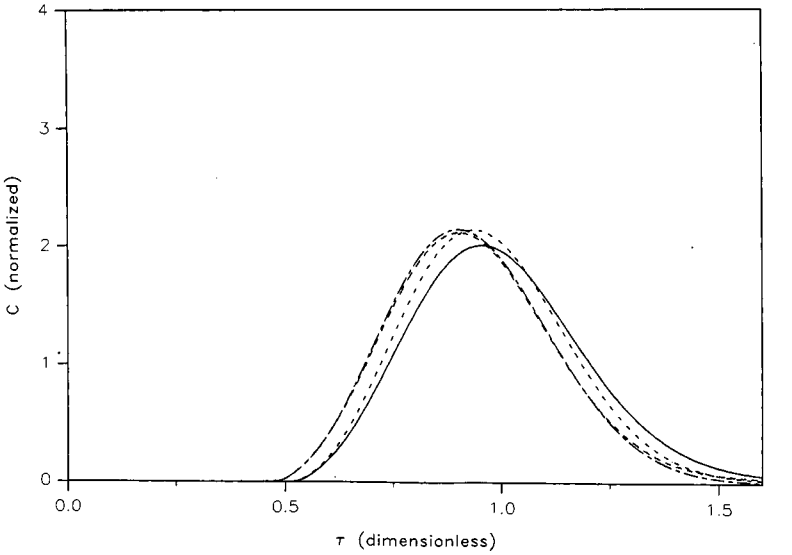

Fig. 10. Comparison of theoretical and experimental elution curves for tubes in series with $\tau_m = 0.447$. Lines as in Fig. 8.

peaks are different in shape from those predicted by the widely used Taylor–Aris theory, which is unlikely to be adequate for the tube geometries most frequently used in chromatographic practice.

The second issue addressed was that of predicting elution curves from a system consisting of multiple components in series. When radial mixing between components is adequate, the convolution approach allows the individual RTDs to be combined fairly accurately, so that under these conditions variances should indeed be additive, as is usually assumed. Although the convolution approach proved to be inaccurate in some systems studied here, only relatively poor radial mixing could be accomplished under the conditions studied; the lateral mixing occurring naturally during flow through a packed columns should help to justify the assumption of additivity of variances in actual chromatographic systems. However, it is important that the proper approach be used to find the variances of the individual components, especially the connecting tubing. Another consequence under conditions where convolution is warranted is that much of the "fine structure" of the individual elution curves, such as convection peaks, is smoothed out by the convolution process, so that anomalous peaks are unlikely to arise due to extra-column effects under normal chromatographic conditions.

ACKNOWLEDGEMENTS

This work was supported by the National Science Foundation under grant no. CBT-8657185. We thank Dr. C. N. Trumbore for the loan of the syringe pump and the injection valve.

REFERENCES

1 K. Hupe, R. J. Jonker and G. Rozing, *J. Chromatogr.*, 285 (1984) 253.
2 K. W. Freebairn and J. H. Knox, *Chromatographia*, 19 (1985) 37.
3 J. C. Sternberg, *Adv. Chromatogr.*, 2 (1966) 205.
4 G. Taylor, *Proc. R. Soc. London, Ser. A*, 317 (1953) 186.
5 R. Aris, *Proc. R. Soc. London, Ser. A*, 235 (1956) 67.
6 M. J. E. Golay and J. G. Atwood, *J. Chromatogr.*, 186 (1979) 353.
7 J. G. Atwood and M. J. E. Golay, *J. Chromatogr.*, 218 (1981) 97.
8 W. N. Gill and V. Ananthakrishnan, *AIChE J.*, 13 (1967) 801.
9 J. S. Yu, *ASME J. Appl. Mech.*, 46 (1979) 750.
10 J. S. Yu, *ASME J. Appl. Mech.*, 48 (1981) 217.
11 K. P. Mayock, J. M. Tarbell and J. L. Duda, *Sep. Sci. Technol.*, 15 (1980) 1285.
12 A. Shankar and A. M. Lenhoff, *AIChE J.*, 35 (1989) 2048.
13 C. G. Caro, *J. Physicol.*, 185 (1966) 501.
14 F. M. Kelleher and C. N. Trumbore, *Anal. Biochem.*, 137 (1984) 20.
15 C. N. Trumbore, M. Grehlinger, M. Stowe and F. M. Kelleher, *J. Chromatogr.*, 322 (1985) 443.
16 T. Korenaga, F. Shen and T. Takahashi, *AIChE J.*, 35 (1989) 1395.
17 J. S. Vrentas and C. M. Vrentas, *AIChE J.*, 34 (1988) 1423.
18 J. C. Wang and W. E. Stewart, *AIChE J.*, 29 (1983) 493.
19 R. B. Bird, W. E. Stewart and E. N. Lightfoot, *Transport Phenomena*, Wiley, New York, 1960, p. 297.
20 O. Levenspiel, *Chemical Reaction Engineering*, J. Wiley, New York, 2nd ed., 1972, pp. 253–265.
21 G. F. Froment and K. B. Bischoff, *Chemical Reactor Analysis and Design*, Wiley, New York, 1979, pp. 592–606.
22 R. C. Reid, J. M. Prausnitz and T. K. Sherwood, *The Properties of Gases and Liquids*, McGraw-Hill, New York, 3rd ed., 1977, p. 577.

Journal of Chromatography, 556 (1991) 249–262
Elsevier Science Publishers B.V., Amsterdam

CHROM. 23 198

Peak-shape analysis and noise evaluation in suppressed ion chromatography for ultra-trace ion analysis

GABRIELLA BLO* and MAURIZIO REMELLI
Analytical Chemistry Laboratory, Department of Chemistry, University of Ferrara, Via Luigi Borsari 46, I-44100 Ferrara (Italy)
FRANCESCO PEDRIELLI
Department of Physics, University of Ferrara, Via Paradiso 12, I-44100 Ferrara (Italy)
LUISA BALCONI and FABIO SIGON
ENEL–DSR, Research and Development Division, Thermal and Nuclear Research Centre, Via Rubattino 54, I-20134 Milan (Italy)
and
FRANCESCO DONDI
Analytical Chemistry Laboratory, Department of Chemistry, University of Ferrara, Via Luigi Borsari 46, I-44100 Ferrara (Italy)

ABSTRACT

Numerical analysis was used to study the performance of a suppressed ion chromatographic system with on-line preconcentration for ultra-trace ion determination in ultra-pure power plant waters. Peak-shape analysis by the Edgeworth–Cramér series fitting method was applied in order to check non-linear concentration-dependent effects, so as to evaluate the best experimental practice with regard to the linear calibration range. Noise evaluation by Edgeworth–Cramér fitting residuals and Fourier analysis is discussed in order to establish the detection limits. Results of the checks made for strictly linear conditions and determination of the quantification limits for sodium, chloride and sulphate ions are reported.

INTRODUCTION

Ion chromatography (IC) is among the most recent and rapidly growing chromatographic techniques employed in inorganic and organic ion analysis [1,3]. Coupled with a preconcentration step, IC is a powerful technique for trace and ultra-trace analysis [4–8]. Among the various applications presented to date, the determination of common trace anions, such as Cl^-, SO_4^{2-} and NO_3^-, by IC seems the most promising for its sensitivity, versatility, precision and rapidity. A knowledge of parameters such as the detection limit, linearity and accuracy is of practical importance.

In ultra-trace analysis, these fundamental requirements cannot easily be satisfied from IC data or from experiments reported in the literature. In fact, the procedures and experimental conditions followed differ widely. First, the data obtained by one detection method do not correspond to those obtained by another (*e.g.*, UV data

0021-9673/91/$03.50

cannot be transferred to conductivity values measured by chemical suppression). Further, noise contributions are strictly linked to the type of apparatus used (pumping system, electronics). Second, detection limits expressed as the absolute amount detected, obtained with direct injection, cannot be simply transferred to ultra-trace analysis by means of a preconcentration step. The same may also be said about linearity and all the above are also dependent on column type. A third point is the type of signal measured, peak height or peak area, and the way in which these signals are detected (*e.g.*, manual measurement, integration device or other more complex computational methods). Moreover, attention must be paid to the way in which the detection limits are obtained (*e.g.*, extrapolation method, simple noise structure evaluation) [9].

Although there is general agreement in accepting a large linear dynamic range for the IC technique [10–13], a wide linearity range in ultra-trace analysis is not often required. What is more important is a reliable calibration, which proves difficult to achieve in the ppt and ppb[a] ranges because of uncontrolled contamination, wall memory and matrix effects. The best results are obtained by using a completely automatic system including both the sampling and calibration steps, thus preventing sample contamination from the environment. Such a system for on-line ultra-trace ion monitoring in the power plant "condensate–feedwater" cycle has already been described by Balconi *et al.* [14]. By processing linear calibration plots, they obtained linearity ranges and detection limits. The data reported proved to be dependent on the calibration range. For example, for SO_4^{2-} the detection limit is as low as 0.3 ppb in the concentration range 0–10 ppb, but it becomes 6.7 ppb if the concentration range is more extended (to 200 ppm).

These data are contradictory, but this is only apparently so. They reflect the overall determination error, which includes many error sources (*e.g.*, sample handling, sensitivity drift of the instrument and even the non-linearity of some parts of the analytical procedure such as the preconcentration or stripping step). All these factors remain hidden in the overall estimated procedure error unless a careful experimental design is planned in order to isolate the different error sources. Obviously such an analysis is very time consuming and costly, not only because of the large number of factors that must be kept under control, but also because detecting non-linearity effects over a linearity trend requires close, continuous control of the independent variables.

In this paper, a different approach to linearity and detection limit determination is reported for the same ultra-trace ion monitoring system mentioned above. It consists in controlling all the information contained within the analytical signal (chromatographic peak) rather than an individual part of it, such as just considering the peak area or peak height. In practice, a complete peak-shape analysis using the Edgeworth–Cramér (E.C.) series fitting method [15–17] is applied in order to compare peak shapes for different injected amounts and to detect the onset of concentration-dependent, non-linearity effects [18]. In this manner, complementary, but conceptually different, information is obtained which can more clearly aid in understanding the previously reported experimental results [14] and can also give indications as to how to improve the method.

---

[a] Throughout this article, the American trillion (10^{12}) and billion (10^9) are meant.

As the chromatographic signal is always affected by unwanted noise components of a random or deterministic nature which reduce the instrumental detectability, characterization of the noise by Fourier analysis was the second point studied. In fact, a knowledge of the noise structure not only makes it possible to define unambiguously method detection limits but also suggests how to improve them by filtering or instrumental improvements [19].

The results obtained in this study obviously cannot be extended to entirely different experimental conditions; however, to date, very few linearity studies have been reported using rigorous peak-shape analysis and, of these, none simultaneously report a study of the noise. The advantages and the drawbacks of such an approach will also be interesting for different chromatographic fields.

EXPERIMENTAL AND DATA HANDLING

Chromatographic analyses were performed with a Dionex (Sunnyvale, CA, USA) Qic ion chromatograph. Experimental conditions for cation and anion determinations are given in Table I. Dionex concentration columns (50 × 3 mm I.D.), TCC-1 for cations and TAC1 for anions, were connected to the injector instead of the sample loop for sampling with preconcentration. Enrichment factors of 250 for anions and 125 for cations were applied. Analytical-reagent grade chemicals (Merck, Darmstadt, Germany; Baker, Philipsburg, NJ, USA) were used and standard solutions were prepared by on-line dilution with power plant water of the best quality and also with the water obtained from a Millipore (Milford, MA, USA) Milli-Q water purification system (background ion concentrations in power plant water: Cl^- *ca.* 5 ppb, Na^+ and $SO_4^{2-} \leqslant 5$ ppb). Standard solutions of sodium, chloride and sulphate ranged from 10 to 200 ppb.

The detector signal was digitized at a rate of 4 data per second using an HP 3455A model voltmeter (Hewlett-Packard, Avondale, PA, USA). The data were transferred to a mainframe computer for E.C. series fitting by means of a non-linear least-squares minimization procedure. Noise was evaluated by a boxcar five-point

TABLE I

EXPERIMENTAL CONDITIONS FOR ION CHROMATOGRAPHIC ANALYSIS

Samples: sodium, chloride and sulphate. Concentration range: 10–200 ppb.

Parameter	Anion determination	Cation determination
Preconcentration column	HPIC-AG4	CGl
Separation column	HPIC-AS4	CSl
Suppression column	AFS[a]	CFS[a]
Eluent	2 m*M* NaOH–3 m*M* Na_2CO_3	5 m*M* HCl
Regenerant	0.0125 *M* H_2SO_4	0.04 *M* TMAOH[b]
Eluent flow-rate (ml min^{-1})	2	2.3
Regenerant flow-rate (ml min^{-1})	2.5–3	2.5–3
Sampling time (min)	10	5
Sampling rate (ml min^{-1})	2.5	2.5
Conductimeter range (μS)	100	100

[a] Dionex fibre suppressor.
[b] Tetramethylammonium hydroxide.

cubic least-squares approximation on digitized data according to a Fortran IBM (IBM Instruments, Danbury, CT, USA) routine [20] and by computing the root-mean-square deviation between experimental (YE) and smoothed (YS) data:

$$N_{RMS} = \sum_{i=1}^{N_p} (YE - YS)_i^2/(N_p - 1)^{1/2} \quad (1)$$

where N_p is the number of data points.

For analysed peaks (standard deviation range 10–40 s) the smoothing window proved to be 1.2 s. The signal-to-noise ratio (S/N) was measured as the ratio between maximum peak height (after removing drift and baseline contribution to signal), $YMAX$, and peak-to-peak noise, computed as four times the N_{RMS} value [9]:

$$S/N = YMAX/4N_{RMS} \quad (2)$$

As N_{RMS} is taken as the standard deviation of the "analytical blank", the quantification limit (L_q), defined as the concentration that provides a signal 20 times the blank [21], is computed from eqn. 2 as

$$L_q = \frac{5c}{S/N} \quad (3)$$

where c is the concentration of the analyte solute. Peak parameters were obtained as explained previously [15]. All calculations for peak-shape analysis were run on a CDC Cyber 76 computer (Cineca, Casalecchio, Bologna, Italy). Fourier analysis was performed on an M24 personal computer (Olivetti-Italy) applying the fast Fourier transform (FFT) procedure according to the Cooley–Tukey algorithm [22], to digitized peak data by using the Labtech Notebook software (Laboratory Technologics, Wilmington, MA, USA). Noise was reduced by filtering in the Fourier domain using a rectangular low-pass filter as discussed under Results and Discussion.

THEORY AND PROCEDURE

An experimental chromatographic peak, considered as a time function signal $y(t)$, can be related to a frequency function $f(x)$, normalized to unit area and unit width, as follows:

$$y(t) = f(x)\ A/\sigma \quad (4)$$

where σ is the peak standard deviation and area A and the normalized time variable x are defined as follows:

$$A = \int_{-\infty}^{+\infty} y(t)\ \mathrm{d}t \quad (5)$$

$$x = (t - m)/\sigma \quad (6)$$

where m is the peak mean.

The E.C. series asymptotic expansions, developed to the Kth order [23], make it possible to approximate a chromatographic peak expressed as a frequency function $f(x)$ for linear non-ideal chromatography according to the following equation:

$$f(x) = Z(x) + \sum_{v=1}^{K} Q_v(-Z) + R_K(x) \tag{7}$$

where $Q_v(-Z)$ is a linear aggregate of the derivatives of the normal frequency function $Z(x)$, maximum order $3v$, and contains the cumulant coefficients, of maximum order v, of the frequency function $f(x)$ [23]. Of particular interest in peak-shape characterization are the first two cumulant coefficients, namely the skewness (S) and the excess (E). They measure the peak asymmetry and the degree of peak flattening, respectively. For normal curves, the S and E values are both zero. For tailed peaks, skewness values are positive and conversely for fronted peaks; excess values are positive when the peak is more tall and slim than the normal curve and conversely in the opposite case. Detailed expressions for $Q_v(-Z)$ terms and cumulant coefficients are reported elsewhere [15,23].

The remainder, $R_K(x)$, is a function showing a structured behaviour: *e.g.*, the number of nodes increases as the K-grade rises, and this is almost symmetrical with respect to $x = 0$. The residual function is practically expressed as a percentage difference, $D\%$, between experimental (YE) and calculated E.C. series expansion (YC) peak data. This is defined *versus* the normalized time variable, x, as follows:

$$[D\%(x)]_K = [YE(x) - YC_K(x)] \cdot 100/YMAX \tag{8}$$

Using a non-linear least-squares fitting procedure, an unbiased estimate of statistical peak parameters (area A, mean m, variance σ^2, skewness S, excess E and other cumulant coefficients: γ_3, γ_4, etc.) is made with satisfactory precision [15,16]. Fitting can be evaluated by the mean approximation error, $CV\%$, which is the coefficient of variation of the fitting at the peak maximum in percent [15]:

$$(CV\%)_K = [\sum_{i=1}^{N_p} (YE - YC_K)_i^2/(N_p - n_p - 1)]^{1/2} \cdot (100/YMAX) \tag{9}$$

where N_p and n_p are the number of points and the number of parameters, respectively. The approximation degree of a peak can also be estimated by the approximation-to-noise ratio (ANR) parameter, defined as

$$ANR_K = [\sum_{i=1}^{N_p} (YE - YC_K)_i^2/(N_p - n_p - 1)]^{1/2}/N_{RMS} \tag{10}$$

where N_{RMS} is the root-mean-square noise defined by eqn. 1. As residuals include the non-fitting of the E.C. series and the system noise [15,23], $ANR = 1$ only when fitting residuals are exactly consistent with noise. High ANR values suggest that incomplete fitting makes a contribution within residuals.

On increasing the series expansion order, the peak approximation improves (lower $CV\%$ values) up to a maximum level, depending on the peak shape (skewness) and the signal-to-noise ratio [17]. It has been proved that, under linear chromatographic conditions, E.C. series fitting is able to approximate peaks in a skewness range from 0.03 up to 0.8 with $CV\%$ values ranging between 0.002% and 1% [17].

In the E.C. series fitting pattern, four rules are to be considered when evaluating the goodness of a fit:

(1) for peaks with skewness values <0.8, there must be consistency between maximum expansion order (K_{max}), noise values and skewness values; K_{max} increases with increasing S and noise [17];

(2) under best-fit conditions, the residual values must be consistent with the intrinsic noise level, as reported previously [17]; the residual analysis provides information about the IC system noise;

(3) the statistical parameters (A, m, σ^2, S, E, γ_3, γ_4, ...) calculated by fitting are almost stable when K is increased to its optimum value and, further, they do not depend on solute concentration [18];

(4) for very skewed peaks ($S > 0.8$), an increase in expansion order K, even over 3–4, does not decrease the $CV\%$ value, nor does it improve fitting; under these conditions the peak parameter values obtained from the fitting are meaningless [17].

The simultaneous consistency of the general features mentioned above is a necessary condition for a linear non-ideal chromatographic process. A breakdown of these conditions when the amount injected is increased usually signifies the onset of non-linearity effects. Such behaviour has been demonstrated for both theoretically generated peaks [17] and different experimental systems such as gas chromatographic packed and capillary columns [18,24] and also field flow fractionation peaks [25]. Graphic peak-shape analysis is also useful in checking non-linearity effects [24,26]. In fact, the peak shape, and statistical peak parameters, must remain the same as concentration is increased until the chromatographic process reaches non-linear conditions.

Fourier analysis is a well known procedure for analysing the frequency components of waveforms, not necessarily periodic, such as chromatographic peaks. By converting the time domain (t) signal to its frequency (ν) counterpart, a chromatographic signal has its own unique frequency spectrum where peak information is usually at lower frequencies than the noise components [19]. In the frequency domain noise frequencies can thus be removed by using a digital low-pass filter [27,28].

Various methods have been considered for determining the appropriate cut-off frequency. The first, suggested by Maldacker *et al.* [29], takes as the cut-off frequency the point at which the Fourier power spectrum amplitude, $F^2(\nu)$ [27], drops to less than 0.1% of the maximum. The second method involves the concept of the equivalent width time (EWT) [22]. This quantity is calculated from area A and height $YMAX$ of the peak to be filtered as follows:

$$EWT = A/YMAX \tag{11}$$

The cut-off frequency is the reciprocal of the EWT parameter as described by Lam and Isenhour [30]. The last method, applied by Bush [31], takes as the cut-off frequency the point at which the standard deviation of the Fourier power spectrum amplitudes, computed from higher to lower noise components, remains constant.

The filtering performance of these methods was evaluated by computing the root-mean-square (RMS_F) difference between experimental (YE) and filtered (YF) signals as follows:

$$RMS_F = [\sum_{i=1}^{N_p} (YE - YF)_i^2/(N_p - 1)]^{1/2} \quad (12)$$

RESULTS AND DISCUSSION

Linear range determination by peak-shape analysis

Ion chromatographic peaks, here collected and analysed under different experimental conditions, are the outputs of a complex ion trace analysis apparatus which includes the following steps: preconcentration, stripping and injection, separation and detection. For a critical evaluation of the overall linearity of this analytical procedure, the E.C. series fitting method provides two key tools: peak parameters and peak shapes.

Table II reports the numerical results of peak-shape analysis for sodium, chloride and sulphate ions under different concentrations. The statistical peak parameters, signal-to-noise ratio (S/N), coefficient of variation of the fitting ($CV\%$) and approximation-to-noise ratio (ANR) are listed for the series expansion order of the best fitting (K_{max}).

The S/N values at which different peaks were recorded increased with increase in concentration, as expected since noise is approximately constant whereas the signal increases as the amount analysed is increased. In contrast the approximation degree of the E.C. series fitting ($CV\%$) does not improve at the same rate. In particular for Cl^- and SO_4^{2-}, it worsens as the concentration increases. ANR expresses more clearly the progressive inability of the E.C. series to approximate Cl^- and SO_4^{2-} peaks at

TABLE II

PEAK PARAMETERS BY THE E.C. SERIES FITTING METHOD

Parameters: c = analysed concentration; σ^2 = variance; S = skewness; E = excess; K_{max} = optimum E.C. series expansion order; S/N = signal-to-noise ratio; $CV\%$ = fitting coefficient of variation (%); ANR = approximation-to-noise ratio.

Ion	c(ppb)	$\sigma^2(s^2)$	S	E	K_{max}	S/N	$CV\%$	ANR
Na^+	11.5	301	0.31	0.78	6	108	0.58	2.5
	113.5	317	0.19	0.63	4	1050	0.22	9.3
	225.5	323	0.24	0.74	6	1350	0.28	15
Cl^-	10.2	121	0.46	0.55	4	374	0.19	2.8
	10.2	126	0.52	0.85	6	318	0.34	4.3
	100.5	136	0.73	1.61	5	2190	0.72	63
	200.0	127	0.78	1.75	5	4180	0.93	156
SO_4^{2-}	10.2	1480	0.26	0.31	6	68	0.49	1.3
	100.5	1508	0.68	0.82	6	480	0.28	5.4
	200.0	1644	0.71	1.73	5	1495	0.72	43

increasing concentrations. In fact, this quantity is very low for Cl^- only at 10.2 ppb and for SO_4^{2-} only at 10.2 and 100.5 ppb (see Table II).

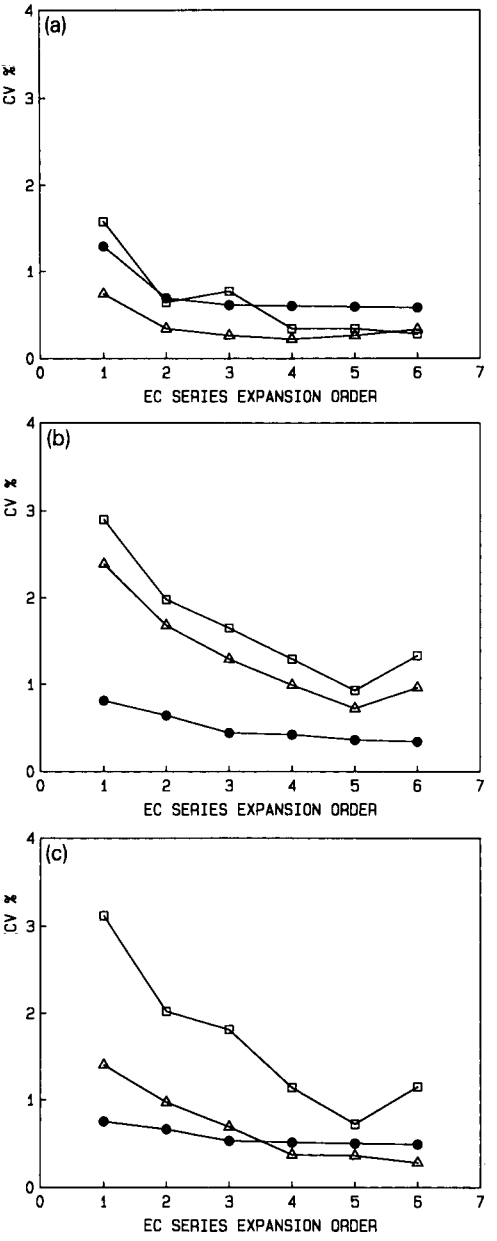

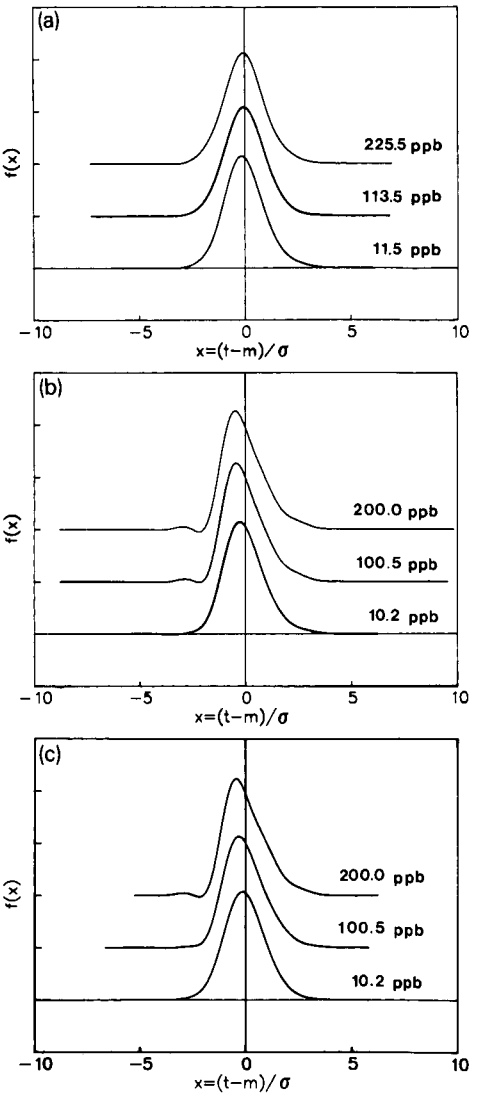

Fig. 1. Fitting coefficient of variation (*CV*%) *vs.* E.C. series expansion order at different concentrations: (a) sodium (● = 11.5 ppb; △ = 113.5 ppb; □ = 225.5 ppb); (b) chloride (● = 10.2 ppb; △ = 100.5 ppb; □ = 200.0 ppb); (c) sulphate (● = 10.2 ppb; △ = 100.5 ppb; □ = 200.0 ppb).

Fig. 2. Normalized fitted peaks *vs.* the normalized time variable (x) at different concentrations: (a) sodium; (b) chloride; (c) sulphate.

Let us now analyse in detail the E.C. fitting patterns as the series expansion order increases. In Fig. 1, the $CV\%$ for the ions considered at different concentrations is plotted against expansion order K. It can be observed that the best fitting conditions are soon obtained for all the Na^+ concentration values, even with E.C. series expansion order $K \approx 2$. A further expansion of the series only slightly improves the degree of approximation. In contrast, Cl^- behaves as Na^+ at the lowest concentration, whereas at higher values (100.5 and 200 ppb), the fitting minimum is found only when the expansion order has reached a value of 5. Sulphate behaves like chloride.

The skewness and excess parameters behave similarly to $CV\%$: with Na^+ these parameters are independent of both concentration and E.C. series expansion order, whereas for Cl^- and SO_4^{2-} this does not hold true except at concentrations lower than 10.2 ppb.

In order to establish exactly to what extent the fitting pattern is or is not congruent with the intrinsic properties of the E.C. series, and thus to check non-linear behaviour, reference can be made to the simulation study cases analysed elsewhere [17]. Peaks generated by theoretical peak-shape functions in linear chromatography and having skewness values comparable to those encountered here, should be approximated with a $CV\%$ value lower than 0.3%. This behaviour is obeyed by Na^+ at all the concentrations considered, whereas Cl^- and SO_4^{2-} have this property only at the lowest concentration analysed (10.2 ppb). E.C. series, applied to fit Cl^- and SO_4^{2-} peaks at higher concentrations, behave as a fitting function without precise meaning.

Graphic peak-shape analysis pictorially represents the previously described evidence. In Fig. 2 a comparison of fitted peaks, normalized at unit area, at different concentrations is shown for the ions considered. Whereas the sodium peak shape remains the same, the peaks of both anions do not maintain the same shape with respect to concentration.

The inability of the E.C. series to approximate non-linear cases is even clearly seen in the oscillatory nature of the fitting residual function, $D\%$, shown in Fig. 3. Note also that in the cases which were recognized as "linear", the degree of fitting is not only good but also homogeneous over the whole peak and with a large number of nodes, as expected from the properties of E.C. series [15]. This does not hold true in those cases of non-linearity.

It can be observed at this point that it is the oscillatory behaviour of the E.C. series which prevents the residual from being identical with the noise, even under the best approximation conditions (see the Na^+ case). Thus the ANR values reached (ranging between 2 and 15; see Table II: Na^+ cases, Cl^- at 10.2 ppb, SO_4^{2-} at 10.2 and 100 ppb) are to be considered as much more than acceptable.

From the results presented, it can be concluded that E.C. series peak-shape analysis is unambiguously able to detect linearity limits. The linearity limits determined here are identified as the highest concentration where the E.C. series is able to approximate the response peak shape coherently. Such values, 200 ppb for sodium and 10 ppb for chloride and sulphate, appear much lower when compared with linearity ranges reported elsewhere for IC with or without preconcentration.

Wetzel *et al.* [4] reported linear dynamic ranges of 10^4 for phosphate, nitrate and sulphate from 2 to 10^4 ppb and of 10^3 for chloride from 2 to 10^3 ppb; Haddad and Heckenberg [3] investigated the linearity for other anions (nitrite, nitrate and bromide) between 0 and 20 ppb. These values were determined using peak height or

area, which can be linear over a broader concentration range than that determined here, whereas the peak-shape analysis is a more sensitive approach and is much more stringent with respect to concentration effects than is either peak area or peak height.

Taking into account what has been reported elsewhere about linearity in IC [3,4,10–13], the origin of the non-linearity, detected here especially for Cl^- and SO_4^{2-}, cannot be ascribed to the separation column, but to other instrumental components of the considered IC system. A detailed investigation on the single band broadening and tailing contributions due to different extra-column effects is beyond the aims of this work.

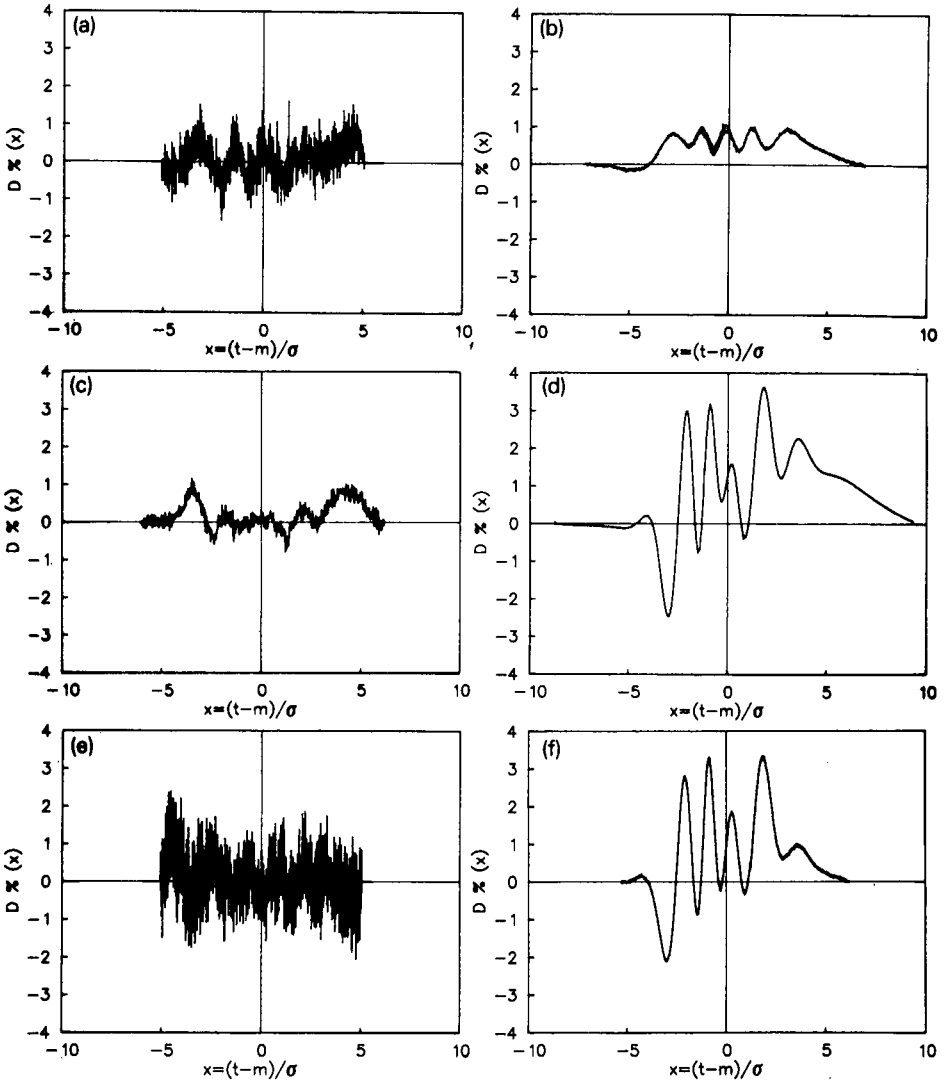

Fig. 3. Residuals of the best E.C. series fittings *vs.* the normalized time variable (x): (a) sodium, 11.5 ppb; (b) sodium, 225.5 ppb; (c) chloride, 10.2 ppb; (d) chloride, 200.0 ppb; (e) sulphate, 10.2 ppb; (f) sulphate, 200.0 ppb.

Noise analysis and quantification limits

As the chromatographic signal has been approximated at its best and a linear range is made evident, it can be assumed that this status also holds true at lower concentrations and that quantification limits are consequently determined by the existing noise. First information regarding system noise is included in the residual function $D\%$ by virtue of its peculiar properties. In fact, $D\%$ plots (Fig. 3) exhibit three different components: high-, intermediate- and low-frequency terms. The first

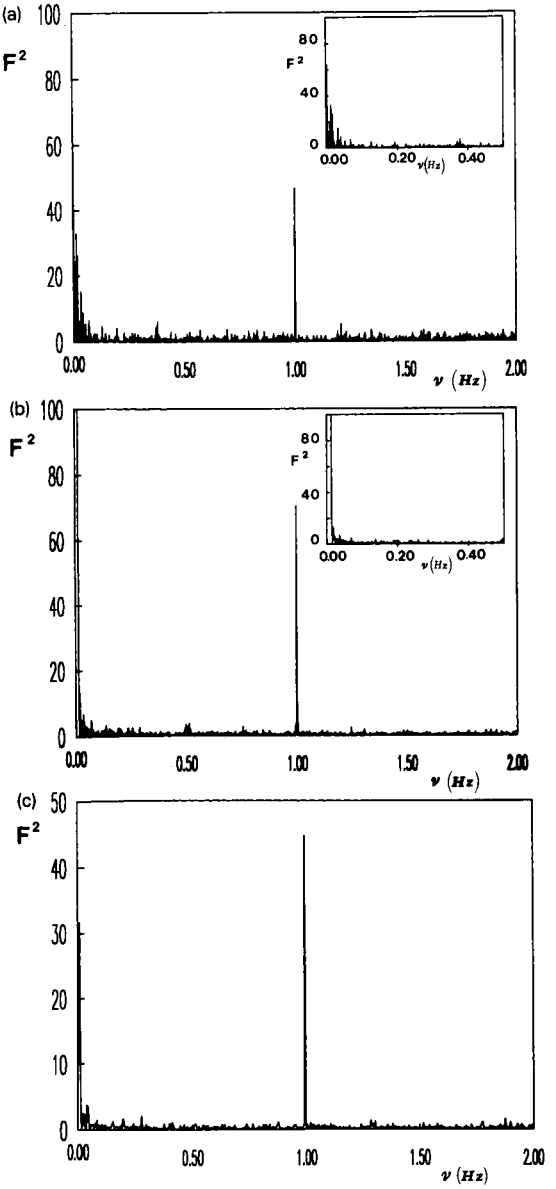

Fig. 4. Fourier power spectra of chromatographic signals: (a) baseline; (b) sulphate, 10.2 ppb; (c) its E.C. fitting $D\%$ residual.

TABLE III

QUANTIFICATION LIMITS IN ION CHROMATOGRAPHY WITH ON-LINE PRECONCENTRATION

Enrichment factor: 250 (anions); 125 (cations).

Ion	L_q (ppb)	
	Without FFT filtering	With FFT filtering
Na^+	0.5	0.030
Cl^-	0.1	0.007
SO_4^{2-}	1	0.080

two components can be explained as noise contributions. The last, however, arises from the kind of fitting considered (E.C. series) and becomes more evident when the signal-to-noise ratio rises and the other two components become negligible.

In order to characterize in detail the noise structure on the chromatographic signal, the fast Fourier transform procedure (FFT) was applied to the baseline, to peaks and also to residuals of the E.C. series fitting. Each chromatographic signal is described by its power spectrum in the frequency domain.

Fig. 4 shows the power spectra of (a) the baseline, (b) an SO_4^{2-} peak at 10.2 ppb and (c) the corresponding E.C. fitting D% residual. The peak frequency components (peak information) are located at the lowest frequencies whereas noise components spread at higher frequencies. The last correspond in all spectra to the white type of noise. The sharp noise component present at 1 Hz is related to the eluent pumping system of the kind of chromatograph used; it is present in all power spectra and proves to represent a deterministic noise component.

The precision level having been set, the quantification limit can be obtained by defining it as the concentration that provides a certain signal multiple of the noise (see eqn. 3). Several quantification limits can be defined in this manner, depending on what is taken as the noise. In the present instance the noise component at 1 Hz, clearly deterministic, is far from the low-frequency signal components and can easily be eliminated. In order to reduce noise appropriately, the use of a low-pass filter in the

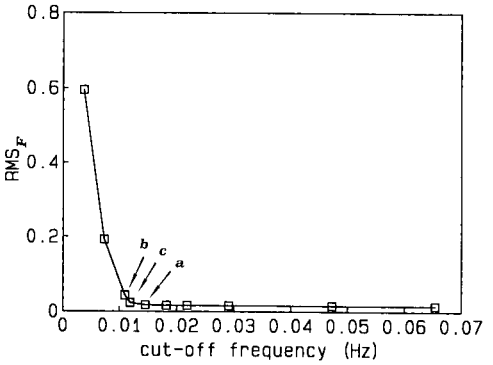

Fig. 5. Root mean square difference (RMS_F) between original and filtered signals *vs.* cut-off frequency: sulphate peak, 10.2 ppb; (a) 0.1% of power spectrum maximum criterion; (b) *EWT* criterion; (c) constant power spectrum amplitude standard deviation criterion.

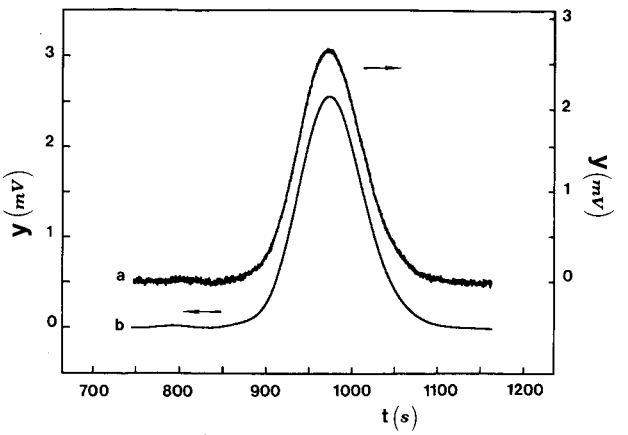

Fig. 6. Filtering: sulphate peak, 10.2 ppb; cut-off frequency 0.015 Hz: (a) original peak; (b) filtered peak.

frequency domain is considered. To select the optimum cut-off frequency, the three different criteria described under Theory and Procedure were applied [(a) power spectrum amplitude $<0.1\%$ of the maximum; (b) reciprocal to the *EWT* parameter; (c) constant standard deviation of the power spectrum amplitudes].

In Fig. 5, the RMS_F difference between the original and filtered peaks *vs.* the cut-off frequency is plotted for an SO_4^{2-} peak at 10.2 ppb and the three criteria labelled as a, b and c are shown. It can be seen that the cut-off graphically determined according to criterion c provides the lowest RMS_F value among the three methods applied. At the same time this filtering is satisfactory as it preserves the original peak shape, as can be seen in Fig. 6 where the original and filtered sulphate peaks are shown. By this filtering procedure, the signal-to-noise ratio is obviously enhanced and it has been estimated that it can be improved at least 20-fold. Under the latter safe condition, allowance is also made for a limited signal drift. On this basis two hypotheses of quantification limits are reported in Table III. The first is computed according to eqn. 3 and the second is a value enhanced 20-fold if the filtering procedure is employed. It can be seen that the quantification limits determined by this approach appear significantly lower than those obtained by linear calibration plots [14].

CONCLUSIONS

IC with a preconcentration step appears to be a very sensitive method for ultra-trace ion determinations. The peak-shape analysis, employed here to check anomalous concentration-dependent behaviours, even minimal, in the overall analytical system, proved to be a powerful tool in determining the correct linearity range, in order to plan the routine use of the IC technique, *e.g.*, in ultra-trace ion monitoring in power plant "condensate–feed water" cycle already described [14].

ACKNOWLEDGEMENTS

This work was supported by ENEL (Central Electricity Generating Board of Italy) in collaboration with the Research and Development Division, Thermal and Nuclear Research Centre, and by the Italian Ministry of Research and University (MURST).

REFERENCES

1 D. T. Gjerde and J. S. Fritz, *Ion Chromatography*, Hüthig, New York, 2nd ed., 1987.
2 F. C. Smith and R. C. Chang, *The Practice of Ion Chromatography*, Wiley-Interscience, New York, 1983.
3 P. R. Haddad and A. L. Heckenberg, *J. Chromatogr.*, 300 (1984) 357.
4 R. A. Wetzel, C. L. Anderson, H. Schleicher and G. D. Crook, *Anal. Chem.*, 51 (1979) 1532.
5 K. M. Roberts, D. T. Gjerde and J. S. Fritz, *Anal. Chem.*, 53 (1981) 1691.
6 P. R. Haddad and A. L. Heckenberg, *J. Chromatogr.*, 318 (1985) 279.
7 A. L. Heckenberg and P. R. Haddad, *J. Chromatogr.*, 330 (1985) 95.
8 D. C. Gan and J. G. Tarter, *J. Chromatogr.*, 404 (1987) 285.
9 J. P. Foley and J. G. Dorsey, *Chromatographia*, 18 (1984) 503.
10 J. A. Mosko, *Anal. Chem.*, 56 (1984) 629.
11 C. A. Pohl and E. L. Johnson, *J. Chromatogr. Sci.*, 18 (1980) 442.
12 T. Okada and T. Kuwamoto, *J. Chromatogr.*, 350 (1985) 317.
13 L. N. Polite, H. McNair and R. D. Rocklin, *J. Liq. Chromatogr.*, 10 (1987) 829.
14 L. Balconi, R. Pascali and F. Sigon, *Anal. Chim. Acta*, 179 (1986) 419.
15 F. Dondi, A. Betti, G. Blo and C. Bighi, *Anal. Chem.*, 53 (1981) 496.
16 F. Dondi, *Anal. Chem.*, 54 (1982) 473.
17 F. Dondi and F. Pulidori, *J. Chromatogr.*, 284 (1984) 293.
18 F. Dondi and M. Remelli, *J. Chromatogr.*, 315 (1984) 67.
19 R. Annino, *Adv. Chromatogr.*, 15 (1977) 33.
20 *IBM Application Program—System/360 Scientific Subroutine Package (360A–CM–03X), Version III, Programmer's Manual*, IBM Technological Publications, White Plains, NY, 4th ed., 1968.
21 D. L. Massart, B. G. M. Vandeginste, S. N. Deming, Y. Michotte and L. Kaufman, *Chemometrics. A Textbook*, Elsevier, Amsterdam, 1988.
22 R. M. Bracewell, *The Fourier Transform and Its Applications*, McGraw-Hill, New York, 2nd ed., 1986.
23 H. Cramér, *Mathematical Methods of Statistics*, Princeton University Press, Princeton, NJ, 7th ed., 1957, Ch. 17.
24 M. Remelli, G. Blo, F. Dondi, M. C. Vidal-Madjar and G. Guiochon, *Anal. Chem.*, 61 (1989) 1489.
25 P. Reschiglian, G. Blo and F. Dondi, *Anal. Chem.*, 63 (1991) 120.
26 J. L. Excoffier, A. Jaulmes, M. C. Vidal-Madjiar and G. Guiochon, *Anal. Chem.*, 54 (1982) 1941.
27 M. A. Sharaf, D. L. Illman and B. R. Kowalski, *Chemometrics*, Wiley-Interscience, New York, 1986.
28 T. Hevesi, J. Krupcik, E. Benicka, D. Repka and J. Garaj, *Trends Anal. Chem.*, 9 (1990) 132.
29 T. A. Maldacker, J. E. Davis and L. B. Rogers, *Anal. Chem.*, 46 (1974) 637.
30 R. B. Lam and T. L. Isenhour, *Anal. Chem.*, 53 (1981) 1179.
31 C. A. Bush, *Anal. Chem.*, 46 (1974) 890.

Journal of Chromatography, 556 (1991) 263–275
Elsevier Science Publishers B.V., Amsterdam

CHROM. 23 408

Investigation of the causes of reduced efficiency in micellar liquid chromatography

ALAIN BERTHOD*
Université Claude Bernard, Lyon 1, Laboratoire des Sciences Analytiques, UA CNRS 435 (J. M. Mermet), 69622 Villeurbanne Cedex (France)
MICHAEL F. BORGERDING
R. J. Reynolds Tobacco Company, Bowman Gray Technical Center, Winston-Salem, NC 27102 (USA)
and
WILLIE L. HINZE
Department of Chemistry, Wake Forest University, P.O. Box 7486, Winston-Salem, NC 27109 (USA)

ABSTRACT

Reduced chromatographic efficiency is a major drawback of micellar liquid chromatography (MLC). The Knox equation $h = Av^{1/3} + B/v + Cv$, was used to determine the individual contribution of the flow anisotropy (A term), molecular band broadening (B term) and mass transfer processes (C term) to the final band broadening. Knox plots of h, the reduced plate height, *versus* v, the reduced linear flow-rate, were determined on the same column (i) with an aqueous–organic mobile phase, (ii) with a micellar mobile phase and (iii) with the same aqueous–organic phase. The changes in the A, B and C terms are discussed. Two stationary phases were used: a classical C_{18} monomer phase and a densely grafted (3.5 μmol/m^2) C_{14} phase. Two micellar solutions were used: a non-ionic micellar solution of Brij 35 and an anionic solution of sodium dodecyl sulfate (SDS). Test solute diffusion coefficients were measured in each mobile phase used. The increase in A is mainly responsible for reduced MLC efficiency. However, the B and C terms also increased significantly with micellar solutions. It is shown that the observed changes in the Knox parameters can be explained by the change in the stationary phase produced by surfactant adsorption; 6% of the adsorbed SDS (0.14 μmol/m^2) was irreversibly adsorbed on the C_{14} phase whose initial efficiency could not be restored. Such a small amount of adsorbed surfactant was able to degrade completely the initial efficiency of the C_{14} stationary phase. A model explaining how that irreversible adsorption may occur with ionic long-chain surfactants and densely grafted stationary phases with long-chain ($>C_8$) bonding moieties is proposed.

INTRODUCTION

Since the inception of micellar liquid chromatography (MLC) by Armstrong and co-workers [1,2], the technique has been extensively studied to determine the advantages and disadvantages associated with the substitution of a surfactant, present at a concentration higher than the critical micellar concentration (CMC), for the typical organic solvent component of a classical LC mobile phase. Unique separation selectivities, enhanced detection modes and practical advantages such as non-toxicity, non-flammability, low cost or simplified waste disposal have been reported in several

0021-9673/91/$03.50

recent reviews of MLC [3–6]. A serious disadvantage, common to all MLC systems studied to date, however, has been reduced chromatographic efficiency. The significance of this deficiency is most apparent when viewed in the context of resolution: about 30–50% fewer components can be resolved per unit time with the chromatographic efficiencies typically observed in MLC, when compared to commonly used aqueous–organic mobile phases.

Several workers have addressed this problem. Dorsey *et al.* [7] showed that MLC chromatographic efficiency can be improved by the addition of 3% of *n*-propanol to the micellar mobile phase, which serves to overcome the postulated poor mobile phase wetting of the stationary phase. Yarmchuck *et al.* [8] suggested that reduced MLC efficiency is caused by slow solute exit rate from the micelle and the stationary phase which produces poor mass transfer between the bulk phases., They recommended the use of low mobile phase flow-rates, elevated operating temperatures and minimum surfactant concentrations.

Surfactant adsorption on the stationary phase was also suspected to have a major impact on the MLC efficiency. Surfactants were found to absorb on the stationary phase in amounts approximating that of the bonded hydrocarbon [9,10]. The increase in the film thickness of the stationary phase due to adsorbed surfactant was thought to be responsible for the decreased MLC efficiency [9,11,12]. It was shown that the efficiency improvement induced by addition of a short-chain alcohol was due to surfactant desorption out of the stationary phase [13]. Pentanol was the most efficient additive for efficiency improvement [14].

In this work, MLC efficiency was studied by applying a rate equation to determine the contributions to the final solute band width. The Knox equation has been widely used in liquid chromatography for this purpose [15,16]. It can be expressed as

$$h = Av^{1/3} + \frac{B}{v} + Cv \tag{1}$$

where A, B and C are the constants of the Knox equation, h is the reduced plate height calculated as $h = H/d_p$, where H is the column plate height ($H = L/N$, L being the column length and N the number of theoretical plates), d_p is the stationary phase particle diameter, v is the reduced mobile phase velocity, *i.e.*, $v = \mu d_p/D_m$ (μ being the mobile phase velocity in cm/s and D_m the solute diffusion coefficient in the mobile phase in cm^2/s).

The A, B and C terms of the Knox equation are related to the flow anisotropy, molecular longitudinal diffusion and mass transfer processes, respectively. These three terms were determined for the same column on the same chromatographic system with a reference aqueous–organic mobile phase and with a micellar phase. The variations of the A, B and C terms with micellar phases allow one to highlight changes attributable to a particular effect.

EXPERIMENTAL

Chromatographic system

Two systems were used. The first consisted of components from Waters Assoc. (Milford, MA, USA) *viz.* a Model M6000 A pump, Model 441 UV detector and

Model 720 system controller. The second system was constructed in the laboratory with a Shimadzu LC-5A pump, Rheodyne Model 7520 0.5-μl injection valve and Shimadzu SPD-6A UV detector (Touzard et Matignon, Paris, France). Two columns were used. A 10 cm × 5 mm I.D. Radial Pak cartridge (Waters Assoc.) packed with C_{18}, non-end-capped 10-μm particles was used with Brij 35 micellar solutions and an acetonitrile (ACN)–water (30:70, v/v) reference solution. The second column was a 15 cm × 4 mm I.D. column packed with a laboratory-grafted C_{14} phase with a maximum bonding density of the monomer type (particle diameter 5 μm, surface area 210 m^2/g, pore volume 0.45 ml/g, mean pore diameter 9 nm, carbon load 17.9% and C_{14} monomer bonding coverage 3.5 $\mu mol/m^2$ [17]). It was used with sodium dodecyl sulfate (SDS) micellar solutions and a methanol–water (70:30, v/v) reference solution.

Chemicals

Table I gives the physico-chemical properties of the two surfactants used. The non-ionic polyoxyethylene 23 dodecyl ether (Brij 35) was obtained from Sigma (St. Louis, MO, USA), SDS and methanol from Merck (Darmstadt, Germany), ACN and benzene from Burdick & Jackson (Muskegon, MI, USA), benzyl alcohol and benzaldehyde from Fisher Scientific (Raleigh, NC, USA) and toluene and ethyl-, propyl- and butylbenzene from Fluka (Buchs, Switzerland). Water was distilled, deionized and filtered with a Barnstead Nanopure system.

Determination of diffusion coefficient

Diffusion coefficients were determined using the Taylor dispersion technique [19], as described in recent papers [11,20]. Five replicate measurements were made in all instances.

Determination of the A, B and C terms of the Knox equation

Chromatograms were obtained with mobile phase flow-rates ranging from 0.1 to 1.6 ml/min with the 15-cm C_{14} column and from 0.4 to 3 ml/min with the 10-cm C_{18} column. All parameters were determined from digitally acquired data after cor-

TABLE I

PHYSICO-CHEMICAL PROPERTIES OF SURFACTANTS AND MICELLES

Data from refs. 4 and 18.

Surfactant	Molecular weight (g/mol)	CMC[a]		Micelle		
		mol/l	ppm	Radius (nm)	Aggregation No.	V^b (l/mol)
SDS ($C_{12}H_{25}SO_3^-Na^+$)	288.4	$8.2 \cdot 10^{-3}$	2360	2.6	62	0.246
Brij 22 [$C_{12}H_{25}(OCH_2CH_2)_{10}OH$]	626	$8 \cdot 10^{-5}$	50	2.8	97	0.6
Brij 35 [$C_{12}H_{25}(OCH_2CH_2)_{25}OH$]	1200	$9 \cdot 10^{-5}$	108	2.6	40	1.07

[a] Critical micellar concentration.

[b] Micellar molar volume.

recting for extra-column contributions as described [20]. The number of theoretical plates, N, was calculated by use of the inflection point method:

$$N_{0.6h} = 4\left(\frac{t_r}{W_{0.6h}}\right)^2 \tag{2}$$

the method derived by Foley and Dorsey [21]

$$N_{0.1h} = 41.7 \cdot \frac{(t_r/W_{0.1h})^2}{(b/a) + 1.25} \tag{3}$$

or by the moment method:

$$N_{\text{moment}} = \frac{M_1^2}{M_2} \tag{4}$$

where t_r is the retention time, W_{xh} is the peak width, expressed in time units, and measured at proportion x of the peak height, h, a and b refer to the $0.1h$ peak width and the retention time [21] with $a+b=W_{0.1h}$. M_i is the ith moment: M_o is the peak area defined as

$$M_0 = \int C(t)\,dt \tag{5}$$

where $C(t)$ is the detector signal at time t,

$$M_1 = \frac{1}{M_0}\int t\,C(t)\,dt \tag{6}$$

is the first reduced moment corresponding to the peak retention time [22] and

$$M_2 = \frac{1}{M_0}\int (t - M_1)^2\,C(t)\,dt \tag{7}$$

is the second central reduced moment corresponding to the peak variance.

The efficiency measurement method employed may significantly affect the Knox parameters, as pointed out recently [23]. In this work, the moment method was most often employed. Each plate count value, obtained using the moment method, was double-checked using the Foley–Dorsey equation [24]. In one instance (C_{14} column and methanol–water mobile phase, after SDS exposure), the peak tailings were so large that the computer could not find the peak terminations. In that case, the inflection point method was used for efficiency measurements. The A, B and C terms of the Knox equation were determined using a computer fitting method [24]. The uncertainty margin that can be as high as $\pm 50\%$ of a fitted value for tailing peaks is always given in parentheses after every Knox parameter listed.

RESULTS AND DISCUSSION

Solute diffusion in micellar solutions

Molecular diffusion is the predominant plate height contribution at low mobile phase velocities [20,25]. This parameter, D_m, is essential in the calculation of v ($v = \mu d_p / D_m$). It was directly determined in the different micellar phases and in the reference aqueous–organic phases. Table II lists the diffusion coefficients obtained by

TABLE II

DIFFUSION COEFFICIENTS IN VARIOUS MOBILE PHASES AT 24°C

Micellar phases

Solute	Micellar partition coefficient[a]	Diffusion coefficient ($\times 10^6$ cm^2/s)
Brij 22, (5%, w/v; 8·10^{-2} mol/l)		
Benzyl alcohol	1600 ± 200	5.1 ± 0.1
Benzaldehyde	2100 ± 300	4.7 ± 0.1
Benzene	7000 ± 800	2.88 ± 0.01
Micelle	–	0.87[b]
Brij 35, (5%, w/v; 4.2·10^{-2} mol/l)		
Benzyl alcohol	400 ± 40	6.3 ± 0.1
Benzaldehyde	640 ± 50	5.5 ± 0.1
Benzene	1800 ± 200	4.4 ± 0.2
Micelle	–	0.94[b]
SDS, (1.4%, w/v; 5·10^{-2} mol/l)		
Benzene	4800 ± 500	6.8 ± 0.3
Toluene	15 000 ± 1000	3.4 ± 0.2
Ethylbenzene	43 000 ± 3000	1.7 ± 0.1
Propylbenzene	120 000 ± 10 000	0.94 ± 0.08
Butylbenzene	340 000 ± 40 000	0.68 ± 0.07
SDS micelle	–	0.57[c]

Hydro-organic mobile phases

Solute	Diffusion coefficient ($\times 10^6$ cm^2/s)		
	Water[d]	ACN–water (30:70, v/v)	Methanol–water (70:3, v/v)
Benzene	11.2 ± 0.7	11.4 ± 0.1	8.65 ± 0.06
Toluene	10.5 ± 0.7	–	8.0 ± 0.05
Ethylbenzene	9.9 ± 0.7	–	7.4 ± 0.05
Propylbenzene	8.4 ± 0.6	–	6.5 ± 0.05
Butylbenzene	7.0 ± 0.5	–	5.5 ± 0.05
Benzyl alcohol	8.7 ± 0.4	9.6 ± 0.4	–
Benzaldehyde	8.9 ± 0.3	10.08 ± 0.03	–

[a] Data from refs. 9, 12, 14, 26, 27.
[b] Calculated from the Stokes-Einstein equation using the micelle radii given in Table I.
[c] From ref. 11.
[d] Calculated using eqn. 9 in ref. 11.

the Taylor dispersion technique. Measurements were done in SDS, Brij 35 and Brij 22 solutions. The last surfactant was not utilized for efficiency comparison in this work but it will be used in future work.

As demonstrated previously [11], the inclusion of a solute in a micelle produces a significant decrease in its diffusion coefficient, D_m. The equation expressing D_m as a function of D_{mic} and D_{aq}, the diffusion coeffcient of the micelle and the solute diffusion coefficient in water, respectively, is [11]

$$D_m = \frac{D_{mic}}{1 + \Psi} + \frac{D_{aq}}{1 + \frac{1}{\Psi}} \tag{8}$$

where

$$\Psi = \frac{N(1 - CV)}{PCV} \tag{9}$$

N is the micellar aggregation number, C is the surfactant concentration in the micelle, *i.e.*, the total surfactant concentration minus the CMC, and V is the surfactant micellar molar volume. N, CMC and V values are listed in Table I. The diffusion coefficients, D_{aq}, in water without micelles were calculated from the experimental D_m values obtained in the three different micellar solutions. They are in close agreement, within $\pm 5\%$. For example, the benzene D_{aq} values calculated from the D_m values in Brij 22, Brij 35 and SDS solutions at 25°C were $1.02 \cdot 10^{-5}$, $1.17 \cdot 10^{-5}$ and $1.18 \cdot 10^{-5}$ cm^2/s, respectively.

A, B and C Knox parameters

Fig. 1 shows the theoretical contributions of each term for a "good" column ($A = 1$, $B = 2$, $C = 0.035$). As already stated, the B term, related to molecular diffusion, is the predominant plate height contribution at low reduced velocities ($v < 2$). The stationary phase mass transfer processes (C term), in contrast, become increasingly

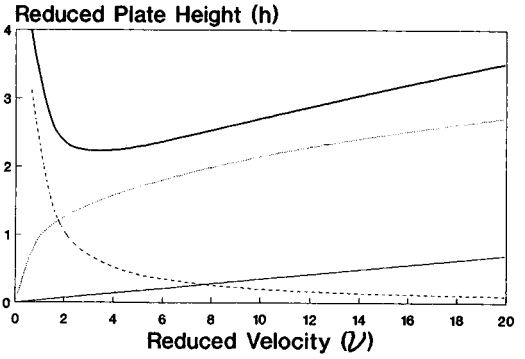

Fig. 1. Theoretical h *versus* v plot for a good column. Dotted line: flow anisotropy contribution, $Av^{1/3}$, with $A = 1$. Dashed line: longitudinal molecular diffusion contribution, B/v, with $B = 2$. Full line: mass transfer contribution, Cv, with $C = 0.035$. Bold line: the Knox plot, sum of the three contributions.

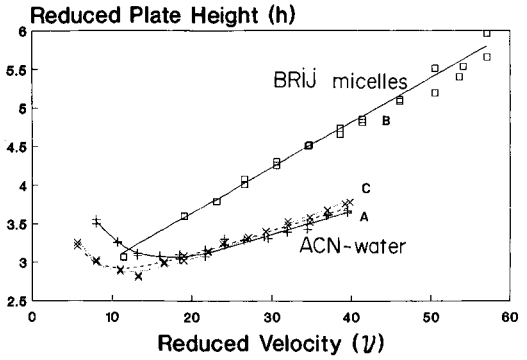

Fig. 2. Knox plots with a C_{18} column and the solute benzene. (A) +, ACN–water (30:70, v/v) on the new column; $A = 0.65$, $B = 16.4$, $C = 0.026$. (B) □, Brij 35 (5%, w/v) mobile phase; $A = 1.0$, $B = 6$, $C = 0.03$. (C) ×, ACN–water (30:70, v/v) after Brij exposure. Dotted line: $A = 0.75$, $B = 10.2$, $C = 0.025$. Dashed line: $A = 0.91$, $B = 8.6$, $C = 0.10$.

significant as the reduced velocity increases. The flow anisotropy (A term) contributes to *ca.* 50% or more of the plate height at all reduced flow velocities greater than 2.

Fig. 2 shows the reduced plate height *versus* reduced efficiency for the solute benzene on the 10 cm × 5 mm I.D. C_{18} column with (A) ACN–water (30:70, v/v) on the new column, (B) a 5% (w/v) Brij 35 mobile phase and (C) ACN–water (30:70, v/v) again after a column wash with the aqueous–organic mobile phase. Fig. 3 shows the same set of h *versus* ν plots on the 15 cm × 4 mm I.D. C_{14} column: (A) with methanol–water (70:30, v/v) on the new column, (B) with 1.4% (w/w) SDS (0.05 M), (C) with methanol–water (70:30, v/v) after a column wash with methanol. Table III lists the capacity factors and A, B and C terms of the Knox equation obtained with the different mobile phases using the fitting procedure described in ref. 24. The uncertainty margin, indicated with every fitted term, is illustrated in Fig. 2C. Table III lists the parameters $A = 0.83 \pm 0.08$, $B = 9.4 \pm 0.8$, $C = 0.017 \pm 0.007$. The dotted line in Fig. 2 is the theoretical Knox plot with $A = 0.75$, $B = 10.2$ and $C = 0.025$, which are the

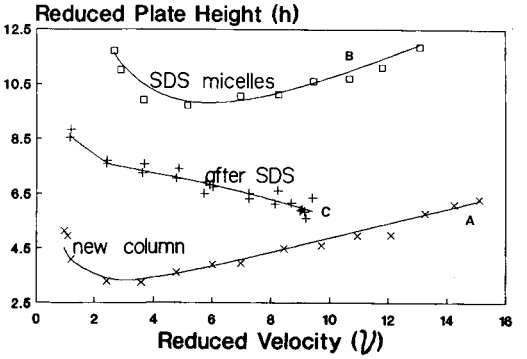

Fig. 3. Knox plots with a C_{14} column and the solute benzene. (A) ×, methanol–water (70:30, v/v) on the new column; $A = 1.1$, $B = 3.1$, $C = 0.22$. (B) □, SDS (1.4%, w/v) mobile phase; $A = 3.2$, $B = 20$, $C = 0.20$. (C) +, methanol–water (70:30, v/v) after SDS exposure; $A = 0.70$, $B = 5.7$, $C = -0.7$.

TABLE III

PARAMETERS OF THE KNOX EQUATION WITH DIFFERENT MOBILE PHASES

Mobile phase	Solute	k'	A	B	C
Acetonitrile–water (30:70, v/v)	Benzyl alcohol	2.2	1.4 ± 0.1	2.5 ± 0.6	0.029 ± 0.009
	Benzaldehyde	6.6	1.0 ± 0.04	10 ± 0.5	0.027 ± 0.004
	Benzene	17.3	0.65 ± 0.03	16.4 ± 0.6	0.026 ± 0.004
Water–Brij 35 (5%, w/v)	Benzyl alcohol	4.5	1.3 ± 0.15	10 ± 3	0.15 ± 0.03
	Benzaldehyde	11.0	1.4 ± 0.15	8 ± 2.5	0.04 ± 0.015
	Benzene	26.1	1.0 ± 0.12	6 ± 2	0.03 ± 0.01
Acetonitrile–water (30:70, v/v) after Brij exposure	Benzyl alcohol	1.9	1.3 ± 0.1	11.2 ± 1.1	0.08 ± 0.02
	Benzaldehyde	5.2	1.0 ± 0.1	10.8 ± 0.9	0.04 ± 0.01
	Benzene	15.2	0.83 ± 0.08	9.4 ± 0.8	0.017 ± 0.007
Methanol–water (70:30, v/v)	Benzene	1.1	1.1 ± 0.15	3.1 ± 0.2	0.22 ± 0.02
	Toluene	2.1	1.05 ± 0.15	3.5 ± 0.2	0.16 ± 0.02
	Ethylbenzene	3.5	1.1 ± 0.15	3.8 ± 0.4	0.15 ± 0.02
	Propylbenzene	6.0	1.3 ± 0.15	5.0 ± 0.4	0.09 ± 0.02
Water–SDS (1.4%, v/v)	Benzene	15.6	3.2 ± 0.6	20 ± 5	0.2 ± 0.1
	Toluene	29.0	3.0 ± 0.7	25 ± 6	0.5 ± 0.2
	Ethylbenzene	45.0	3.1 ± 0.7	23 ± 6	0.5 ± 0.2
	Propylbenzene	60.5	3.0 ± 0.7	20 ± 6	0.7 ± 0.3
Methanol–water (70:30, v/v) after SDS exposure	Benzene	0.70	5.7 ± 0.3	4 ± 0.4	−0.7 ± 0.1
	Toluene	1.47	5.2 ± 0.3	4.2 ± 0.4	−0.64 ± 0.08
	Ethylbenzene	2.54	4.6 ± 0.2	4.4 ± 0.5	−0.54 ± 0.06
	Propylbenzene	4.54	4.0 ± 0.2	4.7 ± 0.6	−0.42 ± 0.05

minimum A value and the maximum B and C values. The dashed line is the theoretical Knox plot with the maximum A value ($A=0.91$) and the minimum B and C values ($B=8.6$, $C=0.01$). Both lines fit the experimental set of points within the error margins. This illustrates that the Knox equation must be used with care to obtain information on band broadening contributions. For the same set of experimental points, the maximum C value ($C=0.025$) is 2.5 times greater than the minimum C value ($C=0.01$). As pointed out [24], the uncertainty in the B adjustment can be very high when the h *versus* v plot does not present a minimum. This was often the case with micellar solutions and explains the high error margins in the parameters obtained with micellar mobile phases. As will be discussed later, the validity of the use of the Knox equation with micelle-exposed columns may be questioned [26].

A term. The A term depends on flow anisotropy. The A term for benzene was 0.65 in an ACN–water mobile phase and 1.0 in the Brij 35 micellar mobile phase, *i.e.*, 40% higher. At a reduced velocity $v=20$, the reduced plate height was $h=3.10$ with the ACN–water phase and $h=3.62$ with the Brij 35 micellar phase (Fig. 2). The A contribution, *i.e.*, $Av^{1/3}$, was 1.76 (56% of the whole band broadening) and 2.71 (75%) with the ACN–water and the Brij 35 micellar phase, respectively. The 40% increase in A is the main factor responsible for micellar efficiency loss. A threefold increase in A induced by the SDS micellar phase was observed for the four alkylbenzenes studied. For benzene, at a reduced velocity $v=10$, the reduced plate height was $h=4.9$ with the methanol–water phase and $h=10.9$ with the SDS micellar phase (Fig. 3). The A contribution was 2.36 (48%) and 6.9 (63%) with the methanol–water and the SDS micellar phase, respectively. Again, the increase in A was the main factor responsible for micellar efficiency loss.

In only one case, propylbenzene and C_{14} phase, the micellar efficiency loss was due to both A and C increases. The A value for propylbenzene was 1.3 in methanol–water and 3.0 in SDS. The corresponding C values were 0.09 and 0.7, respectively (Table III). At a reduced velocity $v=10$, the reduced plate height was $h=4.2$ with the methanol–water phase and 15.5 with the SDS phase. The A contribution was 2.8 (66%) and 6.5 (only 42%) with the methanol–water phase and the SDS micellar mobile phase, respectively. The C contribution, *i.e.*, Cv, increased from 0.9 (22%) to 7 (45%). The particular case of propylbenzene is discussed further below.

It seems that the presence of micelles and the surfactant-induced stationary phase modifications significantly increase the flow anisotropy. The surfactant adsorbed layer may change the column porosity and permeability [12,26]. This point will be discussed later.

B term. According to Giddings [25], the B term can be written as

$$B = 2\left[\gamma_m + \gamma_s\left(\frac{D_s}{D_m}\right)k'\right] \tag{10}$$

where γ_m and γ_s are the obstruction factors for diffusion through granular and/or porous materials. Subscripts m and s refer to the mobile and stationary phase, respectively. The D terms are the solute diffusion coefficient in the mobile (m) and stationary (s) phase, and k' is the solute capacity factor.

B is related to band broadening due to molecular diffusion. The lowering of the

solute diffusion coefficient produced by micellar inclusion (Table II) should cause an increase in the B term. This was the case for all solutes studied, except for the benzene and Brij 35 system, where a decrease in the B term was observed. As shown by Khaledi [28], the relative eluent strength of micellar mobile phase is much lower than that of aqueous–organic phases. In this study, the capacity factors obtained with micellar phases were always higher than the corresponding values obtained with aqueous–organic phases and the same stationary phase. The k' value for benzene was 17.3 with the ACN–water mobile phase and 26.1 with the Brij 35 mobile phase. As the B term decreased from 16.4 to 6, this means that the D_s/D_m ratio was drastically reduced (eqn. 10). The B value obtained with SDS solutions were *ca.* 20 (Table III) with no increase as the capacity factors increased from 15.6 (benzene) to 60.5 (propylbenzene). Given the D_m values listed in Table II, it can be estimated than the D_s values became lower as the hydrophobic character of the solute increased. This observation supports the solubility limit theory proposed by Borgerding and co-workers [27,29]. Very hydrophobic solutes are directly transferred from the micelle interior to the stationary phase organic layer. They do not and cannot go into the aqueous phase because their water solubility is too low. The solute diffusion in the surfactant-modified stationary phase is very restricted.

C term. The C term of the Knox equation represents the mass transfer contribution to solute band broadening. It was written as [25]

$$C = q\left(\frac{k' + \varphi}{1 + k'}\right)^2 \left(\frac{D_m}{\gamma_{sm}\varphi D_m + k'\gamma_s D_s}\right) \tag{11}$$

where the γ terms are obstruction factors, the subscripts s, m and sm represent the mobile, stationary and pore stagnant mobile phase, respectively, φ is the stagnant mobile phase fraction and q is a geometrical factor dependent on porosity [25].

The micellar mobile phase induced an increase in the C term that was as high as 700%, as already noted (propylbenzene and SDS phase). The reduced mass transfer induced by micellar phases was attributed to poor wetting of the stationary phase [5,7] or to surfactant adsorption [9–11,13,26,27] on the stationary phase. This latter point is the most important and warrants further discussion.

Surfactant adsorption

The decrease in efficiency caused by micellar mobile phases is revealed by increases in the three terms of the Knox equation. Micellar mobile phases seem to increase the flow anisotropy, which increases the A term, and to decrease drastically the solute diffusion coefficients in both the stationary and mobile phases, which increases the B and C terms. Both effects can be explained by surfactant adsorption. It was demonstrated by Berthod *et al.* [30] that the important differences between a C_1, C_8, C_{18} or CN bonded stationary phase were reduced in micellar chromatography. All of the surfactant-covered phases behaved similarly.

The surfactant adsorption was *ca.* 70 mg of Brij 35 per gram of C_{18} stationary phase and 140 mg of SDS per gram of C_{14} phase or 2.3 μmol/m^2. As described by Borgerding *et al.* [12,26], the volumes occupied by the surfactants were 63 and 120 mm^3, respectively, producing a decrease in the stationary phase pore volume of 22%

and 28%, respectively. The surfactant tends to clog the smallest pores, with diameters smaller than 7 nm, dramatically decreasing the stationary phase surface area [12,26]. Such changes in the stationary phase physico-chemical characteristics may modify the mobile phase circulation, thus explaining the A term increases.

The surfactant adsorption increases the stationary phase organic layer thickness and decreases the mass transfer rate and D_s, the solute diffusion coefficient in the stationary phase [9,13,26,27,29]. This adsorption may explain the increases in the B (eqn. 10) and C terms (eqn. 11). The significant improvement in efficiency obtained with addition of small amounts of a short-chain organic modifier (propanol [7], pentanol or tetrahydrofuran [13]) is primarily due to the displacement of adsorbed surfactant. Pentanol, which best desorbs ionic surfactants, is the best organic additive for micellar efficiency improvement [14].

Surfactant adsorption reversiblity

An important point has not been well addressed in the literature, namely the question of whether it is possible to desorb completely the surfactant adsorbed on a bonded stationary phase. Fig. 2 shows that the Knox plot obtained with a new C_{18} column roughly corresponds to the plot obtained with the same solute and column after surfactant exposure. The column was washed with ACN–water (30:70, v/v) solution; a column wash with pure methanol or pure isopropanol would have completely eliminated any trace of adsorbed Brij 35, restoring the initial column efficiency. However, this was not observed with the C_{14} column. After SDS exposure, the C_{14} column was washed overnight with pure methanol as recommended by Berthod and Roussel [13]. Fig. 3C shows the unusual *h versus v* plot obtained with the surfactant-exposed C_{14} column. After looking at the results, the column was washed one more time with pure isopropanol. Another identical (within experimental error) *h versus v* plot was obtained (Fig. 3C). The peak tailings were so large that the computer software could not find the peak terminations. The inflection point method was used for plate count computation, which may explain the unusual decrease in the *h versus v* plot observed in Fig. 3C.

It was not possible to restore the initial efficiency of this column. Irreversible adsorption of SDS was suspected. The column was opened and drained, pushing with methanol. The stationary phase was collected, dried and sent for elemental analysis. Trace amounts of sulfur ($0.09 \pm 0.03\%$, w/w) were found. This corresponds to about 9 mg of SDS irreversibly adsorbed on the C_{14} phase; 9 mg of SDS represents only 32 μmol, or 0.14 μmol/m^2, which is only 6% of the SDS initially adsorbed on the C_{14} phase. This small amount of irreversibly adsorbed SDS is enough to modify critically the organic bonded C_{14} layer, producing very low chromatographic efficiency. It is not possible to discuss the Knox parameters obtained with such a modified stationary phase because the peak efficiencies may not have been accurately evaluated and the Knox equation may not correctly depict the efficiency evolution *versus* flow-rate. Theoretically (eqn. 11), is not possible to obtain negative C values. If the C values are not correct, the corresponding A and B terms have no meaning.

Such an irreversible SDS adsorption was observed by Knox and Hartwick [31] on a monomeric C_{18} bonded phase. However, we observed fully reversible SDS adsorption on the same kind of C_{18} phases [10,13]. We have never observed irreversible adsorption on short-chain bonded phases [10,13,30]. Further, irreversible ad-

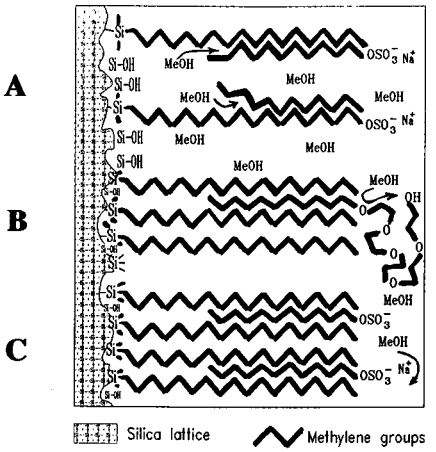

Fig. 4. Surfactant adsorption–desorption. (A) On a medium-density bonded stationary phase, methanol can go inside the bonded layer to desorb the surfactant molecules. (B) On a densely grafted stationary phase, the hydrophobic chain of an nonionic surfactant is inserted in the bonded organic layer, but its bulky hydrophilic part is an easy grasp to extract the molecule. (C) On a densely grafted stationary phase, the long hydrophobic chain of an ionic surfactant is tightly inserted in the bonded organic layer. Organic solvents cannot grap the small polar head, the surfactant adsorption is irreversible. The high efficiency of the column is irreversibly lost after surfactant exposure. MeOH = methanol.

sorption was not observed with short-chain surfactants [31]. It seems that irreversible surfactant adsorption is more likely with densely grafted monomer stationary phases and small polar head group surfactants, with both the surfactant and bonding moiety having hydrophobic chains longer than C_8. Fig. 4 illustrates this mechanism. With a low bonding density (<2.5 μmol/m^2) stationary phase (Fig. 4A), the hydrocarbon tail of the surfactant molecule is not tightly inserted in the bonded hydrocarbon layer. The surfactant molecules can be washed out by methanol. The long polar chain of a nonionic surfactant provides an easy "handle" with which to extract the inserted part of the molecule (Fig. 4B). With a long-chain ionic surfactant and a densely grafted stationary phase (Fig. 4C), it is difficult to get a grip on the surfactant molecule and to extract it from the bonded layer. The inserted SDS molecules may induce some local rigid crystallinity which restrains solute–stationary phase exchanges. Fig. 4C shows also that the surfactant ionic groups face the mobile phase. The ion-exchange properties of such surfactant-exposed stationary phases have been shown to be useful for ion analysis [31-33]. The polarity increase of the C_{14}–SDS surfactant-exposed stationary phase was evidenced by the decrease in the capacity factor of the hydrophobic solutes after exposure to the surfactant [compare the data for methanol–water (70:30, v/v) before and after SDS exposure, Table III].

CONCLUSIONS

As far as the Knox equation can be significantly used to study the efficiency changes in micellar liquid chromatography, the efficiency loss produced by a micellar mobile phase in mainly due to an increase in the A term. The B and C terms also

increased, contributing to the decrease in efficiency. These changes can be explained by the significant surfactant adsorption on the stationary phase that occurs with aqueous micellar solutions. The adsorbed surfactant decreases the column porosity, permeability and tortuosity (A increase); it also decreases the solute diffusion in the stationary phase, and the solute mass transfer (C increase). The surfactant adsorbed on the stationary phase can be washed out by a pure organic solvent. However, the adsorption can be partially irreversible, especially when the stationary phase is a high-density "brush-type" monomer phase and the surfactant is an ionic, small polar head group molecule.

REFERENCES

1 D. W. Armstrong and R. Q. Terrill, *Anal. Chem.*, 51 (1979) 2160.
2 D. W. Armstrong and F. Nome, *Anal. Chem.*, 53 (1981) 1662.
3 D. W. Armstrong, *Sep. Purif. Methods*, 14 (1985) 212.
4 W. L. Hinze, in W. L. Hinze and D. W. Armstrong (Editors), *Ordered Media in Chemical Separations*, (*ACS Symposium Series*, Vol. 342), American Chemical Society, Washington, DC, 1987, Ch. 1, pp. 2–82.
5 J. G. Dorsey, *Adv. Chromatogr.*, 27 (1987) 167.
6 A. Berthod and J. G. Dorsey, *Analusis*, 16 (1988) 75.
7 J. G. Dorsey, M. T. DeEchegaray and J. S. Landy, *Anal. Chem.*, 55 (1983) 924.
8 P. Yarmchuck, R. Weinberger, R. F. Hirsch and L. J. Cline-Love, *J. Chromatogr.*, 283 (1984) 47.
9 M. F. Borgerding and W. L. Hinze, *Anal. Chem.*, 57 (1985) 2183.
10 A. Berthod, I. Girard and C. Gonnet, *Anal. Chem.*, 58 (1986) 1356.
11 D. W. Armstrong, T. J. Ward and A. Berthod, *Anal. Chem.*, 58 (1986) 579.
12 M. F. Borgerding, W. L. Jinze, L. D. Stafford, G. W. Fulp and W. C. Hamlin, *Anal. Chem.*, 61 (1989) 1353.
13 A. Berthod and A. Roussel, *J. Chromatogr.*, 449 (1988) 349.
14 W. L. Hinze, Z. S. Fu, R. W. Williams, F. S. Sadek and A. Berthod, *J. Chromatogr.*, submitted for publication.
15 J. H. Knox and J. N. Done, *J. Chromatogr. Sci.*, 10 (1972) 606.
16 J. H. Knox, *J. Chromatogr. Sci.*, 15 (1977) 352.
17 A. Chartier, C. Gonnet, D. Morel, J. L. Rocca and J. Serpinet, *J. Chromatogr.*, 438 (1988) 263.
18 K. L. Mittal and B. Lindman (Editor), *Surfactants in Solution*, Plenum Press, New York, 1984.
19 G. I. Taylor, *Proc. R. Soc. London, Ser. A*, 223 (1954) 446.
20 A. Berthod, F. Chartier and J. L. Rocca, *J. Chromatogr.*, 469 (1989) 53.
21 J. P. Foley and J. G. Dorsey, *Anal. Chem.*, 55 (1983) 730.
22 B. A. Bidlingmeyer and F. V. Warren, *Anal. Chem.*, 56 (1984) 1583A.
23 A. Berthod, *J. Liq. Chromatogr.*, 12 (1989) 1187.
24 A. Berthod, *J. Liq. Chromatogr.*, 12 (1989) 1169.
25 J. C. Giddings, *Dynamics of Chromatography*, Marcel Dekker, New York, 1965.
26 M. F. Borgerding, *Ph. D. Dissertation*, Wake Forest University, Winston-Salem, NC, 1988.
27 M. F. Borgerding, F. H. Quina, W. L. Hinze, J. Bowermaster and H. McNair, *Anal. Chem.*, 60 (1988) 2520.
28 M. G. Khaledi, *Anal. Chem.*, 60 (1988) 876.
29 M. F. Borgerding, R. L. Williams, W. L. Hinze and F. H. Quina, *J. Liq. Chromatogr.*, 12 (1989) 1367.
30 A. Berthod, I. Girard and C. Gonnet, in W. L. Hinze and D. W. Armstrong (Editors), *Ordered Media in Chemical Separations*, (*ACS Symposium Series*, Vol. 342), American Chemical Society, Washington, DC, 1987, Ch. 5, pp. 130–141.
31 J. H. Knox and R. A. Hartwick, *J. Chromatogr.*, 204 (1981) 3.
32 A. Berthod, I. Girard and C. Gonnet, *Anal. Chem.*, 58 (1986) 1359.
33 F. G. P. Mullins, in W. L. Hinze and D. W. Armstrong (Editors), *Ordered Media in Chemical Separations*, (*ACS Symposium Series*, Vol. 342, American Chemical Society, Washington, DC, 1987, Ch. 4, pp. 115–129.

Journal of Chromatography, 556 (1991) 277–285
Elsevier Science Publishers B.V., Amsterdam

CHROM. 23 101

Adsorption isotherms of phenylalanine in a chromatographic column measured simultaneously by system peaks analysis and frontal analysis

SHULAMIT LEVIN* and SALEH ABU-LAFI
Pharmaceutical Chemistry Department, School of Pharmacy, P.O.B. 12065, The Hebrew University of Jerusalem, Jerusalem 91120 (Israel)

ABSTRACT

Adsorption isotherms of phenylalanine dissolved in acetate buffer of three concentrations, 0.001, 0.01 and 0.1 *M*, were measured using frontal analysis and system peaks analysis simultaneously. The adsorption isotherms measured by the two methods were identical. System peaks were induced by injecting a small vacancy, pure water, just after the plateau was reached in each step of the frontal analysis. The capacity factor of the system peak corresponding to phenylalanine was used in the calculation of the adsorption isotherm. The use of system peaks for the measurement of adsorption isotherms is promising, especially for multi-component systems where mixed isotherms are needed for rational formulation of a preparative separation.

INTRODUCTION

Often when there is a need for a preparative separation, optimization is based on the conditions used in the analytical separation and amounts are increased up to overloading concentrations thereafter. However, the procedure for optimization of the separation should be formulated using a rational design and prediction of the prospects of a good separation rather than by a trial and error sequence. An extensive rational approach to preparative separations in chromatography was described by Guiochon and co-workers [1–9], Snyder and co-workers [10–12] and Knox and Pyper [13].

A good preparative separation can be rationally formulated by using adsorption isotherms of the sample components. The sample is run through the column as a mobile phase solution, and the concentration of each solute i in the stationary phase, $C_{s,i}$, is measured as a function of the concentrations of the sample constituents in the mobile phase, $C_{m,i}$. The dependence is described by the adsorption isotherm. When there is more than one component in the mobile phase, the system is referred to as a multi-component system. In a multi-component system there is a need for more than one adsorption isotherm for each solute to describe the mutual dependence on the various components, $C_{m,i}$.

0021-9673/91/$03.50

Adsorption isotherms can be implemented in the prediction of peak shape and retention at overloading concentrations [1–13]. There are several methods for the measurement of adsorption isotherms [14]. Frequently, the method of choice for the measurement of an adsorption isotherm is frontal analysis. We suggest here another method, a system peaks analysis.

System peaks have been discussed during the last few years by Levin and Grushka [15–17], Levin and Abu-Lafi [18] and Golshan-Shirazi and Guiochon [19–23] and by Westerlund and co-workers [24–27]. An excellent theoretical study of system peaks in linear chromatography was presented by Golshan-Shirazi and Guiochon [23]. With a multi-component mobile phase where one or more components are adsorbed on the stationary phase, injection of a sample different in any sense from the mobile phase itself induces system peaks. Identification and quantitative treatment of these peaks allowed the calculation of capacity factors of mobile phase components and column void volumes using the appropriate detection [15,16]. It has also been shown that the adsorption isotherm of a particular mobile phase component can be calculated from the corresponding system peak [15–18].

A detailed explanation of the principle behind the use of system peaks for the measurement of adsorption isotherms was given previously [18]. A system peak in the vacancy mode is the outcome of a small equilibrium perturbation at the column head when an additive-free mobile phase solution is injected. The equilibrium of each component of the mobile phase is disturbed and thereby manifested by at least one system peak using the appropriate detection conditions. The small perturbation in the concentration of a mobile phase component i moves down the column at a constant velocity u_i, dictated by the adsorption properties of component i, according to the expression

$$u_i = \frac{u_0}{1 + \mathrm{d}C_{\mathrm{s},i}/\mathrm{d}C_{\mathrm{m},i}} \tag{1}$$

where u_0 is the mobile phase velocity and $\mathrm{d}C_{\mathrm{s},i}$ and $\mathrm{d}C_{\mathrm{m},i}$ are the infinitesimal disturbances in the concentrations at the stationary and mobile phases, respectively, or the slope of the adsorption isotherm of component i.

Theoretical and experimental treatments of system peaks in non-linear chromatography were made by Golshan-Shirazi and Guiochon [19–22] using conditions under which competition between the solute and mobile phase components occurs. It was shown that injection of a solute into a binary mobile phase was accompanied by two system peaks in addition to the solute peak. One of the two system peaks was eluted according to the capacity factor of a corresponding mobile phase component, and the other accompanied the solute peak. Therefore, in principle, a mobile phase component can show up in more than one peak. However, there is always one system peak that elutes according to a particular corresponding component's capacity factor k'_i, and can serve for the measurement of this component's adsorption isotherms. We used such a peak for the measurement of the adsorption isotherm of phenylalanine at various buffer concentrations. Identical adsorption isotherms were obtained using system peaks analysis and frontal analysis.

EXPERIMENTAL

Materials

The mobile phase was prepared by dissolving the appropriate amount of phenylalanine (Merck, Darmstadt, Germany) in acetate buffer (pH 3.7), prepared from analytical-reagent grade sodium acetate (Merck) and acetic acid (Frutarom, Haifa, Israel) (1:9).

Instrumentation

The chromatographic system, which was used in all of the experiments, was an HP1050 (Hewlett-Packard, Palo Alto, CA, U.S.A.) modular system with a diode-array UV detector and an HPCHEM IBM-compatible data system with a ThinkJet or LaserJet Series II printer when needed. A Rheodyne (Cotati, CA, U.S.A.) injection valve was used, equipped with a 20- or 2000-μl loop as needed. The temperature was kept constant within ± 0.5°C using a circulating water-bath.

Procedure

All the chromatographic runs were done with a LiChrosorb RP-18 cartridge, 125 × 4 mm I.D. (Merck). The temperature was kept constant at 30°C throughout the experiments. The flow-rate was 1.5 ml/min in all the experiments except for the injection of phenylalanine at overload, where it was 1 ml/min. The system was thoroughly washed with acetonitrile–water between changes in the mobile phase composition.

RESULTS AND DISCUSSION

The chromatographic system consisted of a reversed-phase column and aqueous acetate buffer and phenylalanine in the mobile phase, as described previously [18]. A chromatogram of pure water injected into 0.025 *M* phenylalanine dissolved in 0.1 *M* acetate buffer is shown in Fig. 1. The wavelength of detection was 254 nm, so phenylalanine could serve for the visualization of all three system peaks, marked A, B and C in Fig. 1. Peak A corresponds to an unretained species, whereas B and C can both be related to species adsorbed on the stationary phase. The retention times of peaks A and B can be related to acetate salt and acetic acid, respectively, in agreement with previously described sytems which included acetate buffer [15–18].

Peak C eluted at a capacity factor corresponding to phenylalanine. The system peaks here were negative. A peak appears negative, when the detector response to the sample zone is lower than that to the mobile phase. At low acetate concentrations peaks A and B were small, because interference of phenylalanine with the other components was low [18].

Measurement of adsorption isotherms

System peaks analysis. The adsorption isotherm of phenyalanine in 0.001, 0.01 and 0.1 *M* acetate buffer (pH 3.7) was measured from system peak C. The column was equilibrated with phenylalanine and acetate buffer, then a small vacancy (pure water) was injected. Three system peaks appeared as demonstrated in Fig. 1. The capacity factor of peak C was characteristic of phenylalanine (k'_p) and was used for the

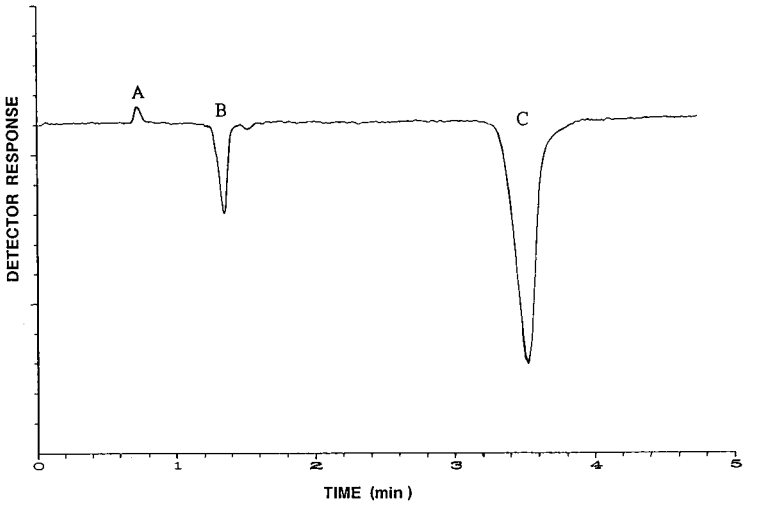

Fig. 1. System peaks A, B and C detected at 254 nm when 20 μl of water were injected into a mobile phase of 0.025 *M* phenylalanine in 0.1 *M* acetate buffer (pH 3.7).

calculation of the adsorption isotherm. The concentration of phenylalanine in the mobile phase, $C_{m,p}$, was changed stepwise, and k'_p (peak C) was measured at each step. The concentration of phenylalanine in the stationary phase was calculated at every step using the following equation [17]:

$$C_{s,p} = \frac{1}{\varphi} \int_0^{C_{m,p}} k'_p \, dC_{m,p} \tag{2}$$

where φ is the phase ratio and $dC_{m,p}$ is the difference in concentration between every two consecutive steps, *i.e.*, at each step k'_p is multiplied by $dC_{m,p}$ and summed over the range of concentrations from 0 to $C_{m,p}$.

Frontal analysis. The adsorption isotherms of phenylalanine measured by system peaks analysis were compared with the most commonly used method, frontal analysis. The column was equilibrated with phenylalanine-free mobile phase (0.001, 0.01 and 0.1 *M* acetate buffer, pH 3.7), then the mobile phase composition was changed abruptly and buffer containing a new concentration of phenylalanine, $C_{m,p}$, entered the column. A front that had a retention volume $V_{R,p}$ characteristic of the concentration of phenylalanine in the new mobile phase, $C_{m,p}$, appeared as shown in Fig. 2. The concentration of phenyalanine in the stationary phase can be calculated according to the equation normally used in frontal analysis:

$$C_{s,p} = \frac{(V_{R,p} - V_0 - V_h)}{V_s} \cdot C_{m,p} \tag{3}$$

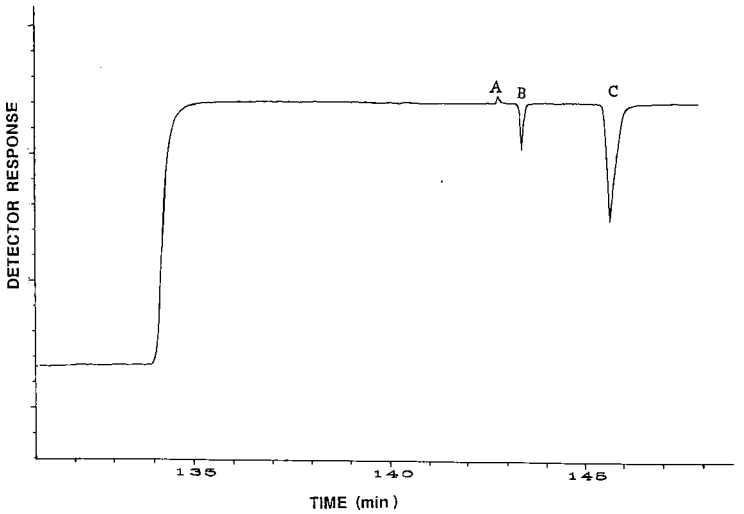

Fig. 2. Front obtained during one step in the frontal analysis of phenylalanine dissolved in 0.1 *M* acetate buffer (pH 3.7). Water (20 μl) was injected after the plateau was reached and induced the three system peaks.

where V_0 is the column void volume, V_s is the stationary phase volume (calculated by subtracting the void volume from the volume of the empty column) and V_h is the hold-up volume from the pump to the detector (measured by placing a zero dead volume union instead of the column). The concentration was increased stepwise in our experiment rather than beginning from the phenylalanine-free solution in every step, and therefore the following expression was used rather than eqn. 3:

$$C_{s,p} = \int_0^{C_{m,p}} \frac{(V_{R,p} - V_0 - V_h)}{V_s} \cdot dC_{m,p} \tag{4}$$

where $dC_{m,p}$ is the difference in concentrations between two consecutive steps.

Combination of frontal analysis and system peaks analysis. Formation of system peaks can be associated with frontal analysis by injecting a small vacancy just after the plateau has been reached. At this point the column is equilibrated with the mobile phase containing the new composition. Normally, in an independent measurement of the adsorption isotherm using system peaks analysis the detector is zeroed on the plateau. Consequently, the plateau becomes the baseline and then a vacancy is injected [15–18].

A 20-μl volume of water was injected over the plateau using 0.1 *M* acetate buffer containing the new concentration of phenylalanine in each step and the corresponding system peaks appeared superimposed on the plateau as shown in Fig. 2. The sequence of steps obtained at 0.1 *M* acetate buffer is shown in Fig. 3. A similar sequence was obtained using 0.01 *M* acetate buffer. However, the combination of both the frontal analysis and system peaks analysis methods was difficult to achieve with 0.001 *M* buffer, relatively small system peaks being obtained. As a rule, the large fronts were

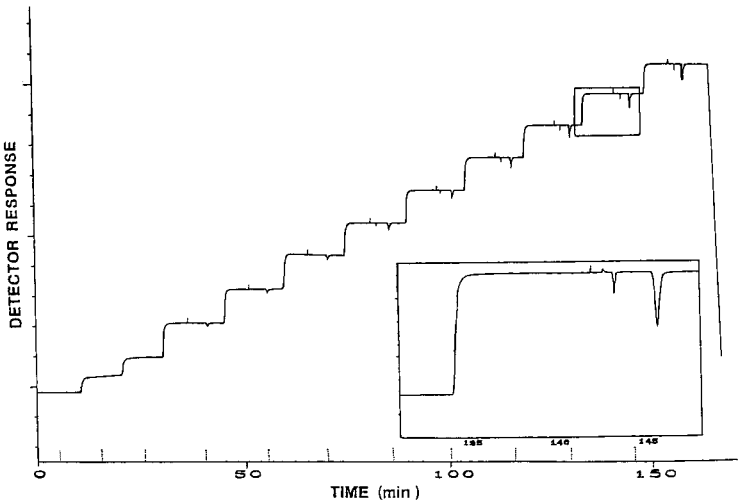

Fig. 3. Sequence of steps in which the adsorption isotherm of phenylalanine was simultaneously measured using both the frontal analysis and system peaks analysis methods. The solute-free mobile phase was 0.1 *M* acetate buffer (pH 3.7). The small vacancy injected on the plateau was 20 μl of pure water. The inset is an enlargement of one step in the combined analysis for illustration. The broken lines on the time axis mark the times when the concentration of phenylalanine in the mobile phase was changed. The injection point is marked on the plateau for each step.

detected using a relatively low sensitivity of the detector, whereas the superimposing system peaks were detected using a relatively high sensitivity. A compromise could not be attained using the 0.001 *M* buffer, so the two measurements were made separately. Generally, the retention volume of the fronts decreased with the concentration of phenylalanine, as well as the capacity factor of system peak C.

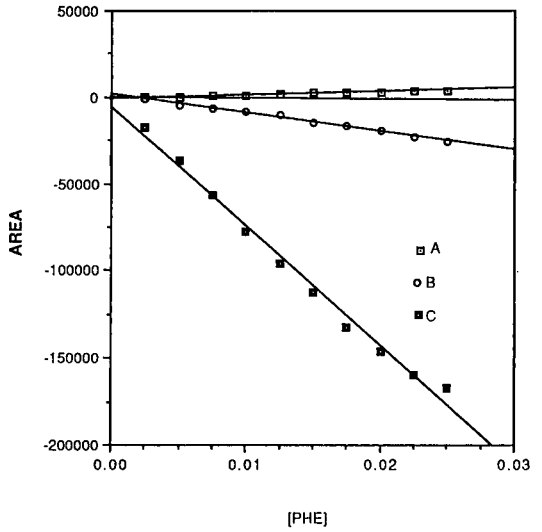

Fig. 4. Areas of peaks A, B and C when 20 μl were injected on the plateau during a stepwise increase in phenylalanine concentration in 0.1 *M* acetate buffer (pH 3.7).

An interesting point in Fig. 3 is the behaviour of the peak areas of the three system peaks with increase in phenylalanine concentration in the mobile phase. All three peaks areas were measured at each step and the results are shown in Fig. 4. Peak A became more and more positive whereas peaks B (with k' of acetic acid) and C (with k' of phenylalanine) became more and more negative as the concentration increased, as was observed in previous work [15–18]. The relationship between the system peaks areas and the distribution equilibria in the column is under study.

The three adsorption isotherms of phenyalanine at three different buffer concentrations measured by both the frontal analysis and system peaks analysis methods, are shown in Fig. 5. The similarity between the adsorption isotherms obtained by the two methods is striking; differences fell within the experimental error.

Peak shape at overload conditions

The relationship between adsorption isotherms and peak shape in non-linear chromatography has frequently been discussed in the literature [1–13]. The chromatograms of phenylalanine at volume and concentration overload (2 ml of 0.025 *M* solution) injected into two different mobile phases are shown in Fig. 6. Points of

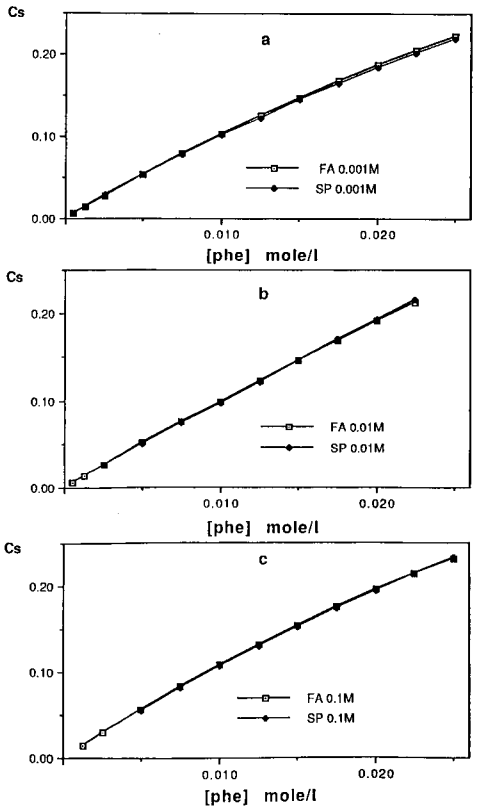

Fig. 5. Adsorption isotherms of phenylalanine measured by (□) frontal analysis and (◆) system peaks analysis. Phenylalanine was dissolved in (a) 0.001, (b) 0.01 and (c) 0.1 *M* acetate buffer (pH 3.7).

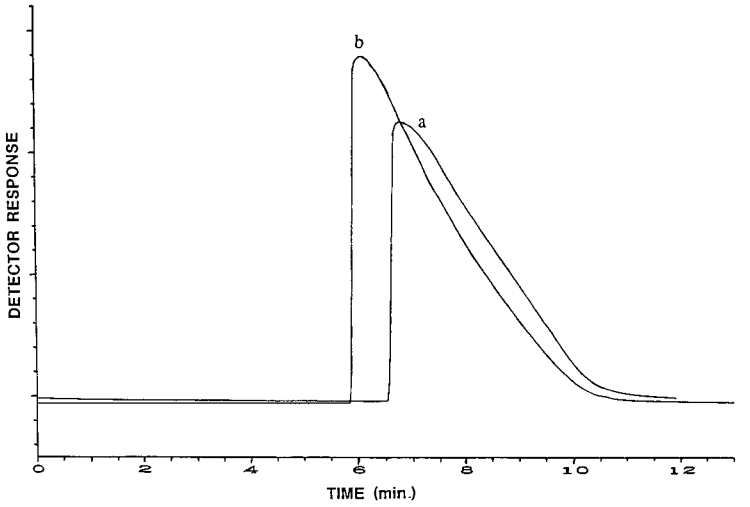

Fig. 6. Injection of 0.025 *M* phenylalanine using a 2-μl loop. The mobile phase was (a) 0.001 and (b) 0.1 *M* acetate buffer (pH 3.7).

interest are the peaks shapes and retention. The peaks have a sharp front and diffuse rear, as expected from their slightly concave adsorption isotherms. Generally, retention was smaller than the linear range. The retention at a 0.1 *M* buffer concentration was smaller than that at 0.001 *M*, as predicted by the adsorption isotherm.

In principle, one peak at overloading concentrations can be used for measurements of adsorption isotherms by elution of a characteristic point (ECP) [28]. In this method, retention volumes of various points on the rear boundary of the peak are taken for the analysis using eqn. 4. The detector response is calibrated to actual concentrations, so the rear boundary can be represented as a series of points with characteristic concentrations in the stationary and mobile phases, *i.e.*, it can represent a whole adsorption isotherm in one injection.

The peaks shown in Fig. 6 were used for the measurement of adsorption isotherms by ECP. The heights of the fronts obtained by frontal analysis were used for detector response calibration. The concentrations of the solute in the stationary phase calculated from ECP were far above the values obtained by frontal analysis and system peaks analysis. The discrepancy between the isotherms obtained by frontal analysis and ECP is well documented in the literature (see ref. 28 and references cited therein). It is believed to arise from axial dispersion, which produces more diffuse rear boundaries and hence the higher results for the concentrations in the stationary phase.

CONCLUSION

Adsorption isotherms can be measured using system peaks analysis as they are identical with the adsorption isotherms obtained by frontal analysis. The use of system peaks for the measurement of adsorption isotherms is especially favourable for multi-component systems. Mixed adsorption isotherms cannot be readily measured

experimentally by current methods. We believe that system peaks analysis can be used where mixed isotherms are needed for a rational formulation of a preparative separation. There is a need for a definite assignment of each of the peaks obtained in a multi-component system. Once the system peaks have been defined, their capacity factors can be used for the measurement of the adsorption isotherm of each component in the mobile phase.

REFERENCES

1 B. C. Lin, Z. Ma, S. Golshan-Shirazi and G. Guiochon, *J. Chromatogr.*, 500 (1990) 185–213.
2 G. Guiochon and A. Katti, *Chromatographia*, 24 (1987) 165–189.
3 G. Guiochon, S. Ghodbane, S. Golshan-Shirazi, J. X. Huang, A. Katti, B. C. Lin and Z. Ma, *Talanta*, 36 (1989) 19.
4 S. Golshan-Shirazi and G. Guiochon, *Anal. Chem.*, 60 (1988) 1856.
5 A. M. Katti and G. Guiochon, *J. Chromatogr.*, 449 (1988) 25–40.
6 S. Golshan-Shirazi and G. Guiochon, *Anal. Chem.*, 61 (1989) 462.
7 A. M. Katti and G. Guiochon, *J. Chromatogr.*, 499 (1990) 21–35.
8 S. Golshan-Shirazi and G. Guiochon, *Anal. Chem.*, 61 (1989) 1276.
9 S. Golshan-Shirazi and G. Guiochon, *Anal. Chem.*, 61 (1989) 1368 and 2464.
10 L. R. Snyder, J. W. Dolan and G. B. Cox, *J. Chromatogr.*, 483 (1989) 63–84.
11 L. R. Snyder and G. B. Cox, *J. Chromatogr.*, 483 (1989) 85–94.
12 G. B. Cox and L. R. Snyder, *J. Chromatogr.*, 483 (1989) 95–110.
13 J. H. Knox and H. M. Pyper, *J. Chromatogr.*, 363 (1986) 1–30.
14 E. Grushka and S. Levin, in E. Katz (Editor), *Quantitative Analysis Using Chromatographic Techniques*, Wiley, New York, 1987, p. 359.
15 S. Levin and E. Grushka, *Anal. Chem.*, 58 (1986) 1602–1607.
16 S. Levin and E. Grushka, *Anal. Chem.*, 59 (1987) 1157–1164.
17 S. Levin and E. Grushka, *Anal. Chem.*, 61 (1989) 2428–2433.
18 S. Levin and S. Abu-Lafi, *J. Chromatogr.*, 517 (1990) 285–295.
19 S. Golshan-Shirazi and G. Guiochon, *J. Chromatogr.*, 461 (1989) 1–18.
20 S. Golshan-Shirazi and G. Guiochon, *J. Chromatogr.*, 461 (1989) 19–34.
21 S. Golshan-Shirazi and G. Guiochon, *Anal. Chem.*, 61 (1989) 2373–2380.
22 S. Golshan-Shirazi and G. Guiochon, *Anal. Chem.*, 61 (1989) 2380.
23 S. Golshan-Shirazi and G. Guiochon, *Anal. Chem.*, 62 (1990) 923–932.
24 A. Sokolowski, T. Fornstedt and D. Westerlund, *J. Liq. Chromatogr.*, 10 (1987) 1629–1662.
25 J. Crommen, G. Schill, D. Westerlund and Z. Hackzell, *Chromatographia*, 24 (1987) 252.
26 M. Johannsson and D. Westerlund, *J. Chromatogr.*, 452 (1988) 241–255.
27 E. Arvidsson, J. Crommen, G. Schill and D. Westerlund, *J. Chromatogr.*, 461 (1989) 429.
28 J. Jacobson, J. Frenz and C. Horvath, *J. Chromatogr.*, 316 (1984) 53–68.

Journal of Chromatography, 556 (1991) 287–304
Elsevier Science Publishers B.V., Amsterdam

CHROM. 23 299

Optimisation pentaparamétrique de la résolution en chromatographie phase gazeuse par la technique du diagramme à fenêtres

Cas du couplage de deux colonnes

J. M. FOUGNION, C. DAVID, A. CROCQ[a] et C. GENTY*
Conservatoire National des Arts et Métiers, Laboratoire Méthodes Physico-Chimiques d'Analyse, 292 Rue St. Martin, 75141 Paris Cedex 03 (France)

ABSTRACT

Pentaparametric optimization of resolution in gas chromatography. Case of two serially connected columns

The window diagram method is used to approach the optimization of both resolution and analysis time in gas phase chromatography with two serially coupled columns. The influence of five parameters is studied: temperatures of both columns, flow-rate, total column length and relative lengths.

A computer program allows, with few experimental results, to foresee the value to be set for each parameter in order to achieve the best separation. The experimental verifications carried out lead to results which are in good agreement with the values foreseen by the window diagram.

INTRODUCTION

Dès 1975 Laub et Purnell [1] décrivent l'optimisation d'un mélange de phases stationnaires par la technique du diagramme à fenêtre (DAF) et en 1978 [2], ils prennent en compte l'influence de la température d'une colonne. Smuts *et al.* [3], en 1980 couplent deux colonnes à température différente. En 1984, Purnell et Williams [4] publient une approche théorique permettant le couplage de colonnes capillaires, reprenant ainsi une idée ancienne due notamment à Hildebrand et Reilley [5], puis en 1985 [6] ils proposent le couplage de colonnes remplies. En 1987, Guiochon et Gutierrez [7] publient les résultats d'une étude concernant l'efficacité de colonnes capillaires couplées. Le grand nombre de publications sur l'optimisation du couplage de colonnes en chromatographie en phase gazeuse (CPG) montre l'intérêt d'obtenir des conditions opératoires qui soient les meilleures, ceci dans un but essentiellement économique.

Dans la plupart des cas les auteurs préconisent la sélectivité α, comme critère de réponse, Purnell et Williams [8] conseillant toutefois en 1985 de choisir le temps

[a] Adresse actuelle: Compagnie Générale des Eaux, 52 Rue d'Anjou, 75008 Paris, France.

0021-9673/91/$03.50

d'analyse. Lors du *16th International Symposium on Chromatography*, en 1986, un poster [9] montrant l'intérêt d'utiliser la résolution plutôt que la sélectivité pour critère de réponse à été présenté par notre laboratoire.

Dans cette optique, le présent article se propose de décrire la démarche suivie lors du développement d'un programme informatique, permettant d'optimiser la résolution (critère principal) et le temps d'analyse (critère secondaire) dans le cas du couplage de deux colonnes (capillaires ou remplies) en fonction des cinq paramètres suivants:

(1) la température de la colonne A;
(2) la température de la colonne B;
(3) le débit;
(4) la longueur totale des 2 colonnes;
(5) la fraction de longueur de la colonne de tête.

Ce programme utilise soit des relations connues, parfois modifiées afin de prendre en compte plus finement l'influence de certains paramètres, soit des relations obtenues expérimentalement et qui s'appliquent correctement dans le domaine étudié. Plus particulièrement on met à profit une approche proposée par Ceulemans [10] définissant une efficacité de la colonne indépendante des composés. L'optimisation décrite comporte deux phases: la première consiste en l'acquisition de grandeurs caractéristiques des colonnes et des solutés, la seconde concerne la simulation proprement dite.

THÉORIE

Pour mener à bien l'optimisation multiparamétrique de la résolution R, on utilise la relation bien connue

$$R = \frac{1}{2}\frac{\alpha - 1}{\alpha + 1}\sqrt{\bar{n}_{\text{eff}}} \tag{1}$$

où $\bar{n}_{\text{eff}}$ = nombre de plateaux effectifs moyen entre les deux solutés et α = sélectivité. Le calcul de R impose de déterminer α et n_{eff} pour toutes les valeurs pouvant être prises par les variables qui sont: les températures des colonnes de tête (T_a) et de queue (T_b), la fraction de longueur de la colonne de tête (l_f), le débit (F_c) et la longueur totale des deux colonnes (L_c).

Détermination de α

La sélectivité α s'exprime par le rapport des facteurs de capacité (k') de deux solutés

$$\alpha = \frac{k'_2}{k'_1} \tag{2}$$

avec $k'_2 \geqslant k'_1$. Pour déterminer α, on doit donc connaître les valeurs de k' quels que soient la température et le rapport des longueurs des deux colonnes.

Influence de la température sur le facteur de capacité k'

On utilise la relation

$$\ln (k'/T) = A/T + B \tag{3}$$

dans laquelle A et B sont des coefficients typiques d'un soluté et de la colonne utilisée. Ceux-ci sont calculés préalablement sur chaque colonne et pour chaque composé par des mesures effectuées au minimum à deux températures.

Influence du couplage de colonnes sur le facteur de capacité

Dans ce cas on détermine le facteur de capacité résultant d'un composé en utilisant la relation proposée par Purnell et Williams [6]

$$k' = \frac{Q\, k'_a + k'_b}{Q + 1} \tag{4}$$

où k'_a = facteur de capacité d'un soluté pour la colonne de tête A, k'_b = facteur de capacité du même soluté pour la colonne de queue B et Q = rapport des temps morts entre la colonne de tête et la colonne de queue

$$Q = t_{m_a}/t_{m_b} \tag{5}$$

Pour obtenir Q on doit calculer les temps morts sur chaque fraction de colonne. Pour cela on utilise l'approche développée par Purnell et Williams [6], que nous avons modifiée de manière à prendre en compte l'influence de la température [*cf.* annexe].

$$Q = \frac{\bar{R}_{F_b}}{\bar{R}_{F_a}} \frac{\bar{V}^2_{m_a}}{\bar{V}^2_{m_b}} \frac{T_b{}^2}{T_a{}^2} \frac{p_e^3 - p_j^3}{p_j^3 - p_s^3} \tag{6}$$

Cette relation fait intervenir les caractéristiques physiques de chacune des colonnes comme le volume mort par unité de longueur ($\bar{V}_{m_a}$ et $\bar{V}_{m_b}$) et la résistance au flux gazeux par unité de longueur ($\bar{R}_{F_a}$ pour la température T_a et $\bar{R}_{F_b}$ pour la température T_b), les pressions en tête (p_e), à la jonction (p_j) et à la sortie (p_s) des colonnes, ainsi que les températures des colonnes.

La procédure pour calculer ces différents facteurs lors de l'optimisation est décrite ci-après.

Détermination de $\bar{V}_m$

On détermine le volume mort d'une colonne (V_m) à partir de la relation de définition par des mesures de temps mort, de pression et de température pour un débit donné (Purnell et Williams [6]).

$$V_m = jF_c t_m \frac{T_c}{T_d} \tag{7}$$

où j = facteur de James et Martin, $j = 3/2[(p_e/p_s)^2 - 1]/[(p_e/p_s)^3 - 1]$; T_c = température de la colonne; et T_d = température du débitmètre. On définit $\bar{V}_m$, valeur de V_m par unité de longueur de colonne: $\bar{V}_m = V_m/L$, dont L = longueur de la colonne sous test.

Détermination de $\bar{R}_F$

La notion de résistance au passage d'un flux gazeux (R_F) a été introduite par Hildebrand et Reilley [5] puis reprise par Purnell et Williams [4] dans le cadre de l'optimisation. Sous sa forme d'origine et pour une colonne déterminée, R_F s'écrit

$$R_F = \frac{p_e^2 - p_s^2}{p_s u_s} \tag{8}$$

où u_s = vitesse du gaz vecteur à la sortie de la colonne.

On définit $\bar{R}_F$, valeur de R_F par unité de longueur de colonne: $\bar{R}_F = R_F/L$. Après réarrangement de éqn. 8 et en tenant compte des relations $\bar{u} = L/t_m$ et $u_s = \bar{u}/j$ on obtient

$$t_m = \frac{2\,L^2 \bar{R}_F}{3} \frac{p_e^3 - p_s^3}{(p_e^2 - p_s^2)^2} \tag{9}$$

Cette expression permet de calculer préalablement la valeur de $\bar{R}_F$, par régression linéaire, à partir de la connaissance des pressions d'entrée et de sortie d'une colonne ainsi que du temps mort, pour différents débits.

Influence de la température sur $\bar{R}_F$

R_F peut également s'écrire, dans le cas d'une colonne remplie

$$R_F = \frac{2\,\varepsilon\,\eta\,L}{B_0} \tag{10}$$

où η = viscosité du gaz vecteur; ε = porosité du support; B_0 = perméabilité du support; et L = longueur de la colonne. Cette relation montre que R_F est directement proportionnel à la viscosité du gaz. En admettant que la porosité et la perméabilité du support soient indépendantes de la température, on peut calculer $\bar{R}_F(T)$ à l'aide de la relation

$$\bar{R}_F(T) = \bar{R}_F(T_x) \frac{\eta(T)}{\eta(T_x)} \tag{11}$$

où T_x = température de mesure de $\bar{R}_F$.

Ettre [11] a comparé les différentes voies pour exprimer la variation de la viscosité de l'hélium en fonction de la température. Il retient $\eta = 0{,}3993T + 186{,}6$ pour un

domaine de température limité. Nous préférons, du fait de la non-linéarité de la viscosité en fonction de la température, utiliser des coefficients obtenus par un ajustement polynomial de degré deux, à partir des valeurs tabulées dans le Handbook of Chemistry and Physics [12].

Calcul de la pression intermédiaire p_j entre les deux colonnes

Celle-ci est obtenue à partir d'une équation proposée par Purnell et Williams [6] et modifiée de façon à prendre en compte la température (*cf.* annexe)

$$p_j^2 = p_s^2 + \frac{p_s F_c}{T_d} \frac{T_b \bar{R}_{F_b} L_b}{\bar{V}_{m_b}} \tag{12}$$

où F_c = débit volumique de gaz vecteur à la température du débitmètre pour la pression atmosphérique; L_b = longueur de la colonne de queue; et T_d = température du débitmètre.

Calcul de la pression d'entrée p_e en fonction des conditions opératoires et des caractéristiques physiques des deux colonnes couplées

En exprimant les relations de base de la chromatographie en fonction des cinq paramètres retenus: le débit de gaz vecteur imposé aux colonnes (F_c), la longueur totale des deux colonnes (L_c), la fraction de longueur de la colonne de tête (l_f) et les températures des deux colonnes (T_a et T_b) on obtient pour p_e la relation suivante (*cf.* annexe)

$$p_e^2 = p_s^2 + \frac{p_s F_c L_c}{T_d} \left[\frac{l_f T_a \bar{R}_{F_a}}{\bar{V}_{m_a}} + \frac{(1 - l_f) T_b \bar{R}_{F_b}}{\bar{V}_{m_b}} \right] \tag{13}$$

avec $l_f = L_a/L_c$ (L_a = longueur de la colonne de tête, L_c = longueur totale de deux colonnes).

Détermination de n_{eff}

Dans le cas de colonnes couplées, on utilise pour chaque soluté la relation

$$\frac{1}{n_{eff}} = \frac{c^2/n_{eff_a} + 1/n_{eff_b}}{(c+1)^2} \tag{14}$$

avec $c = t'_{r_a}/t'_{r_b}$; où n_{eff} = efficacité globale, en nombre de plateaux effectifs; t'_{r_a} = temps de rétention réduit sur la colonne A; t'_{r_b} = temps de rétention réduit sur la colonne B; n_{eff_a} = efficacité sur la colonne A, en nombre de plateaux effectifs; et n_{eff_b} = efficacité sur la colonne B, en nombre de plateaux effectifs. Cette relation est semblable à celle proposée par Purnell et Williams [8] qui prenait en compte des efficacités théoriques. L'utilisation de plateaux effectifs permet de considérer des paramètres plus proches de la réalité physique. On calcule ainsi l'efficacité globale pour chaque soluté en fonction de l'efficacité sur chaque fraction de colonne. Malheureuse-

ment, n_{eff_a} et n_{eff_b} sont liés au soluté étudié et pour faire abstraction du facteur de capacité, donc du composé, nous avons opté pour l'approche proposée par Ceulemans [10].

Détermination de n_{eff_a} ou n_{eff_b}

L'observation de la quasi-linéarité de la largeur des pics, en fonction du temps de rétention, a conduit Ceulemans [10] à la notion de "plateaux théoriques à facteur de capacité infini" notée n_{inf}. Il définit alors

$$n_{\text{inf}} = 16[(t_r - t_c)/w]^2 \tag{15}$$

et

$$t_q = t_c - t_m \tag{16}$$

où t_r = temps de rétention; w = largeur à la base d'un pic; t_m = temps mort; et t_c = constante. Ce qui donne une relation directe entre n_{eff} et n_{inf}

$$n_{\text{eff}} = n_{\text{inf}} \frac{t_r'^2}{(t_r' - t_q)^2} \tag{17}$$

n_{inf} et t_q qui sont caractéristiques de la colonne ayant été déterminés initialement, la simple mesure du temps de rétention permettra d'obtenir la valeur de n_{eff} pour chacun des solutés. t_q constitue une mesure de la décroissance de n_{eff} avec la diminution du temps de rétention. n_{inf} représente l'efficacité maximale que l'on obtiendrait pour un composé dont le temps de rétention tendrait vers l'infini.

Variation de n_{inf} et t_q avec la température

La formule précédente ne prend pas en compte la variation de l'efficacité avec la température. Nous nous sommes donc attachés à mettre en évidence l'influence de celle-ci sur n_{inf} et t_q (voir la Partie Expérimentale).

A partir des résultats, on constate que l'on commet une erreur faible en considérant constants n_{inf} et t_q pour des températures d'utilisation courantes des colonnes. Cependant, si l'on désire prendre en compte la faible variation de ces grandeurs, il sera toujours possible d'entrer les lois de variation dans l'ordinateur, et d'en tenir compte pour les calculs.

Variation de n_{inf} et t_q en fonction du débit

La notion de n_{inf} conduit à celle de h_{inf}

$$h_{\text{inf}} = L/n_{\text{inf}} \tag{18}$$

h_{inf} correspond à la hauteur d'un plateau effectif pour un soluté dont le facteur de capacité tend vers l'infini. Gaget et Serpinet [13] ont étudié les différentes formes possibles de l'expression de la hauteur équivalente à un plateau théorique (h) en

fonction du débit. Pour la suite, on a utilisé l'expression due à Brennan et Kemball [14] qui s'est révélée bien adaptée à notre approche d'optimisation

$$h_{\text{inf}} = A_h + \frac{B_h}{p_s u_s} + C_h p_s u_s + D_h j u_s \tag{19}$$

A_h, B_h, C_h, D_h étant des constantes. Cette expression permet de prendre en compte pression et débit en sortie de colonne. Les différents coefficients mathématiques sont déterminés au préalable à partir de mesures expérimentales et ne prétendent en aucun cas être les vrais coefficients de l'équation cinétique. Ils permettent d'obtenir par calcul la valeur de l'efficacité en tout point de notre domaine.

Comme $t_q = t_c - t_m$ (16), la variation de t_q en fonction du débit se ramène à suivre celle de t_m et de t_c. On a trouvé expérimentalement que t_c varie selon la relation suivante

$$t_c = A_c/p_s u_s + B_c \tag{20}$$

où A_c et B_c sont des constantes. Toutes ces relations montrent la complexité d'un système où l'interaction entre paramètres est la règle quasi générale. Pour illustrer ce fait on a représenté un synoptique, s'inspirant de celui de Bounine et Guiochon [15], montrant l'influence des variables sur le critère de réponse (Fig. 1).

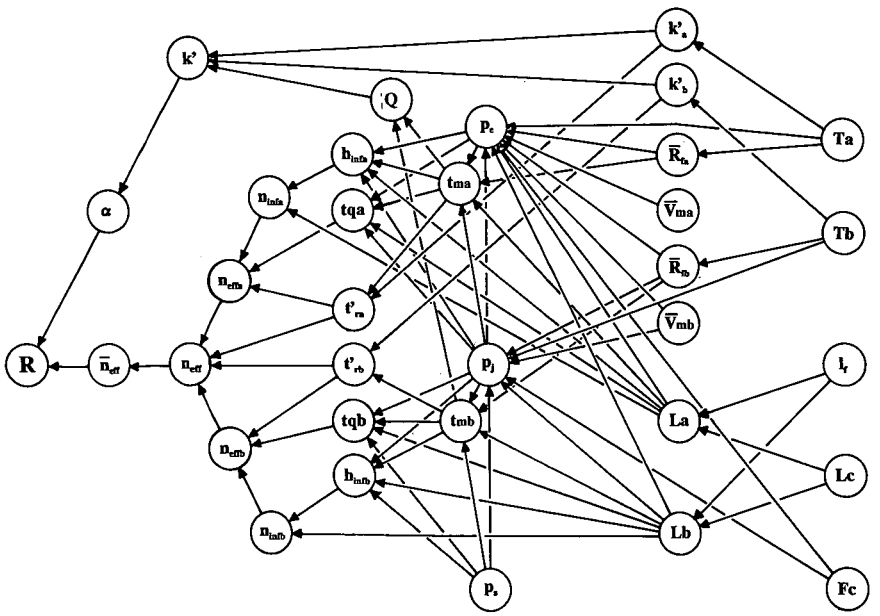

Fig. 1. Synoptique montrant l'influence des variables sur le critère de réponse cas d'une régulation de débit massique de gaz vecteur.

PARTIE EXPÉRIMENTALE

Chromatographe

L'étude est faite sur chromatographe DI 700 de Delsi Instrument (Argenteuil, France) sur lequel a été adaptée une deuxième enceinte thermostatée à 0,5°C près (Fig. 2). L'appareil est muni d'un injecteur pour colonnes remplies porté à 250°C; d'un système à deux fours, régulés indépendamment en température; d'un détecteur à ionisation de flamme porté à 250°C; d'un régulateur de débit massique et de son coffret de commande (RDM-280 et CRDM-280) de l'Air Liquide division Alphagaz, Paris, France); d'une mesure de pression par un manomètre électronique M2-500 de l'Air Liquide division Alphagaz, placé à l'entrée de l'injecteur. Le signal fourni par le détecteur est traité à l'aide d'un enregistreur intégrateur Enica 21 de Delsi Instrument.

Colonnes

On utilise des colonnes en acier inoxydable de 3 m × 3.2 mm O.D. remplies à 10% de phase Superox 20M (polyéthylène glycol) ou à 10% de phase OV-25 (25% de méthyl–75% phényl silicone) sur Chromosorb W HP 80–100 mesh. Les phases stationnaires étaient fournies préimprégnées et préconditionnées par la société Alltech France (Templeuve, France). Ces colonnes ont été remplies dans notre laboratoire à partir d'un même lot de tubes, ce qui nous garantit un diamètre identique pour chacune d'elles.

Gaz vecteur

On a choisi de l'hélium N55 de l'Air Liquide division Alphagaz, pour une plus grande stabilité des colonnes dans le temps.

Produits

On a réalisé un mélange de douze solutés comprenant du tridécane, tétradécane, pentadécane de l'hexanol-1, heptanol-1 et octanol-1 (Janssen Chimica, Pantin, France), nonanol-1, heptylbenzène et du cyclooctanol (Aldrich, Strasbourg, France), de l'hexylbenzène et de la méthyl 5-hexanone (Polyscience Corp., USA, distribué par Interchim, Paris, France) et de l'acétophénone (Prolabo, Paris, France) dans de l'heptane (Merck Clevenot, Nogent-sur-Marne, France).

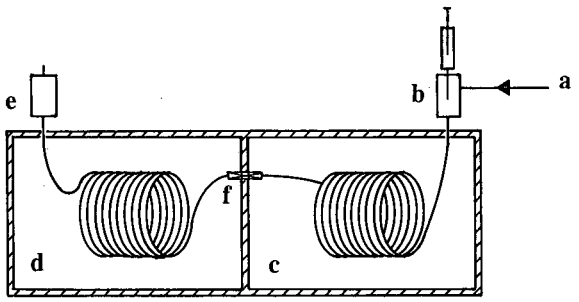

Fig. 2. Schéma du chromatographe. (a) Gaz vecteur; (b) injecteur; (c) four de la colonne A; (d) four de la colonne B; (e) détecteur; (f) jonction.

RÉSULTATS ET DISCUSSION

Influence de la température sur n_{inf} et t_q

On a étudié [16] sur les phases stationnaires Superox 20M et OV-25, la variation de n_{inf} et de t_q en fonction de la température (Fig. 3).

Pour cela, on a injecté des séries homologues d'alcanes et d'alcools à différentes températures de colonne, tout en gardant le débit massique de gaz vecteur (He) à 30 ml/min. Pour chaque valeur de température, les valeurs de n_{inf} et t_q sont déterminées par régression linéaire à partir des points expérimentaux correspondant à la relation $w = f(t_r)$. On constate, pour des températures d'utilisation courantes des colonnes (par exemple entre 120 et 230°C pour la colonne OV-25), d'une part, que l'efficacité reste à peu près constante si l'on considère la répartition des points de mesure et, d'autre part, que l'incertitude sur le résultat final demeure faible puisque l'efficacité n'intervient dans la valeur de la résolution que par sa racine carrée. De même, t_q est constant sur la colonne Superox 20M, ou varie linéairement avec une très faible pente sur la colonne OV-25. D'autres essais effectués sur phases OV-101 et OV-210 ont confirmé ces résultats. Par ailleurs, la détermination de n_{inf} et t_q reste valable pour un grand nombre d'analyses à partir du moment où il n'y a pas de dégradation de la colonne, mais il est évident que celle ci évolue lentement en fonction du temps.

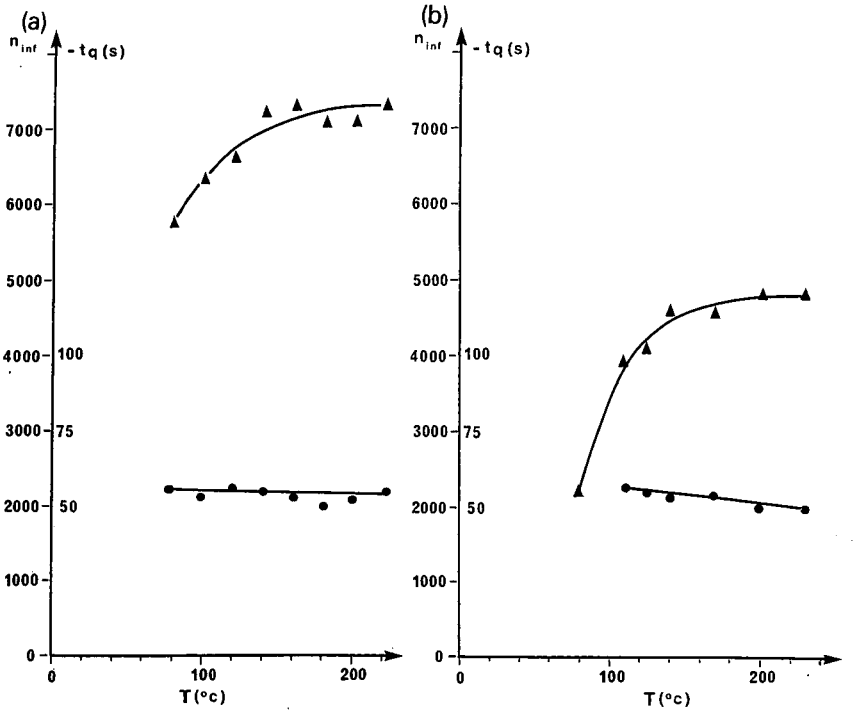

Fig. 3. Variations de n_{inf} et t_q en fonction de la température. (▲) n_{inf}; (●) t_q. (a) Colonne Superox 20M de 3 m, taux d'imprégnation de 10% sur Chromosorb W HP 80–100 mesh; (b) colonne OV-25 de 3 m, taux d'imprégnation de 10% sur Chromosorb W HP 80–100 mesh. Débit d'helium: 30 ml/min.

Mesures des grandeurs caracteristiques

On les acquiert pour une température de 140°C à partir des mesures de pressions p_e et p_s, de débits, de temps morts, de temps de rétention et de largeurs de pics. Pour cela on emploie des mélanges test d'alcanes, d'alcools et de cétones, étudiés de manière à minimiser le nombre d'injections. On se sert du méthane pour connaître la valeur du temps mort.

Les valeurs de $\bar{R}_{F_a}$ et $\bar{R}_{F_b}$ sont obtenues à l'aide de la relation 9 et celles de $\bar{V}_{m_a}$ et $\bar{V}_{m_b}$ avec la relation 7. Les coefficients de h_{inf} et de t_c sont calculés par régression à partir des relations 19 et 20 et portés dans le Tableau I.

Les différents solutés du mélange à analyser sont injectés par famille à 140°C et à 200°C, sur chaque colonne, afin d'obtenir les valeurs des facteurs de capacité, présentées dans le Tableau II. Ces valeurs permettent de déterminer les coefficients A et B de l'équation 3.

Toutes ces grandeurs caractéristiques sont entrées dans le logiciel qui calcule point par point, avec un pas que l'on choisit, les valeurs de résolution pour tout le domaine expérimental.

Simulation sur ordinateur

Le DAF monoparamétrique de la résolution en fonction de la température montre que l'on n'atteint pas 1,5 de résolution pour chacune des deux colonnes, prise isolément. Par contre le DAF de simulation, réalisé avec les cinq variables, en plaçant la colonne OV-25 en tête, montre qu'il existe de nombreuses fenêtres intéressantes, pour lesquelles le critère principal $R \geqslant 1{,}5$ est satisfait. Parmi celles ci, on a choisi celle qui correspond au temps d'analyse le plus court (critère secondaire). Les conditions opératoires déterminées par ordinateur sont: $F_c = 40$ ml/min, $L_c = 4{,}25$ m, $T_a = 171$°C, $T_b = 144$°C, $l_f = 0{,}655$, $R = 1{,}50$, temps d'analyse assimilé au temps de sortie du dernier pic. = 658 s.

On présente, dans le Tableau III, un exemple très simplifié de balayage systématique réalisé à l'aide du logiciel. Au départ, on doit indiquer les valeurs extrêmes pouvant être prises par les variables, ainsi que leur pas de variation.

TABLEAU I

CARACTERISTIQUES DES COLONNES: MESURES PRÉLIMINAIRES POUR RÉALISATION DU LOGICIEL DE SIMULATION

F_c = 3–60 ml/min, L_c = 3 m, T_a = 140°C, T_b = 140°C.

Caracteristiques	Colonne OV-25	Colonne Superox 20M
$\bar{R}_F$ (Nsm^{-4})	37,8	35,4
$\bar{V}_m$ (cm^3/m)	2,97	2,98
Coefficients de h_{inf}		
A_h	$1{,}51 \cdot 10^{-4}$	$1{,}21 \cdot 10^{-4}$
B_h	$3{,}72 \cdot 10^{-5}$	$2{,}96 \cdot 10^{-5}$
C_h	$7{,}63 \cdot 10^{-4}$	$9{,}04 \cdot 10^{-4}$
D_h	$1{,}53 \cdot 10^{-3}$	$2{,}40 \cdot 10^{-4}$
Coefficients de t_c		
A_c	−2,29	−2,58
B_c	−16,9	0,56

TABLEAU II

VALEURS EXPÉRIMENTALES DES FACTEURS DE CAPACITÉ OBTENUS SUR LES DEUX COLONNES, POUR DEUX TEMPÉRATURES: MESURES PRÉLIMINAIRES POUR RÉALISATION DU LOGICIEL DE SIMULATION

F_c = 30 ml/min, L_c = 3 m.

Soluté	No.	OV-25		Superox 20M	
		140°C	200°C	140°C	200°C
Tridécane	1	8,06	1,64	3,73	0,93
Tétradécane	2	13,32	2,39	5,91	1,31
Pentadécane	3	21,97	3,47	9,34	1,85
Hexanol-1	4	1,85	0,54	4,33	1,00
Heptanol-1	5	3,13	0,81	7,01	1,44
Octanol-1	6	5,26	1,20	11,29	2,07
Nonanol-1	7	8,78	1,76	18,08	2,95
Hexylbenzène	8	14,61	2,84	11,18	2,37
Heptylbenzène	9	24,02	4,12	17,63	3,34
Methyl 5-hexanone	10	1,71	0,51	1,90	0,58
Cyclooctanol	11	12,74	2,73	23,56	4,24
Acétophénone	12	11,01	2,37	19,21	3,76

TABLEAU III

EXEMPLE DE BALAYAGE POUR DÉTERMINATION DES FENÊTRES

Balayage en F_c: de 35 ml/min à 45 ml/min, sauts de 5 ml/min; balayage en L_c: de 4 m à 4,5 m, sauts de 0,25 m; balayage en T_a: de 168°C á 172°C, sauts de 2°C; balayage en T_b: de 140°C à 146°C, sauts de 2°C; balayage en l_f: de 0,600 à 0,700, sauts de 0,025; résolution minimale demandée: 1,4.

F_c (ml/min)	L_c (m)	T_a (°C)	T_b (°C)	l_f	α	R	Temps d'analyse (s)
35	4,00	168	146	0,625	1,259	1,46	667
35	4,25	168	146	0,625	1,258	1,49	729
35	4,25	170	144	0,650	1,085	1,51	724
35	4,25	172	142	0,675	1,083	1,46	699
35	4,25	172	146	0,650	1,084	1,49	682
35	4,50	168	142	0,650	1,080	1,47	837
35	4,50	168	146	0,625	1,258	1,52	793
35	4,50	170	144	0,650	1,084	1,57	787
35	4,50	172	142	0,675	1,084	1,52	760
35	4,50	172	146	0,650	1,084	1,54	741
40	4,25	170	144	0,650	1,084	1,47	674
40	4,25	172	142	0,675	1,085	1,46	651
40	4,50	168	142	0,650	1,081	1,47	780
40	4,50	168	146	0,625	1,257	1,45	739
40	4,50	170	144	0,650	1,083	1,51	734
40	4,50	172	142	0,675	1,083	1,50	708
40	4,50	172	146	0,650	1,082	1,49	691
45	4,50	168	142	0,650	1,081	1,45	733
45	4,50	170	144	0,650	1,082	1,46	689

Vérification expérimentale et commentaires

On réalise une vérification expérimentale en se plaçant dans les conditions indiquées par le DAF de simulation. Pour cela on coupe la colonne OV-25 à 2,78 m et la colonne Superox 20M à 1,47 m et on met bout à bout les deux fractions, à l'aide d'un raccord rempli de laine de verre silanisée, tout en respectant le sens du passage du gaz vecteur dans les colonnes. On compare les valeurs prévues par le programme à celles effectivement obtenues (Tableau IV).

On note une très bonne correspondance entre les valeurs de k'. Ces résultats montrent de toute évidence que l'approche proposée par Purnell [6] s'applique bien. Les valeurs d'efficacité mesurées sont systématiquement meilleures que celles calculées mais elles restent du même ordre de grandeur. Nous avons observé ce fait de manière quasi générale mais avec des écarts plus ou moins grands selon le cas. Ceux ci peuvent s'expliquer tout à la fois à partir de considérations expérimentales, comme la précision des mesures, la stabilité en température du chromatographe ou la régulation massique de gaz vecteur et de considérations théoriques telles que la forme retenue pour l'équation de la hauteur équivalente à un plateau théorique (HEPT) ou l'influence des familles de composés sur la valeur de n_{inf}.

Pour ce qui est de la forme retenue pour la HEPT, on utilise une relation connue et admise permettant de prendre en compte pression et vitesse du gaz vecteur pour chacune des colonnes mises bout à bout. Cette relation, bien que simple mais correcte, s'avère suffisante au titre de l'optimisation.

Les coefficients B_h, C_h et D_h, varient sans nul doute avec la température, mais comme l'ont signalé en particulier Purnell [17], Harris et Habgood [18], il est très difficile de connaître précisément leur variation. Les essais expérimentaux que nous avons effectués pour estimer l'influence de la température sur ces coefficients ont été plutôt décevants, les variations observées étant, compte tenu des incertitudes de me-

TABLEAU IV

COMPARAISON DES VALEURS CALCULÉES PAR LE PROGRAMME DE SIMULATION ET DES VALEURS EXPÉRIMENTALES DE k' ET DE n_{eff}

F_c = 40 ml/min, L_c = 4,25 m, T_a = 171°C, T_b = 144°C, l_f = 0,655.

Soluté No.	k' calculé	k' obtenu	n_{eff} calculé	n_{eff} obtenu	Écarts[a] (%)
10	1,06	1,07	1640	1835	+12
4	1,57	1,57	2490	2600	+4,4
5	2,51	2,51	3465	3590	+3,6
1	3,34	3,34	3675	3850	+4,8
6	3,97	3,97	4345	4570	+5,2
2	5,18	5,17	4490	4820	+7,3
7	6,25	6,24	5030	5175	+2,9
8	6,79	6,78	5290	6110	+15
12	7,37	7,38	5415	6010	+11
3	8,01	7,98	5125	5440	+6,1
11	8,74	8,73	5580	5950	+6,6
9	10,48	10,48	5905	6965	+18

[a] Écarts relatifs observés entre les efficacités obtenues et calculées.

TABLEAU V

COMPARAISON DES RÉSOLUTIONS CALCULÉES PAR LE PROGRAMME ET MESURÉES EXPÉRIMENTALEMENT

F_c = 40 ml/min, L_c = 4,25 m, l_f = 0,655.

T_a (°C)	T_b (°C)	R calculée	R mesurée
171	142	1,14	1,14
171	144	1,50	1,49
171	146	1,23	1,33
171	148	0,87	0,90

sure, à la limite de la signification. C'est la raison pour laquelle on a considéré, en première approximation, que n_{inf} et t_q étaient indépendants de la température, mais la Figure 3 montre que ce n'est pas strictement le cas. Pour les efficacités obtenues, les variations observées mettent en évidence le fait que n_{inf} et t_q ne sont pas totalement indépendants des familles de composés; par exemple, on remarque que les écarts les moins importants se produisent pour les alcools et les plus importants pour les aromatiques.

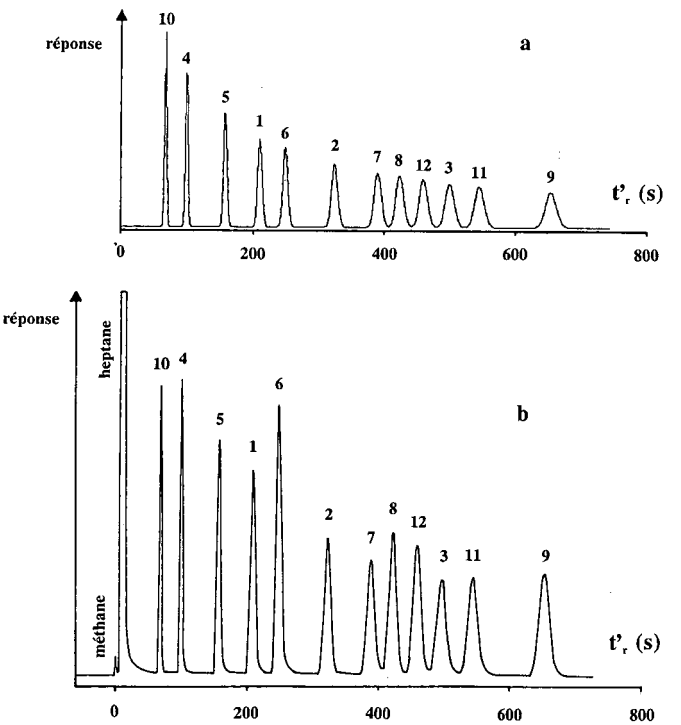

Fig. 4. Comparaison du chromatogramme simulé et obtenu pour la fenêtre. (a) Simulation; (b) chromatogramme obtenu. Pics: 1 = tridécane; 2 = tétradécane; 3 = pentadécane; 4 = hexanol-1; 5 = heptanol-1; 6 = octanol-1; 7 = nonanol-1; 8 = hexylbenzène; 9 = heptylbenzène; 10 = methyl 5-hexanone; 11 = cyclooctanol; 12 = acétophénone.

Quoi qu'il en soit, l'approche développée ici nous donne globalement des résultats satisfaisants et meilleurs que si seule la sélectivité avait été retenue pour critère de réponse. En effet, la variation rapide de l'efficacité d'un couple soluté–colonne en fonction de la température pourrait entraîner parfois à des conclusions trompeuses, si on ne considérait que la sélectivité. Par exemple, à des valeurs fortes de α pourrait correspondre une résolution faible et inversement (voir Tableau III).

On vérifie l'existence de la fenêtre en fixant la température de la colonne OV-25 à 171°C et en faisant varier celle de la colonne Superox 20M de 142 à 148°C. On confirme bien la présence de la fenêtre et on remarque sa forme assez pointue (voir Tableau V) en fonction de la température de la colonne B. Ces résultats montrent l'importance du couplage à deux températures et notamment l'apport d'une optimisation pentaparamétrique (T_a, T_b, l_f, L_c, F_c) par rapport à une optimisation tétraparamétrique (T_c, l_f, L_c, F_c) où l_f est le paramètre principal.

Le logiciel étant muni d'un programme de simulation de chromatogrammes, on présente la comparaison entre la prévision et le résultat expérimental, au travers de la Figure 4, qui correspond aux valeurs du Tableau IV. On remarque la bonne concordance de l'allure des chromatogrammes.

CONCLUSION

L'approche d'optimisation à l'aide de cinq paramètres, par la technique du DAF, s'avère très efficace. Les variables les plus influentes sur la résolution sont T_a, T_b et l_f. L_c et F_c jouent principalement sur le temps d'analyse. Les essais ont été réalisés avec des colonnes remplies, mais l'optimisation peut s'appliquer avec encore plus de facilité à des colonnes capillaires, l'effet de compressibilité des gaz ayant un impact moindre.

REMERCIEMENTS

A. C. remercie l'Agence Nationale pour la Valorisation de la Recherche (ANVAR) pour le financement qui lui a permis de réaliser le dispositif expérimental. Les renseignements et les conditions d'obtention du logiciel peuvent être obtenus à l'adresse indiquée, auprès de J. M. F., auteur de ce programme.

ANNEXE

Flux gazeux dans deux colonnes couplées portées à 2 températures différentes

Prenons le cas d'un débit massique constant au travers de deux colonnes couplées uniformément remplies. Plaçons la colonne A, de longueur L_a en tête à la température T_a et la colonne B de longueur L_b en queue à la température T_b. La pression à l'entrée du système est p_e, à la jonction p_j et à la sortie p_s. Les débits volumiques à l'entrée et à la sortie de la colonne A respectivement F_{ae} et F_{as} et pour la colonne B, F_{be} et F_{bs} et les vitesses du gaz vecteur seront de même u_{ae}, u_{as}, u_{be}, u_{bs}.

Colonne A		Colonne B	
p_c	p_j		p_s
F_{ae}	F_{as} F_{be}		F_{bs}
u_{ae}	u_{as} u_{be}		u_{bs}
T_a, L_a		T_b, L_b	

Si nous mesurons le débit volumique (F_c) à la température ambiante (T_d), alors pour la colonne B

$$F_{bs} = F_c \frac{T_b}{T_d} \tag{A1}$$

et

$$F_{be} = F_{bs} \frac{p_s}{p_j} = F_c \frac{p_s}{p_j} \frac{T_b}{T_d} \tag{A2}$$

pour la colonne A

$$F_{as} = F_{be} \frac{T_a}{T_b} = F_{bs} \frac{p_s}{p_j} \frac{T_a}{T_b} \tag{A3}$$

et

$$F_{ae} = F_{as} \frac{p_j}{p_e} = F_c \frac{p_s}{p_e} \frac{T_a}{T_d} \tag{A4}$$

avec $F = \pi r^2 \varepsilon u$, où F = débit gazeux; ε = porosité; r = rayon interne de la colonne; et u = vitesse du gaz vecteur. On peut écrire pour la colonne B

$$\frac{p_s F_{bs}}{\pi} = p_s r_b^2 \varepsilon_b u_{bs} = p_j r_b^2 \varepsilon_b u_{be} \tag{A5}$$

et pour la colonne A

$$\frac{p_j F_{as}}{\pi} = p_j r_a^2 \varepsilon_a u_{as} = p_e r_a^2 \varepsilon_a u_{ae} \tag{A6}$$

d'où l'on obtient

$$\frac{p_s F_{bs}}{\pi} = p_s r_b^2 \varepsilon_b u_{bs} = p_j r_b^2 \varepsilon_b u_{be} = p_j r_a^2 \varepsilon_a u_{as} \frac{T_b}{T_a} = p_e r_a^2 \varepsilon_a u_{ae} \frac{T_b}{T_a} \tag{A7}$$

Pression intermédiaire pour deux colonnes couplées à températures différentes

Le calcul de p_j revient à déterminer la pression en tête de la colonne B. On peut écrire à partir de $V_{m_b} = \pi r_b^2 \varepsilon_b L_b$ et de l'équation A5

$$F_{bs} = u_{bs} \frac{V_{m_b}}{L_b} \tag{A8}$$

et à partir de l'équation 8

$$u_{bs} = \frac{p_j^2 - p_s^2}{p_s R_{F_b}} \tag{A9}$$

d'où

$$F_{bs} = \frac{V_{m_b}}{L_b} \frac{p_j^2 - p_s^2}{p_s R_{F_b}} \tag{A10}$$

Après réarrangement on obtient

$$p_j^2 = p_s^2 + F_{bs} L_b p_s \frac{R_{F_b}}{V_{m_b}} \tag{A11}$$

et en entrant le débit gazeux F_c, mesuré à la température ambiante T_d, on arrive à

$$p_j^2 = p_s^2 + F_c p_s \frac{T_b}{T_d} \frac{L_b R_{F_b}}{V_{m_b}} \tag{A12}$$

ou

$$p_j^2 = p_s^2 + F_c p_s \frac{T_b}{T_d} \frac{L_b \bar{R}_{F_b}}{\bar{V}_{m_b}} \tag{12}$$

Pression à l'entrée de deux colonnes couplées a températures différentes

Le calcul de p_e revient à déterminer la pression en tête de la colonne A. On peut écrire à partir de $V_{m_a} = \pi r_a^2 \varepsilon_a L_a$ et de l'équation A6

$$F_{as} = \frac{V_{m_a}}{L_a} \frac{p_e^2 - p_j^2}{p_j R_{F_a}} \tag{A13}$$

et à l'aide de l'équation A3

$$F_{bs} = \frac{T_b}{T_a} \frac{V_{m_a}}{L_a} \frac{p_e^2 - p_j^2}{p_s R_{F_a}} \tag{A14}$$

d'où à l'aide de l'équation A1

$$p_e^2 = p_j^2 + F_c p_s \frac{T_a}{T_d} \frac{L_a R_{F_a}}{V_{m_a}} \tag{A15}$$

en éliminant p_j^2 à l'aide de la relation A12 et en réarrangeant l'équation on arrive finalement à

$$p_e^2 = p_s^2 + \frac{p_s F_c}{T_d} \left(\frac{T_a R_{F_a} L_a}{V_{m_a}} + \frac{T_b R_{F_b} L_b}{V_{m_b}} \right) \tag{A16}$$

où T_d = température du débitmètre et F_c = débit de gaz vecteur, ou en faisant intervenir L_c et l_f et en utilisant $\bar{V}_m$ et $\bar{R}_F$

$$p_e^2 = p_s^2 + \frac{p_s F_c L_c}{T_d}\left[\frac{l_f T_a \bar{R}_{F_a}}{\bar{V}_{m_a}} + \frac{(1-l_f)T_b \bar{R}_{F_b}}{\bar{V}_{m_b}}\right] \tag{13}$$

Calcul du rapport des temps morts pour les deux colonnes

Pour la colonne A on aura

$$t_{m_a} = \frac{2}{3}\frac{L_a R_{F_a}}{(p_e^2 - p_j^2)^2}\frac{p_e^3 - p_j^3}{} \tag{A17}$$

de même pour la colonne B

$$t_{m_b} = \frac{2}{3}\frac{L_b R_{F_b}}{(p_j^2 - p_s^2)^2}\frac{p_j^3 - p_s^3}{} \tag{A18}$$

en faisant le rapport

$$Q = \frac{t_{m_a}}{t_{m_b}} = \frac{L_a}{L_b}\frac{R_{F_a}}{R_{F_b}}\frac{(p_e^3 - p_j^3)}{(p_j^3 - p_s^3)}\frac{(p_j^2 - p_s^2)^2}{(p_e^2 - p_j^2)^2} \tag{A19}$$

À partir des équations A12 et A15 on peut écrire

$$p_e^2 - p_j^2 = F_c p_s \frac{T_a}{T_d}\frac{L_a R_{F_a}}{V_{m_a}} \tag{A20}$$

et

$$p_j^2 - p_s^2 = F_c p_s \frac{T_b}{T_d}\frac{L_b R_{F_b}}{V_{m_b}} \tag{A21}$$

Après réarrangement on obtient

$$Q = \frac{L_b R_{F_b}}{L_a R_{F_a}}\frac{V_{m_a}^2}{V_{m_b}^2}\frac{T_b{}^2}{T_a{}^2}\frac{p_e^3 - p_j^3}{p_j^3 - p_s^3} \tag{A22}$$

et en fonction de $\bar{R}_F$ et $\bar{V}_m$

$$Q = \frac{\bar{R}_{F_b}}{\bar{R}_{F_a}}\frac{\bar{V}_{m_a}^2}{\bar{V}_{m_b}^2}\frac{T_b{}^2}{T_a{}^2}\frac{p_e^3 - p_j^3}{p_j^3 - p_s^3} \tag{6}$$

RÉSUMÉ

La technique du diagramme à fenêtre permet de réaliser une approche de l'optimisation de la résolution et du temps d'analyse en chromatographie en phase gazeuse, dans le cas de deux colonnes couplées. L'influence des cinq paramètres suivants est étudiée: la température de chaque colonne, le débit, la longueur totale de colonne et la fraction de longueur de la colonne de tête. Un programme informatique permet, à partir d'un nombre réduit de données expérimentales, de prévoir la valeur à donner à chaque paramètre pour réaliser une séparation optimale. Les vérifications expérimentales conduisent à des résultats qui sont globalement en bon accord avec les valeurs prévues par le diagramme à fenêtre.

BIBLIOGRAPHIE

1 R. J. Laub et J. H. Purnell, *J. Chromatogr.*, 112 (1975) 71.
2 R. J. Laub et J. H. Purnell, *J. Chromatogr.*, 161 (1978) 49.
3 T. W. Smuts, K. de Clerk, T. G. du Toit et T. S. Buys, *J. High Resolut. Chromatogr. Chromatogr. Commun.*, 3 (1980) 124.
4 J. H. Purnell et P. S. Williams, *J. Chromatogr.*, 292 (1984) 197.
5 G. P. Hildebrand et C. N. Reilley, *Anal. Chem.*, 36 (1) (1964) 47.
6 J. H. Purnell et P. S. Williams, *J. Chromatogr.*, 321 (1985) 249.
7 G. Guiochon et E. N. Gutierrez, *J. Chromatogr.*, 406 (1987) 3.
8 J. H. Purnell et P. S. Williams, *J. Chromatogr.*, 325 (1985) 1.
9 J. M. Fougnion, C. David et C. Genty, *16th International Symposium on Chromatography, Abstracts*, GAMS, Paris, 1986, p. 112.
10 J. Ceulemans, *J. Chromatogr. Sci.*, 22 (1984) 296.
11 L. S. Ettre, *Chromatographia*, 18 (5) (1984) 243.
12 R. C. Weast et M. J. Astle (Rédacteurs), *CRC Handbook of Chemistry and Physics*, CRC Press, Boca Raton, FL, 61st ed., 1981.
13 C. Gaget et J. Serpinet, *Analusis*, 14 (2) (1986) 55.
14 R. Brennan et G. Kemball, *J. Inst. Pet.*, 44 (1958) 14.
15 J. P. Bounine et G. Guiochon, *Analusis*, 12 (4) (1984) 175.
16 A. Crocq, *Mémoire Ingénieur*, Conservatoire National des Arts et Métiers, Paris, 1989.
17 J. H. Purnell, *Gas Chromatography*, Wiley, New York, 1962, p. 194.
18 W. E. Harris et H. W. Habgood, *Programmed Temperature Gas Chromatography*, Wiley, New York, 1966, p. 44.

Journal of Chromatography, 556 (1991) 305–316
Elsevier Science Publishers B.V., Amsterdam

CHROM. 23 273

Quantitative resolution of severely overlapping gas chromatographic peaks

Isothermal and temperature-programmed operation

JEFFREY T. LUNDEEN[a] and RICHARD S. JUVET, Jr.*
Department of Chemistry, Arizona State University, Tempe, AZ 85287-1604 (USA)

ABSTRACT

Severely overlapping gas chromatographic peaks ($R \leqslant 0.35$) are quantitatively resolved by a mathematical method. Accurate analyses may be obtained under the worst of overlapping conditions even with simple chromatographic instrumentation. For the method to be successful either the peak shapes of each component must differ if the retention times are identical, or their retention times must be slightly different if the peak shapes are identical. The method has been tested on both isothermal and temperature-programmed data. The computer method proposed requires correction for fluctuations in carrier gas flow-rate and programmed column temperature, both of which cause irreproducibility in peak position. A procedure for accomplishing this correction is presented.

INTRODUCTION

Quantitative analysis of severely overlapping gas chromatographic (GC) peaks has been a serious problem since the introduction of the technique. Whenever possible, resolution has historically been increased by varying the experimental conditions of separation, *i.e.*, column packing, temperature, flow-rate, choice of liquid stationary phase, etc. As samples become more complex, however, the problem of overlapping peaks becomes more acute, and changing the conditions to resolve one set of components generally causes another set to become unresolved. The selection of proper conditions for satisfactory separation can be extremely time consuming, and for complex systems sufficient resolution for accurate analysis by conventional methods is often impossible. Rather than physically resolving the peaks, another approach is to resolve them mathematically.

In an earlier paper on the theory of this approach, Lundeen and Juvet [1] reviewed previous mathematical methods and proposed a new method which gave promising results with computer-simulated data. D'Allura and Juvet [2] applied this method successfully to liquid chromatography. In this work, the method is applied

[a] Present address: James River Corp. Central Research, Camas, WA, USA.

0021-9673/91/$03.50

to both isothermal and temperature-programmed gas chromatography. The detector response is measured at numerous locations throughout the width of the peak. Since peak shapes change with sample size, linear calibration graphs are not obtained except near the peak maxima. An example of experimentally measured calibration graphs obtained from various regions of a chromatographic peak is given in Fig. 1. Pure standards are used to fit the detector response at a given time to a second-degree polynomial of each component's concentration. With higher order polynomials, calibration points can be fitted exactly; random fluctuations, however, are better smoothed by using lower order polynomials [3]. The response from the overlapping mixture is taken as the sum of the responses from each of the components present in the mixture. A series of simultaneous equations are solved to give the concentration of each component of the mixture. Although no instance has been found in any of our studies for the non-additivity of component detector responses, if a possibility were to exist for interference in the flame ionization detection (FID) of two substances eluted simultaneously, the suitability of the analysis would best be tested using a test mixture of the pair at known concentrations. The method is successful if either the peak shape of each overlapping component is slightly different or if there is a slight difference in retention. The analysis of isotopic mixtures in which peak shapes are identical but retentions slightly different has been reported elsewhere [4].

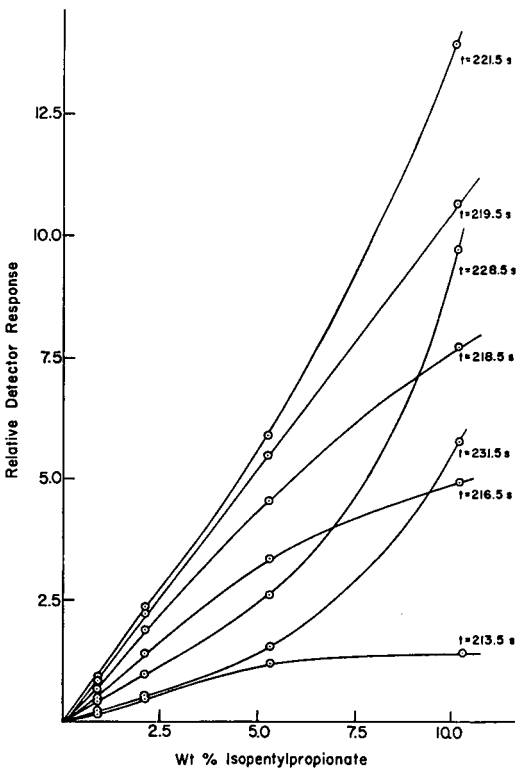

Fig. 1. Calibration graphs for isopentyl propionate. Variation in detector response with sample size at various positions throughout the width of the chromatographic peak. Times given are from moment of injection.

The peak positions must be accurately reproduced between the chromatograms of the standards and that of the unknown mixture. Changes in anything that affects the peak position, such as unexpected variations in flow-rate or in column temperature, affect the accuracy of the proposed method if proper corrections are not made. Therefore, either the flow-rate and column temperature must be held constant so that the peak position doet not vary or else these parameters must be accurately measured and the peak position adjusted to the position it would have had these parameters not varied. The latter approach was chosen.

THEORY

A well established equation in gas chromatography [5,6] is

$$1 = \int_0^{t_R} (\bar{F}/V_R^0)\,dt \tag{1}$$

where dt is the time element, t_R is the observed retention time, V_R^0 is the corrected retention volume and $\bar{F}$ is the average flow-rate in the column. This equation applies to both isothermal and to temperature-programmed gas chromatography as long as the flow-rate and corrected retention volume are both expressed at the same temperature. Both $\bar{F}$ and V_R^0 have the gas compressibility factor applied so that eqn. 1 may be rewritten using the directly observed quantities rather than the pressure-corrected quantities:

$$1 = \int_0^{t_R} (F_c/V_R)\,dt \tag{2}$$

where F_c is the corrected flow-rate expressed at the column outlet and V_R is the observed retention volume. If the flow-rates and volumes are expressed at some standard temperature, T_S, such as 25°C, rather than being expressed at the column temperature, T_c, then

$$F_S = (T_S/T_c)F_c \tag{3}$$

$$V_S = (T_S/T_c)V_R \tag{4}$$

where F_S and V_S correspond to F_c and V_R, respectively, corrected to the standard temperature. Eqn. 1 may therefore be written in terms of these new quantities as

$$1 = \int_0^{t_R} (F_S/V_S)\,dt \tag{5}$$

The adjusted retention volume, V_R', of a compound is the observed retention volume of the compound, V_R, minus the volume of the mobile phase, V_M, generally measured from the retention volume of some unretained compound such as air, V_a:

$$V_R' = V_R - V_M \tag{6}$$

The adjusted retention volume varies with the absolute temperature of the column [5] according to

$$V'_R = A \exp(-\Delta H_S/RT_c) \tag{7}$$

where ΔH_S is the heat of solution of the solute in the stationary phase, R is the gas constant and A is a constant for the particular solute. Both ΔH_S and A vary slightly with temperature, but over a temperature range of 40–60°C can be assumed to be constant. The observed retention volume is then

$$V_R = V_M + A \exp(-\Delta H_S/RT_c) \tag{8}$$

Habgood and Harris [5] have shown that this equation is more accurate if the volume are expressed at a standard temperature rather than at the column temperature. The following approximate equation will be substituted:

$$V_S = B \exp(C/RT_c) \tag{9}$$

Fig. 2 shows a plot of eqn. 9 for *o*-xylene and dodecane. It can be seen that the relationship is sufficiently linear over the temperature range studied to justify the use of eqn. 9. Substituting eqn. 9 into eqn. 5 yields

$$1 = \int_0^{t_R} F_S/[B \exp(C/RT_c)]\, dt \tag{10}$$

The integration could be carried to some time t_i rather than t_R. If $t_i < t_R$ then the integral would be <1, and if $t_i > t_R$, then the integral would be >1.

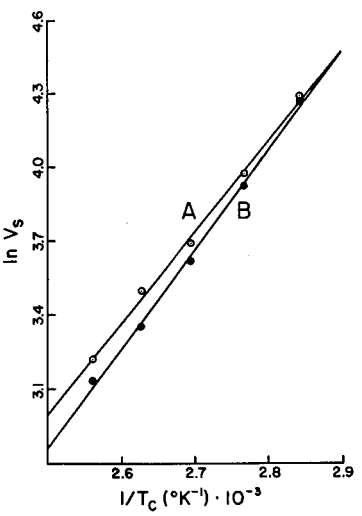

Fig. 2. Retention volume *vs.* $1/T$. Observed retention volumes corrected to 25.00°C. (A) *o*-Xylene; (B) dodecane.

Assume that the same compound is injected two different times under slightly different conditions of temperature and flow-rate. If one of the runs is chosen as standard and the second run is compared with it, the ratio of the two integrals is

$$K = \frac{\int_0^{t_i} (F_S)_2 \exp[-C/R(T_c)_2]\,dt}{\int_0^{t_i} (F_S)_1 \exp[-C/R(T_c)_1]\,dt} \tag{11}$$

As two runs with the same compound are being compared, the constant B will be the same in both integrals and will cancel. If $K > 1$, then under the second set of conditions the compound eluted earlier, and its retention time is

$$(t_R)_2 = (t_R)_1/K \tag{12}$$

This equation is not limited to the retention times of peak maxima but can be used to relate any time within a peak from one set of conditions to the other. If $K < 1$, then the compound eluted later under the second set of conditions but its retention time and other corresponding points on the peak are still given by eqn. 12. By using this equation, the position of a compound injected several times may be corrected for variation in the column temperature and flow-rate of the carrier gas. This equation is applicable for both isothermal and temperature-programmed gas chromatography.

Determination of the exact value of C for both compounds to be resolved would make the above corrections time consuming and impractical for day-to-day use. In order to simplify the procedure, an average value of C may be assumed for all compounds. This assumption implies that the B value for each overlapping component will also be identical since the components elute together.

Therefore, by monitoring the flow-rate and column temperature, the position of peaks eluting under different sets of conditions may be corrected to a set of standard conditions.

EXPERIMENTAL

Gas chromatograph

A Perkin-Elmer (Norwalk, CT, USA) Model 3920 gas chromatograph was used, equipped with a dual flame ionization detector and a 5 ft. × 1/8 in. I.D. column containing 12% Carbowax 20M (Supelco, Bellefonte, PA, USA) on 60–80-mesh Chromosorb W AW. A Model CXSS-18E-12 Chromel–Constantan thermocouple (Omega Engineering, Stamford, CT, USA) was installed through a hole drilled in the side of the column so that the temperature-measuring junction was near the center of the column and in contact with the column packing. The thermocouple was referenced against an ice-bath and calibrated against a precision thermometer. The thermocouple could read to 0.01°C over the temperature range 80–120°C. The injection port was replaced with a Seiscor (Seismograph Service, Tulsa, OK, USA) Model VIII

liquid sampling valve. Tubing from the sample valve output was run through a heated aluminum block maintained at 160°C for rapid and reproducible vaporization of the sample. The sample was dissolved in a solvent and ca. 0.5 μl was injected reproducibly with a standard deviation of 1.6% and a maximum deviation of 4.1%. The volume injected was maintained constant to improve reproducibility in sample vaporization. Nitrogen was used as the carrier gas, and no flow controller was required as corrections were made for variations in flow and temperature. Hence accurate analyses may be obtained using this technique with simple instrumentation.

Flow monitor

The flow monitor used was similar to that reported by Juvet *et al.* [7]. The flow monitor was positioned in the carrier gas line before the liquid sample injection valve. Under computer control, a Seiscor Model VIII gas sampling valve was used to inject a small sample of helium periodically into the carrier gas. The helium introduced passed through the first pair of cells of a Gow-Mac micro-thermal conductivity cell (Model 10-952; Gow-Mac Instrument, Bridgewater, NJ, USA), through an empty capillary delay loop to the second pair of cells. Both thermal conductivity cell pairs were wired to form the four arms of a Wheatstone bridge. The capillary delay loop was made of a 6-ft. length of 1/16-in. O.D. stainless-steel tubing. The time required for the helium to travel through the delay loop was a function of the flow-rate of the carrier gas. A computer automatically injected a 30-μl sample of helium every 30 s and then sampled the output from the Wheatstone bridge at a rate of 200 Hz. The time required for the helium to travel through the delay loop was calibrated over the flow-range 16–22 ml/min against a soap-bubble flow meter. Flow-rates were then converted to a standard temperature of 25°C. Using the flow monitor, the flow-rate of the carrier gas could be measured to ± 0.02 ml/min. Results from the flow monitor are not affected by changes in the temperature of the GC oven. The presence of helium from time to time in the carrier gas had no effect on the FID of the organic compounds injected owing to the insensitivity of the detector to helium.

Computer

A Digital Equipment (Maynard, MA, USA) PDP-8/E computer was used for taking the data reported here, although a Commodore (Santa Clara, CA, USA) 32K microcomputer has been programmed for similar studies involving GC analysis of isotopic mixtures reported elsewhere [4]. The PDP-8/E was equipped with 16K of memory, a KL8-E asynchronous data control board, a DK8-EP real-time programmable clock, an RX02 dual density floppy disk system and a DECwriter II. Programs written used the OS8 V3D operating system. An interface was built to control a Phoenix Data (Phoenix, AZ, USA) Model ADC-312 12-bit analog-to-digital converter (ADC), an eight-channel multiplexer, four relay lines and four switch-sensing lines. Three Analog Devices Model 610K instrumental amplifiers were used to adjust the signals from the thermocouple, flame ionization detector and flow monitor to the 0–5 V range required for the ADC. A Rikadenki-Kogyo (Tokyo, Japan) Model B-161 recorder was sometimes attached to the output of the amplifiers for visual monitoring of the signals.

Procedure

An assembly language program was used to collect data during each injection from the three signal sources. The program sampled the temperature and FID signals at a selectable rate (0.25–100 points/s) and calculated the flow-rate once every 30 s. With 16K of memory both the temperature and FID channel buffers have a maximum data capacity of 3938 points. The buffer on the flow channel will not fill before the other buffers. The order of sampling was four standards of the first component, four standards of the second component, and as many sample mixtures as desired. The data were then analyzed by three BASIC programs. The first program corrected the data for fluctuations in flow and temperature, the second was used to find the peaks of interest and subtract off the baseline and the third did the resolution calculations.

Chemicals

Samples were dissolved in a mixture of hexane isomers (Certified ACS grade, Fisher Scientific, Fair Lawn, NJ, USA). Other reagents were analytical-reagent grade isopentyl propionate, dodecane (99% pure), *o*-xylene (97% pure), tridecane (99+% pure) and 2-octanone (95% pure) (Aldrich, Milwaukee, WI, USA).

RESULTS AND DISCUSSION

Fig. 3 shows typical chromatograms of mixtures of two components with almost identical retentions that have been resolved by this resolution method. Note that no shoulder is apparent on the two peaks eluting at 100 and 160 s in Fig. 3A and B, respectively. No other mathematical resolution method can handle the analysis of such mixtures. The output signals from the flame ionization detector and the thermocouple together with the calculated flow-rates are shown along a common time axis. The off-scale peak and the small peak on its tail in both chromatograms are from the hexane solvent. The temperature of the column packing was measured rather than that of the oven, as partitioning of the sample takes place in the packing. Under isothermal conditions, the packing temperature was constant with a standard deviation of only 0.028°C. With temperature programming, the temperature inside the column shows a significant lag behind the oven temperature owing to the insulating properties of the solid support. The flow-rate is greatest at the time of injection because of vaporization of the sample. It then returns over a period of several seconds to a more constant value. Since the flow monitor averages the flow over the *ca.* 10 s of measurement made each 30 s, any rapid oscillations in flow-rate that might occur at injection are not observed. Flow-rates varied by 0.06 ml/min or *ca.* 0.3% over the period of a chromatographic run if the momentary initial flow increase is disregarded. If it is not, the flow varied by 0.30 ml/min or about 1.3%. Measured flow-rates are used in making retention time corrections rather than an average of these values.

In Fig. 3A the single peak at *ca.* 100 s actually consists of two severely overlapping peaks of *o*-xylene and dodecane with a resolution of only 0.35. Quantitative results for this chromatogram and other mixtures of the same two compounds are given in Table I. The average error before corrections for variations in flow-rate and temperature was *ca.* 13%, and this was reduced to *ca.* 7% after making retention time corrections, an error not much larger than the 2–5% error generally quoted for completely resolved peaks in conventional GC analyses. The corrections were made

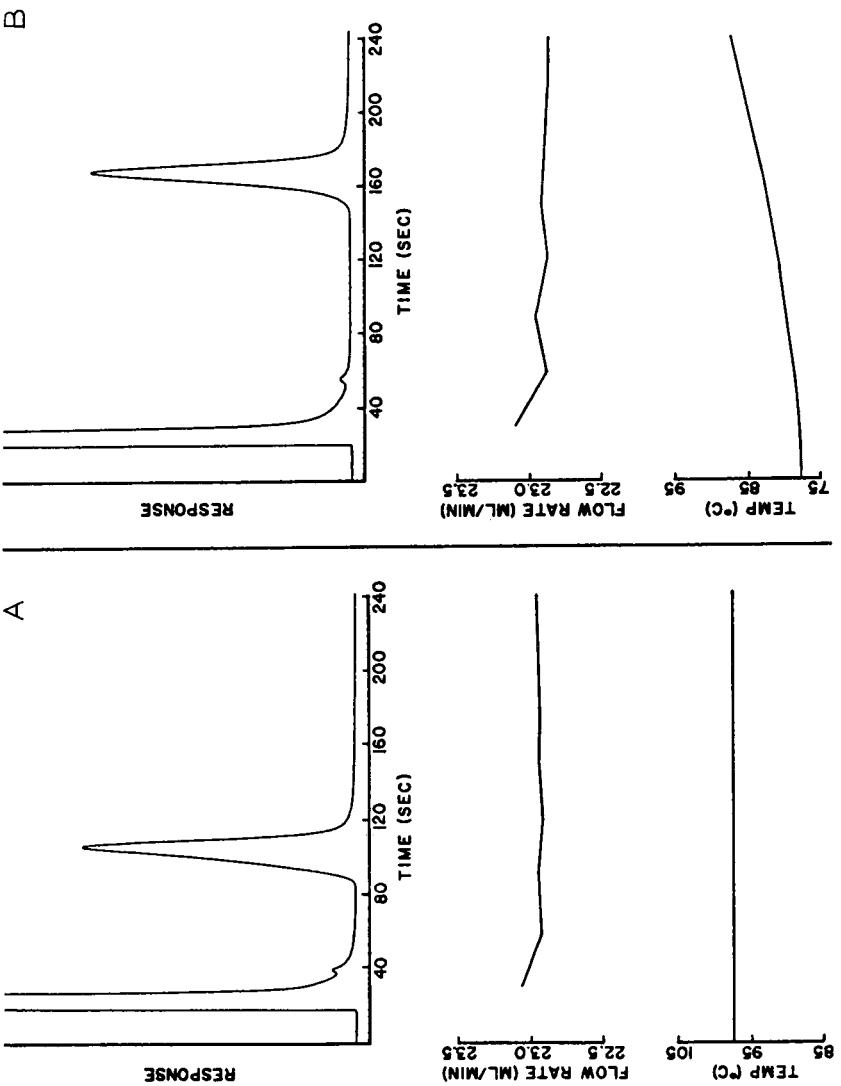

Fig. 3. (A) Isothermal analysis of dodecane and *o*-xylene. Column temperature: 97.4°C. Peak resolution: 0.35. Mixture: 3.00% (v/v) *o*-xylene and 3.00% (v/v) dodecane in hexane (first two peaks from hexane solvent). Measured flow-rate and column temperature shown at the time indicated. Column: 12% Carbowax 20M on 60–80-mesh Chromosorb W AW. (B) Temperature-programmed analysis of dodecane and *o*-xylene. Oven temperature: initially 77.9°C, then programmed at *ca.* 3.5°C/min for 4 min. Peak resolution: 0.24. Mixture, measured flow-rate and column temperature and column as in (A).

using a C value of 8.0 kcal/mol. The corrections were made using a range of C values of $\pm 20\%$ from this value, and the quantitative results varied by less than 1%. Hence correction is not strongly dependent on the choice of C when variations in temperature are small.

Table II gives the results for the resolution of tridecane and 2-octanone analyzed isothermally. The peaks had a resolution of only 0.20, a value so small that no indication of a shoulder is evident on the peak. However, the average error in composition after corrections for fluctuations in flow-rate and temperature is only *ca.* 9%.

Fig. 3B is a typical temperature-programmed chromatogram. The peak eluting at *ca.* 160 s is composed of a mixture of dodecane and *o*-xylene, the resolution of which is only 0.24 under the experimental conditions used. Table III gives the analytical results for various mixtures of these two components. The average error before corrections for variations in temperature and flow-rate was *ca.* 28% and after corrections was *ca.* 24%. As expected, these errors are considerably larger than those found under isothermal conditions. Not only is the flow changing during the analysis, but also the temperature is being deliberately changed. Changes in temperature have a dramatic effect on retention times, hence any small irregularities in the rate of heating between different samples will affect the results. Equally important, peak shapes are more symmetrical and similar in temperature-programmed GC than in isothermal determinations. The correction method was designed to correct for these changes in temperature and flow-rate, and it did improve the results. Considering that the two components involved had almost identical retention times ($R = 0.24$), any result at all under such conditions must be considered remarkable. No other method of resolution can approach the accuracy obtained for these severely overlapping peaks. The small difference in retention and the similarity in peak shapes contribute significantly to the errors obtained in temperature-programmed operation.

CONCLUSIONS

The resolution method developed earlier by Lundeen and Juvet [1] using computer-simulated chromatographic peaks has been shown to work well in practice under isothermal conditions and reasonably well in temperature-programmed determinations under conditions of resolution that no other mathematical resolution method can handle. As this method provides relatively good accuracy with isothermal determinations of severely overlapping peaks, some might choose to analyze the sample isothermally at higher temperatures, accepting overlapping of early eluting peaks, rather than to use temperature-programmed elution. A large part of the error is undoubtedly caused by the $\pm 1.6\%$ sampling error. The flow monitor measures the average flow-rate for periods of 10 s once every 30 s. If this period could be reduced or a continous monitor designed, as was done for our work in liquid chromatography [2], a more accurate profile of the flow-rate could be made. This should further improve retention corrections. Moreover, in this work all peaks were measured using the same amplifier gain from the gas chromatograph. This meant that on the smaller peaks only about 15% of the range of the ADC was used. If the gain of the amplifier were accurately calibrated at different gain settings, the height of each peak could be adjusted to take full advantage of the ADC, probably leading to further improvements in accuracy.

TABLE I

ISOTHERMAL ANALYSIS OF DODECANE AND *o*-XYLENE

Improvement in quantitative results through correction for flow and temperature variations. Conditions as in Fig. 3A. Peak resolution: 0.35. Component 1 is *o*-xylene and 2 is dodecane.

Actual		Uncorrected				Corrected			
Amount of 1 (%, v/v)	Amount of 2 (%, v/v)	Amount of 1 (%, v/v)	Error (%)	Amount of 2 (%, v/v)	Error (%)	Amount of 1 (%, v/v)	Error (%)	Amount of 2 (%, v/v)	Error (%)
3.00	3.00	3.44	+14.7	2.48	−17.3	3.33	+11.0	2.74	−8.7
2.00	4.00	2.39	+19.5	3.73	− 6.8	2.30	+15.0	3.90	−2.5
4.00	2.00	4.38	+ 9.5	1.84	− 8.0	4.29	+ 7.2	2.00	0.0

TABLE II

ISOTHERMAL ANALYSIS OF TRIDECANE AND 2-OCTANONE

Improvement in quantitative results through correction for flow and temperature variations. Column temperature: 87.7°C. Peak resolution: 0.20. Component 1 is tridecane and 2 is 2-octanone.

Actual		Uncorrected				Corrected			
Amount of 1 (%, v/v)	Amount of 2 (%, v/v)	Amount of 1 (%, v/v)	Error (%)	Amount of 2 (%, v/v)	Error (%)	Amount of 1 (%, v/v)	Error (%)	Amount of 2 (%, v/v)	Error (%)
2.00	4.00	1.92	−4.0	4.37	+ 9.2	2.03	+ 1.5	4.31	+ 7.8
2.00	4.00	1.93	−3.5	4.39	+ 9.8	2.04	+ 2.0	4.34	+ 8.5
3.00	3.00	3.22	+7.3	3.59	+19.7	3.32	+10.7	3.47	+15.7
3.00	3.00	3.23	+7.7	3.58	+19.3	3.34	+11.3	3.47	+15.7
2.00	4.00	1.93	−3.5	4.43	+10.8	1.91	− 4.5	4.45	+11.2
2.00	4.00	2.03	+1.5	4.41	+10.2	1.95	− 2.5	4.45	+11.2
3.00	3.00	3.18	+6.0	3.57	+19.0	3.27	+ 9.0	3.46	+15.3
3.00	3.00	3.14	+4.7	3.60	+20.0	3.26	+ 8.7	3.47	+15.7

TABLE III

PROGRAMMED TEMPERATURE ANALYSIS OF DODECANE AND *o*-XYLENE

Improvement in quantitative results through correction for flow and temperature variations. Conditions as in Fig. 3B. Peak resolution: 0.24. Component 1 is *o*-xylene and 2 is dodecane.

Actual		Uncorrected				Corrected			
Amount of 1 (%, v/v)	Amount of 2 (%, v/v)	Amount of 1 (%, v/v)	Error (%)	Amount of 2 (%, v/v)	Error (%)	Amount of 1 (%, v/v)	Error (%)	Amount of 2 (%, v/v)	Error (%)
3.00	3.00	3.10	+ 3.3	4.29	+43.0	2.93	− 2.3	4.51	+50.3
3.00	3.00	3.16	+ 5.3	4.44	+48.0	3.01	+ 0.3	4.53	+51.0
2.00	4.00	2.76	+38.0	3.82	− 4.5	2.49	+24.5	4.20	+ 5.0
2.00	4.00	2.74	+37.0	3.83	− 4.2	2.46	+23.0	4.27	+ 6.8
4.00	2.00	5.28	+32.0	0.72	−64.0	4.33	+ 8.3	3.27	+63.5

Although only packed columns have been employed in the study reported here, peak widths of 20–30 s were handled with ease. Since temperature and FID signals can be sampled as rapidly as 100 points/s, open-tubular columns with a good quality, chemically bonded liquid stationary phase could possibly be used.

ACKNOWLEDGEMENTS

The idea for this work was generated while one of us (R.S.J.) was on sabbatical leave in Professor Guiochon's laboratory at the École Polytechnique. The authors thank Professor Guiochon for the use of his equipment for preliminary research and Marie-France Gonnard and Claire Videl-Madjar for laboratory assistance during these early studies.

REFERENCES

1 J. T. Lundeen and R. S. Juvet, *Anal. Chem.*, 53 (1981) 1369.
2 N. J. D'Allura and R. S. Juvet, *J. Chromatogr.*, 239 (1982) 439.
3 S. D. Christian and E. E. Tucker, *Am. Lab.*, 15, No. 9 (1983) 35.
4 Y. W. Fan and R. S. Juvet, in preparation.
5 H. W. Habgood and W. E. Harris, *Anal. Chem.*, 32 (1960) 450.
6 W. E. Harris and H. W. Habgood, *Programmed Temperature Gas Chromatography*, Wiley, New York, 1966, Ch. 2–4.
7 R. S. Juvet, J. P. Olivo and G. Guiochon, *Anal. Chem.*, 55 (1983) 1614.

Journal of Chromatography, 556 (1991) 317–330
Elsevier Science Publishers B.V., Amsterdam

CHROM. 23 235

Thermodynamics of solution of non-mesomorphic solutes at infinite dilution in the smectic-A, nematic and isotropic phases of *p*-*n*-octyl-*p'*-cyanobiphenyl

A gas–liquid chromatographic study

SAMIR GHODBANE[a], GHASSAN A. OWEIMREEN[b] and DANIEL E. MARTIRE*
Department of Chemistry, Georgetown University, Washington, DC 20057 (USA)

ABSTRACT

From specific retention volumes measured at four temperatures in each of the three fluid phases of *p*-*n*-octyl-*p'*-cyanobiphenyl (8CB), infinite-dilution solute activity coefficients, partial molar excess enthalpies and entropies, and enthalpies and entropies of solution were determined for 21 solutes varying in molecular size, shape and flexibility. The reported results and their trends are discussed in terms of a previously proposed solution model. The results for 8CB are compared with those for the lower alkyl homologs in this liquid-crystalline solvent series, 5CB, 6CB and 7CB. The thermodynamic behavior within each of five solute groups is interpreted.

INTRODUCTION

Gas–liquid chromatography (GLC) has become an established technique for the determination of reliable thermodynamic data for volatile solutes at "infinite dilution" in non-volatile solvents. In the Henry's law region, GLC has become the method of choice because of the speed and ease with which data can be obtained for a wide variety of solutes. As the solute diffusion rate in both the liquid and vapor phases is extremely fast, instantaneous equilibrium takes place at all points in the column. Accordingly, the dynamic equilibrium of GLC can be approximated by true static equilibrium. Two comprehensive studies (one undertaken in this laboratory [1] and one inter-laboratory [2]) comparing GLC and extrapolated static data have confirmed that inifinite-dilution solute activity coefficients accurate to better than ± 1% can be obtained by GLC.

[a] Present address: Analytical Research Department, Merck & Co., P.O. Box 2000, R80L-106, Rahway, NJ 07065, USA.
[b] Present address: Department of Chemistry, King Fahd University of Petroleum and Minerals, Dhahran 31261, Saudi Arabia.

0021-9673/91/$03.50

Of particular interest to the present authors is the reliability [3–5] and application of GLC [6–17] for the determination of thermodynamic properties of non-mesomorphic solutes in the mesophases and isotropic phase of liquid crystals. The purpose of these studies was to achieve a better understanding of the effect of solute characteristics (size, shape, flexibility, polarity and polarizability) on the solution process in ordered and disordered assemblies of rod-like molecules.

In this work, thermodynamic data were obtained by GLC for 21 non-mesomorphic solutes in the smectic-A (S_A), nematic (N) and isotropic (I) phases of *p-n*-octyl-*p'*-cyanobiphenyl (8CB). This study complements previous work on *p-n*-pentyl-*p'*-cyanobiphenyl (5CB) [6], *p-n*-hexyl-*p'*-cyanobiphenyl (6CB) [17] and *p-n*-heptyl-*p'*-cyanobiphenyl (7CB) [16], and forms part of a systematic study on the members of this important series [18]. Of the four liquid crystals listed, 8CB is the only one to exhibit the more ordered smectic-A mesophase. The data, which are examined in the light of an infinite-dilution solution model [7,9,19], are compared with previous results.

EXPERIMENTAL

The liquid stationary phase was obtained in sealed ampoules from BDH (Poole, UK) and was used without purification. Its quoted purity of 99.5% was evident from its sharp crystal to smectic-A endotherm observed by differential scanning calorimetry (DSC) [20]. Shown in Table I are the observed transition temperatures and enthalpies (ΔH) for 8CB [20]. The very small ΔH value obtained for the smectic-A to nematic ($S_A \rightarrow N$) transition indicates a very weakly first-order phase transition. Other investigators, using X-ray scattering and DSC [21] or high-precision calorimetry [22], have come to the conclusion that the $S_A \rightarrow N$ transition is virtually second order ($\Delta H \approx 0$).

8CB was coated on Johns-Manville 60–80 mesh, acid-washed and DMCS-treated Chromosorb W HP (Alltech, Deerfield, IL, USA). Details of the column preparation are given elsewhere [6,23]. The weight percentage of liquid phase in the packing (*i.e.*, the liquid phase loading) was determined by careful ashing [24] of three samples of about 1 g of packing, done before and after combustion of 8CB. The column used to obtain the thermodynamic data contained a loading of 11.50 ± 0.03%.

The 21 non-mesomorphic solutes chosen for this study (see Table II) exhibit a range of solute sizes, shapes and flexibilities. They were obtained from various standard sources and fall into five main categories: normal alkanes (*n*-C_5 to *n*-C_9), branched hexanes, branched heptanes, quasi-spherical molecules (3,3-diethylpentane

TABLE I

TRANSITION TEMPERATURES AND ENTHALPIES OF 8CB [20]

Transition	t(°C)	ΔH (cal mol^{-1})
Crystal → smectic A (C→S_A)	21.2	5900 ± 150
Smectic A → nematic (S_A→N)	33.4	16 ± 2
Nematic → isotropic (N→I)	40.6	187 ± 9

TABLE II

LIST OF SOLUTES

Solute	Compound	Molecular weight	Boiling point (°C)
1	*n*-Pentane	72.15	36.07
2	*n*-Hexane	86.18	68.74
3	*n*-Heptane	100.21	98.43
4	*n*-Octane	114.20	125.66
5	*n*-Nonane	128.26	150.80
6	2-Methylpentane	86.17	60.27
7	3-Methylpentane	86.17	63.28
8	2,2-Dimethylbutane	86.17	49.74
9	2,3-Dimethylbutane	86.17	57.99
10	2-Methylhexane	100.21	90.05
11	3-Methylhexane	100.21	91.85
12	3-Ethylpentane	100.21	93.47
13	2,2-Dimethylpentane	100.21	79.20
14	2,3-Dimethylpentane	100.21	89.78
15	2,4-Dimethylpentane	100.21	80.50
16	3,3-Dimethylpentane	100.21	86.06
17	2,2,3-Trimethylbutane	100.21	80.88
18	Tetramethyltin	178.84	78.0
19	3,3-Diethylpentane	128.26	146.17
20	Benzene	78.12	80.11
21	Toluene	92.14	110.62

and tetramethyltin) and aromatics (benzene and toluene). All solutes were sufficiently volatile at the experimental temperatures and were used without further purification. Except for tetramethyltin, their required physical properties (molar volumes, saturated vapor pressure and second virial coefficients) were available or could be accurately determined [9].

A dual-column GLC apparatus, equipped with a Gow-Mac (Madison, NJ, USA) hot-wire thermal conductivity detector (Model 10-952) with AuW elements) in conjunction with a Gow-Mac bridge control and power supply (Model 40-001) and a well stirred and thermally regulated water-bath to maintain the column temperature to within ± 0.03°C, was used. The column was installed and conditioned with a gentle flow of carrier gas (helium) for 24 h at 50°C. Before entering the column, the carrier gas was passed through a trap packed with 5A molecular sieve to adsorb moisture and contaminants. The carrier gas flow continued through a Negretti-Zambra (London, UK) precision pressure regulator (Model R/182) and finally to a Hamilton (Whittier, CA, USA) injection port (inlet part No. 86800, heated to about 200°C) and into the column. Inlet pressures were selected to give convenient elution times and reasonable column efficiency. The procedure followed to obtain accurate results is described elsewhere [6]. The use of internal standards showed that column bleeding and decomposition were negligible during the period of operation. Finally, all the usual, necessary steps were taken to ensure the attainment of the infinite-dilution condition [6] and the absence of interfacial effects [6,25].

RESULTS

Specific retention volumes, V_g^0, [2,24] were obtained at four temperatures in each of the smectic-A (23.0, 25.5, 28.5 and 31.0°C), nematic (35.5, 36.5, 37.5 and 38.5°C) and isotropic (43.0, 45.5, 48.5 and 50.5°C) phases. By remaining at least 2.5°C below the smectic-A to nematic transition temperature and at least 2°C below the nematic to isotropic transition temperature, we ensured that the passage of the solute band through the column did not induce a phase transition [8,20]. The V_g^0 values reported in Tables III–V represent the average of three separate measurements for each point. The fugacity-corrected infinite-dilution solute activity coefficients, γ_f^∞, were calculated from V_g^0 using the following equation [6]:

$$\ln(\gamma_f^\infty) = \ln(273.2R/M_1P_2^0V_g^0) - B_{22}P_2^0/RT \quad (1)$$

where R is the gas constant, M_1 is the solvent molecular weight and P_2^0 and B_{22} are the saturated vapor pressure and second virial coefficient, respectively, of the pure solute at the experimental temperature T. The vapor pressures were calculated from the Antoine equation, by use of the constants contained in Dreisbach's compilation [26]. The virial coefficients were calculated from the modified corresponding states equation of McGlashgan, Wormald and co-workers [27–29], using the critical constants from ref. 26. The resulting γ_f^∞ values are reported in Tables VI–VIII. The

TABLE III

SOLUTE SPECIFIC RETENTION VOLUMES (V_g^0, ml g^{-1}) IN SMECTIC 8CB

Solute No.	23.0°C	25.5°C	28.5°C	31.0°C
1	37.76	35.03	32.28	30.23
2	118.8	108.5	96.37	89.34
3	364.5	327.9	287.5	260.9
4	1095	972.8	832.7	743.9
5	3307	2865	2409	2130
6	78.29	71.84	64.56	59.04
7	93.23	84.71	75.94	69.40
8	49.84	46.04	41.65	38.84
9	72.59	66.93	60.39	55.33
10	229.5	207.5	182.8	165.4
11	256.0	232.5	203.3	184.5
12	281.7	256.5	224.2	203.0
13	134.8	123.4	109.9	100.6
14	235.5	212.3	187.9	170.2
15	141.0	128.6	114.0	104.4
16	194.9	176.6	156.3	142.8
17	152.1	136.7	123.4	112.2
18	146.6	132.6	119.3	109.0
19	2116	1882	1604	1431
20	542.6	488.3	433.5	395.3
21	1787	1589	1377	1246

TABLE IV

SOLUTE SPECIFIC RETENTION VOLUMES (V_g^0, ml g^{-1}) IN NEMATIC 8CB

Solute No.	35.5°C	36.5°C	37.5°C	38.5°C
1	27.01	26.50	25.91	25.62
2	77.05	75.97	74.10	72.14
3	219.6	213.9	208.8	203.6
4	618.1	598.1	585.8	563.6
5	1741	1671	1624	1558
6	52.66	51.52	50.14	49.80
7	61.44	60.60	59.20	58.79
8	34.29	33.95	33.15	33.10
9	49.71	49.01	48.09	47.41
10	142.7	139.8	135.7	133.0
11	159.6	155.9	151.6	149.0
12	175.2	171.5	167.4	164.8
13	86.41	84.28	82.87	81.18
14	148.4	145.3	142.5	140.3
15	91.81	89.03	87.34	85.55
16	125.4	122.7	120.7	119.2
17	98.92	97.97	96.14	95.70
18	97.95	95.95	94.11	91.93
19	1237	1199	1178	1149
20	346.1	338.1	329.3	323.9
21	1078	1042	1011.6	984.5

TABLE V

SOLUTE SPECIFIC RETENTION VOLUMES (V_g^0, ml g^{-1}) IN ISOTROPIC 8CB

Solute No.	43.0°C	45.5°C	48.5°C	50.5°C
1	27.14	25.29	23.56	22.43
2	73.30	68.77	63.05	59.13
3	199.8	183.6	167.0	155.1
4	540.4	490.7	435.1	401.8
5	1451	1296	1131	1039.6
6	51.18	47.78	44.57	42.10
7	59.97	56.31	52.29	49.66
8	34.48	32.32	30.88	29.38
9	49.48	46.28	43.21	41.17
10	134.1	124.5	114.8	106.8
11	150.5	139.5	128.1	119.0
12	167.5	154.9	142.4	132.8
13	84.87	78.90	73.32	68.28
14	141.7	132.9	122.5	113.8
15	88.41	82.67	76.77	73.56
16	122.4	113.4	105.7	99.01
17	98.14	92.36	85.60	80.39
18	92.76	85.93	80.10	75.55
19	1131	1017	906.4	846.6
20	321.6	296.1	266.1	247.5
21	941.1	848.3	750.4	696.0

TABLE VI

SOLUTE ACTIVITY COEFFICIENTS (γ_f^∞) IN SMECTIC 8CB

Solute No.	23.0°C	25.5°C	28.5°C	31.0°C
1	3.36	3.30	3.22	3.15
2	3.60	3.54	3.51	3.42
3	3.90	3.83	3.77	3.69
4	4.28	4.19	4.15	4.06
5	4.62	4.55	4.50	4.38
6	3.91	3.84	3.79	3.76
7	3.66	3.63	3.59	3.55
8	4.08	4.02	3.97	3.89
9	3.80	3.73	3.68	3.65
10	4.29	4.22	4.16	4.11
11	4.12	4.02	4.00	3.93
12	3.97	3.87	3.84	3.78
13	4.56	4.46	4.40	4.33
14	4.00	3.95	3.89	3.84
15	4.67	4.58	4.53	4.44
16	4.01	3.96	3.92	3.85
17	4.16	4.15	4.04	4.00
19	4.35	4.22	4.16	4.06
20	1.25	1.24	1.22	1.20
21	1.28	1.27	1.25	1.23

TABLE VII

SOLUTE ACTIVITY COEFFICIENTS (γ_f^∞) IN NEMATIC 8CB

Solute No.	35.5°C	36.5°C	37.5°C	38.5°C
1	3.03	2.99	2.96	2.89
2	3.31	3.23	3.18	3.14
3	3.56	3.49	3.42	3.36
4	3.85	3.78	3.67	3.62
5	4.11	4.04	3.93	3.87
6	3.55	3.50	3.46	3.36
7	3.38	3.30	3.25	3.15
8	3.76	3.67	3.63	3.52
9	3.44	3.36	3.31	3.24
10	3.90	3.81	3.77	3.68
11	3.72	3.65	3.59	3.50
12	3.59	3.51	3.44	3.35
13	4.19	4.12	4.03	3.95
14	3.62	3.54	3.46	3.37
15	4.18	4.14	4.05	3.98
16	3.63	3.56	3.48	3.38
17	3.78	3.67	3.59	3.47
19	3.67	3.59	3.47	3.38
20	1.13	1.11	1.09	1.07
21	1.14	1.12	1.10	1.08

TABLE VIII

SOLUTE ACTIVITY COEFFICENTS (γ_1^∞) IN ISOTROPIC 8CB

Solute No.	43.0°C	45.5°C	48.5°C	50.5°C
1	2.37	2.35	2.30	2.28
2	2.61	2.54	2.49	2.47
3	2.81	2.75	2.67	2.65
4	3.02	2.95	2.89	2.85
5	3.24	3.17	3.10	3.04
6	2.78	2.73	2.65	2.62
7	2.63	2.56	2.49	2.45
8	2.91	2.86	2.72	2.69
9	2.65	2.60	2.52	2.48
10	3.03	2.95	2.84	2.83
11	2.87	2.80	2.70	2.69
12	2.73	2.66	2.57	2.55
13	3.18	3.11	3.00	2.99
14	2.78	2.68	2.59	2.58
15	3.22	3.13	3.02	2.93
16	2.76	2.70	2.59	2.57
17	2.85	2.76	2.67	2.65
19	2.73	2.68	2.60	2.53
20	0.89	0.88	0.87	0.87
21	0.92	0.92	0.91	0.90

TABLE IX

SOLUTE PARTIAL MOLAR EXCESS ENTHALPIES ($\bar{H}^e$, kcal mol^{-1})

Solute	Smectic	Nematic	Isotropic
1	1.43 ± 0.06	2.83 ± 0.25	1.07 ± 0.10
2	1.10 ± 0.16	3.18 ± 0.34	1.50 ± 0.18
3	1.21 ± 0.08	3.77 ± 0.04	1.66 ± 0.12
4	1.13 ± 0.12	4.08 ± 0.37	1.62 ± 0.07
5	1.14 ± 0.15	3.98 ± 0.28	1.67 ± 0.05
6	0.85 ± 0.07	3.33 ± 0.46	1.73 ± 0.12
7	0.66 ± 0.02	4.17 ± 0.33	1.93 ± 0.04
8	1.02 ± 0.09	4.06 ± 0.45	2.27 ± 0.25
9	0.90 ± 0.09	3.80 ± 0.11	1.83 ± 0.08
10	0.96 ± 0.06	3.58 ± 0.21	2.00 ± 0.21
11	0.97 ± 0.14	3.77 ± 0.22	1.84 ± 0.20
12	1.00 ± 0.16	4.32 ± 0.18	1.93 ± 0.16
13	1.14 ± 0.08	3.72 ± 0.16	1.75 ± 0.24
14	0.92 ± 0.01	4.46 ± 0.14	2.06 ± 0.29
15	1.09 ± 0.08	3.32 ± 0.28	2.62 ± 0.10
16	0.88 ± 0.07	4.56 ± 0.22	2.05 ± 0.20
17	0.94 ± 0.15	5.28 ± 0.28	2.07 ± 0.19
19	1.45 ± 0.15	5.48 ± 0.25	2.00 ± 0.16
20	0.98 ± 0.07	3.65 ± 0.21	0.71 ± 0.12
21	0.90 ± 0.10	3.17 ± 0.15	0.62 ± 0.06

infinite-dilution solute partial molar excess enthalpy ($\bar{H}^e$) and entropy $\bar{S}^e$) were determined from the usual thermodynamic relationship:

$$\ln(\gamma_f^\infty) = \bar{H}^e/RT - \bar{S}^e/R \tag{2}$$

Hence, a linear least-squares fit of ln (γ_f^∞) as a function of $1/T$ gives $\bar{H}^e$ (from the slope) and $\bar{S}^e$ (from the intercept) (Tables IX and X). The high linear correlation coefficients (most of them in excess of 0.999) reflect the quality of the data. A typical plot of ln γ_f^∞ *vs.* $1/T$ is shown in Fig. 1. It is important to point out that only a very small discontinuity in ln γ_f^∞, if any, is observed at the $S_A \rightarrow N$ transition temperatue. This is the case for all the solutes studied and is consistent with the weakly first or second-order nature of the $S_A \rightarrow N$ transition.

The inifinite-dilution solute partial molar enthalpy and entropy of solution ($\Delta\bar{H}$ and $\Delta\bar{S}$) were obtained by means of the following equation [7,30]:

$$\ln(V_g^0) = -\Delta\bar{H}/RT + \Delta\bar{S}/R - \ln(M_1/273.2\,R) \tag{3}$$

A linear least-squares fit of ln V_g^0 *vs.* $1/T$ yields $\Delta\bar{H}$ (from the slope) and $\Delta\bar{S}$ (from the intercept) (Tables XI and XII). Virtually all of the linear correlation coefficients of the fits were in excess of 0.999.

TABLE X

SOLUTE PARTIAL MOLAR EXCESS ENTROPIES ($\bar{S}^e$, cal mol^{-1} K^{-1})

Solute No.	Smectic	Nematic	Isotropic
1	2.40 ± 0.18	6.95 ± 0.79	1.65 ± 0.30
2	1.16 ± 0.54	7.95 ± 1.09	2.85 ± 0.56
3	1.38 ± 0.25	9,70 ± 0.12	3.19 ± 0.39
4	0.92 ± 0.39	10.53 ± 1.18	2.94 ± 0.23
5	0.82 ± 0.50	10.07 ± 0.89	2.95 ± 0.14
6	0.17 ± 0.22	8.28 ± 1.48	3.45 ± 0.37
7	0.35 ± 0.07	11.08 ± 1.06	4.20 ± 0.13
8	0.64 ± 0.30	10.52 ± 1.44	5.05 ± 0.78
9	0.40 ± 0.30	9.85 ± 0.34	3.84 ± 0.24
10	0.35 ± 0.20	8.88 ± 0.69	4.14 ± 0.66
11	0.45 ± 0.46	9.61 ± 0.72	3.73 ± 0.63
12	0.63 ± 0.55	11.46 ± 0.58	4.12 ± 0.49
13	0.85 ± 0.27	9.22 ± 0.53	3.25 ± 0.75
14	0.35 ± 0.02	11.90 ± 0.44	4.49 ± 0.90
15	0.62 ± 0.27	7.92 ± 0.90	5.96 ± 0.31
16	0.21 ± 0.25	12.21 ± 0.70	4.46 ± 0.64
17	0.33 ± 0.49	14.46 ± 0.92	4.47 ± 0.59
19	1.97 ± 0.51	15.17 ± 0.80	4.34 ± 0.50
20	2.87 ± 0.24	11.57 ± 0.67	2.47 ± 0.36
21	2.54 ± 0.35	10.02 ± 0.49	2.13 ± 0.18

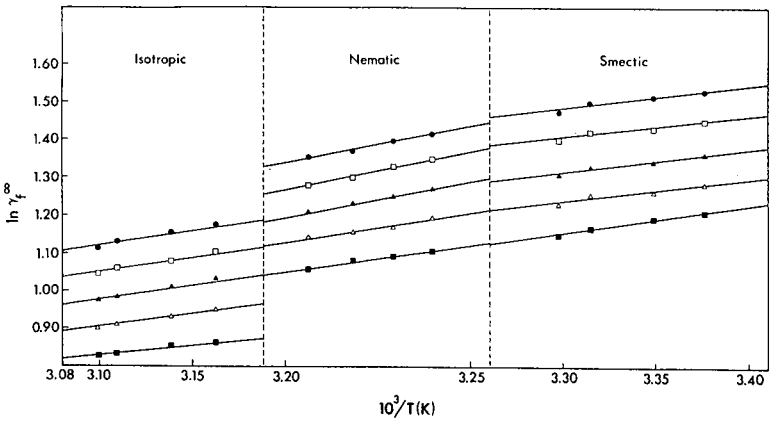

Fig. 1. Logarithm of the solute acitivity coefficient at infinite dilution (ln γ_f^∞) *versus* reciprocal temperature ($10^3/T$). ■ = *n*-Pentane; △ = *n*-hexane; ▲ = *n*-heptane; □ = *n*-octane; ● = *n*-nonane. Phase transition temperatures are indicated by dashed vertical lines.

TABLE XI

SOLUTE PARTIAL MOLAR ENTHALPIES OF SOLUTION ($\Delta\bar{H}$, kcal mol^{-1})

Solute No.	Smectic	Nematic	Isotropic
1	−4.97 ± 0.06	−3.46 ± 0.25	−5.13 ± 0.10
2	−6.46 ± 0.17	−4.25 ± 0.34	−5.82 ± 0.17
3	−7.53 ± 0.08	−4.82 ± 0.04	−6.80 ± 0.12
4	−8.75 ± 0.12	−5.69 ± 0.37	−8.05 ± 0.07
5	−9.91 ± 0.16	−6.92 ± 0.28	−9.07 ± 0.05
6	−6.32 ± 0.06	−3.72 ± 0.46	−5.21 ± 0.12
7	−6.60 ± 0.03	−2.98 ± 0.33	−5.10 ± 0.04
8	−5.63 ± 0.09	−2.48 ± 0.45	−4.11 ± 0.33
9	−6.08 ± 0.08	−3.08 ± 0.10	−4.94 ± 0.08
10	−7.36 ± 0.06	−4.61 ± 0.21	−6.05 ± 0.21
11	−7.41 ± 0.14	−4.47 ± 0.23	−6.27 ± 0.19
12	−7.42 ± 0.16	−3.95 ± 0.18	−6.21 ± 0.15
13	−6.61 ± 0.08	−3.90 ± 0.17	−5.76 ± 0.24
14	−7.26 ± 0.01	−3.59 ± 0.14	−5.87 ± 0.28
15	−6.78 ± 0.08	−4.42 ± 0.28	−5.00 ± 0.11
16	−7.01 ± 0.08	−3.21 ± 0.22	−5.61 ± 0.20
17	−6.71 ± 0.15	−2.26 ± 0.29	−5.36 ± 0.18
18	−6.60 ± 0.08	−4.01 ± 0.10	−5.46 ± 0.16
19	−8.85 ± 0.15	−4.59 ± 0.25	−7.87 ± 0.17
20	−7.09 ± 0.08	−4.30 ± 0.21	−7.12 ± 0.11
21	−8.20 ± 0.11	−5.78 ± 0.15	−8.21 ± 0.06

TABLE XII

SOLUTE PARTIAL MOLAR ENTROPIES OF SOLUTION, $\Delta\bar{S}$ (cal mol^{-1} K^{-1})

Solute No.	Smectic	Nematic	Isotropic
1	−18.18 ± 0.21	−13.30 ± 0.80	−18.28 ± 0.32
2	−20.95 ± 0.55	−13.76 ± 1.08	−18.49 ± 0.54
3	−22.34 ± 0.27	−13.54 ± 0.13	−19.62 ± 0.37
4	−24.25 ± 0.39	−14.29 ± 1.18	−21.57 ± 0.21
5	−25.99 ± 0.53	−16.21 ± 0.89	−22.86 ± 0.16
6	−21.31 ± 0.19	−12.82 ± 1.49	−17.30 ± 0.37
7	−21.89 ± 0.09	−10.09 ± 1.07	−16.62 ± 0.11
8	−19.87 ± 0.32	−9.65 ± 1.45	−14.61 ± 1.02
9	−20.64 ± 0.27	−10.84 ± 0.34	−16.52 ± 0.25
10	−22.68 ± 0.18	−13.70 ± 0.69	−18.04 ± 0.64
11	−22.63 ± 0.45	−13.02 ± 0.73	−18.49 ± 0.61
12	−22.45 ± 0.53	−11.17 ± 0.59	−18.11 ± 0.48
13	−21.19 ± 0.26	−12.42 ± 0.53	−18.01 ± 0.74
14	−22.30 ± 0.04	−10.32 ± 0.45	−17.35 ± 0.88
15	−21.69 ± 0.27	−13.97 ± 0.91	−15.54 ± 0.33
16	−21.81 ± 0.26	−9.42 ± 0.71	−16.81 ± 0.63
17	−21.32 ± 0.50	−6.82 ± 0.92	−16.46 ± 0.57
18	−21.01 ± 0.28	−12.50 ± 0.31	−16.89 ± 0.50
19	−23.29 ± 0.50	−9.35 ± 0.81	−19.55 ± 0.54
20	−20.07 ± 0.27	−10.94 ± 0.68	−19.67 ± 0.34
21	−21.43 ± 0.37	−13.50 ± 0.50	−20.98 ± 0.20

DISCUSSION

Although many trends have been identified and analyzed through extensive thermodynamic studies by GLC [6–17,31], a definitive molecular-level description of retention and selectivity in nematic liquid-crystalline phases is still lacking. In 1971, Chow and Martire [9] proposed an infinite-dilution solution model for the interpretation of thermodynamic results (γ_f^∞, $\bar{H}^e$, $\bar{S}^e$, $\Delta\bar{H}$ and $\Delta\bar{S}$) from GLC. Although several workers have applied the model with some success [6–17] and it was later refined [19], the model remains semi-quantitative, at best. Clearly, additional systematic experimental studies (thermodynamic, spectroscopic and structural) and extension of a recent, promising, molecular theory based on a lattice model [32,33] are needed to further a more detailed understanding. Nevertheless, the refined solution model [6,7,9,19] can, at this stage, be reasonably used to discuss and analyze trends in the thermodynamic results.

We begin by comparing 5CB [6], 6CB [17], 7CB [16] and 8CB. The trends within each of five solute groups (*n*-alkanes, isomeric hexanes, heptanes, nonanes and the aromatic solutes) are then examined. Note that the discontinuities in ln γ_f^∞ as a function of $1/T$ at the phase-transition temperatures (see Fig. 1) are discussed elsewhere [8,20].

General trends with 5CB, 6CB, 7CB and 8CB

In both the isotropic and nematic phases, the general trends observed with 8CB

as the solvent are similar to those previously encountered with 5CB, 6CB and 7CB. The infinite-dilution solute activity coefficients exhibit positive deviations from Raoult's law ($\gamma_f^\infty > 1$), except for the aromatic solutes in the isotropic phase of 6CB, 7CB and 8CB, and all excess enthapies and excess entropies are positive. This indicates that, in general, the non-mesomorphic solutes are incompatible with both phases of these liquid-crystalline solvents.

Comparing the results for the nematic (N) and isotropic (I) phases, we note, without exception, the following trends in all four solvents:

(a) $(\Delta\bar{H})_I < (\Delta\bar{H})_N$ and $(\bar{H}^e)_I < (\bar{H}^e)_N$

(b) $(\Delta\bar{S})_I < (\Delta\bar{S})_N$ and $(\bar{S}^e)_I < (\bar{S}^e)_N$

(c) $(\gamma_f^\infty)_I < (\gamma_f^\infty)_N$

The small value of ΔH_{NI} (Table I) indicates that solvent–solvent interactions in the nematic phase are only slightly stronger than those in the isotropic phase. Therefore, trend (a) can only be interpreted as resulting from effectively stronger solute–solvent interactions in the isotropic phase. Trend (b) is less straightforward. In the nematic phase, rotational and conformational restrictions reduce solute entropy, while weaker solute–solvent interactions lead to an increase in solute (translational) entropy. Experiment shows that the latter prevails and the nematic phase is entropically favored. Trend (c) indicates that the lower solute excess Gibbs free energy in the isotropic phase is enthalpic in origin.

8CB is the only member of the series to exhibit a smectic phase. Let us compare the results for the different phases of 8CB. The trends are as follows:

(a) $(\Delta\bar{H})_{S_A} < (\Delta\bar{H})_I < (\Delta\bar{H})_N$ and $(\bar{H}^e)_{S_A} < (\bar{H}^e)_I < (\bar{H}^e)_N$

(b) $(\Delta\bar{S})_{S_A} < (\Delta\bar{S})_I < (\Delta\bar{S})_N$ and $(\bar{S}^e)_{S_A} < (\bar{S}^e)_I < (\bar{S}^e)_N$

(c) $(\gamma_f^\infty)_I < (\gamma_f^\infty)_N < (\gamma_f^\infty)_{S_A}$

In the light of our DSC measurements (Table I), solvent–solvent interactions are clearly not governing trend (a). The determining factor is the relative strength of solute–solvent interactions which are greater (more negative) in the smectic phase than in the other two phases. Strong solute–solvent interactions tend to restrict the solute's translational freedom and decrease its entropy. Further, the lack of long-range alignment of solvent molecules in the isotropic phase tends to increase solute entropy (through greater rotational and conformation freedom) relative to its smectic and nematic phase values. Again, the experimental results indicate that the first effect predominates and the nematic phase is found to be the most entropically favored. It is also the least favored in terms of enthalpy.

From (a) and (b) we conclude that the smaller γ_f^∞ (the lower solute excess Gibss free energy) in the isotropic phase is caused by a more favorable enthalpy relative to the nematic phase and a more favorable entropy relative to the smectic phase, and the slightly smaller γ_f^∞ in the nematic phase relative to the smectic phase is achieved through more favorable entropic effects.

In the following sections, we drop the subscript f in the activity coefficient notation and adopt the terminology with respect to $\Delta\bar{H}$ and $\Delta\bar{S}$ that larger refers to more negative values and smaller to less negative values.

n-Alkanes (solutes 1–5)

In the nematic phase, $\Delta\bar{H}$,$\Delta\bar{S}$ and γ^{∞} increase with increasing solute chain-length. This may be explained as follows: (a) as the solute chain length increases, the molecular polarizability increases, leading to stronger solute–solvent interactions (through dispersion forces) and larger $\Delta\bar{H}$ and $\Delta\bar{S}$ values; (b) with increasing solute chain length the solute-to-solvent size ratio increases and the combinatorial entropy contribution leads to larger $\Delta\bar{S}$ and less positive $\bar{S}^{e}$ values; and (c) a more elongated and more flexible molecule loses more rotational and conformational freedom on solvation, hence leading to larger $\Delta\bar{S}$ and more negative $\bar{S}^{e}$ values. The trend in γ^{∞} indicates that the enthalpy of solution increases less rapidly with increasing chain length than do the combined entropy of solution effects.

The same trends in γ^{∞}, $\Delta\bar{H}$ and $\Delta\bar{S}$ are observed in the isotropic phase where rotational and conformational entropy losses are relatively small, and in the smectic phase where these losses are greater than in the nematic phase, thus making $(\Delta\bar{S})_{S_A}$ larger than $(\Delta\bar{S})_{N}$ (*i.e.*, more negative) for all *n*-alkanes.

Isomeric hexanes (solutes 2 and 6–9)

The hexanes vary in shape from that of the straight-chain and relatively flexible *n*-hexane to the more globular and conformationally more rigid 2,2-dimethylbutane. However, their γ^{∞}, $\Delta\bar{H}$ and $\Delta\bar{S}$ values are too close to permit a clear interpretation. Nevertheless, when *n*-hexane is contrasted with 2,2- and 2,3-dimethylbutane, the trend observed is not unlike that encountered with the isomeric heptanes, which are discussed next.

Isomeric heptanes (solutes 3 and 10–17)

They vary widely in shape from that of the straight-chain and relatively flexible *n*-heptane to that of the more globular and conformationally more rigid 2,2,3-trimethylbutane. $\Delta\bar{H}$ and $\Delta\bar{S}$ tend to increase as the solute molecule becomes less branched because, as proposed [6,7,9,19], (a) rotational and conformational entropy losses increase, leading to larger $\Delta\bar{S}$ values, and (b) the effective strength of solute–solvent attractive interactions increases, leading to larger $\Delta\bar{H}$ and $\Delta\bar{S}$ values.

However, this effect is less marked in the isotropic phase and, even more so, in the smectic phase. The absence of a general trend in the γ^{∞} values of isomeric alkanes (which generally exceed those of their *n*-alkane counterparts) is due to a complex interplay between smaller $\Delta\bar{H}$ (tending to increase γ^{∞}) and smaller $\Delta\bar{S}$ (tending to decrease γ^{∞}) values resulting from increased branching. The absence of a general trend in the γ^{∞} suggests a subtle balance between enthalpy and entropy effects, which is difficult to interpret without a knowledge of the structure of the solution, the molecular conformations, etc.

The available data indicate that, for the same number of carbon atoms in the solute molecule, the branched alkane has, in general, a higher γ^{∞} value than the *n*-alkane. Exceptions to this rule, where the γ^{∞} values are comparable and/or the trend is reversed (7CB[16]), are encountered among solutes with centrally located

branches. For heptanes and hexanes at least, the more centrally located the branches are, the closer is the γ^{∞} value to that of the straight-chain isomer. Comparison of 2-methylhexane and 3-methylhexane shows a lower γ^{∞} value for the latter, *i.e.*, solute compatibility with the solvent increases as the branching is more centrally located. A similar trend is observed when 2,2-dimethylpentane and 3,3-dimethylpentane are contrasted.

Isomeric nonanes (solutes 5 and 19)

Two extremes in molecular structure were studied: *n*-nonane and the quasi-spherical 3,3-diethylphentane. The analysis proposed above also applies here. We simply note again that solution of the *n*-alkane is enthalpically favored (smaller $\bar{H}^{e}$ and larger $\Delta\bar{H}$) due to stronger effective solute–solvent interactions, but entropically unfavored (smaller $\bar{S}^{e}$ and larger $\Delta\bar{S}$) due to the conformational, rotational and enhanced translational entropy losses. In this case, however, the less favorable entropy prevails, and *n*-nonane has the higher γ^{∞} values.

Aromatic solutes (solutes 20 and 21)

For the three phases, the trends in $\Delta\bar{H}$ and $\Delta\bar{S}$ are toluene > benzene, while the γ^{∞} values are slightly higher for toluene. The $\Delta\bar{H}$ trend may be rationalized on the basis of molecular size and dispersion forces. The larger toluene molecule (with greater molecular polarizability) should have stronger solute–solvent interactions and, therefore, larger $\Delta\bar{H}$ values than the smaller benzene molecule. The trend in $\Delta\bar{S}$ follows both the trend in $\Delta\bar{H}$ (stronger interactions should result in greater translational entropy loss) and the trend expected from the combinatorial entropy ($\bar{S}^{e}$ increases and $\Delta\bar{S}$ decreases with decreasing solute size). The trend in γ^{∞} indicates that the enthalpy trend predominates, as was previously observed with 5CB, 6CB and 7CB.

Finally, comparing collectively the aromatic and aliphatic solutes, we observe that the latter have higher γ^{∞} values in all phases and solvents. This can be atrributed to more positive interchange energies (hence, less favorable enthalpies) and, in part, to the unfavorable conformational contribution of the more flexible alkanes.

ACKNOWLEDGEMENTS

This material is based on work supported by the National Science Foundation under Grant CHE-8902735.

The authors are pleased to dedicate this paper to Professor Georges Guiochon on the occasion of his 60th birthday. We wish him continued health, happiness and productivity, and gratefully acknowledge the impact his generously shared insights and knowledge have had on our research.

REFERENCES

1 G. L. Vogel, M. A. Hamzavi-Abedi and D. E. Martire, *J. Chem. Thermodyn.*, 15 (1983) 739.
2 R. J. Laub, J. H. Purnell, P. S. Williams, M. W. P. Harbison and D. E. Martire, *J. Chromatogr.*, 155 (1978) 233.
3 L. C. Chow and D. E. Martire, *J. Phys. Chem.*, 73 (1969) 1127.
4 J. M. Schnur and D. E. Martire, *Anal. Chem.*, 43 (1971) 1201.

5 H. T. Peterson, D. E. Martire and W. Lindner, *J. Phys. Chem.*, 76 (1972) 596.
6 G. A. Oweimreen, G. C. Lin and D. E. Martire, *J. Phys. Chem.*, 83 (1979) 2111; and references cited therein.
7 D. E. Martire, A. Nikolic and K. L. Vasanth, *J. Chromatogr.*, 178 (1979) 401; and references cited therein.
8 G. A. Oweimreen and D. E. Martire, *J. Chem. Phys.*, 72 (1980) 2500.
9 L. C. Chow and D. E. Martire, *J. Phys. Chem.*, 75 (1971) 2005.
10 D. G. Willey and G. H. Brown, *J. Phys. Chem.*, 76 (1972) 99.
11 J. M. Schnur and D. E. Martire, *Mol. Cryst. Liq. Cryst.*, 26 (1974) 213.
12 G. Kraus, K. Seifert and H. Schubert, *J. Chromatogr.*, 100 (1974) 101.
13 A. A. Jeknavorian and E. F. Barry, *J. Chromatogr.*, 101 (1974) 299.
14 A. A. Jeknavorian, P. Barrett, A. C. Watterson and E. F. Barry, *J. Chromatogr.*, 107 (1975) 317.
15 E. G. Rippie and H. G. Ibrahim, *Thermochim. Acta*, 11 (1975) 125.
16 G. A. Oweimreen, *Mol. Cryst. Liq. Cryst.*, 68 (1981) 257.
17 G. A. Oweimreen, *J. Solution Chem.*, 11 (1982) 105.
18 G. W. Gray, K. J. Harrison, J. A. Nash, J. Constant, D. S. Hulme, J. Kirton and E. P. Raynes, *Liq. Cryst. Org. Fluids*. 2 (1974) 617.
19 D. E. Martire, *Mol. Cryst. Liq. Cryst.*, 28 (1974) 63.
20 S. Ghodbane and D. E. Martire, *J. Phys. Chem.*, 91 (1987) 6410.
21 P. Navard and R. Cox, *Mol. Cryst. Liq. Cryst. Lett.*, 102 (1984) 261; and references cited therein.
22 H. Marynissen, J. Thoen and W. Van Dael, *Mol. Cryst. Liq. Cryst.*, 97 (1983) 149.
23 D. G. Willey and D. E. Martire, *Mol. Cryst. Liq. Cryst.*, 18 (1972) 55.
24 D. E. Martire and P. Riedl, *J. Phys. Chem.*, 72 (1968) 3478.
25 H. L. Liao and D. E. Martire, *Anal. Chem.*, 44 (1972) 498.
26 R., R. Dreisbach, *Adv. Chem. Ser.*, No. 15 (1955) and No. 22 (1959).
27 M. L. McGlashan and D. J. B. Potter, *Proc. R. Soc. London, Ser. A*, 267 (1972) 478.
28 M. L. McGlashan and C. J. Wormald, *Trans. Faraday Soc.*, 60 (1964) 646.
29 E. A. Guggenheim and C. J. Wormald, *J. Chem. Phys.*, 74 (1965) 3775.
30 E. F. Meyer, *J. Chem. Educ.*, 50 (1973) 191.
31 M. S. Vigdergauz, R. V. Vigalok and G. V. Dmitrieva, *Russ. Chem. Rev. (Eng. Transl.)*, 50 (1981) 498.
32 D. E. Martire, *J. Chromatogr.*, 406 (1987) 27; and references cited therein.
33 D. E. Martire and S. Ghodbane, *J. Phys. Chem.*, 91 (1987) 6403.

Journal of Chromatography, 556 (1991) 331–351
Elsevier Science Publishers B.V., Amsterdam

CHROM. 23 410

High-speed gas chromatography

Theoretical and practical aspects

GUY GASPAR*,[a]
Chrompack France, B.P. 20, F-91941 Les Ulis Cedex (France)

ABSTRACT

The performance of a gas chromatographic (GC) system depends mainly on the column efficiency and for fast separations, on the equipment design. A theoretical and practical study shows the importance of the various phenomena involved in the optimization of a GC system. An original approach, the performance concept, is introduced. Exact and simplified, approximate expressions are given for the calculation of the optimum practical velocity, the optimum column length and the minimum analysis time. The calculated values are in good agreement wit experimental valves from other sources. In the experimental part two cases are distinguished: fast chromatography using conventional equipment and ultra-fast chromatography requiring specially designed instrumentation. The most important considerations for the practical realization of high-speed separations are discussed in detail: column parameters, choice of working conditions and extra-column parts, such as the sampling device, detector, amplifier and data acquisition system. Some examples of extremely fast analyses (analysis times a few of seconds or less) are shown.

INTRODUCTION

Gas chromatographic (GC) analyses can potentially be performed much faster than they are practised at present. This fact was clearly understood by Desty and Goldup [1,2] soon after the introduction of open-tubular capillary columns; they published very impressive fast separations (analysis times of a few seconds) by using short, narrow-bore columns. Later, the team at the Ecole Polytechnique (France) directed by Guiochon performed systematic investigations to study instrumental contributions to the system efficiency and to the analysis time; several very rapidly obtained chromatograms (analysis time 2 s or less) were shown [3–7], these analyses being realized with a special laboratory-built equipment. These experiments were followed by studies by Cramers' research group at Eindhoven University of Technology; in particular, work by Schutjes and co-workers [8–10] showed the potential of high-speed GC for real application problems. At that time all these studies represented real technical exploits because of the lack of adequate instrumentation. Now-

[a] Present address: Fisons Instruments, 85, Av. Aristide Briand, 94 110 Arcueil, France.
Bon Anniversaire Professeur Guiochon.

0021-9673/91/$03.50

adays the great progress achieved in electronics, computer techniques, silicon micromachining and column technology (narrow-bore packed or open-tubular fused-silica columns) has allowed the construction and even the commercialization of reliable, moderate cost portable high-speed gas chromatographs; the pioneering work in this field by Microsensor Technology (Fremont, CA, USA) must be mentioned [11–13].

First we have to answer the common question of whether there is a need for very high-speed GC and what its benefits would be. The most current argument against fast chromatography is that the sample preparation itself is often a time-consuming procedure and the time saving resulting from fast analysis becomes negligible.

Naturally, the situation is simpler when there are pure samples to be injected, as in gas analyses, process measurements and field applications. A very promising application would be the continuous control of the air composition in operating rooms or of the air expired by anaesthetized patients. With complicated sample preparations the advantage of fast analyses should be interpreted differently: they allow an increase in precision or signal-to-noise ratio. If an analysis can be carried out 100 times faster, the same sample can be injected 100 times, resulting in a tenfold higher precision. Under certain conditions, it is possible to achieve extremely high reproducibility [14], and consequently the superposition of consecutive runs gives better signal-to-noise ratios; by superposing 100 runs of the same sample we obtain tenfold higher signal-to-noise ratios, resulting in tenfold lower detection limits.

This paper will focus on those aspects which are of special importance for fast (possible with conventional equipment) and for ultra-fast (requiring special instrumentation) chromatography.

THEORY

System efficiency and performance

Conventional packed columns having poor efficiency do not give a good perspective for fast separations. Although some rapid analyses with packed capillary columns have been reported [12], the most promising way seems to be the use of open-tubular columns, which have the additional advantage of much higher permeability. Consequently, we limit our discussion to the properties of these columns, which implies the use of the Golay equation to calculate the column theoretical plate height (HETP):

$$H = \frac{2D_G}{u} + \left[\frac{2k'}{3(k'+1)^2}\cdot\frac{d_f^2}{D_L} + \frac{1+6k'+11k'^2}{96(k'+1)^2}\cdot\frac{d_c^2}{D_G}\right]u \tag{1}$$

or in its simplified form:

$$H = \frac{B}{u} + (C_L + C_G)u = \frac{B}{u} + Cu \tag{2}$$

In order to obtain fast separations, let us assume that we are working with short columns and with hydrogen as the carrier gas; consequently, the influence of the pressure gradient on the band broadening is negligible, that is, the James–Martin and Giddings pressure drop correction factors are equal to 1. In other words, in our

equations the velocity u can be considered as the average carrier gas velocity. By derivation we can obtain from eqn. 2 the optimum velocity:

$$u_{opt} = (B/C)^{1/2} \tag{3}$$

and the minimum HETP value:

$$H_{min} = 2(BC)^{1/2} \tag{4}$$

For thin liquid films, the C_L coefficient can be neglected in comparison with C_G; hence by replacing B and C_G from eqn. 1, we obtain

$$u_{opt} = 8 \cdot \frac{D_G}{d_c}\left[\frac{3(k' + 1)^2}{1 + 6k' + 11k'^2}\right]^{1/2} = 8 \cdot \frac{D_G}{d_c} \cdot f(k') \tag{5}$$

and

$$H_{min} = d_c/f(k') \tag{6}$$

The fundamental assumption of the Golay model is that band broadening occurs only in the column. This hypothesis is valid when the column is long and the linear gas velocity is low (normal current practice). Under high-speed conditions (short columns and high velocities), the instrumental contribution becomes important. Gaspar *et al.* [6] showed the effect of extra-column parts on the system efficiency:

$$H = \frac{B}{u} + Cu + Du^2 \tag{7}$$

This equation was also proved experimentally and excellent agreement was found between measured and predicted values. In eqn. 7, the last term, proportional to the square of the gas velocity, describes all extra-column contributions (injector, connections, detector, electrometer, recording or data handling device) in the following manner:

$$D = \frac{\sigma^2_{EC}}{(k' + 1)^2 L} \tag{8}$$

where σ^2_{EC} is the sum of extra-column variances expressed in time units. The meaning of D is logical: the column is longer and the efficiency loss caused by the instrumentation is smaller; the solute is more retained and the extra-column contribution is smaller.

The existence of a quadratic term in eqn. 7 has the following consequences: (a) the minimum HETP is higher than that one given by eqn. 4, that is, the system is less efficient; and (b) the optimum velocity is smaller than the value given by eqn. 3, that is, to obtain the highest possible efficiency we are obliged to work more slowly.

These effects are negligible with conventional (long) capillary columns if they are properly connected and other parts (injector, detector, etc.) are also functioning normally. For instance, with conventional equipment the magnitude of the sum of all extra-column variances can be estimated as 0.001 s^2; using a 25 m × 0.25 mm I.D. column for a compound having a capacity factor of 1.5, eqns. 3 and 4 give u_{opt} =

58.7 cm/s and H_{min} = 0.170 mm, and a plate number of 146 910. By considering also the Du^2 term, these values become 57.0 cm/s, 0.172 mm and 145 027, respectively (substituting D_G = 0.25 cm^2/s in the Golay equation, corresponding to *n*-octane at room temperature with hydrogen as carrier gas). The differences are negligible. However, with a specially designed system for ultra-fast analyses (85 cm × 0.065 mm I.D. column and total extra column variance only 0.0000685 s^2, calculated from Fig. 1) extra-column effects become dramatic: the optimum velocity falls to 110 cm/s instead of 226 cm/s, the minimum HETP is 0.072 mm instead of 0.044 mm and we have only 11 834 instead of 19 211 plates; the Du^2 term will amount to 21.7% of the total HETP value calculated at u = 110 cm/s.

It would be possible to characterize simultaneously the resolution and the rapidity by a new, not yet defined, chromatographic term, which we can call "performance". We shall use it in the following manner: (a) for two chromatographic systems, that with the higher performance gives the same resolution in a shorter analysis time; or (b) the performance is higher if the system gives a higher resolution in the same time. In both instances we assume that the same mixture is injected and the same type of stationary phase is used.

Gaspar *et al.* [7] introduced the notion of the time necessary to generate a theoretical plate (*TH*), defined as

$$TH = \frac{\sigma^2}{t_R} \tag{9}$$

which gives the zone broadening as the time-based variance increase per unit time spent in the chromatographic system and which can characterize the system performance. Considering eqn. 10 also, *TH* is the inverse of the magnitude already used, *i.e.*, the number of plates generated per unit time. *TH* is an analogous quantity to HETP; while the classical theory of GC is based on the efficiency, we shall use the performance measured by *TH*. The best performing system is the one which results in the smallest increase in band time variance in a given time. By transformations, we obtain from eqn. 9

$$TH = \frac{\sigma^2}{t_R^2} \cdot t_R = \frac{t_R}{N} = (k' + 1)\frac{L}{u} \cdot \frac{H}{L} = (k' + 1)\frac{H}{u} \tag{10}$$

and from eqn. 7

$$TH = (k' + 1)\left(\frac{B}{u^2} + C + Du\right) \tag{11}$$

By derivation, we can show that *TH* has a minimum at an optimum velocity given by

$$u' = (2B/D)^{1/3} \tag{12}$$

It is easy to show that this is the velocity at which the tangent, through the origin, touches the *H*–*u* curve (*cf.*, Fig. 1). We have to understand the meaning of u' in the following way: starting from the optimum velocity (which gives the minimum HETP value) and increasing the carrier gas velocity up to u', the increase in analysis speed is

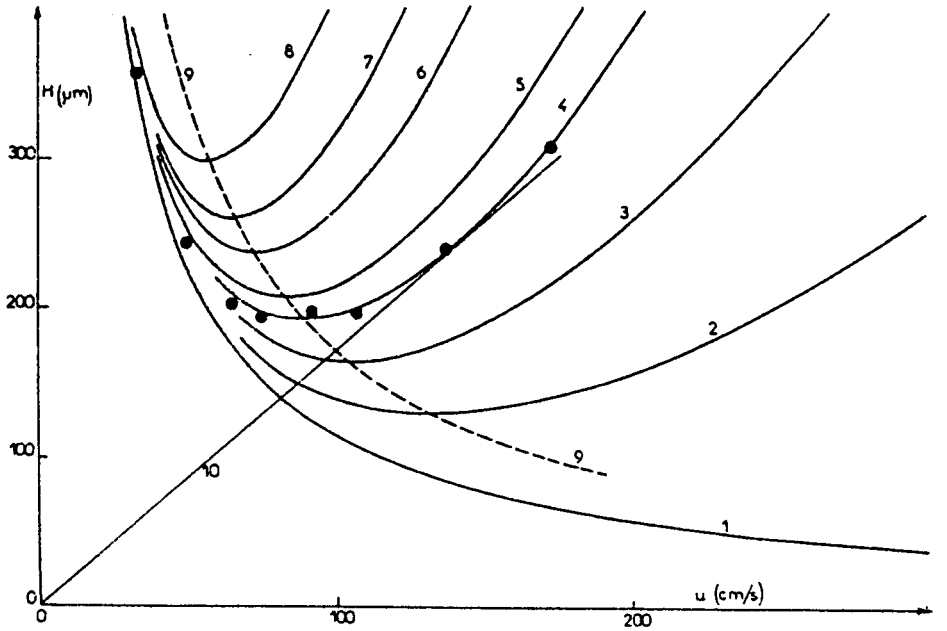

Fig. 1. Plot of HETP *versus* carrier gas velocity. Carrier gas, hydrogen; sample, methane; column, 85 cm × 65 μm I.D.; temperature, 25°C. *D*: (1) O; (2) $2.5 \cdot 10^{-7}$; (3) $5 \cdot 10^{-7}$; (4) $8.1 \cdot 10^{-7}$ with experimental points; (5) $1 \cdot 10^{-6}$; (6) $1.5 \cdot 10^{-6}$; (7) $2 \cdot 10^{-6}$; (8) $3 \cdot 10^{-6}$ s^2/cm. Curve 9 links the minima of all the $H - U$ plots. Line 10 is the tangent from the origin to curve 4, corresponding to minimum *TH*.

greater than the decrease in efficiency, but at higher gas velocities the situation is completely reversed and the efficiency decreases rapidly.

In the early days of capillary GC, Scott and Hazeldean [15] defined the optimum practical gas velocity (OPGV) as that at which H/u is minimum. It is easy to find a similarity and even an identity between OPGV and u' but, whereas the classical theory results an infinite value for the OPGV, now u' has a concrete value.

The plate height at velocity u' is

$$H' = \frac{3}{2}(2B)^{2/3} D^{1/3} + \frac{C}{D^{1/3}}(2B)^{1/3} \tag{13}$$

It is important to note that this value is not the minimum but that one which corresponds to the optimum practical gas velocity.

Analysis time

The retention time of a compound is given by the well known expression

$$t_R = (k' + 1)t_0 = (k' + 1)\frac{L}{u} = N \cdot \frac{H}{u}(k' + 1) \tag{14}$$

If we compare it with eqn. 10, we obtain the following very simple relationship:

$$t_R = N \cdot TH \tag{15}$$

The target of chromatography is to separate the components of a mixture. Therefore, in order to obtain the minimum retention time:

(1) we have to use a system without any redundancy or, in other words, the minimum necessary plate number sufficient for a given separation is

$$N_{ne} = 16R_s^2\left(\frac{\alpha}{\alpha - 1}\right)^2\left(\frac{k' + 1}{k'}\right)^2 \tag{16}$$

(2) we have to set the velocity u' (see eqn. 12) giving the minimum value of TH:

$$TH' = (k' + 1)\left[\frac{3}{2}(2B)^{1/3} D^{2/3} + C\right] \tag{17}$$

(3) the previous conditions involve using the shortest column, its length being

$$L' = N_{ne}H' \tag{18}$$

However, eqns. 12, 15 and 18 are not valid for calculations because they depend on the column length via D. As Gaspar *et al.* [7] have shown, by introducing a quantity $\mathscr{D}$ independent of the column length:

$$\mathscr{D} = DL = \frac{\sigma_{EC}^2}{(k' + 1)^2} \tag{19}$$

the shortest column length will be

$$L' = \frac{7.35\mathscr{D}B^{1/2}}{\left[\left(C^2 + \frac{6\mathscr{D}}{N_{ne}}\right)^{1/2} - C\right]^{3/2}} \tag{20}$$

and now the following form of the optimum practical gas velocity is also independent of L:

$$u' = \left[\frac{6B}{\left(C^2 + \frac{6\mathscr{D}}{N_{ne}}\right)^{1/2} - C}\right]^{1/2} \tag{21}$$

It is interesting that contrary to eqn. 12, this velocity is independent of column length, but it is a function of the necessary plate number. Finally, the retention time is

$$t_R' = N_{ne}TH' = 0.5(k' + 1)N_{ne}\left[C + \left(C^2 + \frac{6\mathscr{D}}{N_{ne}}\right)^{1/2}\right] \tag{22}$$

If the "critical pair" to be separated is the last one in the chromatogram, eqn. 22 gives the minimum analysis time. If there are other peaks eluted after the critical pair, we can use another expression which resembles eqn. 22:

$$t_{A,min} = 0.5(nk' + 1)N_{ne}\left[C + \left(C^2 + \frac{6\mathscr{D}}{N_{ne}}\right)^{1/2}\right] \quad (23)$$

where n is the ratio of the column capacity factor of the last compound and the k' value of the second peak of the critical pair.

Eqns. 22 and 23 give a direct correlation between the analysis time and equipment contribution. These results are not surprising: the decrease in the coefficients of plate-height equation increases the system efficiency and also the "performance", that is, the analysis speed.

When we have a simple separation to do (requiring a few thousand plates or less) and if we use very efficient columns (narrow bore and very thin films), it is possible to show that

$$\frac{6\mathscr{D}}{N_{ne}} \gg C^2 \quad (24)$$

Combination of eqns. 19, 22 and 24 leads to a simpler form of the analysis time:

$$t_R = 0.5(k' + 1)CN_{ne} + 1.23\sqrt{\sigma^2_{EC}N_{ne}} \quad (25)$$

assuming always that we are working at the optimum practical gas velocity and with the minimum column length. This expression gives smaller values than eqn. 22; the error is less than 1% for small k' values (0.5–4), but it increases up to 4–8% in the k' range 10–15 using a narrow (0.05 mm I.D.) column.

As an example it will be interesting to replace real data in the analysis time equation (eqn. 25) with the following values: $d_c = 50\ \mu m$, $d_f = 0.05\ \mu m$, $D_G = 0.25$ cm^2/s and $D_L = 9 \times 10^{-7}\ cm^2/s$ (which correspond to n-octane at room temperature in hydrogen as carrier gas and on a squalane-type stationary phase and gives roughly $k' = 2$. Further, by using $6.85 \cdot 10^{-5}\ s^2$ as the extra-column variance, one obtains for the plate height coefficients: $C = 8.65 \cdot 10^{-6}$ s and $\mathscr{D} = 9.6 \cdot 10^{-6}\ s^2$.

With a simple analysis requiring only $N_{ne} = 10\,000$ plates, we obtain for the analysis time 1.14 s. The exact expression eqn. 22 would give 1.15 s; these values are in good agreement with analysis times reported by several workers under similar conditions. The numerical value of the first term $[0.5(k' + 1)CN_{ne}]$ is equal to 0.13 s, corresponding only to 11% of the total time. If the necessary plate number were only 3000, the first term would be 6% of the analysis time. This result means also that by using very efficient columns most of the zone broadening occurs in the extra-column part of the chromatographic system; on the other, hand for very simple separations, in addition to eqn. 24 the following condition is also valid:

$$\left(\frac{6\mathscr{D}}{N_{ne}}\right)^{1/2} \gg C \quad (26)$$

TABLE I

ANALOGOUS MAGNITUDES

	Efficiency concept		Performance concept		
E 1	Length-based zone variance	${}_L\sigma^2$	Time-based zone variance	σ^2	P 1
E 2	Height equivalent to a theoretical plate	$H = {}_L\sigma^2/L$	Time necessary to generate a theoretical plate	$TH = \sigma^2/t_R$	P 2
E 3	Theoretical plate number	$N = L^2/{}_L\sigma^2$	Theoretical plate number	$N = t_R^2/\sigma^2$	P 3
E 4	Column length	$L = N \cdot H$	Retention time	$t_R = N \cdot TH$	P 4
1st degree optimization					
E 5	Column length	$L = N_{ne} \cdot H$	Retention time	$t_R = N_{ne} \cdot TH$	P 5
2nd degree optimization					
E 6	Column length	$L = N_{ne} \cdot H_{min}$	Retention time	$t'_R = N_{ne} \cdot TH'$	P 6

which allows further simplifications both for the optimum column length:

$$L' = 1.92\left(\frac{\sigma_{EC}^2 B^2 N_{ne}^3}{(k'+1)^2}\right)^{1/4} \tag{27}$$

and also for the optimum practical velocity:

$$u' = 1.56\left[\frac{B^2 N_{ne}(k'+1)^2}{\sigma_{EC}^2}\right]^{1/4} \tag{28}$$

It is important to note that the above expressions are only approximate, allowing a rapid estimation of the column length and velocity, respectively; the exact equations are eqns. 20 and 21. These approximate equations lead to smaller values than the exact values, with errors of 15–50% for the optimum length and 5–20% for the optimum velocity (depending on the k' range), using always narrow columns (0.05 mm I.D.). For columns with I.D. = 0.15 mm or larger, the errors are much more important because condition 26 is no longer valid.

"Efficiency" and "performance" concepts

During the progress of GC, most efforts were dedicated to the development of very efficient columns (or GC systems), and the main goal of optimization approaches or theories was to find operating optimum conditions giving the highest efficiency (minimum HETP), the analysis speed being of only secondary or no interest. Many papers (even this one) show H/u plots, which indicates a kind of myth around the notion of HETP. Hence it is easy to understand that the starting point of all theoretical arguments was the efficiency concept.

When process control or routine analyses are to be performed, it is also important to optimize the analysis speed, which gives a supplementary advantage in sensitivity (see Figs. 2 and 7). Naturally, the chromatographic system always has to effect the required separation, and no concessions are admitted here, so the analysis time optimization must not be self-contained. As we have shown above, the "performance" concept is more extended, involving both efficiency and speed. Table I offers a comparison of the classical efficiency and the more extended performance concepts.

Some remarks can be made about Table I:

(1) Band broadenings are characterized by their length- or time-based variance.

(2) The plate number notion is interpreted in the same way in both concepts.

(3) HETP and TH in addition to column length and retention time are symmetrical in the two concepts.

(4) The values σ^2, ${}_L\sigma^2$, H, TH, N, L and t_R are specific for a given compounds and for a given chromatographic system working under given operating conditions.

(5) The necessary plate number N_{ne} calculated by eqn. 16 is a value determined by the analytical problem and it is independent of the chromatographic system itself.

(6) Consequently, if $N \gg N_{ne}$, the system has a redundancy, and the column length and analysis time are larger than is strictly necessary.

(7) The first-degree optimization means shortening the column to obtain sufficient (but not more) plate numbers. Consequently, we can also save analysis time.

(8) The second-degree optimization is intended to optimize the operating conditions (gas velocity); in the efficiency concept to choose the optimum velocity giving the minimum HETP and in the performance concept another velocity to obtain the minimum *TH* (*TH'*; see eqn. 17). We have to interpret these results very carefully: expression E6 in Table I gives the shortest column of all, whereas expression P6 gives the smallest analysis time of all, but not by using the same column length as given by E6. Expression P6 assumes we use the column length given by eqn. 22 and we set the gas velocity given by eqn. 21. Both are larger than the minimum column length and optimum gas velocity determined by the efficiency concept, but all together they give a shorter analysis time. This is in complete harmony with what was pointed out by Scott and Hazeldean [15], *i.e.*, a longer column operated at a higher velocity gives a more rapid analysis than a shorter column operated at the optimum velocity for minimum HETP, with equivalent resolution. This statement was later confirmed experimentally by Villalobos and Annino [21].

PRACTICAL ASPECTS

In most of following discussions we shall distinguish two cases:

(a) "pseudo" fast analyses, which can be performed by means of conventional equipment; in this case, the typical analysis times are of the order of minutes and separations can be carried out by respecting some simple rules;

(b) truly high-speed analyses, which need specially designed instrumentation in order to achieve analysis times of a few seconds. In this latter instance, it is assumed that we are working with simple sample mixtures (5–10 compounds or quantification of some key compounds only).

Column parameters

Column inside diameter. As eqn. 3 shows, the optimum gas velocity is inversely proportional to the inner diameter. This velocity increases as the inner diameter decreases, so that a shorter analysis time can be obtained by using columns with a smaller diameter. Another phenomenon is that the minimum HETP decreases with decreasing column radius (see eqn. 4) so that, with a short, narrow-bore column, the same separation can be obtained as with a long, wider bore column, which increases the analysis speed even more (*cf.*, Fig. 2).

Nowadays, there are no technical limitations to the manufacture of (fused-silica) columns with diameters of 50 μm or less, but the construction of commercially available gas chromatographs prevents unlimited miniaturization. Sample introduction in particular raises problems with diameters smaller than 100 μm. The use of 150 μm (0.15 mm) columns seems to be the best compromise, as they can easily be installed in any capillary gas chromatograph and are completely compatible with the split injection technique. Fig. 3 shows a chromatogram obtained using such a column.

Really fast analyses can only carried out by using narrow columns (I.D. < 0.1 mm), but special equipment is needed in order to reduce instrumental contributions (*cf.*, Figs. 4 and 5).

As an interesting approach, Lee *et al.* [12] used packed capillary columns to analyse natural gas (Fig. 6).

Film thickness. The stationary phase film thickness influences the column effi-

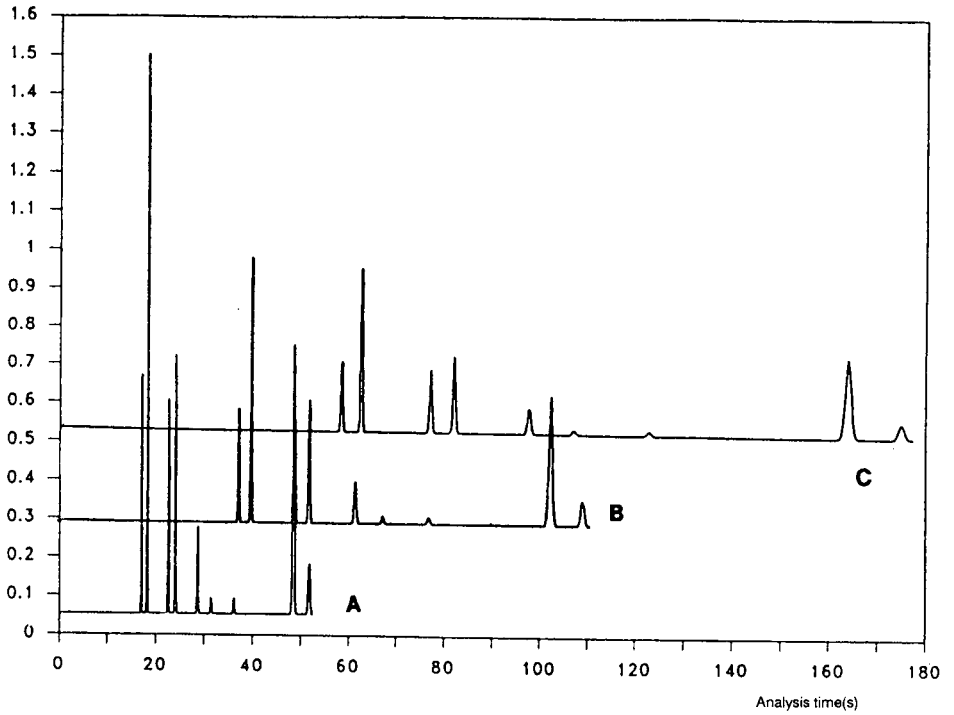

Fig. 2. Effect of column diameter peak height and analysis time. Columns: A = 10 m × 0.15 mm; B = 16 m × 0.25 mm; C = 21 m × 0.32 mm. Columns have the same phase ratio (same capacity factor) and plate number (same resolution). (Reprinted from Chrompack brochure.)

ciency directly (see the Golay equation), and indirectly via k' values because of the well known relationship

$$k' = \frac{4Kd_f}{d_c} \tag{29}$$

An increase in liquid film thickness has several complicated effects. As a first approximation, the result is a loss of efficiency because of increases in C_L. This effect is negligible as far as the condition $C_L \ll C_G$ can be respected. Most of the fast applications were carried out with a film thickness inferior to 0.1 μm, that is on very efficient columns. Exceptions are when very volatile compounds are to be separated (see Fig. 3).

Column length. For really short analyses, very short columns (0.15–4 m) are used in order to obain analysis times of a few seconds or less. Eqns. 20 and 27 permit the calculation of the column length necessary for a given analytical problem, assuming we set the optimum practical gas velocity at a value calculated by eqn. 21 or 28. To obtain these expressions we neglected the gas compressibility effect; therefore, in practice it is better to use 10–15% longer columns and 10–15% smaller values for the optimum velocity, which together give 20–30% longer analysis times.

Using the same values as above (see *Analysis time*), eqn. 20 gives 86 cm for the column length, which is also in good agreement with literature data.

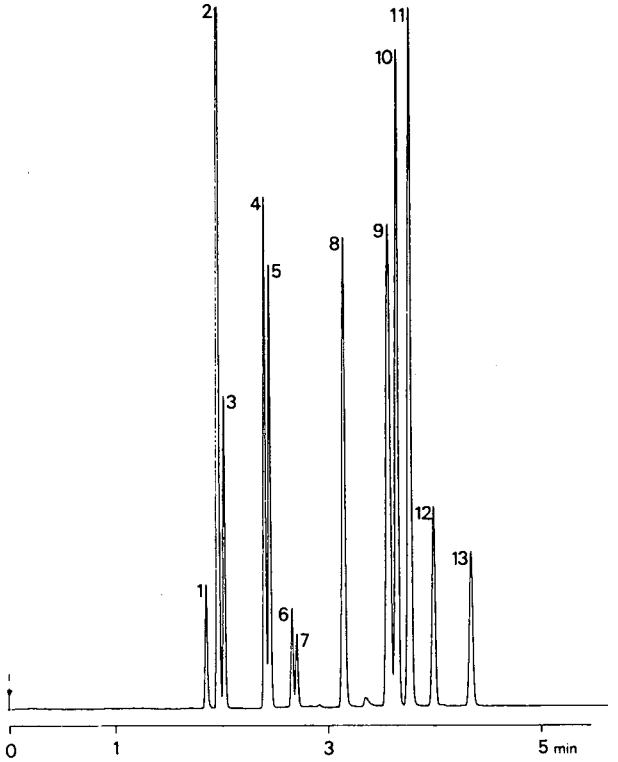

Fig. 3. Separation of C_1–C_4 hydrocarbons. Column, 25 m × 0.15 mm I.D., coated with CP-Sil 5 CB (1.2 μm); temperature, 25°C; carrier gas, hydrogen; flow-rate 53 cm/s; split injection with slitting ratio 133; flame ionization detector. Peaks: 1 = methane; 2 = ethene; 3 = ethane, ethyne; 4 = propene; 5 = propane; 6 = propadiene; 7 = propyne; 8 = isobutane; 9 = isobutene, 1-butene; 10 = 1,3-butadiene; 11 = *n*-butane; 12 = *trans*-2-butene; 13 = *cis*-2-butene. (Reprinted from Chrompack brochure.)

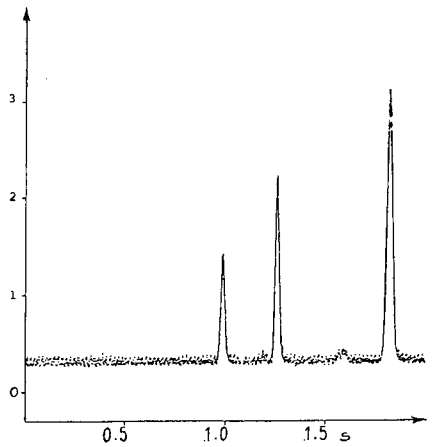

Fig. 4. High-speed chromatogram 1. Column, 120 cm × 0.065 mm I.D., coated with squalane (0.03 μm); temperature 20°C; carrier gas, hydrogen; flow-rate, 121 cm/s; fluidic logic gate injector; digital reconstruction of chromatogram. Compounds in their elution order: methane, *n*-heptane, *n*-octane.

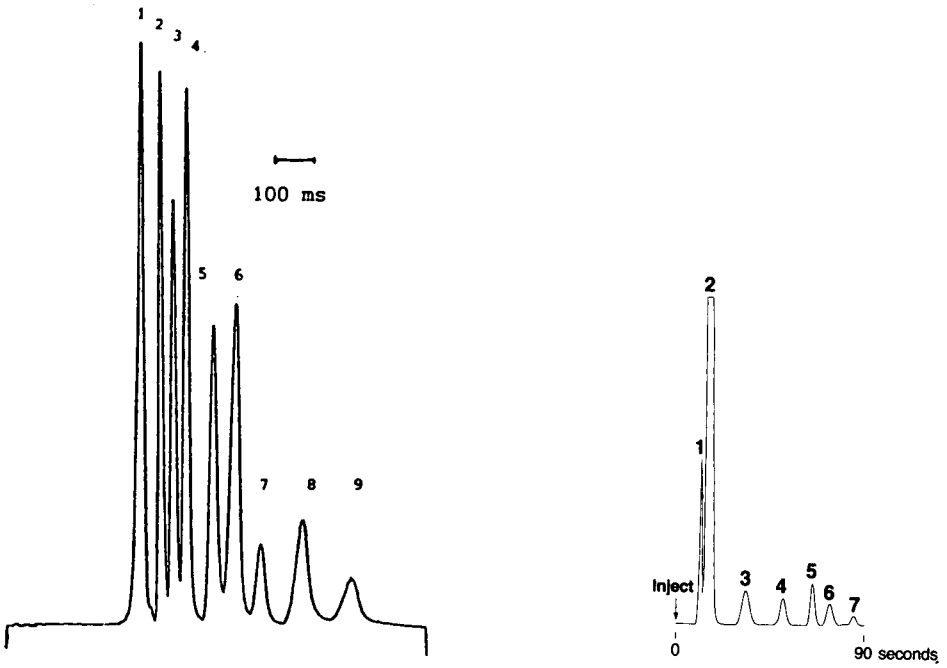

Fig. 5. High-speed chromatogram 2. Column, 30 cm × 0.050 mm I.D. coated with squalane; temperature, 72°C; carrier gas, helium; flow-rate, 470 cm/s; on-column cold-trap injector. Peaks: 1 = n-C_6; 2 = cyclohexane; 3 = n-C_7; 4 = methylcyclohexane; 5 = toluene; 6 = n-C_8; 7 = 1,2-dimethylhexane; 8 = ethylhexane; 9 = n-C_9. (Reproduced from ref. 16 with permission).

Fig. 6 Analysis of natural gas. Column, 25 cm × 0.5 mm I.D. PLOT Molsieve 5A column packed with 100–120-mesh HayeSep A; silicon microvalve injector; thermal conductivity detector. Peaks: 1 = air; 2 = methane; 3 = carbon dioxide; 4 = ethane; 5 = carbonyl sulphide; 6 = hydrogen sulphide; 7 = propane. (Reproduced with permission of Microsensor Technology).

It is interesting to observe that L', as given by eqn. 20, has a minimum of the function $\mathscr{D}$. It is easier to explain the increase in L' with the increase in $\mathscr{D}$: the system efficiency becomes lower and we must compensate for this loss by using a longer column, but it also increases with decreasing $\mathscr{D}$ at small values of $\mathscr{D}$. The reason is that we must now operate the column at a very high velocity (*cf.* eqn. 21) and again, but for a different reason (large velocity allowed by small extra-column contributions; we must not forget that this velocity is not the one giving the highest efficiency, but the minimum of the ratio H/u), the column length must become large. As pointed out by Grant [17], "...the fastest analysis possible will always be at OPGV provided that column length is increased to compensate for the theoretical plate loss...". It is important to note that this is by no means the shortest analysis time. The shortest analysis time is always that given by eqn. 22, this phenomenon being of only mathematical and secondary interest. The simplified form eqn. 27, of the column length is unambiguous.

Operating conditions

First, we should point out that really fast analyses can only be carried out under isothermal conditions; with temperature-programmed runs the cooling time and the system stabilization period would be too long, and consequently the main benefit would be lost. Possibly further developments in micromachining technology ("cartridge" chromatographs, injector, column and detector integrated on a low heat capacity wafer; the chromatograph itself becomes a consumable part of the whole system) and adoption of Peltier elements as heating and cooling devices will allow temperature-programmed high-speed separations also to be performed. Until that time we have to consider only two parameters as degrees of freedom: the carrier gas velocity and the column temperature. In addition, we shall discuss briefly how to choose the carrier gas.

Choice of carrier gas. According to eqn. 5, the best carrier gas for fast analyses is the one in which the diffusion coefficient of the component is the highest. Hydrogen is obviously the best choice. In helium it is slightly smaller, and this gas could be a secondary choice, but as its viscosity is high the pressure gradients would be too large.

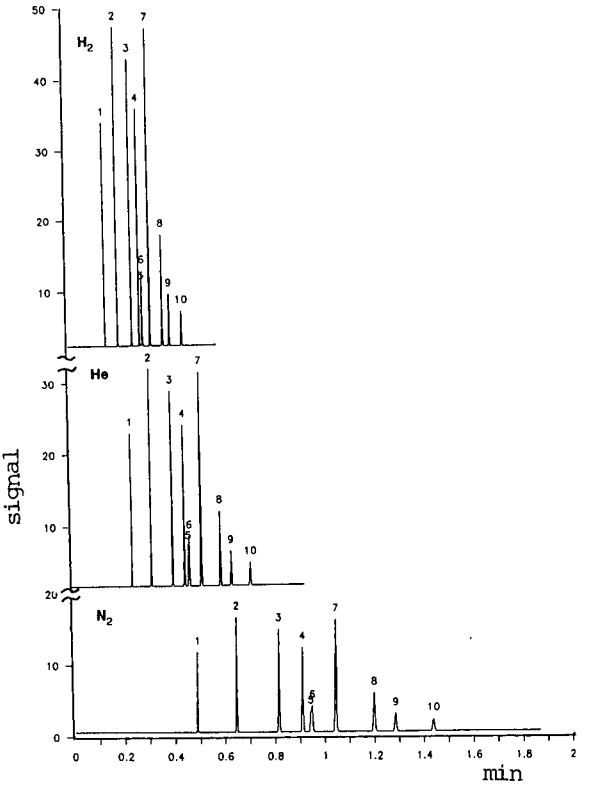

Fig. 7. Separation of aromatic hydrocarbons with different carrier gases. Column, 50 m × 0.32 mm I.D., coated with CP-Sil 5CB, film thickness 1.20 μm; temperature 100°C; optimum gas velocities, hydrogen 47 cm/s, helium 30 cm cm/s and nitrogen 15 cm/s. Peaks: 1 = benzene; 2 = toluene; 3 = vinylcyclohexane; 4 = ethylbenzene; 5 = *m*-xylene; 6 = *p*-xylene; 7 = styrene; 8 = isopropylbenzene; 9 = benzaldehyde; 10 = *n*-propylbenzene. (Reprinted from Chrompack brochure).

Other gases giving small diffusion coefficients are approximately three times slower than hydrogen (see Fig. 7).

Carrier gas velocity. Eqn. 21 or 28 permits the calculation of the optimum practical velocity as a function of instrumental variance and of the necessary plate number for a given analytical problem. As was mentioned above, slightly smaller values are recommended because of gas compressibility effects.

According to eqn. 21, the smaller the amount of all the extra-column variances, the higher is the optimum velocity. Using again the same values as above (analysis time calculation), we obtain 224 cm/s for the carrier gas velocity.

Column temperature. Temperature changes influence the values of the diffusion coefficients D_G and D_L and mainly the partition constant K, which is directly related to the column capacity factor k' (see eqn. 29). We shall focus only on the temperature dependence of k', which is the strongest. In other words, we have to examine how the column length and the optimum practical velocity depend on the capacity factor. These dependences are complicated because the necessary plate number (N_{ne}) and the plate-height coefficients C and D depend on k'.

We are interested in optimization of the analysis time with a satisfactory resolution between the two critical components of the sample mixture. We therefore have to look for the minimum analysis time. Two completely different cases will prove to give similar results (*cf.*, Fig. 8). In both instances, the analytical problem is the same: separation of these components with a resolution factor of 1.3 (baseline separation) and a liquid-phase selectivity of 1.1. In the first instance, let us assume that we use a specially designed fast chromatographic system, with the same parameters as in the above calculations. In the second instance, let us assume that we use conventional equipment with a split injector and a 0.15 mm I.D. column.

On examining Fig. 8A–D, several features may seem surprising or even contradictory:

(a) Under certain conditions (low initial values of k'), a temperature decrease (k' increasing) accelerates the analysis speed (Fig. 8B). We must not forget that we want to optimize the system using eqns. 16, 20, 21 and 22. Thus, the reason is simple: the necessary plate number is smaller at higher k' values (Fig. 8A), a shorter column is

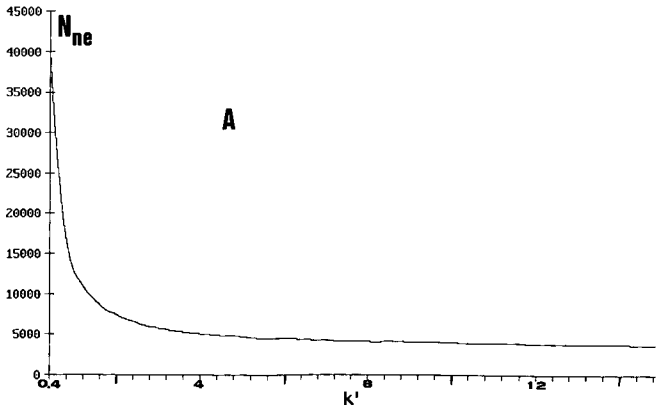

Fig. 8.

(Continued on p. 346)

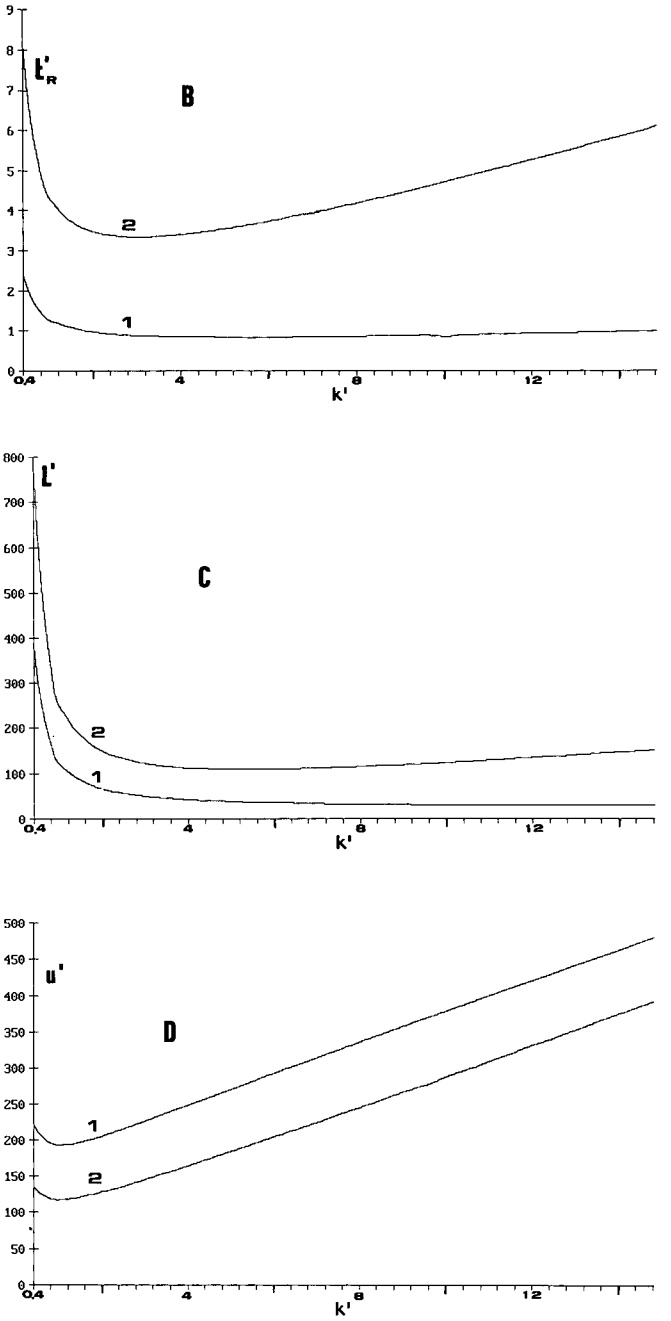

Fig. 8. Effect of column capacity factor (A) necessary plate number, (B) minimum analysis time (s), (C) minimum column length (cm) and (D) optimum practical velocity (cm/s). Phase selectivity = 1.3; required resolution factor = 1.3. Curves 1: column I.D. = 0.05 mm, film thickness = 0.05 μm, equipment variance = 0.0000685 s^2. Curves 2: column I.D. = 0.15 mm, film thickness = 0.1 μm, equipment variance = 0.000625 s^2, corresponding to well designed conventional equipment.

required (Fig. 8C) and a higher gas velocity is allowed (Fig. 8D). On the other hand, an increase in k' also has a beneficial effect on the D term, as is shown by eqn. 8, and the system efficiency also increases.

(b) The analysis time has a minimum as a function of k'. After the decrease mentioned above, the necessary plate number becomes virtually constant and the increase in the $(k' + 1)$ term is stronger than the decrease in the H/u ratio (see eqn. 14). The k' dependence of D (eqn. 19) also becomes negligible. This minimum is less marked when specially designed equipment is used (lower curve in Fig. 8B); with very efficient columns, conditions 24 and even 26 are valid and the contribution of the first term of eqn. 25 is slight compared with the second term.

(c) The carrier gas velocity has a minimum as a function of k'. The coefficient C has a very marked maximum as a function of k'. For large k' values, the gas velocity becomes infinite according to the classical OPGV concept (D becomes negligible).

From all these results, we can conclude that the optimum working k' range is roughly 1–10. For simple sample mixtures, it seems convenient to set the column temperature so that the chromatogram is placed in the k' range 1–5 (the classical theory gives $k' = 2$ as the optimum value to obtain the minimum analysis time).

Equipment

It was shown above that using very efficient, narrow-bore, short columns, zone broadening occurs mainly in the extra-column parts of the chromatographic system. Usually, the contributions of the various parts of the equipment (injector, connections, detector, electrometer, even the data acquisition and handling system) are independent of each other [18]. Thus, the equipment constant σ^2_{EC} can be broken down and expressed as the sum of individual contributions from different parts of the equipment:

$$\sigma^2_{EC} = \sum\sigma_i^2 = \sum\lambda_i\tau_i^2 \tag{30}$$

where τ_i are characteristic time (*e.g.*, time constant) and λ_i are factors depending on the choice of the characteristic times and on their profile. As examples, for a rectangular profile $\lambda = 1/12$ if τ is its width and for a Gaussian profile $\lambda = 1$ if $\tau = \sigma$. The contributions of different profiles were discussed in detail by Sternberg [18]. Below we give a review from a practical point of view.

Sample injection. The first fast injector was realized by Desty and Goldup [1,2] achieved by hitting a syringe with a hammer; with this technique, and injection duration of a few tens of milliseconds was achieved and very spectacular fast chromatograms were obtained; syringe consumption was not reported!

Conventional, commercially available capillary sample introduction systems can hardly be used to perform fast analyses because of their well known limitations (band broadening in space or in time). Only the split injector seems to allow "pseudo-fast" separations (*cf.*, Fig. 3). The contribution to band broadening of this type of injector can be estimated by the following expression:

$$\sigma_I = \tau_I = \frac{V_v}{F} \tag{31}$$

where V_v is the volume occupied by the sample in the vapour phase in the injector chamber at the injector temperature and at the inlet pressure, and F is the total flow-rate in the injector chamber. Estimating $V_v = 50$ μl (injecting 0.1 μl of liquid sample) and $F = 120$ ml/min, we obtain $\tau_I = 25$ ms as a charateristic time ($\lambda_I = 1$), which means that the injector contribution to the σ^2_{EC} equipment constant should be $6.25 \cdot 10^{-4}$ s^2. If other extra-column contributions are negligible ($\sigma^2_{EC} \approx \sigma^2_I$) and assuming $N_{ne} = 10\,000$ plates, the second term of eqn. 25 gives 2.77 s as the ultimate lower limit of the analysis time.

Gaspar and co-workers [4,5] described a fast sampling device (injection profiles of a few milliseconds) based on a fluidic logic gate; this injector was inspired by the idea of Wade and Cram [19]. Fluidic logic elements are pneumatic devices without moving parts, which allows fast operations with switching times less than 1 ms. They were developed for automation and process control because of their resistance to high temperatures and electromagnetic fields. The essential component is an inhibited OR/NOR gate. The fluidic injector is extremely reliable and stable; owing to its exceptional reproducibility, it was used later to study peak distortion profiles in non-linear chromatography [20].

To overcome the limitations of conventional equipment, Van Es *et al.* [16] had the clever idea of using an on-column cold-trap reinjection system to obtain very narrow input bands (1.1 ms), and they performed high-speed separations using very short, narrow-bore columns (*cf.*, Fig. 5). They installed a 10-cm long external aluminium-caoted fused-silica column (cold trap) between the on-column injector and the short (10–35 cm) analytical column, *ca.* 2 cm of the trap being cooled to -70°C with nitrogen. The injected sample can be liberated (reinjected) from the cold trap by a fast thermal desorption step made by means of high-power electrical heating in the form of short pulses. This reinjection device allows conventional equipment to be used.

A revolutionary approach was described by Lee *et al.* [12]. Silicon micromachining technology permits the integration (Fig. 9) of low-dead-volume (4-nl) microvalves and sample loops (internal volume *ca.* 25–250 nl). A typical switching time is *ca.* 1.5 ms; the injection valve can be opened from 5 to 255 ms, this duration being controlled by a microprocessor. The input band of such a valve can be considered to be rectangular, the characteristic time τ is the pulse width and λ is equal to 1/12; consequently, for a 10-ms pulse, the extra-column contribution σ^2_I is only $8.3 \cdot 10^{-6}$ s^2, which is extremely low.

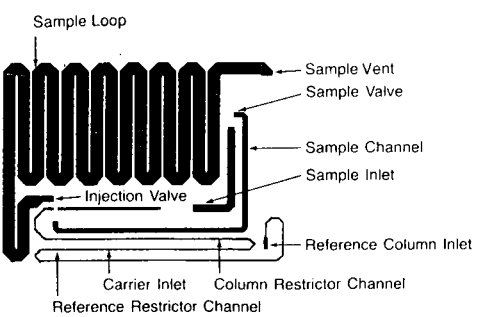

Fig. 9. Silicon wafer injection pattern. (Reproduced with permission of Microsensor Technology).

Detector. The detector time constant can have two origins: (a) purging time of internal volume given by the ratio V/F and (b) time constant arising from the principle of operation.

The flame ionization detector seems potentially to be the best detector for fast analyses. The column can be installed directly in the burner tip; the dead volume between the column outlet and the flame is estimated to be *ca.* 500–1000 nl. This volume is flushed at a relatively high flow-rate (carrier gas + hydrogen, 30–40 ml/min) and the characteristic time is about 1 ms ($\lambda = 1$). Characteristic times of the process taking place in the flame itself are a few microseconds, which is negligible compared with the previous value.

For a long time the thermal conductivity detector was disregarded from the point of view of sensitivity and rapidity. Recent developments [12] by the Microsensor Technology R & D group have given a completely new horizon for this type of detector: the Microsensor thermal conductivity detector has a dead volume of only 2 nl. Considering 0.6 ml/min as a typical flow-rate through the cell (optimum flow-rate for 0.15 mm I.D. columns), the flushing time constant is about 2 ms. Usually thermal characteristic times are much larger; however, advances in silicon technology allow a very compact, low heat capacity geometry to be realized and the total time constant remains less than 10 ms.

Amplifier (electrometer). When speaking about the amplifier we mean the electrometer (typical for flame ionization detection) and all other electronic devices for signal amplification. The contribution of the amplifier to band broadening was studied by Gaspar *et al.* [6] and later by Villalobos and Annino [21,22]. As the latter workers showed, an electrometer time constant larger than 20 ms (the usual value for modern commercially available chromatographs) results in a perceptible peak broadening even when using columns with conventional dimensions (10 m × 0.25 mm I.D.). For truly fast analyses, a specially designed preamplifier installed directly on the detector is recommended. Only in this way is it possible to achieve small enough time constants (1 ms or less); otherwise, the capacity of the input cable results in large time constants, mainly when high sensitivities (high input impedance) are required.

Data acquisition system. For truly fast analyses, ordinary chart recorders are far too slow, and only high-speed UV recorders or storage oscilloscopes can be used. The best way is to use digital data acquisition devices; here two important aspect must be considered:

(a) Choice of the A/D converter: an 8-bit A/D converter can resolve 1 part in 256 (which is not sufficient), a 12-bit converter 1 part in 4096 and a 16-bit converter 1 part in 65 536. The best compromise (considering cost) seems to be to use a 12-bit converter, considering also that the linear dynamic range of amplifiers usually does not exceed three orders of magnitude.

(b) Sampling time set-up: on increasing the sampling time (decreasing sampling frequency), two things happen: the signal-to-noise ratio increases, this ratio being proportional to the square root of the sampling period; with too high a sampling frequency undersirable baseline noise will be detected and measured; and over a certain limit decrease in accuracy occurs.

Integrator manufacturers suggest a practical rule for optimum data bunching, *i.e.* 10–20 bunches per peak half-width; thus, when working with peak standard deviations, we obtain the following relationship:

$$\frac{\sigma}{4.31} > T_s > \frac{\sigma}{8.62} \tag{32}$$

Truly fast chromatograms have standard deviations of 5–10 ms, which means that a sampling time of 1–2 ms gives the best compromise for sufficient accuracy and efficient numerical filtering.

CONCLUSIONS

Fast separations (analyses lasting a few minutes) can be carried out by means of conventional equipment, using commercially available narrow-bore (0.15 mm I.D.) columns and by respecting some simple rules, such as (a) choice of carrier gas (hydrogen), (b) setting the column temperature to optimize the capacity factor range (1–5), (c) choice of injection technique (split preferred, or cold trapping and thermaldesorption) and (d) the use of modern, sophisticated instrumentation having low time constants.

The realization of extremely fast analyses (a few seconds) is no longer a dream, the existing state of fused-silica column technology, of micromachining and of the microcomputer field giving real possibilities for manufacture specially designed high-speed chromatographs. The expressions given for analysis time, for optimum practical velocity and for optimum column length permit the best performance of such a chromatograph to be exploited.

SYMBOLS

B	coefficient of HETP equation
C_G	coefficient of HETP equation (gas phase)
C_L	coefficient of HETP equation (liquid phase)
C	Sum of C_G and C_L
D	coefficient of modified HETP equation
$\mathscr{D}$	product of D by column length
d_c	column inner diameter
d_f	liquid film thickness
F	flow-rate
H	height equivalent to a theoretical plate (HETP)
H_{min}	minimum value of HETP
H'	value of HETP at velocity u'
K	partition constant
k'	column capacity factor
L	column length
N	theoretical plate number
N_{ne}	number of theoretical plates necessary to resolve two compounds
R_s	resolution factor
T_s	sampling period time for digital data acquisition
TH	time necessary to generate a theoretical plate
TH'	minimum value of TH
t_R	retention time
u	average carrier gas velocity
u_{opt}	optimum velocity to obtain a minimum HETP
u'	optimum practical velocity to obtain a minimum TH

V	volume
α	liquid-phase selectivity
σ	time-based peak standard deviation
${}_{\mathrm{L}}\sigma^2$	length-based peak variance
σ^2	time-based peak variance
σ_i^2	time-based variance of an extra-column device
σ_{EC}^2	sum of extra-column variance (time-based)
λ	multiplication factor
τ	characteristic time of an extra-column device

ACKNOWLEDGEMENTS

The author is indebted to J. P. Grenotton and F. Sebregts for their advice and to J. Olek for technical help.

REFERENCES

1 D. H. Desty and A. Goldup, in R. P. W. Scott (Editor), *Gas Chromatography 1960*, Butterworths, London, 1960, p. 162.
2 D. H. Desty, *Adv. Chromatogr.*, 1 (1965) 199.
3 G. Guiochon, *Anal. Chem.*, 50 (1978) 1812.
4 G. Gaspar, P. Arpino and G. Guiochon, *J. Chromatogr. Sci.*, 15 (1977) 256.
5 G. Gaspar, J. P. Olivo and G. Guiochon, *Chromatographia*, 11 (1978) 321.
6 G. Gaspar, R. Annino, C. Vidal-Madjar and G. Guiochon, *Anal. Chem.*, 50 (1978) 1512.
7 G. Gaspar, C. Vidal-Madjar and G. Guiochon, *Chromatographia*, 15 (1982) 125.
8 C. Schutjes, E. Vermeer, J. Rijks and C. Cramers, *J. Chromatogr.*, 253 (1982) 1.
9 C. Schutjes, E. Vermeer and C. Cramers, *J. Chromatogr.*, 279 (1983) 49.
10 C. P. M. Schutjes, *Thesis*, Eindhoven, 1983.
11 S. Saadat and S. Terry, *Am. Lab.*, 5 (1984) 90.
12 G. Lee, C. Ray, R. Siemers and R. Moore, *Am. Lab.*, 10 (1985) 124.
13 C. A. Ray, paper presented at the *Conference on Natural Energy Measurement, Rosemont, IL, June 27–28, 1988.*
14 G. Gaspar, *Thesis*, Academy of Sciences, Budapest, 1978.
15 R. P. W. Scott and G. S. F. Hazeldean, in R. P. W. Scott (Editor) *Gas Chromatography 1960*, Butterworths, London, 1960, p. 144.
16 A. Van Es, J. Janssen, C. Cramers and J. Rijks, *J. High Resolut. Chromatogr. Chromatogr. Commun.*, 11 (1988) 852.
17 D. V. Grant, *J. Chromatogr.*, 122 (1976) 107.
18 J. C. Sternberg, *Adv. Chromatogr.*, 2 (1966) 205.
19 R. L. Wade and S. P. Cram, *Anal. Chem.*, 44 (1972) 131.
20 P. Cardot, I. Ignatiadis, A. Jaulmes, C. Vidal-Madjar and G. Guiochon, *J. High Resolut. Chromatogr. Chromatogr. Commun.*, 8 (1985) 591.
21 R. Villalobos and R. Annino, *J. High Resolut. Chromatogr.*, 12 (1989) 149.
22 R. Villalobos, *J. Chromatogr. Sci.*, 28 (1990) 341.

Journal of Chromatography, 556 (1991) 353–362
Elsevier Science Publishers B.V., Amsterdam

CHROM. 23 320

High-performance liquid chromatography on dynamically modified silica

IX[a]. Modification of silica with 3-(N,N-dimethylpalmitylammonium) propanesulphonate for reversed-phase chromatography

STEEN HONORÉ HANSEN* and JETTE TJØRNELUND
PharmaBiotec Research Center, Department of Organic Chemistry, The Royal Danish School of Pharmacy, 2 Universitetsparken, DK-2100 Copenhagen (Denmark)

ABSTRACT

Reversed-phase high-performance liquid chromatography on silica has been performed using 3-(N,N-dimethylpalmitylammonium) propanesulphonate as an additive to the aqueous mobile phases. The adsorption of the surfactant has been investigated as a function of its concentration in the eluent and the pH of the eluents. The separation mechanisms are reversed-phase as well as silanolophilic interactions, and are compared with those observed when using quaternary long-chain alkyltrimethylammonium ions as the additive to generate the reversed phase.

INTRODUCTION

Reversed-phase high-performance liquid chromatography (RP-HPLC) on dynamically modified silica using quaternary long-chain alkyltrimethylammonium ions as the modifying agent has been thoroughly investigated during the last decade [1–3]. It has been shown that these RP-HPLC systems exhibit an excellent reproducibility of selectivity even when using silica column packing materials of various origins [4,5]. The reproducibility of selectivity as well as the peak shape of the amine solutes are superior to deactivated chemically bonded octadecylsilyl (ODS) column packing materials [6,7].

A few investigations of the use of 3-(N,N-dimethylalkylammonium) propanesulphonates as additives to the eluents in RP-HPLC on chemically bonded phases have been reported [8–10].

This paper reports the modification of bare silica with 3-(N,N-dimethyl-

[a] For Part VIII, see ref. 3.

0021-9673/91/$03.50

palmitylammonium) propanesulphonate (PAPS) as a function of the concentration of PAPS in the eluent and the pH of the eluent. The retention mechanisms of the solutes are discussed and compared with the retention mechanisms observed when using quaternary long-chain alkyltrimethylammonium compounds for the modification of the silica surface. The structures of the two types of modifiers are shown in Fig 1.

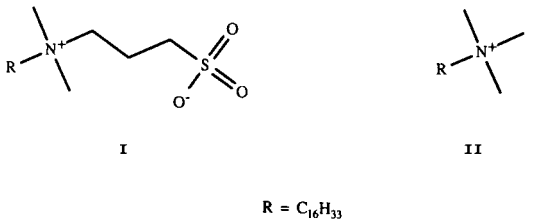

I II

R = $C_{16}H_{33}$

Fig. 1. (I) 3-(N,N-Dimethylpalmitylammonium) propanesulphonate (PAPS) and (II) N,N,N-trimethylhexadecylammonium (CTMA) ion.

EXPERIMENTAL

Chemicals

3-(N,N-Dimethyldodecylammonium) propanesulphonate (DAPS), 3-(N,N-dimethylmyristylammonium) propanesulphonate (MAPS), PAPS and 3-(N,N-dimethylstearylammonium) propanesulphonate (SAPS) were obtained from Fluka (Buchs, Switzerland). 4,4'-Diethoxyazobenzene was prepared by coupling diazotized 4-ethoxyaniline to phenol followed by ethylation using diethyl sulphate; the crude product was recrystallized from methanol–water.

The column packing materials were as follows: Partisil (Whatman, NJ, USA), Zorbaxsil (DuPont, Cheshire, UK), Spherosil XOA 600 (Prolabo, Paris, France), LiChrosorb Si 60 (Merck, Darmstadt, Germany), Chromosorb LC6 (Johns-Manville, Denver CO, USA) and Spherisorb S5W (Phase Separations, Clwyd, UK).

All other chemicals were of analytical-reagent grade from Merck.

Apparatus

The chromatographic investigations were performed using one of two systems. The first system consisted of a Waters (Millipore, Milford, MA, USA) liquid chromatograph with a 6000A pump, a 710B WISP autoinjector, a Shimadzu (Tokyo, Japan) CTO-6A column oven and a 490E programmable multiwavelength detector operated at 254 nm and controlled by a Waters Maxima 820 data system. The second system used a Kontron (Tegimenta, Switzerland) chromatograph consisting of an Anacomp 220 HPLC controller, a 220 pump, an MSI 660 autosampler, a 480 column oven, a 432 UV detector operated at 254 nm and a Model 800 plotter.

All analytical columns from Knauer (Bad Homburg, Germany), 120 × 4.6 mm I.D., were slurry-packed in methanol with the respective column packing material. The column systems were operated at 40°C, and the analytical columns were protected against dissolution by the use of saturation columns, 150 × 4.6 mm I.D., packed with LiChroprep Si 60 (15–25 μm) and situated between the pump and the autoinjector.

The hold-up volumes of the chromatographic systems were determined using deuterium oxide.

A Shimadzu UV-265 UV–VIS spectrophotometer was used for the determination of the critical micelle concentration (CMC) by solubilization of 4,4′-diethoxyazobenzene. A Waters 431 conductivity detector was used for the determination of the CMC by conductance measurements.

Determination of adsorption isotherm

Eluents consisting of methanol–water–potassium phosphate buffer pH 7.5 (50:45:5, v/v/v) with 0–50 m*M* of PAPS were used for the experiments. The amount of PAPS adsorbed was determined as described in the following sections. The contents of the column packing materials were determined as described previously [4]. The surface area of LiChrosorb Si 60 was determined as described by Hansen *et al.* [11].

Determination of CMC

The CMC was determined by two methods. The first method, the solubilization of 4,4′-diethoxyazobenzene, was performed as described previously [12]. The determination of the CMC was also performed by measuring the conductance of solutions consisting of methanol–water–0.2 *M* potassium phosphate buffer pH 7.5 (50:45:5 v/v/v) with 0–20 m*M* of PAPS. The conductance data were normalized by division by the conductance of the solution without added PAPS. These results were plotted as a function of the concentration of PAPS. The CMC was determined as the concentration of PAPS corresponding to a minimum in the relative resistance [10].

HPLC of 3-(N,N-dimethylalkylammonium) propanesulphonates

The determination of the amounts of PAPS absorbed on to the silica surface was performed by an elution method. After equilibration the analytical column was disconnected from the system and eluted with methanol–water (90:10, v/v) into a 50-ml calibrated flask. The concentration of PAPS in the 50-ml eluate was determined by the following HPLC method.

The purity of PAPS was investigated using a 120 × 4.6 mm I.D. Knauer column packed with Spherisorb octyl 5 μm (Phase Separations) and operated at ambient temperature. The mobile phase consisted of methanol–water–0.2 *M* potassium phosphate buffer pH 7.5 (80:17:3, v/v/v), and the flow-rate was 1.0 ml/min. A Waters 410 differential refractometer was used for the quantitative determination of the compounds. A linear response was obtained in the range 0.012–50 m*M* for all four 3-(N,N-dimethylalkylammonium) propanesulphonates. The k' values for DAPS, MAPS, PAPS and SAPS were 1.32, 2.08, 3.35 and 5.49, respectively.

RESULTS AND DISCUSSION

Adsorption isotherm

A standard chromatographic system similar to those used for the modification of silica with quaternary long-chain alkyltrimethylammonium compounds was chosen [12]. The columns packed with bare silica were equilibrated with methanol–0.2 *M* potassium phosphate buffer pH 7.5–water (50:5:45, v/v/v) containing different amounts of PAPS. The adsorption isotherm (Fig. 2) does not show a Langmuir

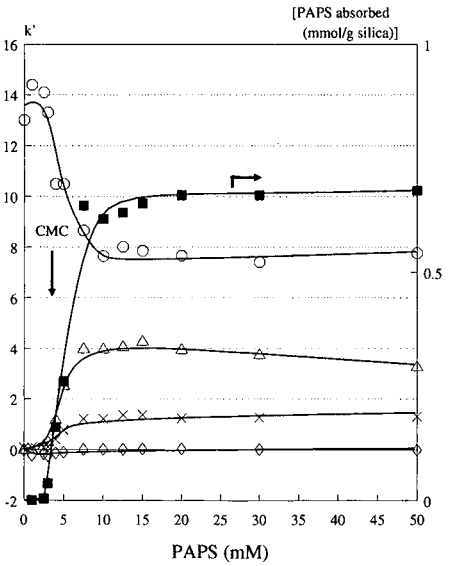

Fig. 2. Adsorption isotherm for PAPS (■). Retention (k' values) *versus* the concentration of PAPS in the eluent for: × = phenol; △ = toluene; ◇ = benzoic acid; o = N,N,N-trimethylanilinium ion. Chromatographic conditions: column, LiChrosorb Si 60, 5 μm, 120 × 4.6 mm I.D.; eluent, methanol–water–0.2 *M* potassium phosphate pH 7.5 (50:45:5, v/v/v) with different amounts of PAPS added; flow-rate 1.5 ml/min at 40°C.

behaviour. At low concentrations of PAPS only a very small amount of the surfactant is adsorbed on to the silica surface. At a certain concentration, corresponding to the CMC, a steep increase in the amount of PAPS adsorbed is observed until a plateau is reached, corresponding to an adsorption of about 0.7 mmol/g of silica. The surface area of LiChrosorb Si 60 is about 550 m^2/g, and the adsorbed amount therefore corresponds to a coverage of about 1.2 $\mu mol/m^2$ of silica, which should be compared to the about 8 $\mu mol/m^2$ of silanol groups normally considered to be available on a fully hydroxylated silica surface.

The CMC of PAPS in the eluent was determined to be 3.2 m*M* by the solubilization method and 4 m*M* by measuring the conductance of the mobile phases. By HPLC analysis PAPS was found to contain 1.1% DAPS, 1.4% MAPS and 2.0% SAPS.

Influence of pH

The effect of the pH of the eluents on the retention of solutes was investigated in the pH range 2–10 (Fig. 3). The change in the retention of the solutes when changing the pH is very similar to that observed in RP-HPLC on chemically bonded ODS phases.

The retention of non-ionic solutes is virtually constant throughout the pH interval investigated, which indicates the constant amount of PAPS absorbed on to the surface of the silica. Anionic solutes are only retained in the system at a pH where they are non-ionized, *i.e.* at low pH values. The anionic solutes have negative capacity

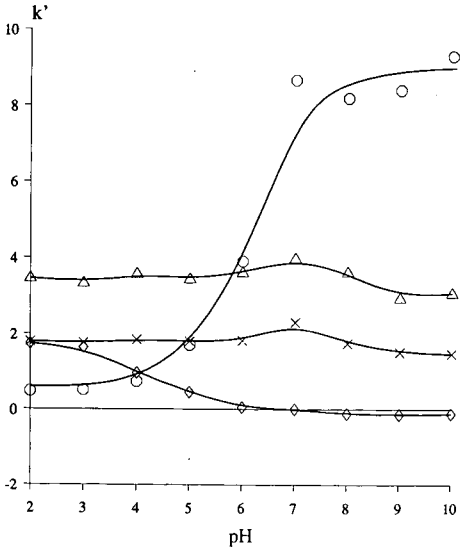

Fig. 3. Retention (k' values) *versus* pH of buffer solutions in eluent. Symbols as in Fig. 2. Chromatographic conditions as in Fig. 2, with various pH values in buffer solutions and with 7.5 mM PAPS added.

factors k' at higher pH values, indicating ionic exclusion from the partly ionized silica column packing material. The retention of the quaternary ammonium compound increases with the ionization of the silanols corresponding to the pK_a value (about 7) of the silica. The retention of amines also increases with the increase in ionization of the silanols (Fig. 4). At high pH values (about 8–10), where the retention is due to a mixture of reversed-phase and ion-exchange interactions (Fig. 4C), the retention decreases as a result of the increasing deprotonization of the amines.

The retention of cationic solutes was studied in detail to compare the modification of silica with N,N,N-trimethylhexadecylammonium (CTMA) ions (Fig. 4A) and PAPS (Fig. 4C). The relative retention between imipramine and some related cations at pH values above 8 (Fig. 4C) are similar to that found when chromatographing these substances on bare silica with the same mobile phases but without adding any surfactant (Fig. 4B). However, larger k' values are obtained due to the additional reversed-phase effect, and due to the additional separation mechanism some changes in selectivity are observed. Comparing the PAPS system (Fig. 4C) with the CTMA system (Fig. 4A) reveals fundamental differences in the separation mechanisms as the quaternary ammonium ion only exhibits a small retention in the latter system, whereas it has the largest retention time of the solutes using no modification (Fig. 4B) or modification with PAPS.

Retention mechanisms

When no or only a small amount of PAPS is adsorbed on the silica surface, no RP effect is observed, but above the CMC reversed-phase separations are performed (Fig. 5), similar to those seen in RP-HPLC on chemically bonded phases.

Only a small reduction of the cationic capacity is seen when PAPS is absorbed

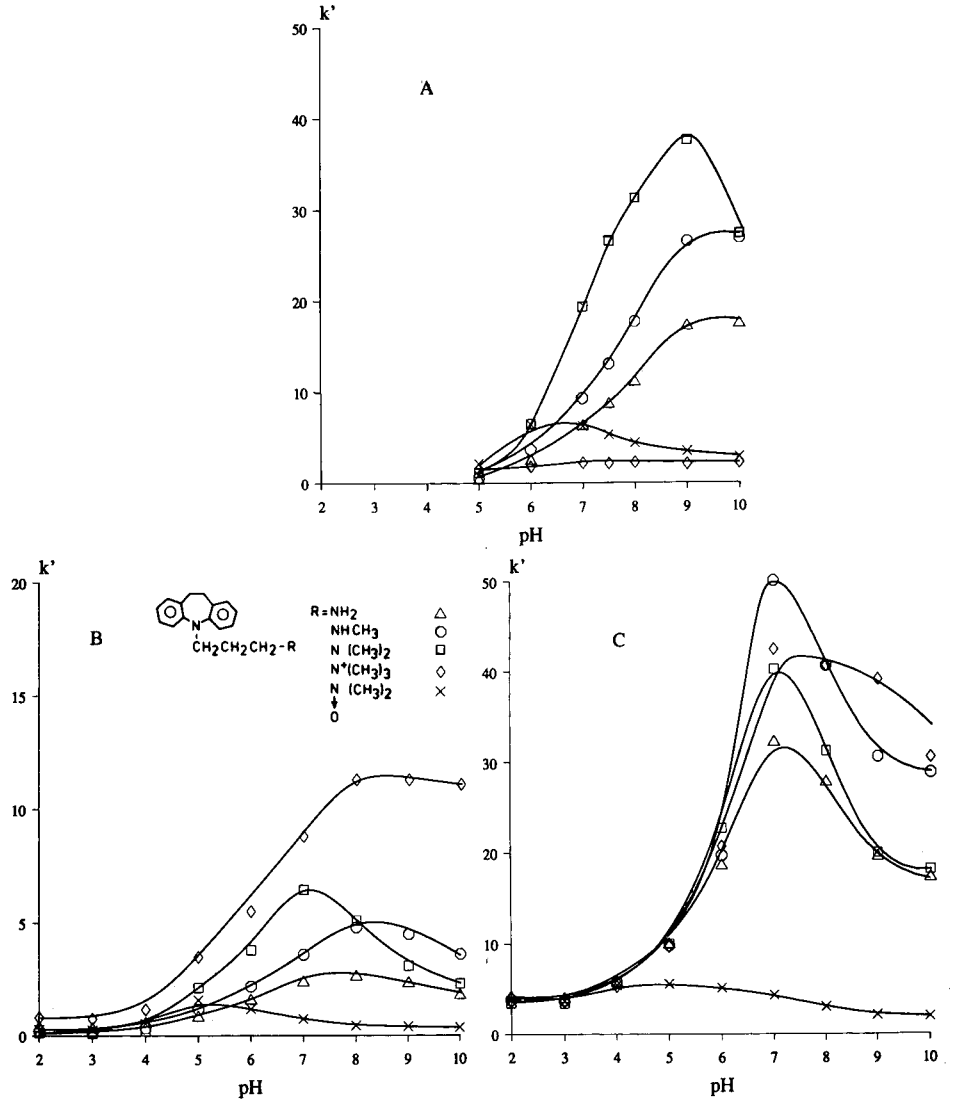

Fig. 4. Retention (k' values) of imipramine and some closely related compounds *versus* pH of buffer solutions in eluent. Chromatographic conditions: column as in Fig. 2; eluents, methanol–water–0.2 *M* potassium phosphate pH 7.5 (50:45:5, v/v/v). (A) With 2.5 m*M* of N,N,N-trimethylhexadecylammonium bromide added; (B) with no surfactant added; (C) with 7.5 m*M* of PAPS added. Flow-rate, 1.5 ml/min at 40°C.

on to the surface at pH values above 5 (Fig. 4C), as indicated by the retention of the quaternary ammonium compound. When using quaternary long-chain alkyltrimethylammonium ions, the cation-exchange properties of the silica are effectively eliminated (Fig. 4A).

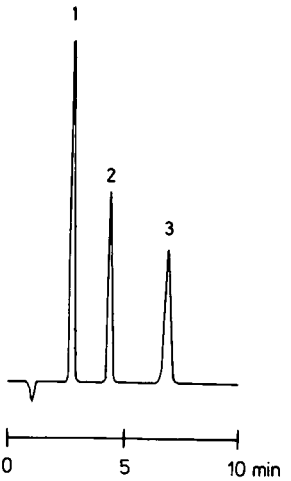

Fig. 5. Separation of (1) phenol, (2) toluene and (3) *m*-xylene on Spherisorb S5W 5 μm, 120 × 4.6 mm I.D., using methanol–water–0.2 *M* potassium phosphate pH 7.5 (50:45:5, v/v/v) with 7.5 m*M* of PAPS added as eluent. Flow-rate, 1.5 ml/min at 40°C.

If the adsorption of PAPS on to the silica surface is accomplished by interactions between the quaternary ammonium groups and the silanol groups in the same way as with quaternary long-chain alkyltrimethylammonium ions, but leaving free sulphonate groups for cation-exchange, differences in the silanol activity are masked. Thus, the reversed-phase system generated may be expected to show a high reproducibility of selectivity between solutes using different brands of silica.

The data in Table I show a poor reproducibility of selectivity when using different brands of silica. It has been shown previously [4–7, 13–14] that very reproducible selectivities (relative standard deviations typically 5% or below) between solutes may be obtained on different brands of silica if the silica is dynamically modified with CTMA. For comparison, data from Hansen *et al.* [6] are reprinted in Table II.

There is straightforward correlation between the surface area of the silica, the amount of CTMA adsorbed and the k' value for benzene when silica is modified with CTMA [11,13]. If the interaction between PAPS and the silica surface is due to interactions between the quaternary ammonium group and the silanols, a correlation between the retention of benzene or toluene and the surface area is expected as the retention of neutral solutes in these systems is due only to reversed-phase interactions with the long carbon chains of the absorbed surfactant. No such correlation was found, and, in addition, the adsorption of PAPS on to the silica surface is independent of the pH value of the buffer in the eluent, as indicated by the constant retention of toluene (Fig. 3) throughout the pH interval investigated.

If the adsorption of PAPS on to the silica is due to ionic interactions between the quaternary ammonium group and the silanols, an increase in the retention of neutral solutes with an increase in the ionization of silica is expected, but this was not observed. At pH values below 5, PAPS is probably adsorbed as a result of dipolar–dipolar interactions as the ammonium propanesulphonate is a strong dipole. Above

TABLE I

SEPARATION FACTORS (α) BETWEEN PHENOL AND EIGHT DIFFERENT SOLUTES ON SEVEN DIFFERENT BRANDS OF SILICA COLUMN PACKING MATERIALS

Eluent: methanol–0.2 *M* potassium phosphate buffer pH 3.0 or 7.5–water (50:5:45, v/v/v) with 7.5 m*M* PAPS added. Temperature 40°C. – = No retention; R.S.D. = relative standard deviation.

Solute	α															
	Partisil		Zorbaxsil		Hypersil		Spherosil XOA 600		LiChrosorb Si 60		Spherisorb S5W		Chromosorb LC6		R.S.D. (%)	
	pH 3.0	pH 7.5	pH 3.0	pH 7.5	pH 3.0	pH 7.5	pH 3.0	pH 7.5	pH 3.0	pH 7.5	pH 3.0	pH 7.5	pH 3.0	pH 7.5	pH 3.0	pH 7.5
Benzoic acid	0.99	–	0.93	–	0.92	–	0.95	–	0.93	–	0.93	–	0.78	–	1.8	–
Phenylethylamine	0.18	1.43	0.33	2.83	0.26	1.04	0.22	0.68	0.14	1.12	0.29	1.37	0.22	1.02	27.6	51.3
Benzene	1.09	1.09	1.12	1.72	1.11	1.07	1.11	1.60	1.07	1.01	1.09	1.21	1.11	1.06	1.6	23.0
Toluene	1.92	1.90	1.95	2.85	1.93	1.76	1.86	2.69	1.94	1.73	1.90	1.74	1.89	1.88	1.6	23.1
Phthalic acid	1.15	–	0.63	–	0.73	–	0.77	–	0.79	–	0.61	–	0.85	–	22.8	–
Diethylaniline	0.29	3.37	0.60	4.97	0.36	3.00	0.38	4.67	0.15	3.03	0.38	3.51	0.31	3.32	38.3	21.5
Morphine	0.23	1.89	0.66	3.55	0.35	1.27	0.28	2.76	0.13	1.83	0.47	1.36	0.27	1.29	51.3	43.6
Salicylic acid	0.57	0.16	1.31	0.33	1.34	0.35	0.57	0.42	0.58	0.21	1.17	0.14	1.41	0.28	40.2	38.6

TABLE II

SELECTIVITY (α) BETWEEN IMIPRAMINE AND TEN BASIC DRUGS ON ELEVEN DIFFERENT SILICA COLUMN PACKING MATERIALS (NO. 11–21) DYNAMICALLY MODIFIED WITH 2.5 m*M* CTMA IN THE ELUENT.

For further details see ref. 6.

		Column packing material											R.S.D. (%)
		11	12	13	14	15	16	17	18	19	20	21	
Imipramine	k'	12.7	6.7	9.4	15.9	9.1	6.5	19.0	13.1	9.3	6.5	17.5	
	A_s	0.9	0.8	0.9	1.1	0.9	0.9	1.9	1.0	1.7	1.2	0.9	
Desipramine	α	0.55	0.55	0.54	0.56	0.54	0.58	0.57	0.55	0.56	0.58	0.54	2.7
Imipramine N-oxide	α	0.27	0.28	0.26	0.27	0.27	0.26	0.23	0.26	0.26	0.27	0.25	5.1
cis-Clopenthixol	α	0.91	0.88	0.85	0.89	0.87	0.86	0.82	0.91	0.88	0.89	0.92	3.3
	A_s	1.0	0.8	1.0	1.1	0.8	0.9	1.1	1.0	1.1	0.8	1.0	
trans-Clopenthixol	α	1.04	0.99	0.97	1.01	0.98	0.96	0.92	1.03	0.98	0.99	1.06	4.0
Prochlorperazine	α	2.43	2.23	2.13	2.50	2.25	2.07	1.84	2.17	2.04	2.11	2.49	9.2
	A_s	1.3	1.2	1.2	1.5	1.3	1.4	1.4	1.2	1.7	1.7	1.5	
Chlorpromazine	α	1.92	1.79	1.63	1.96	1.85	1.76	1.74	1.70	1.74	1.80	1.92	5.7
	A_s	1.0	0.9	0.8	0.8	0.7	1.0	1.0	0.9	1.0	0.9	0.9	
Perphenazine	α	0.93	0.88	0.78	0.93	0.88	0.85	0.82	0.85	0.92	0.89	0.93	5.6
Propranolol	α	0.37	0.37	0.38	0.38	0.38	0.35	0.29	0.35	0.32	0.34	0.38	8.2
	A_s	2.4	1.7	1.9	2.9	2.2	2.0	2.9	2.0	2.5	1.6	2.1	
Nortriptylin	α	0.54	0.56	0.52	0.57	0.54	0.57	0.52	0.54	0.54	0.57	0.53	3.5
Amitriptylin	α	0.95	0.97	0.94	0.98	0.97	0.95	0.90	0.94	0.94	0.97	0.97	2.4
	A_s	1.0	1.0	0.8	0.9	0.7	1.0	1.3	1.0	1.3	1.0	2.1	

pH 5 the ionization of the silanols increases with increasing pH values. Whether the adsorption process at high pH values is due to dipolar–dipolar interactions, to ionic interactions, or to a mixture thereof between the quaternary ammonium group and the ionized silanols, leaving a free sulphonate group, cannot be distinguished from the results obtained in these experiments. However, the system exhibits only a small change in the cation-exchange capacity at pH values above 5.

When using quaternary long-chain alkyltrimethylammonium ions for the modification of silica, a similar reversed-phase effect is obtained, but the silanol activity and thus the cation-exchange capacity is effectively masked as a result of the ionic interaction between the quaternary ammonium group and the silanols. This results in a highly reproducible selectivity from various brands of silica [15].

CONCLUSIONS

An RP-HPLC system has been generated using bare silica as the column packing material and aqueous eluents with PAPS added. However, the system does not provide the high reproducibility of selectivity using different brands of silica which is obtained when using silica dynamically modified with quanternary long-chain alkyltrimethylammonium ions.

ACKNOWLEDGEMENT

This work was supported by The Alfred Benzon Foundation.

REFERENCES

1 S. H. Hansen, *J. Chromatogr.*, 209 (1981) 203.
2 S. H. Hansen, P. Helboe and M. Thomsen, *J. Pharm. Biomed. Anal.*, 2 (1984) 165.
3 S. H. Hansen, P. Helboe and M. Thomsen, *J. Chromatogr.*, 447 (1988) 182.
4 S. H. Hansen, P. Helboe, M. Thomsen and U. Lund, *J. Chromatogr.*, 210 (1981) 453.
5 P. Helboe, *J. Chromatogr.*, 245 (1982) 229.
6 S. H. Hansen, P. Helboe and M. Thomsen, *J. Chromatogr.*, 409 (1987) 71.
7 S. H. Hansen, P. Helboe and M. Thomsen, *Trends Anal. Chem.*, 7 (1988) 389.
8 S. G. Weber and W. G. Tramposch, *Anal. Chem.*, 55 (1983) 1771.
9 W. G. Tramposch and S. G. Weber, *Anal. Chem.*, 56 (1984) 2567.
10 W. G. Tramposch and S. G. Weber, *Anal. Chem.*, 58 (1986) 3006.
11 S. H. Hansen, P. Helboe and U. Lund, *J. Chromatogr.*, 260 (1983) 156.
12 S. H. Hansen, P. Helboe and U. Lund, *J. Chromatogr.*, 240 (1982) 319.
13 S. H. Hansen, P. Helboe and M. Thomsen, *J. Chromatogr.*, 360 (1986) 53.
14 S. H. Hansen, *J. Chromatogr.*, 491 (1989) 175.
15 P. Helboe, S. H. Hansen and M. Thomsen, *Adv. Chromatogr.*, 28 (1989) 195.

Journal of Chromatography, 556 (1991) 363–372
Elsevier Science Publishers B.V., Amsterdam

CHROM. 23 284

Chromatographic characterization of ion exchangers for high-performance liquid chromatography of proteins

I. Chromatographic determination of loading capacity for low- and high-molecular mass anions[a]

D. BENTROP and H. ENGELHARDT*
Angewandte Physikalische Chemie, Universität des Saarlandes, D-6600 Saarbrücken (Germany)

ABSTRACT

The capacity of silica-based anion exchangers was determined by three independent methods (potentiometric titration, calculation from elemental analysis data and frontal analysis with sodium nitrate). All three methods gave almost identical results. Breakthrough experiments with sodium nitrate were carried out at different concentrations and flow-rates. The capacity of a large-pore ion exchanger for macromolecular anions such as chondroitin sulphate and bovine serum albumin (BSA) was also determined by frontal analysis. The capacity is much lower than that for small anions and is influenced by the irreversible adsorption of sample ions onto the stationary phase. The capacity for the linear polyanion of chondroitin sulphate was independent of its concentration in the carrier solution (within the range 1–10 g/l). For both biological samples the binding capacity depends on the eluent velocity; the capacity for chondroitin sulphate clearly increases with decreasing flow-rate, whereas globular BSA shows little dependence of capacity on flow-rate. The influence of band spreading on the determination of binding capacity by frontal analysis is discussed.

INTRODUCTION

The number of stationary phases available for the ion-exchange chromatography of proteins is abundant and still growing [1]. However, there is a remarkable lack of pragmatic chromatographic criteria for the characterization of these media. As individual proteins show different chromatographic behaviours it does not seem to be possible to develop a simple, generally applicable test procedure such as that described for reversed-phase chromatography [2]. Therefore, a number of chromatographic techniques have been used to obtain practically useful information on the interactions of proteins with ion exchangers.

[a] Part of this work was presented at the *14th International Symposium on Column Liquid Chromatography, Boston, MA, May 20–25, 1990.*

0021-9673/91/$03.50

One of the most important properties of ion exchangers in terms of their analytical and preparative applications is their exchange capacity, which can be measured easily and reliably by frontal chromatography [3,4]. There are several papers dealing with the determination and/or theoretical modelling of adsorption isotherms of model proteins on ion exchangers [5–9]. Some workers [10–12] investigating the protein binding capacities of ion exchangers found a decrease in capacity with increasing flow-rate, which was explained by factors such as mass transfer resistances and hindered diffusion of the macromolecules in the pores because of their low molecular diffusion coefficients. As these workers determined the binding capacity via the breakthrough volume or from the sample load volume at which the sample concentration of the effluent, monitored by UV absorbance, is 10 or 20% of the feed stream, there might be another explanation for the observed decrease of this capacity with increasing flow-rate. (The knowledge of this binding capacity is important for practical purposes in preparative chromatography; usually, it is smaller than the "true" capacity that has to be determined via the retention volume of the protein front). Fig. 1 is a schematic representation of band spreading in elution and frontal chromatography. As can be easily seen, the breakthrough volume (*i.e.* capacity) decreases with increasing flow-rate because of increasing band spreading, which is especially significant for proteins as a result of their small diffusion coefficients.

There is an ongoing contradictory discussion on the flow-rate dependence of protein loading capacity, even when it is calculated via the retention volume of the breakthrough curve. Recently, Blanco *et al.* [13] investigated the adsorption of β-lactoglobulin onto a weakly hydrophobic surface. They measured the adsorbed amount of protein via the retention volume of the protein front and found the capacity to be independent of the flow-rate. However, Huang *et al.* [9], who studied the adsorption of chicken albumin onto TSK-DEAE 5 PW anion exchanger at pH 8.6, found a dramatic decrease of the adsorbed amount of protein at linear velocities above 1.3 mm/s, although they determined the capacity via the retention volume of the front.

This paper discusses, from a practical point of view, the binding capacities of a

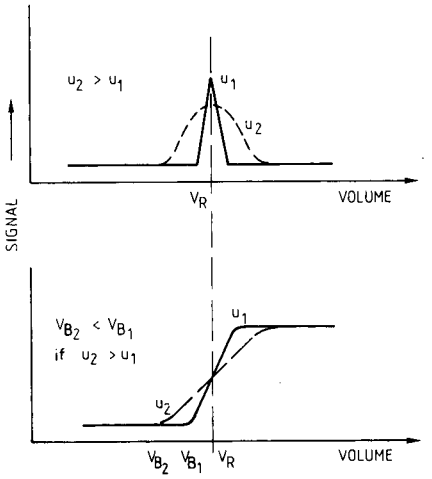

Fig. 1. Schematic representation of band spreading in elution and frontal chromatography. Symbols: u = linear velocity; V_R = retention volume; V_B = breakthrough volume.

silica-based, polymer-encapsulated anion exchanger for low- and high-molecular mass solutes and its dependence on the flow-rate used during the breakthrough measurement. A simple measure for the accessibility of exchange sites on the chromatographic surface for macromolecules can be obtained by comparing their capacity with that for nitrate.

EXPERIMENTAL

Chromatographic instrumentation

Breakthrough measurements were carried out with a modular high-performance liquid chromatography (HPLC) system consisting of a low-pressure eluent selection valve (Rheodyne, Berkeley, CA, USA), a Model 64 HPLC pump from Knauer (Berlin, Germany) or Model 2150 from LKB (Bromma, Sweden), a pulsation dampener (Orlita, Giessen, Germany), a modified Model 7125 sample injector (Rheodyne) without a sample loop, a laboratory-made UV detector (254 nm, flow cell volume, 8 μl) or a Model R401 refractive index detector from Waters Assoc. (Milford, MA, USA) and a strip-chart recorder. All tubings and connections downstream of the injector valve were kept as small as possible.

Materials

Sodium nitrate and the other inorganic chemicals used throughout this study (NaCl, LiCl, $Na_2HPO_4 \cdot 12H_2O$, $NaH_2PO_4 \cdot 2H_2O$, H_3PO_4) were of analytical-reagent grade from either Merck (Darmstadt, Germany) or Fluka (Buchs, Switzerland). HPLC-grade water was delivered by a Milli-Q water purification system (Millipore, Bedford, MA, USA). Bovine serum albumin (BSA) (fraction V) was purchased from J. T. Baker (Phillipsburg, NJ, USA) and Sigma (St. Louis, MO, USA) and the sodium salt of chondroitin sulphate (puriss) was obtained from Serva (Heidelberg, Germany). All chemicals were used as received, without further purification. Sodium azide (Merck) was added to the solutions of chondroitin sulphate and BSA at a concentration of 10 mg/l to prevent microbial growth.

Columns

The polymer-encapsulated strong anion exchanger with quaternary ammonium

TABLE I

PROPERTIES OF THE STRONG ANION EXCHANGERS USED FOR THE BREAKTHROUGH EXPERIMENTS DESCRIBED IN THIS STUDY

Property	SAX100	SAX300
Particle size (μm)	10	7
Surface area (m^2/g)	320	100
Pore size (nm)	10	30
Carbon content (% w/w)	13.60	4.56
Nitrogen content (% w/w)	2.63	0.78
Capacity (μmol/g)		
from nitrogen content	939	279
by potentiometric titration	899	253

groups (SAX) which was used throughout this study was synthesized according to the procedure described in ref. 14. The characteristic properties of the ion exchangers based on either LiChrosorb Si100 (SAX100) or Nucleosil 300-7 (SAX300) are summarized in Table I. The stationary phases were slurry-packed into stainless-steel columns 25 or 15 cm in length and 0.41 cm I.D.

Procedures

The column loading capacities for sodium nitrate, chondroitin sulphate and BSA were determined using frontal chromatography at different flow-rates and sample concentrations. The employed measurement procedure was discontinuous and similar to that described by Kopaciewicz *et al.* [10].

The column was equilibrated with carrier solution [water for nitrate and chondroitin sulphate, 20 m*M* sodium phosphate buffer (pH 7.5) for BSA] at 2 ml/min. After switching the injector valve to the load position the pumping system was purged with sample solution. Thereafter, the valve was switched to the inject position so that the pump delivered the sample solution to the column. The flow-rates were measured volumetrically during each frontal analysis run. After each breakthrough measurement the ion-exchange column was washed with a solution of sodium chloride (0.5 *M* and 2 *M* for nitrate and chondroitin sulphate, respectively) and re-equilibrated with water. After every loading of BSA the column was washed with 50 m*M* phosphoric acid and 0.5 *M* sodium chloride before re-equilibration with the buffer.

The ion-exchange capacity for nitrate was calculated from the retention volume of its almost symmetrical breakthrough curves, whereas for chondroitin sulphate and BSA the breakthrough point of the curve was used for the determination of binding capacity [15].

RESULTS AND DISCUSSION

Exchange capacity for nitrate

The capacity of the ion exchanger SAX100 for low-molecular-mass anions was determined by frontal analysis with sodium nitrate at different nitrate concentrations and flow-rates, which corresponded to linear velocities up to 7.1 mm/s.

Surprisingly, the binding capacity for nitrate depended on its concentration in the mobile phase. Fig. 2 shows the exchange isotherm of nitrate, illustrating a decrease of capacity with increasing nitrate concentration. Chemistry does not offer an obvious explanation for this behaviour. It is not due to a lack of stability of the stationary phase (data not shown), but it may have been caused by a systematic error linked to the discontinuous experimental technique and to the fact that the retention times of the nitrate fronts were shorter at higher nitrate concentrations. Consequently, the data at high concentrations are less reliable. Linear regression of the isotherm data gives a straight line which intercepts the y-axis at a capacity of 879 μmol/g. This extrapolation to a nitrate concentration of zero yields a capacity value that is close to the result of 899 μmol/g obtained by potentiometric titration and to the capacity of 939 μmol/g calculated from nitrogen content. Thus, frontal analysis with low-molecular mass ions is a suitable method for the determination of the capacity of ion-exchange columns without unpacking the column or the destruction of the stationary phase.

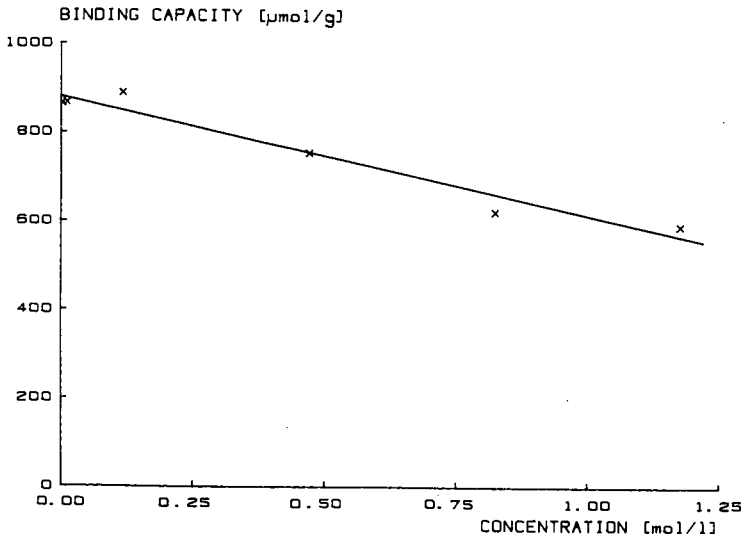

Fig. 2. Exchange isotherm of sodium nitrate on SAX100. Flow-rate, 1.0 ml/min.

Fig. 3. shows a plot of the nitrate binding capacity *versus* flow-rate for two nitrate concentrations. Within the range of experimental error, the capacity is independent of the mobile phase flow-rate, indicating that the nitrate ions can penetrate all the pores and that there are not mass transfer resistances in this instance.

The polymer-encapsulated ion exchanger SAX300 was synthesized on a wide-pore silica column (Nucleosil 300-7) to evaluate its capacity for biological macromolecules. Its actual capacity was also determined by three independent methods that gave almost identical results: (1) calculation from nitrogen content, 279 μmol/g; (2) potentiometric titration, 253 μmol/g; and (3) frontal analysis with sodium nitrate 252 μmol/g. Again, the nitrate binding capacity was independent of the flow-rate.

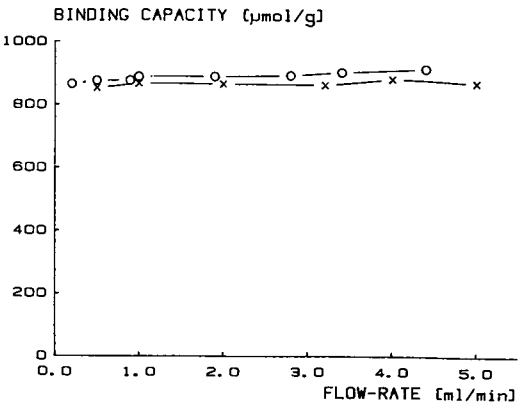

Fig. 3. Plot of nitrate binding capacity *versus* flow-rate for concentrations of 0.012 (×) and 0.118 mol/l (o). Stationary phase, SAX100.

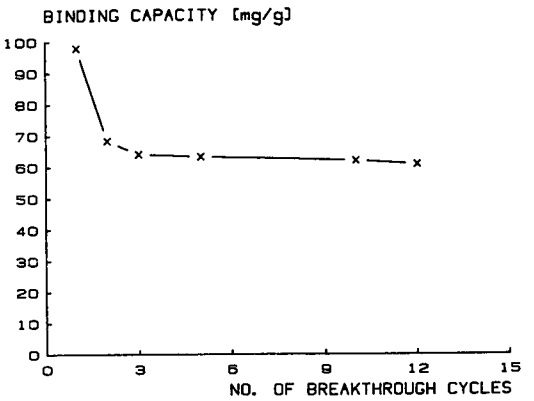

Fig. 4. Influence of the number of breakthrough cycles on the binding capacity of SAX300 for BSA. Flow-rate, 0.5 ml/min. Mobile phase, 4.87 g/l BSA in carrier solution.

Binding capacity for bovine serum albumin

During the first breakthrough cycles the SAX300 irreversibly adsorbed a considerable amount of BSA. Fig. 4 shows a *ca.* 35% loss of protein binding capacity until the most active sites of the stationary phase were saturated with protein after the first three cycles. The irreversible adsorption of such a large amount of BSA (34 mg/g) may have been caused by hydrophobic interactions of protein molecules with the polymeric ion exchanger (which is known to exert a certain hydrophobicity [14]) and their subsequent denaturation on the chromatographic surface.

The irreversible binding of BSA is also well reflected by a 10% reduction of the nitrate binding capacity and an increase of the carbon content from 4.56 to 5.12% (w/w). A calculation of the irreversibly adsorbed amount of BSA via the increase of the nitrogen content by 0.39% (w/w) and the nitrogen content of the BSA used [15.4% (w/w)] yields a value of 25 mg/g, which is in good agreement with that from frontal analysis data.

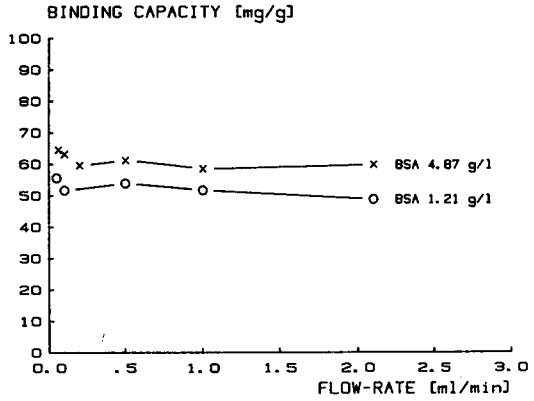

Fig. 5. Plot of BSA binding capacity *versus* flow-rate for concentrations of 4.87 and 1.21 g/l BSA in carrier solution. Stationary phase, SAX300.

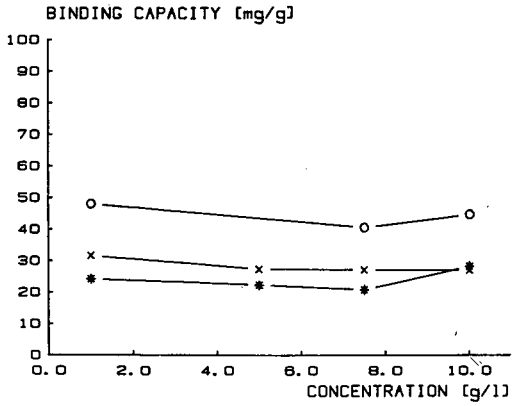

Fig. 6. Influence of mobile phase flow-rate on the exchange isotherm of the sodium salt of chondroitin sulphate. Flow-rates: o = 0.1; × = 0.5; * = 2 ml/min. Stationary phase, SAX300.

Fig. 5 shows the dependence of the capacity for BSA on the flow-rate, which was measured only after the irreversible adsorption had occurred. The linear velocities of the mobile phase were in the range 0.1–3.6 mm/s. Within this range, the BSA capacity was almost independent of the flow-rate; there was only a slight increase of capacity at flow-rates below 0.2 ml/min. Thus the mass transport of BSA was not significantly hindered; this is not surprising as BSA is a fast-diffusing transport protein [16].

Frontal analysis with the sodium salt of chondroitin sulphate

The linear polyanion of chondroitin sulphate also underwent irreversible adsorption onto the polymer-encapsulated anion exchanger SAX300. The blocking of exchange sites by this irreversible binding led to a 14% reduction of the capacity for nitrate, which can be considered as a minor change in the stationary phase properties

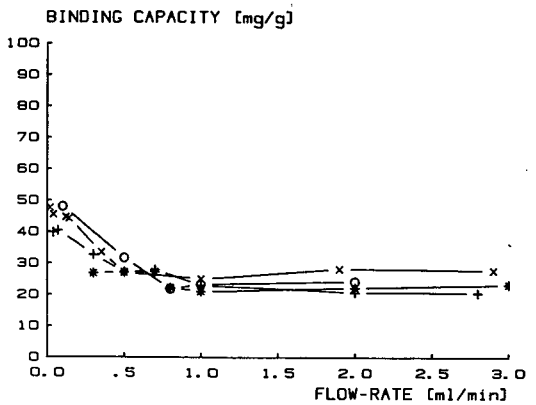

Fig. 7. Plot of binding capacity *versus* flow-rate for different concentrations of the sodium salt of chondroitin sulphate. Concentrations: o = 1.0; * = 5.0; + = 7.5; × = 10.0 g/l. Stationary phase, SAX300.

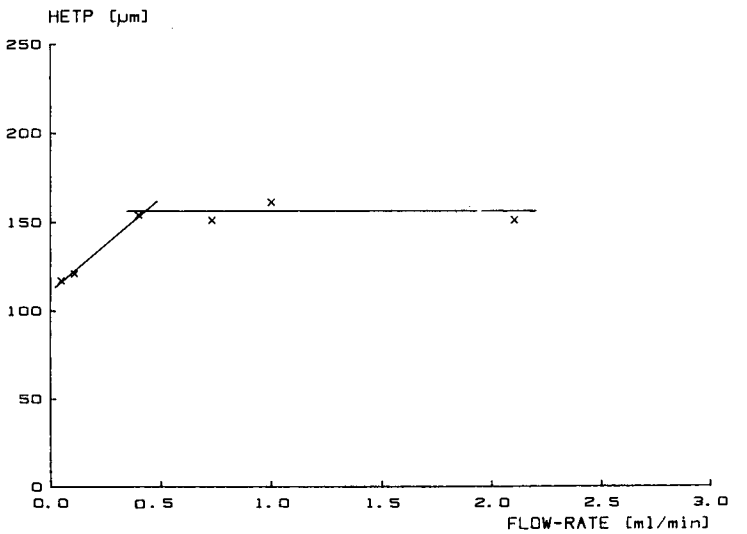

Fig. 8. Plot of HETP *versus* flow-rate for the sodium salt of chondroitin sulphate. Mobile phase, aqueous solution of sodium chloride (1 mol/l). Stationary phase, SAX300 (15 cm column).

compared with the conversion of a silica-based DEAE anion exchanger to a cation exchanger by the adsorption of chondroitin sulphate described by Liao *et al.* [17].

Frontal experiments with chondroitin sulphate after the saturation of the irreversibly adsorbing sites revealed that the capacity was independent of the sample concentration (in the range 1–10 g/l) in the carrier solution (Fig. 6). In contrast, the binding of chondroitin sulphate was strongly influenced by the flow-rate. Fig. 7 shows that there was a significant increase in the binding capacity at flow-rates below 0.8 ml/min (1.4 mm/s linear velocity), leading to a doubling of the capacity at flow-rates below 0.1 ml/min (0.2 mm/s linear velocity). This behaviour can be explained by a restricted mass transfer and slow adsorption kinetics, which are also reflected by asymmetric breakthrough curves that do not allow an unequivocal judgement as to whether equilibrium (*i.e.* complete saturation of the stationary phase or a plateau of the breakthough curve, respectively) has been reached. Anspach *et al.* [18] attribute this phenomenon to the rearrangement of adsorbed molecules on the chromatographic surface.

The increase in capacity at low flow-rates can also be correlated with the height equivalent to a theoretical plate (HETP) *versus* flow-rate curve of chondroitin sulphate (Fig. 8). In principle, the shape of this graph is typical for polymeric solutes [19] that do not necessarily show a minimum in the HETP *versus* flow-rate plot. There is a significant decrease in band spreading at flow-rates below 0.5 ml/min which corresponds well to the flow-rate dependence of the binding capacity calculated from the breakthrough point (cf. Figs 1 and 7). A comparison of the capacity *versus* flow-rate plots for BSA and chondroitin sulphate reveals that the diffusion of the linear polyanion into the pores is much more restricted than that of globular BSA, probably due to the high number of electrostatic interactions that are possible between chondroitin sulphate and the anion exchanger.

Comparison of exchange capacities

The capacity of the wide-pore anion exchanger SAX300 for low-molecular mass anions such as nitrate is 250 μmol/g. Its capacity for macromolecular anions is much lower because high-molecular mass anions cover or block a large number of exchange sites. The maximum exchange capacity for chondroitin sulphate is 0.87 μmol/g, which means that each adsorbed anion of chondroitin sulphate with a molecular mass of approximately 50 000 and two acidic groups per monomer unit covers about 290 quaternary ammonium groups. Thus, it can be assumed that there is an approximately stoichiometric ion exchange between the stationary phase and the (calculated) *ca.* 220 negative charges of a linear chondroitin sulphate anion.

The maximum capacity for globular BSA is 0.93 μmol/g. At this maximum load each BSA molecule covers or blocks 270 exchange sites, although its negative net charge at pH 7.5 is only *ca.* 20 [20][a]. This low binding capacity for BSA can be attributed to a certain inaccessibility of the exchange sites on the chromatographic surface for the negative charges of BSA that are likely to be spread all over the protein molecule.

CONCLUSIONS

Frontal analysis is a fast and reliable technique for the determination of the binding capacities of ion-exchange columns for both low and high molecular weight solutes.

For low-molecular mass ions the exchange capacity is independent of the flow-rate, whereas the capacity for macromolecular samples is influenced by chromatographic band spreading, which increases strongly with increasing eluent velocity due to the small diffusion coefficients of macromolecules. For mainly practical reasons, it is not possible to work with high-molecular mass solutes at the optimum linear velocity where the contribution of mass transfer resistance to peak broadening can be neglected. Consequently, the flow-rate dependence of the binding capacity has to be measured individually for each sample and each stationary phase according to specific differences in the type and number of interactions.

REFERENCES

1 R. E. Majors, *LC · GC Int.*, 3 (1990) 10.
2 H. Engelhardt and M. Jungheim, *Chromatographia*, 29 (1990) 59.
3 J. R. Conder and C. L. Young, *Physicochemical Measurement by Gas Chromatography*, Wiley, Chichester, 1979, Ch. 9.
4 A. W. J. de Jong, J. C. Kraak, H. Poppe and F. Nooitgedacht, *J. Chromatogr.*, 193 (1980) 181.
5 J. X. Huang and Cs. Horváth, *J. Chromatogr.*, 406 (1987) 285.
6 R. D. Whitley, J. M. Brown, N. P. Karajgikar and N. H. L. Wang, *J. Chromatogr.*, 483 (1989) 263.
7 G. L. Skidmore, B. J. Horstmann and H. A. Chase, *J. Chromatogr.*, 498 (1990) 113.
8 G. L. Skidmore and H. A. Chase, *J. Chromatogr.*, 505 (1990) 329.
9 J. X. Huang, J. Schudel and G. Guiochon, *J. Chromatogr.*, 504 (1990) 335.
10 W. Kopaciewicz, S. Fulton and S. Y. Lee, *J. Chromatogr.*, 409 (1987) 111.
11 J. A. J. Schutyser, T. J. W. Buser, D. van Olden and T. Overeem, *J. Liq. Chromatogr.*, 10 (1987) 2151.

[a] In ref. 20, the value of net charge is given for human serum albumin (HSA), but there is hardly any difference in the amino acid composition of BSA and HSA [21].

12 A. M. Tsai, D. Englert and E. E. Graham, J. Chromatogr., 504 (1990) 89.
13 R. Blanco, A. Arai, N. Grinberg, D. M. Yarmush and B. L. Karger, *J. Chromatogr.*, 482 (1989) 1.
14 H. Engelhardt, H. Löw, W. Eberhardt and M. Mauss, *Chromatographia*, 27 (1989) 535.
15 I. Mazsaroff, R. Bischoff, P. A. Tice and F. E. Regnier, *J. Chromatogr.*, 437 (1988) 429.
16 A. L. Lehninger, *Biochemistry*, Worth, New York, 1970, p. 137.
17 A. W. Liao, Z. ElRassi, D. M. LeMaster and Cs. Horváth, *Chromatographia*, 24 (1987) 881.
18 F. B. Anspach, A. Johnston, H.-J. Wirth, K. K. Unger and M. T. W. Hearn, *J. Chromatogr.*, 499 (1990) 103.
19 P. Wichner, *Ph. D. Thesis*, University of the Saarland, Saarbrücken, 1985.
20 *The Merck Index*, Merck, Rahway, NJ, 1983, p. 1217.
21 F. W. Putnam, in H. Neurath (Editor), *The Proteins – Composition, Structure and Function*, Academic Press, New York, 1965, p. 189.

Journal of Chromatography, 556 (1991) 373–381
Elsevier Science Publishers B.V., Amsterdam

CHROM. 23 272

Synthesis of chemically bonded liquid crystals for high-performance liquid chromatography

New phases via the organochlorosilane pathway

JOSEPH J. PESEK*, MARK A. VIDENSEK and MARY MILLER
Department of Chemistry, San Jose State University, San Jose, CA 95192 (USA)

ABSTRACT

Two bonded nematic liquid crystal stationary phases for use in high-performance liquid chromatography were prepared by reacting the silanized forms of [4-(allyloxy)benzoyl]biphenyl and 4-{[4-(allyloxy)-benzoyl]oxy}-4′-methoxybiphenyl with the surface of silica. The diffuse reflectance infrared Fourier transform and carbon-13 cross-polarization magic angle spinning NMR spectra of the two bonded phases confirmed that the reaction was successful. Carbon elemental analysis indicated a high loading of the liquid crystal on the surface. Van 't Hoff plots using polyaromatic hydrocarbons as the solutes in an acetonitrile–water mobile phase indicated that phase transitions are occurring. The relative retention of anthracene and phenanthrene as a function of temperature is also sensitive to changes in the stationary phase morphology and reveals that more than a single transition is occurring over the temperature range studied.

INTRODUCTION

Since the introduction of liquid crystals as stationary phases more than 25 years ago [1,2], many applications have been developed for gas chromatography (GC) [3]. More recently, it has been shown that liquid crystals are suitable stationary phases for supercritical fluid chromatography (SFC) [4,5]. However, the same properties that make these materials desirable as stationary phases in GC and SFC also make them potentially just as useful in high-performance liquid chromatography (HPLC). These properties include phase transitions which can be controlled by experimental conditions in order to change the retention mechanism. It has now been demonstrated that liquid crystal materials can be synthesized and bonded to porous silica [6] so that they possess properties which are clearly different than those of ordinary reversed-phase materials for HPLC [7,8].

The previous studies have all utilized a material which was shown to have liquid crystal properties when bonded to a polysiloxane backbone [9]. Because the preliminary results on this material suggest a phase that might possess unique capabilities for HPLC, it is now necessary to verify further the synthetic approach for the original material and the resulting physical and chromatographic properties.

0021-9673/91/$03.50

The successful pathway originally chosen involves the synthesis of a liquid crystal silane reagent using standard hydrosilylation chemistry [10]. It involves a reaction between a terminal olefin, which is a liquid crystal for one compound in this study, and dimethylchlorosilane to produce the silane reagent:

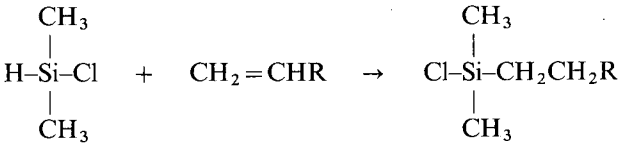

The silane reagent is then reacted with the silica surface to produce the bonded phase:

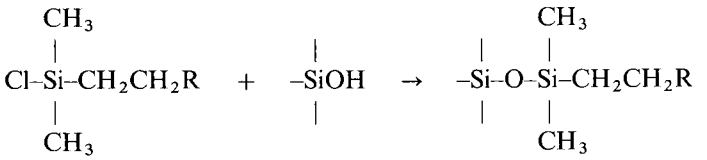

The same reaction pathway was utilized in this study in order to determine its general usefulness and to characterize further the resulting chromatographic properties that bonded liquid crystals possess as stationary phases in HPLC.

EXPERIMENTAL

Materials

All chemicals used in the synthetic procedures and the chromatographic characterizations were of analytical-reagent grade. Solvents in the HPLC experiments were of chromatographic grade. All liquid reagents and solvents used in moisture-sensitive reactions were distilled and collected over type 4A molecular seives. All solid materials used in moisture-sensitive reactions were dried at 110°C for 24 h prior to the start of the experiment. The dried solids were then cooled to 25°C over Drierite in a vacuum desiccator. The solid suport was Nucleosil 300-10. Deuterated chloroform was used as the solvent for proton NMR spectra.

Apparatus

All glassware for moisture-sensitive synthetic work was dried at 110°C for 24 h prior to use and assembled hot with a nitrogen purge. Infrared spectra were obtained in the diffuse reflectance infrared Fourier transform (DRIFT) mode on a Perkin-Elmer (Norwalk, CT, USA) Model 1800 spectrometer. Proton NMR spectral studies were performed on a Varian (Palo Alto, CA, USA) EM 390 spectrometer. Carbon-13 cross-polarization magic angle spinning (CP-MAS) NMR spectra were obtained on a Bruker (Billerica, MA, USA) MSL 300 spectrometer operated in the TOSS mode to eliminate sidebands. Elemental analyses were done at the University of California Berkeley Micro Lab. Differential scanning calorimetric (DSC) measurements were made on a Perkin-Elmer Series 7 thermal analysis system. Surface area measurements (BET) were made on a Micromeritics (Norcross, GA, USA) Model ASAP 2400

analyser. Chromatographic studies were done with a Dionex (Sunnyvale, CA, USA) Model GPM-2 gradient pump module, a Dionex VDM-2 detector, a Pickering (Moutain View, CA, USA) Model CHX 650 column heater and a Spectra-Physics (San Jose, CA, USA) Model SP8875 autosampler.

Synthesis of [4-(allyloxy)benzoyl]biphenyl [9]

To a two-necked, 250-ml, round-bottomed flask equipped with a 50-cm reflux condenser, a Teflon septum with a nitrogen line, a magnetic stirring bar and an oil-bath, 4.93 g of 4-phenylphenol dissolved in 50 ml of dry pyridine were added under nitrogen. Next, 6.13 g of 4-(allyloxy)benzoyl chloride were added with stirring. The mixture was stirred for 3 h at 25°C and then heated at 60°C for an additional 2 h. After the reaction mixture had cooled to 25°C, 200 ml of acidic (20% HCl) deionized water were added. The resulting precipitate was collected by vacuum filtration and washed with 200 ml of cold deionized water. The crude product was recrystallized from acetone–ethanol (1:1) yielding 8.45 g (88%), m.p. 138–140°C.

Synthesis of 4-{[4-(allyloxy)benzoyl]oxy}-4'-methoxybiphenyl [9]

A 400-ml volume of 10% sodium hydroxide solution cooled to 0°C was placed in a three-necked, 1000-ml, round-bottomed flask equipped with a self-equalizing addition funnel, a 50-cm reflux condenser, a Teflon septum with a nitrogen line, a magnetic strirring bar and an ice-bath. Next, 75.50 g of 4,4'-dihydroxybiphenyl were added with vigorous stirring. To this 48.64 g of dimethyl sulphate were added with vigorous stirring over a 1-h period. After the addition was complete, the resulting precipitate was recovered by vacuum filtration with a sintered-glass filter and was redissolved in 400 ml of 10% sodium hydroxide solution. The solution was heated briefly to boiling and was allowed to cool for filtration. The solid was placed in 200 ml of water and was heated to boiling and filtered while hot. The filtrate was then heated to 70°C and acidified with 20% hydrochloric acid, causing crude 4-hydroxy-4'-methoxybiphenyl to precipitate. The product was recrystallized twice from ethanol.

The recrystallized material (3.62 g), dissolved in 100 ml of dry pyridine and under a nitrogen blanket, was placed in a three-necked, 250-ml, round-bottomed flask equipped with a 100-ml self-equalizing addition funnel, a 50-cm reflux condenser, a magnetic stirrer and an oil-bath. Then 4.19 g of 4-(allyloxy)benzoyl chloride dissolved in 20 ml of dry pyridine were added with stirring over a 1-h period. The reaction mixture was stirred for an additional 3 h at 25°C and then heated at 60°C for a further 2 h. The reaction mixture was cooled to 25°C and 400 ml of water were added. The solution was acidified with 20% hydrochloric acid. The precipitate was recovered by vacuum filtration and washed with 400 ml of saturated sodium hydrogencarbonate solution and then with 400 ml of deionized water. The crude product was recrystallized twice from acetone yielding 4.27 g (84%) with the following melting points: crystalline to nematic, 147°C, and nematic to isotropic liquid, 249°C.

Synthesis of silane reagents and silica bonding [6,10]

The organic moiety dissolved in 20 ml of dry toluene was placed in a two-necked, 100-ml, round-bottomed flask equipped with a 50-cm reflux condenser, a Teflon septum with a nitrogen line, a magnetic stirrer and an oil-bath. Next, 11.8 mmol of dimethylchlorosilane were added to the reaction flask while stirring and purging with

nitrogen. After 5 min, 8 mg of hexachloroplatinic acid were added. The reaction mixture was heated to 65°C and stirred for 10 days under nitrogen. Then 20 ml of freshly distilled toluene were added followed by 6.5 g of silica (Nucleosil 300-10) and 0.5 ml of dry pyridine. The reaction mixture was stirred for 10 days at 40°C under nitrogen. The solid was then collected and washed with 60 ml of toluene followed by 60 ml of ethanol. The washing procedure was repeated six times.

RESULTS AND DISCUSSION

Fig. 1 depicts the structures of the starting liquid crystals and the silane reagents which were used to bond the material to porous silica. Each of these materials was characterized by both IR and proton NMR spectra. Compound **a** displayed peaks in the IR region at 3072 cm^{-1} for the C–H stretch of the terminal alkene, at 1647 cm^{-1} for the C=C double bond stretch, at 1608 and 1511 cm^{-1} for aromatic C–H bending, at 1731 cm^{-1} for the C=O stretch, at 1260 and 1169 cm^{-1} for the C–O ester stretch and also peaks between 3072 and 3017 cm^{-1} representing aromatic C–H stretching and between 2980 and 2893 cm^{-1} representing aliphatic C–H stretching.

The essential features of the proton NMR spectrum include a complex pattern centered at 7.50 ppm due to the aromatic hydrogens (thirteen from integration data), a multiplet at 6.10 ppm due to a single vinyl hydrogen, another multiplet at 5.45 ppm due to two vinyl hydrogens and a doublet at 4.75 ppm which is assigned to the methylene protons of the $=CHCH_2O$ segment of the molecule.

The IR spectrum of compound **b** contains the same essential features as that of compound **a** as the structures are very similar. The proton NMR spectrum of **b** also has

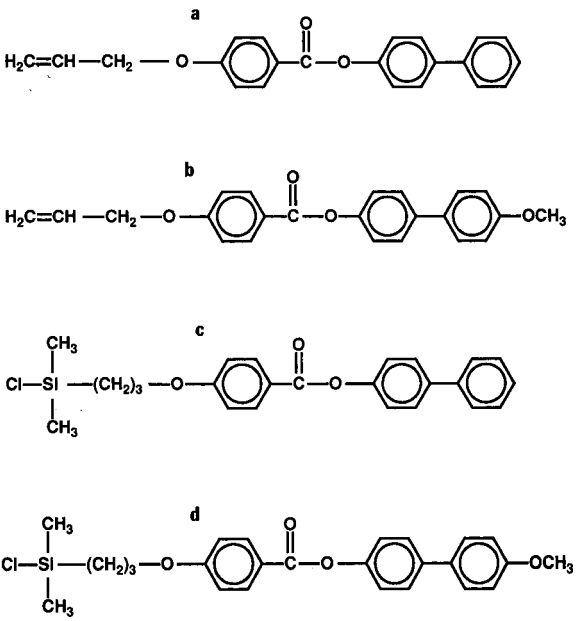

Fig. 1. Structures of (**a**) [4-(allyloxy)benzoyl]biphenyl, (**b**) 4-{[4-(allyloxy)benzoyl]oxy}-4′-methoxybiphenyl, (**c**) silane reagent of compound **a** and (**d**) silane reagent of compound **b**.

the same peaks as observed for **a** and an additional peak (singlet) at 3.80 ppm. This peak corresponds to the methoxy group and represents the only major structural difference between the two compounds.

The IR spectrum can be used to confirm the success of the hydrosilylation reaction to produce compound **c**. It displays increased intensity in the aliphatic C–H stretching region due to th two methyl groups and a disappearance of the bands at 3072 cm^{-1} from the C–H olefinic stretch and at 1647 cm^{-1} from the C=C double bond stretch. The proton NMR of **c** has no peaks in the vinyl region and a large singlet at 0.25 ppm which corresponds to the two methyl groups attached to silicon. Similar results are observed in both the IR and NMR spectra of compound **d**. Therefore, as in the previous study [6], spectral data confirm the success of the syntheses of both starting materials and the liquid crystal silane reagents.

Once the silane reagent has been synthesized, the bonding chemistry to the silica surface is identical with that used for the production of all commercially available monomeric stationary phases. Again, both IR and NMR can be used to verify the success of the bonding reaction. Fig. 2 (top) shows the DRIFT spectrum of the product from the reaction of compound **c** and silica (phase 1). Significant aromatic and

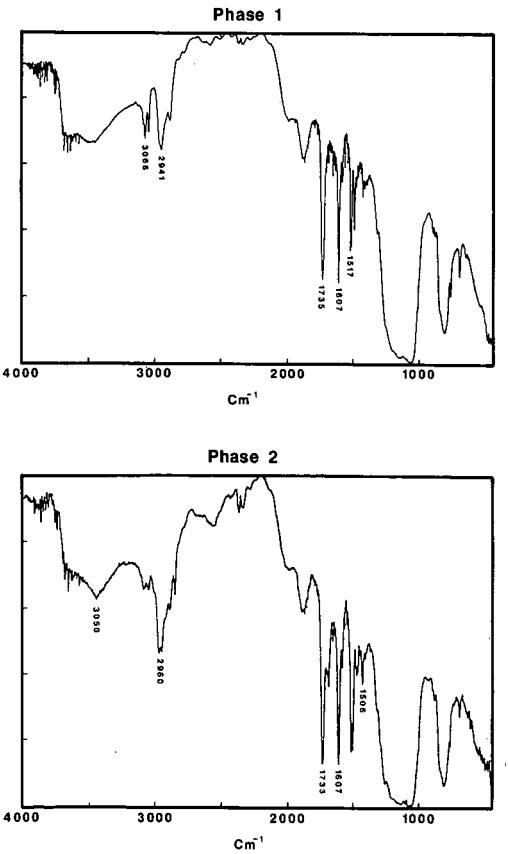

Fig. 2. DRIFT spectra of phase 1 and phase 2 on silica.

aliphatic C–H stretching is observed, in addition to three peaks (1735, 1607 and 1517 cm^{-1}) which correspond approximately to bands observed in both the liquid crystal starting material and liquid crystal silane reagent as described above. Fig. 2 (bottom) shows the DRIFT spectrum for the product from the reaction of compound **d** and silica (phase 2). As expected, its spectrum is similar to that of phase 1 with the same essential features as described above.

The carbon-13 CP-MAS spectrum of phase 1 is shown in Fig. 3 (top). The large peak at 0 ppm is due to the two methyl groups attached to the silicon of the silane reagent, the peaks between 10 and 30 ppm are the methylene groups, the peak near 70 ppm is the OCH_2–carbon, the peaks between 100 and 150 ppm are the aromatic carbons and the peak near 163 ppm is the carbonyl carbon. The spectrum of phase 2 shown in Fig. 3 (bottom) is essentially the same as phase 1 except for the peak at 57 ppm, which is the result of the methoxy carbon. An additional peak near the carbonyl may be due to incomplete suppression of the sidebands. However, it is clear from both the DRIFT and carbon-13 CP-MAS spectra that the bonding reactions were successful so that chromatographic characterizations could be done with the assumption that the stationary phase consisted of a bonded liquid crystal material.

The carbon content of phase 1 as determined by elemental analysis was 9.69%. This corresponds to a surface coverage [11] of 3.55 $\mu mol/m^2$. The values for phase 2 were 12.75% carbon with a coverage of 4.74 $\mu mol/m^2$. These results can be compared with the *ca.* 3.5 $\mu mol/m^2$ obtained in a previous study [6]. Both the phase used in the previous work (ABMP) and phase 1 in this study involve materials that only become liquid crystals when bonded to a polysiloxane backbone. Phase 2, however, is a true liquid crystal when in the form of compound **b**. This might account for the higher loading obtained, as a higher degree of ordering is already present when the bonding occurs. Even the 3.5 $\mu mol/m^2$ realized with the other two phases is high considering the size of the molecules. Phase 1 is approximately equivalent in chain length to a normal C_{18} alkyl but is considerably bulkier. The bonding density is better than the 3.3 $\mu mol/m^2$ achieved with monomeric C_{18} phases [11].

DSC measurements are the simplest means for detecting phase transitions in

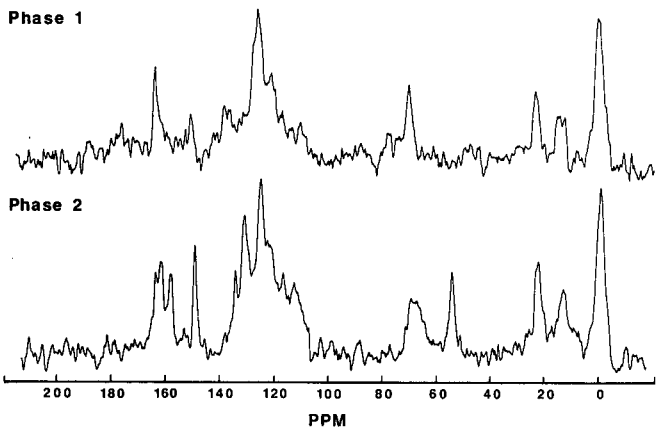

Fig. 3. Carbon-13 CP-MAS-NMR spectra of phase 1 and phase 2 on silica.

liquid crystals. However, the previous study [6] showed only a very broad, positive heat flow rather than a sharp transition that is expected with pure materials. Indeed, compound **b** gave such a sharp transition at 147°C, which agrees with the literature value [9], for the crystalline to nematic phase change. However, no sharp transitions were observed in the DSC data for either phase 1 or phase 2 on silica. A comparison of the DSC measurements for bare silica, phase 1 and phase 2 over the temperature range 300–425°C gave slopes of 0.088, 0.109 and 0.120 mW/°C, respectively. This increased positive heat flow is similar to that observed in the early study and indicates a broad transition temperature (probably nematic to isotropic) due to the variable contact between adjacent molecules that reflects the irregular nature of the porous silica surface.

Some preliminary chromatographic testing has been initiated on phase 1 in order to ascertain if its properties are similar to those observed for the ABMP phase in the previous study [6]. Fig. 4 is the Van 't Hoff plot for phenanthrene and anthracene in acetonitrile–water (50:50). A distinct transition is observed near 65°C for both solutes. This compares with the 55°C transition temperature observed for the ABMP phase. A higher transition temperature for phase 1 would be expected as it exhibits higher values than ABMP when bonded to polysiloxane [9].

Another perspective on the behavior of the bonded phase is seen in Fig. 5, which is a plot of the relative retention of anthracene and phenanthrene (k'_2/k'_1) *vs.* temperature. While the Van 't Hoff plots for these compounds show a single transition, this plot indicates that the bonded phase behavior may be more complex. Certainly the general trend to less discrimination between the two molecules as temperature increases is reasonable. The order in the phase becomes less so that the slot model proposed [12] becomes less likely to exist under these conditions. As the order in the

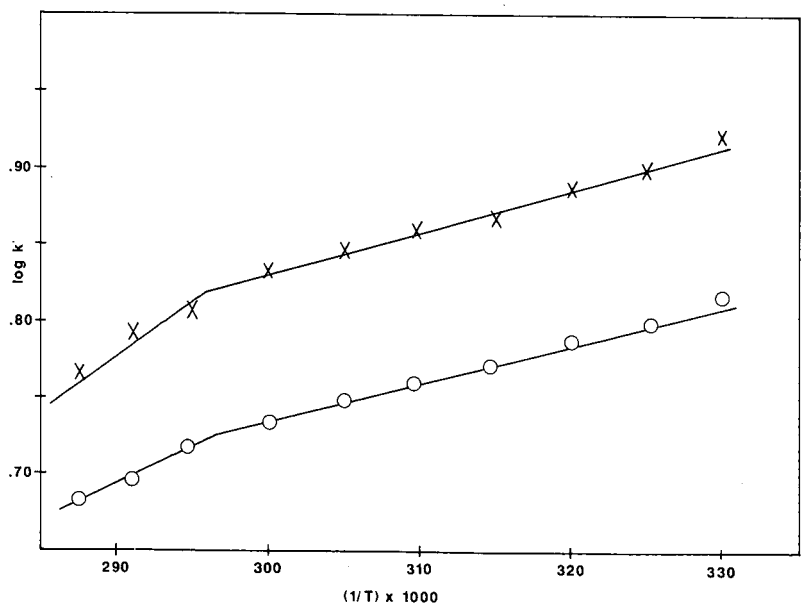

Fig. 4. Log k' *vs.* $1/T$ (K) for (○) phenanthrene and (×) anthracene on phase 1.

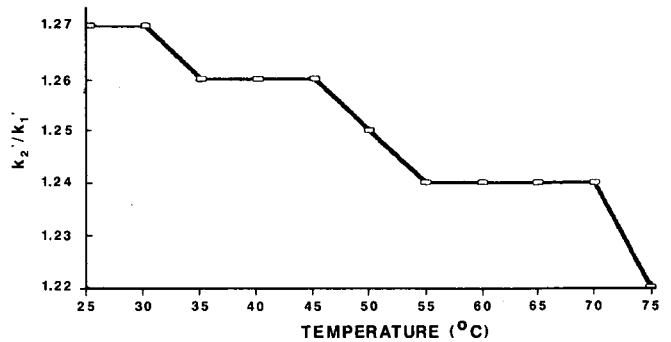

Fig. 5. Plot of k'_2 (anthracene)/k'_1 (phenanthrene) *vs.* temperature on phase 1.

phase decreases, the ability to discriminate on the basis of molecular shape (length-to-width ratio) also begins to decrease. The relative retention plot also indicates that the nature of the transition may not be uniform as three separate changes in the ratio take place over the temperature range studied. Because the surface is not homogeneous it is expected that there would be variable contact between the adjacent bonded moieties. This may account for the variations observed in relative retention as the order in the bonded liquid crystal is not being disrupted uniformly. As these changes are small, it appears that the relative retention is more sensitive to the subtle variations in bonded phase structure not seen in the normal Van 't Hoff plot.

Finally, it should be noted that the relative retention for anthracene and phenanthrene at 25°C (1.27) is very close to that measured for ABMP (1.29) at the same temperature but with a slightly different mobile phase composition (30:70). According to previous results [7], the relative retention might increase as the amount of water in the mobile phase increases owing to the tendency of all hydrophobic phases, especially alkyls, to aggregate under these conditions. This would ensure that a greater fraction of a liquid crystal phase would be a in slot-like configuration. In addition, no measurable changes were recorded in k' values during the course of the characterization experiments, indicating that the phase was stable and that changes in phase morphology induced by temperature and/or solvent composition were reversible.

CONCLUSIONS

It has been shown that the organochlorosilane pathway is a useful method for bonding liquid crystals to silica surfaces. Preliminary results indicate that these new materials possess the same type of behavior that was identified in an earlier study and that these characteristics are consistent with liquid crystal behavior. Further chromatographic measurements must be done on these and other materials to understand fully their behavior and potential as stationary phases for HPLC. Additional synthetic work and extensive chromatographic characterization are currently being undertaken in our laboratory as well as at a number of other collaborating institutions.

ACKNOWLEDGEMENTS

Partial support of this research was provided by the National Science Foundation (grant CHE-8814849). Carbon-13 CP-MAS spectra and BET measurements were provided by Dr. John Fetzer, Chevron Research and Technology (Richmond, CA, USA).

REFERENCES

1 H. Kelker, *Fresenius' Z. Anal. Chem.*, 198 (1963) 254.
2 H. Kelker, *Ber. Bunsenges. Phys. Chem.*, 80 (1963) 698.
3 Z. Witkiewicz, *J. Chromatogr.*, 251 (1982) 698.
4 S. Rokushika, K. P. Naikwadi, A. L. Jadhav and H. Hatano, *Chromatographia*, 22 (1988) 280.
5 D. R. Luffer and M. Novotny, *J. Phys. Chem.*, 94 (1990) 3161.
6 J. Pesek and T. Cash, *Chromatographia*, 27 (1989) 559.
7 J. J. Pesek and A. M. Siouffi, *Anal. Chem.*, 61 (1989) 1928.
8 J. J. Pesek, Y. Lu, A. M. Siouffi and F. Grandperrin, *Chromatographia*, 31 (1991) 147.
9 M. A. Apfel, H. Finkelman, G. M. Janini, R. J. Laub, B. H. Luhmann, A. Price, W. L. Roberts and T. J. Shaw, *Anal. Chem.*, 57 (1985) 651.
10 J. Kohler, *Chromatographia*, 21 (1986) 573.
11 W. Cheng and M. McCown, *J. Chromatogr.*, 318 (1985) 173.
12 S. A. Wise and L. C. Sander, *J. High Resolut. Chromatogr. Chromatogr. Commun.*, 8 (1985) 248.

Journal of Chromatography, 556 (1991) 383–394
Elsevier Science Publishers B.V., Amsterdam

CHROM. 23 238

Hydroquinone oxidation kinetics in adsorptive liquid chromatographic beds

CHAWN-YING JENG and STANLEY H. LANGER*
Department of Chemical Engineering, University of Wisconsin, Madison, WI 53706 (USA)

ABSTRACT

Catalytic properties of chromatographic silicas modified with ferric ions using a batch preparation process are compared with those modified *in situ* in a column on the basis of the hydroquinone oxidation to benzoquinone in a liquid chromatographic reactor. This is done through application of a statistical moment method for kinetic parameter estimation from reactor chromatograms. The first absolute moment of the overall elution profile is utilized to evaluate the pseudo-first order rate constants for oxidation both with and without consideration of hydroquinone sorption processes. In general, hydroquinone adsorption processes are found to have a significant role in the overall process and affect the intrinsic reaction rate measurements. On comparing the two modified silicas, it is found that the influence of adsorption in models is less pronounced with the batch-treated material. The decrease in reaction rate effects with the material prepared by a batch process can be attributed to increased quenching of strongly adsorptive sites on the silica surface as a result of prolonged exposure to metal ions in solution. Retention behavior is consistent with a decrease in the influence of hydrogen bonding hydroxyl groups on the batch-treated material.

INTRODUCTION

Complications from solutes reacting during liquid chromatographic separation due to the catalytic activities of adsorbent beds have been observed and summarized by Snyder [1]. While reactions catalyzed by acidic or basic packings can often be eliminated by special surface treatments [2], the presence of active trace metal ions in columns often causes more serious problems in the course of separation, due to complexation and irreversible adsorption [3–6]. We have previously demonstrated how hydroquinone oxidation could be used as a probe reaction for detecting catalytic activity which probably stems from transition metal ions associated with silica columns in high-performance liquid chromatography [7]. The active sites in the column were located through flow-rate and flow direction variations; the redox nature of the active sites were also characterized to some extent. Difficulties with similar reactions during liquid chromatographic separations have also been described for reversed-phase [8] and ion-exclusion [9] columns.

Recently, we have initiated studies of more homogeneous packings containing associated metal ions in columns used as liquid chromatographic reactors (LCRs) in

0021-9673/91/$03.50

order to increase our knowledge about the properties of these packings and potential analytical complications, and to investigate further possibilities for utilizing these types of reactors. Because of complications in interpreting reactant and product profiles during kinetic studies, a convenient statistical moment method for parameter estimation was introduced [10]. It is based on the overall elution curve of the reaction chromatogram from the liquid chromatographic reactor and eliminates difficulties which occur when attempting to resolve these curves. Rate constants for a hydroquinone oxidation performed on an *in situ* iron (Fe^{3+})-modified silica column were obtained utilizing this method. The influence of mass transfer processes occurring in the column on reaction rate processes was evaluated and hydroquinone adsorption processes were found to influence reaction rate constant determinations significantly. Two models were developed: model I treated a first-order chemical reaction as the only kinetically controlling process; model II incorporated consideration of finite adsorption and desorption rates for the reactant together with the first-order reaction. The latter showed a better fit to the kinetic data for on-column hydroquinone oxidation on *in situ* iron-modified silica. Other investigators have also addressed the importance of adsorption and desorption mechanisms in chromatographic performance [11–17].

Here, further studies of the hydroquinone oxidation reaction catalyzed by iron (Fe^{3+})-modified silica packing in organic solvents are described to illustrate the kinds of information which can be obtained about packings from using the liquid chromatographic column as a reactor for kinetic studies. Specifically, kinetic analyses based on the two models are applied to an iron-modified silica packing obtained through batch treatment so that comparison can be made with the *in situ* prepared packing as well as to further demonstrate the useful nature of the statistical moment approach for kinetic parameter estimation. Similarities and differences in performance between chromatographic reactors using packings from the batch silica treatment and the previously studied *in situ* treatment are discussed together with variations in retentions of several pertinent materials on the columns.

THEORY

Two models based on the first absolute statistical moment of the overall elution curve (reactant plus product) have been developed for the rate evaluation of a (pseudo-)first-order irreversible reaction in a linear liquid–solid chromatographic reactor [10]. Model I is applicable to an ideal chromatographic reactor situation [18,19] in which the rate of a single chemical reaction determines the overall reactor performance; model II also considers the chemical reaction but incorporates consideration of reactant adsorption and desorption rates which are commensurate with reaction rates. The effects of other kinetic processes on reaction rate evaluation including axial dispersion, external mass transfer resistance across the particle boundary, and intraparticle diffusion have been shown to be negligible [10,19].

Model I: LCR with equilibrium distribution between two phases for both reactant and product

When distribution equilibria between the mobile and stationary phases are established instantaneously and linear isotherms can be utilized for both reactant and

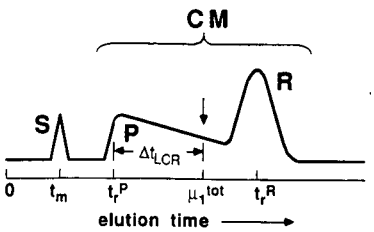

Fig. 1. Hypothetical reactor chromatogram showing parameters of this study: S = standard, R = reactant, P = product, CM = center of mass for the elution profile reactant and product. The first absolute moment for the overall elution curve (μ_1^{tot}) is located at the center of mass of the profile. See text for details.

product, the first absolute moment for the overall elution curve [10] containing both reactant and product, μ_1^{tot}, can be expressed as

$$\mu_1^{tot} = t_r^P + \Delta t_{LCR} \tag{1}$$

Its physical significance together with that of other relevant parameters is illustrated in Fig. 1. Here, t_r^P is the characteristic retention time of the product and Δt_{LCR} represents the shift of the first moment due to liquid chromatographic reaction. The shift can be shown to be equal to

$$\Delta t_{LCR} = \frac{K^R - K^P}{k_{app,I}}[1 - \exp(-k_{app,I} t_m)] \tag{2}$$

where the apparent reaction rate constant for model I is

$$k_{app,I} = k_m + K^R k_{s,I} \tag{3}$$

K^R and K^P are the indicated distribution equilibrium constants for the reactant (R) and product (P) respectively; t_m and k_m are the mobile phase residence time and reaction rate constant respectively; $k_{app,I}$ is the "apparent rate constant" which is the sum of the reaction rates in the mobile and stationary phases for model I while $k_{s,I}$ is the corresponding stationary phase rate constant.

The physical meaning of μ_1^{tot} has been discussed in an earlier development [10]: it is essentially the "average retention time" of the overall elution profile and is located at the center of mass of the P + R distribution as illustrated in Fig. 1. It is expressed in eqn. 1 as the sum of the product retention time and an LCR reaction-dependent term, Δt_{LCR}, which accounts for contributions from the remaining reactant peak and broadening of the chromatogram due to continuous product formation during elution. An analogy to the "unreacted fraction" used in chemical kinetics can be made for the normalized quantity $\Delta \bar{t}_{LCR}$, defined as

$$\Delta \bar{t}_{LCR} = \frac{\mu_1^{tot} - t_r^P}{t_r^R - t_r^P} \tag{4a}$$

$$= \frac{1 - \exp(-k_{app} t_m)}{k_{app} t_m} \tag{4b}$$

where t_r^R is the characteristic retention time of the reactant and $t_r^R - t_r^P$ of eqn. 4a represents the maximum possible shifting of μ_1^{tot} from its initial position t_r^R when the column is utilized as a separator only and no reaction occurs in the column; then, μ_1^{tot} is equal to t_r^R and $\Delta\bar{t}_{LCR}$ becomes unity. On the other hand, if the reaction is complete immediately upon reactant introduction to the column and the pulse is eluted as a single product peak, μ_1^{tot} is equal to t_r^P and $\Delta\bar{t}_{LCR}$ becomes zero. These correspond to a zero and infinite k_{app} value respectively, which also results in $\Delta\bar{t}_{LCR}$ values of 1 and 0 in eqn. 4b. In the liquid chromatographic reactor operation, this dimensionless group has a value between zero and unity and relates to the percentage or extent of reaction occurring inside the column. Thus, it relates to the fraction of unreacted species often used in chemical kinetics and reactor design, *i.e.* $(1 - X)$, where X is the fractional conversion [20].

Model II: LCR without equilibrium distribution between two phases for the reactant

When reactant adsorption and desorption rates are commensurate with chemical reaction rates and other mass transfer processes have negligible effects on reaction rate, the overall first absolute moment for model II can again be written in the form of eqn. 1 and parameters illustrated in Figure 1 are still applicable, but with the value of Δt_{LCR} now having a different dependence on kinetic parameters [10]:

$$\Delta t_{LCR} = \frac{\dfrac{K_{ad}^R}{(1 + k_{s,II}/k_d)} - K^P}{k_{app,II}}[1 - \exp(-k_{app,II}t_m)] \tag{5}$$

$$k_{app,II} = k_m + K_{ad}^R \frac{k_{s,II}}{1 + k_{s,II}/k_d} \tag{6}$$

Now, K_{ad}^R is the adsorption equilibrium constant for the reactant ($=k_a/k_d$, where k_a and k_d are the adsorption and desorption rate constants), and $k_{app,II}$ and $k_{s,II}$ are the apparent and stationary phase rate constants respectively of model II. Although adsorption and desorption rate constants cannot be determined directly from eqn. 5 due to coupling between these kinetic parameters in the expression, model II can be distinguished from model I on the basis of the different dependences of Δt_{LCR} on the stationary reaction rate constant in the two models.

Utilization of μ_1^{tot} in rate evaluation can readily overcome the problem resulting from overlap between reactant and product profiles [21]. The use of the total elution curve also eliminates a need for applying internal or external standard methods together with associated complications. In practice, μ_1^{tot} can be measured directly from the experimental elution curve of a reaction chromatogram as a function of the mobile phase residence time.

Consequently, Δt_{LCR} is calculated from eqn. 1 with its dependence on t_m shown in eqns. 2 and 5 for models I and II respectively. By varying flow rates in the LCR system, data at different t_m values are generated and kinetic parameters can then be estimated by a non-linear regression routine and compared for each model.

EXPERIMENTAL

Liquid chromatographic reactor system

The standard liquid chromatographic system employed here as a liquid chromatographic reactor, incorporated a Waters 590 solvent delivery pump (Milford, MA, USA), an LDC/Milton Roy SpectroMonitor D absorbance detector (Riviera Beach, FL, USA) set at the wavelength of 267.5 nm, and a special glass column (10 cm × 3 mm I.D., Omnifit, Atlantic Beach, NY, USA) to minimize potential contact with metal while permitting observation of color changes from silica surface modification by ferric ions. The assembly and other details have been described elsewhere [10]. Digitized chromatographic signals were acquired and stored using a Hewlett-Packard 3396A integrator equipped with a 9114A disc drive (Palo Alto, CA, USA). Data processing for conversion of the reactor chromatogram signals to the first absolute moment (see Fig. 1) was also performed in this system which possesses a BASIC language capability.

Batch procedure for preparing iron-modified silica

Packing material (Spherisorb S10W 10 μm silica gel from Phase Separations, Norwalk, CT, USA) was dried in an oven (150°C) overnight. It was then equilibrated with a buffered isopropanol solution [0.04 M potassium acetate + 1% (v/v) acetic acid] in an erlenmeyer flask on a stirrer for 5 h before washing with neat isopropanol several times. This activation step was needed for effective metal doping onto the silica surface [22]. Subsequently, the silica sample was treated with a 2.72 m*M* $FeCl_3$–isopropanol solution overnight during which time the coated silica slurry attained a light yellow color. This modified silica was then centrifuged and washed with isopropanol to remove free ferric material, and dried under nitrogen at 50°C. The final product was slurry-packed into the glass column with an in-house constructed slurry packing apparatus.

A similar procedure for *in situ* modification of the silica surface by pulse injections of ferric ions into a pre-packed silica column has been described earlier [10]. This procedure also provided a column of uniform color comparable to the one from slurry packing. The pulse injection technique with a glass column allows observation of color change as the yellow zone develops along the column. In this particular situation, it also eliminates unnecessary metal contacting in the pump. Ferric chloride can be a strong hydrometallurgical leaching agent under some conditions. For other types of surface modification, one might treat columns *in situ* by continuously pumping solutions containing modifiers. Results from an inductively coupled plasma (ICP) emission spectrometer analysis showed an iron loading of *ca.* 0.1% (w/w) on silica packing for both batch-treated and *in situ* samples.

Chromatographic reactor study and reagents

The kinetic study for hydroquinone oxidation in the batch-treated iron/silica column was conducted at temperatures between 20 and 40°C and flow-rates between 0.75 and 1.5 ml/min. Temperature control was obtained in the same way as in the *in situ*-treated column using a column jacket [10]. The mobile phase used for the batch-treated column was a 4% solution of *tert.*-butanol in hexane, while the solvent composition was 8% *tert.*-butanol/hexane mixture with the *in situ*-modified column.

Capacity factors of hydroquinone and benzoquinone were measured for the silica column before and after *in situ* treatment as well as for the batch-treated column. The column void volume was determined with a toluene standard and corrected for the extra-column volume. All solvents and chemicals used in this study were purchased from Baxter (McGaw Park, IL, USA) and Aldrich (Milwaukee, WI, USA).

RESULTS AND DISCUSSION

A representative series of liquid reactor chromatograms at various flow rates for the iron-catalyzed hydroquinone oxidation in the batch-treated silica column are illustrated in Fig. 2 for both 25 and 35°C. The first absolute moment of the overall elution profile μ_1^{tot} for a particular flow-rate can be obtained directly from a reactor chromatogram with the data processing system described earlier and the equation

$$\mu_1^{tot} = \frac{\sum_{t=t_1}^{t_2} [C^R(t) + C^P(t)]t\Delta t}{\sum_{t=t_1}^{t_2} [C^R(t) + C^P(t)]\Delta t} \tag{7}$$

where $C^R(t)$ and $C^P(t)$ are the reactant and product concentrations at elution time t; these quantities correspond to the detector response with the wavelength set at 267.5 nm where the absorptivities of hydroquinone reactant and benzoquinone product are equal. Here, the summations cover the time range of the total elution curve between t_1 and t_2, and are calculated at the data acquisition speed of 20 points/s ($\Delta t = 0.05$ s). Now, data for the normalized μ_1 shift, $\Delta \bar{t}_{LCR}$, can be calculated from eqn. 4a and plotted against flow-rate for various reaction temperatures as shown in Fig. 3 for the indicated reaction chromatogram series. The normalized value at the ordinate resembles the fraction of reactant remaining in the effluent stream ($1 - X$) as explained

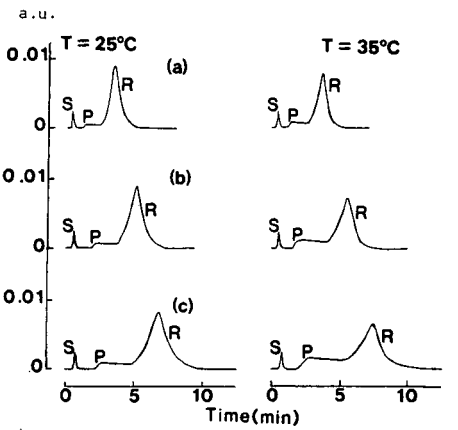

Fig. 2. Series of liquid reactor chromatograms for hydroquinone oxidation catalyzed by batch-treated iron/silica at 25 and 35°C. R = Hydroquinone reactant; P = benzoquinone product; S = toluene standard; mobile phase: 4% *tert.*-butanol in hexane; sample: 20 μl of 0.72 m*M* hydroquinone; wavelength: 267.5 nm. Flow-rates: (a) 1.5 ml/min; (b) 1.0 ml/min; (c) 0.75 ml/min.

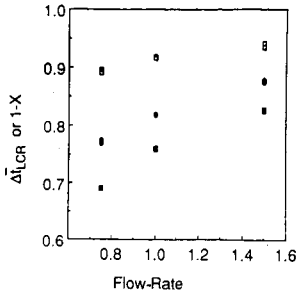

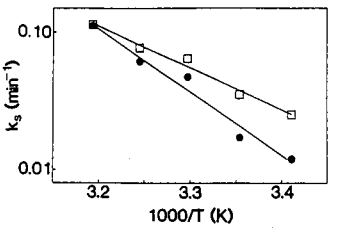

Fig. 3. Dependence of $\Delta\bar{t}_{LCR}$ on mobile phase flow-rates (in ml/min) at various column temperatures; operating conditions same as Fig. 2. □ = 25°C; ◆ = 35°C; ■ = 40°C.

Fig. 4. Arrhenius plots of stationary phase reaction rate constants *versus* temperatures for models I (□) and II (●) in the batch, iron-modified silica column.

earlier and can be used to study the effects of reaction time and temperature on extent of reaction occurring in a column. The reaction time for the hydroquinone oxidation in the column increases with decreasing flow-rate, and results in higher conversions as shown in the series of chromatograms of Fig. 2. This gives larger X values, and thus lower $\Delta\bar{t}_{LCR}$ values as illustrated in Fig. 3 for all temperatures. Also shown in Fig. 3 is the effect of increasing reaction temperature; the resulting higher reaction rate gives a lower $\Delta\bar{t}_{LCR}$ value for the same flow-rate. At the limit of an infinite flow-rate which corresponds to no chemical reaction in the column ($X = 0$), the ordinate values should approach unity for all temperatures.

Reaction kinetic parameter estimation

Hydroquinone oxidation kinetic data analysis for the batch-treated column can be performed in a manner resembling that of the *in situ* case. Neglecting any uncatalyzed mobile phase reactions, eqns. 2 and 5 become [10]

$$\Delta t_{LCR,I} = \frac{1 - (K^P/K^R)}{k_{s,I}}[1 - \exp(-K^R k_{s,I} t_m)] \tag{8}$$

and

$$\Delta t_{LCR,II} = \left(\frac{1}{k_{s,II}} - \frac{K^P}{k_{app,II}}\right)[1 - \exp(-k_{app,II} t_m)] \tag{9}$$

Now, $k_{s,I}$ for Model I and $k_{s,II}$ and $k_{app,II}$ for Model II can be fitted by a non-linear regression routine. The kinetic parameters in eqns. 8 and 9 were determined with a VAX 11/785 computer using the GREG (general regression) program, a FORTRAN package of the least-square algorithm to estimate the parameters of a user-defined model developed by Stewart [23]. The stationary phase rate constants for models I and II determined by GREG are plotted against reaction temperature in Fig. 4 for the batch-treated column. In Fig. 4, it can be seen that values of k_s for model I deviate from those from model II at low temperatures but give more comparable values at higher

TABLE I

COMPARISON OF KINETIC PARAMETERS FOR STATIONARY PHASE RATE CONSTANTS FOR BATCH AND *IN SITU* TREATMENTS

	Kinetic parameter[a]	Batch treatment	*In situ* treatment [10]
Model I	$\ln k_s(T_B)$ (min^{-1})	−3.096	−1.208
	E_s (kcal/mol)	13.22	4.10
Model II	$\ln k_s(T_B)$ (min^{-1})	−3.592	−2.343
	E_s (kcal/mol)	20.06	13.04

[a] Arrhenius relation: $\ln k_s = \ln k_s(T_B) - (E_s/R)(1/T - 1/T_B)$, where R is the gas constant and T_B is a base temperature (=303.15 K); $k_s(T_B)$ is the stationary phase reaction rate constant at 303.15 K and E_s is the activation energy for stationary phase reaction.

temperatures (*ca* 40°C). This reflects the importance of the effect of finite hydroquinone sorption rates at low temperatures. The result is consistent with the *in situ*-treated case since a greater contribution to the elution curve from unreacted hydroquinone reactant is expected at low temperatures where the conversion is low. Thus, a general hydroquinone adsorption effect on rate evaluation is present in the modified silica packings generated for both treatments.

Values of the fitted Arrhenius kinetic parameters in the range of experimental reaction temperatures for the stationary phase rate constants in the two models can also be compared for the batch and *in situ* treatments; these are listed in Table I. The deviations for both kinetic parameters, E_s and k_s, are significantly less for the batch-treated packing than for the *in situ*-treated packing as shown in Table I. This is an indication that the contribution of the hydroquinone adsorption mechanism on intrinsic kinetic evaluation is less important with the former. Table I also indicates a difference in the catalytic activity of the iron-modified silica produced from these two treatments. The *in situ* treated material is more catalytically active as reflected in the rate constant values. Possible explanations for variations between the two iron-modified silica packings are discussed below.

Model discrimination

"Goodness" of model fits to the experimental data from the *in situ*-treated

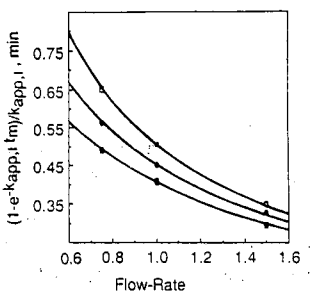

Fig. 5. Simulation curve comparison for Δt_{LCR} (corrected to account for the kinetic contribution alone, see eqn. 2) with experimental data in the batch-treated silica column for model I: □ = 25°C; ◆ = 35°C; ■ = 40°C. Flow-rate scale in ml/min.

column were examined earlier by calculating predicted responses from estimated parameters as a function of flow-rates at several temperatures [10]. For that packing, model II showed superiority over model I under operating conditions of high flow-rates and low temperatures where adsorption of hydroquinone is important. A similar analysis was conducted for the column packed with batch-treated material using model I as shown in Fig. 5. Analysis with model II did not improve the results significantly. Here then, kinetic evidence from parameter estimation for a significant adsorption effect is less obvious since both models can provide relatively good data fit under all operating conditions. The different behavior of the column packings resulting from the batch and *in situ* procedures can be related to variations in the silica surface properties during the treatments.

Longer and milder contacting treatment of the batch reaction apparently tends to generate a more homogeneously modified silica sample than the *in situ* treatment. The resulting product is likely to contain fewer strongly adsorptive sites on the silica surface, including isolated and vicinal silanol groups as noted by others [24–26]. It is quite likely that these associated hydroxyl groups are responsible for the strong adsorption of hydroquinone and thus, for the greater deviation between the two models in the *in situ* case. This is consistent with the results from comparing retention behavior of the samples (capacity factors) in the two columns, as shown in Table II. Less resolution of hydroquinone from benzoquinone was achieved on packings prepared by the batch procedure using a mobile phase of 8% of *tert.*-butanol in hexane. While retentions of benzoquinone were comparable on both packings, hydroquinone was retained significantly less on the batch-treated packing. This can be explained by a significant loss of hydrogen bonding surface silanol groups (especially vicinal groups) during the batch reaction; these and other associated groups might give longer hydroquinone retention [24]. With the loss of hydroquinone retention relative to benzoquinone, it became appropriate to use an eluting solvent with only 4% *tert.*-butanol to achieve resolution. Additional support for this view is the fact that the batch-treated column gives reaction chromatograms showing less tailing for the hydroquinone reactant peak than the *in situ*-treated column (even with the weaker mobile phase).

A likelihood ratio test [27,28] can be utilized to discriminate between the two "nested" models in order to determine which provides a better fit for the hydroquinone oxidation kinetic data on a statistical basis. The likelihood ratio test is based on the principle of variance ratio, usually known as the F ratio, for analysis between a full and

TABLE II

CAPACITY FACTORS FOR THE HYDROQUINONE OXIDATION SYSTEM (8% *tert.*-BUTANOL IN HEXANE AT 25°C)

Column	Benzoquinone	Hydroquinone
Silica before treatment	1.55	5.55
In situ iron treatment	1.27	3.01
Batch iron treatment	1.31	2.26
	(1.75)[a]	(8.43)[a]

[a] Values for the mobile phase of 4% *tert.*-butanol in hexane.

TABLE III

EXTRA SUM OF SQUARE ANALYSIS[a] FOR MODEL DISCRIMINATION

Packing treatment	Source	Residual sum of squares (RSS)	Degrees of freedom (n_f)	Mean square (RSS/n_f)	Mean square ratio
In situ	Model I (1 parameter)	0.04690	11		
	Model II (2 parameters)	0.00182	10	0.00018	
	Extra parameter	0.04508	1	0.04508	250
Batch	Model I (1 parameter)	0.01981	11		
	Model II (2 parameters)	0.00444	10	0.00044	
	Extra parameter	0.01537	1	0.01537	35.0

[a] Kinetic data at 35°C for *in situ* (CYJ4-34) and batch (CYJ4-44) treatments.

a partial model. Results of a representative calculation for examination of the effect of addition of the extra parameter in model II are illustrated in Table III for the two iron treatments. In Table III, the mean square can be determined by dividing the degrees of freedom into the residual sum of squares for the full model as well as for the extra kinetic parameter added into the partial model. Then, the calculated mean square ratio value between the extra parameter and the full model is compared with the F ratio from statistical distribution tables at proper degrees of freedom (n_f = 1 for the extra parameter and 10 for the full model) and a chosen probability α that the test is significant (*e.g.* F = 10.0 and 1.5 for α = 99% and 75%, respectively). If the calculated ratio is greater than the table value, the extra parameter should be retained and the full model is statistically better than the partial model; otherwise, one should accept the partial model. Results from Table III indicate that the extra parameter is important in both treatments, but particularly for the *in situ* packing. The mean square ratios from some data sets are plotted against temperature in Fig. 6. It is found that the test ratios are larger than standard F values with α = 99% in most cases and even more so when α = 75% is chosen. This implies that the extra parameter in model II to describe the reactant adsorption and desorption process is statistically important and model II is a better representation of the LCR system than model I in general, although the batch-treated packing shows less of this effect especially in comparing conversions with flow (Fig. 5). A trend of decreasing mean square ratio values as temperature increases can also be detected in Fig. 6. Large F values at low temperatures guarantee

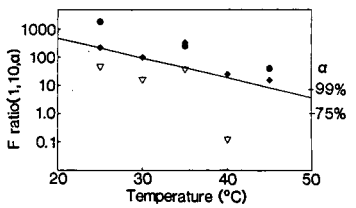

Fig. 6. Results of the likelihood ratio test between model I and model II at various reaction temperatures. Filled symbols (● = CYJ4-34; ◆ = CYJ4-47) = *in situ* treatment, open symbols (▽ = CYJ4-44) = batch treatment.

the superiority of model II over model I there since only a small fraction of reactant was converted to product and the hydroquinone adsorption process is a controlling process. At higher temperatures, a larger portion of hydroquinone was converted to benzoquinone and the importance of the reactant adsorption rate relative to the chemical reaction is diminished. The result is smaller F values so that the advantage of using model II over model I at higher temperatures becomes less significant especially with the batch treatment.

CONCLUSIONS

A statistical moment approach based on an overall elution curve has been applied successfully for the on-column hydroquinone oxidation catalyzed by iron-modified silica. Results from batch and *in situ* procedures for modifying the silica surface with ferric ions are compared. A reactor model which incorporates consideration of finite reactant adsorption and desorption processes generally shows a better fit to the experimental data than a simple model where only chemical reaction is considered. The former is particularly advantageous at low temperatures where the reactant species is predominant in the chromatogram. The *in situ*-treated sample shows larger discrepancies between the two models and indicates a more significant effect of hydroquinone adsorption on reaction rate evaluation than the batch-treated one. Differences in the performance as a result of the two treatments can be attributed to variations in the loss of hydrogen bonding silanol groups of the treated samples. Further investigations of modified silicas of the type described here are continuing in our laboratory.

ACKNOWLEDGEMENT

We appreciate support from the US Army Research Office and the University of Wisconsin. We also thank Professor Warren Stewart for making the GREG program available.

REFERENCES

1 L. R. Snyder, *Principles of Adsorption Chromatography*, Marcel Dekker, New York, 1968, p. 357.
2 S. H. Langer, J. Y. Yurchak and C. M. Shaughnessy, *Anal. Chem.*, 40 (1968) 1747.
3 Y.-T. Shih and P. W. Carr, *Talanta*, 28 (1981) 411.
4 S. R. Hutchins, P. R. Haddad and S. Dilli, *J. Chromatogr.*, 252 (1982) 18.
5 S. M. Cramer, B. Nathanael and Cs. Horváth, *J. Chromatogr.*, 295 (1984) 405.
6 P. C. Sadek, P. W. Carr, L. D. Bowers and L. C. Haddad, *Anal. Biochem.*, 144 (1985) 128.
7 C. Y. Jeng and S. H. Langer, *J. Chromatogr. Sci.*, 27 (1989) 549.
8 J.-X. Huang, J. D. Stuart, W. R. Melander and Cs. Horváth, *J. Chromatogr.*, 316 (1984) 151.
9 M. A. Gattrell and D. W. Kirk, *J. Chromatogr.*, 409 (1987) 404.
10 C. Y. Jeng and S. H. Langer, *Ind. Eng. Chem. Res.*, 30 (1991) 1489.
11 M. Suzuki and J. M. Smith, *Chem. Eng. Sci.*, 26 (1971) 221.
12 C. Vidal-Madjar and G. Guiochon, *J. Chromatogr.*, 142 (1977) 61.
13 Cs. Horváth and J. H. Lin, *J. Chromatogr.*, 149 (1978) 43.
14 A. J. Muller and P. W. Carr, *J. Chromatogr.*, 357 (1986) 11.
15 D. S. Hage, R. R. Walters and H. W. Hethcote, *Anal. Chem.*, 58 (1986) 274.
16 D. B. Marshall, J. W. Burns and D. E. Connolly, *J. Chromatogr.*, 360 (1986) 13.
17 Y. S. Lin and Y. H. Ma, *Ind. Eng. Chem. Res.*, 28 (1989) 622.

18 S. H. Langer, J. Y. Yurchak and J. E. Patton, *Ind. Eng. Chem.*, 61 (1969) 10.
19 A. H. T. Chu and S. H. Langer, *Anal. Chem.*, 58 (1986) 1617.
20 O. Levenspiel, *Chemical Reaction Engineering*, Wiley, New York, 1972, p. 46.
21 S. H. Langer and J. E. Patton, *J. Phys. Chem.*, 76 (1972) 2159.
22 G. A. Eiceman and F. A. Janecka, *J. Chromatogr. Sci.*, 21 (1983) 555.
23 W. E. Stewart, *GREG Manual*, Chemical Engineering Department, University of Wisconsin, Madison, WI, 1986.
24 M. Mauss and H. Engelhardt, *J. Chromatogr.*, 371 (1986) 235.
25 J. Köhler, D. B. Chase, R. D. Farlee, A. J. Vega and J. J. Kirkland, *J. Chromatogr.*, 352 (1986) 275.
26 D. B. Marshall, C. L. Cole and D. E. Connolly, *J. Chromatogr.*, 361 (1986) 71.
27 N. R. Draper and H. Smith, *Applied Regression Analysis*, 2nd ed., Wiley, New York, 1981.
28 D. M. Bates and D. G. Watts, *Nonlinear Regression Analysis and Its Applications*, Wiley, New York, 1988, p. 103.

Journal of Chromatography, 556 (1991) 395–406
Elsevier Science Publishers B.V., Amsterdam

CHROM. 23 158

Impact of acidic/hydrothermal treatment on pore structural and chromatographic properties of porous silicas

I. The conventional approach

K. K. UNGER* and K. D. LORK
Institut für Anorganische Chemie und Analytische Chemie, Johannes Gutenberg-Universität, W-6500 Mainz (Germany)
and
B. PFLEIDERER, K. ALBERT and E. BAYER
Institut für Organische Chemie, Universität Tübingen, W-7400 Tübingen (Germany)

ABSTRACT

A series of commercial silicas and a laboratory made product were subjected to acidic/hydrothermal treatment with solutions of HCl, HNO_3, H_2SO_4 and HF. The concentration of acid and the temperature and duration of treatment were varied. The specific surface area, content of metal impurities, types and concentration of surface hydroxyl and siloxane groups and crystallinity were determined for native and treated silicas. Only changes in the structural order of the surface could be assessed by means of ^{29}Si cross-polarization magic angle spinning NMR spectrometry and electron diffraction. The native and acid-treated silicas were surface modified to *n*-octyl derivatives and tested under reversed-phase conditions. A notable improvement in the column plate number and the asymmetry of the peaks was observed, whereas the solute capacity factors remained nearly unchanged. The effect of the conditions of acidic treatment (concentration, temperature and duration) was established by factorial experiments. Acidic/hydrothermal treatment caused a more ordered surface structure with quasi-crystalline domains, which improved the chromatographic mass-transfer kinetics and hence the column performance of acid-treated silicas.

INTRODUCTION

Surface treatment of silica adsorbents before use has been a common procedure in classical column liquid chromatography. Simply, the aim was to remove inorganic impurities, mainly metal compounds, to clean and to activate the silica. As silicas in those days were mainly of technical grade and not specifically manufactured for application in column liquid chromatography, such a procedure was certainly required. In a typical procedure the silica was refluxed in a suspension with 2 *M* hydrochloric acid for a given period and then washed to neutrality [1].

Hydrothermal treatment of silicas with water and water vapour at elevated temperatures between 373 and 573 K and atmospheric or higher pressures served as a

0021-9673/91/$03.50

suitable means to obtain materials of large pore size from small-pore silicas [2–7]. Depending on the temperature and duration of treatment, the pore diameter of the silica was enlarged at a constant specific pore volume. Correspondingly, the specific surface area decreased. In this way, silicas with average pore diameters larger than 50 nm and a fully hydroxylated surface were prepared. With the advances in high-performance liquid chromatography (HPLC) in pharmaceutical and bioanalysis, stronger requirements were put on silica-based reversed-phase packings, particularly those applied for the analysis of basic compounds. Basic analytes were often strongly retained with tailed peaks in reversed-phase chromatography owing to the residual adsorptivity of the silica base material. To overcome this obstacle, amines such as trimethylamine were added to the mobile phase as modifiers, which were then adsorbed on the surface, blocking the remaining active acidic centres [8,9]. However, the addition of mobile phase modifiers did not prove a satisfactory approach.

In recent years, attempts have been made to subject the silicas to specific procedures prior to the bonding reactions to create a deactivated and stable surface with regard to the chromatography of basic compounds. These procedures included treatment with complexing agents, dehydroxylation and rehydroxylation with acids such as hydrofluoric acid [10], treatment with acids combined with gentle hydrothermal treatment [11] and partial dissolution of the silica by treatment with ammonium hydrogen fluoride $(NH_4)HF_2$ [12]. As a result, a family of base-deactivated reversed-phase silicas were introduced by column manufacturers [13].

Despite the large number of studies in this area, the real effect of surface treatment on the structural properties of silicas remained poorly understood, although a substantial improvement in terms of column performance and column stability was achieved. It was generally assumed that the surface treatment led to a high extent of homogenization of the originally heterogeneous surface. Köhler and Kirkland [10] ascribed the effect to the formation of associated, less adsorptive hydroxyl groups which were monitored by diffuse reflectance Fourier transform infrared spectroscopy. Eisenbeiss [14] suggested a reorganization of the surface in energetic and geometric terms without providing convincing evidence.

The aim of this work was to examine the structural properties of a series of silicas for HPLC before and after treatment with acids such as HCl, HNO_3, H_2SO_4 and HF under mild hydrothermal conditions. After conversion of the acid-treated silicas into their reversed-phase derivatives, the chromatographic properties were assessed in terms of solute retention, column plate number and peak shape.

EXPERIMENTAL

Chemicals

Commercial silicas were LiChrosorb Si 100-7 and LiChrospher Si 100-10 from E. Merck (Darmstadt, Germany), G 250-10 from Grace (Worms, Germany) and Nucleosil 100-7 from Macherey, Nagel & Co. (Düren, Germany). Silica BE-0 was laboratory-made preparation synthesized from tetraethoxysilane according to a procedure described elsewhere [15]. The properties of the silicas are listed in Table I. The same batch of each silica was employed for surface modifications.

All chemicals and reagents were of analytical-reagent grade and a gift from E. Merck. HPLC-grade solvents for chromatographic measurements were also obtained

TABLE I

CHARACTERISTIC DATA FOR NATIVE SILICAS

d_p = Average particle diameter; a_s = specific surface area; v_p = specific pore volume; p_d = average pore diameter.

Silica	d_p (μm)	a_s (m^2/g)	v_p (ml/g)	p_d (nm)
LiChrosorb Si 100-7	7	355	1.1	10
LiChrospher Si 100-10	10	388	–	10
G 250-10	10	250	–	25
Nucleosil 100-7	7	377	–	10
BE-0	10	246	0.97	12

from E. Merck. The synthesis and purification of silanes employed for the modification of silicas were described previously [16].

Treatment of silicas

Hydrochloric, sulphuric, nitric and hydrofluoric acid were used. Three parameters were varied at two levels at acid treatment: the concentration of acid [0.1 and 10 *M*, except for HF (0.01 and 0.1 *M*)], the temperature of treatment (273 and 363 K) and the duration of treatment (0.1 and 24 h). The experiments were carried out on the basis of factorial design. The statistical evaluation on the significance of parameters was performed according to the method of Yates [17]; see also Retzlaff *et al.* [18].

Silica (6 g) suspended in 50 ml of the acid was stirred in a closed 100-ml two-necked flask using a specially designed PTFE stirrer [11] at two temperatures, namely 273 K using an ice-bath and 363 K using a thermostat. The treatment of silicas with HF was performed in a 250-ml polypropylene erlenmeyer flask. After treatment for 0.1 and 24 h, the silicas were washed to neutrality with deionized water. The silicas were then dried at 423 K and 20 Pa for 24 h. A blank experiment with pure water at 363 K for 0.1 and 24 h was carried out under the same conditions.

Characterization of native silicas and reversed-phase derivatives

Specific surface area, a_s. After activation at 423 K and 20 Pa for 24 h, the specific surface area was determined by nitrogen sorption using an Accusorb 2100 E instrument (Micromeritics, Norcross, GA, USA) and by the BET method [19].

Specific pore volume, v_p. The specific pore volume was determined by titration with water according to the method of Fisher and Mottlau [20].

Pore-size distribution and average pore diameter (p_d). The pore-size distribution was measured by mercury intrusion using a laboratory-made porosimeter with a maximum pressure of 400 MPa, and was calculated from the corrected intrusion curve by means of the Washburn equation using a contact angle of mercury of 140°C and a surface tension of mercury of 0.48 mN/m [21]. The average pore diameter was the mean pore diameter at 50% of the cumulative pore volume distribution curve.

Concentration of surface hydroxyl groups. The concentration of surface hydroxyl groups was determined by means of isotopic exchange with deuterated trifluoroacetic acid followed by ^{1}H NMR spectroscopy according to a method of Holik and Matejkova [22]. The procedure is described in detail in ref. 11. The precision of the determination was ±2.5%.

pH of the silica suspension. The apparent pH was measured in a 1% (w/w) suspension of silica in 0.1 *M* sodium chloride solution using an E50 glass electrode (WTW, Weilheim, Germany) and a Type PH 530 pH meter (WTW).

Content of inorganic impurites. The metal content was determined by X-ray fluorescence spectrometry (XRF) using a instrument PW 100 (Philips, Kassel, Germany) and by atomic absorption spectrometry (AAS) using an ARL 310,000 Quantometer (Philips).

Pellets for XRF were made by employing a mixture of silica and a polyalcohol (Mowviol N 50-98; Hoechst, Frankfurt/M, Germany) in the ratio 30:70 (w/w). For the AAS measurements, about 500 mg of silica were suspended in 5 ml of 40% HF (w/w) (Suprapur; E. Merck) in a platinum crucible. On heating the silica was evaporated as SiF_4. The residue was dissolved in 5 ml of 16% (w/w) HCl (Suprapur; E. Merck).

^{29}Si cross-polarization magic angle spinning nuclear magnetic resonance (CP-MAS NMR) spectrometry. The measurements were conducted at the Institut für Organische Chemie, Universität Tübingen, using a Bruker (Karlsruhe, Germany) MSL 200 Fourier transform NMR spectrometer with samples of 200–300 mg in double-bearing rotors of Al_2O_3. For further details, see ref. 23.

Electron diffraction measurements. The silica was milled to a fine powder in a ball-mill for 2 h prior to measurement in an Model EN 240 80-kV instrument (Philips) employing thallium chloride as reference material.

Fourier transform infrared (FT-IR) spectrometry. The measurements were conducted at the Haber-Bosch Institut of the Max-Planck Gesellschaft (Berlin, Germany) by Dr. H. Karge. Self-supporting disks of silica were prepared with a thickness between 5 and 13 mg/cm^2. A Model 325 spectrometer (Perkin-Elmer, Überlingen, Germany) fitted with a vacuum cell which could be heated to 700 K was used. IR spectra were run on native silicas after heat treatment at 375, 475, 575 and 673 K. Spectra were also recorded after adsorption of pyridine at 298 K and after desorption of pyridine at 473 K.

Chromatographic measurements. The native silicas were reacted after activation at 423 K and 20 Pa for 24 h with N,N′-dimethylaminodimethyl-*n*-octylsilane according to a procedure described elsewhere [16]. The products were slurry packed in 125 mm × 4.6 mm I.D. stainless-steel columns (Hyperchrom; Bischoff Analysentechnik, Leonberg, Germany). The HPLC system consisted of a pump (Model 2150; LKB, Bromma, Sweden), a Rheodyne Type 2105 injection valve (Latek, Heidelberg, Germany), an oven to thermostat the column (Model 2155; LKB), a variable-wavelength UV detector (Model 2151; LKB) and an integrator (Model CR-3A; Shimadzu Europe, Duisburg, Germany).

The test solutes were mixtures of N-methylaniline and N,N′-diethylaniline (sample mixture I) and of methyl, propyl, *n*-butyl and *n*-pentyl benzoate (sample mixture II). The sample concentration was 0.1 mg/ml, the injection volume 20 μl, the flow-rate 1.0 ml/min, the wavelength of detection 254 nm and the column temperature 301 K. The mobile pase was methanol–water (70:30, v/v). Sodium azide was used as a t_0 marker. Three columns were packed and tested for each silica. Injection of test mixtures was repeated twice.

The chromatographic solute capacity factor (k'), plate number (N) and the peak asymmetry factor (A) were calculated according to the following equations:

$$k' = (t_R - t_o)/t_o$$

where t_R is the retention time of the solute,

$$N = 5.54\,(t_r/w_{1/2})^2$$

where $w_{1/2}$ is the peak width at half-height of the peak and

$$A = b_{0.1}/a_{0.1}$$

where $a_{0.1}$ is the distance from the peak front to the maximum at 10% of the peak height and $b_{0.1}$ the distance from the maximum of the peak to its tail at 10% of the peak height.

RESULTS AND DISCUSSION

Effect of acidic/hydrothermal treatment on the structural properties of silicas

As series of silicas (LiChrosorb Si 100-7, LiChrospher Si 100-10, G 250-10 and a laboratory-made silica Be-0) were treated with solutions of hydrochloric, sulphuric, nitric and hydrofluoric acid under different conditions (see Experimental). The experiments were conducted on the basis of factorial design. The data obtained were subjected to statistical tests to evaluate the statistical significance of the treatment conditions on the structural properties. The structural parameters determined for the native and treated silicas were the specific surface area, a_s, the metal content, the apparent pH of the silica suspension, the total concentration of the surface hydroxyl groups, the types of surface hydroxyl groups and the crystallinity.

Specific surface area, a_s, assessed by means of nitrogen sorption and the BET method. The effect of acid treatment (363 K, 24 h) on a_s was investigated for LiChrosorb Si 100-7 and BE-0 silicas. For LiChrosorb Si 100-7, the a_s values were as follows: native silica, 355 ± 8 m^2/g; 0.1 *M* HF treated, 337 ± 5 m^2/g; 0.1 *M* HCl treated, 358 ± 10 m^2/g; 10 *M* HCl treated, 360 ± 9 m^2/g; and 10 *M* H_2SO_4 treated, 363 ± 4 m^2/g. For BE-0, the a_s values were as follows: native silica, 246 ± 6 m^2/g; 0.1 *M* HF treated, 222 ± 8 m^2/g; and 10 *M* H_2SO_4 treated, 252 ± 11 m^2/g.

Within the limits of the precision of the method the specific surface area of the treated silicas remained unchanged compared with that of the native product, except for the HF-treated silica, for which a 10% decrease in a_s was observed, caused by the slight dissolution of silica from small pore regions by reaction with HF, forming SiF_4.

Metal content determined by AAS. LiChrosorb Si 100-7 contained the impurities Al 640, Fe 60, Ti 175, Ca 170 and Na 660 ppm. Treatment with 0.1 and 10 *M* HCl, 10 *M* H_2SO_4 and 0.1 *M* HF at 363 K for 24 h reduced the content of metal impurities by about half (for details, see ref. 11). The acidic/hydrothermal treatment of LiChrospher Si 100-10 and BE-0 had only a minor effect on the metal content. The latter was a highly pure silica containing *ca.* 10 ppm of Fe.

Content of surface hydroxyl groups, α_{OH}, by the method of Holik and Matejkova [22]. The treatment conditions were 363 K for 24 h. The precision of the method was ±3% [11]. For LiChrosorb Si 100-7, the α_{OH} values were as follows: native silica, 8.55 $\mu mol/m^2$; 0.1 *M* HF treated, 9.03 $\mu mol/m^2$; 10 *M* H_2SO_4 treated, 9.18 $\mu mol/m^2$; and

10 *M* HCl treated, 8.60 μmol/m^2. For LiChrospher Si 100-10, the α_{OH} values were as follows: native silica, 8.38 μmol/m^2; and 10 *M* HCl treated, 8.45 μmol/m^2. For BE-0, the α_{OH} values were as follows: native silica, 8.12 μmol/m^2; 0.1 *M* HF treated, 8.69 μmol/m^2; and 10 *M* H_2SO_4 treated, 9.37 μmol/m^2.

The results indicate that the total concentration of surface hydroxyl groups increased by up to 10% compared with the native silica. The most drastic effect was observed for silicas treated with H_2SO_4.

Apparent pH of the silica suspension. The treatment conditions were 363 K for 24 h. For LiChrosorb Si 100-7, the native silica had pH 7.7, 0.1 *M* HF treated pH 7.3, 10 *M* HCl treated pH 7.2 and 10 *M* H_2SO_4 treated pH 3.0. For LiChrospher Si 100-10, the native silica had pH 5.8 and 10 *M* HCl treated 5.7.

Except for the silica treated with H_2SO_4, the pH remained the same after the acidic/hydrothermal treatment.

Identification of the types of hydroxyl groups and their determination by ^{29}Si CP-MAS NMR spectroscopy. ^{29}Si CP-MAS NMR spectroscopy allows the detection of geminal hydroxyl groups, Q_2, isolated hydroxyl groups, Q_3, and siloxane groups, Q_4, from their chemical shifts of -91, -100 and -109 ppm, respectively [24–26]. The absolute amounts of silanol and siloxane groups cannot be determined owing to their different relaxation behaviours [23]. However, it is possible to compare the peak intensities under the same measuring conditions. Fig. 1 shows the spectrum of (a) the native and (b) acid-treated (0.1 *M* HCl, 363 K, 24 h) LiChrosorb Si 100-7. Compari-

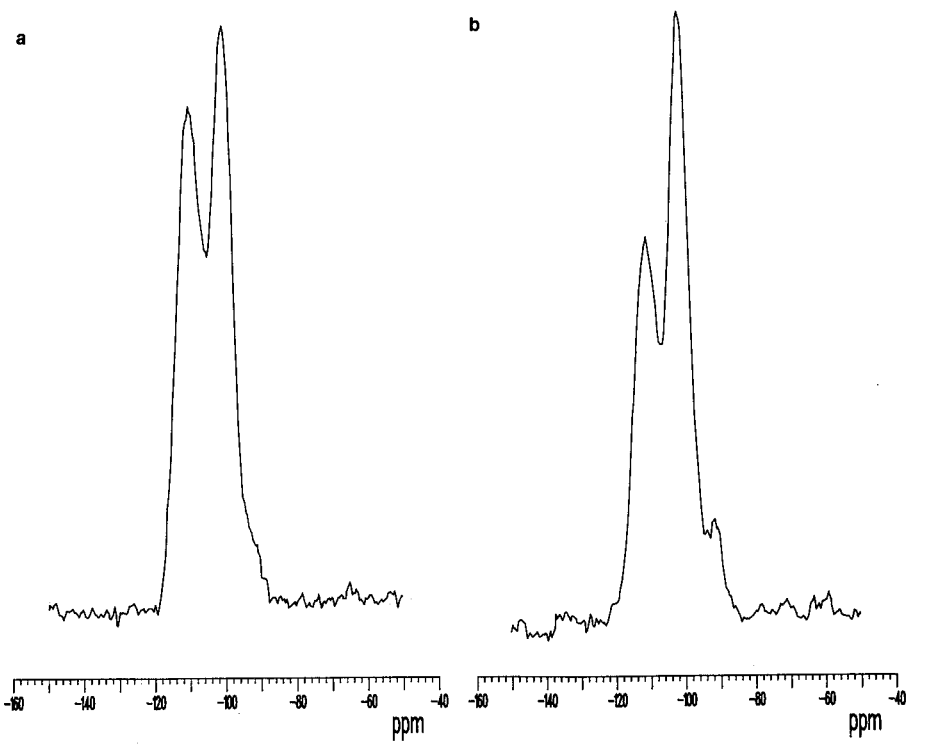

Fig. 1. ^{29}Si CP-MAS NMR spectra of (a) native and (b) acid-treated LiChrosorb Si 100-7. Conditions of treatment: 0.1 *M* HCl, 363 K, 24 h.

son of the two spectra indicates that the content of geminal and isolated hydroxyl groups increased at the expense of siloxane groups as a result of acid treatment. By peak deconvolution the relative amounts of Q_2, Q_3 and Q_4 were calculated based on peak-area measurements. The results were as follows: for the native silica, Q_2 1.0 ± 0.05%, Q_3 43.9 ± 2.2% and Q_4 54.9 ± 2.7%; and for the acid-treated silica, Q_2 4.6 ± 0.2%, Q_3 50.2 ± 2.5% and 45.1 ± 2.2%. Similar results were found for native and acid-treated (10 *M* H_2SO_4, 10 *M* HNO_3, 0.1 *M* HF; 363 K, 24 h) BE-0.

It should be emphasized, however, that after silanization of the acid-treated silicas with N,N′-dimethylaminodimethyl-n-octylsilane, geminal hydroxyl groups completely disappeared in the ^{29}Si CP-MAS NMR spectrum of the silanized silicas.

By measuring the amplitude of the Q_4 signal as a function of the contact time in milliseconds, a notable shift of the curves of the native BE-0 and the acid-treated derivative (10 *M* H_2SO_4, 363 K, 24 h) was observed (see Fig. 2). While one broad maximum was obtained at about 15 ms for the native silica, two maxima appeared at 8 and 33 ms for the treated product. The occurrence of the two maxima indicates two types of siloxane groups with different relaxation behaviours [23]. Siloxane groups with the "maximum" in the CP curve at 8 ms show shorter relaxation times than those with the "maximum" at 33 ms. Shorter relaxation times can be ascribed to a more ordered structure with a lower mobility of siloxane groups. There exist at least two different types of domains at the surface of acid-treated silica: regions with polycrystalline structure interfere with regions with amorphous structure.

Assessment of the crystallinity of silicas by electron diffraction measurements. Electron diffraction measurements on the native LiChrosorb Si 100-7 yielded no detectable reflection pattern whereas on the acid-treated product (10 *M* HCl, 363 K,

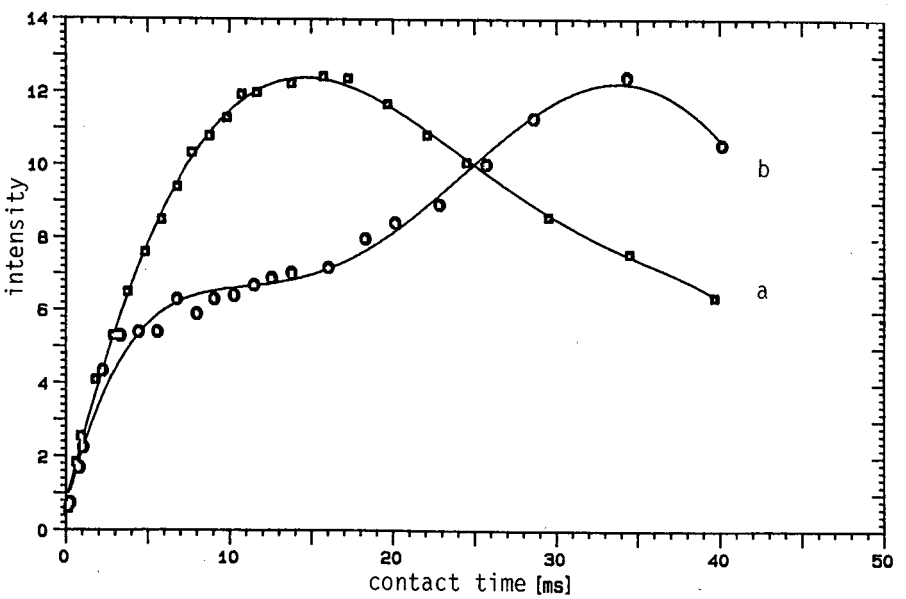

Fig. 2. Amplitude of Q_4 signal as a function of the contact time for (a) native and (b) acid-treated BE-0 silica. Conditions of treatment: 10 *M* H_2SO_4, 363 K, 24 h.

24 h) a distinct pattern was observed which was identified as a hexagonal structure. Of the possible crystalline polymorphs with a hexagonal structure, β-tridymite seems to be favoured over α-quartz, but a final decision cannot yet be made.

FT-IR spectrometry. FT-IR spectra of native and acid-treated silicas were measured at different activation temperatures. Spectra were also measured after adsorption and desorption of pyridine on the silicas. No differences in the spectra between the native and acid-treated silicas could be observed. Table II summarizes the results of the structural characterization of the native and acid-treated silicas.

Except for the HF-treated silicas, no changes in the specific surface area between the native and treated products were found. Generally, it is questionable whether subtle changes in the microstructure of the surface can be detected by using nitrogen, which has a kinetic diameter of about 0.36 nm [27], as an adsorptive molecule. Smaller adsorptive molecules as sensitive standards for probing geometric changes of the surface structure, such as helium or argon, should preferably be employed.

The decrease in inorganic impurities as a result of acid treatment is trivial and should be seen in the context of an increase in the structural order of the surface. As the impurities are detected as elements, no statements can be made about the chemical composition and structure of surface impurities which have been removed and remained on the surface.

The observed slight increase in the total concentration of surface hydroxyl groups is probably caused by the mild hydrothermal treatment. The result is in agreement with the observation obtained from ^{29}Si CP-MAS NMR spectrometry where the concentration of isolated and geminal groups increased on acidic/hydrothermal treatment.

The pH of a silica suspension is a too crude a measure to detect possible changes in the chemical composition of the silica surface. It appears that the impurities

TABLE II

RESULTS OF STRUCTURAL CHANGES OF SILICAS ON ACIDIC/HYDROTHERMAL TREATMENT

Parameter	Effect of acidic treatment
a_s (BET)	a_s remains constant after treatment with HNO_3, H_2SO_4 and HCl and decreases with HF.
Inorganic impurities	Decrease in metal impurities by about half with LiChrosorb Si 100-7, little effect with the other silicas.
Total concentration of surface hydroxyl groups	OH increases slightly. The effect is most pronounced for H_2SO_4-treated silicas (about 10%).
Geminal hydroxyl, free hydroxyl and siloxane groups	The content of geminal and free hydroxyl groups increased on acidic treatment. Siloxane groups became less mobile and more structured.
Electron diffraction	A reflection pattern arose with acid-treated silicas which could be assigned to a hexagonal structure.
IR spectrometry	No notable changes in the spectra between the native and acid-treated silicas could be observed.

removed from the surface by the treatment did not contribute to the acidic properties of the silica surface to a large extent.

The most notable alteration in the surface structure is the change in the mobility of siloxane groups, which was demonstrated for the first time for a porous silica. Additional methods for detecting changes in the long-range structural order of about 1 nm are needed in other to be able to interpret the NMR data. The occurence of a reflection for the acid-treated silica in the electron diffraction measurements supports the conclusion that a change towards a higher degree of structural ordering had occurred. However, an interpretation in quantitative terms cannot be given.

Tranmission IR spectrometry is too insenstive to diagnose minor changes in the hydroxyl group population as observed by means of isotopic exchange with deuterated trifluoroacetic acid.

In conclusion, it appears that the formation of quasi-crystalline domains at the silica surface occurs as a result of acidic/hydrothermal treatment. The effect is detectable but not very pronounced and requires more intensive examinations by solid-state NMR and diffraction methods.

Effect of acidic/hydrothermal treatment on the chromatographic properties of reversed-phase silicas made from acid-treated base materials

Native and acid-treated silicas (LiChrosorb Si 100-7, LiChrospher Si 100-10, Nucleosil 100-5 and silica BE-0) were reacted with N,N′-dimethylamino-*n*-octylsilane under such conditions that a constant ligand density of $\alpha_{n\text{-octyl}} = 3.2 \pm 0.1$ μmol/m^2 was obtained. The reversed-phase materials were packed into 125 mm × 4.6 mm I.D. columns. The mobile phase was methanol–water (70:30, v/v). Anilines (sample mixture I) and *n*-alkyl benzoates (sample mixture II) were chromatographed on these columns. From the chromatograms the solute capacity factor, the plate number and the asymmetry factor were calculated. Table III gives typical results for dimethylaniline and *n*-butyl benzoate as test solutes.

Solute capacity factor, k′. The data in Table III show that no consistent changes in k' occurred on al the acid-treated silicas. Hence the results must be considered specifically for each silica. On the silanized BE-0 silica which was treated with HF a decrease in k' of about 20% occurred.The treatment with other acids had only a minor effect on the k' values of the solutes compared with the untreated reversed-phase BE-0 silica. A similar observation can be made on acid-treated and silanized LiChrospher Si 100-10 silicas.

Plate number and asymmetry factor. As the dependences of the plate number (N) and the asymmetry factor (A) on the treatment parameters followed similar trends, but N was determined with a smaller relative standard deviation than A, the discussion of the results will focus on the changes in N as a function of acid treatment. For illustration, Table IV presents the parameters for acid-treated and silanized LiChrosorb Si 100-7 silicas which had a statistically significant impact on N. The results are grouped according to the type of acid employed.

With a given acid, the temperature and the duration of acid treatment affected the plate number significantly, whereas the influence of the concentration of the acid was less pronounced. In some instances the effect of the acid concentration on N was negative, *i.e.*, N decreased with increasing concentration of acid. It can be also seen from Table IV that the sum of the effects of two parameters often exerted a negative influence on N.

TABLE III

EFFECT OF ACIDIC TREATMENT ON THE CHROMATOGRAPHIC PARAMETERS OF REVERSED PHASE SILICAS MADE FROM NATIVE AND ACID-TREATED PRECURSORS

Standard deviations of the parameters: $0.05 < \sigma_{k'} < 0.12$; $250 < \sigma_N < 400$; $0.08 < \sigma_A < 0.27$.

Silica	Type of treatment	Solute					
		Dimethylaniline			*n*-Butyl benzoate		
		k'	N/m	A	k'	N/m	A
LiChrospher Si 100-10	None	2.78	30 100	2.25	4.72	31 500	1.69
	0.1 *M* HF, 298 K	2.90	32 300	1.81	4.75	34 300	1.60
	10 *M* HCl, 298 K	2.92	30 900	1.90	4.70	32 300	1.54
	10 *M* HCl, 363 K	2.99	31 400	1.75	4.77	33 000	1.58
BE-0	None	1.52	10 200	2.04	2.31	7600	1.83
	0.1 *M* HF, 363 K	1.21	9900	2.00	1.97	8600	1.55
	10 *M* H_2SO_4, 363 K	1.51	11 000	1.82	2.29	7400	1.82
	0.1 *M* HNO_3, 363 K	1.46	10 700	1.81	2.26	7600	1.80
	10 *M* HNO_3, 363 K	1.60	11 800	1.73	2.38	9400	1.19

In detail the results can be summarized as follows. The acid treatment of LiChrosorb Si 100-7 with HCl and HNO_3 led to similar results: increasing treatment temperature and duration gave an improvement in the plate number. An increase in the concentration of acid had the reverse effect, namely a decrease in N.

With HF-treated LiChrosorb Si 100-7 all three parameters, temperature, duration and concentration of HF, in particular the last parameter, brought about a substantial improvement in the plate number.

LiChrosorb Si 100-7 treated with H_2SO_4 and silanised showed exceptional behaviour in comparison with the other acids: for the benzoates an improvement in N was obtained on variation of all three parameters, whereas the opposite occurred with

TABLE IV

SURVEY OF STATISTICALLY SIGNIFICANT PARAMETERS OF ACID TREATMENT ON THE PLATE NUMBER OF REVERSED-PHASE SILICA COLUMNS

Silica: LiChrosorb Si 100-7. Parameters: A = temperature, B = duration, C = concentration. Statistical significance >97.5% (marked with asterisks), otherwise >95%.

Acid used for treatment	Solute	Significant parameters
HCl	Dimethylaniline	$A^*, B^*, -(A + B)$
	n-Butyl benzoate	$A, B^* - (A + B)$
HNO_3	Dimethylaniline	$A^*, B^*, (A + B)$
	n-Butyl benzoate	$A^*, B^* - C, -(A + B)$
HF	Dimethylaniline	A^*, B^*, C^*
	n-Butyl benzoate	$A^*, B^*, C^*, (A + C)$
H_2SO_4	Dimethylaniline	$A^*, B, -C, (A + B), -(A + C), -(B + C)$
	n-Butyl benzoate	$A, B^* - (A + C), -B + C)$

anilines as test solutes. The decrease in N for the anilines was most pronounced with 10 M H_2SO_4 and was accompanied by an increase in k' (data not shown). Blank experiments with pure water also showed an improvement in the plate number for LiChrosorb Si 100-7, which increased with increase in treatment temperature.

Similar dependences were obtained on acid-treated and silanized LiChrospher Si 100-10 and BE-0 silicas. However, the effects were less pronounced than those on LiChrosorb Si 100-7.

CONCLUSIONS

Acid treatment of native silicas prior to silanization improved the column performance in terms of plate number and peak symmetry. The extent of improvement increased with increasing temperature and duration of treatment and concentration of the acid, and was partly dependent on the type of native silica.

Considering the changes in the structural properties that result from acidic treatment and combining the results of acid treatment on the column performance, it appears that significant changes in the surface chemistry do not occur on acid treatment and thus the retention of solutes remains unaffected, with some exceptions, and that minor improvements in the structural ordering of the native silica surface on acid treatment exert a statistically significant increase in the column performance of the reversed-phase silicas made from acid-treated precursors. The correlation between these two parameters cannot yet be quantified owing to the lack of precise and reliable structural data for the acid-treated silica surface.

ACKNOWLEDGEMENTS

The authors are gratefully indebted to Dr. Voigt-Martin, Institut für Physikalische Chemie, Johannes Gutenberg-Universität, Mainz, and to Dr. H. Karge, Haber-Bosch Institut of the Max Planck Gesellschaft, Berlin, for conducting the electron diffraction and IR measurements. The generous support of E. Merck is also gratefully acknowledged. The project was supported by the Deutsche Forschungsgemeinschaft.

REFERENCES

1 O. E. Brust, I. Sebestian and I. Halász, *J. Chromatogr.*, 83 (1973) 15.
2 N. V. Akshinskaya, A. V. Kiselev and Yu. S. Nikitin, *Russ. J. Phys. Chem.*, 37 (1963) 491.
3 N. V. Akshinskaya, V. A. Davydov, L.T. Zhuravlev, G. Curthoys, A. V. Kiselev, B.V. Kuznetsov, Yu. S. Nikitin and V. V. Rybina, *Kolloidn. Zh.*, 26 (1964) 529.
4 V. M. Chertov, D. B. Dzhambaeva and I. E. Neimark, *Kolloidn.Zh.*, 27 (1965) 279.
5 A. V. Kiselev, Yu. S. Nikitin, A. J. Sarakhov and E. B. Oganesyan, *Koloidn. Zh.*, 30 (1968) 842.
6 A. V. Kiselev, Yu. S. Nikitin and E. B. Oganesyan, *Kolloidn. Zh.*, 31 (1969) 525.
7 A. V. Kiselev, V. M. Lukyanovich, Yu. S. Nikitin, E. B. Oganesyan and A. J. Sarakhov, *Kolloidn. Zh.*, 31 (1969) 388.
8 E. Bayer and A. Paulus, *J. Chromatogr.*, 400 (1987) 1.
9 A. Sokolowski and K. G. Wahlund, *J. Chromatogr.*, 189 (1980) 299.
10 J. Köhler and J. J. Kirkland, *J. Chromatogr.*, 385 (1987) 125.
11 K. D. Lork, *Ph. D. Thesis*, Johannes Gutenberg-Universität, Mainz, 1988.
12 R. Stout, G. B. Cox and T. J. Odiorne, presented at the *11th International Symposium on Column Liquid Chromatography, June 28–July 3, 1987, Amsterdam*, poster MO-P-35.
13 R. Majors, *LC · GC Int.*, 3, No. 4 (1990) 12 and 3, No. 5 (1990) 10.

14 F. Eisenbeiss, *Ber. Bunsenges. Phys. Chem.*, 93 (1989) 1026.
15 K. Unger and J.Schick-Kalb, *Ger. Pat.*, 2 155 281, 1971.
16 K. D. Lork and K. K. Unger, *Chromatographia,* 26 (1988) 115.
17 F. Yates, *Design and Analysis of Factorial Experiments*, Imperial Bureau of Soil Science, London, 1937.
18 G. Retzlaff, G. Rust and J. Waibel, *Statistische Versuchsplanung*, Verlag Chemie, Weinheim, 2nd ed., 1978.
19 S. J. Greeg and K.S. W. Sing, *Adsorption, Surface Area and Porosity*, Academic Press, London, 1982, pp. 41–110.
20 N. E. Fisher and A. Y. Mottlau, *Anal. Chem.*, 34 (1962) 714.
21 S. J. Gregg and K. S. W. Sing, *Adsorption, Surface Area and Porosity,* Academic Press, London, 1982, pp. 173–194.
22 M. Holik and B. Matejkova, *J. Chromatogr.*, 213 (1981) 33.
23 B. Pfleiderer, K. Albert, E. Bayer, L. van de Ven, J. de Haan and C. Cramers, *J. Phys. Chem.*, 94 (1990) 4189.
24 G. E. Maciel and D. W. Sindorf, *J. Am. Chem. Soc.*, 102 (1980) 7607.
25 D. W. Sindorf and G. E. Maciel, *J. Am. Chem. Soc.*, 105 (1983) 1487.
26 G. Engelhardt and D. Michel, *High-Resolution Solid State NMR of Silicates and Zeolites*, Wiley Interscience, New York, 1987.
27 D. W. Breck, *Zeolite Molecular Sieves*, Wiley-Interscience, New York, 1974, pp. 634–641.

Journal of Chromatography, 556 (1991) 407–414
Elsevier Science Publishers B.V., Amsterdam

CHROM. 23 199

Effect of silanol groups on heat-treated silicas by calcination and retention behaviour in high-performance liquid chromatography

MITSUYOSHI OKAMOTO*
Gifu Prefectural Tajimi Hospital, 5-161, Maehata cho, Tajimi, Gifu 507 (Japan)
KAZUNORI NOBUHARA
Fuji-Davison Chemical Ltd., 2-Chome, Kozoji cho, Kasugai, Aichi 487 (Japan)
and
KIYOKATSU JINNO
Toyohashi University of Technology, 1-1, Hibarigaoka, Tempaku cho, Toyohashi 440 (Japan)

ABSTRACT

The effect of silanol groups on heat-treated silicas by calcination has been studied by high-performance liquid chromatography. After heat-treating at various temperatures, the silicas were used for the measurement of physical parameters and chemical analysis. From elemental analysis data for carbon and hydrogen, the reactive silanol group concentrations, $\alpha_{OH(s)}$, were determined to be 2.3% from C or 2.9% from H for 180°C-treated silica, and 1.6% from C or 1.6% from H for 950°C-treated silica (original silica: mean pore diameter 11.6 nm, specific surface area 298 m^2/g, pore volume 1.22 ml/g, particle size 5.0 μm). The capacity factors of dioctylphthalate, dibutylphthalate and dimethylphthalate generally increased with increasing-heat treatment from 180 to 950°C, using methanol–hexane mixtures as the eluent. On the basis of the physico-chemical and chromatographic data the heat-treated silicas by calcination have been compared.

INTRODUCTION

Chemically modified phases are used mostly in high-performance liquid chromatography (HPLC). Thus, it is very important to investigate the mechanical, thermal and solvolytic resistance of these phases. Up to now silicas have been used preferentially as supports for chemically bonded phases. These materials consist of organic functional groups, such as octadecyl, octyl, ethyl and phenyl groups, bonded to silicas. In previous papers [1–8], we have suggested that the important parameters of silica with respect to the number of accessible alkylamino or phenyl groups per 100 $Å^2$ (1 nm^2) are the pore diameter and the specific surface area. On the other hand, with respect to the surface hydroxyl group concentration, $\alpha_{OH(s)}$, there have been few reports of HPLC analyses on heat-treated silica by calcination in physical and chemical research [9]. Therefore we studied the effect of silanol groups on heat-treated silicas by calcination and the retention behaviour in HPLC.

0021-9673/91/$03.50

EXPERIMENTAL

Reagent

Hexamethyldisilazane (HMDS) was obtained from Petrarch Systems (Bristol, PA, USA). Benzene, dioctylphthalate (DOP), dibutylphthalate (DBP) and dimethylphthalate (DMP) were obtained from Wako (Osaka, Japan). Porous silicas (Table I) were prepared in our laboratories. The other reagents and organic solvents were of analytical-reagent grade.

TABLE I

CHARACTERISTICS OF ORIGINAL SILICA

Sample[a]	Mean particle size (μm)	Mean pore diameter (nm)	Specific surface area (m^2/g)	Pore volume (ml/g)
Silica	5.0	11.6	298	1.22

[a] The designation is for convenience and has no commercial significance.

Apparatus

The HPLC measurements were carried out on a Twincle instrument (Jasco, Tokyo, Japan), equipped with a Uvidec-100IV variable-wavelength detector (Jasco) and a column of 250 × 4.6 mm I.D., packed with heat-treated silicas by calcination.

Stationary phase and elemental analysis

Porous silicas (Table I) were heated for 12 h at the required temperature (Table II). Then, according to the method of Buszewski [10], after 7 g of dried silica-180, silica-300, silica-500, silica-700 or silica-950 had been added to 70 ml of toluene and 4 ml of HMDS, silica-180-T, silica-300-T, silica-500-T, silica-700-T and Silica-950-T (which are listed in Table III) were prepared. Hereafter, silica-180-T to silica-950-T will be abbreviated to "column gel". The characteristics of these materials are also given in Tables II and III. The carbon and hydrogen contents of the treated silicas were de-

TABLE II

CHARACTERISTICS OF HEAT-TREATED SILICAS BY CALCINATION

DOP = Dioctylphthalate; DBP = dibutylphthalate; DMP = dimethylphthalate.

Treated gel[a]	Specific surface area (m^2/g)	Total silanol group concentration, $\alpha_{OH(s)}$	Capacity factor, k'		
			DOP	DBP	DMP
Silica-180	298	9.1	0.16	0.38	1.03
Silica-300	285	9.4	0.17	0.38	1.03
Silica-500	301	7.3	0.19	0.43	1.14
Silica-700	306	3.9	0.24	0.56	1.38
Silica-950	257	1.9	0.27	0.65	1.60

[a] The number indicates the heat-treatment temperature.

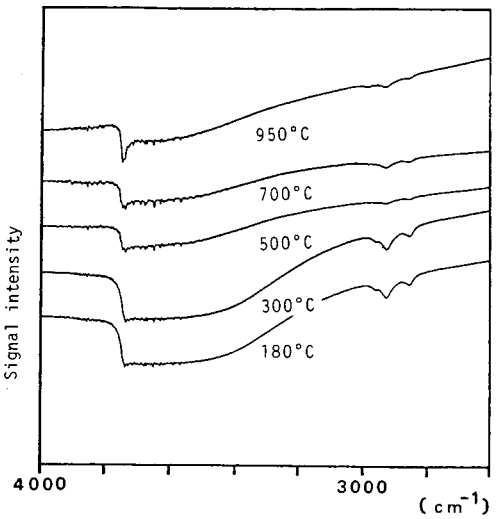

Fig. 1. Infrared spectra of the various heat-treated silicas by calcination.

termined by elemental analysis using an MT-3 CHN elemental analyser (Yanagimoto, Kyoto, Japan). The specific surface areas, mean pore diameters and pore volumes of the column silicas were determined with an MOD-220 porosimeter (Carlo Erba, Milan, Italy), SA-1000 surface-area pore-volume analyser (Shibata, Tokyo, Japan), FT-IR 1640 infrared spectrophotometer (Perkin-Elmer, CT, USA), and the data are shown in Tables II and III and Fig. 1.

Column preparation

The column silicas were packed into the stainless-steel column (250 × 4.6 mm I.D.) by the slurry technique.

RESULTS AND DISCUSSION

As is well known [9,11], the broad absorption band between 3800 and 3000 cm^{-1} (in Fig. 1) can be assigned generally to the OH bond of silanol groups. By elevating the

TABLE III

HEXAMETHYLDISILAZANE TREATMENTS AND REACTIVE SILANOL GROUPS PER 100 Å^2 (1 nm^2)

Column gel	C found (%)	H found (%)	Reactive silanol groups concentration, $\alpha_{OH(s)}$	
			From C	From H
Silica-180-T	4.09	1.28	2.3	2.9
Silica-300-T	3.62	1.20	2.1	2.8
Silica-500-T	4.07	1.25	2.3	2.8
Silica-700-T	3.50	0.97	1.9	2.1
Silica-950-T	2.47	0.62	1.6	1.6

heat-treatment temperature, this broad band at 180°C becomes narrower, and at 950°C the band shape is sharp as a result of the condensation and dehydration reaction of silanol, which gives rise to a sharp absorption band at 3747 cm^{-1}.

If HMDS is substituted monofunctionally on silica, the change of the surface structure of the saturated silica-180-T to silica-950-T can be described by the following formulae:

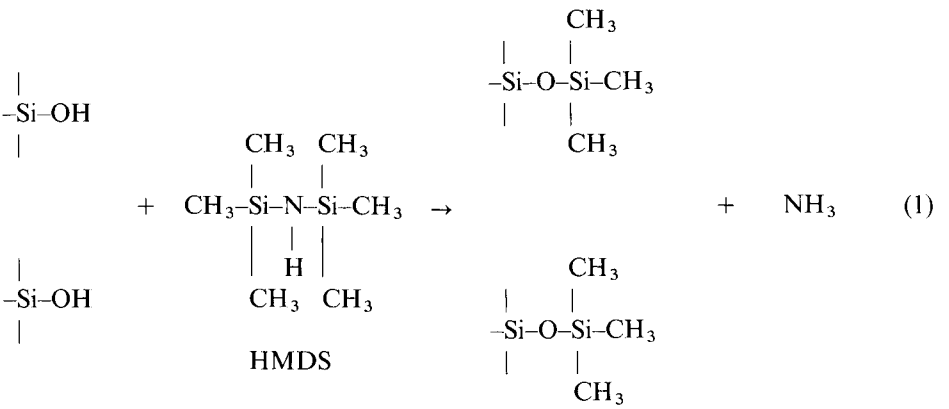

The reactive silanol groups per 100 $Å^2$ (1 nm^2) of silica is given by

$$[(H/100)/1.0079 \cdot 9] \cdot 6.022 \cdot 10^{23}/S \cdot 10^{18} \tag{2}$$

or

$$[(C/100)/12.011 \cdot 3] \cdot 6.022 \cdot 10^{23}/S \cdot 10^{18} \tag{3}$$

where H = weight percentage of hydrogen, C = weight percentage of carbon, $6.022 \cdot 10^{23}$ = Avogadro's number and S = specific surface area (m^2/g) of treated silica.

Substitution of the values of H and C found by elemental analysis into eqns. 2 and 3 gives the number of reactive silanol groups per 100 $Å^2$ (1 nm^2) of silica surface, indicated as "found" in Table III.

Tables II and III and Fig. 2 show the relation between the total and reactive silanol group concentration and the heat-treatment temperature of the silica sorbent. As can be seen from the "found" data in Table III, the reactive silanol group concentration decreases only slightly with respect to the increasing heat-treatment temperature and certainly shows smaller variability compared with the change of total silanol group concentration with temperature (Table II).

As shown in Fig. 2, the total silanol group concentration decreases distinctly by elevating the heat-treatment temperature, while the reactive silanol group concentration is shown to be almost constant, decreasing slightly with increasing temperature of calcination.

Fig. 3 shows the relation of the capacity factors (k') of phthalic acid esters *versus* the various silicas treated by calcination. As can be seen from Fig. 3, the k' of phthalic acid esters increases with elevating heat-treatment temperature.

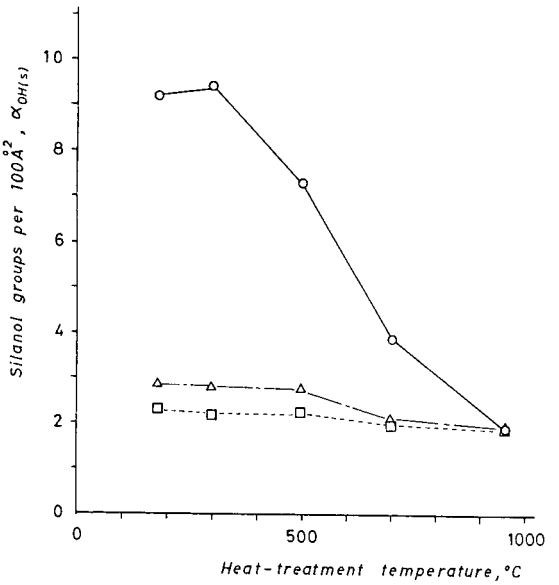

Fig. 2. Relation of the total silanol group concentration *versus* the reactive silanol group concentration to the various heat-treatment temperatures. ○ = Total silanol groups; △ = reactive silanol groups (calculated from hydrogen percentages in Table III); □ = reactive silanol groups (calculated from carbon percentages in Table III).

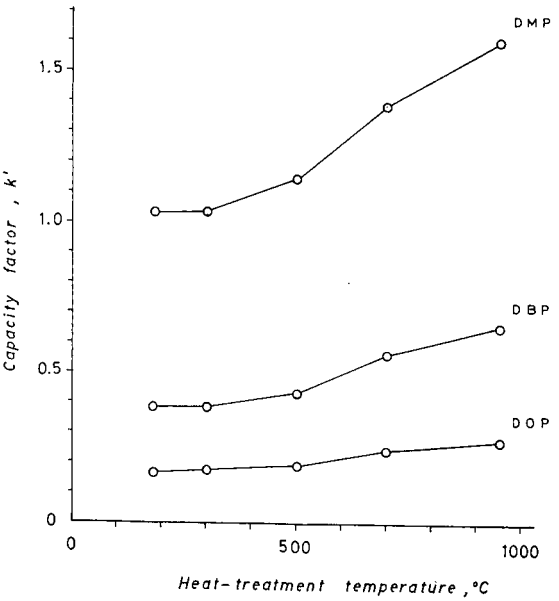

Fig. 3. Relation of the capacity factors (k') of phthalic acid esters *versus* the various heat-treated silicas by calcination. HPLC conditions: Mobile phase; Methanol–*n*-hexane (1:99, v/v); flow-rate: 1.0 ml/min; detection: 254 nm UV; DOP = dioctylphthalate; DBP = dibutylphthalate; DMP = dimethylphthalate.

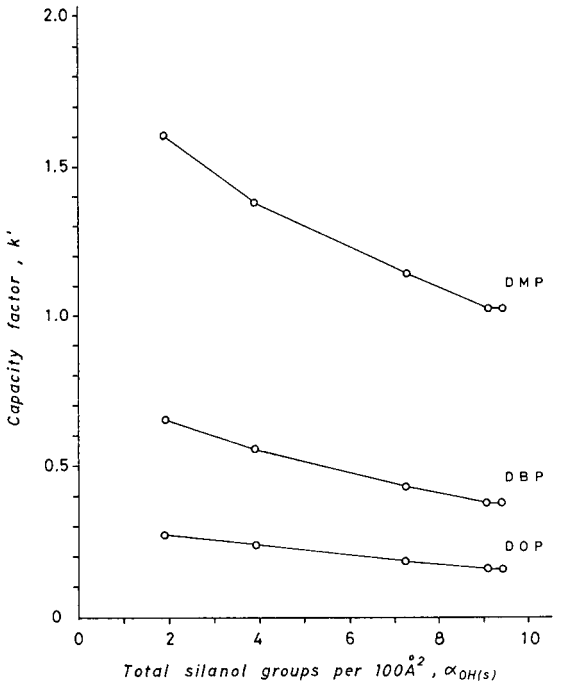

Fig. 4. Relation of the capacity factors (k') of phthalic acid esters *versus* the total silanol groups per 100 Å^2 (1 μm^2). HPLC conditions as in Fig. 3.

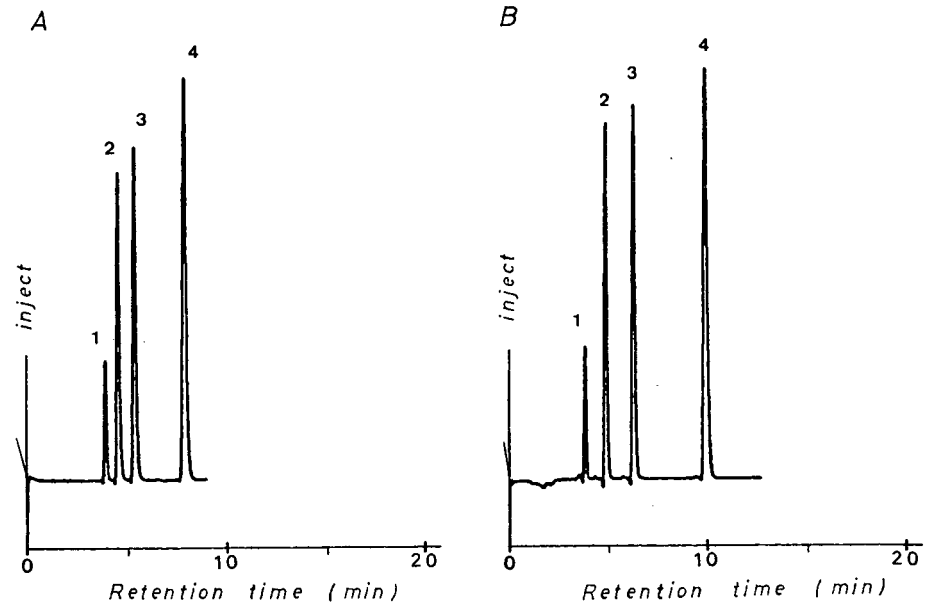

Fig. 5. Comparative typical chromatograms of phthalic acid esters on the 180°C-treated silica (A) *versus* the 950°C-treated silica (B). HPLC conditions as in Fig. 3. Peaks: 1 = benzene (t_0); 2 = dioctylphthalate; 3 = dibutylphthalate; 4 = dimethylphthalate.

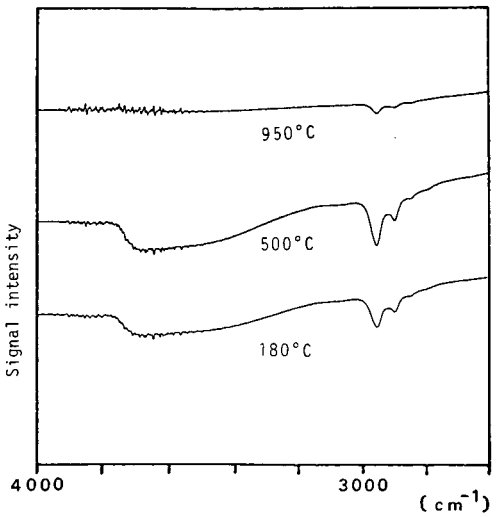

Fig. 6. Infrared spectra showing the effect of hexamethyldisilazane treatment on various heat-treated silica. Samples as in Table III.

From the studies on liquid chromatography with silica as sorbent, it is generally known that the interaction of the silica surface with the solute depends on the silanol groups. The silanol group concentration $\alpha_{OH(s)}$ decreased by calcination with higher heat-treatment temperature; on the contrary, the k' values of DOP, DBP and DMP were increased under the same HPLC conditions, as is shown in Table II.

Fig. 4 shows the relation of the k' of phthalic acid esters *versus* the total silanol groups per 100 Å^2 (1 nm^2). As can be seen from Fig. 4, the k' of phthalic acid esters decreases by increasing the total silanol groups per 100 Å^2 (1 nm^2).

Fig. 5 shows the comparative chromatograms of phthalic acid esters on two types of heat-treated silicas (calcination temperatures at 180 and 950°C).

As can be seen from Figs. 2, 4 and 5, the results indicate that the retention effect was not proportional to the number of silanol groups and the silanol group concentration, $\alpha_{OH(s)}$, on the silica surface.

It was assumed that the hydrogen-bonded silanol groups on the silica surface have an inhibitory effect on the retention of the solute and that the retention effect was due mainly to free silanol groups on the silica surface. This idea is supported by showing that the broad absorption band between 3800 and 3000 cm^{-1} decreased as a result of elevating heat-treatment temperature (Fig. 6). As can be seen from Figs. 1 and 6, the amount of hydrogen-bonded silanol groups decreases as a result of the condensation and dehydration reactions during calcination. On the other hand, it was proven that free silanol groups exist even after the heat treatment of the sorbent at 950°C. It was also shown that the silanol group concentration, $\alpha_{OH(s)}$, of the reactive silanol is almost constant (about two groups per 100 Å^2 = 1 nm^2); these are mainly the free silanol groups on the heat-treated silica surface.

ACKNOWLEDGEMENTS

The authors acknowledge helpful discussions with Professor Hiroshi Kishimoto at Nagoya City University and a research subsidy from the Toyoda Foundation.

REFERENCES

1 M. Okamoto, *J. Chromatogr.*, 202 (1980) 55.
2 M. Okamoto and H. Kishimoto, *J. Chromatogr.*, 212 (1981) 251.
3 M. Okamoto and F. Yamada, *J. Chromatogr.*, 247 (1982) 167.
4 M. Okamoto and F. Yamada, *J. Chromatogr.*, 283 (1984) 61.
5 M. Okamoto and K. Jinno, *Chromatographia*, 21 (1986) 467.
6 M. Okamoto and K. Jinno, *J. Chromatogr.*, 395 (1987) 171.
7 M. Okamoto, K. Jinno, M. Yamagami, K. Nobuhara and K. Fukushima, *J. Chromatogr.*, 396 (1987) 345.
8 M. Okamoto, I. Yoshida, M. Utsumi, K. Nobuhara and K. Jinno, *J. Chromatogr.*, 515 (1990) 43.
9 K. K. Unger, *Porous Silica*, Elsevier, Amsterdam, 1979.
10 B. Buszewski, *Chromatographia*, 28 (1989) 574.
11 S. Kondo, M. Muroya and K. Fujii, *Bull. Chem. Soc. Jpn.*, 47 (1974) 553.

Journal of Chromatography, 556 (1991) 415–424
Elsevier Science Publishers B.V., Amsterdam

CHROM. 23 202

Use of the reordering/resolvation of alkyl-modified silica to characterize the microscopic heterogeneity of silica via liquid chromatography

R. K. GILPIN* and L. WU
Department of Chemistry, Kent State University, Kent, OH 44242 (USA)

ABSTRACT

The microscopic heterogeneity of the surface silanols of silica was studied by liquid chromatography. By examining thermally induced reordering/resolvation of bonded alkyl chains (*i.e.*, octyl groups) in contact with water, it is possible to deduce fundamental information about differences in the microscopic surface structure of silica prepared by different manufacturing processes. In addition, deuterium exchange–mass spectrometry was used to measure the bulk silanol concentration on the same silica.

INTRODUCTION

For over two decades, chemically modified silicas have been used as liquid chromatographic stationary phases. During this time, in order to improve the performance of existing phases and to develop novel new phases, a better understanding of the bonding chemistry and the surface structure has been of paramount importance. Initially, most phases were prepared using multi-reactive silanes because of increased stability. However, present synthetic routes often employ monoreactive silanes as the reaction is more controllable and reproducible. Even so, the surfaces formed and the nature of these surfaces with respect to their chromatographic selectivities vary between manufacturers and in-house preparations among laboratories. To a large extent these differences can be attributed to the silicas used to prepare the bonded phases in terms of geometric properties such as pore structure and surface area in addition to the general nature of the surface in terms of the number and types of silanol groups present and their distribution.

The key to explaining differences in chromatographic selectivity for a given immobilized ligand, especially when using monoreactive chemistry, lies in developing a better understanding of the surface structure. Two modified silicas with nearly identical surface areas, pore structures and coverages in terms of the total amounts of bound carbon often vary in chromatographic selectivity. Hence, although the surface coverages on a macroscopic level are equivalent, on a microscopic level the distributions of the bound ligands on the surface differ. The two extremes of this variable

0021-9673/91/$03.50

bonding model are either surfaces where the chains are uniformly distributed in a homogeneous arrangement or surfaces which are made up of varying spots or patches of bound ligands distributed in a non-homogeneous fashion with tightly packed organic areas and areas of non-bonding. This latter case has been shown by many investigators to reflect more closely the bonding heterogeneity of chromatographic phases.

A large number of investigators have studied silica and derivatized silica. Because of the extensive volume of work in this area it is not possible to cite all of the references; Iler [1] and Unger [2] have written extensive texts which summarize both the physical and chemical properties of silica. Based on geometric considerations, Iler [1] suggested that amorphous silica theoretically should have a surface silanol concentration of about 8 groups/nm^2. However, experimentally determined concentrations typically vary from this predicted value. In part, this can be attributed to the technique employed to quantify the silanols, especially if they involve either a chemical derivatization or a physical sorption process. Steric effects arising from the size of the reagent, the spacing of the silanols and the pore structure of the silica (*i.e.*, higher surface area materials that may contain a number of micropores) may result in lower than expected values. A number of procedures have been reported for determining the silanol concentration, including (1) adsorbed dye methods [3], (2) chemical reactions with methyllithium and Grignard reagents [4,5], (3) infrared spectrometry [6] or (4) treatment with deuterium oxide followed by either nuclear magnetic resonance spectrometry (NMR) [7–9], mass spectrometry (MS) [10] or chromatography [4,11] to monitor the degree of isotopic exchange.

In addition to the above considerations, the processes used to synthesize and thermally treat the silica during manufacturing and drying prior to analysis influence the number, types and distribution of surface silanols. Iler [12] suggested that the hydrated surface of amorphous silica dried at 150°C in air should contain 4.5–8.0 SiOH groups/nm^2. Similarly, according to Unger [13] the maximum silanol concentration on porous silica dried at 200°C should be 4.8–5.4 groups/nm^2. Recently published experimental results are in good agreement with the latter predictions. Measured silanol concentrations for various types of chromatographic silicas have been found to range between 3 and 5 groups/nm^2 [4,5,7–11].

The idea of characterizing the microscopic heterogeneity of silica by a method which requires no assumptions to be made about surface area, pore geometry and silanol distribution is appealing and should be potentially useful in explaining differences in chromatographic selectivity for similar bonded phases prepared on different silica substrates. In an effort to develop such a method a series of silicas produced by different manufactures were chemically modified by derivatization with *n*-octyltrichlorosilane. Subsequently, the reordering/resolvation of these materials in contact with water were studied by liquid chromatography [14]. Under such conditions the surface immobilized chains can be made thermally to undergo changes in their conformation. These changes have been described in terms of a characteristic reordering/resolvation temperature which is dependent on chain length and functionality of the bound ligand, but is independent of bonding chemistry and surface coverage within a certain critical range [15–18]. To date all previous investigations of reordering/resolvation have been carried out on a single type of silica, LiChrosorb Si-60. This work represents an extension of previous work to examine the influence of the substrate on

reordering/resolvation and the use of these data to characterize the microscopic nature of the surface.

EXPERIMENTAL

Materials

n-Octyltrichlorosilane and deuterium oxide (99.8 atom% of D) were purchased from Huls America (Levittown, PA, USA) and Aldrich (Milwaukee, WI, USA), respectively. Analytical-reagent grade toluene and high performance liquid chromatographic grade acetonitrile were obtained from Fisher Scientific (Pittsburgh, PA, USA). Deionized water was produced in-house with a Milli-Q reagent water purification system (Millipore, El Paso, TX, USA).

Chromatographic-grade silicas were purchased from various manufactures: LiChrosorb Si-100 and Si-60 from E. Merck (Darmstadt, Germany), Partisil-10 from Whatman (Clifton, NJ, USA), Zorbax SIL from Rockland Technologies (Newport, DE, USA) and ICN 7–12 was from ICN Biochemicals (Cleveland, OH, USA). The physical properties of these materials are listed in Table I.

Water-saturated toluene was prepared by vigorously mixing toluene with water and allowing it to separate into two layers. Dry toluene was made by refluxing toluene with calcium hydride overnight.

Synthesis

About 1.7 g of a given silica were added to 30 ml of deionized water, the mixture was shaken, allowed to stand for 2–3 h and the excess water was decanted off. The resulting silica was dried at 120°C for 3 h then it was transferred to a special reaction vessel with a fritted-glass bottom [15] and 170 ml of water-saturated toluene were added. After allowing the silica to equilibrate overnight the water-saturated toluene was removed and the silica was reacted under reflux conditions with 30 ml of a 15% solution of *n*-octyltrichlorosilane in dry toluene for 8 h. During the modification, dry nitrogen was bubbled through the bottom of the reaction vessel to stir the mixture and to expel the HCl generated. Subsequently, the silica was washed four times with 50-ml portions of both dry and water-saturated toluene and then twice with 50 ml portions of diethyl ether. The material was dried at 120°C.

TABLE I

PHYSICAL PROPERTIES OF THE SILICA STUDIED

Data are from manufacturers' literature.

Silica	Particle size (μm)	Surface area (m^2/g)	Pore size (Å)
LiChrosorb Si-60	10	550	60
LiChrosorb Si-100	10	420	100
Zorbax SIL	7	350	70–80
Partisil-10	10	>400	80
ICN 7–12	7–12	500–600	60

Column packing

A slurry was prepared by combining about 0.8 g of a given modified silica with *ca.* 30 ml of 2-propanol in a dynamic packing apparatus. The mixture was stirred for about 15 min and the apparatus sealed. The modified silica was packed by the ascending technique into 25 cm × 2.4 mm I.D. stainless-steel columns using a Haskel (Burbank, CA, USA) Model DSTV-52-C air-driven fluid pump and a packing pressure of 6000 p.s.i. [19]. Methanol was used as the delivery solvent.

Equipment

A Hewlett-Packard (Palo Alto, CA, USA) Model HP5995 gas chromatograph–mass spectrometer equipped with a Model 9825A desktop computer was used to make the deuterium exchange measurements. In doing this, the gas chromatograph was not employed. Rather, the samples were introduced directly into the quadrupole mass analyzer by slowly bleeding the vapors developed above small L-shaped glass tubes (1/4 in. O.D.) which were attached through the auxiliary mass calibration inlet port. To maximize sensitivity and minimize interferences, the analyzer was set to scan over a mass range from 16.0 to 22.0 u. The mass analyzer temperature was 200°C and the electron impact (70 eV) ionization source was set at 150°C.

The liquid chromatographic system consisted of a Laboratory Data Control (Riviera Beach, FL, USA) Constametric III pump, an Altex Model 152 UV detector set at 254 nm and a Rheodyne (Berkeley, CA, USA) Model 7010 injection valve with a Model 7012 loop filler port. The column temperature was controlled in a water-bath equipped with a Fisher Scientific Model 730 isotemp immersion circulator and a Neslab Instrument (Portsmouth, NH, USA) Model EN-350 flow-through liquid cooler. The flow-rate of the mobile phase was measured by a Phase Separation (Queensberry, Clwyd, UK) Model FLOSOA electronic flow meter which was connected to the outlet of the UV detector. The detector output signal was recorded and analyzed using an IBM Instruments (Danbury, CT, USA) Model 9000 computer system and chromatographic applications program (CAP).

Deuterium exchange and mass spectrometric measurements

A set of standard solutions were prepared by adding from 1–5% of water to D_2O. The different silica samples were dried at 150°C under vacuum for 24 h to remove adsorbed water. After cooling to room temperature in a desiccator, 60–80 mg of silica were weighed into L-shaped glass sample tubes, 200 μl of deuterium oxide which contained 1% of water were added and the tubes were sealed. To facilitate complete wetting of the material (*i.e.*, to release the gas from the pores) the sealed sample tubes were placed in an ultrasonic bath and sonicated for at least 30 min. Subsequently, the samples were allowed to stand for at least 4 h before analysis.

Before each standard and sample measurement, a pure deuterium oxide background was run to insure that no exchange peaks were present in the mass spectrum. Samples were introduced directly into the analyser section via the auxiliary calibration inlet port at a pressure of $2 \cdot 10^{-5}$ Torr (1 Torr = 133.3 Pa) (monitored by a vacuum ionization gauge). Spectra were recorded for a minimum of 10 min. Plateau values were reached after about 0.5 min of sample introduction time. At least ten values were averaged from the reported ion tables over the last 5 min of acquired spectra. Separate sample introductions and mass spectra were collected a minimum of

three times on each tube. Each silica was studied a minimum of at least three complete times on separate days.

Liquid chromatographic measurements

Each column was first conditioned with 100 ml of acetonitrile followed by an equal amount of water at the lowest temperature studied, 10°C. Acetonitrile was used to minimize entrapment problems [20]. After conditioning, the retention times of three test solutes (resorcinol, phenol and *p*-cresol) were measured every 5°C up to 80°C (initial evaluation). This was carried out using deionized water as the mobile phase at a flow-rate of 1.0 ml/min. At least two injections of each solute were made at all temperatures. After completing the initial evaluation, the column was cooled to 10°C and the retention times of the test solutes were measured again over the same temperature range (re-evaluation). Between all temperature changes the pump was switched off until the column had reached thermal equilibrium. All columns were studied at least twice by the above procedure (*i.e.*, conditioning, initial evaluation and re-evaluation).

The mean capacity factors, k', were calculated from multiple injections of the test solutes using deuterium oxide to determine the void volume. Void volume measurements were made at each temperature studied.

RESULTS AND DISCUSSION

Although there are a number of methods for determining the number and types of silanol groups on the surface of silica, the results obtained typically give macroscopic information about the system. In order to reduce these macroscopic data to a microscopic level, assumptions must first be made in terms of the surface area and pore geometry of the support and the distribution of the silanols on its surface. In the current study the surface silanol concentrations for several different silicas were measured using a conventional bulk characterization procedure, deuterium exchange followed by mass spectrometry. Subsequently, these same silicas were initially modified via chemical derivatization with *n*-octyltrichlorosilane and then the reordering/resolvation of the materials in contact with water measured by liquid chromatography. The resulting data appear to reflect differences in microscopic heterogeneity of the surfaces as discussed below.

Deuterium exchange and mass spectrometric measurements

The surface silanol concentrations for the five different chromatographic-grade porous silicas were measured by deuterium exchange–mass spectrometry. Prior to making these measurements each material was treated as described under Experimental. During the development stages of this work, it was found to be necessary to add 1% of water to the deuterium oxide in order to reach a total level of exchanged water which gave reproducible mass spectrometric readings and which fit in the linear region of calibration graphs generated by adding known amounts of water (*i.e.*, from 1 to 5%) to deuterium oxide.

Fig. 1 shows a representative calibration graph obtained by plotting the exchange ratio for the 19–20 peaks *vs.* the logarithm of the percentage of water added. At water levels between 1 and 5% the graphs were linear with correlation coefficients

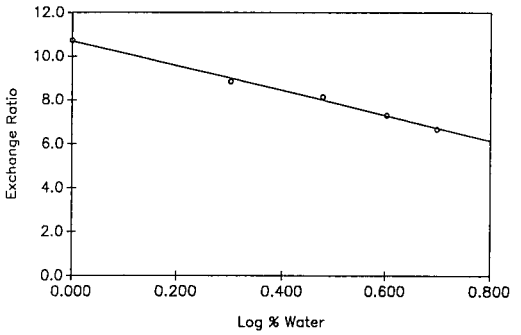

Fig. 1. Representative calibration graph: exchange ratio of the 19–20 u peaks *vs.* log (% water added).

of 0.99 or better. Before each calibration and sample measurement, a pure deuterium oxide background was run to insure the absence of a 19 u peak in the mass spectrum. Readings were taken by alternating samples and standards.

The concentration of surface silanols in moles per gram of material are given in Table II for the five silicas studied. The surface concentrations are also reported in terms of the number of silanol groups per nm^2 based on the manufacturers' listed surface area data summarized in Table I. The measured values ranged between 3.4 and 4.9 silanols/nm^2. These data are in good agreement with values reported by Iler [12] and other recently published data [4,5,7–11]. For LiChrosorb-100 where a direct comparison can be made, the current value of 4.42 groups/nm^2 and an earlier reported value by Welsch and Frank [4] of 4.40 groups/nm^2 are identical. However, both the current value and that of Welsch and Frank are slightly lower than that reported by an alternative deuterium exchange method [11] (*i.e.*, 5.1 groups/nm^2). For Zorbax SIL, the current value of 4.41 silanols/nm^2 is slightly higher than that previously obtained by solid-state NMR methods [8,9] of 3.0–3.6 groups/nm^2. It seems reasonable that some of this difference might be attributed to variations in surface area between manufactured batches of Zorbax or treatment and drying steps in the manufacturing and preanalysis handling of the silica. However, it is unclear whether these factors would account for all of the difference.

TABLE II

MEASURED SILANOL CONCENTRATIONS FOR THE SILICAS STUDIED

Silica	Silanol concentration (mmol/g)	Groups/nm^2 [a]
LiChrosorb Si-60	3.14	3.44 ± 0.24
LiChrosorb Si-100	3.09	4.42 ± 0.09
Zorbax SIL	2.56	4.41 ± 0.82
Partisil-10	3.22	4.86 ± 0.13
ICN 7–12	3.07	3.37 ± 0.76

[a] Data were measured by deuterium exchange–mass spectrometry and are based on the manufacturers' reported surface areas listed in Table I.

The value of 3.44 groups/nm^2 for LiChrosorb Si-60 seems low compared with that obtained for LiChrosorb Si-100 and may reflect differences in pore structure and wetting. Similar numbers were obtained for another higher surface area material, *i.e.*, 3.37 groups/nm^2 for ICN 7–12. The current results are consistent with data reported for other materials with smaller pores such as Porasil 60 silica [7]. In all instances the above calculated values (column 2 in Table II) assume a homogeneous distribution of the silanol groups on the surface.

Liquid chromatographic studies of reordering/resolvation

The orientation of silica-immobilized alkyl chains in contact with water are influenced by cohesive, hydrophobic and specific interactions between the chain, solvent and surface. [16]. A two-state model has been proposed where the bonded chains may be in either an aggregated/collapsed conformation or in a more extended/solvated conformation, depending on the thermal conditons. These conformational differences have been studied as a function of various properties of the bonded groups, including their size, shape and polarity (*i.e.*, the presence of functional groups) as well as the bonding chemistry [15–18,19–27]. To date, all previous investigations have been carried out using a single type of silica substrate, LiChrosorb Si-60.

In the current study, columns were packed with different octyl-modified silicas, conditioned with acetonitrile, and the retentions of three solutes were measured as a function of temperature using water as the mobile phase. These experiments were conducted in a similar fashion to those reported by Gilpin's group [15–18, 27].

Representative plots of ln k' *vs.* $1/T$, where T(K) is the column temperature, are shown in Fig. 2 for phenol chromatographed on the Zorbax- and Partisil-modified silicas. Plots were also constructed for the other test solutes on these same modified

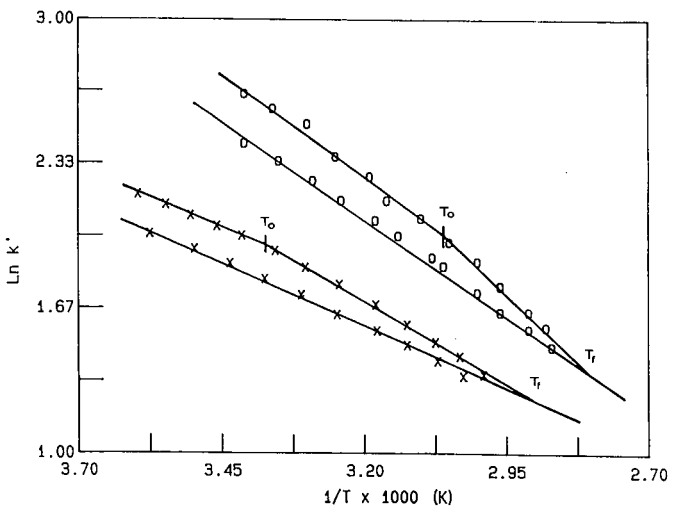

Fig. 2. Representative plots of ln k' *vs.* $1/T$ which illustrate the differences in thermally induced reordering/resolvation for octyl groups chemically bonded to two different silica substrates. T_o and T_f represent the initial and final surface reordening/resolvation temperatures, respectively. (○) Zorbax silica; (×) Partisil silica.

silicas and on the other modified silicas. The general shapes of all the curves were similar to each other and to curves reported previously [15] for octyl-modified LiChrosorb Si-60. However, the curves differed in the onset temperature (T_0) for reordering/resolvation and the temperature range (ΔT) over which thermal reordering/resolvation occurred.

Summarized in the Table III are T_0 values for the various octyl-modified silicas. These data are averages from at least duplicate injections for the three different solutes, resorcinol, phenol and *p*-cresol. In all instances at least two different reaction batches for a given silica were studied. For comparative purposes the data for LiChrosorb Si-60 reported earlier [15] are also included in Table III. The data in Table III show that the reordering/resolvation temperature is independent of surface coverage (*i.e.*, at least for the range studied) for a given silica. This trend is also in agreement with results from earlier studies [15,17]. For example, although the surface coverages of the different reaction batches of octyl-modified Partisil range from 8.8 to 11.0% bound carbon, the average reordering/resolvation temperatures are statistically not significantly different. This is also true of the other materials listed in Table III. These results imply that within a critical range of chain density bonding occurs in subunits or patches on the surface. Increasing the extent of the reaction may increase the size of a subunit or the formation of more subunits but it does not increase the bonding density within a subunit. Thus, the reordering/resolvation temperature is independent of the number of subunits but depends on the spacing (*i.e.*, distribution/heterogeneity of the surface silanols) of the bonded groups within a subunit.

Different silicas produced via different processes should vary in the number and

TABLE III

SURFACE COVERAGE AND REORDERING/RESOLVATION TEMPERATURE FOR THE OCTYL-MODIFIED SILICAS

Silica	Column	Carbon (%)	Onset temperature[a] (°C)
LiChrosorb Si-60		9.5[b]	Av. 44.7 ± 0.7[b]
LiChrosorb Si-100	a	7.4	44.1
	b	7.2	45.5
	c	6.8	44.1
			Av. 44.6 ± 0.7
Zorbax SIL	a	10.0	54.5
	b	7.2	56.2
	c	7.2	52.5
			Av. 54.5 ± 1.5
Partisil-10	a	11.0	22.4
	b	8.8	24.9
			Av. 23.7 ± 1.3
ICN 7–12	a	8.9	35.4
	b	9.3	35.7
			Av. 35.6 ± 0.2

[a] Determined from linear fits of ln k' *vs.* $1/T$ data labeled point T_0 in Fig. 2.
[b] Data from ref. 15.

average spacing of silanol groups. As shown in Table III, the reordering/resolvation temperatures for the octyl-modified surfaces are significantly different for silicas produced by different manufacturers. On the other hand, for LiChrosorb Si-60 and Si-100, which are manufactured by a similar process, the reordering/resolvation temperatures are similar. For Zorbax and Partisil, reordering/resolvation start at about 54 and 24°C, respectively. Their physical properties such as pore size and surface area (Table I) are similar, but their reordering/resolvation temperatures differ by more than 30°C. These observations further support the idea that resolvation is controlled by the microscopic distribution of the bound chains (*i.e.*, the silanol distribution), not gross physical properties of the silica.

Table IV gives mean data for T_o and T_f, the initial and final surface reordering/resolvation temperatures, for the various octyl-modified silicas. The total temperature ranges (ΔT) over which thermally induced reordering/resolvation occurred are also listed in Table IV. As cohesive and hydrophobic interactions are dependent on chain length, for a given chain length, T_o, T_f and ΔT should be related to the distribution and spacing of the bonded groups on the surface and thus should reflect differences in the heterogeneity and concentration of the silanols on the silica substrate. Again, comparing Zorbax and Partisil, the range for Partisil, $\Delta T = 44.5$°C, is about twice that for Zorbax, $\Delta T = 25.3$°C. These results imply that there is a greater degree of heterogeneity in terms of the silanol distribution of Partisil compared with Zorbax.

CONCLUSION

Deuterium exchange–mass spectrometry was used to measure the macroscopic silanol concentrations of silica produced by different manufacturers, which ranged from 3 to 5 groups/nm^2. These data show neither a significant difference between the materials nor a direct relationship with reordering/resolvation of the materials in contact with water. As macroscopic measurements such as surface coverage and silanol concentration determined by gas chromatography–mass spectrometry give only average properties of the surface, they do not satisfactorily characterize the heterogeneity of the surface of silica. It is this latter aspect that the chromatographic method described in the current work has addressed.

Based on the reordering/resolvation data obtained in this or in similar studies applied to other substrates, it may be possible to explain either similarities of differences in the chromatographic performance of bonded phases prepared on various types of silica. As reordering/resolvation of the surface are dependent on chain length

TABLE IV

TEMPERATURE RANGE OVER WHICH SURFACE REORDERING/RESOLVATION OCCURS

Silica	T_o(°C)	T_f(°C)[a]	$\Delta T = T_f - T_o$ (°C)
LiChrosorb Si-100	44.6	71.8	27.2
Zorbax SIL	54.4	79.7	25.3
Partisil-10	23.7	68.2	44.5
ICN 7–12	35.6	76.8	41.2

[a] T_f is the final temperature where all the surface is solvated.

[16], for a given chain length, T_o and ΔT should be related to the distribution and spacing of the bonded groups on the surface and should reflect differences in the heterogeneity and concentration of silanols on the silica substrate which arise during manufacture.

REFERENCES

1 R. K. Iler, *The Chemistry of Silica*, Wiley, New York, 1979.
2 K. K. Unger, *Porous Silica*, Elsevier, Amsterdam, 1979.
3 W. K. Lowen and E. C. Broge, *J. Phys. Chem.*, 65 (1961) 16.
4 T. Welsch and H. Frank, *J. Chromatogr.*, 267 (1983) 39.
5 S. C. Antakli and J. Serpinet, *Chromatographia*, 23 (1987) 767.
6 G. Wirzing, *Naturwissenschaften*, 51 (1964) 211.
7 M. Holik and B. Matejkova, *J. Chromatogr.*, 213 (1981) 33.
8 J. Kohler, D. B. Chase, R. D. Farlee, A. J. Vega and J. J. Kirkland, *J. Chromatogr.*,352 (1986) 275.
9 J. Kohler and J. J. Kirkland, *J. Chromatogr.*, 385 (1987) 125.
10 L. T. Zhuravlev, *Langmuir*, 3 (1987) 316.
11 G. Foti and E. Sz. Kováts, *Langmuir*, 5 (1989) 232.
12 R. K. Iler, *J. Chromatogr.*, 209 (1981) 341.
13 K. K. Unger, *Angew. Chem., Int. Ed. Engl.*, 11 (1972) 267.
14 L. Wu, *M.S. Thesis*, Kent State University, Kent, OH, 1990.
15 R. K. Gilpin and J. A. Squires, *J. Chromatogr. Sci.*, 19 (1981) 195.
16 S. S. Yang and R. K. Gilpin, *J. Chromatogr.*, 394 (1987) 295.
17 S. S. Yang and R. K. Gilpin, *J. Chromatogr.*, 408 (1987) 93.
18 S. S. Yang and R. K. Gilpin, *J. Chromatogr.*, 449 (1988) 115.
19 R. K. Gilpin and W. R. Sisco, *Anal. Chem.*, 50 (1978) 1337.
20 R. K. Gilpin, M. E. Gangoda and A. E. Krishen, *J. Chromatogr. Sci.*, 20 (1982) 345.
21 R. K. Gilpin, *Am. Lab.*, 14 (1982) 164.
22 R. K. Gilpin, *J. Chromatogr. Sci.*, 22 (1984) 371.
23 R. K. Gilpin, *Anal. Chem.*, 57 (1985) 1465A.
24 R. K. Gilpin and M. E. Gangoda, *J. Chromatogr. Sci.*, 21 (1983) 352.
25 M. E. Gangoda, R. K. Gilpin and B. M. Fung, *J. Magn. Reson.*, 74 (1987) 134.
26 B. R. Suffolk and R. K. Gilpin, *Anal. Chem.*, 57 (1985) 596.
27 S. S. Yang and R. K. Gilpin, *Talanta*, 36 (1989) 327.

Journal of Chromatography, 556 (1991) 425–432
Elsevier Science Publishers B.V., Amsterdam

CHROM. 23 321

New solid adsorbents for the separation of lower hydrocarbons and permanent gases

II. Ammonium molybdophosphate

VIKRAM S. NAYAK
Guelph Chemical Laboratories Ltd., 246 Silvercreek Parkway N, Guelph, Ontario, N1H 1E7 (Canada)

ABSTRACT

Ammonium molybdophosphate [$(NH_4)_3PMo_{12}O_{40}$] has been tried as a solid adsorbent in the gas chromatographic separation of lower hydrocarbons and permanent gases. It appears to be an effective adsorbent for the separation of methane, ethane, ethylene, acetylene, propane, propylene and butane. The retention characteristics of C_1–C_4 hydrocarbons in both isothermal and temperature-programmed runs using a 20% ammonium molybdophosphate column were obtained. The retention times and peak-area percentages of lower hydrocarbons are highly reproducible in both isothermal and temperature-programmed runs. The separation of lower hydrocarbons and permanent gases obtained using ammonium molybdophosphate appears to be comparable to that obtained using either ammonium tungstophosphate or ammonium tungstosilicate.

INTRODUCTION

Analyses of lower hydrocarbons and permanent gases are generally carried out by gas–solid chromatography (GSC). With the development of capillary gas chromatography by Golay in 1960 [1] and the subsequent introduction of porous-layer open-tubular (PLOT) columns, high-resolution GSC has been gaining importance in the separation of a wide variety of organic compounds and permanent gases. Although the solid adsorbents used in GSC generally have high thermal stability and offer negligible column bleeding, they suffer from limitations such as irreversible adsorption of polar compounds and inapplicability towards the separation of higher hydrocarbons because of very long retention times. Broadening of peaks is also commonly observed in GSC. In GSC, Gaussian-shaped peaks can be produced only under ideal conditions such as high selectivity for non-specific interaction between the solid adsorbent and the adsorbate species, linear adsorption, homogeneous distribution of adsorption sites, particle size and pore size and the absence of diffusional effects [2–4]. Deviations from ideal behaviour have been observed with all the homogeneously macroporous solids, homogeneously microporous solids, inhomogeneously porous

0021-9673/91/$03.50

solids and non-porous solids [5–16]. In GSC the selection of a solid adsorbent is merely based on surface area, thermal stability and pore-size distribution.

Recent studies have shown that some of the heteropoly oxometalates such as ammonium tungstophosphate and ammoniun tungstosilicate are capable of separating lower hydrocarbons and permanent gases [17,18]. Another microporous heteropoly oxometalate, ammonium molybdophosphate, also appears to be a promising solid adsorbent for the separation of lower hydrocarbons and permanent gases. Like ammonium tungstophosphate and ammonium tungstosilicate, ammonium molybdophosphate has a moderately high surface area (>150 m^2/g) and high thermal stability (at least up to 623 K). It is generally prepared by treating an aqueous solution of 12-molybdophosphoric acid with an aqueous solution of an ammonium salt. The structure of ammonium molybdophosphate is very similar to that of ammonium tungstophosphate except that the twelve octahedra which surround the central tetrahedron have molybdenum atoms at the centers.

TABLE I

SORPTION AND DIFFUSION OF ORGANIC COMPOUNDS IN AMMONIUM MOLYBDOPHOSPHATE AT 293 K

Sorbate	Sorption capacity (g/g)	Diffusivity, $D \times 10^{11}$ (cm^2/s)
Alcohols [22]		
Methanol	0.032	4.2
Ethanol	0.035	2.7
1-Propanol	0.041	2.1
1-Butanol	0.043	1.6
2-Methyl-2-butanol	0.039	10.3
1-Hexanol	0.048	0.5
Aromatics [19]		
Benzene	0.036	11.0
Toluene	0.037	6.0
p-Xylene	0.034	3.7
m-Xylene	0.011	1.5
o-Xylene	0.009	1.8
Mesitylene	0.006	0.8
m-Diethylbenzene	0.035	0.5
Saturates [20]		
n-Hexane	0.028	25.0
3-Methylpentane	0.028	23.0
Cyclohexane	0.027	10.0
n-Heptane	0.030	18.0
n-Octane	0.033	12.0
Isooctane	0.031	8.8
Unsaturates [21]		
1-Hexene	0.030	11.0
2,3-Dimethyl-1-butene	0.029	6.6
1-Heptene	0.032	8.5
1-Octene	0.034	3.5
Cyclohexene	0.031	6.0
4-Methyl-1-cyclohexene	0.033	3.9

The sorption on and diffusion in ammonium molybdophosphate of different hydrocarbons and alcohols have already been reported [19–22]. A summary of the sorption capacity and the diffusivity of different hydrocarbons and alcohols on ammonium molybdophosphate is given in Table I. As no information on the use of ammonium molybdophosphate for the separation of lower hydrocarbons and permanent gases is available in the literature, it appeared worth exploring the possibility of using it as an adsorbent in GSC. This paper reports a study of the GSC separation of lower hydrocarbons and permanent gases using ammonium molybdophosphate as solid adsorbent.

EXPERIMENTAL

12-Molybdophosphoric acid (BDH), ammonium chloride (BDH) and all the gases (Matheson) were the highest purity available and were used as received. A stoichiometric amount of ammonium chloride solution was added slowly with constant stirring to 12-molybdophosphoric acid solution. Bright yellow ammonium molybdophosphate crystals were separated by centrifugation, washed with distilled water and dried at 110°C in an air oven for 4 h.

The chromatographic column was prepared as follows. Ammonium molybdophosphate (5 g) was added with stirring to a beaker containing about 50 ml of distilled water and 20 g of acid-washed non-porous glass beads (0.4 mm). The slurry was heated slowly with contant stirring until a dry mass was obtained. The glass bead-supported ammonium molybdophosphate crystals were dried at 100°C in an air oven for 2 h and finally transferred to a stainless-steel column (6 ft. × 1/8 in. O.D.). The separations of lower hydrocarbons and permanent gases were carried out using a Hewlett-Packard gas chromatograph equipped with flame ionization and thermal conductivity detectors. The size and shape of the ammonium molybdophosphate crystals were determined with a JEOL scanning electron microscope.

RESULTS AND DISCUSSION

Like ammonium tungstophosphate and ammonium tungstosilicate, ammonium molybdophosphate seems to be a good adsorbent for the separation of lower hydrocarbons and permanent gases. The order of retention times of lower hydrocarbons and permanent gases appears to be the same on all three adsorbents. With ammonium molybdophosphate highly reproducible retention times and peak-area percentages for different gases were obtained in both isothermal and temperature-programmed runs.

Separation of C_1–C_4 hydrocarbons

The separation of methane, ethane, ethylene, acetylene, propane, propylene and *n*-butane using the ammonium molybdophosphate column (6 ft × 1/8 in. O.D., 20% on non-porous glass beads) in a temperature-programmed run is shown in Fig. 1. The column temperature was initially held at 35°C for 4 min, increased linearly at 10°C/min to 160°C and maintained there for 30 min. Both the peak-area percentages and the retention times of the hydrocarbons showed good reproducibility.

Attempts to use a column filled with ammonium molybdophosphate only for

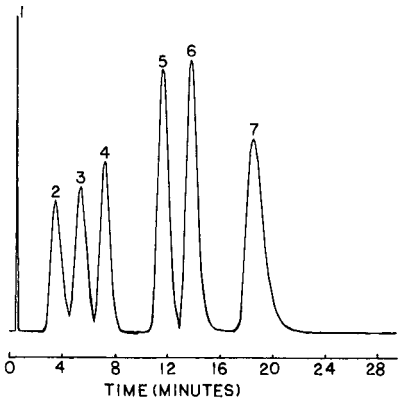

Fig. 1. Chromatogram showing the separation of (1) methane, (2) ethane, (3) ethylene, (4) acetylene, (5) propane, (6) propylene and (7) *n*-butane. Column: 20% ammonium molybdophosphate on glass beads (6 ft. × 1/8 in. O.D.); oven temperature, 35°C for 4 min, then increased at 10°C/min to 160°C, held for 30 min; carrier gas, nitrogen; flow-rate, 8 ml/min; flame ionization detection.

the separation of lower hydrocarbons and permanent gases were unsuccessful as appropriate carrier gas flow-rates could not be maintained owing to a large pressure drop across the column. In order to reduce the pressure drop across the column, non-porous glass beads (0.4 mm) were used as a diluent. Even after loading 20% (w/w) ammonium molybdophosphate, the glass beads still appeared to be free-flowing, indicating that the Van der Waals force of attraction is strong enough to hold the glass beads and the ammonium molybdophosphate crystals together.

The possible contribution of non-porous glass beads to the separation of hydrocarbons was evaluated by injecting the C_1–C_4 mixture into a 6 ft. × 1/8 in. O.D. column filled with non-porous glass beads. It was found that all the constituents of the hydrocarbon mixture eluted together as one sharp peak. The retention time of this

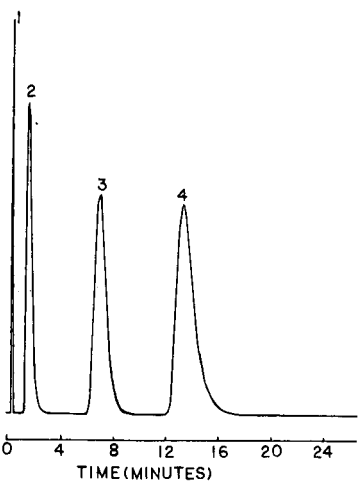

Fig. 2. Chromatogram showing the separation of C_1–C_4 alkanes. Column as in Fig. 1; oven temperature, 50°C for 2 min, then increased at 10°C/min to 160°C, held for 15 min; carrier gas, nitrogen; flow-rate, 15 ml/min; flame ionization detection. Peaks: 1 = methane; 2 = ethane; 3 = propane; 4 = *n*-butane.

TABLE II

RETENTION CHARACTERISTICS OF C_1–C_4 ALKANES OBTAINED IN FIVE SUCCESSIVE TEMPERATURE-PROGRAMMED RUNS WITH A 20% AMMONIUM MOLYBDOPHOSPHATE COLUMN (6 ft. x 1/8 in. O.D.)

Oven temperature, 50°C for 2 min, then increased at 10°C/min to 160°C, maintained for 15 min; carrier gas, nitrogen; flow-rate, 15 ml/min; sample size, 0.05 ml.

Alkane	Mean retention time (s)	Mean peak area (%)	Relative standard deviation of retention time (%)	Relative standard deviation of peak area (%)
Methane	20.76	1.65	2.31	0.85
Ethane	91.32	18.08	1.05	0.77
Propane	417.4	32.52	0.22	0.67
n-Butane	804.5	47.76	0.3	0.73

unresolved peak matched that of methane obtained with the ammonium molybdophosphate column under identical conditions.

Separation of C_1–C_4 alkanes

It appears that the separation of methane, ethane, propane and *n*-butane can be achieved rapidly by using a 20% ammonium molybdophosphate (6 ft. × 1/8 in. O.D.) column. Their baseline separation in a temperature-programmed run is shown in Fig. 2. The column temperature was initially maintained at 50°C for 2 min, then increased at 10°C/min to 160°C and maintained there for 15 min. Both the peak-area percentages and the retention times showed good reproducibility. The retention characteristics of the alkanes obtained with five successive temperature programmed runs are given in Table II.

It appears that the 20% ammonium molybdophosphate column is capable of separating C_1–C_4 alkanes even under isothermal conditions. A representative chromatogram showing baseline separation at 120°C is shown in Fig. 3. The reproducibil-

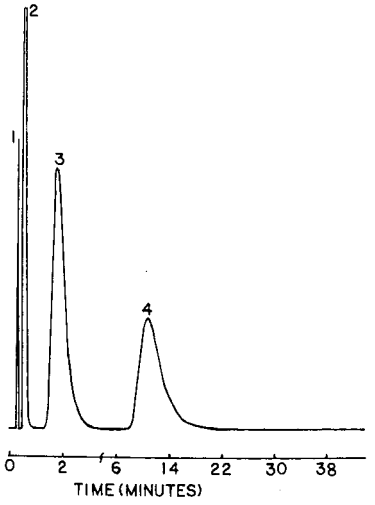

Fig. 3. Chromatogram showing the separation of C_1–C_4 alkanes under isothermal conditions. Conditions as in Fig. 2 except oven temperature (120°C). Peaks as in Fig. 2.

TABLE III

RETENTION CHARACTERISTICS OF C_1–C_4 ALKANES OBTAINED IN FIVE SUCCESSIVE ISOTHERMAL RUNS WITH A 20% AMMONIUM MOLYBDOPHOSPHATE COLUMN (6 ft. x 1/8 in. O.D.)

Oven temperature, 120°C. Carrier gas, nitrogen; flow-rate, 15 ml/min; sample size, 0.05 ml.

Alkane	Mean retention time (s)	Mean peak area (%)	Relative standard deviation of retention time (%)	Relative standard deviation of peak area (%)
Methane	19.32	1.70	1.24	2.54
Ethane	32.52	17.37	0.74	0.99
Propane	108.8	32.46	0.44	0.66
n-Butane	634.0	48.47	0.36	0.86

ity of the peak-area percentages and retention times was good. The retention characteristics obtained in five successive runs are given in Table III.

Separation of permanent gases

Like ammonium tungstophosphate [17] and ammonium tungstosilicate [18], ammonium molybdophosphate seems to be capable of separating permanent gases, with the same order of retention times. The separation of nitrogen, methane and carbon dioxde achieved by using the 20% ammonium molybdophosphate column (6 ft. × 1/8 in. O.D.) is shown in Fig. 4. The order of retention times of C_1–C_2 hydrocarbons observed with the three heteropoly oxometalates, *i.e.*, methane < ethane < ethylene < acetylene, appears to match that observed with SP-1700 or alumina PLOT columns. However with other columns, such as Carbosieve G or S series, the retention times of C_1–C_2 hydrocarbons follow the increasing order of their boiling points, *i.e.*, methane < acetylene < ethylene < ethane.

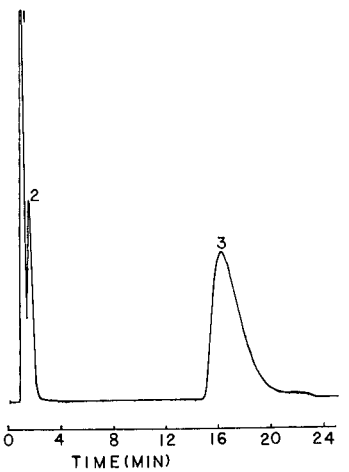

Fig. 4. Separation of permanent gases under isothermal conditions. Column as in Fig. 1. Oven temperature, 25°C; carrier gas, helium; flow-rate, 10 ml/min; thermal conductivity detection. Peaks: 1 = nitrogen; 2 = methane; 3 = carbon dioxide.

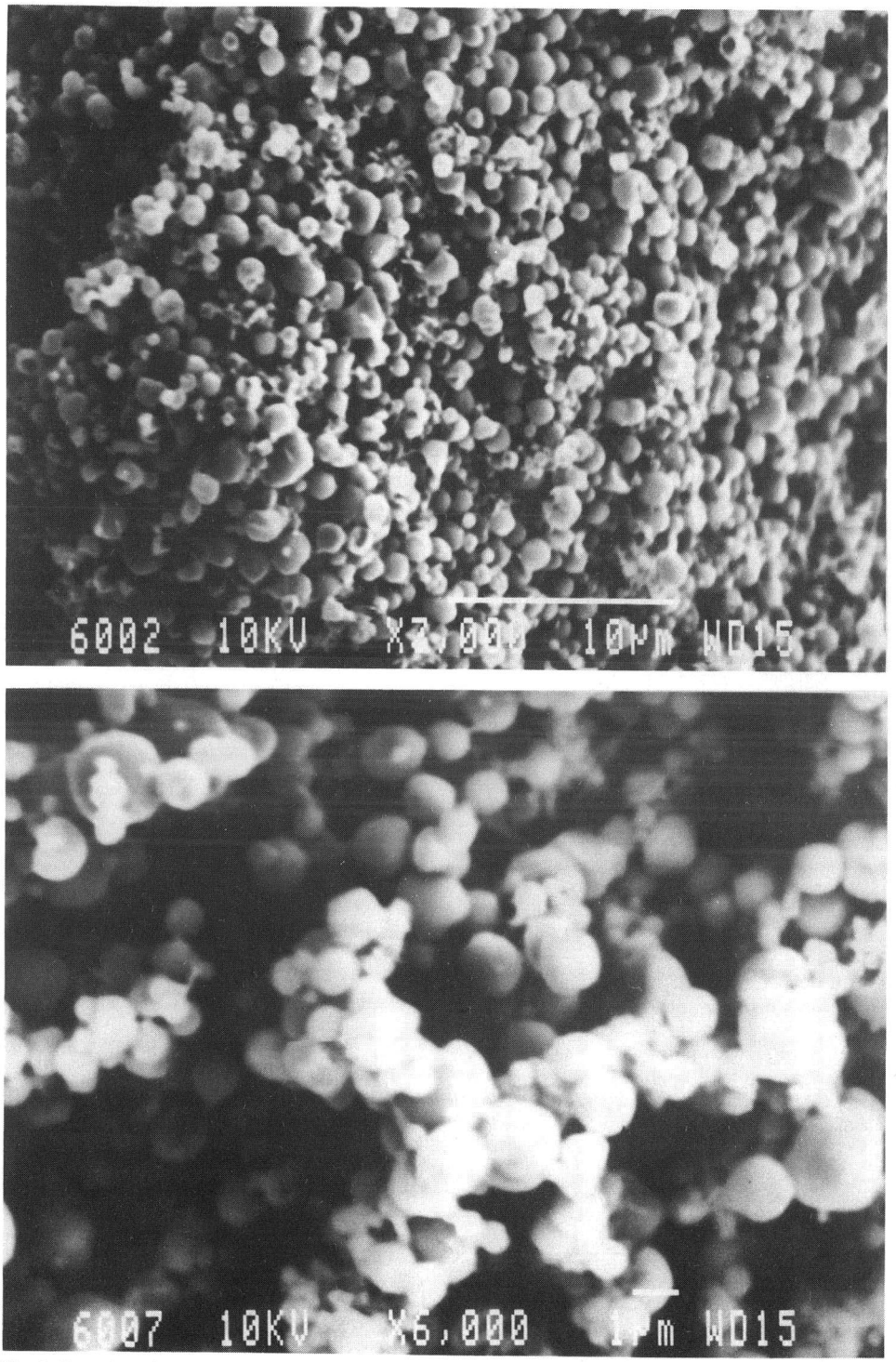

Fig. 5. Scanning electron micrographs of ammonium molybdophosphate.

From the order of retention times of C_1–C_2 hydrocarbons it can be said that the interaction between the heteropoly oxometalates and the adsorbates is specific in nature. The elution peaks of lower hydrocarbons obtained with the 20% ammonium molybdophosphate column are fairly sharp and symmetrical and have a quasi-Guassian shape. The elution of quasi-Guassian-shaped peaks is an indication that the distribution of adsorption sites on ammonium molybdophosphate is homogeneous, the adsorption is linear, the interaction of ammonium molybdophosphate with the lower hydrocarbons is weak and diffusional phenomena are negligibly small. In GSC, as it is almost impossible to eliminate completely the effects of diffusional phenomena, broadening of elution peaks, at least to some extent, is expected. Like other solid adsorbents which are used in GSC, ammonium molybdophosphate appears to contain a small number of smaller and larger crystals (Fig. 5). The observed slight broadening of the elution peaks can be attributed mainly to the diffusional effects due to the particle-size distribution.

REFERENCES

1 M. J. Golay, *US Pat.*, 920 478 (1960).
2 H. C. Thomas, *Ann. N.Y. Acad. Sci.*, 49 (1948) 161.
3 D. White and C. T. Cowan, in D. H. Desty (Editor), *Gas Chromatography 1958*, Butterworths, London, 1958, p. 116.
4 J. C. Giddings, *Anal. Chem.*, 36 (1964) 1170.
5 A. V. Kiselev and Y. I. Yashin, *Gas-Adsorption Chromatography*, Plenum Press, New York, London, 1969.
6 E. Cremer, *Angew. Chem.*, 72 (1959) 512.
7 A. V. Kiselev, E. A. Paskonova, R. S. Petrova and K. D. Shcherbakova, *Zh. Fiz. Khim.*, 38 (1964) 161.
8 S. Ross, J. K. Saelens and J. P. Olivier, *J. Phys. Chem.*, 66 (1962) 696.
9 A. V. Kiselev, in D. H. Everett and F. Stone (Editors), *The Structure and Properties of Porous Materials*, Butterworths, London, 1958, p. 195.
10 M. M. Dubinin, in P. L. Walker (Editor), *Chemistry and Physics of Carbon*, Marcel Dekker, New York, 1966, p. 51.
11 J. R. Dacey and J. A. Fendley, in D. H. Everett and F. Stone (Editors), *The Structure and Properties of Porous Materials*, Butterworths, London, 1958, p. 142.
12 R. M. Barrer, in D. H. Everett and F. Stone (Editors), *The Structure and Properties of Porous Materials*, Butterworths, London, 1958, p. 6.
13 R. M. Barrer, in L. Dondelcorn (Editor), *Non-Stoichiometric Compounds*, Academic Press, New York, 1963, p. 309.
14 A. V. Kiselev and A. A. Lopatkin, *Kinet. Katal.*, 4 (1963) 786.
15 G. T. Minkoff and R. H. E. Duffett, *Br. Pet. Mag.*, No. 13 (1964) 16.
16 A. V. Kiselev, *Dokl. Akad. Nauk SSSR*, 98 (1954) 431.
17 V. S. Nayak, *J. Chromatogr.*, 498 (1990) 349.
18 V. S. Nayak and R. N. Pandey, *J. Chromatogr. Sci.*, 28 (1990) 617.
19 V. S. Nayak and J. B. Moffat, *J. Colloid Interface Sci.*, 120 (1987) 301.
20 V. S. Nayak and J. B. Moffat, *J. Colloid Interface Sci.*, 122 (1988) 475.
21 V. S. Nayak and J. B. Moffat, *J. Phys. Chem.*, 92 (1988) 2256.
22 V. S. Nayak and J. B. Moffat, *J. Phys. Chem.*, 92 (1988) 7097.

Journal of Chromatography, 556 (1991) 433–440
Elsevier Science Publishers B.V., Amsterdam

CHROM. 23 294

Dynamic gas–solid chromatographic techniques for characterizing carbon molecular sieves

W. R. BETZ* and S. J. LAMBIASE
Supelco Inc., Supelco Park, Bellefonte, PA 16823-0048 (USA)

ABSTRACT

Gas–solid chromatography (GSC) was used for the evaluation of carbon molecular sieves and provided an insight into their kinetic and thermodynamic properties in both column chromatography and sample enrichment studies. GSC studies of the column chromatographic performance characteristics of these sieves allowed the derivation, from Van Deemter plots, of permeability, capacity ratio, HETP and *C*-term values. Both conventional (4 and 2 mm I.D.) and micropacked (0.75 mm I.D.) GSC columns were evaluated. GSC studies of the sample enrichment performance characteristics of these sieves allowed the derivation of adsorbate breakthrough volumes, adsorption isotherms and equations of state. Using probe molecules such as dichloromethane, various adsorbent surface areas were extracted from the isotherm plots. Both conventional and micro-packed GSC columns were evaluated.

INTRODUCTION

In the early 1950s, gas–solid chromatography (GSC) evolved as an analytical separation tool in addition to a method for characterizing solid supports [1,2]. The physico-chemical measurements obtained by GSC described both the kinetic and thermodynamic processes occurring at the adsorbate/adsorbent interface, and remain viable measurements for understanding these phenomena. Since then, considerable attention has been given to the development of adsorbents with physico-chemical properties [3] that facilitate the separation of complex mixtures by GSC, and with adsorption–desorption properties effective for sample enrichment purposes. Considerable attention was also given to the characterization of the kinetic and thermodynamic properties of these porous solids in chromatographic systems. These investigations provided valuable insights into the technique of GSC, which still remain useful [4]. The porous solids typically used in the fields of GSC and sample enrichment were, and remain, activated charcoals, activated silica gels, porous polymers, zeolites, carbon molecular sieves and graphitized carbon blacks.

The use of GSC for characterizing adsorbents, as described here, evolved over a 6-year period. This study began by using 4 mm I.D. GC columns designed to emulate adsorbent tubes [5], progressed to 2 mm I.D. columns [6] and ultimately led to the use of 0.75 mm I.D. micropacked columns. The use of these micropacked columns for

0021-9673/91/$03.50

determining the kinetic and thermodynamic interactions occurring between the adsorbate and adsorbent surfaces is the basis for this study.

EXPERIMENTAL

Gas–solid kinetic study

Chromatographic columns were prepared using standard column packing techniques [7]. Silanized glass columns (2 m × 0.25 in. O.D.), of both 2.0 and 0.75 mm I.D., were chosen. They were packed with the same carbon molecular sieve, Carboxen-1000 (Supelco), with 20–45, 45–60, 60–80 and 80–100 mesh particle size distributions. The columns were installed in a Varian Model 3700 gas chromatograph equipped with a thermal conductivity detector. Kinetic information was extracted from the Van Deemter plots for carbon dioxide (125°C) and ethane (225°C), using getted helium as the carrier gas. A Spectra-Physics Model 4270 integrator was used to determine adsorbate retention data, and a Macintosh II personal computer was used to generate the plots. Chromatographic profiles were obtained with a Houston Instruments strip-chart recorder.

Adsorption isotherm study

These columns were also prepared using standard column packing techniques. Silanized glass columns (1 ft. × 0.25 in. O.D.) of 0.75 mm I.D. were packed with 10.0 mg of each of the eight chosen adsorbents (see Table II). The particle size distribution was 60–80 or 80–100 mesh, depending on the availability of the smaller fraction. The columns were installed in a Varian Model 3700 gas chromatograph equipped with a flame ionization detector. Adsorption isotherm data for the chosen adsorbate, dichloromethane, were determined at 80°C using the peak maxima elution method [8,9]. Peak-height and peak-area data were obtained using a Spectra-Physics Model 4270 integrator. Detector linearity was determined for an adsorbate concentration range chosen to obtain $p/p_0 = 1$ values. Adsorption isotherm plots were generated with a Macintosh II personal computer and chromatographic profiles were obtained with a Houston Instruments strip-chart recorder.

RESULTS AND DISCUSSION

Gas–solid kinetic study

The data obtained from the kinetic study of Carboxen 1000, using columns of 2.0 and 0.75 mm I.D. packed with different particle size distributions of the same spherical carbon molecular sieve, are presented in Table I. These data, extracted from the Van Deemter plots [10], represent an improvement in chromatographic performance over sieves previously prepared and evaluated in this laboratory, hence this material was chosen as the example discussed here. The Van Deemter plots obtained for carbon dioxide and ethane are illustrated in Figs. 1 and 2, respectively (the plot for ethane with the 20–45 mesh fraction, with HETP values of 4.04–13.3 mm, was omitted from Fig. 2 so the ordinate scale could be expanded in the region of values between 0 and 4). The HETP values of 0.76 (CO_2) and 0.72 (C_2H_6) for the 80–100 mesh (0.149–0.177 mm) sieve packed in 0.75 mm I.D. columns indicate optimum efficiency for this work. This level of efficiency is accompanied by a decrease in the k'

TABLE I

PARAMETERS FOR CARBON MOLECULAR SIEVE (CARBOXEN-1000) COLUMN KINETICS-STUDY

Parameter	Values					
Column length (m)	2.0	2.0	2.0	2.0	2.0	2.0
d_c (mm)	2.0	2.0	2.0	2.0	0.75	0.75
d_p (mesh)	80–100	60–80	45–60	20–45	80–100	60–80
d_p/d_c	0.08	0.11	0.15	0.30	0.22	0.28
HETP (mm) (CO_2)	0.80	1.21	1.41	3.80	0.76	1.93
HETP (mm) (C_2H_6)	0.80	1.23	1.42	4.04	0.72	1.77
k' (CO_2)	22.6	11.6	11.0	6.0	20.2	10.7
k' (C_2H_6)	23.7	15.2	13.2	5.9	21.1	11.7
n (CO_2)	2500	1658	1418	526	2635	1036
n (C_2H_6)	2500	1626	1408	495	2778	1130
μ (cm/s) (CO_2)	18.9	11.4	11.4	3.79	22.7	18.9
μ (cm/s) (C_2H_6)	18.9	18.9	15.2	3.79	18.9	18.9
C ($s \times 10^{-4}$) (CO_2)	5.34	16.5	32.5	295	5.90	18.9
C ($s \times 10^{-4}$) (C_2H_6)	7.80	16.0	23.5	270	4.80	15.5
K ($cm^2 \times 10^{-7}$) (CO_2)	1.42	3.12	3.72	25.1	1.53	4.84
K ($cm^2 \times 10^{-7}$) (C_2H_6)	1.46	3.38	3.28	29.3	1.36	4.36

values for both adsorbates, hence shorter analysis times without a decrease in efficiency are expected with the micropacked columns. A decrease in efficiency is seen with an increase in particle size, hence HETP values are dependent on both column diameter and sieve particle size. This trend is in good agreement with previous studies [11,12]. Fig. 3 illustrates a reduction in analysis time without a decrease in efficiency

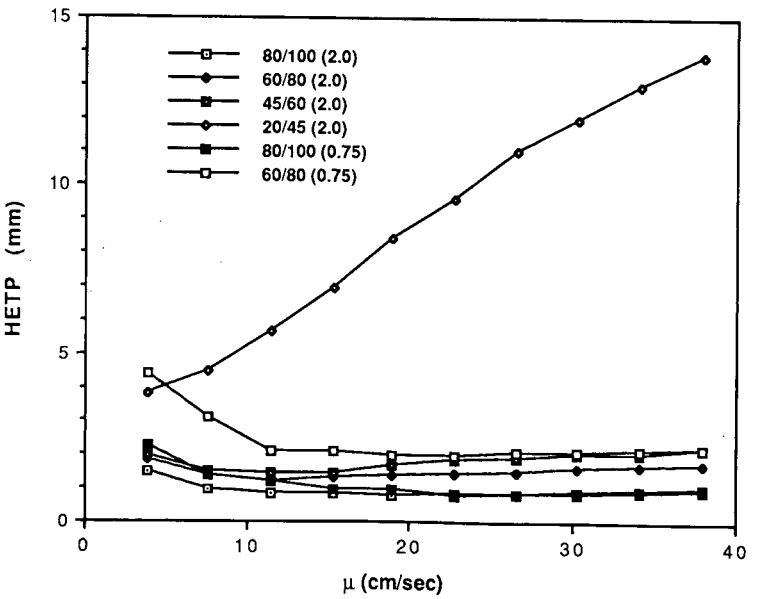

Fig. 1. Van Deemter plots for carbon dioxide with Carboxen 1000. Sieve mesh size and (in parentheses) column I.D. (mm) are given.

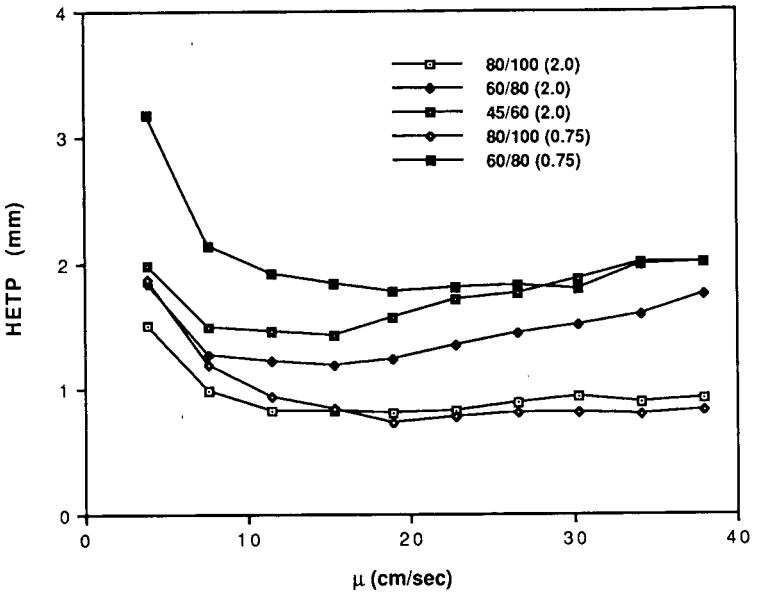

Fig. 2. Van Deemter plots for ethane with Carboxen 1000. Sieve mesh size and (in parentheses) column I.D. (mm) are given.

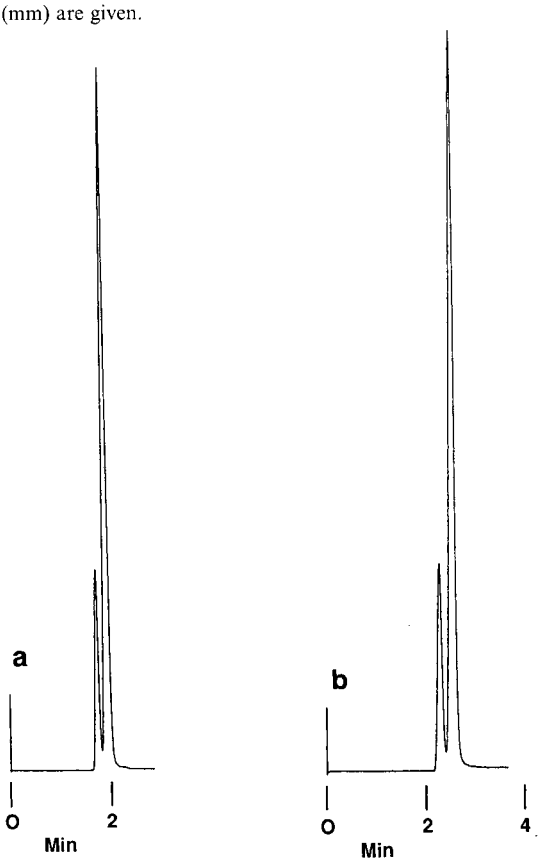

Fig. 3. Reduced analysis time without a decrease in efficiency for chromatographic analysis of oxygen and nitrogen with (a) a 0.75 mm I.D. column *versus* (b) a 2.0 mm I.D. column packed with 80–100 mesh Carboxen 1000. Oxygen is first peak eluted.

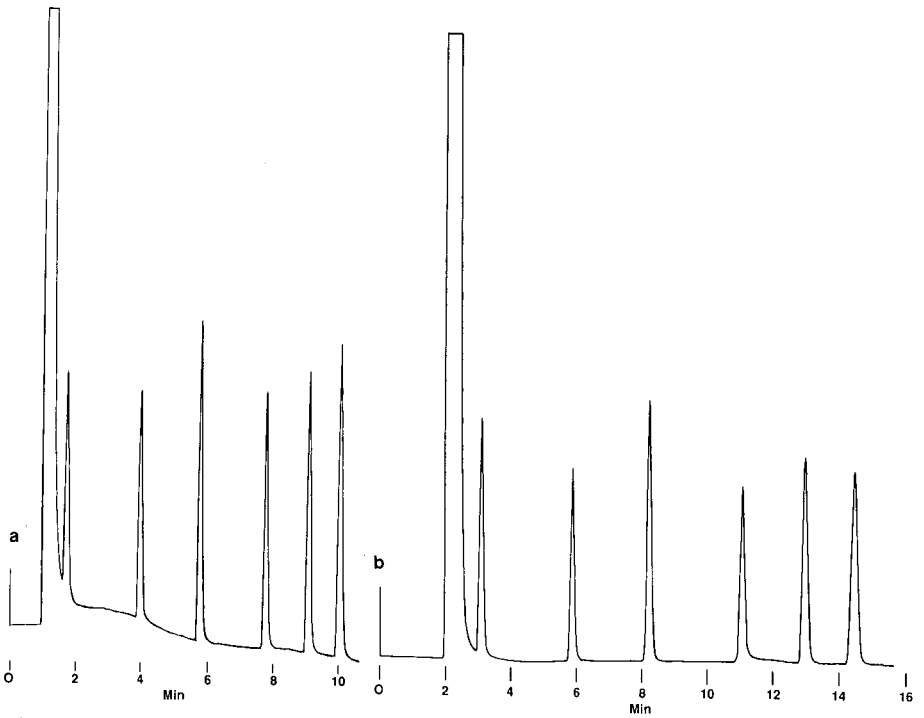

Fig. 4. Separation of permanent gases and light hydrocarbons with (a) a 0.75 mm I.D. column and (b) a 2.0 mm I.D. column. GC oven temperature: 35°C for 1 min, then increased to 225°C at 16°C/min. Peak identification (left to right): nitrogen (large), carbon monoxide, methane, carbon dioxide, acetylene, ethylene, ethane.

for the separation of oxygen and nitrogen with a 0.75 mm I.D. column at 35°C. This trend also exists for a wide temperature range, such as the 35–225°C range used to separate some permanent gases and light hydrocarbons (Fig. 4).

A comparison of the *C*-terms obtained for ethane indicates that no significant decrease in efficiency is expected when using increased linear velocities with the 0.75 mm I.D. column, hence a higher linear velocity was chosen for the micropacked column in Fig. 4 (25.6 cm/s, *versus* 18.9 cm/s for the 2.0 mm I.D. column). Also, the p_1 values were similar for both column I.D.s with the 80–100 mesh sieve throughout the temperature range studied (32 p.s.i.g. at 35°C and 52 p.s.i.g. at 225°C, at 18.9 cm/s). These ranges of particle size distributions and pressures allow for the use of micropacked columns possessing similar physical characteristics under normal packed column GC pressure conditions.

The permeability (K_{exp}; Darcy equation [12]) data indicate a decrease in permeability with an increase in column diameter, and a decrease in K_{exp} with decreasing particle diameter for a fixed column diameter. These trends are in agreement with previous studies [4,12]. K_{exp} values and K values were also in good agreement when using the Kozeny–Carman [13] equation. Permeability also decreases with a decrease in the d_p/d_c ratio, and is optimum at a ratio between 0.20 and 0.25 [12]. This optimum is exemplified by an increase in the permeability values for ethane, relative to values

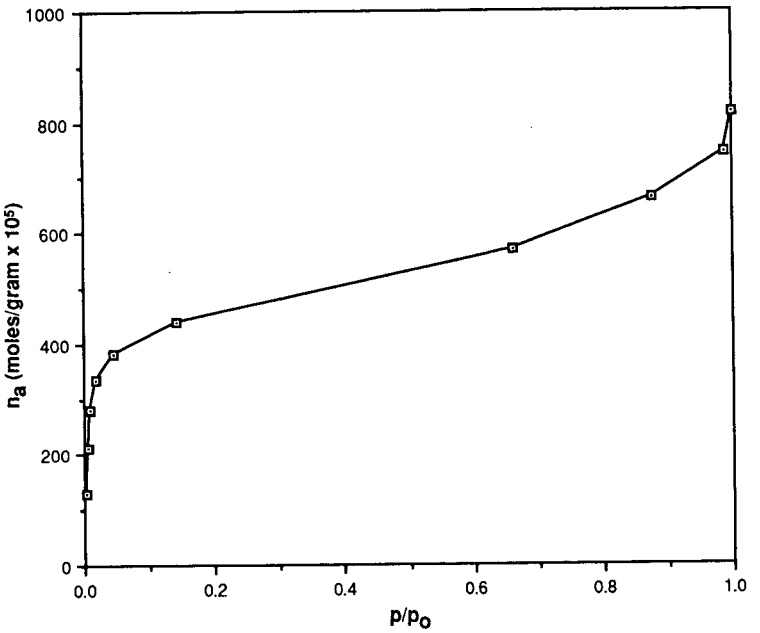

Fig. 5. Adsorption isotherm for dichloromethane with Carboxen 1000. Injection volumes: 0.1–5.0 μl.

for carbon dioxide, when the d_p/d_c values are outside the experimental range of 0.15–0.28. Typically, a decrease would be expected as the adsorbate molecular size is increased.

Adsorption isotherm study

Previous work with 2.0 mm I.D. columns [6] provided effective characterization of non-porous solids such as graphitized carbon blacks [14]. The large internal surface areas characteristic of the carbon sieve adsorbents were more readily characterized with the 0.75 mm I.D. columns. The adsorption isotherms generated for the eight carbon adsorbents are indicative of Type IV isotherms [15] (Fig. 5). The choice of a 1 ft. (0.3 m) × 0.75 mm I.D. column packed with 10.0 mg of the adsorbent allowed

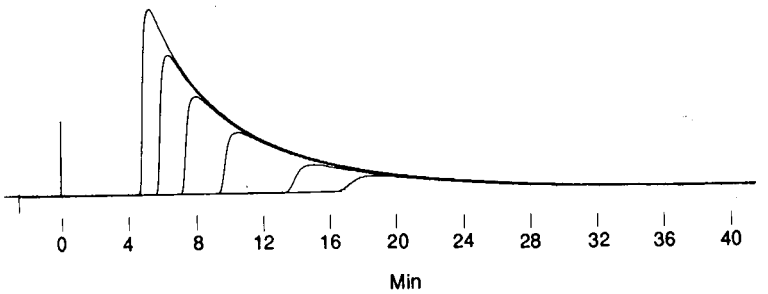

Fig. 6. Chromatographic profile for dichloromethane with Carboxen 569. Injection volumes: 0.2–1.2 μl.

TABLE II
BREAKTHROUGH VOLUMES AND SURFACE AREAS FOR CARBON-BASED ADSORBENTS

Adsorbent	BTV [16] (l)	Surface area (m^2/g)	
		CH_2Cl_2	N_2
Carbosieve S-III	66.2	697	820
Carboxen 569	43.2	466	485
Activated charcoal	39.2	526	1070
Carbosieve S-II	31.5	506	1060
Carboxen 564	31.5	380	400
Purasieve	5.05	364	950
Carboxen 563	1.56	291	510
Spherocarb	1.05	291	880

sufficient internal column pressures to be applied so that $p/p_0 = 1$ values could be achieved with reasonable sample sizes (< 80 μmol).

Detector linearity for a halogenated molecule such as dichloromethane also was considered when choosing the column I.D. Fig. 6 illustrates the chromatographic behavior of dichloromethane with a porous carbon sieve which possesses a large microporous region and sufficient mesoporous/macroporous regions to access the micropores. This chromatographic behaviour justifies the use of GSC for the determination of adsorption isotherms. The Type IV isotherm is similar to Type II [15] isotherms in its characteristic shape. Multiple adsorbate layers are absent in the mesoporous and macroporous regions, however, and therefore pressure unity can be readily achieved.

The lack of correlation between nitrogen surface area data and the breakthrough volume (BTV) data [16] (Table II) led to the generation of these isotherm data at 80°C. The BTV data were obtained at infinite dilution (*i.e.*, the extreme lower end of the Henry's Law region) and thus represent a migration volume rather than a saturation, or capacity, volume. This region of adsorbate coverage is applicable to sample enrichment modes, for which trace level analyses are required (*i.e.*, ambient air monitoring). Alternatively, the data obtained from static nitrogen surface area measurements represent microporous volume data rather than microporous surface area data, and may, therefore, be limited in the assistance provided when examining various adsorbent strengths. Typically, a large micropore diameter (*i.e.*, 10–20 Å) allows for effective sieve kinetics with subsequent diminished adsorption strength. These large diameters, however, provide large micropore volume values (*i.e.*, overestimates of micropore surface area) when the data are obtained via static nitrogen measurements. Correspondingly, surface area data generated by this dynamic GSC technique at the boiling points of the adsorbate probe molecules (40.7°C for dichloromethane) also provided micropore volume data which do not correlate well with the BTV values desired for trace level sample enrichment. Construction of BET plots [15] extracted from the lower end of the Henry's law region using a GSC column temperature of 80°C, however, allowed for an understanding of the sieve microporous surface area that the dichloromethane probe molecules actually encounter in this region. The surface area data obtained using this approach indicate a correlation between the BTV values and the dichloromethane surface area data.

CONCLUSION

The dynamic technique of GSC has assisted in understanding the physicochemical characteristics of several carbon molecular sieves. The use of micropacked columns has led to an improved understanding of the kinetic and thermodynamic properties of these sieves functioning for the separation of permanent gases and light hydrocarbons. GSC has also assisted in providing an insight into the use of sieve surface area for molecules, other than nitrogen, typically encountered in sample enrichment studies.

REFERENCES

1 J. R. Conder and C. L. Young, *Physicochemical Measurements by Gas Chromatography*, Wiley, New York, 1979.
2 R. J. Laub and R. L. Pecsok, *Physicochemical Applications of Gas Chromatography*, Wiley, New York, 1978.
3 A. V. Kiselev and Y. I. Yashin, *Gas Adsorption Chromatography*, Plenum Press, New York, 1969.
4 G. Guiochon, *Adv. Chromatogr.*, 8 (1969) 179.
5 W. R. Betz and W. R. Supina, *Pure Appl. Chem.*, 61 (1989) 2047.
6 W. R. Betz and W. R. Supina, *J. Chromatogr.*, 471 (1989) 105.
7 C. F. Poole and S. A. Schuette (Editors), *Contemporary Practice of Chromatography*, Elsevier, New York, 1984.
8 J. F. K. Huber and R. G. Gerritse, *J. Chromatogr.*, 58 (1971) 137.
9 M. Domingo-García, F. J. López-Garzón, R. López-Garzón and C. Moreno-Castilla, *J. Chromatogr.*, 324 (1985) 19.
10 J. J. van Deemter, F. J. Zuiderweg and A. Klinkenberg, *Chem. Eng. Sci.*, 5 (1956) 271.
11 T. Welsch, W. Engelwald and J. Poerschmann, *J. Chromatogr.*, 148 (1978) 143.
12 J. A. Rijks, C. A. Cramers and P. Bocek, *Chromatographia*, 8 (1975) 482.
13 I. Halasz and E. Heine, *Adv. Chromatogr.*, 4 (1967) 207.
14 F. Bruner, P. Ciccioli, G. Crescentini and M. T. Pistolesi, *Anal. Chem.*, 45 (1973) 1851.
15 S. J. Gregg and K. S. W. Sing, *Adsorption, Surface Area and Porosity*, Academic Press, New York, 1982.
16 W. R. Betz, S. G. Maroldo, G. D. Wachob and M. C. Firth, *Am. Ind. Hyg. Assoc. J.*, 50 (1989) 181.

Journal of Chromatography, 556 (1991) 441–456
Elsevier Science Publishers B.V., Amsterdam

CHROM. 23 288

Chromatographic determination of the physico-chemical parameters of adsorption on active carbons

ZYGFRYD WITKIEWICZ*, HENRYK GRAJEK and JERZY CHOMA
Institute of Chemistry, Military Technical Academy, 01-489 Warsaw 49 (Poland)

ABSTRACT

The adsorption isotherms of several polar and non-polar compounds on active carbons with modified surfaces were determined chromatographically at different temperatures. The results were compared with those obtained by the static method. The entropies and heats of adsorption were calculated from the adsorption isotherms and compared with the values obtained from calorimetric measurements. The results were closest for adsorbents with a weakly developed microporous structure. The effect of the carrier gas flow-rate through the adsorbent bed in the column on the shape of the chromatographically determined adsorption isotherm was tested. The linear forms of equations corresponding to the BET, Hüttig, Kiselev and Hill physical adsorption models were used. The adsorption isotherms of aliphatic alcohols chromatographically were best described in terms of the Hill model.

INTRODUCTION

In recent years, a good knowledge of the processes taking place on the phase boundary has become very important. The most important of these processes include, for both practical and theoretical reasons, primarily adsorption and heterogeneous catalysis [1]. The explanation of processes proceeding on the surfaces of adsorbents and catalysts requires the determination of their surface area and porous structure, in addition to the adsorption isotherms and thermodynamic functions. For this purpose common and widely used static methods are applied. These methods are fairly accurate but time consuming.

A more rapid method of testing adsorbents and catalysts is afforded by adsorption gas chromatography [2,3]. The possibility of applying it in physico-chemical investigations follows from the fact that chromatographic separation is related to the properties and physico-chemical interactions of the column filling (*e.g.*, adsorbent or catalyst) with the chromatographed substances. The carrier gas also has some influence, but its effect is minor so in practice the course of the chromatographic process depends predominantly on the properties of the adsorbent and the chromatographed substance (adsorbate). The properties of the adsorbate–absorbent system can be characterized by adsorption isotherms. The latter can be determined chromatographically and from them the basic physico-chemical quantities characterizing the adsorbent can be found. The chromatographic method supplements the static proce-

0021-9673/91/$03.50

dures which are fundamental for studying the adsorption mechanism, and the adsorbate–adsorbent as well as the competetive adsorbate–adsorbate interactions. Chromatography allows adsorption to be studied at very small coverages of the surface and at elevated temperatures. Static measurements are very difficult and in some instances impossible under these conditions.

In the literature one can find many examples showing that the chromatographic method is useful in investigations of adsorption. However, there are still doubts, mainly as to the range of its application and the related reliability of the results obtained. It was therefore decided that a systematic study of the usefulness of the chromatographic method for investigating carbon adsorbents, with surfaces modified by superficial oxidation, deposition of transition metal cations and silanization, using different adsorbents was necessary.

The chromatographically determined adsorption isotherms were used to test the suitability of equations corresponding to the models of physical adsorption on homogeneous surfaces for interpreting the adsorbate–adsorbent and adsorbate–adsorbate interactions on the surfaces of several active carbons. The results obtained by adsorption gas chromatography are compared with those obtained by static methods.

EXPERIMENTAL

Adsorbents

The following carbon adsorbents were used in the study: active carbon, obtained by the steam-gas method from hard coal, and denoted A-2, and its modifications obtained by mild oxidation in aqueous nitric acid by the method of Rychlicki [4] (denoted A-2o), by deposition of copper and chromium salts by the Alves and Clark method [5] and by silanization with trimethylchlorosilane (TMCS) by the Wójcik and Karpiński method [6] (denoted S1–S6); and active carbon SKS-2, obtained from commercial porous styrene–divinylbenzene copolymers in the form of spherical particles (supplied by the Institute of General and Inorganic Chemistry, Kiev, USSR).

The active carbons and their modifications were fractionated and degassed in a vacuum drier at 453 K and 1.5–2.5 kN m^{-2} for 10 h. For adsorbents A-2, A-2o and S1–S6 the 0.250–0.300 mm fraction and for SKS-2 the 0.250–0.315 mm fraction was used.

In order to characterize the adsorbents, their apparent and real densities were measured, using toluene as the pycnometric liquid, and the volumes of the micropores and mesopores and the constants in the two-term Dubinin–Radushkevich (DR) equation [7,8] were calculated from the isotherms benzene vapour adsorption determined at 293 K after degassing at $1.33 \cdot 10^{-3}$ N m^{-2}. The characteristics of the tested adsorbents are given in Table I.

Chromatographic measurements

The chromatographic investigations were carried out using a Mera-Elwro 504 gas chromatograph with a thermal conductivity detector. The adsorbents were placed in glass columns (65 cm × 2 mm I.D.) with an absorbent bed length of 8–15 cm, which corresponded to 0.12–0.35 g depending on the kind of active carbon used. The part of the column that was not occupied by the adsorbent was filled with glass beads

TABLE I

CHARACTERISTICS OF THE PORE STRUCTURE OF THE ADSORBENTS USED

Parameter	A-2	A-2o	Amount of catalyst on support A-2o (%)						SKS-2
			0.99 Cr(VI): S1	2.00 Cr(VI): S2	2.69 Cr(VI): S3	4.27 Cu(II): S4	2.00 Cr(VI), 6.44 Cu(II): S5	2.00 Cr(VI), 6.44 Cu(II), TMCS: S6	
Apparent density, d_{app} (g dm^{-3})	1.015	1.150	1.020	1.100	1.140	1.010	0.995	1.055	0.800
Solid density, d_{real} (g dm^{-3})	1.600	1.700	1.620	1.640	1.700	1.650	1.680	1.780	1.680
Volume of micropores, V_{mi} (cm^3 g^{-1})	0.306	0.284	0.280	0.276	0.268	0.240	0.218	0.200	0.399
Volume of mesopores, V_{me} (cm^3 g^{-1})	0.235	0.231	0.235	0.214	0.217	0.170	0.157	0.130	0.322
$\frac{100V_{mi}}{V_{mi}+V_{me}}$ (%)	55.67	55.18	54.36	56.33	55.26	58.54	58.13	60.61	64.25
Constants of the Dubinin–Radushkevich equation:									
W_{o1} (cm^3 g^{-1})	0.151	0.192	0.152	0.155	0.157	0.155	0.162	0.166	0.220
W_{o2} (cm^3 g^{-1})	0.182	0.126	0.122	0.118	0.115	0.097	0.078	0.070	0.182
$B_1 \cdot 10^6$ (K^{-2})	0.460	0.580	0.480	0.520	0.550	0.580	0.630	0.650	0.630
$B_2 \cdot 10^6$ (K^{-2})	2.310	2.510	2.420	2.480	2.450	2.490	2.520	2.580	2.600

of the same mesh size [9]. The packed column was mounted in the chromatograph thermostat and heated for 8 h at 453 K in stream of argon at a flow-rate of 50 cm^3 min^{-1}.

The following adsorbates were used in the tests: benzene and cyclohexane (pure for chromatography) and methanol, ethanol and *n*-propanol (analytical-reagent grade). The purities were additionnally checked chromatographically in a capillary column filled with a liquid crystal stattionary phase.

The adsorbates were injected into the column by means of a Hamilton microsyringe. The amount of sample introduced depended on the method used to determine the isotherm. Two procedures were used for this purpose: determination from the peak maximum and determination from the peak profile [2]. In the first procedure different amounts of the adsorbates ranging from 3 to 50 μl were injected. In the second procedure the size of the sample was 30–50 μl or 12 μl. When larger amounts of the adsorbates were injected it was possible to determine the isotherms up to a relative pressure of about 0.3. With smaller samples a more accurate determination of the initial section of the isotherm was possible up to a relative pressure of about 0.1.

The adsorption isotherms were determined at 298 K and in the range from 373–423 K in 10 K steps at carrier gas flow-rates (measured by means of a bubble gauge) ranging from 30 to 70 cm^3 min^{-1} in 10 cm^3 min^{-1} steps. The temperature of the injection device and of the detector was 473 K. The fluctuations of the thermostat temperature, as measured by means of Anschütz thermometers, did not exceed 0.1 K.

In the determination of the isotherms, the carrier gases used, purified and dried

on Carbosorbit N active carbon and on molecular sieves 5A, were argon, helium and hydrogen. When helium or hydrogen was used, after the initial heat treatment of the carbon in a stream of argon the latter was replaced with helium or hydrogen and the selected gas was passed through the column for at least 2 h before starting the measurements.

The pressures (p) and the corresponding adsorption values (a) were calculated from the following equations:

$$p = \frac{m_a q R T_c h}{S_{peak} v_0} \tag{1}$$

$$a = \frac{m_a S_{ads}}{m S_{peak}} \tag{2}$$

where

m_a = amount of the adsorbate injected (mmol); m = mass of adsorbent in the column (g); v_o = reduced carrier gas flow-rate ($cm^3\ min^{-1}$);

$$v_0 = \frac{v T_c (p_0 - p_{H_2O})}{T_0 p_0} \cdot \frac{3\left(\frac{p_i}{p_o}\right)^2 - 1}{2\left(\frac{p_i}{p_o}\right)^3 - 1};$$

v = carrier gas flow-rate at the column temperature, as measured in the flow meter at ambient temperature ($cm^3\ min^{-1}$); q = speed of the recording paper ($cm\ min^{-1}$); R = universal gas constant; T_c = temperature of the column (K); T_o = temperature of the environment (K); p_i = pressure at the column inlet ($kN\ m^{-2}$); p_o = pressure at the column outlet ($kN\ m^{-2}$); h = height of the peak (cm); p_{H_2O} = pressure of water vapour at the temperature of the environment ($kN\ m^{-2}$); S_{peak} = total surface area of the peak (cm^2).

When the isotherms were determined from the peak maximum, the quantity S_{ads} corresponded to the adsorption surface area (in cm^2) of the adsorbate sample treated. When the peak profile method was used, the quantity S_{ads} was found by dividing the adsorption surface area into n parts.

The peaks obtained were unsymmetrical for all the adsorption systems. This points to the dominating effect of diffusion on the rate of establishment of adsorption equilibrium. Therefore, in both methods of calculating the adsorption isotherms account was taken of the effect of diffusion of the adsorbate in the carbon bed on adsorption according to Dollimore *et al.* [10].

Calorimetric measurements

The differential molar heat of adsorption of methanol was measured by means of a conductance calorimeter of the Tiana–Calve type [11], the dosing system of which permitted the measurement of the amount of adsorbate by the volumetric method with an accuracy of 0.1 μmol. The minimum heat effect per unit recorder paper surface area at a paper speed of $8.33 \cdot 10^{-5}\ ms^{-1}$ was $32.8 \cdot 10^{-1}$ J.

RESULTS AND DISCUSSION

In Fig. 1 the adsorption isotherms for benzene vapour determined at 373 K by the static method (involving calorimetric determination of the differential molar heat of adsorption) are compared with those found chromatographically from the peak profile with the use of argon, helium and hydrogen as the carrier gas for the adsorbents S5 and SKS-2. Fig. 1 indicates that the chromatographic measurements yield lower adsorption values than the static method. The differences in adsorption increase with increase in the micropore volume (at a relative pressure of 0.002 this difference amounts to 0.18 and 0.36 mmol g^{-1} for sorbent S5 and carbon SKS-2, respectively).

The results of chromatographic measurements of adsorption were closest to those obtained by the static method when hydrogen was used as the carrier gas. Lower adsorption values were obtained when helium was the carrier gas and the lowest values when argon was used. This is probably due to the fact that the adsorption of hydrogen is the poorest and that this gas penetrates better the adsorbent bed in the column, which renders the transport of the adsorbate molecules to the

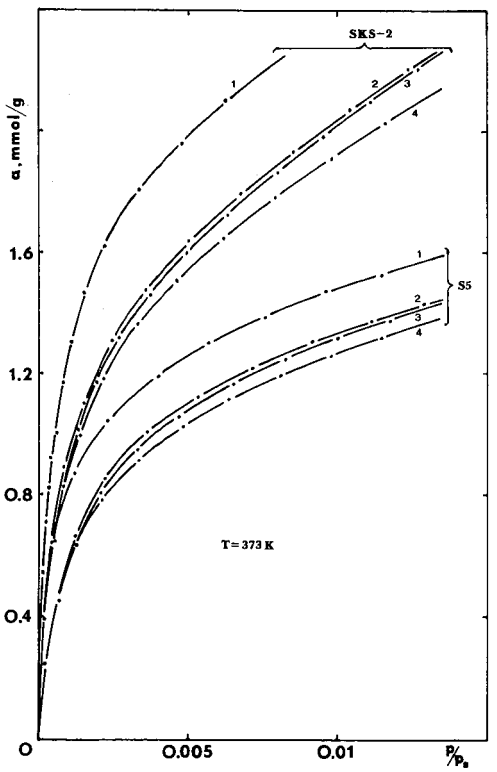

Fig. 1. Adsorption isotherms of benzene determined at 373 K (1) statically and chromatographically by the peak profile method using (2) hydrogen, (3) helium and (4) argon as the carrier gas on adsorbents S5 and SKS-2.

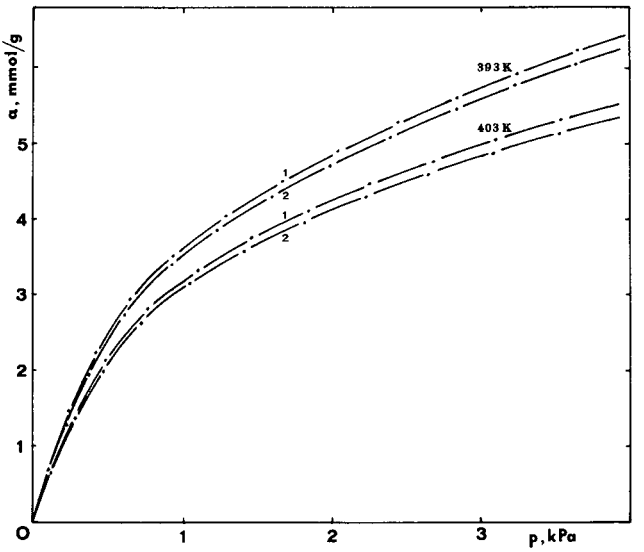

Fig. 2. Adsorption isotherms of ethanol determined chromatographically using (1) the peak profile and (2). the peak maximum method on carbon A-2 at 393 and 403 K.

adsorbent surface easier than with argon and helium. Therefore, for subsequent studies hydrogen was adopted as the carrier gas.

In Fig. 2 the ethanol adsorption isotherms obtained by the peak maximum and peak profile methods are compared [1,2]. It can be seen that the peak profile method

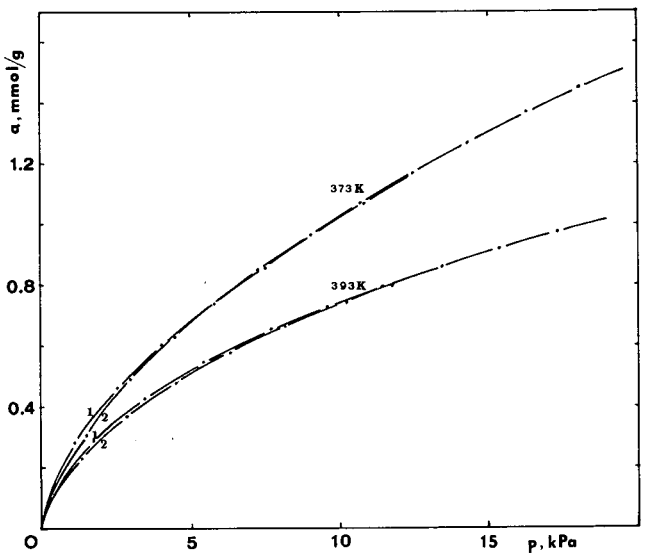

Fig. 3. Adsorption isotherms of ethanol on sorbent S5 at 373 and 393 K determined chromatographically using the profile peak method for (1) small samples of adsorbate in the range up to $p/p_s = 0.05$ and (2) for large samples up to $p/p_s = 0.2$.

always yields higher adsorption values than the peak maximum method (*e.g.*, at about 2 kN m^{-2} the difference in adsoption values is 160 μmol, which when referred to the adsorption corresponding to that pressure, amount to about 4%). The isotherms determined by the peak profile method are therefore close to those found by the static procedure. Considering the shorter time required to determine the adsorption isotherm by the peak profile method, this method was adopted in further studies.

The ethanol adsorption isotherms on S5 at 373 and 393 K determined for small samples of the adsorbate (in the range up to $p/p_s = 0.05$, where p_s is the saturated vapour pressure of the adsorbate at the given temperature) are compared in Fig. 3 with those determined for large adsorbate samples (up to $p/p_s = 0.2$). In the range of relative pressures of 0.005–0.05 the plots overlap. The greatest differences in adsorption occur in the range 0.005–0.02 and amount to about 0.055 mmol, which represents 5.8% when referred to the mean adsorption in this range or relative pressures.

The adsorption isotherms of benzene and ethanol determined chromatographically at 373 K on adsorbents A-2, A-2o, S5, and SKS-2 are shown in Fig. 4. Both adsorbates are very well adsorbed on SKS-2. The adsorption isotherms for benzene and ethanol on A-2 and A-2o have similar shapes. The lowest adsorptivity is observed for S5.

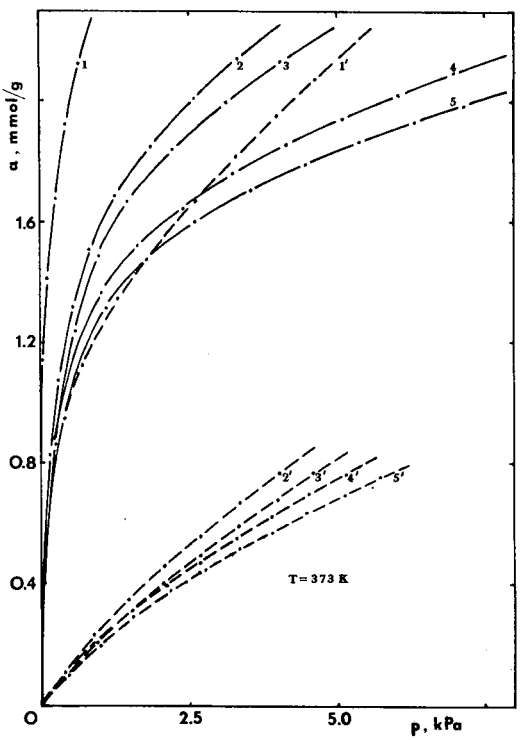

Fig. 4. Adsorption isotherms of (1–5) benzene and (1'–5') ethanol determined chromatographically at 373 K on adsorbents (1,1') SKS-2, (2,2') A-2, (3,3') A-2o, (4,4') S4 and (5,5') S5.

Fig. 5 shows the adsorption isotherms for methanol, ethanol and *n*-propanol determined at 298 and 373 K on the initial carbon A-2 and on its modifications S1, S4 and S6. It can be seen that the modification of the surface, especially its silanization, results in a decrease in the adsorptivity of the carbons with respect to alcohols. The decrease in adsorption at low relative pressures seems to suggest that in addition to physical adsorption a process of chemical adsorption also occurs or that an excessive flow-rate of the carrier gas through the adsorbent bed in the column hinders the penetration of the adsorbate molecules from the carrier gas stream to the carbon surface. The adsorption isotherms of methanol, ethanol and *n*-propanol determined chromatographically at 298 and 373 K on S5 are plotted in Fig. 6 as volume of the adsorbed substance *versus* relative pressure [$v = f(p/p_s)$]. The greatest decrease in adsorption at low relative pressures is observed for methanol probably because the methanol molecule contains a polar group and an apolar group of similar size. The strong mutual interaction of the methanol molecules, competetive with the adsorbate–adsorbent interactions, reduces the adsorption potential and hence the adsorption energy.

In Fig. 7, adsorption isotherms are shown for methanol and ethanol determined at 373 K by the static and chromatographic methods at different flow-rates of the carrier gas through the S5 bed. The initial sections of the chromatographically determined isotherms are lower than those determined statically, and the extent is independent of the flow-rate of the carrier gas up to about 50 $cm^3\ min^{-1}$. However, above this value there is a decrease in adsorption proportional to the flow-rate. A similar

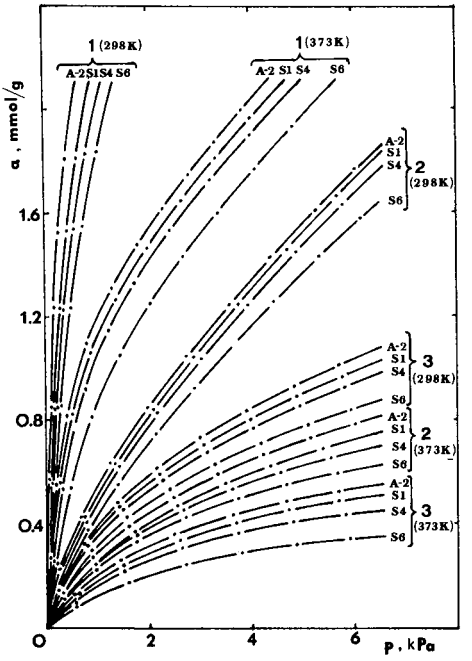

Fig. 5. Adsorption isotherms of (1) methanol, (2) ethanol and (3) *n*-propanol determined chromatographically at 298 and 373 K on the carbon A-2 and on its modifications S1, S4 and S6 (see Table I).

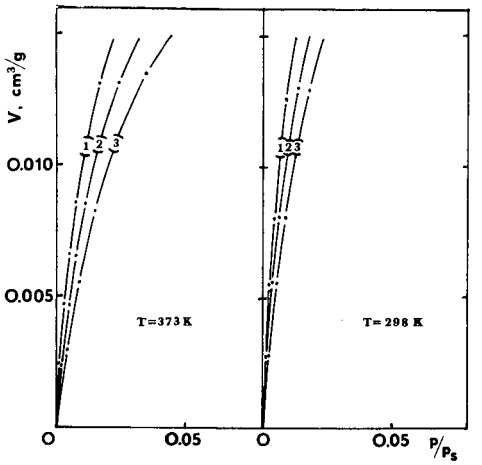

Fig. 6. Adsorption isotherms of (1) methanol, (2) ethanol and (3) *n*-propanol determined chromatographically at 298 and 373 K on sorbent S5.

effect was observed for the other aliphatic alcohol–adsorbent systems. It was therefore decided to conduct subsequent investigations on the active carbons at carrier gas flow-rates not exceeding 50 $cm^3\ min^{-1}$.

The decrease in the adsorption of alcohols on silanized adsorbents with respect

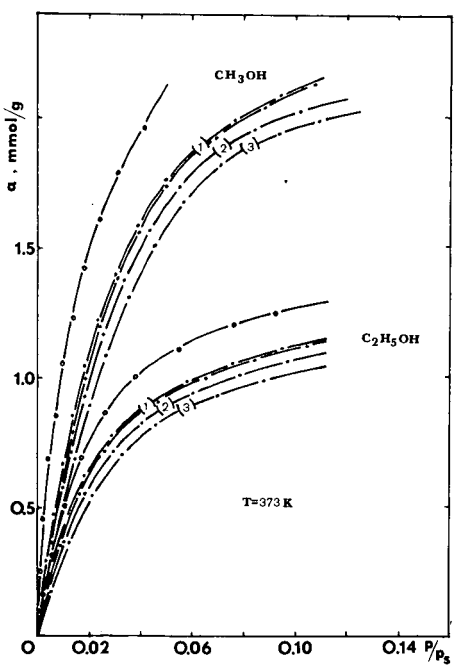

Fig. 7. Adsorption isotherms of methanol and ethanol determined at 373 K by (○) static and (●) chromatographic methods. The latter method was applied at different flow-rates of the carrier gas through the S5 bed: (1) 30 and 50, (2) 60 and (3) 70 $cm^3\ min^{-1}$.

to other adsorbents may be due to either the lowering of the lyophilic properties of the surface of silanized carbons and a consequent decrease in the adsorptivity of compounds with polar groups, or strong adsorbate–adsorbate interactions [12–15].

On the basis of the adsorption isotherms determined chromatographically at different temperatures, the adsorption isosteres were calculated and the relationships $\ln p = f(1/T)$ were found. From the slope of the straight lines obtained, the isosteric heat of adsorption was calculated according to

$$q = = R\left[\frac{\partial \ln p}{\partial\left(\frac{1}{T}\right)}\right]_{a=\text{const.}} \tag{3}$$

In Fig. 8 the differential molar heat of adsorption of benzene, calculated from chromatographic measurements ($q_{diff} = q_{st} - RT$) [16,17], is compared with the heats of adsorption found calorimetrically at 373 K for adsorbents A-2, A-2o, S5 and SKS-2. The closest values of the heats of adsorption were obtained for A-2, A-2o and S5, the differences for these adsorbents not exceeding 2.6 kJ mol^{-1}. The largest difference (*ca.* 12.0 kJ mol^{-1}) was obtained for SKS-2.

The differential molar heats of adsorption and the entropy of adsorption were calculated from the statically and chromatographically determined benzene adsorption isotherms, by the method suggested by Bering and Serpinsky (BS) [18–20] according to

$$q = L + \alpha RT^2\left[\frac{\Delta \ln\left(\frac{p}{p_s}\right)}{\Delta \ln a}\right] - RT\ln\left(\frac{p}{p_s}\right) \tag{4}$$

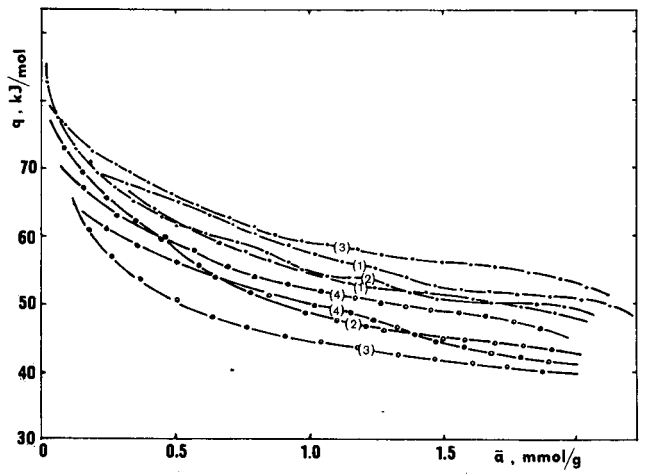

Fig. 8. Changes in the differential molar heats of adsorption of benzene (○) calculated from chromatographic measurements and (●)determined calorimetrically at 373 K on adsorbents (1) A-2, (2) A-2o, (3) SKS-2 and (4) S5.

where L = heat of adsorbate condensation, α = coefficient of thermal expansion of the adsorbate and

$$\Delta S = -\alpha RT \left[\frac{\Delta \ln a}{\Delta \ln \left(\frac{p}{p_s} \right)} \right] \tag{5}$$

The values calculated in this way were compared with those found calorimetrically and chromatographically on sorbent S5 (Fig. 9). The results obtained for carbons A-2, A-2o and S5 were closer to the heats determined calorimetrically than the differential molar heats of adsorption calculated from the isosteres. The largest differences in the values occur for the initial coverages of all the adsorbents used.

The differential molar heats of adsorption of ethanol determined calorimetrically at 373 K on A-2, A-2o, S5 and SKS-2 are compared in Fig. 10 with the heats calculated by the BS method from the chromatographically determined adsorption isotherm. Comparable values were obtained for carbons A-2 and A-2o. The ethanol–SKS-2 system is characterized by higher heats (by *ca.* 20 kJ mol^{-1}). For the above adsorbents the heats of adsorption in the initial range of coverages differ only slightly from those calculated at higher coverages.

The behaviour of the ethanol–S5 sorbent system was different. In the initial range of coverages the heat of adsorption is larger than that on carbons A-2 and A-2o by *ca.* 115 kJ mol^{-1}. As the degree of coverage increased, this heat decreased to values comparable to those found for carbons A-2 and A-2o.

In Fig. 11 the plots of the differential molar heats of adsorption of methanol determined calorimetrically and calculated by the BS method from the chromato-

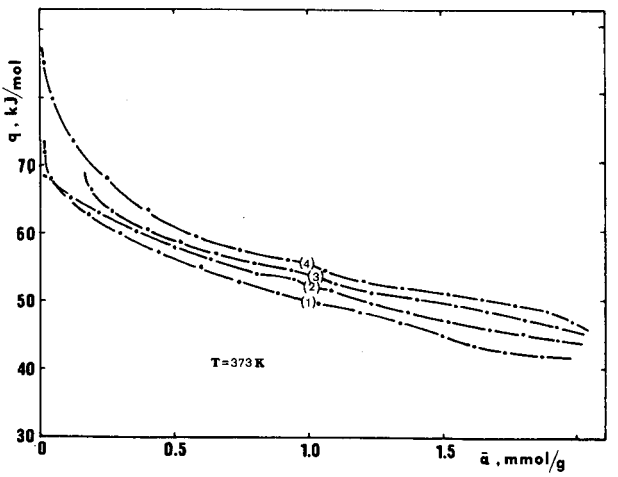

Fig. 9. Changes in the differential molar heats of adsorption of benzene on sorbent S5 at 373 K: (1) calculated from chromatographic measurements of isosteric heats of adsorption; (2) calculated from chromatographically determined adsorption isotherm using BS method; (3) calculated from statically determined isotherm using BS method; (4) determined calorimetrically.

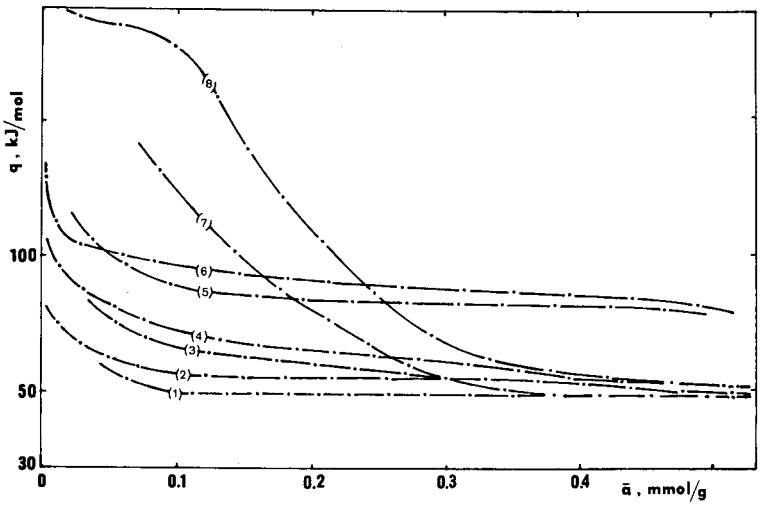

Fig. 10 Changes in the differential molar heats of adsorption of ethanol on carbons (1,2) A-2, (3,4) A-2o, (5,6) SKS-2 and (7,8) S5 at 373 K: (1,3,5,7) calculated from chromatographically determined adsorption isotherms using BS method; (2,4,6,8) determined calorimetrically.

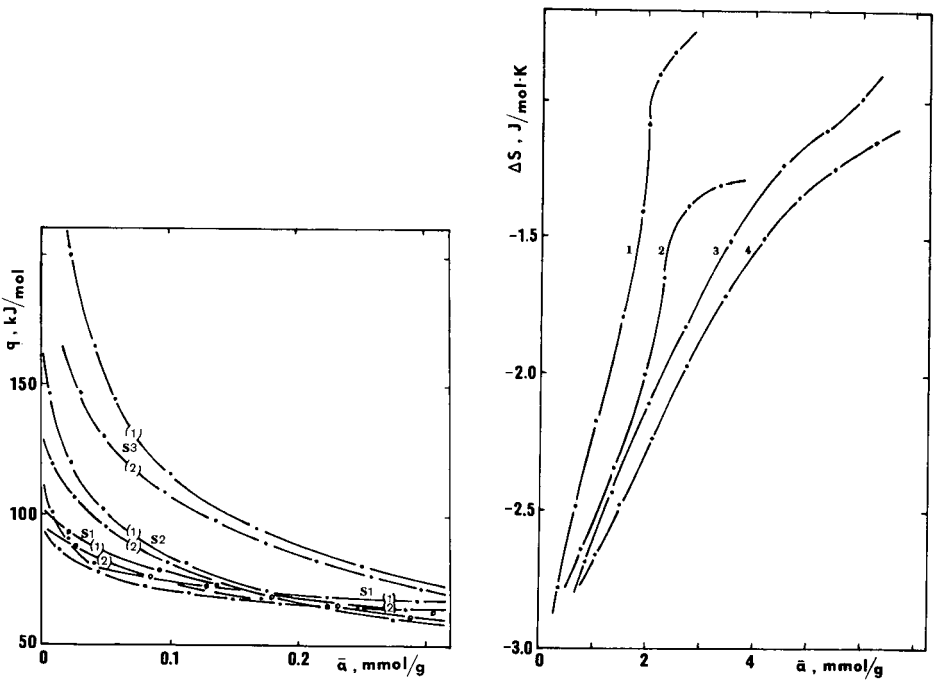

Fig. 11. Changes in the differential molar heats of adsorption of methanol (1) determined calorimetrically and (2) calculated from chromatographic isotherms using the BS method at (○) 298 and (●) 373 K on sorbents S1, S2 and S3.

Fig. 12 Changes in the differential molar entropy of adsorption of (1) cyclohexane, (2) benzene, (3) ethanol and (4) *n*-propanol on carbon A-2. T = 373 K.

graphically determined isotherm at 298 and 373 K are compared. The heat of adsorption of methanol increases in the range of the initial coverages of the adsorbent surface with increasing content of Cr(VI) on the carbon surface. An increase in temperature of about 75 K produces no significant decrease in the differential molar heat of adsorption, which seems to support the earlier conclusion that in addition to physical adsorption, chemical adsorption may also occur on carbons with cations deposited on their surface.

In Fig. 12 the variation of the entropy of adsorption of the adsorbates on carbon A-2 is shown. All adsorption systems were characterized by a negative entropy which increased with temperature and with the coverage of the surface. The increase in entropy with temperature indicated the progress of delocalization of the adsorbate molecules on the carbon surface and a decrease in the interactions of these molecules with the carbon surface.

The energy of interaction of methanol and ethanol with the modified active carbon surfaces was larger than that on non-polar compounds (see Fig. 10 and 11). We therefore decided to check the adequacy of the theory of physical adsorption on homogeneous surfaces for describing adsorption on carbon adsorbents in terms of the Brunauer, Emmett and Teller (BET) model [21]:

$$\frac{h}{a(1-h)} = \frac{1}{a_m C_{BET}} + \frac{C_{BET}-1}{a_m C_{BET}} \cdot h \tag{6}$$

the Hüttig model [22]:

$$\frac{(1-h)h}{a} = \frac{1}{a_m C_H} + \frac{1}{a_m} \cdot h \tag{7}$$

the Kiselev model [23,24]:

$$\frac{\theta}{(1-\theta)h} = K_1 + K_1 K_n \tag{8}$$

and the Hill model [25–27]:

$$\ln\left\{\frac{\theta(1-h)^2}{h[1-\theta(1-h)]}\right\} + \frac{\theta(1-h)}{1-\theta(1-h)} = \ln K_1 + K_2\theta(1-h) \tag{9}$$

where:

a = adsorption at relative pressure $h = p/p_s$ (mmol g^{-1}); a_m = amount of adsorbate necessary to cover the adsorbent surface area accessible for its molecules with a compact monolayer (mmol g^{-1}); p = pressure of the adsorbate vapour (N m^{-2}); θ = coverage of the adsorbent surface; C_{BET}, C_H, K_1 = constants characterizing the adsorbate–adsorbent interactions; K_2, K_n = constants characterizing the adsorbate–adsorbate interactions.

In the calculations, use was made of chromatographically determined adsorption isotherms for adsorbates undergoing reversible adsorption on carbon adsorbents, *i.e.*, methanol and ethanol, so the above considerations have a full physical

TABLE II

PARAMETERS OF BET [21], HÜTTIG [22], KISELEV [23,24] AND HILL [25,26] EQUATIONS FOR ETHANOL AT 373 K

Equation	Parameter	A-2	A-2o	S1	S4	S5	S6
BET	a_m (mmol g^{-1})	7.93	9.78	4.63	2.29	8.60	2.16
	C_{BET}	7.8	5.5	8.6	21.5	10.2	22.7
	Linearity: from h =	0.045	0.090	0.030	0.027	0.048	0.080
	to h =	0.239	0.236	0.238	0.241	0.230	0.244
Hüttig	a_m (mmol g^{-1})	6.07	5.95	6.25	3.67	4.85	2.88
	C_H	31.1	29.4	22.1	22.6	26.2	19.6
	Linearity: from h =	0.050	0.055	0.070	0.085	0.043	0.072
	to h =	0.239	0.236	0.238	0.241	0.230	0.244
Kiselev	K_1	3.82	3.83	3.05	3.65	1.86	3.61
	K_n	1.05	1.02	0.91	0.93	0.94	0.75
	Linearity: from h =	0.095	0.070	0.043	0.043	0.051	0.038
	to h =	0.239	0.236	0.238	0.241	0.218	0.244
Hill	K_1	0.78	0.76	0.70	0.92	0.83	0.91
	K_2	1.81	1.69	1.38	1.20	1.54	1.62
	Linearity: from h =	0.045	0.060	0.067	0.030	0.055	0.058
	to h =	0.139	0.236	0.238	0.241	0.228	0.244

meaning. The intervals in which the adsorption isotherms of alcohols on the tested absorbents fulfilled the above equations and the corresponding characteristic quantities are summarized in Table II for several adsorbents. The characteristic quantities were determined by the least-squares method [28]. The results given in Table II can be regarded as satisfactory despite the fact that some workers question the validity of eqns. 6–9 in which homogeneity of the adsorbent is assumed [29–31].

At low coverages the BET [21] and Hüttig [22] adsorption models hold well, but as the coverage increases the effect of intermolecular interactions becomes greater. In addition to the vertical interactions, accounted for in the BET and Hüttig models, an even greater part is played by steric interactions. The effect of the latter interaction with delocalized adsorption is accounted for by the Kiselev model [23]. This model does not account, however, for the change in intermolecular interaction energy with the change in molecule coordination in surface complexes, and this is probably the reason why it does not hold in cases of strong adsorbate–adsorbate interactions. In the cases considered Kiselev's model is fulfilled the worst.

Hill's model [25–27] assumes, in contrast to that of Kiselev [23,24], non-localized adsorption. Here, the effect of lateral interactions is accounted for and it is assumed that the adsorbate molecules do not have to be completely immobile, and, depending on the character of interactions with the adsorbate molecules, they can, in the unadsorbed state, move freely on the surface according to the adsorption–desorption mechanism.

The equations for models of adsorption on homogeneous surfaces may be applied to dynamic adsorption on active carbons at low coverages of the surface area and relatively high temperatures (attainable in chromatographic processes) when the adsorption energy is controlled primarily by the adsorbate–adsorbent interactions. The

considered equations do not, however, provide for strong intermolecular interactions, especially hydrogen bonds, which result in the formation of surface associates. If the alcohols studied are associated in the liquid phase, then, depending on their concentration, they will also be associated to some extent in the adsorbent field of forces [32]. This is probably why the effects of intermolecular interactions that occur may be comparable to the effects of heterogeneity of the surface only at low coverages, when the effect of association can be neglected [33]. The use of equations for different models of adsorption on homogeneous surfaces for microporous adsorbent is therefore justified.

CONCLUSIONS

The isotherms obtained for the systems studied are convex with respect to the pressure axis, which indicates that the adsorbate–adsorbent interactions have a dominant effect on the initial progress of adsorption of all the adsorbates and that the part played by association dominates in the overall interaction of adsorbates with the surface of the carbons.

The observed differences in the adsorption values and heats of adsorption found from static and dynamic measurements may be due to blocking of the active adsorption sites on the adsorbent surface by the carrier gas molecules, a molecular sieve effect connected with the similarity of the dimensions of the adsorbate molecules and the entrances to the pores, or not filling of the whole adsorption volume of the micropores with the adsorbate in the chromatographic process.

The change in the chemical character of the active carbon surface due to silanization with trimethylchlorosilane vapour produces a lowering of the lyophilic properties of this surface with respect to alcohols and a decrease in their total adsorption. The heats of adsorption of aliphatic alcohols depend on the kind of surface groups present, so on this basis it is possible to illustrate the character of the adsorbate–adsorbent interactions. From the point of view of these interactions the alcohols may be arranged in the order *n*-propanol > ethanol > methanol. This is confirmed by the isotherms shown in Fig. 6.

The negative values of the differential molar adsorption entropy are indicative of the localization of the adsorbate molecules on the surfaces of the adsorbents. However, the entropy values indicate low values of the energy of the bonds.

It is advantageous to conduct the investigations of adsorbents by adsorption gas chromatography with the use of gases that are poorly adsorbed in the bed (*e.g.*, helium of hydrogen). On the basis of certain premises in the literature [3], it should be noted, however, that the use of hydrogen as the carrier gas may lead to a decrease in the concentratiom of surface oxides on the adsorbents used (*e.g.*, A-2o).

The decrease in adsorption at carrier gas flow-rates exceeding 50 $cm^3\ min^{-1}$ indicates that under these conditions polar adsorbates do not reach adsorption equilibrium, whereas the non-polar adsorbates do [34].

REFERENCES

1 A. V. Kiselev and Ya. I. Yashin, *Adsorpcyjna Chromatografia Gazowa*, PWN, Warsaw 1969.
2 T. Paryjczak, *Gas Chromatography in Adsorption and Catalysis*, Polish Scientific Publishers, Warsaw and Ellis Horwood, Chichester, 1986.

3 F. Dondi, M. F. Gonnord and G. Guiochon, *J. Colloid Interface Sci.*, 62 (1977) 303.
4 G. Rychlicki, *Rola Chemizmu Powierzchni Węgla w Procesach Adsorpcji i Katalizy*, Nicholas Copernicus University, Toruń, 1985.
5 B. R. Alves and A. J. Clark, *Carbon*, 24 (1986) 287.
6 G. Wójcik and K. Karpiński, *Chem. Stosow.*, 22 (1978) 351.
7 M. M. Dubinin and Ya. E. Polstyanov, *Izv. Akad. Nauk SSSR, Ser. Khim.*, (1966) 793.
8 M. Marsh and B. Rand, *J. Colloid Interface Sci.*, 33 (1979) 101.
9 J. Volf, J. Kaubek and J. Pasek, *J. Chromatogr.*, 81 (1973) 9.
10 D. Dollimore, G. R. Heal and D. R. Martin, *J. Chromatogr.*, 50 (1970) 209.
11 J. Garbacz and G. Rychlicki, *Podstawy Termodynamiki i Kalorymetrii Procesu Adsorpcyjnego*, Nicholas Copernicus University, Toruń, 1986.
12 U. B. Mohlin and D. G. Gray, *J. Colloid Interface Sci.*, 47 (1974) 747.
13 G. M. Dorris and D. G. Gray, *J. Colloid Interface Sci.*, 71 (1979) 93.
14 W. T. Cooper and J. M. Hayes, *J. Chromatogr.*, 314 (1984) 111.
15 M. Domingo-García, F. J. López-Garzón, R. López-Garzón and C. Moreno-Castilla, *J. Chromatogr.*, 324 (1985) 19.
16 S. Ross and J. P. Olivier, *On Physical Adsorption*, Wiley-Interscience, New York, 1964.
17 G. Deininger, J. Asshauer and I. Halasz, *Chromatographia*, 8 (1975) 143.
18 V. P. Bering and V. V. Serpinsky, *Dokl. Akad. Nauk SSSR*, 114 (1957) 1249.
19 V. P. Bering and V. V. Serpinsky, *Izv. Akad. Nauk SSSR*, (1957) 1254.
20 V. P. Bering and V. V. Serpinsky, *Dokl. Akad. Nauk SSSR*, 148 (1963) 1331.
21 S. Brunauer, P. H. Emmett and E. Teller, *J. Am. Chem. Soc.*, 60 (1938) 309.
22 G. F. Hüttig, *Monatsh. Chem.*, 78 (1948) 177.
23 A. V. Kiselev, *Kolloid. Zh.*, 20 (1958) 338.
24 N. N. Avgul, A. V. Kiselev and A. I. Lygina, *Kolloid. Zh.*, 23 (1961) 369.
25 T. L. Hill, *J. Chem. Phys.*, 14 (1946) 441.
26 T. L. Hill, in W. G. Frankenburg (Editor), *Advances in Catalysis and Related Subjects*, Vol. 4, Academic Press, New York, 1952, p. 211.
27 F. Dondi, M.-F. Gonnord and G. Guiochon, *J. Colloid Interface Sci.*, 62 (1977) 316.
28 C. J. H. Beaven and P. Eadington, *Chem. Ind. (London)*, (1966) 1484.
29 G. D. Halsey, in W. G. Frankenburg (Editor), *Advances in Catalysis and Related Subjects*, Vol. 4, Academic Press, New York, 1952, p. 259.
30 M. M. Dubinin and E. D. Zhukovskaja, *Izv. Akad. Nauk. SSSR, Otd. Khim. Nauk*, (1958) 535.
31 M. M. Dubinin, *Carbon*, 21 (1983) 359.
32 A. Zukal and O. Kadlec, *Collect. Czech. Chem. Commun.*, 38 (1973) 321.
33 L. M. Dormant and A. W. Adamson, *J. Colloid Interface Sci.*, 38 (1972) 285.
34 W. W. Raczyński, *Zarys Teorii Dynamiki Sorpcji i Chromatograffii*, WNT, Warsaw, 1966.

Journal of Chromatography, 556 (1991) 457–484
Elsevier Science Publishers B.V., Amsterdam

CHROM. 23 099

Influence of solute size and the non-polar interaction term on the selection of test solutes for the classification of stationary phase selectivity in gas chromatography

THEOPHILUS O. KOLLIE and COLIN F. POOLE*
Department of Chemistry, Wayne State University, Detroit, MI 48202 (USA)

ABSTRACT

A new parameter ΔG_S^{INT} (X) is introduced for the determination of the capacity of a stationary phase to enter into orientation and hydrogen-bonding interactions. ΔG_S^{INT} (X) is defined as the component of the free energy of solution that is equivalent to the solute–solvent interactions of solute (X) that exceeds those interactions typified by an *n*-alkane of identical volume in solvent S reduced by the identical interactions of solute (X) in a hydrocarbon solvent (squalane). ΔG_S^{INT} (X) provides a quantitative scale of orientation and proton donor–acceptor interactions that is independent of solute size and non-polar solute–solvent interactions. Multivariate analysis of ΔG_S^{INT} (X) values for 21 test solutes on 20 stationary phases was used to identify acceptable test solutes for characterizing specific intermolecular interactions and to classify the stationary phases based on their capacity for these interactions. Several highly correlated solutes were identified as suitable for determining orientation and solvent proton acceptor capacity of which nitrobenzene and *n*-octanol, respectively, are recommended as the preferred solutes. Benzene and dioxane were identified as the most favorable test solutes for solvent proton donor capacity within the data set. It seems likely that a more appropriate solute could be found for this interaction. The classification of stationary phases by ΔG_S^{INT} (X) is informative and shows a logical clustering of phases of similar type and a linearly related change in properties for the homologous series of poly(methylphenylsiloxane) solvents as the mole percentage of phenyl groups is increased.

INTRODUCTION

The properties of a stationary phase that are considered important in the selection process for a particular application are its useful temperature operating range, ability to provide columns of acceptable efficiency and its characteristics as a solvent determined by its solvent strength and selectivity. The first two parameters can be determined unambiguously for any phase and limiting boundary conditions established [1]. The strength of a solvent (synonymous with the general concept of polarity) is a measure of the capacity of a stationary phase to enter into all intermolecular interactions. No exact method has emerged for calculating or determining this term, however, and its current usage is based on common sense [2,3]. It is not important to the studies reported here and will not be discussed further. The solvent selectivity is a measure of the capacity of a stationary phase to enter into specific intermolecular

0021-9673/91/$03.50

interactions represented by dispersion, induction, orientation and donor–acceptor complexation (*e.g.*, hydrogen bonding). Molecular mechanics has not reached a state of maturity, to date, that would permit the *a priori* calculation of the above forces in the complex systems represented by solute–stationary phase interactions of interest in gas chromatography. In the absence of an exact method of calculation chromatographers have come to rely upon a number of empirical experimental approaches to characterize these forces [1–6]. Of these approaches, the system of stationary phase selectivity constants introduced by Rohrschneider and later extended by McReynolds has been the most widely used and virtually all popular stationary phases have been characterized by this method. Certain theoretical and experimental deficiencies in the McReynolds approach have been recognized recently (and also in other methods based on retention index differences) and can be briefly summarized as follows [2,3,7–10]: poor retention of test solutes on some phases prevents the accurate determination of retention index values; the calculation method ignores the importance of interfacial adsorption as a retention mechanism (interfacial adsorption is often the dominant retention mechanism for *n*-alkanes on polar phases); individual phase constants are composite values defined by the retention characteristics of both the retention index standards and test solutes (the retention characteristics of the *n*-alkanes dominate in many instances); and the original data of McReynolds contains experimental uncertainties that affect their reliability. It has been suggested that the McReynolds approach to stationary phase characterization should be abandoned in favor of thermodynamic approaches which can be related to rigorous models describing the transfer of a solute from the gas phase to the stationary phase. Early thermodynamic approaches to the measurement of selectivity were based on the determination of the partial molar Gibbs free energy of solution for either functional groups [11] or specific test solutes, such as the first five test solutes suggested by McReynolds [12,13]. The sum of the retention index increments for the first five McReynolds' test solutes, suggested as a general scale of solvent polarity, was shown to correlate with the partial molar excess, Gibbs free energy of solution of a methylene group [14,15]. In more recent studies the molal standard state was adopted to minimize inconsistencies from a lack of an exact knowledge of the molecular weight of common polymeric phases [3,8,16] and multivariate analysis techniques were used to identify suitable test solutes to characterize stationary phase interactions [8,17]. For highly cohesive phases such as OV-275, TCEP and DEGS, the selectivity parameters were found to be solute-size dependent [17]. It was speculated that the size dependence for the test solutes could be removed by separating the free energy into a cavity term and an interaction term, the latter being independent of solute size and representative of polar solute–solvent interactions. The elaboration of this interaction term into a quantitative scale of solvent selectivity and the selection of test solutes to characterize specific molecular interactions are the focus of this paper.

To accommodate differences in solute size in the selectivity scale it will be necessary to employ a model which specifically incorporates a size-dependent term in the decomposition of the free energy of solution for the test solutes. Linear solvation energy relationships employing solvatochromic parameters have been very successfully applied to the prediction of a wide range of solvent properties [18–20]. In this model the solvation process is considered to involve three steps: (1) the creation of a cavity in the solvent of a suitable size to accommodate the solute; (2) reorganization

of the solvent molecules around the cavity (the free-energy change for this process is probably small or zero); and (3) interaction of a solute molecule with the surrounding solvent molecules. For transfer from the gas phase to the stationary phase the overall free energy change must be negative, the cavity formation process is endoergic (positive free-energy change) and the solute–solvent interaction term is exoergic (negative free-energy change). The solvation process is described by the general equation

$$SP = SP_o + mV_2/100 + S(\pi_2^* + d\delta_2) + a\alpha_2 + b\beta_2 \quad (1)$$

where SP is some solvent property to be correlated and SP_o is a constant. V_2 is a volume term characteristic of the solute (*e.g.*, molar volume, Van der Waals volume). The term mV_2 describes the endoergic process of cavity formation. The three solute terms π_2^*, α_2 and β_2 are the monomer solute dipolarity, hydrogen-bond acidity and hydrogen-bond basicity, respectively, and are used to characterize the exoergic solute–solvent interactions. The term containing δ_2 is a solute polarizability correction factor. There is no explicit term in eqn. 1 that corresponds to a dispersion interaction. This does not seem to matter for processes that involve condensed phases, *e.g.*, liquid–liquid distribution, because the dispersion interactions in each phase will largely cancel. However, this term cannot be neglected for the process of transferring a solute from the gas phase to solution. For such processes, the alternative eqn. 2 is preferred, with the solute parameter log K_L^{16} replacing the solute parameter $V_2/100$ [21–23]:

$$SP = SP_o + l(\log K_L^{16}) + s\pi_2^* + a\alpha_2 + b\beta_2 \quad (2)$$

Log K_L^{16} is the logarithm of the solute gas–liquid partition coefficient for hexadecane as solvent at 298 K. The function $l(\log K_L^{16})$ is related to the endoergic work of creating a cavity in the solvent and the endoergic solute–solvent dispersion interactions. Abraham *et al.* [24] have used a modified version of eqn. 2 to characterize the solvent properties of the 77 stationary phase data set of McReynolds:

$$\log V_g^o = C + rR_2 + s\pi_2^* + a\alpha_2 + b\beta_2 + l \log K_L^{16} \quad (3)$$

where V_g^o is the specific retention volume for the solute and R_2 is a term describing the solute molar refraction. The coefficients r,s,a,b and l, obtained by multiple linear regression, determine quantitatively the susceptibility of a stationary phase to enter into specific interactions and can be used to characterize stationary phase properties. The r coefficient determines the tendency of the phase to interact with π- or n-solute electron pairs, s phase dipolarity, a phase hydrogen-bond basicity, b phase hydrogen-bond acidity and l a combination of general dispersion interactions and cavity effects. In order to separate out effects due to cavity formation and to allow, at least partly, for solute–solvent dispersion interactions, several workers have referenced solvation properties, such as partition coefficients, to those of a non-polar solute (usually an n-alkane) with a similar volume to the solute in question [25–30]. This was the basis of the Snyder selectivity triangle approach for classifying solvents in terms of the relative strength of their orientation and hydrogen bonding interactions using nitromethane, ethanol and dioxane as test solutes [25,26,30]. In Snyder's treatment, the contribution of induction and entropy effects, etc., to the solute gas–liquid partition coefficient

were removed by subtracting the partition coefficient for a particular test solute in a hydrocarbon solvent (in fact, the average value for hexane, isooctane and cyclohexane) from the value of the partition coefficient found for the same test solute in a polar solvent. Rutan *et al.* [29] have argued that the above model may not account completely for all the details of the solvent reorganization process given that an *n*-alkane would probably not be as effective as a polar solute at disrupting the intermolecular bonding among solvent molecules. The cavity formation process, therefore, would be different for an *n*-alkane and a polar solute. At least three common models have been advanced that would allow the independent calculation of the Gibbs free energy of cavity formation based on the Hildebrand solubility parameter theory, scaled particle theory and Sinanoglu–Reis–Moura Ramos (SRMR) solvophobic theory [31,32]. However, it is difficult to see how these approaches could be applied to a diverse group of stationary phases with all the variations represented by polarity and size as well as the fact that most of the physical parameters required for the calculations are not available in the literature. In this paper we propose a new model to characterize solute–solvent polar interactions based on the general premise of linear solvation energy relationships and Snyder's treatment of the cavity/dispersion term. Multivariate analysis techniques are then applied to the size-independent free-energy interaction term to identify suitable test solutes for characterizing specific stationary phase polar interactions and to classify the stationary phases into clusters based on the similarity of their capacity for specific intermolecular interactions using a data set consisting of the partial molal Gibbs free energy of solution for 28 solutes on 23 stationary phases [17].

EXPERIMENTAL

The names, abbreviations and compositions of the 22 stationary phases and 25 test solutes used in this study are summarized in Table I. The data for the partial molal Gibbs free energy of solution for the test solutes at 121.4°C on each stationary phase are collected and summarized in ref. 17. The partial molal Gibbs free energy of solution for the *n*-alkanes on the phases used in this study were taken from several sources [3,8,9,33,34] and are summarized in Table II. The Van der Waals volume for the test solutes and *n*-alkanes were calculated by several methods. The Van der Waals volume according to Bondi, V_B, was calculated by summing the contribution of fragmental constants given by Bondi [35]. In a similar manner, the characteristic Van der Waals volume, V_X, was calculated from fragmental constants as described by McGowan [36,37] and Abraham and McGowan [38]. The intrinsic Van der Waals volume, V_I, introduced by Leahy [39] and Leahy *et al.* [40], was estimated in an approximate form using the correlation equation between the intrinsic and characteristic volume presented by Abraham and co-workers [38,41]. The Van der Waals volume, V_A, and Van der Waals total surface area and solvent accessible surface area were calculated with the molecular modeling program MacroModel version 2.0 (Department of Chemistry, Columbia University, New York) [42–44] executed on a VAX II/750 computer with version 4.7 of VMS (Digital Equipment, Merrimack, NH, USA). Multivariate analysis was performed on an Epson Apex 200 computer using Ein*Sight version 2.5 (Infometrix, Seattle, WA, USA) software for data analysis and pattern recgnition. The data were entered via a standard spreadsheet program, VP-

TABLE I

IDENTIFICATION AND ABBREVIATIONS FOR STATIONARY PHASES AND TEST SOLUTES

Stationary phases

No.	Abbreviation	Name
1	SE-30	Poly(dimethylsiloxane)
2	DDP	Didecyl phthalate
3	OV-105	Poly(cyanopropylmethyldimethylsiloxane)
4	OV-3	Poly(dimethylmethylphenylsiloxane), 10 mol% phenyl groups
5	OV-7	Poly(dimethylmethylphenylsiloxane), 20 mol% phenyl groups
6	OV-11	Poly(dimethylmethylphenylsiloxane), 35 mol% phenyl groups
7	OV-17	Poly(methylphenylsiloxane)
8	OV-22	Poly(methylphenyldiphenylsiloxane), 65 mol% phenyl groups
9	PPE-5	1,3-Bis(3-phenoxyphenoxy)benzene
10	OV-330	Poly(dimethylsiloxane)–Carbowax copolymer
11	QMES	Tetra-*n*-butylammonium 4-morpholinoethanesulfonate
12	OV-25	Poly(methylphenyldiphenylsiloxane), 75 mol% phenyl groups
13	CW20M	Poly(ethylene glycol)
14	QPIC	Tetra-*n*-butylammonium 4-picrate
15	QpTS	Tetra-*n*-butylammonium 4-toluenesulfonate
16	QF-1	Poly(trifluoropropylmethylsiloxane)
17	QACES	Tetra-*n*-butylammonium 2-(2-acetamido)aminoethanesulfonate
18	QTAPSO	Tetra-*n*-butylammonium 3-tris(hydroxymethyl)methylamino-2-hydroxy-1-propanesulfonate
19	DEGS	Poly(diethylene glycol succinate)
20	TCEP	1,2,3-Tris(2-cyanoethoxypropane)
21	OV-225	Poly(cyanopropylmethylphenylmethylsiloxane)
22	OV-275	Poly(dicyanoallylsiloxane)

Test solutes

No.	Name
1	Benzene
2	*n*-Butylbenzene
3	2-Methyl-2-pentanol
4	1-Nitropropane
5	1-Nitropentane
6	Nitrobenzene
7	Benzonitrile
8	Pyridine
9	2-Octanone
10	1,1,2,2-Tetrachloroethane
11	*n*-Butanol
12	*n*-Octanol
13	1-Dodecyne
14	Nonanal
15	1,4-Dioxane
16	Benzodioxane
17	N,N-Dimethylaniline
18	Anisole
19	Aniline
20	N-Methylaniline
21	2,6-Dimethylaniline
22	2-Octyne
23	*cis*-Hydrindane
24	Dihexyl ether
25	2,4,6-Trimethylpyridine

TABLE II

PARTIAL MOLAL GIBBS FREE ENERGY OF SOLUTON FOR *n*-ALKANES (kcal/mol) AT 121.4°C

Stationary phase	Hexane	Heptane	Octane	Nonane	Decane	Undecane	Dodecane	Tridecane	Tetradecane	Pentadecane
SQ			−3.944	−4.470	−4.991	−5.508	−6.026	−6.543		
OV-3				−3.756	−4.198	−4.671	−5.126	−5.577		
OV-7				−3.672	−4.140	−4.602	−5.065	−5.524		
OV-11				−3.528	−4.002	−4.464	−4.929	−5.390		
OV-17					−3.876	−4.345	−4.804	−5.260	−5.715	−6.169
OV-22					−3.674	−4.119	−4.563	−5.003	−5.444	−5.883
OV-25						−4.006	−4.436	−4.862	−5.312	−5.727
OV-105				−3.705	−4.155	−4.600	−5.043	−5.483	−5.922	
OV-225						−3.609	−3.998	−4.410	−4.822	−5.279
OV-375					−3.492	−3.921	−4.362	−4.789	−5.204	−5.638
QF-1					−3.147	−3.531	−3.915	−4.291	−4.668	−5.034
CW20M						−3.451	−3.812	−4.193	−4.592	−4.977
DEGS						−2.034	−2.226	−2.365	−2.828	−3.144
TCEP					−1.499	−1.935	−2.246	−2.548	−2.817	−3.037
PPE-5				−3.319	−3.803	−4.280	−4.756	−5.230		
QpTS						−3.325	−3.763	−4.079	−4.466	−4.772
QPIC						−3.326	−3.763	−4.155	−4.544	−4.942
QMES						−3.316	−3.712	−4.097	−4.368	−4.704
QACES						−2.350	−2.711	−2.713	−3.013	−3.321
QTAPSO						−1.857	−2.007	−2.318	−2.388	−2.581
DPP	−2.514	−3.059	−3.543	−4.071	−4.576	−5.081				
SE-30		−2.838	−3.323	−3.770	−4.224	−4.669	−5.122			

Planner, version 2.0 (Paperback Software International, Berkeley, CA, USA). Missing data points were added as described in ref. 17.

RESULTS AND DISCUSSION

In a previous study, multivariate analysis was applied to a collection of data in the form of the partial molal Gibbs free energy of solution for 28 test solutes on 23 stationary phases to identify suitable test solutes for the classification of stationary phases based on their capacity to enter into specific intermolecular interactions (dispersion, induction, orientation and proton donor–acceptor properties) [17]. For members of a homologous series, *e.g.*, Fig. 1, a good correlation was found between individual members of the series for the partial molal Gibbs free energy of solution except for a group of highly cohesive polar phases that behaved in a different manner to the other phases. This different behavior was speculated to result from the differences in the free energy of cavity formation for the two groups of stationary phases indicating that a more rigorous interpretation of the data was required to separate the contribution of solute size from terms describing the selective solute–solvent interactions that could be used as a basis for the classification of stationary phases.

If we assume that the total free energy change for the transfer of solute X from the gas phase to the stationary phase (with molecular interactions characteristic of infinite dilution) is the linear sum of the individual free energy contributions to the

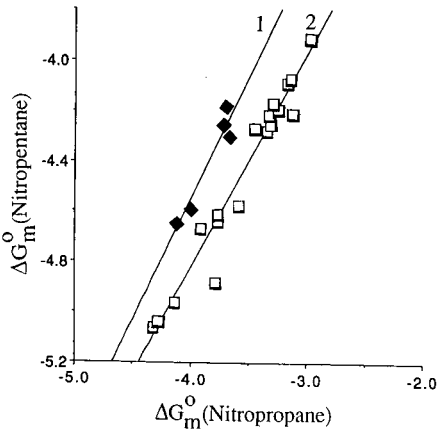

Fig. 1. Plot of the partial molal Gibbs free energy of solution for nitropentane against nitropropane for the stationary phases identified in Table I. Group 1 phases (DEGS, TCEP, QACES, QTAPSO, OV-275) are of high cohesive energy and are displaced from the remaining phases, Group 2, in the correlation plots.

transfer process, then a general expression for the solution process, can be written as follows:

$$\Delta G_S^{SOLN}(X) = \Delta G_S^{CAV}(X) + \Delta G_S^{NP}(X) + \Delta G_S^{P}(X) \quad (4)$$

where $\Delta G_S^{SOLN}(X)$ is the partial Gibbs free energy of solution for the transfer of solute X from the gas phase to the stationary phase S, $\Delta G_S^{CAV}(X)$ the partial Gibbs free energy of cavity formation for solute (X), $\Delta G_S^{NP}(X)$ the partial Gibbs free energy of interaction of the non-polar contribution of solute (X) with the surrounding solvent and $\Delta G_S^{P}(X)$ the partial Gibbs free energy of interaction for the polar contribution of solute (X) with the surrouding solvent. The cavity term is a measure of the free energy required to separate the solvent molecules to create a cavity of a suitable size to hold the solute. It depends only on the size of the solute and the strength of intermolecular interactions between the solvent molecules. However, the independent calculation of the cavity term is not a simple task and requires the input of solvent parameters that are largely unavailable for the stationary phases employed in this study [31,32]. Also, there are no suitable methods that enable either ΔG_S^{NP} or ΔG_S^{P} to be calculated directly. A practical solution can be found if a few simplifying assumptions are made. The polar contribution of the free energy of solution of solute (X) is assumed to be equal to the difference between the free energy of solution of solute (X) in stationary phase S and the free energy of solution for a hypothetical *n*-alkane with an identical molecular volume in the same stationary phase. Thus,

$$\Delta G_S^{SOLN}(HC)^{V} = \Delta G_S^{CAV}(X) + \Delta G_S^{NP}(X) \quad (5)$$

and the difference between eqns. 4 and 5 provides a value for $\Delta G_S^{P}(X)$ in terms of experimentally derived values:

$$\Delta G_S^{P}(X) = \Delta G_S^{SOLN}(X) - \Delta G_S^{SOLN}(HC)^{V} \quad (6)$$

where $(HC)^V$ identifies a parameter representing a property of an *n*-alkane with a volume V identical with that of solute (X). An exact value for $\Delta G_S^{SOLN}\,(HC)^V$ can be obtained by linear regression from a plot of the partial molal Gibbs free energy of solution for a series of *n*-alkanes against their molecular volume. The induction component to $\Delta G_S^P\,(X)$ can be removed by assuming that this equivalent to the polar contribution to the free energy of solution of solute (X) in a non-polar hydrocarbon solvent, such as squalane. This can be calculated in a manner similar to solvent S and is given by

$$\Delta G_{SQ}^P\,(X) = \Delta G_{SQ}^{SOLN}\,(X) - \Delta G_{SQ}^{SOLN}\,(HC)^V \tag{7}$$

The solvent interaction term for polar interactions can then be formally defined as

$$\Delta G_S^{INT}\,(X) = \Delta G_S^P\,(X) - \Delta G_{SQ}^P\,(X) \tag{8}$$

and is equivalent to the solute–solvent interactions of solute (X) that exceed those interactions typified by an *n*-alkane of identical molecular volume in solvent S reduced by the identical interactions of solute (X) in a hydrocarbon solvent (SQ). The partial Gibbs free energy contributions to solution from cavity formation, dispersion, induction and reorganization entropy changes should be largely eliminated making $\Delta G_S^{INT}\,(X)$ the most logical term to probe the importance of solute orientation and hydrogen-bonding interactions. It should be noted that during the above discussion no mention was made of the standard state for the solution. As differences in free energies are involved, which are proportional to differences in logarithmic terms, all constants for the standard state (molarity, mole fraction or molality) are self-cancelling, resulting in identical numerical values for $\Delta G_S^{INT}\,(X)$. All absolute values for free energies of solution are quoted as the partial molal Gibbs free energy of solution in this paper.

The electron cloud surrounding the nucleus of an atom has no clearly defined boundary surface and consequently, an atom has no absolute volume [45,46]. From studies in interatomic bonding an empirical volume, the Van der Waals volume, has been widely used to describe the size of atoms and molecules in studies of their physical properties. In the Van der Waals volume concept each atom of a molecule is represented as a sphere centered at the equilibrium position of the atomic nucleus and having a radius equal to the Van der Waals radius of the atom. The Van der Waals surface can be defined as the exterior surface of the union of all such Van der Waals spheres in the molecule. Clearly the Van der Waals surface and hence volume of a molecule will depend on the empirically based choice of the atomic Van der Waals radii. The simplest approach for approximating the Van der Waals volume of a molecule is to add up appropriate chemical group contributions (increments) using tabulated atomic volumes such as those proposed by Bondi [35]. Such table-based methods can only address in an approximate manner multiple overlaps of atomic Van der Waals spheres in complex molecules and isomers. Empirical force field methods (molecular mechanics) have advanced to a level where accurate geometries, and therefore volumes, can be obtained for most simple organic structures. Differences between methods can be expected, however, owing to differences in force-field approximations and the selected empirical atomic radii. The intrinsic volume of Leahy *et al.* is one example of a widely used approach to predicting molecular volumes [39–41]. In this study we used the program MacroModel [42–44] to calculate molecular volumes

which takes a similar approach to that of Leahy *et al.*, but is not necessarily identical with it. McGowan also proposed a characteristic volume for a molecule that is calculated from considerations of parachor [36,37]. The characteristic volume is defined as the volume of 1 mole of liquid when the molecules are not in motion (absolute zero) and, like the method of Bondi, has the advantage that molecular volumes can be simply built up by addition of atomic values followed by subtraction of a fixed constant for each bond regardless of hybridization. Characteristic volumes are larger than Van der Waals volumes calculated by Bondi methods or molecular mechanics. Abraham and co-workers [38,41] have shown that there is a very good correlation between the computer-calculated intrinsic volume (V_I) and McGowans characteristic volume (V_X):

$$V_I = 0.597 + 0.6823\ V_X \qquad r = 0.99;\ n = 209 \tag{9}$$

The molar volume has also been widely used to correlate the size of a molecule with intrinsic physical properties and is easily calculated from the molecular weight and density of a substance. However, the molar volume has certain theoretical disadvantages compared with the Van der Waals volume [38–41]. The molar volume is a bulk property conditioned by the strength of intermolecular interactions and its magnitude reflects not only the intrinsic volume of the molecule but also its bulk structure. In solute–solvent interactions correlations involving the molar volume result in an underestimate of the contribution of polar interactions which have to be empirically corrected for by modifying the cavity term. Thus the molar volume was considered a poor choice compared with the Van der Waals volume for the purpose of our studies. However, the question remained of how to select the most appropriate Van der Waals volume from the several methods available for its calculation.

The Van der Waals volumes calculated according to Bondi [35], V_B, McGowan [35,37] and Abraham and McGowan [38], V_X, from the MacroModel program, V_A, and the intrinsic volume, V_I, estimated by eqn. 9 and compared with literature values [39–41] are summarized in Table III. The characteristic volume is considerably larger than the other estimates of the Van der Waals volume but is linearly correlated with the intrinsic volume [38] (eqn. 9) and with the Bondi volume (eqn. 10) and the MacroModel calculated volume (eqn. 11):

$$V_I = -0.38 + 0.72\ V_B \qquad r = 1.00;\ n = 35 \tag{10}$$

$$V_I = -1.14 + 0.73\ V_A \qquad r = 1.00;\ n = 35 \tag{11}$$

Likewise, the Bondi volume and the computed volume using the MacroModel program are very similar numerically (Table III) and are correlated:

$$V_B = 0.60 + 1.01\ V_A \qquad r = 1.00;\ n = 35 \tag{12}$$

There are absolute differences between the computed intrinsic volumes calculated by Leahy [39] and those obtained using the MacroModel program, which in general produces values similar to those of Bondi [35]. Differences between V_A and V_B are due to allowance for deviations from a hard-sphere volume caused by overlap in the computer calculated volumes. Because of the good correlations between individual methods for calculating Van der Waals volumes, the choice of method in the relative sense is not too important as any differences between individual methods reflect only

TABLE III

VAN DER WAALS VOLUMES AND SURFACE AREAS CALCULATED BY DIFFERENT METHODS

Test solute	Van der Waals volume (cm^3/mol)					Surface area ($Å^2$)	
	Characteristic, V_X	Intrinsic, V_I		Bondi, V_B	MacroModel, V_A	Total	Solvent Accessible[a]
		Estm.	Calc.				
Dioxane	68.1	46.5		49.00	52.99	114.1	184.1
Butanol	73.1	49.9	49.9	52.65	53.42	124.3	180.2
Nitropropane	70.6	48.2		50.83	49.32	125.5	214.7
Nitropentane	98.7	67.3		71.33	69.61	170.6	258.6
Nitrobenzene	89.1	60.8	63.1	64.33	61.61	138.8	206.5
Octanol	129.5	88.4	88.2	93.81	94.79	215.6	269.3
Benzodioxane	107.3	73.2		77.58	72.81	152.2	201.2
Dihexyl ether	185.8	126.8		134.90	135.56	304.7	407.8
Benzene	71.6	48.9	49.1	51.56	50.46	106.7	159.9
Butylbenzene	128.0	87.3		92.72	92.72	194.4	245.3
cis-Hydrindane	116.0	79.1		83.92	85.15	142.8	251.3
2-Octyne	115.0	78.5		83.21	81.84	182.5	264.8
1-Dodecyne	171.3	116.9		124.34	122.79	278.2	371.1
2-Methyl-2-pentanol	101.3	69.1		73.21	73.59	164.3	213.0
Benzonitrile	87.1	59.4	59.0	62.87	61.30	124.3	178.8
Tetrachloroethane	86.9	59.3	61.7	62.74	65.28	132.3	224.1
Pyridine	67.5	46.1		48.58	47.75	98.2	153.6
Trimethylpyridine	109.8	74.9		79.43	77.44	161.2	220.1
Aniline	81.6	55.7		58.87	57.03	113.9	163.1
N-Methylaniline	95.7	65.3		69.15	67.15	139.1	193.2
N,N-Dimethylaniline	109.8	74.9	75.2	79.43	78.29	162.0	215.7
2,6-Dimethylaniline	109.8	74.9		79.43	77.02	156.1	197.7
Anisole	91.6	62.5	63.0	66.15	64.86	138.7	189.3
Nonanal	139.2	95.0		100.92	99.85	234.6	284.5
2-Octanone	125.2	85.4		90.64	88.58	210.2	277.5
Butane	67.2	45.9		47.80	47.88	115.1	193.8
Pentane	81.3	55.5	55.3	58.03	57.99	138.7	223.9
Hexane	95.4	65.1	64.8	68.26	68.29	161.9	240.7
Heptane	109.5	74.7	74.5	78.49	78.35	184.9	269.0
Octane	123.6	84.3	84.2	88.72	88.76	206.4	280.5
Nonane	137.7	93.9		98.85	98.88	229.4	300.9
Decane	151.8	193.5		109.18	109.12	248.5	343.3
Undecane	165.9	113.2		119.41	119.48	274.2	368.1
Dodecane	179.9	122.8		129.64	130.08	296.8	392.9
Tridecane	194.0	132.4		139.87	139.59	320.4	411.5

[a] Calculated for water as solvent.

subtle changes in volumes which will not have a significant impact on the final results calculated using eqn. 6. For calculations using the Van der Waals volume in this paper we adopted the volume, V_A, calculated by the MacroModel program.

As molecules interact at their surfaces, the cavity surface area might be more appropriate than the cavity volume for accessing the ability of a solute to interact with surrouding solvent molecules [43,45–47]. The Van der Waals surface area is

defined as the surface of the intersection of all Van der Waals spheres in a molecule and is often referred to as the total surface area (*TSA*) (Table III). The total surface area is correlated with the Van der Waals volume:

$$V_A = 0.70\ (TSA) + 7.34 \qquad r = 0.99;\ n = 35 \tag{13}$$

although in this case individual molecular variations are much greater than was observed for the different volume terms (Fig. 2). The total surface area may reveal subtle structural features not apparent in the volume term but should not lead to gross differences in the computation of the solvent interaction terms. As the dimensions of molecules are always finite compared with the dimensions over which they interact, the total surface area may not be the most appropriate parameter for gauging solute–solvent interactions [45,46,48]. A solvent–accessible surface area can be defined as the locus of the center of a solvent sphere of fixed radius as it is rolled over the Van der Waals surface of the solute. The accessible surface area is directly related to the number of solvent molecules which could be packed around the solute and is thus indirectly related to the energy of solute–solvent interactions. However, as the choice of solvent radius is ill-defined, it has been suggested that the contact surface area could be a better alternative to the solvent-accessible area. The contact surface area is defined as those parts of the Van der Waals surface that can actually make contact with the surface of the probe. Unfortunately, both the solvent–accessible and contact surface areas require a detailed knowledge of the solvent molecules, which would be difficult for us to compute given the wide range of solvent types and size represented by the stationary phases listed in Table I. For comparative purposes we have computed the solvent-accessible surface area of the test solutes for water as solvent (spherical radius 1.4 Å), which are listed in Table III. There is generally only a poor correlation between the solvent–accessible surface area and the total surface area (for water $r = 0.97$, $n = 35$) or molecular volume, V_A (for water $r = 0.95$, $n = 35$), indicating that whereas substituting the total surface area for the molecular

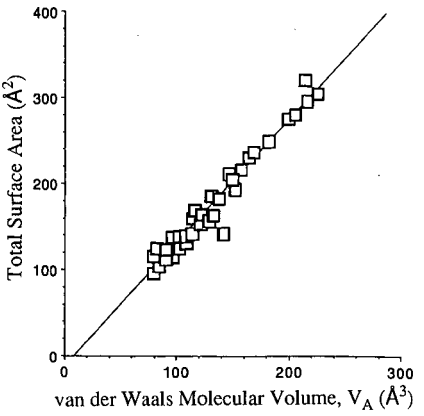

Fig. 2. Plot of the Van der Waals total surface area against the Van der Waals volume, V_A, for the 35 test solutes identified in Table III.

volume would only fine tune the solvent selectivity calculations, the use of the solvent–accessible or contact surface area could significantly modify the predictions obtained. However, the calculation of the solvent-accessible and contact areas is not a trivial task and exceeds our current capabilities for molecular modeling.

In the remaining portion of this paper the Van der Waals volume, V_A, has been used as the basis for the correction term to eliminate the influence of solute size on the solvent selectivity parameter. This is done through the solvent polar interaction parameter (eqn. 6), by subtracting from the partial Gibbs free energy of solution for the equivalent free energy of solution for a hypothetical *n*-alkane with an identical Van der Waals volume. The numerical value of the polar contribution to the free energy of solution corresponds to

$$\Delta G_S^P (X) = - 2.303\ RT \log (K_L^X/K_L^{n'V}) \quad (14)$$

where K_L^X is the gas–liquid partition coefficient for solute (X) and $K_L^{n'V}$ is the gas–liquid partition coefficient for a hypothetical *n*-alkane with an identical Van der Waals volume to solute (X). Values for the latter are simply obtained from the linear relationship between log K_L^{alkane} and the Van der Waals volume:

$$\log K_L^{alkane} = m_S\ V_A (alkane) + b_S \quad (15)$$

where m_S and b_S are the solvent-dependent regression coefficients summarized in Table IV. The limiting factor for the accurate determination of m_S and b_S is the

TABLE IV

REGRESSION COEFFICIENTS AND CORRELATION COEFFICIENTS FOR USE WITH EQN. 15

Stationary Phase	m_S	b_S	r
Squalane	0.0281	−0.5519	1.00
OV-3	0.0247	−0.5313	1.00
OV-7	0.0251	−0.5813	1.00
OV-11	0.0252	−0.6420	1.00
OV-17	0.0249	−0.6609	1.00
OV-22	0.0240	−0.6670	1.00
OV-25	0.0234	−0.6496	1.00
OV-105	0.0240	−0.4791	1.00
OV-225	0.0227	−0.8199	1.00
OV-275	0.0144	−1.4185	0.91
OV-330	0.0233	−0.6978	1.00
QF-1	0.0204	−0.5132	1.00
CW20M	0.0217	−0.7959	1.00
DEGS	0.0156	−0.8136	0.99
TCEP	0.0152	−0.8589	0.99
PPE-5	0.0260	−0.7931	1.00
QpTS	0.0199	−0.6247	1.00
QPIC	0.0215	−0.7857	1.00
QMES	0.0188	−0.4994	1.00
QACES	0.0126	−0.2860	0.99
QTAPSO	0.0091	−0.1254	0.98
DPP	0.0277	−0.6585	1.00
SE-30	0.0244	−0.5263	1.00

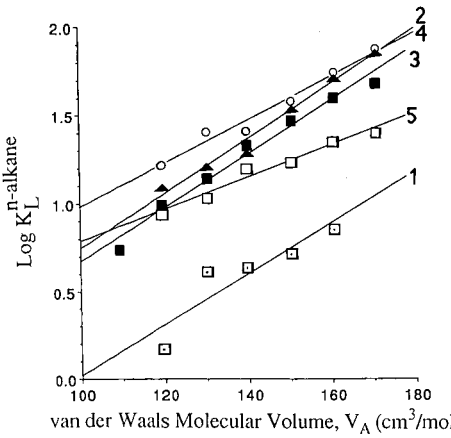

Fig. 3. Plot of the logarithm of the gas–liquid partition coefficient for *n*-alkanes against the Van der Waals volume, V_A, for the stationary phases of high cohesive energy. 1 = OV-275; 2 = DEGS; 3 = TCEP; 4 = QACES; 5 = QTAPSO.

relative magnitude of K_L^{alkane}, which depends on the solubility of the *n*-alkane in the solvent. On the most polar phases *n*-alkanes are retained largely by interfacial adsorption resulting in very small gas–liquid partition coefficients [2,3,8,9]. Log K_L^{alkane} as a function of the Van der Waals volume for the most cohesive phases, the worse case situation, are shown in Fig. 3. The data seems reasonable for DEGS, TCEP, QACES and QTAPSO, but for OV-275 the scatter is too great to believe that the coefficients m_S and b_S in Table IV are any more than roughly determined for this phase.

As an alternative to eqn. 7, it was considered that the cavity and non-polar interaction term might be approximated by

$$\Delta G^{CAV} + \Delta G^{NP} = [V_A/V_{(CH_2)}]\,\Delta G^{CH_2} \tag{16}$$

where $V_{(CH_2)}$ is the van der Waals volume of a methylene group and ΔG^{CH_2} the partial Gibbs free energy of solution for a methylene group. ΔG^{CH_2} can be determined from the periodic change in free energy for any homologous series, such as 2-alkanones, which have much larger gas–liquid partition coefficients on polar phases and show good linear correlations for plots similar to Fig. 3, even for OV-275 [8,9]. However, this approach leads to an overestimate of the left-hand term in eqn. 16 and positive Gibbs free energy of solution values for *n*-alkanes and other non-polar solutes on several phases, which, of course, are theoretically impossible. A plot of the partial molal Gibbs free energy of solution for homologous *n*-alkanes and 2-alkanones as a function of the Van der Waals volume on two different phases is shown in Fig. 4. The intercept term corresponding to the transfer of a solute of zero van der Waals volume is substantial, and further depends on both the identities of the solute and the solvent. This prevents any simple correction term being developed to modify eqn. 16 for its overestimate of the free-energy term. The physical significance of the intercept and its dependence on the identities of the solute and the solvent is not clear. Others have speculated on similar or related findings, but their arguments are not very convincing [26,27,45,46].

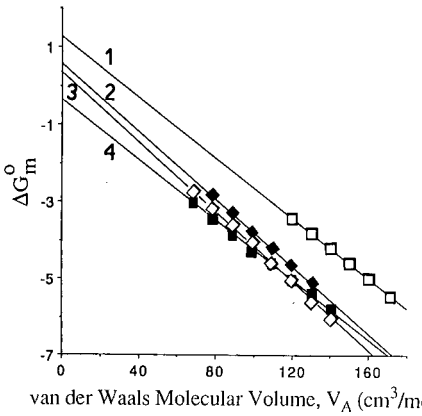

Fig. 4. Plot of the partial molal Gibbs free energy of solution for *n*-alkanes (1 and 2) and 2-alkanones (3 and 4) on SE-30 (2 and 3) and CW20M (1 and 4).

TABLE V

PARTIAL GIBBS FREE ENERGY OF SOLUTION FOR CAVITY FORMATION AND NON-POLAR INTERACTIONS ($\Delta G^{CAV} + \Delta G^{NP}$) AND POLAR INTERACTIONS (ΔG^{P}) ON THE HYDROCARBON STATIONARY PHASE SQUALANE

Test Solute	$\Delta G^{CAV} + \Delta G^{NP}$ (kcal/mol)	ΔG^{P} (kcal/mol)
Benzene	−2.004	−1.156
n-Butylbenzene	−4.058	−1.151
Dihexyl ether	−6.322	−0.044
cis-Hydrindane	−3.713	−1.317
2-Octyne	−3.596	−0.564
1-Dodecyne	−5.674	−0.276
Nonanal	−4.510	−0.675
Dioxane	−2.133	−1.011
Benzodioxane	−3.138	−2.367
N,N-Dimethylaniline	−3.416	−1.877
Anisole	−2.734	−1.636
2,4,6-Trimethylpyridine	−3.373	−1.417
2-Octanone	−3.938	−0.676
1,1,2,2-Tetrachloroethane	−2.756	−1.569
Butanol	−2.154	−0.557
Octanol	−4.253	−0.716
2-Methyl-2-pentanol	−3.178	−0.138
Nitropropane	−1.946	−1.195
Nitropentane	−2.976	−1.241
Nitrobenzene	−2.569	−2.486
Benzonitrile	−2.554	−1.907
Pyridine	−1.867	−1.534
Aniline	−2.337	−2.132
N-Methylaniline	−2.851	−2.185
2,6-Dimethylaniline	−3.352	−2.223

Returning to eqn. 7 and considering the polar interaction term for the test solutes on the hydrocarbon stationary phase squalane (Table V), the polar interaction term characterizes the partial Gibbs free energy of solution which exceeds those interactions of an *n*-alkane of identical Van der Waals volume, and in the case of the hydrocarbon squalane is expected to arise primarily from induction interactions since orientation and proton donor–acceptor interactions should be absent. In all cases ($\Delta G_{SQ}^{CAV} + \Delta G_{SQ}^{NP}$) is greater than ΔG_{SQ}^{P}, which would be expected for squalane. For the homologous test solutes benzene–*n*-butylbenzene, butanol–octonal and nitropropane–nitropentane, the values for ΔG_{SQ}^{P} are very similar, which would be predicted if the estimates of $\Delta G_{SQ}^{CAV} + \Delta G_{SQ}^{NP}$ were realistic. Similarly, the magnitude of ΔG_{SQ}^{P} for the non-polar solutes dihexyl ether, 2-octyne, 1-dodecyne, nonanal and 2-octanone are small with respect to the magnitude of $\Delta G_{SQ}^{CAV} + \Delta G_{SQ}^{NP}$ in agreement with intuition. On the other hand, ΔG_{SQ}^{P} values seem relatively too large for all the aromatic solutes and *cis*-hydrindane, for example, benzene has $\Delta G_{SQ}^{CAV} + \Delta G_{SQ}^{NP} = -2.004$ kcal/mol and $\Delta G_{SQ}^{P} = -1.156$ kcal/mol. It would seem likely that the hardcore Van der Waals volumes are a poor estimate of the size of the cavity and its accessible surface for solvent interactions for aromatic and cyclic solutes. This is part of the justification for referencing ΔG_{S}^{INT} (X) to ΔG_{SQ}^{P} (X) in the hope of correcting, at least partially, for the non-polar contribution to ΔG_{S}^{P} (X) not accounted for by $\Delta G_{S}^{CAV} + \Delta G_{S}^{NP}$ owing to an incorrect estimate of the solvent–accessible cavity surface by the Van der Waals volume for cyclic and aromatic solutes. The other reason is to remove from the solvent interaction term the solute induction contribution to ΔG_{S}^{P} (X). For the solutes with large dipole moments in Table V this contribution is far from negligible.

The sum of $\Delta G_{S}^{CAV} + \Delta G_{S}^{NP}$ for 25 solutes on 21 stationary phases is summarized in Table VI. The cavity term is endoergic and of opposite sign to the nonpolar partial Gibbs free energy of solution term. All values of $\Delta G_{S}^{CAV} + \Delta G_{S}^{NP}$ are negative and increase in magnitude with the size of the solute. For any particular solute the magnitude of the term $\Delta G_{S}^{CAV} + \Delta G_{S}^{NP}$ decreases with increasing solvent strength, in reasonable agreement with the order predicted by the solvent strength parameter [3,8]. To a first approximation, solutes of the same size will have similar contributions from dispersion to the $\Delta G_{S}^{CAV} + \Delta G_{S}^{NP}$ term. For an individual solute the descending order of the $\Delta G_{S}^{CAV} + \Delta G_{S}^{NP}$ term should be roughly proportional to the cavity term, the free energy required to create a hole in the solvent of a certain size by breaking solvent–solvent bonds. This is borne out by multivariate analysis of the data in Table VI, which indicates that 98.6% of the total variance in the data is accounted for by one component vector. The lowest correlation coefficient for any two solutes on all stationary phases in Table VI is $r = 0.90$ (2,4,6-trimethylpyridine *vs.* dihexyl ether) and most values exceed $r = 0.99$. Thus, it can be concluded that $\Delta G_{S}^{CAV} + \Delta G_{S}^{NP}$ is independent of the identity of the solute, except for its size, and is independent of the magnitude of solute-solvent polar interactions. The relative magnitude of $\Delta G_{S}^{CAV} + \Delta G_{S}^{NP}$ indicates that as solute size increases the term becomes more favorable for transfer from the gas phase as ΔG_{S}^{NP} (X) grows faster in importance than the opposing contribution from ΔG_{S}^{CAV} (X). However, the more cohesive the solvent, the less favorable is the cavity term for the transfer from the gas phase and the term, $\Delta G_{S}^{CAV} + \Delta G_{S}^{NP}$ is always less favorable for solvents of high cohesive energy (that is, solvents with a propensity for significant solvent–solvent polar interactions) than for solvents

TABLE VI

CONTRIBUTIONS FROM CAVITY AND NON-POLAR INTERACTION TERMS TO THE SOLUTION OF TEST SOLUTES IN STATIONARY PHASES OF DIFFERENT POLARITY (kcal/mol)

Stationary phase	Benzene	*n*-Butylbenzene	Dihexyl ether	*cis*-Hydrindane	2-Octyne	2-Methyl-2-pentanol	Nitropropane	Nitropentane	Nitrobenzene
SE-30	−1.880	−3.663	−5.629	−3.364	−3.262	−2.898	−1.829	−2.723	−2.370
DPP	−1.643	−3.667	−5.899	−3.328	−3.212	−2.800	−1.586	−2.601	−2.200
OV-105	−1.612	−3.366	−5.300	−3.072	−2.972	−2.614	−1.562	−2.442	−2.095
OV-3	−1.586	−3.391	−5.382	−3.089	−2.986	−2.618	−1.535	−2.440	−2.083
OV-7	−1.489	−3.323	−5.345	−3.015	−2.911	−2.537	−1.437	−2.357	−1.994
OV-11	−1.333	−3.175	−5.205	−2.866	−2.761	−2.385	−1.281	−2.205	−1.840
OV-17	−1.254	−3.074	−5.080	−2.769	−2.665	−2.294	−1.203	−2.115	−1.755
OV-22	−1.141	−2.894	−4.828	−2.600	−2.500	−2.143	−1.091	−1.971	−1.623
PPE-5	−1.041	−2.941	−5.036	−2.622	−2.514	−2.127	−0.987	−1.940	−1.564
OV-225	−0.764	−2.423	−4.252	−2.145	−2.050	−1.712	−0.717	−1.549	−1.221
OV-330	−1.034	−2.736	−4.614	−2.451	−2.354	−2.006	−0.985	−1.839	−1.502
QMES	−1.017	−2.391	−3.905	−2.160	−2.082	−1.802	−0.978	−1.667	−1.395
OV-25	−1.084	−2.794	−4.679	−2.507	−2.409	−2.061	−1.035	−1.893	−1.554
CW20M	−0.705	−2.291	−4.039	−2.025	−1.934	−1.611	−0.660	−1.455	−1.142
QPIC	−0.673	−2.244	−3.976	−1.980	−1.891	−1.570	−0.628	−1.416	−1.105
QpTS	−0.876	−2.330	−3.934	−2.087	−2.004	−1.707	−0.835	−1.564	−1.276
QF-1	−1.003	−2.494	−4.138	−2.244	−2.159	−1.855	−0.961	−1.709	−1.414
QACES	−0.806	−1.727	−2.742	−1.572	−1.520	−1.332	−0.780	−1.242	−1.059
QTAPSO	−0.755	−1.420	−2.153	−1.309	−1.271	−1.135	−0.736	−1.070	−0.938
DEGS	−0.014	−1.153	−2.410	−0.962	−0.897	−0.665	−0.019	−0.553	−0.327
TCEP	−0.004	−1.115	−2.340	−0.929	−0.865	−0.639	−0.027	−0.530	−0.310

	Benzonitrile	Pyridine	2,4,6-Trimethylpyridine	2-Octanone	1,1,2,2-Tetrachloroethane	Butanol	Octanol	1-Dodecyne
SE-30	−2.357	−1.760	−3.068	−3.559	−2.532	−2.020	−3.832	−5.066
DPP	−2.185	−1.507	−2.992	−3.550	−2.384	−1.790	−3.860	−5.260
OV-105	−2.082	−1.495	−2.781	−3.264	−2.254	−1.740	−3.533	−4.746
OV-3	−2.070	−1.465	−2.790	−3.287	−2.247	−1.718	−3.563	−4.812
OV-7	−1.980	−1.366	−2.711	−3.216	−2.160	−1.622	−3.497	−4.767

OV-11	−1.826	−1.210	−2.561	−3.068	−2.007	−1.467	−3.350	−4.624
OV-17	−1.742	−1.132	−2.467	−2.968	−1.920	−1.387	−3.247	−4.506
OV-22	−1.610	−1.023	−2.310	−2.793	−1.783	−1.269	−3.061	−4.275
PPE-5	−1.550	−0.914	−2.308	−2.831	−1.736	−1.179	−3.122	−4.436
OV-225	−1.209	−0.653	−1.870	−2.327	−1.372	−0.885	−2.581	−3.729
OV-330	−1.490	−0.920	−2.169	−2.637	−1.657	−1.158	−2.898	−4.076
QMES	−1.385	−0.925	−1.933	−2.311	−1.520	−1.117	−2.521	−3.472
OV-25	−1.542	−0.969	−2.224	−2.694	−1.710	−1.208	−2.956	−4.140
CW20M	−1.130	−0.599	−1.762	−2.199	−1.285	−0.821	−2.442	−3.539
QPIC	−1.093	−0.567	−1.720	−2.153	−1.248	−0.787	−2.393	−3.480
QpTS	−1.266	−0.779	−1.846	−2.246	−1.408	−0.982	−2.469	−3.475
QF-1	−1.402	−0.903	−1.997	−2.407	−1.549	−1.112	−2.636	−3.667
QACES	−1.053	−0.744	−1.420	−1.673	−1.143	−0.873	−1.814	−2.451
QTAPSO	−0.933	−0.711	−1.199	−1.382	−0.999	−0.804	−1.484	−1.944
DEGS	−0.319	−0.063	−0.774	−1.087	−0.431	−0.097	−1.262	−2.051
TCEP	−0.302	−0.070	−0.745	−1.051	−0.411	−0.085	−1.221	−1.989

	Nonanal	Dioxane	Benzodioxane	N,N-Dimethylaniline	Anisole	Aniline	N-Methylaniline	2,6-Dimethylaniline
SE-30	−4.055	−1.991	−2.864	−3.105	−2.514	−2.169	−2.614	−3.050
DPP	−4.113	−1.769	−2.760	−3.034	−2.363	−1.971	−2.477	−2.971
OV-105	−3.752	−1.722	−2.580	−2.818	−2.236	−1.896	−2.335	−2.763
OV-3	−3.789	−1.699	−2.583	−2.827	−2.228	−1.879	−2.330	−2.771
OV-7	−3.727	−1.603	−2.501	−2.750	−2.141	−1.786	−2.245	−2.692
OV-11	−3.580	−1.448	−2.350	−2.599	−1.988	−1.632	−2.092	−2.542
OV-17	−3.474	−1.368	−2.259	−2.505	−1.901	−1.549	−2.004	−2.448
OV-22	−3.281	−1.250	−2.109	−2.346	−1.764	−1.425	−1.864	−2.292
PPE-5	−3.359	−1.160	−2.090	−2.347	−1.717	−1.349	−1.824	−2.288
OV-225	−2.788	−0.868	−1.680	−1.905	−1.354	−1.033	−1.448	−1.853
OV-330	−3.111	−1.140	−1.974	−2.204	−1.639	−1.310	−1.735	−2.151
QMES	−2.693	−1.103	−1.775	−1.961	−1.505	−1.240	−1.583	−1.918
OV-25	−3.170	−1.190	−2.028	−2.259	−1.692	−1.361	−1.788	−2.206
CM20M	−2.640	−0.804	−1.580	−1.795	−1.269	−0.962	−1.359	−1.746
QPIC	−2.590	−0.771	−1.540	−1.753	−1.231	−0.927	−1.320	−1.704
QpTS	−2.651	−0.967	−1.679	−1.876	−1.393	−1.112	−1.476	−1.830
QF-1	−2.822	−1.096	−1.826	−2.028	−1.533	−1.245	−1.618	−1.981
QACES	−1.929	−0.863	−1.314	−1.439	−1.133	−0.955	−1.185	−1.410
QTAPSO	−1.567	−0.797	−1.122	−1.212	−0.992	−0.863	−1.029	−1.192
DEGS	−1.405	−0.085	−0.643	−0.797	−0.419	−0.198	−0.483	−0.762
TCEP	−1.360	−0.074	−0.618	−0.768	−0.399	−0.184	−0.462	−0.733

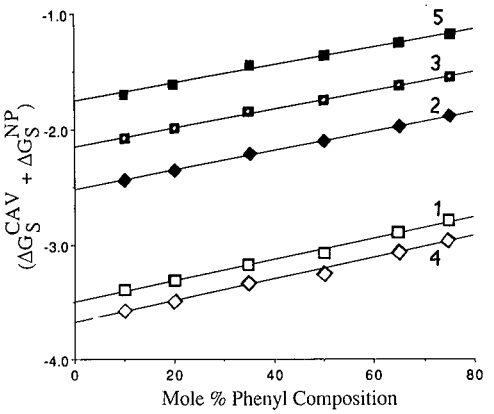

Fig. 5. Plot of $\Delta G_S^{CAV} + \Delta G_S^{NP}$ against mole percentage phenyl composition for a homologous series of poly(methylphenyl)siloxane solvents. 1 = *n*-butylbenzene; 2 = nitropentane; 3 = nitrobenzene; 4 = octanol; 5 = dioxane.

of low cohesive energy. For the homologous series of poly(methylphenyl)siloxanes varying in mole percentage phenyl composition there is a linear decrease in $\Delta G_S^{CAV} + \Delta G_S^{NP}$ with increasing mole percentage phenyl, which is independent of the solute identity (Fig. 5). The linear behavoir supports the view that changes in $\Delta G_S^{CAV} + \Delta G_S^{NP}$ are due to the cavity term, which depends on solvent–solvent interactions only.

The polar interaction term ΔG_S^{INT} (X) for 25 solutes on 21 phases is summarized in Table VII. ΔG_S^{INT} (X) should have values from zero to negative numbers representing solute–solvent interactions that are favorable to the solution process. This is generally the case. A few positive values are observed for weakly selective phase such as SE-30 and/or weakly selective test solutes such as *cis*-hydrindane. In most instances these values are very small and could simply be dismissed as resulting from experimental error [3]; however, as discussed previously for squalane, there may also be a contribution from ΔG_S^{NP} (X) caused by a poor approximation of the solvent-accessible cavity surface by a Van der Waals volume which is only roughly cancelled out by referencing the interactions to those in a hydrocarbon solvent (squalane). This would be particularly true for test solutes such as *cis*-hydrindane. ΔG_S^{INT} (X) should also be independent of solute size for homologous compounds. In Fig. 1 it was shown that of a plot of the partial molal Gibbs free energy of solution for nitropentane against nitropropane did not yield a single correlation with phases of high cohesive energy behaving anomalously compared with the weaker solvents. Fig. 6 shows the behavior for a plot of ΔG_S^{INT} (X) for nitropentane against nitropropane. The highly cohesive phases are no longer behaving anomalously (r = 1.00). The slope, 0.99, is very close to 1.00 and the intercept, −6.77 cal/mol, near zero, indicating that the influence of solute size on the magnitude of polar solute–solvent interactions has been effectively removed. The relevant data for the other homologous solutes are butylbenzene–benzene (r = 0.99, slope = 0.96 and intercept = 43 cal/mol) and octanol–butanol (r = 0.99, slope = 1.06 and intercept = 153.6 cal/mol). For the homologous series of poly(methylphenyl)siloxane solvents, replacing phenyl by methyl should, ignoring secondary interactions as the relative concentration of phenyl groups in-

TABLE VII

CALCULATED VALUES OF $\Delta G_S^{INT}(X)$(kcal/mol)

Stationary phase	Benzene	Butylbenzene	2-Methyl-2-pentanol	1-Nitropropane	1-Nitropentane	Nitrobenzene
OV-3	−0.064	−0.045	−0.272	−0.424	−0.402	−0.252
OV-7	−0.173	−0.154	−0.349	−0.626	−0.609	−0.513
OV-11	−0.303	−0.302	−0.429	−0.857	−0.821	−0.797
OV-17	−0.283	−0.381	−0.467	−0.956	−0.925	−0.947
OV-22	−0.454	−0.478	−0.571	−1.055	−1.014	−1.080
OV-25	−0.580	−0.558	−0.513	−1.076	−1.047	−1.141
OV-105	0.026	0.023	−0.294	−0.418	−0.419	−0.182
OV-225	−1.156	−1.151	−0.138	−1.195	−1.241	−2.486
OV-330	−0.711	−0.685	−1.204	−1.600	−1.539	−1.694
QF-1	−0.105	−0.130	−0.680	−1.316	−1.329	−0.945
CW20M	−1.060	−0.960	−1.582	−2.079	−1.981	−2.294
DEGS	−1.308	−1.409	−2.147	−2.501	−2.518	−2.746
TCEP	−1.546	−1.505	−2.294	−2.965	−2.886	−3.020
PPE-5	−0.786	−0.755	−0.901	−1.427	−1.404	−1.671
QpTS	−0.841	−0.816	−2.359	−2.295	−2.264	−2.480
QPIC	−1.091	−1.038	−1.604	−2.318	−2.315	−2.466
QMES	−0.668	−0.731	−2.347	−2.126	−2.139	−2.336
QACES	−0.584	−0.779	−2.267	−2.035	−2.116	−2.372
QTAPSO	−0.476	−0.791	−2.054	−1.796	−1.956	−2.159
DPP	−0.409	−0.366	−0.666	−1.027	−1.051	−1.100
SE-30	0.092	0.103	−0.143	−0.129	−0.122	0.088

	Benzonitrile	Pyridine	2-Octanone	1,1,2,2-Tetrachloro-ethane	Butanol	Octanol
OV-3	−0.378	−0.227	−0.293	−0.157	−0.461	−0.334
OV-7	−0.569	−0.427	−0.418	−0.375	−0.557	−0.435
OV-11	−0.912	−0.627	−0.562	−0.578	−0.667	−0.571
OV-17	−1.054	−0.734	−0.619	−0.685	−0.740	−0.646
OV-22	−1.200	−0.904	−0.730	−0.793	−0.763	−0.699
OV-25	−1.259	−0.931	−0.606	−0.853	−1.015	−0.726
OV-105	−0.331	−0.135	−0.531	−0.115	−0.462	−0.366
OV-225	−1.907	−1.534	−0.676	−1.569	−0.557	−0.716
OV-330	−1.824	−1.238	−1.051	−1.682	−1.694	−1.590
QF-1	−1.165	−0.638	−1.119	−0.236	−0.723	−0.614
CW20M	−2.444	−1.730	−1.348	−2.198	−2.160	−2.071
DEGS	−2.871	−2.436	−1.992	−2.454	−2.494	−2.570
TCEP	−3.214	−2.493	−2.314	−2.546	−2.748	−2.680
PPE-5	−1.668	−1.233	−1.055	−1.248	−1.155	−1.101
QpTS	−2.627	−1.731	−1.455	−2.636	−3.098	−3.140
QPIC	−2.609	−1.897	−1.818	−1.860	−2.099	−2.074
QMES	−2.477	−1.557	−1.394	−1.683	−3.068	−3.176
QACES	−2.548	−1.589	−1.509	−1.782	−2.926	−3.215
QTAPSO	−2.346	−1.509	−1.535	−1.582	−2.453	−2.827
DPP	−1.182	−0.786	−0.657	−0.787	−0.968	−0.443
SE-30	−0.042	−0.013	−0.121	−0.104	−0.275	−0.177

(Continued on p. 476)

TABLE VII (*continued*)

Stationary phase	1-Dodecyne	Nonanal	Dioxane	Benzodioxane	N,N-Dimethyl-aniline	Anisole
OV-3	−0.175	−0.314	−0.270	−0.209	−0.081	−0.119
OV-7	−0.230	−0.442	−0.430	−0.472	−0.275	−0.291
OV-11	−0.313	−0.587	−0.618	−0.775	−0.514	−0.508
OV-17	−0.364	−0.622	−0.729	−0.944	−0.644	−0.618
OV-22	−0.406	−0.736	−0.834	−1.132	−0.884	−0.763
OV-25	−0.542	−0.771	−0.860	−1.243	−0.915	−0.835
OV-105	−0.148	−0.315	−0.190	−0.084	0	−0.033
OV-225	−0.276	−0.675	−1.011	−2.367	−1.877	−1.636
OV-330	−0.687	−1.050	−1.138	−1.638	−1.161	−1.127
QF-1	−0.226	−1.030	−0.684	−0.386	−0.377	−0.326
CW20M	−0.955	−1.339	−1.569	−2.246	−1.584	−1.585
DEGS	−1.503	−1.976	−2.184	−2.836	−2.154	−2.054
TCEP	−1.274	−2.181	−2.497	−2.981	−2.407	−2.255
PPE-5	−0.572	−1.061	−1.254	−1.614	−1.251	−1.168
QpTS	−0.958	−1.519	−1.327	−2.168	−1.419	−1.432
QPIC	−0.890	−1.740	−1.662	−2.110	−1.814	−1.621
QMES	−0.981	−1.430	−1.182	−2.038	−1.317	−1.298
QACES	−1.018	−1.030	−1.278	−2.205	−1.484	−1.362
QTAPSO	−1.042	−1.619	−1.204	−2.077	−1.520	−1.278
DPP	−0.301	−0.498	−0.610	−0.924	−0.566	−0.129
SE-30	−0.070	−0.135	−0.067	−0.114	−0.163	0.099

	Aniline	N-Methyl-aniline	2,6-Dimethyl-aniline	2-Octyne	*cis*-Hydrindane	Dihexyl ether	Trimethyl-pyridine
OV-3	−0.277	−0.164	−0.144	−0.132	−0.087	−0.145	0.142
OV-7	−0.517	−0.398	−0.377	−0.222	−0.009	−0.177	−0.118
OV-11	−0.792	−0.668	−0.649	−0.327	−0.091	−0.243	−0.341
OV-17	−0.941	−0.817	−0.804	−0.384	−0.136	−0.285	−0.520
OV-22	−1.128	−0.993	−0.985	−0.466	−0.209	−0.344	−0.689
OV-25	−1.222	−1.149	−1.092	−0.524	−0.243	−0.405	−0.734
OV-105	−0.258	−0.121	−0.100	−0.061	−0.183	−0.125	−0.370
OV-225	−2.132	−2.185	−2.223	−0.564	−1.316	0.044	−1.417
OV-330	−2.096	−1.712	−1.686	−0.637	−0.206	−0.395	−0.033
QF-1	−0.606	−0.468	−0.467	−0.016	−0.206	−0.229	−1.049
CW20M	−2.898	−2.335	−2.344	−0.783	−0.313	−0.457	−1.571
DEGS	−3.314	−2.793	−2.962	−1.102	−0.531	−0.877	−2.456
TCEP	−3.662	−3.129	−3.297	−1.161	−0.510	−0.923	−2.154
PPE-5	−1.694	−1.535	−1.518	−0.627	−0.396	−0.410	−1.128
QpTS	−3.427	−2.906	−2.528	−0.488	−0.179	−0.415	−0.897
QPIC	−2.946	−2.537	−1.528	−0.541	−0.363	−0.480	−0.391
QMES	−3.362	−2.840	−2.576	−0.350	−0.065	−0.460	−0.925
QACES	−3.395	−2.869	−2.765	−0.289	−0.016	−0.429	−1.064
QTAPSO	−3.025	−2.567	−2.612	−0.177	−0.013	−0.889	−1.199
DPP	0.069	−0.318	−0.252	−0.237	−0.255	−0.155	−0.897
SE-30	0.012	0.125	0.154	−0.019	0.176	−0.056	−0.109

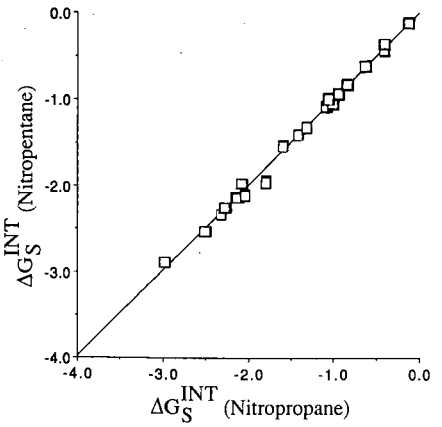

Fig. 6. Plot of ΔG_S^{INT} (nitropentane) against ΔG_S^{INT} (nitropropane) for the normal and highly cohesive stationary phases in Table I except for OV-275 and OV-225.

creases, produce a proportional change in ΔG_S^{INT} (X) for individual solutes. For an individual solute ΔG_S^{INT} (X) should depend only on the relative mole percentage of phenyl groups; for different solutes ΔG_S^{INT} (X) should depend on the strength of the intermolecular interactions with a phenyl group that exceeds those with a methyl group and the relative concentration of phenyl to methyl groups. This, again is shown to be a reasonably good approximation for different test solutes (Fig. 7). Overall, the correlation coefficients for ΔG_S^{INT} (X) against mole percentage phenyl concentration vary from $r = 0.88$ to 0.99 for the poly(methylphenyl)siloxane solvents with an average value of $r = 0.97 \pm 0.02$ ($n = 25$). ΔG_S^{INT} (X) seems to meet reasonable expectations for a solvent–dependent term to measure orientation and hydrogen bond acid–base interactions.

Prior to multivariate analysis of the data matrix of ΔG_S^{INT} (X) in Table VII, a reduction in the matrix was performed to minimize the contributions from those factors behaving anomalously or independently. The data for OV-225 and OV-275

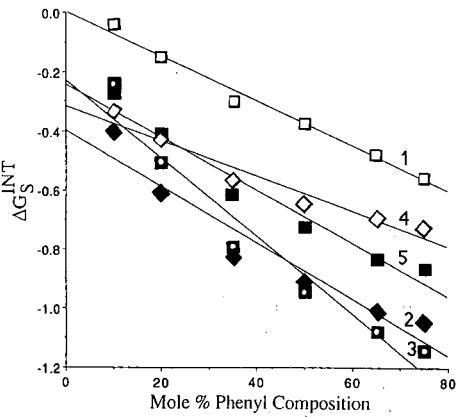

Fig. 7. Plot of ΔG_S^{INT} (X) against mole percentage phenyl for homologous series of poly(methylphenyl) siloxane solvents. 1 = *n*-butylbenzene; 2 = nitropentane; 3 = nitrobenzene; 4 = octanol; 5 = dioxane.

were removed. The low solubility of *n*-alkanes in OV-275 prevented the gas–liquid partition coefficients from being determined with similar accuracy to the other phases, as discussed previously. With OV-225 an unusual dependence on the value of ΔG_S^{INT} (X) with the absolute magnitude of the Van der Waals volume was observed. Some representative values of ΔG_S^{INT} (X) using the different Van der Waals volumes and total surface area are summarized in Table VIII. ΔG_S^{INT} (X) calculated using the

TABLE VIII

COMPARISON OF VALUES FOR ΔG_S^{INT} (X) ON SEVERAL STATIONARY PHASES CALCULATED FROM DIFFERENT VAN DER WAALS VOLUMES AND TOTAL SURFACE AREA (kcal/mol)

Test solute	Stationary phase	Van der Waals volume or surface area			
		V_A	V_I	V_X	*TSA*
Butylbenzene	OV-3	−0.045	−0.050	−0.064	0.013
	OV-17	−0.381	−0.395	−0.417	−0.302
	OV-25	−0.558	−0.555	−0.561	−0.441
	OV-225	−1.151	−1.094	−0.759	−0.622
	CW20M	−0.960	−0.959	−0.982	−0.823
	DEGS	−1.409	−1.438	−1.437	−1.213
	QMES	−0.731	−0.757	−0.760	−0.562
	QTAPSO	−0.791	−0.826	−0.839	−0.505
Nitrobenzene	OV-3	−0.252	−0.265	−0.265	−0.179
	OV-17	−0.947	−0.963	−0.963	−0.813
	OV-25	−1.141	−1.147	−1.147	−0.965
	OV-225	−2.486	−2.374	−2.374	−0.161
	CW20M	−2.294	−2.306	−2.306	−2.091
	DEGS	−2.746	−2.795	−2.795	−2.456
	QMES	−2.372	−2.375	−2.375	−2.090
	QTAPSO	−2.159	−2.232	−2.237	−1.761
Octanol	OV-3	−0.334	−0.322	−0.336	−0.315
	OV-17	−0.646	−0.645	−0.668	−0.618
	OV-25	−0.726	−0.699	−0.705	−0.675
	OV-225	−0.716	−0.800	−1.479	−1.444
	CW20M	−2.071	−2.038	−2.062	−2.020
	DEGS	−2.570	−2.536	−2.536	−2.530
	QMES	−3.176	−3.156	−3.159	−3.125
	QTAPSO	−2.827	−2.767	−2.780	−2.767
Dioxane	OV-3	−0.270	−0.243	−0.252	−0.219
	OV-17	−0.729	−0.704	−0.715	−0.608
	OV-25	−0.860	−0.809	−0.806	−0.707
	OV-225	−1.011	−1.235	−1.240	−1.137
	CW20M	−1.569	−1.504	−1.510	−1.399
	DEGS	−2.184	−2.080	−2.074	−1.964
	QMES	−1.182	−1.107	−1.102	−0.987
	QTAPSO	−1.204	−1.049	−1.050	−0.919
N,N-Dimethylaniline	OV-3	−0.081	−0.084	−0.096	−0.010
	OV-17	−0.644	−0.653	−0.672	−0.762
	OV-25	−0.915	−0.906	−0.909	−0.761
	OV-225	−1.877	−1.849	−1.259	−1.092
	CW20M	−1.584	−1.577	−1.594	−1.404
	DEGS	−2.154	−2.168	−2.166	−1.891
	QMES	−1.317	−1.330	−1.331	−1.094
	QTAPSO	−1.520	−1.536	−1.545	−1.144

total Van der Waals surface area is always less than when calculated using the computer-calculated Van der Waals volume, V_A, but is highly correlated with it. The trends predicted remain the same. For phases other than OV-225, ΔG_S^{INT} (X) calculated using V_A, V_I and V_X show acceptable agreement. OV-225 shows large variations for many solutes when different measures of the Van der Waals volume are used. There seems to be no obvious reason why ΔG_S^{INT} (X) values on OV-225 would be uniquely sensitive to the absolute value of the Van der Waals volume, given the general good correlation among the volume terms, and the fact that similar behavior was not apparent for any of the other phases listed in Table I. The experimental data for OV-225 are reproducible and this aberation is due to a real physical phenomenon on which we reserve judgement. Removing OV-225 from the data set, however, provides a better classification of solute and phase properties by removing the heavy weighting given to the characteristics of this phase by multivariate analysis.

A correlation matrix of the scaled data for ΔG_S^{INT} (X) (each variable was mean centered with a standard deviation of one) was produced to evaluate the relationship between individual variables. A correlation of 0.90 or greater was considered to be a reasonable indication that the variables are correlated, that is, displaying the same retention mechanisms. The variables meeting this test are summarized in Table IX for the two cases where it seems reasonable to assign a particular interaction as a dominant interaction as well as those test solutes that can be classified as behaving independently (uncorrelated with any other test solute with $r > 0.92$). The largest group of highly correlated test solutes have large dipole moments or are easily polarizable and it seems reasonable to associate these test solutes with strong orientation interactions. Dioxane might seem to be anomalous within this group given its small bulk dipole moment, but in fact it has been demonstrated that the local dipole moment preceived by a solvent molecule for dioxane is much greater than that predicted by the bulk dipole moment [28]. The correlation with the alkanols should not be taken as anomalous because of their strong hydrogen-bond donor properties, as they also have substantial dipole moments.

The second group of correlated test solutes is headed by the alkanols and apart from benzonitrile, nitrobenzene and nitropentane, contains solutes with proton donor properties. *n*-Octanol seems to be a reasonable test solute for probing hydrogen-bonding interactions and all the alkanols are highly correlated in the data set. All of the proton-donor solutes have significant dipole moments in addition explaining the modest correlation with benzonitrile, nitrobenzene and nitropentane. The absence of a strong proton acceptor interaction for pyridine, dioxane and benzodioxane has been discussed elsewhere [3,17]. These solutes are either retained predominantly by orientation interactions or the set of stationary phases used for the analysis does not contain a sufficient number of strong hydrogen-bond donor solvents to differentiate this mechanism. The former seems to be the most likely answer [2,3,8,16].

The remaining four solutes in Table IX show few strong correlations with other solutes (dihexyl ether, $r = 0.91$ with 1-dodecyne and nonanal and 0.90 with N,N-dimethylaniline; *cis*-hydrindane, $r = 0.92$ with 2-octyne) and must be considered as behaving independently. Three of them, *cis*-hydrindane, dihexyl ether and 2-octyne, have little orientation or proton donor–acceptor capacity and cannot be considered as selective polar solutes. Their principal interactions must be dispersive interactions and most likely the ΔG_S^{INT} (X) term consists of weak polar interactions and dispersive

TABLE IX

SUMMARY OF CORRELATED VALUES ABSTRACTED FROM THE CORRELATION MATRIX

Solute	Correlation Coefficient	Solute	Correlation Coefficient
(a) Orientation interactions		*(b) Proton donor–acceptor interactions*	
Nitrobenzene	1.00	Octanol	1.00
Benzonitrile	1.00	Butanol	0.99
Nitropentane	0.99	2-Methyl-2-pentanol	0.99
Nitropropane	0.99	Aniline	0.97
Benzodioxane	0.98	N-Methylaniline	0.97
Pyridine	0.98	2,6-Dimethylaniline	0.95
N,N-Dimethylaniline	0.97	Benzonitrile	0.92
N-Methylaniline	0.97	1-Dodecyne	0.91
1,1,2,2-Tetrachloroethane	0.97	Nitrobenzene	0.91
Anisole	0.96	Nitropentane	0.91
1-Dodecyne	0.96	*(c) Solutes behaving independently*	
Aniline	0.96	*cis*-Hydrindane	
Butylbenzene	0.95	Dihexyl ether	
2-Octanone	0.95	2-Octyne	
2,6-Dimethylaniline	0.95	2,4,6-Trimethylpyridine	
Nonanal	0.95		
Dioxane	0.94		
2-Methyl-2-pentanol	0.94		
Butanol	0.94		
Octanol	0.91		
Benzene	0.91		

interactions inadequately accounted for in eqn. 8. 2,4,6-Trimethylpyridine seems to be a genuine outsider and exhibits properties that are not even similar to pyridine [3,17].

To define better the behavior of the test solutes, the scaled data were subjected to principal component analysis. Eigenvectors were extracted from the data such that the maximum information in the form of variance was preserved with a minimum number of eigenvectors. A summary of the results is presented in Table X. Two vectors are sufficient to account for most of the variance. Eliminating the four test solutes behaving independently from the data matrix increases the cumulative variance for the first two principal components from 93.46% to 96.17%. Eliminating OV-225 from the reduced solute data set further increases the cumulative variance to 97.43% for the first two principal components. For each case the variance for the second eigenvector is reduced compared with the first and inspection of the classifications obtained indicated a more logical grouping when the independent test solutes and OV-225 and OV-275 were deleted from the data set. This left a data set containing 21 solutes separated on 20 stationary phases that was used for subsequent pattern recognition analysis.

Scrutinizing the loadings (how much each test solute contributes to the principal component) (Table XI) indicates that the first component was heavily weighted towards solutes recognizable as having a significant capacity for orientation interactions. Loading 2 is heavily weighted towards solutes recognizable as having signif-

TABLE X

SUMMARY OF EIGENVECTOR AND PRINCIPAL COMPONENT ANALYSIS OF THE DATA MATRIX

Eigenvector	Eigenvalue	Percentage variance	Percent cumulative variance
(a) All solutes in Table VII			
1	21.2426	84.97	84.97
2	2.1240	8.49	93.46
3	0.7616	3.04	96.51
4	0.3467	1.38	97.89
(b) Eliminating solutes behaving independently in Table VIII			
1	19.0773	90.84	90.84
2	1.1196	5.33	96.17
3	0.4297	2.04	98.22
(c) Eliminating OV-225 from phases in Table I with same solutes as in (b)			
1	19.6555	93.59	93.59
2	0.8054	3.83	97.43
3	0.2326	1.10	98.53

icant proton donor–acceptor capacity, the proton donor solutes having positive coefficients and the proton acceptor solutes having negative coefficients. The proton donor solutes represented by the alkanols would be expected to have a greater capac-

TABLE XI

SUMMARY OF THE LOADINGS FOR THE FIRST THREE PRINCIPAL COMPONENTS (21 SOLUTES ON 20 PHASES)

Variable	Loading 1	Variable	Loading 2	Variable	Loading 3
Benzonitrile	0.0224	Octanol	0.0439	2-Octanone	−0.0530
Nitrobenzene	0.0224	Benzene	−0.0398	Nonanal	−0.0435
Pyridine	0.0223	Butanol	0.0378	Nitropentane	−0.0300
Benzodioxane	0.0223	2-Methyl-2-pentanol	0.0345	1,1,2,2-Tetrachloroethane	0.0282
Nitropentane	0.0223	Dioxane	−0.0309	Nitropropane	−0.0259
Nitropropane	0.0222	Butylbenzene	−0.0277	Benzodioxane	0.0242
N,N-Dimethylaniline	0.0221	Aniline	0.0213	2,6-Dimethylaniline	0.0223
N-Methylaniline	0.0221	N,N-Dimethylaniline	−0.0188	Benzene	0.0207
Anisole	0.0221	N-Methylaniline	0.0186	Butylbenzene	0.0166
1-Dodecyne	0.0221	2,6-Dimethylaniline	0.0158	Anisole	0.0165
1,1,2,2-Tetrachloroethane	0.0219	Anisole	−0.0158	1-Dodecyne	0.0159
Aniline	0.0219	Pyridine	−0.0148	Aniline	0.0120
2,6-Dimethylaniline	0.0218	Nonanal	−0.0125	N-Methylaniline	0.0118
Butylbenzene	0.0217	2-Octanone	−0.0073	2-Methyl-2-pentanol	−0.0110
2-Octanone	0.0216	Benzodioxane	−0.0063	Benzonitrile	−0.0093
Nonanal	0.0216	Nitropropane	−0.0036	N,N-Dimethylaniline	0.0082
Dioxane	0.0216	1-Dodecyne	0.0032	Dioxane	−0.0048
2-Methyl-2-pentanol	0.0213	Benzonitrile	0.0028	Butanol	0.0042
Butanol	0.0212	Nitrobenzene	0.0010	Nitrobenzene	−0.0040
Octanol	0.0207	Nitropentane	0.0006	Octanol	0.0015
Benzene	0.0207	1,1,2,2-Tetrachloroethane	0.0001	Pyridine	−0.0001

ity for solvent proton acceptor interactions than the proton acceptor solutes typified by benzene, dioxane, butylbenzene and N,N-dimethylaniline as the four most heavily weighted solutes for solvent proton donor interactions. These solutes would normally be considered weak hydrogen-bond bases and most likely better test solutes could be found to represent this interaction. The weak weighting of loading 2 towards orientation solutes indicates reasonable discrimination of properties. Loading 3 seems to be most heavily weighted towards solutes with a combination of moderate dipole and moderate proton donor–acceptor properties and provides a less clearly defined axis for discrimination. However, loading 3 is headed by solutes only moderately weighted in loading 2, so it should provide a complementary classification of stationary phase properties.

The plot of loading 1 (orientation) against loading 2 (proton donor–acceptor) and loading 1 against loading 3 (Fig. 8) provides a classification of the solutes as to type. In the plot of loading 1 against 2 solutes exhibiting essentially orientation interactions are distributed along the central axis. Those solutes with the largest dipole moments are located towards the right-hand side of the figure. The alcohols are closely grouped in the upper left hand portion of the plot and are suitable test solutes for solvent proton acceptor interactions. A secondary group displaced from the central axis consisting of aniline, N-methylaniline and 2,6-dimethylaniline also shows significant proton donor capacity. The test solutes for solvent proton donor capacity are diffusely scattered in the lower proton of the plot and are not as effective as the alkanols at defining a particular interaction. The loading plot 1 against 3 shows little clustering confirming the non-discriminate nature of axis 3 for identifying solutes with significant proton donor–acceptor interactions.

In the same manner that the principal component plots of the loadings can be used to classify the test solutes, the scores plots can be used to classify the stationary phases based on their interactions with the test solutes (Fig. 9). Score 1 against score 2 forms a tight cluster with the liquid organic sulfonate salts (QpTS, QTAPSO, QACES, and QMES) exhibiting strong orientation and proton acceptor properties, uniquely different to the other phases. Slightly more diffuse is the group (TCEP, DEGS, CW 20M, and QPIC, which exhibit strong orientation interactions. The third group contains the poly(siloxanes) SE-30, OV-105, OV-3, OV-7, OV-11, OV-17, OV-22 and OV-25, showing increasing polarity as the mole percentage of phenyl groups is increased. PPE-5 and QF-1 are on the boundary of this group while OV-330 is close to the center of the crosshairs, indicating a balance between orientation and proton donor–acceptor interactions. Score 1 against 3 shows less clustering although groups 1 and 3, discussed above, can still be discerned, if less distinctly than the plot of score 1 against score 2. QF-1 is now seen to behave independently. QF-1 is known to show selectivity for ketone groups. Loading 3 is heavily weighted towards 2-octanone, explaining this change in position. Overall, the score plots provide a logical and intuitive classification of the phases supporting the general usefulness of the solvent model presented in this paper. In general, the method chosen to estimate the molecular volume of solutes and *n*-alkanes is not too important when a reference hydrocarbon solvent is used to compensate for deficiencies in the assumption that the hard sphere volume of the molecules is proportional to the contact surface of the cavity. The strength of the ΔG_S^{INT} (X) parameter is the very high degree of correlation observed for the behavior of solutes of a similar kind in a wide range of solvents and its

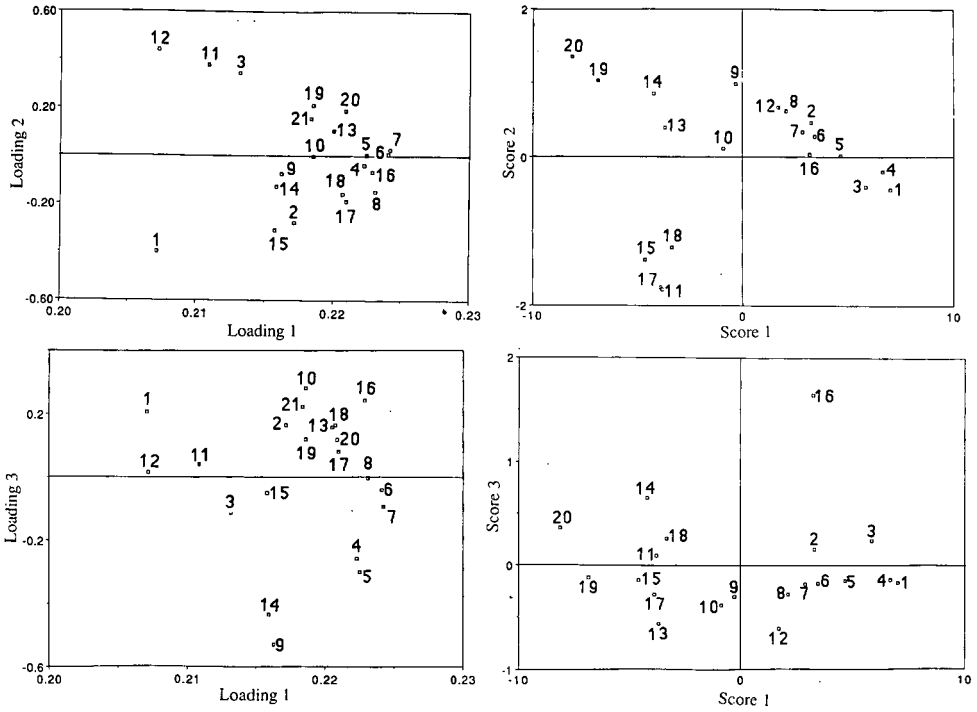

Fig. 8. Principal component plots of loading 2 and loading 3 against loading 1. Test solutes are identified in Table I (number on axis × 10).

Fig. 9. Principal component plots of score 2 and score 3 against score 1. Stationary phases are identified in Table I.

ability to classify solvents in accordance to their capacity for orientation and proton donor–acceptor interactions in a logical manner.

In conclusion, the parameter ΔG_S^{INT} (X) has been shown to provide a quantitative measure of solute–solvent orientation and proton donor–acceptor interactions that are independent of solute size. ΔG_S^{INT} (X) can be simply determined from experimental values for the partial molal Gibbs free energy of solution of solute (X) and appropriate *n*-alkanes on solvent S and squalane and can be determined for any phase in which the solute (X) and *n*-alkanes are sufficiently soluble to provide reasonable values for the gas–liquid partition coefficient.

REFERENCES

1 C. F. Poole and S. A. Schuette, *Contemporary Practice of Chromatography*, Elsevier, Amsterdam, 1984, p. 42.
2 C. F. Poole and S. K. Poole, *Chem. Rev.*, 89 (1989) 377.
3 S. K. Poole and C. F. Poole, *J. Chromatogr.*, 500 (1990) 329.
4 R. V. Golovnya and T. A. Misharina, *J. High Resolut. Chromatogr. Chromatogr. Commun.*, 3 (1980) 4.
5 J. A. Yancey, *J. Chromatogr. Sci.*, 24 (1986) 117.
6 M. V. Budahegyi, E. R. Lombosi, T. S. Lombosi, S. Y. Meszaros, Sz. Nyiredy, G. Tarjan, I. Timar and J. M. Takacs, *J. Chromatogr.*, 271 (1983) 213.

7 B. R. Kersten, C. F. Poole and K. G. Furton, *J. Chromatogr.*, 411 (1987) 43.
8 B. R. Kersten, S. K. Poole and C. F. Poole, *J. Chromatogr.*, 468 (1989) 235.
9 S. K. Poole, B. R. Kersten and C. F. Poole, *J. Chromatogr.*, 471 (1989) 91.
10 C. F. Poole, S. K. Poole, R. M. Pomaville and B. R. Kersten, *J. High Resolut. Chromatogr. Chromatogr. Commun.*, 10 (1987) 670.
11 C. E. Figgins, T. H. Risby and P. C. Jurs. *J. Chromatogr. Sci.*, 14 (1976) 453.
12 R. V. Golovnya and T. A. Misharina, *J. High Resolut. Chromatogr., Chromatogr. Commun.*, 3 (1980) 51.
13 K. G. Furton and C. F. Poole, *J. Chromatogr.*, 399 (1987) 47.
14 J. Novak, *J. Chromatogr.*, 78 (1973) 269.
15 M. Roth and J. Novak, *J. Chromatogr.*, 234 (1982) 337.
16 B. R. Kersten and C. F. Poole, *J. Chromatogr.*, 452 (1988) 191.
17 T. O. Kollie and C. F. Poole, *J. Chromatogr.*, 550 (1991) 213.
18 M. H. Abraham, R. M. Doherty, M. J. Kamlet and R. W. Taft, *Chem. Br.*, 22 (1986) 551.
19 M. J. Kamlet, R. M. Doherty, J.-L. M. Abboud, M. H. Abraham and R. W. Taft, *Chemtech*, (1986) 566.
20 R. W. Taft, J.-L. M. Abboud, M. J. Kamlet and M. H. Abraham, *J. Solution Chem.*, 14 (1985) 153.
21 M. H. Abraham, P. L. Grellier, R. A. McGill, R. M. Doherty, M. J. Kamlet, T. N. Hall, R. W. Taft, P. W. Carr and W. J. Koros, *Polymer*, 28 (1987) 1363.
22 M. H. Abraham and R. Fuchs, *J. Chem. Soc., Perkin Trans. 2*, (1988) 523.
23 M. H. Abraham, P. L. Greillier, I. Hamerton, R. A. McGill, D. V. Prior and G. S. Whiting, *Faraday Discuss. Chem. Soc.*, 85 (1988) 107.
24 M. H. Abraham, G. S. Whiting, R. M. Doherty and W. J. Shuley, *J. Chromatogr.*, 518 (1990) 329.
25 L. R. Snyder, *J. Chromatogr.*, 92 (1974) 223.
26 L. R. Snyder, *J. Chromatogr. Sci.*, 16 (1978) 223.
27 H. Poppe and E. H. Slaats, *Chromatographia*, 14 (1981) 89.
28 M. J. Kamlet, R. W. Taft, P. W. Carr and M. H. Abraham, *J. Chem. Soc., Faraday Trans. 1*, 78 (1982) 1689.
29 S. C. Rutan, P. W. Carr and R. W. Taft, *J. Phys. Chem.*, 93 (1989) 4292.
30 S. C. Rutan, P. W. Carr, W. J. Cheong, J. H. Park and L. R. Snyder, *J. Chromatogr.*, 463 (1989) 21.
31 W. J. Cheong and P. W. Carr, *J. Chromatogr.*, 500 (1990) 215.
32 M. H. Abraham, A. Nasehzadeh, J. J. Moura Ramos and J. Reisse, *J. Chem. Soc., Perkin Trans. 2*, (1980) 854.
33 C. F. Poole, R. M. Pomaville and T. A. Dean, *Anal. Chim. Acta*, 225 (1989) 193.
34 R. M. Pomaville and C. F. Poole, *Anal. Chem.*, 60 (1988) 1103.
35 A. Bondi, *J. Phys. Chem.*, 68 (1964) 441.
36 J. C. McGowan, *J. Appl. Chem. Biotechnol.*, 28 (1978) 599.
37 J. C. McGowan, *J. Chem. Tech. Biotechnol.*, 34A (1984) 38.
38 M. H. Abraham and J. C. McGowan, *Chromatographia*, 23 (1987) 243.
39 D. E. Leahy, *J. Pharm. Sci.*, 75 (1986) 629.
40 D. E. Leahy, P.W. Carr, R. S. Pearlman, R. W. Taft and M. J. Kamlet, *Chromatographia*, 21 (1976) 473.
41 M. J. Kamlet, R. M. Doherty, P. W. Carr, D. Mackay, M. H. Abraham and R. W. Taft, *Environ. Sci. Technol.*, 22 (1988) 503.
42 F. Mohamadi, N. G. J. Richards, W. C. Guida, R. Liskamp, M. Lipton, C. Caufield, G. Chang, T. Hendrickson and W. C. Still, *J. Comput. Chem.*, 11 (1990) 440.
43 J. B. Moon and W. J. Howe, *J. Mol. Graphics*, 7 (1989) 109.
44 R. S. Bohacek and W. C. Guida, *J. Mol. Graphics*, 7 (1989) 113.
45 R. S. Pearlman, in S. H. Valkowsky, A. A. Sinkula and S. C. Valvani (Editor), *Physical and Chemical Properties of Drugs*, Marcel Dekker, New York, 1980, p. 321.
46 W. J. Dunn, J. H. Block, and R. S. Pearlman, *Partition Coefficients. Determination and Estimation*, Pergamon Press, New York, 1986.
47 P. Camilleri, S. A. Watts and J. A. Boraston, *J. Chem. Soc., Perkin Trans. 2*, (1988) 1699.
48 B. K. Lee and F. M. Richards, *J. Mol. Biol.*, 55 (1971) 379.

Journal of Chromatography, 556 (1991) 485–493
Elsevier Science Publishers B.V., Amsterdam

CHROM. 23 407

Gas chromatographic comparative study of Superox 20M immobilized in different ways

E. FERNÁNDEZ-SÁNCHEZ, A. FERNÁNDEZ-TORRES, J. A. GARCÍA-DOMÍNGUEZ* and M. D. SALVADOR-MOYA[a]

Instituto de Química Física "Rocasolano", C.S.I.C. Serrano 119, 28006 Madrid (Spain)

ABSTRACT

Three capillary columns of Superox 20M, two of them immobilized in different ways, were prepared. All columns showed a transition zone from adsorption of the solutes at low temperatures to absorption at higher temperatures. The minimum allowed operating temperature of the column was found to change from 64°C to 50°C when the polymer was immobilized. Partial molar enthalpies of mixing showed that alkanes are poor solvents of the stationary phase, while aromatics are good solvents, with little dependence on the degree of immobilization. It might be expected that Superox 20M will mix well with polymers with phenyl components, and will not mix with polymers of long hydrocarbon-type chains.

INTRODUCTION

Capillary columns have gained more importance in gas chromatography (GC) because of the high resolution which they offer. Immobilization of the polymer used as stationary phase produces additional advantages such as lower bleeding and consequently longer life and a higher maximum operating temperature (MOT) of the column. However, immobilization implies certain chemical reactions of the polymer, and this may lead to a modification of its behaviouur as stationary phase. Differences may come to light by the estimation of the McReynolds' constants [1] of the polymer.

Superox 20M has been considered as one of the preferred liquid phases for GC [2,3], and it is for this reason that it has been chosen here to compare its behaviour under two different immobilization procedures.

Our interest has been focused on the effect of immobilization on two aspects: (a) the phase transition temperature (melting point) and (b) the change in the behaviour of a number of selected probes. The latter point might imply the possibility of prediction of the solubility of Superox 20M in other polymers as deduced from the values of the enthalpies of mixing of the solutes, depending on their functional groups. This would contribute to the understanding of the problem of the use of mixed stationary phases in GC.

[a] Present address: Universidad de Castilla - La Mancha, EUITA, Ronda de Calatrava, s/n. 13004 Ciudad Real, Spain.

0021-9673/91/$03.50

EXPERIMENTAL

The work described here refers to three different columns made of borosilicate glass. Columns were drawn on a Shimadzu GDM-1B drawing machine to a final internal diameter of 0.259 mm, as determined with the help of a NIKON micro-comparator. All three tubes were leached, washed and dehydrated in the same way, as described by Grob [4]. Once deactivated (see later) all three tubes were filled with the appropriate solution and evaporated by the static procedure described by Grob [5]. Column 1 was deactivated with Carbowax 20M [6–9], and then filled with a 0.425% (w/v) solution of Superox 20M on methylene chloride–pentane (50:50). Column 2 was deactivated in the same way, and then filled with the solution of Superox 20M to which dicumyl peroxide (DCP) had been added (20% of the Superox 20M content), according to the immobilization procedure described by Bystricky [10] for Carbowax-type stationary phases. Column 3 was deactivated with glicydoxypropyl trimethoxy-silane (GPTMS) and immobilized with GPTMS and DCP, as described by Traitler [11]. Once prepared, all three columns were conditioned by passing nitrogen while slowly temperature programmed up to 150°C, at which temperature they were maintained for a few hours. Grob's test [12–14] was run on the three columns. Table I describes the physical characteristics of the columns.

TABLE I

CHARACTERISTICS OF THE GLASS CAPILLARY COLUMNS USED IN THIS WORK

	Column 1	Column 2	Column 3
Length (m)	23.36	22.0	25.0
Deactivation	Carbowax 20M	Carbowax 20M	GPTMS
Immobilization	None	DCP	GPTMS + DCP
Film thickness (μm)	0.275	0.261	0.264
Mass of stationary phase (mg)	5.23	4.67	5.35

Solutes used in this work to obtain the results described include: *n*-hexane, *n*-octane, *n*-decane, *n*-undecane, *n*-dodecane, benzene, toluene and *n*-butanol. Other solutes were also used but results have not been included. Chromatograms were run at 16–18 temperatures between 35 and 150°C in each column. Carrier gas flow-rate was measured at the end of the column with a soap film flow meter at every temperature. Three gas chromatographs were used —two HP-9890 and a Varian 3300— all fitted with a flame ionization detector and split injection mode. Column head pressures were monitored with two pressure transducers calibrated in Torr (Felix Mateo Model 2900) and with a mercury manometer. Atmospheric pressure was checked several times during the day with a mercury barometer. The sample amount was always of the order of 0.02 μl, injected with a split ratio of about 1:20. Retention volumes used are always the average of at least three experiments. A mathematical dead time estimation method based on the retention of at least four *n*-alkanes [15] was used to find correct experimental retention volumes.

Whenever several chromatograms were run at different temperatures, the

sequence was always from low to high temperature to prevent any recrystallization of the stationary phase upon cooling of the column. Columns were left at 35°C overnight.

DATA REDUCTION

Specific retention volumes were calculated according to the expression:

$$V_g = \frac{F_0 j}{w_1} \cdot t'_R \cdot \frac{273}{T} \cdot \frac{(p_0 - p_w)}{p_0} \tag{1}$$

were V_g is the specific retention volume of the substance; F_0 is the carrier gas flow-rate, as measured at the column outlet, at ambient temperature (T) and atmospheric pressure (p_0); j is James and Martin's correction factor; w_1 is the mass of the stationary phase in the column; t'_R is the adjusted retention time of the solute: T is the absolute temperature of the carrier gas in the flow meter; p_0 is the pressure of the carrier gas in the flow meter, in our case atmospheric pressure; and p_w is the vapour pressure of the water at the flow meter temperature (T).

Activity coefficients at infinite dilution based on weight fraction, Ω^∞, were calculated [16–23] according to the expression:

$$\ln \Omega^\infty \equiv \ln \frac{a_1}{w_1} = \ln \frac{273.15R}{P_1^0 V_g M_1} - \frac{P_1^0}{RT}(B_{11} - V_1^0) \tag{2}$$

which has the advantage of ignoring the molecular mass of the polymer. In this equation, a_1 and w_1 are the activity and weight fraction of the solute in the polymer, respectively, and M_1, P_1^0, B_{11} and V_1^0 are the molecular masses, saturated vapour pressure, second virial coefficient and molar volume of the solute at the column temperature T, respectively. R is the gas constant.

Vapour pressures were deduced using Antoine coefficients from Boublik *et al.* [24]. Second virial coefficients of *n*-alkanes were calculated by the method of O'Connell and Prausnitz [25]; for other substances, values were interpolated or extrapolated from literature values corresponding to other temperatures [26]. Densities were calculated according to the pertinent equation [27,28].

Partial molar enthalpy of sorption, ΔH_s, was deduced in each case from experimental values according to the expression:

$$\Delta H_s = -R \frac{\partial(\ln V_g)}{\partial(1/T)} \tag{3}$$

Partial molar enthalpy of mixing of the solute at infinite dilution, ΔH_1, was calculated from:

$$\Delta \bar{H}_1^\infty = R \frac{\partial(\ln \Omega^\infty)}{\partial(1/T)} \tag{4}$$

The molar enthalpy of vaporization of the solutes was calculated as the difference:

$$\Delta H_v = \Delta \bar{H}_1^{\infty} - \Delta H_s \tag{5}$$

The activity coefficients at infinite dilution are related to the partial molar free energy of mixing by the expression:

$$\Delta G_m = RT \ln \Omega^{\infty} \tag{6}$$

Partial molar free energies of sorption at infinite dilution can be calculated from:

$$\Delta G_s = RT \ln(M_1 V_g / 273.15) \tag{7}$$

RESULTS AND DISCUSSION

The melting point of the polymer

Fig. 1 shows values of log V_g *versus* $1/T$ for *n*-octane, benzene, toluene and *n*-butanol, obtained on column 1 (not immobilized). The three typical temperature zones of polymers showing a phase transition are clearly seen in all cases. Between 35 and 55°C a zone is defined where adsorption of the solutes takes place. From 55 to 64°C, the values of V_g increase with temperature in a transition zone of non-equilibrium where two phenomena coexist: adsorption and absorption of the solutes in the polymer. From 64°C, upwards, we have the normal temperature zone of use of Superox 20M with reproducible chromatographic results. The temperature 64°C is the minimum allowable operating temperature of the column (MAOT). The value of 64°C is the same as that found by Sandra and co-workers [29,30] for other Superoxes of higher molecular mass.

Figs. 2 and 3 show results obtained with the same set of solutes on columns 2 and 3, both immobilized. Column 2 presents the three temperature zones of the polymer,

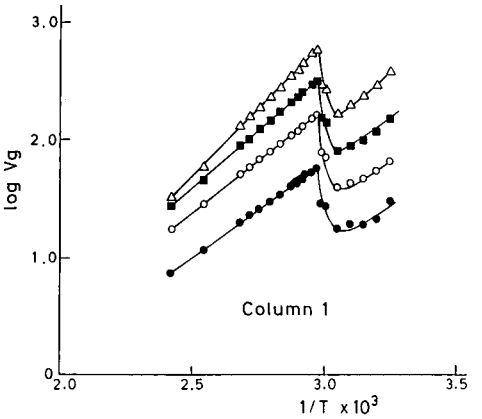

Fig. 1. Representation of log V_g *versus* $1/T$ on column 1 (not immobilized): ● = *n*-octane; ○ = benzene; ■ = toluene; △ = *n*-butanol.

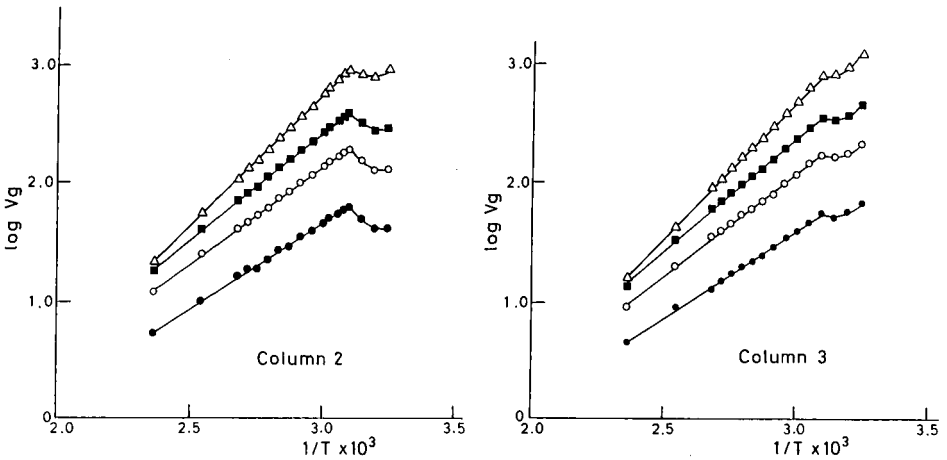

Fig. 2. Representation of log V_g *versus* $1/T$ on column 2 (immobilized with DCP): ● = *n*-octane; ○ = benzene; ■ = toluene; △ = *n*-butanol.

Fig. 3. Representation of log V_g *versus* $1/T$ on column 3 (immobilized with GPTMS and DCP): ● = *n*-octane; ○ = benzene; ■ = toluene; △ = *n*-butanol.

but now the melting point appears at about 40°C and the MAOT is found to be 50°C, 14°C lower than in the case of non-immobilized Superox 20M. Fig. 3 shows plots with shapes that again differ from the previous ones. The non-equilibrium zone appears here between 45 and 50°C as a zone with a slightly different slope. The MAOT of the column is again about 50°C. Sandra *et al.* [31] mention that the minimum useful temperature of a cross-linked polyethylene glycol column is 57°C in the case of a normal run, although it might be as low as 40°C if the column is heated and then cooled very quickly.

The different behaviour of column 1 from that exhibited by columns 2 and 3 with respect to the melting point of the polymer may be explained if we admit that the immobilization process introduces the effect of altering the crystallization of the polymer, decreasing the melting point. In the case of immobilized Superox 20M columns, the MAOT is found to be about 50–52°C. The transition zone of the polymer shows differences that depend on the immobilization procedure followed. It may be observed from Fig. 3 that, as immobilization with GPTMS produces a bonding between the polymer chains and the column surface through the coupling agent (GPTMS), this gives rise to a lower degree of crystallization than that produced with DCP alone (column 2) where only cross-linking of the polymer is supposed to occur. We measured the percentage of crystallinity according to the expression of Stein and Guillet [32]:

$$\text{Crystallinity}\,(\%) = 100\left(1 - \frac{V_g}{V'_g}\right) \tag{8}$$

where V_g is the experimental specific retention volume of a solute at a temperature below the melting point of the stationary phase and V'_g is the hypothetical value for the

TABLE II

PERCENTAGE OF CRYSTALLINITY OF THE STATIONARY PHASES

	Column 1		Column 2		Column 3	
	35°C	40°C	35°C	40°C	35°C	40°C
n-Octane	81	83	59	53	27	24
Benzene	86	86	61	54	32	30
Toluene	86	86	60	53	32	31
n-Butanol	85	85	53	47	27	26

same solute at the same temperature, assuming the polymer to be in a 100% amorphous state. V'_g is found by extrapolation from the values of V_g of the solute above the MAOT. The percentage of crystallinity should not depend on the solute chosen to measure it. Table II lists the values obtained for the three columns. Values are independent of the solute used.

The partial molar enthalpies and the free energies of sorption and mixing

Table III presents the partial molar enthalpies of sorption, mixing (adsorption and absorption) and vaporization, as found with eqns. 3–5, for the four solutes in the

TABLE III

PARTIAL MOLAR ENTHALPIES OF SOLUTION (ΔH_s), MIXING (ΔH_{ad} OR ΔH_{ab}) AND VAPORIZATION (ΔH_v) (kcal/mol^{-1})

	n-Octane	Benzene	Toluene	*n*-Butanol
Column 1 (not immobilized)				
Adsorption zone (35–55°C)				
ΔH_s	−4.79	−5.14	−6.27	− 8.49
ΔH_{ad}	4.95	2.89	2.68	4.23
ΔH_v	9.74	8.03	8.95	12.72
Absorption zone (64–140°C)				
ΔH_s	−7.40	−8.06	−8.97	−10.62
ΔH_{ab}	1.79	−0.33	−0.38	0.77
ΔH_v	9.20	7.73	8.60	11.35
Column 2 (immobilized with DCP)				
Absorption zone (50–150°C)				
ΔH_s	−6.56	−7.44	−8.27	−10.17
ΔH_{ab}	2.71	−0.33	0.37	1.35
ΔH_v	9.27	7.76	8.63	11.52
Column 3 (immobilized with GPTMS and DCP)				
Adsorption zone (35–45°C)				
ΔH_s	−4.80	−4.87	−5.79	− 8.32
ΔH_{ad}	5.01	3.19	3.21	4.57
ΔH_v	9.81	8.06	9.00	12.89
Absorption zone (50–150°C)				
ΔH_s	−6.66	−7.83	−8.66	−10.50
ΔH_{ab}	2.57	−0.06	−0.04	0.97
ΔH_v	9.25	7.76	8.62	11.47

three columns. Columns 1 and 3 show enthalpies of adsorption for all solutes which are higher than the corresponding enthalpies of sorption. Column 2 has an ill-defined adsorption zone, with fewer experimental points and, consequently, values of the partial molar enthalpies cannot be deduced for that zone. In the low-temperature region, when the stationary phase acts as an adsorbent solid, the values of the partial molar enthalpies of solution do not depend much on the degree of immobilization of the polymer. Considering the values of the partial molar enthalpy of mixing in the absorption zone, at temperatures above the phase transition zone, it may be said that *n*-alkane is in all cases the compound that mixes worst with the polymer, but it mixes slightly better with the non-immobilized stationary phase. The aromatic solutes mix better with the polymer than does *n*-butanol, but in this case differences with respect to the immobilization procedure cannot be observed.

With respect to the values of the enthalpies of sorption found in the zone of temperatures above the melting point of the polymer, it may be observed that in the three columns the most negative value is that of the alcohol, followed by those of the aromatics and the least negative value corresponding to the hydrocarbon. The sorption phenomenon implies that the molecules of the solute have transferred from the vapour phase into the polymer. This process depends to a great extent on the interaction of the solute with the Superox 20M, and therefore the entalpy associated with this process will depend on this interaction. In the case we are considering here, we may deduce that the solute–polymer interaction decreases in the order alcohols > aromatics > hydrocarbons. It may also be observed from the table that the values obtained for the non-immobilized stationary phase are somewhat more negative than those of the other two columns. The values of the partial molar free energies of mixing and sorption (Tables IV and V) confirm this.

TABLE IV

PARTIAL MOLAR FREE ENERGIES OF MIXING (kcal/mol)

	Adsorption zone				Absorption zone						
	35°C	40°C	45°C	50°C	70°C	80°C	90°C	100°C	120°C	140°C	150°C
Column 1 (not immobilized)											
n-Octane	3.24	3.34	3.31	3.20	2.24	2.24	2.24	2.24	2.27	2.34	–
Benzene	1.87	1.89	1.90	1.85	0.72	0.76	0.78	0.80	0.89	0.93	–
Toluene	1.98	2.01	2.01	1.98	0.84	0.89	0.91	0.95	1.05	1.08	–
n-Butanol	2.32	2.32	2.29	2.25	1.08	1.10	1.09	1.08	1.17	1.16	–
Column 2 (immobilized with DCP)											
n-Octane	*a*	2.96	*b*	*b*	2.43	2.40	2.47	2.39	2.40	–	2.44
Benzene	*a*	1.39	*b*	*b*	0.92	0.93	0.97	0.98	0.99	–	1.11
Toluene	*a*	1.50	*b*	*b*	1.06	1.07	1.13	1.13	1.16	–	1.25
n-Butanol	*a*	1.73	*b*	*b*	1.24	1.22	1.25	1.24	1.23	–	1.29
Column 3 (immobilized with GPTMS and DCP)											
n-Octane	2.79	2.76	2.72	*b*	2.58	2.56	2.53	2.58	2.51	–	2.60
Benzene	1.17	1.17	1.12	*b*	1.06	1.06	1.08	1.08	1.17	–	1.34
Toluene	1.30	1.30	1.24	*b*	1.18	1.19	1.20	1.23	1.31	–	1.49
n-Butanol	1.62	1.60	1.52	*b*	1.39	1.37	1.36	1.36	1.42	–	1.53

[a] No data available.

[b] Temperature does not correspond to the adsorption zone.

TABLE V

PARTIAL MOLAR FREE ENERGIES OF SORPTION, ΔG_s (kcal/mol)

	Temperature (°C)						
	70	80	90	100	120	140	150
Column 1 (not immobilized)							
n-Octane	−1.56	−1.39	−1.23	−1.07	−0.73	−0.36	–
Benzene	−2.02	−1.83	−1.66	−1.51	−1.09	−0.79	–
Toluene	−2.58	−2.39	−2.21	−2.05	−1.55	−1.29	–
n-Butanol	−2.83	−2.58	−2.37	−2.16	−1.65	−1.25	–
Column 2 (immobilized with DCP)							
n-Octane	−1.31	−1.23	−1.00	−0.92	−0.60	–	−0.10
Benzene	−1.82	−1.66	−1.44	−1.31	−1.10	–	−0.48
Toluene	−2.36	−2.20	−1.99	−1.84	−1.51	–	−0.98
n-Butanol	−2.67	−2.46	−2.20	−2.00	−1.59	–	−0.93
Column 3 (immobilized with GPTMS and DCP)							
n-Octane	−1.16	−1.07	−0.94	−0.73	−0.52	–	+0.05
Benzene	−1.68	−1.53	−1.37	−1.22	−0.84	–	−0.24
Toluene	−2.25	−2.09	−1.92	−1.74	−1.42	–	−0.73
n-Butanol	−2.53	−2.31	−2.10	−1.88	−1.40	–	−0.68

The results just cited might indicate that Superox 20M will mix well with polymers with aromatic rings or an alcoholic function in their chain, while mixing would be difficult with those polymers of long hydrocarbon-type chains [33,34]. Further experimentation with selected solutes would be needed to confirm the generality of this conclusion.

CONCLUSIONS

The MAOT for columns of Superox 20M has been found to be 64°C, the same as that reported for Superoxes of higher molecular weight. When Superox 20M is immobilized in some way, the MAOT changes to about 50°C. The immobilization method used does not affect the value of the MAOT but has a considerable effect on the intensity of the phase transition of the polymer.

According to the values of the partial molar enthalpy of mixing, it is seen that all solutes are better solvents of the non-immobilized stationary phase, with the solubility decreasing for all columns in the order: aromatics > alcohols > *n*-alkanes, the last being non-solvents of the polymer.

A study of the type presented here, based on a selected set of solutes, will allow us to predict polymer–polymer solubilities and is applicable to the problem of the use of mixed stationary phases in GC.

ACKNOWLEDGEMENT

This work was carried out under Project No. PB87/0393 of the Dirección General de Investigación Científica y Técnica (DGI-CYT), of the Ministerio de Educación y Ciencia of Spain.

REFERENCES

1 W. O. McReynolds, *J. Chromatogr. Sci.*, 8 (1970) 685.
2 T. J. Stark, P. A. Larson and R. Dandeneau, *J. Chromatogr.*, 279 (1983) 31.
3 P. Sandra, F. David, M. Proot, G. Diricks, M. Verstappe and M. Verzele, *J. High Resolut. Chromatogr. Chromatogr. Commun.*, 8 (1985) 782.
4 K. Grob, *Making and Manipulating Capillary Columns for Gas Chromatography*, Hüthig, Heidelberg, 1986.
5 K. Grob and G. Grob, *J. High Resolut. Chromatogr. Chromatogr. Commun.*, 5 (1982) 119.
6 W. A. Aue, C. R. Hastings and S. Kapila, *J. Chromatogr.*, 77 (1973) 299.
7 D. A. Cronin, *J. Chromatogr.*, 97 (1974) 263.
8 L. Blomberg, *J. Chromatogr.*, 115 (1975) 365.
9 J. J. Franken, R. C. M. De Nijs and F. L. Schulting, *J. Chromatogr.*, 144 (1977) 253.
10 L. Bystricky, *J. High Resolut. Chromatogr. Chromatogr. Commun.*, 9 (1986) 240.
11 H. Traitler, *J. High Resolut. Chromatogr. Chromatogr. Commun.*, 6 (1983) 60.
12 K. Grob, Jr., G. Grob and K. Grob, *J. Chromatogr.*, 156 (1978) 1.
13 K. Grob, Jr. and K. Grob, *J. Chromatogr.*, 207 (1981) 291.
14 K. Grob, G. Grob and K. Grob, Jr., *J. Chromatogr.*, 219 (1981) 13.
15 J. A. García-Domínguez, J. García-Muñoz, E. Fernández-Sánchez and M. J. Molera, *J. Chromatogr. Sci.*, 15 (1977) 520.
16 D. Patterson, Y. B. Tewari, H. P. Schreiber and J. E. Guillet, *Macromolecules*, 4 (1971) 356.
17 D. D. Deshpande, D. Patterson, H. P. Schreiber and C. S. Su, *Macromolecules*, 7 (1974) 530.
18 C. S. Su, D. Patterson and H. P. Schreiber, *J. Appl. Polym. Sci.*, 20 (1976) 1025.
19 G. DiPaola-Baranyi and J. E. Guillet, *Macromolecules*, 11 (1978) 228.
20 G. DiPaola-Baranyi and P. Degré, *Macromolecules*, 14 (1981) 1456.
21 K. S. Siow, S. H. Goh and J. S. Yap, *J. Chromatogr.*, 354 (1986) 75.
22 A. C. Su and J. R. Freid, *J. Polym. Sci., Polym. Lett.*, 24 (1986) 343.
23 G. J. Price, J. E. Guillet and J. H. Purnell, *J. Chromatogr.*, 369 (1986) 273.
24 T. Boublík, V. Fried and E. Hàla, *The Vapour Pressures of Pure Substances*. Elsevier, Amsterdam, 1975.
25 J. P. O'Connell and J. M. Prausnitz, *Ind. Eng. Chem., Process Des. Dev.*, 6 (1976) 245.
26 J. H. Dymond and E. B. Smith, *The Virial Coefficients of Pure Gases and Mixtures —A critical Compilation*, Clarendon Press, Oxford, 1980.
27 *TRC Thermodynamic Tables*, Thermodynamics Research Center, Texas Engineering Experiment Station, The Texas A & M University System.
28 National Research Council of the USA. *International Critical Tables of Numerical Data. Physics, Chemistry and Technology*, Vol. III. McGraw-Hill, New York, 1928.
29 M. Verzele and P. Sandra, *J. Chromatogr.*, 158 (1978) 111.
30 P. Sandra, M. Verzele, M. Verstappe and J. Verzele, *J. High Resolut. Chromatogr. Chromatogr. Commun.*, 2 (1979) 288.
31 P. Sandra, F. David, K. A. Turner, H. M. McNair and A. D. Brownstein, *J. Chromatogr.*, 477 (1989) 63.
32 A. N. Stein and J. E. Guillet, *Macromolecules*, 3 (1970) 102.
33 M. Galin and L. Maslinko, *Macromolecules*, 18 (1985) 2192.
34 J. I. Iribarren, M. Iriarte, C. Uriarte and J. J. Iruin, *J. Appl. Polym. Sci.*, 37 (1989) 3459.

Journal of Chromatography, 556 (1991) 495–503
Elsevier Science Publishers B.V., Amsterdam

CHROM. 23 373

Fluorescence detection in liquid chromatography with an intensified diode-array detector

TODD L. CECIL and SARAH C. RUTAN*

Department of Chemistry, Box 2006, Virginia Commonwealth University, Richmond, VA 23284-2006 (USA)

ABSTRACT

The capabilities of full fluorescence spectral detection for the analysis of polyaromatic hydrocarbons after a liquid chromatographic separation were evaluated. The limits of detection and the linear dynamic range were determined for three test compounds, benzo[*a*]pyrene, perylene and anthracene. With the instrument used, detection limits in the micromolar concentration range (*ca.* 100 ng injected), and a linear dynamic range of at least three orders of magnitude were observed. In addition, the pair of isomers 1- and 2-aminoanthracene, which are incompletely resolved both spectroscopically and chromatographically, were studied. Finally, a commercially available mixture of polyaromatic hydrocarbons was characterized, and it was possible to resolve the chromatographically unresolved pair of isomers benzo[*a*]anthracene and chrysene. The data analysis methods used included Kalman filter-based methods for adaptive subtraction of background responses, shift correction and linear regression analysis of overlapped responses. The results indicate that full fluorescence spectral detection in liquid chromatography should be an increasingly useful technique.

INTRODUCTION

Fluorescence spectroscopy is one of the most sensitive and inherently selective methods available for liquid chromatographic (LC) detection. Two of the most important applications of fluorescence detection include biomedical and environmental separations [1–4]. In environmental studies, the greatest attention has been paid to polycyclic aromatic hydrocarbons (PAHs), which are on the US Environmental Protection Agency's priority pollutant list [5]. The PAHs fluoresce strongly and are relatively non-volatile, therefore LC with fluorescence detection is one of the best quantitative separation methods available for their analysis.

Most of the work concerned with the fluorescence detection of LC effluents has been conducted using first-order fluorescence detectors, *i.e.*, that supply first-order data (data with one independent variable, *e.g.*, retention time). First-order fluorescence is usually done at a fixed excitation wavelength and either the total fluorescence intensity or a selected emission wavelength is monitored. Although first-order detectors are simple, reliable and inexpensive, they can suffer from problems due to variable retention times and overlapped peaks. Both of these problems can be minimized, but rarely eliminated, with first-order detectors.

0021-9673/91/$03.50

Second-order detectors can alleviate both problems and provide much more information about a mixture [6]. Second-order detectors produce data as a function of two independent variables, in this instance elution time and emission wavelength. Because of the advantages of using second-order detectors, much interest and attention has been devoted to them in the past 10 years. Some of the better known second-order systems include LC–UV–VIS with photodiode-array-based detection [7,8], LC–mass spectrometry [9] and LC–Fourier transform infrared spectrometry [10]. Second-order fluorescence detectors were developed in the 1970s and 1980s but the data analysis methods required to analyze the large amounts of data were not well developed [11,12]. Since then, little work concerning second-order fluorescence detectors has been conducted, but in the same period array detector technology and data analysis methods have advanced significantly. Therefore, second-order fluorescence detection is now a viable technique and should recieve more attention. Recently, papers have appeared that reflect this resurgence of interest [13,14]. The second-order detector examined in this work is based on a commercial spectrofluorimeter with modified optics and an intensified photodiode array (PDA) replacing the photomultiplier tube. A more detailed description of the modifications to the spectrofluorimeter is given below.

Fluorescence detection of LC effluents has several problems at the chemical level that must be addressed in order for this technique to become more widely accepted. These problems include fluorescence intensity fluctuations, spectral distortions, spectral response shifts, scattered light intereferences, variable background contributions and the qualitative and quantitative analysis of overlapped spectral and chromatographic data. These problems are examined here because they seem to represent the limitations to the acceptance of photodiode-array fluorescence detectors for routine analyses. We show that our detector is capable of reasonable detection limits and a good linear dynamic range. Further, methods for the analysis of chromatograms and the component fluorescence spectra that should be applicable to any second-order fluorescence detection method are examined. Finally, some of the advantages of the second-order fluorescence detection method are discussed.

EXPERIMENTAL

Chromatography

The chromatographic portion of the apparatus consisted of two Rainin (Woburn, MA, USA) HP pumps, each equipped with a 5-ml pump head. A Rainin pressure monitor and zero-dead-volume solvent-mixing chamber were also used. Injection was accomplished with a Rheodyne six-port injection valve with a 20-μl sample loop and an injection event marker. The columns used included two 15 cm × 1 cm I.D. Microsorb ODS C_{18} columns and a Spherisorb 10 cm × 1 cm I.D. ODS2 C_{18} column. All columns had 5-μm packing material.

The solvents used included methanol, acetonitrile and water. Methanol and acetonitrile were of Omnisolv (EM Scientific) spectroscopic grade and were used as received. Water was de-ionized, filtered through a 10-μm membrane and degassed with a helium sparge for 30 min before each run. The sample loop was rinsed with 500 μl of acetonitrile between injections. A sample volume of at least ten times the sample loop volume was injected each time.

All of the neat PAHs were obtained from Foxboro/Analabs (North Haven CT, USA) and were at least 98% pure. Aminoanthracenes were also purchased from Foxboro/Analabs and were of at least 90% purity and received no further purification. Standard solutions were made using degassed solvents. A standard mixture was purchased from Alltech (Deerfield, IL, USA) and contained anthracene (ANT), fluoranthene (FLA), phenanthrene (PHA), pyrene (PYR), chrysene (CHR) and benzo[*a*]anthracene (BAA) at about 10 ppm levels in toluene. This mixture was used as received.

Detector and optics

Our laboratory-constructed detector is similar to that described by Jadamec *et al.* [11]. The detector consists of a modified Farrand MK1 spectrofluorimeter with a 200-W Hg–Xe arc lamp as a source. The lamp housing was updated with the addition of an internal fan that stabilized the arc. The housing modifications were obtained from Optical Devices/Farrand (Elmsford, NY, USA). The fluorimeter was further modified by the replacement of the 28 000 line/in. gratings with 14 000 line/in. gratings obtained from Edmund Scientific. The excitation grating was blazed for maximum throughput in the first order at 250 nm and the emission grating was blazed at 500 nm. The lower resolution grating causes a larger portion of the first-order spectrum diffracted from the grating to be imaged on the diode array. The slits that were used on the excitation monochromator were both 20 nm, and the entrance slit to the emission polychromator was 1 nm. The cuvette holder in the sample compartment was replaced by an 8-μl flow cell purchased from Farrand. The flow cell was square and included focusing optics. In order to mount the diode array, a 1-in. diameter hole was drilled in the monochromator where the photomultiplier tube had previously been located. An adaptor plate was fabricated, mounted on the exterior of the monochromator and the diode array was attached to it. The final 90°C mirror in the Czerny–Turner monochromator was replaced with one that was wider so that a 200-nm portion of the emission spectrum would fall on the array. The intensified diode-array system was purchased from Tracor Northern and consisted of a TN-6122a intensified diode array, a TN-6600 Intelligent Interface and data acquisition and control software called ISIS. The TN-6122a is an electrothermally cooled PDA and therefore no additional cooling is necessary. The diode array can collect a spectrum every 0.1 s. Longer integration times reduce the noise and increase the signal proportionally. However, if the integration time is too long, the background signal will saturate the array. Therefore, a balance between the intensifier setting and integration time is necessary. In this instance an integration time of 1.1 s was found to be appropriate.

Control and acquisition

The computer that was used to control the LC pumps and the diode array was a PC-type 80386-based clone with a 320-megabyte hard disk, a Metrabyte Dash 16 A/D card, dual RS-422 ports and the TN-6600 interface card. All of the data collection and control programs were designed to run under the Microsoft Windows operating environment. All of the data analysis programs operate under DOS and were written using the PASCAL programming language. The program that controls the LC pumps was written with the Microsoft C compiler and the Microsoft Windows

software development kit. The Windows environment allowed both ISIS and the pump control program to run concurrently so that data could be collected as gradient control was being conducted. The injection was triggered with an injection event marker as a binary on–off switch through a parallel input on the A/D board for the gradient program and through the trigger input on the TN-6600 interface for the ISIS software. The pumps were controlled using the Rainin ASCII pump control protocol via the RS-422 ports.

Experimental conditions

The limit of detection (LOD) and linear dynamic range (LDR) calculations were based on experiments involving benzo[*a*]pyrene (B[*a*]P), perylene (PER) and anthracene (ANT). A standard solution with a concentration of 100 μM was prepared in acetonitrile for each of the PAHs. The standard solution was then diluted to the concentrations shown in Table I. An excitation wavelength of 300 nm was used for these studies. Each of the chromatograms was obtained under isocratic conditions with 100% acetonitrile at a flow-rate of 1.82 ml/min.

The second series of experiments involved 1- and 2-aminoanthracene (1-AANT and 2-AANT, respectively). A solution in acetonitrile was prepared for each of the aminoanthracenes at a concentration of 10 μM. An excitation wavelength of 300 nm was used. Five experiments were conducted. The first two involved obtaining a spectrum of each of the standard solutions of the AANTs injected directly into the flow cell. The intensifier was set so that the 2-AANT was on-scale at this concentration. The intensifier was not changed for the remainder of this series of experiments. The spectra of the pure standard solutions are called the model spectra. Then the standard solutions were injected onto the column using the following gradient conditions: flow-rate, 1.82 ml/min; linear gradient from acetonitrile–water (50:50) to 100% acetonitrile at 2%/min. The chromatograms of the standard solutions are called the model chromatograms. A 50:50 mixture of the AANT isomers was prepared and separated using the above conditions. This chromatogram is the unknown chromatogram.

The next series of experiments involved the separation and identification of a standard mixture of PAHs containing *ca.* 10 ppm of each of the PAH components. The same experimental conditions as described above were used for this analysis. Solutions of pure BAA, CHR, PYR, ANT, FLA and PHA in acetonitrile at *ca.* 50 μM were used as standards.

RESULTS AND DISCUSSION

As with any new detector design or detection method, it is necessary first to identify the capabilities of the method. One approach for instrument characterization is to determine the LDR and the LOD. Using these measures, it is possible to compare different instrument systems. Therefore, the first experiments that were conducted with the above detector included both LOD and LDR measurements. These measurements were done using B[*a*]P, PER and ANT, which were chosen for two reasons: first, they have been used extensively by workers in the fluorescence field for these types of measurements; and second, the fluorescence emission of each of the compounds falls on a different portion of the diode array, thereby allowing the LOD and LDR of the method to be determined over the entire PDA detector spectral range.

This examiniation of the PDA performance was done in order to identify any anomalous behavior over the array. The calibration data for these analytes are given in Table I. The PER data were obtained on a different day to the other two compounds. The concentrations reflect the concentration of the injected solution, not the concentration at the detector. The percentage deviation between the experimental data and the linear least-squares fit of those data is shown in Fig. 1. These residuals show no significant trends over three orders of magnitude, for a single intensifier setting. If more than one setting were used, the LDR could be increased significantly. The curvature at the upper limit of these curves comes from concentration quenching, which commonly occurs in fluorescence detection.

The calibration results for each of these fluorophores are shown in Table II. The LODs can be approximated from the standard deviations of the linear regression intercepts. This gives an estimated LOD for each of the three compounds of *ca.* 1 μM. If a different intensifier setting was used or if several replicates were run close to the detection limit, it would be possible to obtain a lower LOD. For all of these studies the intensifier setting was held constant because the changes in signal intensity brought about by changes in the intensifier setting appear to be non-linear.

TABLE I

CALIBRATION DATA FOR B[*a*]P, ANT AND PER

PAH	Concentration (μM)	Peak height (10^3 counts)
B[*a*]P[a]	100	2893
	50.0	1702
	25.0	873
	12.5	441
	6.25	250
	3.15	147
	1.56	88.0
	0.78	75.0
ANT[b]	100	3114
	50.0	1547
	25.0	858
	12.5	475
	6.25	266
	3.15	147
	1.56	99.0
	0.78	75.1
PER[c]	100	3075
	50.0	1580
	33.3	990
	10.0	347
	5.00	181
	1.00	75.1
	0.10	51.0

[a] Intensifier setting for B[*a*]P at 750.
[b] Intensifier setting for ANT at 850.
[c] Intensifier setting for PER at 800.

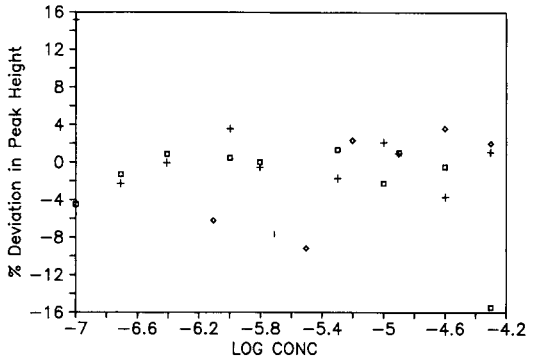

Fig. 1. Percentage deviation in peak height *versus* the log (concentration) for (□) B[*a*]P, (+) ANT and (◇) PER.

The next series of experiments involved 1- and 2-aminoanthracene (1- and 2-AANT), which were chosen because they are strong fluorophores and known carcinogens [15], and have similar spectral and chromatographic characteristics. In addition, the fluorescence efficiency of 1-AANT is an order of magnitude smaller than that of its isomer with 300 nm excitation. The emission spectra of the isomers are shown in Fig. 2. Further, it was found that both isomers undergo solvent-induced spectral response shifts. All of these factors combine to make this system very difficult to analyze using traditional approaches. The data obtained from this second-order detector were analyzed by fitting each of the spectra within the chromatographic peak envelope. The relative concentrations were summed to obtain the overall concentration estimates for each of the two isomers.

The procedure for the analysis of the 50:50 mixture of the aminoanthracene isomers was as follows. First, spectra of pure standard solutions of the aminoanthracenes in acetonitrile were obtained (Fig. 2). These spectra were background corrected using an algorithm developed previously in our laboratory [16], based on the adaptive Kalman filter fit of a measured model background of acetonitrile. In this instance, as the background was relatively featureless, the zeroth derivative was used in the fitting procedure [17]. These background-corrected spectra were used as models for the spectra obtained from a gradient run with a mixture of the isomers. A Kalman filter-based shift correction algorithm developed in our laboratory was applied to determine the spectral shifts [18,19]. The parameters used for this fit were a cut-off

TABLE II

CALIBRATION RESULTS FOR B[*a*]P, ANT AND PER

PAH	Slope (10^3 counts/μM)	Intercept (10^3 counts)
B[*a*]P	29.0 (0.9)	86 (38)
ANT	30.4 (0.3)	65 (12)
PER	30.3 (0.3)	35 (14)

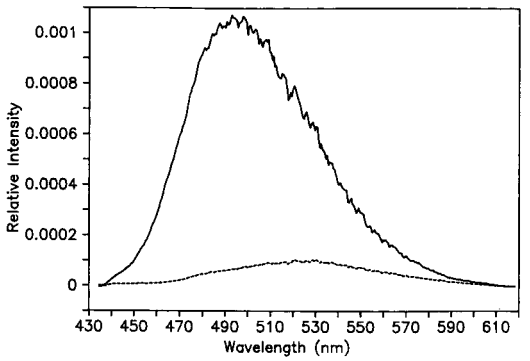

Fig. 2. Fluorescence spectra of (dashed line) 1-aminoanthracene and (solid line) 2-aminoanthracene in acetonitrile.

point of 0.5 and a measurement variance of 1×10^{-8}. Although the results were variable, especially for the weaker fluorophore, 1-AANT, they indicated a +4 nm shift for 1-AANT and a +9 nm shift for the 2-AANT, obtained from the most intense spectra in the chromatographic profile. A red shift of this magnitude is reasonable, as the model spectra were obtained in 100% acetonitrile and the aminoanthracenes elute in a solvent composition of approximately 60:40 acetonitrile–water. All spectra within the chromatographic envelope were then fitted with the regular Kalman filter to this shifted model. The extracted chromatograms are shown in Fig. 3. The chromatogram for 1-AANT shows more noise, as the model for this component had larger noise contributions. The areas under the two peaks are very similar (0.41 and 0.39 for 1- and 2-AANT, respectively). The retention times for these two peaks were identical. As the model used was based on spectra obtained from standard solutions injected directly into the flow cell, a correction factor is required to account for the number of moles flowing through the cell during the integration time. Calculations show that an average of 33.4 μl flows through the cell during this period. Correction by a factor of

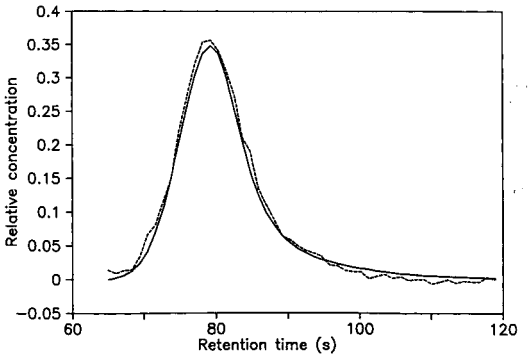

Fig. 3. Extracted chromatograms of (dashed line) 1-aminoanthracene and (solid line) 2-aminoanthracene.

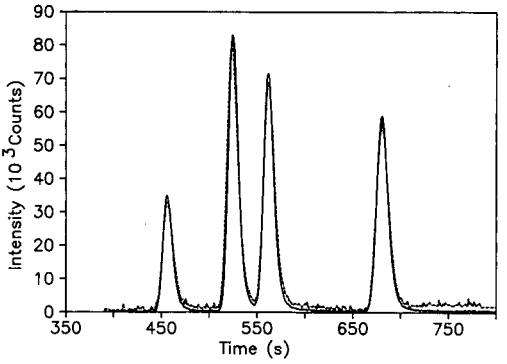

Fig. 4. (Dashed line) chromatogram of the PAH mixture and (solid line) the Kalman fit of the chromatogram. The first peak is ANT, the second is FLA, the third is PYR and the fourth contains both BAA and CHR.

33.4/20 (where 20 μl is the chromatographic injection volume) should yield corrected relative concentrations of 0.68 and 0.65 for 1-AANT and 2-AANT, respectively. The theoretical relative concentrations should be 0.5 for both isomers. Our concentration estimation errors are probably due to a change in the fluorescence efficiency in the chromatographic eluent in comparison with pure acetonitrile. We are currently investigating the reasons for this discrepancy. Note that other methods, such as rank annihilation, could not be used to analyze these data, for two main reasons: first, the spectral shifts would cause majors errors in this algorithm, and second, the two species show no chromatographic resolution, which is a requirement for successful application of the rank annihilation algorithm

Using the method outlined above, a mixture of five PAHs was separated and the concentrations were estimated. The chromatogram for the PAH mixture is shown in Fig. 4. Under these conditions, BAA and CHR co-elute. This chromatogram was fitted using pure component chromatograms for each of the five components using the shift correction technique, and the resulting fit is shown in Fig. 4. The results for the concentration estimates are given in Table III. The method used to fit the aminoanthracene spectra was also used to fit this PAH mixture. The concentration estimates obtained from fitting the spectral data are also shown in Table III. We could

TABLE III

CONCENTRATION ESTIMATES FOR PAH MIXTURE

PAH	Concentration estimate (μM)	
	Chromatographic fit	Spectral fit
ANT	7.2	7.6
FLA	3.7	5.6
PYR	5.1	14.1
BAA	5.0	6.0
CHR	6.7	11.6

not compare these results with the true values, as we found that the standard mixture was not prepared quantitatively by the manufacturer. Although the concentration estimates using the two different methods are not in complete agreement, these results help to illustrate the importance of developing careful data analysis strategies for fluorescence spectral detection in liquid chromatography. More recent studies have found that the most probable cause for this lack of agreement between the two methods is due to the irreproducibility of the gradient separation conditions.

CONCLUSIONS

This work shows that it is possible to build a relatively inexpensive second-order fluorescence detector that yields acceptable detection limits. It also shows that there is a definite need for data analysis strategies that use second-order data more effectively, especially for fluorescence spectroscopy, where several chemical and physical factors can affect the accuracy of the results. Here, a combination of methods for background subtraction, shift correction and peak resolution were used to analyze mixtures of PAHs. We can effectively correct for solvent-dependent spectral shifts and also for retention time variations in gradient methods. The chromatographic profiles of severely overlapped species can be extracted based on analysis of the emission spectral data. Using appropriate data analysis methods it should be possible to identify and quantify fluorescence signals without an extensive calibration procedure. Further work will be focused on understanding the factors affecting accurate quantification in this system.

ACKNOWLEDGEMENTS

The authors acknowledge the donation of the Farrand Mark 1 spectrofluorimeter from Philip Morris, USA, and financial support from the US Department of Energy (Grant DE-FG05-88ER13833).

REFERENCES

1 F. V. Bright, *Anal.Chem.*, 61 (1989) 309.
2 Y. Umegae, H. Nohta and Y. Ohkura, *J. Chromatogr.*, 515 (1990) 495.
3 J. Salamoun, M. Macka, M. Nechutal, M. Matousek and L. Knesel, *J. Chromatogr.*, 514 (1990) 179.
4 S. K. Poole, T. A. Dean, J. W. Oudsema and C. F. Poole, *Anal. Chim. Acta*, 236 (1990) 3.
5 *Fed. Regist.*, December 3rd, 1979, p. 69464.
6 E. Sanchez and B. R. Kowalski, *J. Chemometr.*, 2 (1988) 265.
7 A. F. Fell, B. J. Clark and H. P. Scott, *J. Chromatogr.*, 316 (1984) 423.
8 E. V. Dose and G. Guiochon, *Anal. Chem.*, 61 (1989) 2571.
9 L. J. Deterding, M. A. Moseley, K. B. Tomer and J. W. Jorgensen, *Anal. Chem.*, 61 (1989) 2504.
10 J. W. Hellgeth and L. T. Taylor, *Anal. Chem.*, 59 (1987) 295.
11 J. R. Jadamec, W. A. Saner and Y. Talmi, *Anal. Chem.*, 49 (1977) 1316.
12 J. C. Gluckman, D. C. Shelly and M. V. Novotny, *Anal. Chem.*, 57 (1985) 1546.
13 J. Wegrzyn, G. Patonay, M. Ford and I. Warner, *Anal. Chem.*, 62 (1990) 1754.
14 R. J. Vandernesse, C. Gooijer, G. P. Hoornweg, U. A. T. Brinkman, N. H. Velthorst and S. J. Vanderbent, *Anal. Lett.*, 23 (1990) 1235.
15 R. B. Gammage, in A. Bjorseth (Editor), *Handbook of Polycyclic Aromatic Hydrocarbons*, Marcel Dekker, New York, 1983, p. 659.
16 D. D. Gerow and S. C. Rutan, *Anal. Chim. Acta*, 184 (1986) 53.
17 W.-F. Lien and S. C. Rutan, presented at the *Pittsburgh Conference and Exposition on Analytical Chemistry and Applied Spectroscopy, March 1990, Abstracts*, No. 868.
18 G. H. Webster, T. L. Cecil and S. C. Rutan, *J. Chemometr.*, 3 (1988) 21.
19 T. L. Cecil and S. C. Rutan, *Anal. Chem.*, 62 (1990) 1998.

PUBLICATION SCHEDULE FOR 1991

Journal of Chromatography and Journal of Chromatography, Biomedical Applications

MONTH	D 1990–M 1991	J	J	A	S	O	N	D
Journal of Chromatography	Vols. 535–545/1	545/2 546/1 + 2 547/1 + 2	548/1 + 2 549/1 + 2 550/1 + 2	552/1 + 2 553/1 + 2 554/1 + 2 555/1 + 2	556/1 + 2 557/1 + 2 558/1	558/2 559/1 + 2		
Cumulative Indexes, Vols. 501–550				551/1 + 2				
Bibliography Section	560/1	560/2			561/1			561/1
Biomedical Applications	Vols. 562–566	567/1	567/2 568/1	568/2	569/1 + 2 570/1	570/2	571/1 + 2	572/1 + 2

INFORMATION FOR AUTHORS

(Detailed *Instructions to Authors* were published in Vol. 522, pp. 351–354. A free reprint can be obtained by application to the publisher, Elsevier Science Publishers B.V., P.O. Box 330, 1000 AH Amsterdam, The Netherlands.)

Types of Contributions. The following types of papers are published in the *Journal of Chromatography* and the section on *Biomedical Applications:* Regular research papers (Full-length papers), Review articles and Short Communications. Short Communications are usually descriptions of short investigations, or they can report minor technical improvements of previously published procedures; they reflect the same quality of research as Full-length papers, but should preferably not exceed six printed pages. For Review articles, see inside front cover under Submission of Papers.

Submission. Every paper must be accompanied by a letter from the senior author, stating that he/she is submitting the paper for publication in the *Journal of Chromatography*.

Manuscripts. Manuscripts should be typed in double spacing on consecutively numbered pages of uniform size. The manuscript should be preceded by a sheet of manuscript paper carrying the title of the paper and the name and full postal address of the person to whom the proofs are to be sent. As a rule, papers should be divided into sections, headed by a caption (*e.g.*, Abstract, Introduction, Experimental, Results, Discussion, etc.). All illustrations, photographs, tables, etc., should be on separate sheets.

Introduction. Every paper must have a concise introduction mentioning what has been done before on the topic described, and stating clearly what is new in the paper now submitted.

Abstract. All articles should have an abstract of 50–100 words which clearly and briefly indicates what is new, different and significant.

Illustrations. The figures should be submitted in a form suitable for reproduction, drawn in Indian ink on drawing or tracing paper. Each illustration should have a legend, all the *legends* being typed (with double spacing) together on a *separate sheet.* If structures are given in the text, the original drawings should be supplied. Coloured illustrations are reproduced at the author's expense, the cost being determined by the number of pages and by the number of colours needed. The written permission of the author and publisher must be obtained for the use of any figure already published. Its source must be indicated in the legend.

References. References should be numbered in the order in which they are cited in the text, and listed in numerical sequence on a separate sheet at the end of the article. Please check a recent issue for the layout of the reference list. Abbreviations for the titles of journals should follow the system used by *Chemical Abstracts.* Articles not yet published should be given as "in press" (journal should be specified), "submitted for publication" (journal should be specified), "in preparation" or "personal communication".

Dispatch. Before sending the manuscript to the Editor please check that the envelope contains four copies of the paper complete with references, legends and figures. One of the sets of figures must be the originals suitable for direct reproduction. Please also ensure that permission to publish has been obtained from your institute.

Proofs. One set of proofs will be sent to the author to be carefully checked for printer's errors. Corrections must be restricted to instances in which the proof is at variance with the manuscript. "Extra corrections" will be inserted at the author's expense.

Reprints. Fifty reprints of Full-length papers and Short Communications will be supplied free of charge. Additional reprints can be ordered by the authors. An order form containing price quotations will be sent to the authors together with the proofs of their article.

Advertisements. Advertisement rates are available from the publisher on request. The Editors of the journal accept no responsibility for the contents of the advertisements.

For Superior Chiral Separation From Analytical To Preparative.

The finest from DAICEL……

Why look beyond DAICEL? We have developed the finest CHIRALCEL, CHIRALPAK and CROWNPAK with up to 17 types of HPLC columns, all providing superior resolution of racemic compounds.

NEW CHIRALPAK AS

● CHIRALPAK AS

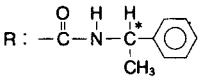

for β-Lactam antibiotics

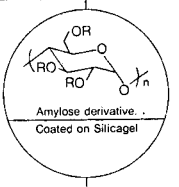

NEW CHIRALPAK AD

● CHIRALPAK AD

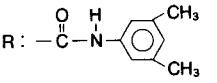

4-Acetoxy-2-azetidine

Eluent : Hexane/Ethanol = 8/2
Flow rate : 1.0mℓ/min
Temperature : r.t.
Detection : UV 254nm

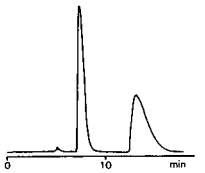

Oxyphencyclimine

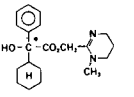

Eluent : Hexane/2-Propanol = 9/1
Flow rate : 1.0mℓ/min
Temperature : r.t.
Detection : UV 254nm

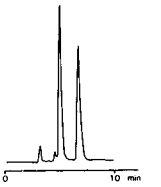

Ofloxacine methyl ester

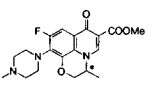

Eluent : Hexane/EtOH = 8/2
Flow rate : 1.2mℓ/min
Temperature : 40°C
Detection : UV 254nm

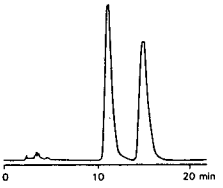

Verapamil

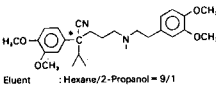

Eluent : Hexane/2-Propanol = 9/1
Flow rate : 1.0mℓ/min
Temperature : r.t.
Detection : UV 254nm

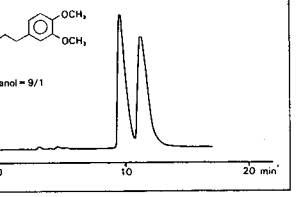

Analytical column 0.46cm × 25cm(10μm)

CHIRALCEL OA
OB
OC
OD
OJ
OF
OG
OK

CHIRALPAK AS
AD

Normal Phase

Semi-preparative column 2cm × 25cm(10μm)

You can have Pure enantiomer quickly!!

■Separation Service

- A pure enantiomer separation in the amount of 100g ~ 10kg is now available.
- Please contact us for additional information regarding the manner of use and application of our chiral columns and how to procure our separation service.

DAICEL CHEMICAL INDUSTRIES, LTD.

chiral chemicals division.
8-1, Kasumigaseki 3-chome, Chiyoda-ku, Tokyo 100, Japan Phone: 03 (507) 3151 FAX: 03 (507) 3193

DAICEL(U.S.A.), INC.
Fort Lee Executive Park
Two Executive Drive, Fort Lee,
New Jersey 07024
Phone: (201) 461-4466
FAX: (201) 461-2776

DAICEL(U.S.A.), INC.
23456 Hawthorne Blvd.
Bldg. 5, Suit 130
Torrance, CA 90505
Phone: (213) 791-2030
FAX: (213) 791-2031

DAICEL(EUROPA)GmbH
Oststr. 22
4000 Düsseldorf 1, F.R. Germany
Phone: (211) 369848
Telex: (41) 8588042 DCEL D
FAX: (211) 364429

DAICEL CHEMICAL(ASIA)PTE. LTD.
65 Chulia Street #40-07
OCBC Centre, Singapore 0104
Phone: 5332511
FAX: 5326454